Investigation of novel pathways causing autoinflammatory disease

Annemarie Steiner

ORCID ID:
0000-0001-8419-4794

from Lutherstadt Wittenberg, Germany

Submitted in total fulfilment of the requirements of the joint degree of
Doctor of Philosophy (PhD)
of the Medical Faculty
The Rheinische Friedrich-Wilhelms-Universität Bonn
and
The Department of Medical Biology
The University of Melbourne

Bonn/Melbourne, 2022

Performed and approved by the Medical Faculty of the Rheinische Friedrich-Wilhelms-Universität Bonn and The University of Melbourne

1. Supervisor: Prof. Matthias Geyer

2. Supervisor: Associate Prof. Seth L. Masters

Date of submission: 5th December 2021
Date of the oral examination: 12th April 2022

Institute of Structural Biology, Bonn,
Director: Prof. Matthias Geyer

Table of contents

Abbreviations

2’3’-cGAMP	2’3’-cyclic GMP-AMP
2’3’-c-di-AM(PS)$_2$	2’3’bisphosphorothioate analog of cyclic adenosine monophosphate (c-di-AMP) (STING ligand)
3D	three-dimensional
5’ppp	5’-triphosphate
µg	microgram
µl	microliter
µm	micrometre
µM	micromolar
°	degree
°C	degree Celsius
x*g*	times gravity

A

Å	Angstrom (0.1 nm)
A	alanine
aa	amino acid
AACOCF3	arachidonyl trifluoromethyl ketone
ADAR	adenosine deaminase acting on RNA
ADP	adenosine diphosphate
AID	autoinflammatory disease
AIFEC	autoinflammation with infantile enterocolitis
AIM2	absent in melanoma 2
ALR	AIM2-like receptors
ALT	alanine aminotransferase
AMP	adenosine monophosphate
AOSD	adult-onset Still’s disease
AP	adapter protein
APAF-1	apoptotic protease activating factor 1
ARF1	ADP-ribosylation factor 1
ASC	apoptosis-associated speck-like protein containing a CARD
ASCE	additional strand catalytic E protein family
AST	aspartate aminotransferase
ATP	adenosine triphosphate

B

bp	base pairs
BFP	blue fluorescent protein
BIR	baculovirus inhibitor of apoptosis protein repeat
BLCL	B cell-derived lymphoblastoid cell lines
BMDCs	murine bone marrow-derived dendritic cells
BMDMs	murine bone marrow-derived macrophages

C

C	cysteine

c.	prefix, referring to coding DNA sequence
CAPS	cryopyrin-associated periodic syndrome
CARD	caspase activation and recruitment domain
CD	cluster of differentiation
CED4	cell death protein 4
cGAS	cyclic GMP-AMP-synthase
CH	connector helix (in STING)
CI	confidence interval
CIITA	class II, major histocompatibility complex transactivator
CL	connector loop (in STING)
cl.	clone
CMV	cytomegalovirus
COP	coat protein complex (coatomer)
COPA	coatomer subunit α
COPB	coatomer subunit β
COPD	coatomer subunit δ
COPE	coatomer subunit ε
COPG1/COPG2	coatomer subunit γ1, γ2
COPZ	coatomer subunit ζ
COX1,2	cyclooxygenase 1 and 2
CpG DNA	cytosine-phosphate-guanine-containing DNA
cPLA2α	cytosolic phospholipase A2 alpha
CRISPR	clustered regularly interspaced short palindromic repeats
CRP	C-reactive protein
cryo-EM	cryogenic electron microscopy
cryo-ET	cryogenic electron tomography
CTT	C-terminal tail (in STING)
CV	column volume

D

D	aspartate
Da	Dalton
DAI	DNA-dependent activator of IRFs
DAH	diffuse alveolar hemorrhage
DAMP	damage-associated molecular pattern
DC	dendritic cell
DDX41	helicase DExD/H-box helicase
del	deletion
DMARD	disease-modifying antirheumatic drug
DNA	desoxyribonucleic acid
Dox	doxycycline
ds	double-stranded
DSB	DNA double strand break
DSS	dextran sodium sulfate

E

E	glutamate

EGFP	enhanced GFP
eIF2α	eukaryotic translation initiation factor 2 alpha
ELISA	enzyme-linked immunosorbent assay
ER	endoplasmic reticulum
ERAD	ER-associated degradation
ERES	ER exit site
ERGIC	ER-Golgi-intermediate compartments
ESR	erythrocyte sedimentation rate
EV	empty vector

F

F	phenylalanine
FACS	fluorescence-activated cell sorting
FBS	fetal bovine serum
FCAS	familial cold autoinflammatory syndrome
FMF	familial Mediterranean fever
fs	frameshift
FSC	forward scatter

G

G	glycine
GFP	green fluorescent protein
GIT	gastrointestinal tract
GMP	guanosine monophosphate
GnomAD	Genome Aggregation Database
GoF	gain of function
GSDMD	gasdermin D
GTP	guanosine triphosphate
gt/gt	golden ticket (mouse strain with missense mutation in STING, STING null phenotype)
GWAS	genome-wide association study

H

H	histidine
h	human
hr(s)	hour(s)
HAMP	homeostasis-altering molecular process
HC	healthy control donor
HD1, HD2	helical domain 1,2
HDR	homology-directed repair
HEK	human embryonic kidney
HIV	human immunodeficiency virus
HLH	hemophagocytic lymphohistiocytosis
HRP	horseradish peroxidase
HSV-1	herpes simplex virus 1
HSCT	hematopoietic stem cell transplantation
HT-DNA	herring testes DNA

I

IBD	inflammatory bowel disease
iBMDMs	immortalized bone marrow-derived macrophages
IEC	intestinal epithelial cells
IF	immunofluorescence
IFI16	interferon-inducible protein 16
IFN	interferon
IFNAR1/2	interferon α/β receptor 1 and 2
IgG, IgA, IgM	immunoglobulin G, A, M
IκB	inhibitor of NF-κB
IKK	IκB kinase
IL	interleukin
IL-18BP	IL-18 binding protein
ILD	interstitial lung disease
indel	insertion and deletion of bases in the genome
iNOS	inducible nitric oxide synthase
iPSC	inducible pluripotent stem cells
IRF	interferon regulatory factor
ISG	interferon-stimulated gene

J

JAK	Janus kinase
JNK1	c-Jun N-terminal kinase 1

K

K	lysine
kb	kilobase
K_d	dissociation constant
kDa	kilodaltons
KDEL	amino acid sequence motif: lysine (K), aspartate (D), glutamate (E), leucine (L)
KDELR	KDEL receptor
KKxx/KxKxx	dilysine (K) motifs
KO	knockout

L

L	leucine
LB	Luria Bertani
LBD	ligand-binding domain
LC3	microtubule-associated protein 1A/1B light chain 3
LDH	lactate dehydrogenase
LIR	LC3-interacting regions
LoF	loss of function
LPS	lipopolysaccharide
LRR	leucine-rich repeat domain
LTB4	leukotriene B4

M

m	mouse/murine
M	molar
MAF	mutant allele frequency
MAPK	mitogen-activated protein kinase
MAVS	mitochondrial antiviral signalling protein
MAS	macrophage activation syndrome
mCit	mCitrine
MDA5	melanoma differentiation-associated protein 5
MDM	monocyte-derived macrophages (human origin)
MDP	muramyl dipeptide
MEF	mouse embryonic fibroblast
MFI	mean fluorescence intensity
min	minutes
ml	milliliters
mTOR	mammalian target of rapamycin
MOI	multiplicity of infection
MS	mass spectrometry
MW	molecular weight
MyD88	myeloid differentiation primary response 88

N

N	asparagine
NACHT	domain present in NAIP, CIITA, HET-E, TP1
NAIP	NLR family of apoptosis inhibitory protein
NBD	nucleotide-binding domain
NEB	New England Biolabs
NF-κB	nuclear factor kappa-light chain enhancer of activated B cells
NHEJ	non-homologous end joining
NK cell	natural killer cell
NLR	NOD-like receptors
NLRC4	NLR family CARD domain containing 4
NLRC4-AID	NLRC4-associated autoinflammatory disease
NLRP3	NLR family pyrin domain containing 3
nm	nanometer
nM	nanomolar
NOD	nucleotide-binding oligomerization domain
NOMID	neonatal-onset multisystem inflammatory disease
NP-40	Nonidet P-40
NPC1	Niemann-Pick disease type C1 protein
NSAID	nonsteroidal anti-inflammatory drug

O

OR	odds ratio

P

P	proline

p.	prefix, referring to amino acid sequence
P3C	Pam3CSK4 (TLR1/2 agonist)
PAM	protospacer adjacent motif
PAMP	pathogen-associated molecular pattern
PBMC	peripheral blood mononuclear cell
PBS	phosphate buffered saline
PCR	polymerase chain reaction
PDB	protein data bank
pegRNA	prime editing guide RNA
PERK	protein kinase R-like ER kinase
PGE2	prostaglandin E2
PI	propidium iodide
PI3K	phosphatidylinositol 3-kinase
PKA, PKR, PKC	protein kinase A, protein kinase R, protein kinase C
PMA	phorbol myristate acetate
PRR	pattern recognition receptor
PTM	post-translational modification
PYD	pyrin domain

Q

Q	glutamine
qRT-PCR	quantitative Real-Time PCR

R

R	arginine
Rab7	Ras-related protein Rab7
RFP	red fluorescent protein
rhIL-18BP	recombinant human IL-18 binding protein
RIG-I	retinoic acid-inducible gene-I
RIPK3	receptor-interacting protein kinase 3
RLR	RIG-I-like receptors
RNA	ribonucleic acid
RNaseH2	ribonuclease H2
rpm	revolutions per minute

S

S	serine
SAA	serum amyloid A
SAMHD1	sterile alpha motif (SAM) domain and HD domain-containing protein 1
SAR1	secretion associated Ras related GTPase 1
SAVI	STING-associated vasculopathy with onset in infancy
SD	standard deviation
SDS-PAGE	sodium dodecyl sulphate-polyacrylamide gel electrophoresis
SEC	size exclusion chromatography
SEC13, 23, 24, 31	COPII subunit proteins
SEM	standard error of the mean

*Sf*9	*Spodoptera frugiperda* 9 immortalized insect cell line
sgRNA	single guide RNA
siRNA	small interfering RNA
SLE	systemic lupus erythematosus
SSC	side scatter
STAND	signal transduction ATPases with numerous domains
STAT	signal transducer and activator of transcription
STEEP	STING ER exit protein
SURF4	surfeit locus protein 4
ss	single-stranded
STIM1	stromal interaction molecule 1
STING	stimulator of interferon genes

T

T	threonine
T3SS	type three secretion system
TBK1	TANK-binding kinase 1
TEV	Tobacco Etch Virus
Th	T helper cell
TLR	Toll-like receptor
Tm	melting temperature
TMD	transmembrane domain
TMED	transmembrane emp24 protein transport domain-containing
TNF	tumour necrosis factor
TNFR	TNF receptor
TRAF	TNF receptor associated factor
TREX1	three-primer repair exonuclease 1
TYK2	tyrosine kinase 2

U

UC	ulcerative colitis
UPR	unfolded protein response

V

V	valine
VPS34	vacuolar protein sorting-associated protein 34
v/v	volume per volume

W

W	tryptophan
WD40	tryptophan (W)-aspartate (D), 40 amino acid motif
WHD	winged helix domain
WIPI2	WD repeat domain phosphoinositide-interacting protein 2
WT	wildtype
w/v	weight per volume

Y

Y	tyrosine

List of Tables

List of Figures

Abstract

Autoinflammatory diseases (AIDs) are rare pathologies caused by mutations in genes associated with innate immune pathways. Investigating the underlying molecular defects contributes to identification of targeted treatment strategies for patients and steadily extends our knowledge of innate signalling pathways and their regulation. Two different diseases were the focus of this thesis: COPA syndrome and NLRC4-AID.

COPA syndrome is an autosomal dominantly inherited immune disorder, caused by loss of function mutations in the coat protein complex I (COPI) subunit α (COPA), which participates in retrograde vesicular trafficking of proteins from the Golgi apparatus to the endoplasmic reticulum (ER) and within Golgi compartments. Deficiency of COPA is associated with ER stress, NF-κB activation and type I interferon (IFN$\alpha\beta$) signalling, although the upstream innate immune sensor that is responsible for this was unknown.

Using a range of biochemical and molecular biological techniques, we established *in vitro* models that recapitulate unprovoked proinflammatory signalling upon CRISPR/Cas9-mediated deletion of *COPA* and identify aberrant activation of immune sensor STING, which was also dependent on upstream cytosolic DNA sensor cyclic GMP-AMP-synthase (cGAS).

Further, we demonstrate that genetic deletion of other COPI subunits, *COPG1* and *COPD*, similarly induces STING activation, which suggests that innate immune diseases associated with mutations in other COPI subunit genes may exist.

Finally in this chapter, we show that inflammation in COPA syndrome patient PBMCs and COPI-deficient cell lines is ameliorated by treatment with the small molecule STING inhibitor H-151, suggesting targeted inhibition of the cGAS-STING pathway as a novel therapeutic approach to treat inflammation associated with COPA syndrome and perhaps other COPI-deficiencies.

In the second and third part of this thesis, we focussed on NLRC4-associated AIDs, which are typically caused by autosomal dominant gain of function mutations in NLR family CARD domain containing 4 (*NLRC4*) that drive hyperactive inflammasome signalling.

Here, we report the first case of a patient with immune dysregulation carrying a recessive mutation in *NLRC4* (c.478G>A, p.A160T). Using historical clinical data, serum cytokine analysis and *in vitro* stimulation of monocyte-derived macrophages we suggest aberrant inflammasome signalling as underlying cause of the inflammatory episodes experienced by the patient.

In vitro, we assessed the pathogenic potential of this mutation and demonstrate ligand-induced increased ASC specking, pyroptosis and cytokine secretion by NLRC4 A160T. Further, using meta-analysis association data we find that heterozygous allele carriers in the general population are at increased risk of developing ulcerative colitis (UC).

Results from subsequently performed structural and biophysical studies aiming to elucidate the conformational changes associated with this mutation point towards a mechanism of action that only affects NLRC4 A160T in the active conformation. Furthermore, since residue A160 is conserved in mice and most primate NLRC4 proteins, but T160 is encoded in the wildtype sequence of NLRC4 in ungulate and carnivore species, the evolutionary relationship between these species is presented. Finally, we discuss potential mechanisms of actions by which NLRC4 A160T may cause aberrant inflammasome activation and evaluate residue T160 as a potential phosphorylation site.

Together, studies described in this thesis identify a direct target for therapeutic intervention in immune diseases associated with defective COPI transport and shape the current understanding of retrograde trafficking as negative regulatory mechanism in STING signalling. Further, we provide *in vitro* evidence for the pathogenic potential of the NLRC4 A160T mutation, which was previously unrecognized and may represent a susceptibility locus for UC.

Declaration

This is to certify that,

(i) the thesis comprises only my original work towards the PhD except where indicated in the preface;
(ii) due acknowledgement has been made in the text to all other material used;
(iii) the thesis is less than 100,000 words in length, exclusive of tables, maps, bibliographies and appendices as approved by the Research Higher Degrees Committee.

Annemarie Steiner

Preface

The work presented in this thesis was conducted in the laboratory of Associate Prof. Seth L. Masters (Walter and Eliza Hall Institute of Medical Research (WEHI), University of Melbourne, Australia) and the laboratory of Prof. Matthias Geyer (Institute of Structural Biology, The Rheinische Friedrich-Wilhelms-Universität Bonn, Germany). Annemarie Steiner was supported by the Melbourne Research Scholarship (Stipend and Fee offset).

My contribution to experiments presented in each chapter of this thesis is listed below:

Chapter 3: 85 %

- The mass spectrometry experiment and proteomics analysis shown in Figure 3.4 A were performed by Dominic De Nardo (WEHI, University of Melbourne and Monash University, Australia) and Laura F. Dagley (WEHI, University of Melbourne, Australia).

- The *ex vivo* flow cytometry analysis of PBMCs isolated from a COPA syndrome patient and healthy control donors (Figure 3.6) was performed by Ignazia Prigione, Stefano Volpi and Marco Gattorno (IRCCS Institute Giannina Gaslini, Genoa, Italy). I performed the data analysis.

- Although the experiments were designed and optimized by me, the final data presented in Figure 3.9 were generated by Katja Hrovat-Schaale and Pawat Laohamonthonkul. Ronnie Ren Jie Low (WEHI, University of Melbourne, Australia) performed the imaging analysis that is part of Figure 3.9 A.

- Data presented in Figure 3.11 and Suppl. Figure 5 was generated by Katja Hrovat-Schaale, Pawat Laohamonthonkul, and Cassandra R.

Harapas (WEHI, University of Melbourne, Australia), however I contributed to the experimental design.

The work presented in chapter 3 is currently under revision following peer review by Nature Communications. A preprint of this work was published on bioRxiv on 9th July 2020.

Chapter 4: 90 %

- Identification of the patient and clinical data was provided by Leonardo Oliveira Mendonça, Fabio Fernandes Morato Castro, Jorge Kalil, (University of São Paulo, Brazil) (Figure 4.2) and genetic analysis performed by Isabella Ceccherini, Francesco Caroli, Alice Grossi and Marco Gattorno (IRCCS Institute Giannina Gaslini, Genoa, Italy) (Figure 4.3 A).

- PBMC isolation and *in vitro* stimulation of monocyte-derived macrophages (Figure 4.4) was performed by Alessandra Pontillo (University of São Paulo, Brazil).

Data presented in chapter 4 (except Figure 4.10) has been published on 16th November 2021 in the Journal of Clinical Immunology.

Chapter 5: 95 %

- Mass spectrometry analysis was performed by Annika Reinelt and Henning Urlaub at the Bioanalytical Mass Spectrometry Facility of the Max Planck Institute for Biophysical Chemistry in Göttingen, Germany (chapter 5.2.6).

Acknowledgements

This thesis would not have been possible without the support of many kind, incredibly smart and inspiring people and I am grateful to each and every one of you for being a part of this journey.

To my primary supervisor in Melbourne, Associate Prof. Seth Masters, thank you so much for taking me on as a PhD student. Your incredible expertise in the field and excitement for science have been a true inspiration. Thank you for your constant encouragement and support, your positivity and focus, critical analysis and patience! Thank you for your understanding during challenging times and creating an environment where everything is possible ☺.

To my primary supervisor in Bonn, Prof. Matthias Geyer, thank you for welcoming me in your lab despite my complete lack of understanding for structural biology and taking the time to teach me! Your enthusiasm for proteins is fascinating and I am very proud that now I can agree and say that protein structures are pretty cool ☺ Thank you for all the encouragement, support and chocolates along the way!

To my committee members, Dr. Vanessa Bryant, Associate Prof. Matt Call and Dr. Nick Wilson, thank you for all your advice, support, encouragement, helpful discussions and always looking out for me.

To Dr. Sophia Davidson, my co-supervisor in Melbourne, thank you so much for being such a wonderful scientist and mentor. Thank you for all the hours of data discussions, tea and biscuit breaks, always making time for me and the countless schemes you drew on benches and hoods! You have taught me so much, professionally and personally, and I could not have wished for a better co-supervisor! ☺

To Dr. Jonas Moecking, my co-supervisor in Bonn, thank you so much for guiding me through the confusing world of proteins. I am very proud to have witnessed your transition from a PhD student to a fantastic postdoc. Thank you for all your expertise, help and open ear at all times! ☺

To all past and present members of the Masters Lab at WEHI and the Geyer Lab in Bonn, thank you so much for creating such a happy work environment, becoming friends and making this time special. Thanks for all the trouble shooting, shared joy and disappointment and the cat memes ☺ A special thank you to Katja, Pawat, Cass and Thomas for your huge help and efforts to finish the paper revisions. Thank you Alan, Dom and Kate for the discussions around cGAS-STING and Fiona and Paul for helping me settle in and transferring your knowledge. Elif, Inga, Anja, Ines, Sophie, Julia, Jale, Martin, Robert, Niels, Max, Christoph, Michael, Larissa thank you all for the warm welcome in Bonn, the coffee breaks, Friday afternoon dances, Karneval and your help answering all my protein questions! A special thank you also to Dr. Gregor Hagelueken for his advice regarding structural biology approaches.

I would also like to thank Prof. Dr. med. Gunther Hartmann for the opportunity to perform experiments at the Institute of Clinical Chemistry and Clinical Pharmacology in Bonn. Dr. Thomas Zillinger and Dr. Eva Bartok, thank you so much for your supervision and scientific guidance. Thanks to everyone in the Hartmann and Bartok Labs, especially Sofia, Kasia, Saskia for all your help and the fun times ☺ A special thank you to my tissue culture buddies Lara, Anna and Christine, I loved working with you (and the cells of course ☺).

To Dr. Florian Schmidt from the Institute of Innate Immunity, thank you for the discussions around NLRC4 and providing reagents and cell lines, which greatly helped to advance this project.

To all collaborators and the here described patient and her family, thank you for your help and participation in this study.

I would also like to thank everyone at WEHI, who contributes to this uniquely friendly, supportive and productive work environment. I have met so many wonderful people, who will (hopefully) remain friends for life. Thank you, Cynthia, Damian, Anna, Suad, Gemma, Ronnie, Farima, Farhad for making me smile every day!

To the IRTG 2168 program, especially Prof. Christian Kurts, Prof. Sammy Bedoui, Dr. Marie Greyer, Lucie Delforge and Sandra Rathmann, thank you for the opportunity to participate in this joint PhD program and all your help and organisational support. A special thank you to all first and second cohort students, especially Alessa and Lara, thanks for everything!

Finally, to my friends and family, thank you for your constant love, support, understanding and endurance and helping me grow into the person I am today. There are no words to describe how forever grateful I am to have you in my life. Thank you for always being there and believing in me. Danke, dass ihr mich in allem unterstützt, immer da seid und an mich glaubt. Ich hab euch lieb!
To Adam and Rollo, although we did not know each other for long before this adventure started, you supported me every single step along the way-from near and far. Thank you for your love and trust, for sharing my excitement when experiments worked, your genuine interest in all the western blots and pretty protein structures and believing in me when I needed it most! Thank you ☺

List of Publications

Davidson, S., **Steiner, A.**, Harapas, C.R. and Masters, S.L. An Update on Autoinflammatory Diseases: Interferonopathies. Curr Rheumatol Rep. 2018; 20; 38

Harapas, C.R., **Steiner, A.**, Davidson, S. and Masters, S.L. An Update on Autoinflammatory Diseases: Inflammasomopathies. Curr Rheumatol Rep. 2018; 20; 40

Steiner, A., Harapas, C.R., Masters, S.L. and Davidson, S. An Update on Autoinflammatory Diseases: Relopathies. Curr Rheumatol Rep. 2018; 20; 39

Steiner, A., Reygaerts, T., Pontillo, A., Ceccherini, I., Moecking, J., Moghaddas, F., Davidson, S., Caroli, F., Grossi, A., Castro, F.F.M., Kalil, J., Gohr, F.N., Schmidt, F.I., Bartok, E., Zillinger, T., Hartmann, G., Geyer, M., Gattorno, M., Mendonça, L.O. and Masters, S.L. Recessive *NLRC4*-Autoinflammatory Disease Reveals an Ulcerative Colitis Locus. J Clin Immunol. 2021
(online ahead of print)

Harapas, C.R., Idiiatullina, E., Al-Azab, M., Hrovat Schaale K., Reygaerts T., **Steiner A.**, Laohamonthonkul P., Davidson S., Yu C.-H., Booty L., Masters S. L., Organellar homeostasis and innate immune sensing. Nat Rev Immunol. 2022
(online ahead of print)

Davidson S., Yu C.-H., **Steiner A.**, Ebstein F., Baker P.J., Jarur-Chamy V., Hrovat Schaale K., Laohamonthonkul P., Kong K., Calleja D.J., Harapas C.R., Balka K.R., Mitchell J., Jackson J.T., Geoghegan N.D., Mlodzianoski M.J., Moghaddas F., Rogers K.L., Mayer-Barber K.D., Almedia De Jesus A., De Nardo D., Kile B.T., Sadler A.J., Poli M.C., Krüger E., Goldbach Mansky R., Masters S.L., PKR is a sensor of proteotoxic stress via accumulation of cytoplasmic IL-24. Sci. Immunol. 2022; 11; 7

1 Literature review

1.1 Innate Immunity

The immune system can be divided into an innate and adaptive arm, which act in concert to fight pathogens and foreign substances. Conceptually, the innate immune system mediates the first line immune response through recognition of highly conserved motifs, which rapidly activates inflammatory pathways. Despite the fast activation mode and the ability to kill invading pathogens directly via non-specific strategies, some infections persist. Therefore, released cytokines, antigen presentation mechanisms and cell-cell interactions trigger adaptive immune system activation, the secondary and specific immune response pathway. Adaptive immunity is mediated through lymphocytes (B, T cells) and antibody responses, which rely on pathogen (antigen) identification upon first exposure, cell expansion and receptor affinity maturation before mechanisms become effective (~4-7 days later). Furthermore, after pathogen clearance, immunological memory is mediated via this arm of the immune system, which provides the basis for vaccine-mediated immunity to disease (Murphy 2017).

Whereas adaptive immunity has developed only in vertebrate species, innate immunity to some extent is evolutionarily conserved in vertebrates, invertebrates as well as plants (Alberts B 2002).

The players of the innate immune system in humans are protective barriers (epithelial layers, mucus), the complement system and cellular components: phagocytes (monocytes/macrophages, neutrophils), dendritic cells (DCs), mast cells, basophils and eosinophils, which function to kill invading pathogens, perform antigen presentation and produce cytokines and chemokines for immune cell recruitment and subsequent adaptive immune system activation (Alberts B 2002).

Microbial motifs recognized by innate immune sensors, so called pattern recognition receptors (PRRs), are functionally important for pathogen survival, fitness and virulence, and therefore evolutionarily conserved and referred to as pathogen-associated molecular patterns (PAMPs) (Janeway et al., 2002).

Additionally, damage-associated molecular patterns (DAMPs), which are defined as self-antigens released upon tissue damage are able to activate PRRs (Matzinger 1994). Various types of PAMPs are confined to pathogens and absent in host cells, thus ensuring self-discrimination. However, nucleic acids provide powerful immunostimulants, which also exist in the host. Therefore, several mechanisms have evolved to prevent PRR activation by self-antigens in healthy cells, including compartmentalization and enzymatic degradation mechanisms (Hartmann 2017). Dysregulation of these pathways caused by genetic defects results in sterile immune system activation, referred to as autoinflammatory disease (Alberts B 2002, McDermott et al., 1999).

1.2 Monogenic autoinflammatory diseases

Monogenic autoinflammatory diseases (AIDs) are a heterogenous class of rare diseases, caused by familial or *de novo* mutations in genes regulating innate immune pathways. Clinically, AIDs present with a broad spectrum of symptoms, which often start early in life and manifest with periodic fevers and inflammation affecting various organs, including skin, joints, muscles, the lung or the gastrointestinal tract (GIT) (Kastner et al., 2010, McGonagle et al., 2006).
The definition of AIDs was initially proposed by McDermott, Daniel Kastner and colleagues in 1999, who described an inherited syndrome in seven unrelated families characterized by unexplained episodes of fever and inflammation. Based on the identified missense mutations in the tumour necrosis factor (TNF) receptor gene (*TNFR1)*, the disease was named tumour necrosis factor receptor associated periodic syndrome (TRAPS) (McDermott et al., 1999). At the time, immune system overactivation in absence of autoantibodies and autoreactive T cells was similarly observed in patients suffering from Familial Mediterranean Fever (FMF), a periodic fever syndrome caused by gain of function (GoF) mutations in the *MEVF* gene, encoding the pyrin inflammasome protein (The French et al., 1997). Thus, these conditions were classified as AIDs, to highlight distinction from autoimmune diseases, which describe overactivation of the

adaptive immunity arm, driven by self-reactive T lymphocytes and/or autoantibodies (Burrows et al., 2000, Cohen 1973, McDermott et al., 1999).
While classification of diseases in general presents a useful strategy to stratify patients with regard to potential treatment options, a meaningful classification of AIDs has remained challenging, likely due to the wide spectrum of dysregulated signalling pathways involved as well as variable phenotypes and severities associated with defects in the same gene. Insufficient prediction of the clinical course and treatment efficacy is further highlighted by the increasing knowledge of the interplay between innate and adaptive immunity and cellular homeostasis (Savic et al., 2020). Although the predominant initial cause may be overactivation of innate immune components, subsequent manifestation of autoinflammation or immunodeficiency is sometimes observed and adds increasing complexity (Wekell et al., 2017). Therefore, features of autoinflammation can also be observed in polygenic and multifactorial disorders, which complicates disease classification (Savic et al., 2020). In fact, the transition from a “gene-centred” view towards a “system-based” concept has recently been suggested to better understand features of systemic AIDs (Savic et al., 2020). This model proposed that disease origin occurs within one of four pathways (proteotoxic stress, cytoskeletal dysregulation, nuclear factor kappa light chain enhancer of activated B cells (NF-κB) pathway, type I interferon (IFN) pathway) which determines the overall clinical course. However, persistently activated signalling pathways subsequently promote adaptive immune system activation, a process which is further influenced by genetic predisposition and environmental impacts (Savic et al., 2020).
Recent advances in sequencing technologies have led to a vastly increased rate of discovery and diagnosis of novel AIDs, where especially monogenic disorders have proven powerful to aid our understanding of innate immune pathway functions and their regulation.

In this thesis, the pathomechanisms of two different diseases are investigated: COPA syndrome and NLRC4-associated AID, which can be classified as type I

IFN-driven (interferonopathies) or inflammasome-associated (inflammasomopathies) diseases, respectively.
The following literature review aims to introduce the involved PRRs and signalling pathways and summarizes the main molecular features that represent the basis of this disease classification.

1.3 Pattern recognition receptors

PRRs are germline-encoded and can be categorized into five main families including Toll-like receptors (TLRs), nucleotide-binding oligomerization domain (NOD)-like receptors (NLRs), retinoic acid-inducible gene-I (RIG-I)-like receptors (RLRs), C-type lectin receptors (CLRs) and absent in melanoma 2 (AIM2)-like receptors (ALRs). Other important and well-studied PRRs include pyrin and cytosolic DNA sensors (Akira et al., 2006, Kawasaki et al., 2014).
The following description of PRRs is not comprehensive and only aims to provide an overview over the diversity of innate immune receptors and the induced pathways relevant for this thesis.

1.3.1 Toll-like receptors

TLRs can reside within the plasma membrane (TLR1,2,4,5,6,10) or within endosomal membranes (TLR3,7,8,9,11,12,13), with slightly different expression patterns in humans (TLR1-10) and mice (TLR1-9, TLR11-13) (Kawasaki et al., 2014). Surface exposed TLRs mainly recognize components of microbial membranes such as lipids, lipopolysaccharides or proteins including the well-defined ligands lipopolysaccharide (LPS, binds TLR4), flagellin (TLR5), or peptidoglycan, lipoteichoic acid, zymosan and mannan (TLR1,2,6) (Kawasaki et al., 2014). Endosomal TLRs monitor cells for intracellular pathogens by recognition of nucleic acids: double-stranded (ds) RNA (TLR3), single-stranded (ss) RNA (TLR7,8) unmethylated cytosine-phosphate-guanine (CpG)-containing DNA (TLR9) or bacterial ribosomal RNA (TLR13) (reviewed in (Kawasaki et al., 2014)).

Downstream signalling occurs via adapter proteins such as Toll-Interleukin-1 receptor (TIR)-domain-containing adapter protein (TIRAP) and myeloid differentiation primary response 88 (MyD88) or TIR-domain containing adapter-inducing interferon β (TRIF) and translocation-associated membrane protein (TRAM), which induce proinflammatory transcription factor activation (nuclear factor (NF)-κB, activator protein-1 (AP-1)) or type I IFN signalling through interferon regulatory factor (IRF) 3 or IRF7, respectively (Kawai et al., 2010, Kawasaki et al., 2014)).

1.3.2 Rig-I-like receptors

The RLR family consists of three structurally-related members: RIG-I (also known as DDX58), melanoma differentiation-associated protein 5 (MDA5, IFIH1) and laboratory of genetics and physiology 2 (LGP2), which initiate key pathways to establish an antiviral immune response following detection of cytoplasmic RNA (Yoneyama et al., 2005). Whereas RIG-I and MDA5 activate downstream signalling via caspase activation and recruitment domain (CARD)-CARD interactions with the signalling adapter mitochondrial antiviral signalling protein (MAVS), LGP2 exhibits regulatory functions due to the lack of the N-terminal CARD domain (Rodriguez et al., 2014). Following MAVS binding at the mitochondrial membrane, receptor polymerization occurs and activates transcription factors IRF3, IRF7 and NF-κB (Kawai et al., 2005, Seth et al., 2005). Despite structural similarities, RIG-I and MDA5 act non-redundantly and recognize distinct RNA species. Whereas RIG-I binds short dsRNAs containing 5'-triphosphates (5'ppp) (Hornung et al., 2006), MDA5 preferably binds long dsRNAs (Kato et al., 2008). Therefore, depending on the provided ligand, viruses may be able to distinctly activate RIG-I or MDA5, or both sensors simultaneously (reviewed in (Saito et al., 2008)).

1.3.3 NOD-like receptors

The family of NLRs encompasses 22 human genes (Ting et al., 2008). The characteristic domain structure comprises the central NACHT domain (present in NLR family apoptosis inhibitor protein (NAIP), CIITA, HET-E and TP-1), which contains highly conserved structural motifs required for nucleotide binding and hydrolysis (chapter 5.1.1). The NACHT domain can be subdivided into the nucleotide-binding domain (NBD), helical domain 1 (HD1), winged helix domain (WHD) and helical domain 2 (HD2). Proteins with these structural features adopt an auto-repressed conformation and undergo structural changes upon activation, which induces oligomerization (Danot et al., 2009).

NLRs are subclassified by their N-terminal domain into NLRA (encode acidic transactivating domain (AD), e.g. MHC class II transactivator (CIITA)), NLRBs (encode baculovirus inhibitor of apoptosis protein repeat (BIR), e.g. NAIP), NLRCs (encode CARD: e.g. NOD1/2, NLRC3-5), NLRPs (encode PYD, e.g. NLRP1-14) and NLRX (encode other domains, e.g. NLRCX1). On the C-terminal end, all NLRs encode LRRs, except NLRP10. As a further exception, NLRP1 encodes an additional function to find domain (FIIND) (Ting et al., 2008).

Only a limited number of NLR family members has been well studied. CIITA was suggested to function as transcriptional regulator of MHC class II gene expression (Steimle et al., 1993), whereas NOD1 (NLRC1) and NOD2 (NLRC2) oligomerize and induce proinflammatory signalling via NF-κB and mitogen-activated protein kinase (MAPK) activation in response to bacterial peptidoglycan fragments, e.g. γ-D-glutamyl-meso-diaminopimelic acid (iE-DAP) and muramyl dipeptide (MDP), respectively (Chamaillard et al., 2003, Franchi et al., 2009, Girardin et al., 2003).

Most NLRs are believed to function as sensors for PAMPs and DAMPs and this has been experimentally confirmed for the best studied family members NLRP1, NLRP3, NLRP6, NLRP7 and NLRC4 (Zheng et al., 2020b). Following ligand binding, conformational changes induce NLR oligomerization and activate immune signalling through the formation of multiprotein signalling platforms, so called inflammasomes (**Figure 1.1**) (Martinon et al., 2002, Schroder et al., 2010).

In contrast, other NLRs may exhibit different functions. For example, NLRP12 has been reported as negative regulator of inflammation, however future studies are essential to determine the exact function and clarify whether signalling occurs through inflammasome formation as previously suggested in response to *Y. pestis* infection (Allen et al., 2012, Zaki et al., 2014, Zheng et al., 2020b).
Other cytosolic PRRs reported to form inflammasomes are sensor proteins pyrin and AIM2, a member of the ALR family, which are not classified as NLRs due to differences in their protein domain structure (lacking the NACHT domain) (Guo et al., 2015).

1.3.3.1 Inflammasomes

Broadly, inflammasome signalling can be differentiated into a canonical or noncanonical pathway.
Canonical inflammasome formation requires a sensor protein, which undergoes structural changes and self-oligomerization upon ligand binding. Homotypic domain interactions between N-terminal PYD-PYD or CARD-CARD domains recruit adaptor protein apoptosis-associated speck-like protein containing a CARD (ASC, composed of 2 domains: PYD-CARD), which subsequently forms large filamentous structures, termed ASC specks that serve as platform for pro-caspase-1 recruitment (Dick et al., 2016, Martinon et al., 2002). To become catalytically active, pro-caspase-1 molecules undergo autoproteolytic cleavage, which is promoted by spatial proximity at the ASC speck (Lu et al., 2014).
Interestingly, ASC specks were also found to be released from macrophages, which is thought to promote immune signalling within the extracellular milieu and following uptake by surrounding phagocytes (Baroja-Mazo et al., 2014, Franklin et al., 2014).
The morphological features of inflammasome complexes have been increasingly investigated over the past decade and structural analysis of filament-forming subdomains of inflammasome proteins, e.g. ASC^{PYD}, ASC^{CARD}, $NLRC4^{CARD}$, caspase-1^{CARD}, revealed important mechanistic details (Li et al., 2018d, Lu et al., 2014, Lu et al., 2016a, Matyszewski et al., 2018). However, the architectural

features and organellar interaction of ASC specks formed within living cells have not yet been conclusively determined. In a recent correlative light and electron microscopy (CLEM) and *in situ* cryogenic electron tomography (cryo-ET) approach, Liu et al. investigated ASC speck formation in a physiological context (preprint (Liu et al., 2021)). Interestingly, following NLRP3 stimulation in immortalized bone marrow-derived macrophages (iBMDMs), the observed ASC filaments (ASC tagged with C-terminal mCerulean) formed an interconnected branched scaffold characterized by different densities and embedded ribosomes and *trans*-Golgi vesicles. Occurrence of multiple regions with higher filament density was suggested to represent simultaneously originating nucleation sites. Whereas the PYD of ASC assembled into tubular filaments, branching was suggested to occur through CARD-CARD interactions of ASC molecules. Therefore, this study provides experimental evidence for the dynamics within the physiological ASC speck that may present a filamentous network and allow for recruitment and free diffusion of signalling molecules and perhaps organellar interaction to mount an efficient proinflammatory signalling cascade (preprint (Liu et al., 2021)).

Active caspase-1 cleaves inactive precursors of interleukin (IL)-1β and IL-18 into their mature biologically activate forms, which are released from the cell to exhibit proinflammatory functions (**Figure 1.1**) (Martinon et al., 2002, Schroder et al., 2010). Additionally, caspase-1 cleaves gasdermin D (GSDMD) between its N- and C-terminal domain, which releases the autoinhibited conformation and allows N-terminus dissociation, oligomerization membranes pore formation (Liu et al., 2016, Shi et al., 2015). Cryogenic electron microscopy (cryo-EM) and atomic force microscopy analysis of artificial liposomes determined a pore diameter between 10~20 nanometers (nm), through which volume loss destabilizes the cellular osmotic gradient and subsequently induces pyroptosis, a lytic form of inflammatory cell death (Ding et al., 2016, Liu et al., 2016, Sborgi et al., 2016). As a consequence, pyroptosis releases large amounts of processed cytokines and intracellular bacteria are exposed for recognition and phagocytosis by immune cells. Additional release of self-DAMPs further promotes inflammation (Miao et al., 2010).

Interestingly, using BMDMs deficient for *Casp1*, *Casp11* and *Gsdmd*, it has been suggested that release of IL-1β and IL-18 (4 nm diameter), which lack typical secretion motifs (Andrei et al., 1999, Rubartelli et al., 1990), depends on GSDMD pores and can occur via a lysis-independent event (Evavold et al., 2018, Heilig et al., 2018). Mechanistically, Heilig et al. suggested size-dependent passive leakage and describeb GSDMD pores as unspecific channels for soluble small cytosolic proteins (25-50 kilodalton (kDa)) (Heilig et al., 2018). Structural comparison of the GSDMD pre- and final pore further revealed a distinct conformational state that exposes negatively charged residues in the pore conduit, which license IL-1β passing (positively charged) only after cleavage of the acidic pro-domain (Xia et al., 2021). However, since pyroptosis is a rapidly occurring event, cell death-independent IL-1β and IL-18 release through GSDMD pores may be a cell type-specific effect and play an important role *in vivo* to prime adjacent cells via paracrine signalling to fine-tune the inflammatory response and avoid cell death (Heilig et al., 2018). Importantly, another regulatory mechanism involves the repair of GSDMD pores using the endosomal sorting complexes required for transport (ESCRT) machinery, which was suggested to limit inflammation following weak inflammasome stimulation (Rühl et al., 2018). Recently, a genetic screen of random mutations in mice revealed cell surface protein ninjurin-1 (encoded by *NINJ1*) as the final regulator of plasma membrane rupture following apoptotic, necroptotic and pyroptotic cell death induction, which is therefore now recognized as an actively regulated process subsequent of GSDMD pore formation (Kayagaki et al., 2021). However, the mechanistic details require further investigation.

Murine caspase-11 and human caspases-4/5 are at the centre of the non-canonical inflammasome pathway, due to their ability to directly sense intracellular LPS and cleave GSDMD (Kayagaki et al., 2011, Viganò et al., 2015). Thus, non-canonical caspases function as combined sensor- and effector-proteins and induce pyroptosis. Although not directly mediated by caspase-11/4/5, IL-1β and IL-18 release occurs via secondary activation of the NLRP3 inflammasome, downstream of potassium efflux as the consequence of

increased cell permeability (Rühl et al., 2015). Therefore, it has been suggested that NLRP3 protein expression levels determine cell-type specific effects downstream of non-canonical inflammasome activation: predominant induction of pyroptosis via this pathway may play an important role in epithelial, endothelial cells and keratinocytes (low NLRP3 expression) (Knodler et al., 2014, Shi et al., 2014), whereas cytokine release was demonstrated in macrophages and DCs (higher NLRP3-expressing cells) (Rathinam et al., 2019).

Robust inflammasome signalling requires two signals including a priming signal (signal 1) prior to ligand-mediated inflammasome assembly (signal 2). Priming is normally provided through NF-κB pathway activation following TLR stimulation or proinflammatory cytokine receptor signalling (e.g. TNF). NF-κB pathway activation potently induces the transcription of genes encoding inflammasome platform and effector proteins, such as *IL1B* (pro-IL-1β) (Hiscott et al., 1993) and transcriptional control of *CASP1* (pro-caspase-1) and *NLRP3* has additionally been suggested in some studies (Bauernfeind et al., 2009, Lee et al., 2015, Qiao et al., 2012). In contrast, the IL-18 precursor is constitutively expressed in intestinal epithelial cells (IEC), keratinocytes, endothelial cells, peripheral blood mononuclear cells (PBMCs) and macrophages (Lamkanfi et al., 2014, Puren et al., 1999, Sugawara et al., 2001). Furthermore, in the case of NLRP3, signal 1 also mediates transcription-independent priming via post-translational modifications (PTMs), including phosphorylation and deubiquitination, which have been suggested to promote structural changes that facilitate inflammasome assembly (**Figure 1.1**) (Juliana et al., 2012, Py et al., 2013, Song et al., 2017).

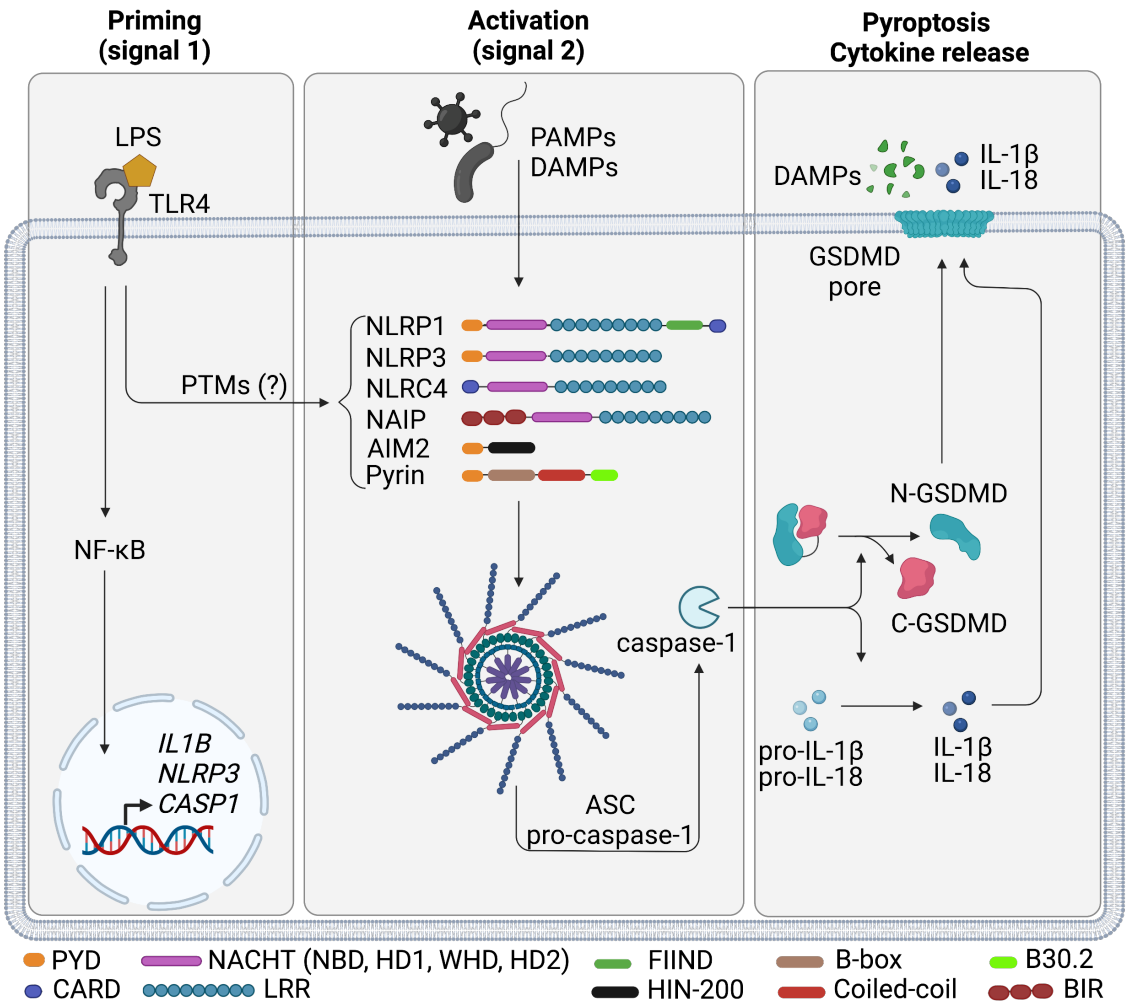

Figure 1.1 | Canonical inflammasome activation and signalling. Protein domain structures of well-studied inflammasome-forming proteins are shown including NOD-like receptors (NLRs) NLRP1, NLRP3, NLRC4, NAIP, absent in melanoma 2 (AIM2) and pyrin. Efficient inflammasome activation typically requires two signals. Signal 1 (priming) induces NF-κB-mediated transcription of inflammasome complex protein-encoding genes, which can occur downstream of Toll-like receptor (TLR) activation, for example through lipopolysaccharide (LPS) binding to TLR4. Additional transcription-independent priming events through post-translational modifications (PTMs) have been identified for NLRP3, but may also play a role in licensing other inflammasomes. Sensing of PAMPs or DAMPs (signal 2) releases the autoinhibited conformation and promotes oligomerization into disc-like or helical structures, which recruit inflammasome adapter apoptosis-associated speck-like protein containing a CARD (ASC) and effector protein pro-caspase-1. Autoproteolytic cleavage activates caspase-1, which subsequently cleaves pro-IL-1β, pro-IL-18 and gasdermin D (GSDMD). The N-terminal cleavage fragment of GSDMD assembles membrane pores that mediates lytic cell death (pyroptosis) and release mature cytokines and DAMPs. Pyrin domain, PYD; caspase activation and recruitment domain, CARD; domain present in NAIP, CIITA, HET-E, TP1, NACHT; nucleotide-binding domain, NBD; helical

domain 1 and 2, HD1, HD2; winged helix domain, WHD; leucine-rich repeat, LRR; baculovirus inhibitor of apoptosis protein repeat, BIR; function to find, FIIND; hematopoietic expression, interferon-inducible nature and nuclear localization domain 200, HIN-200; pathogen-associated molecular patterns, PAMPs; damage-associated molecular patterns, DAMPs). Figure created with BioRender.com.

1.3.3.2 Cytokine effects

Released cytokines IL-1β and IL-18 are potent activators of inflammation and signal via specific receptors: the IL-1 receptor (IL-1R1) or IL-18Rα/β, respectively (Dinarello 2009). Furthermore, a decoy receptor (IL-1R2) and soluble antagonist (IL-1Ra) for IL-1β and an IL-18-specific soluble binding protein (IL-18BP) have been identified, which have important negative regulatory functions (Novick et al., 1999, Symons et al., 1995).

IL-1β is produced by many immune and non-immune cells including neutrophils, monocytes, macrophages, DCs, natural killer (NK) cells and keratinocytes and induces diverse proinflammatory responses (Bakele et al., 2014, Dinarello 2009, Feldmeyer et al., 2010). IL-1β specifically activates cyclooxygenase (COX) 2 and induces TNF and IL-6 release, which clinically manifests in fever, vasodilation and hypotension. Furthermore, IL-1β induces the expression of chemokines and adhesion molecules to recruit neutrophils and other immune cells to the site of inflammation and promotes co-stimulation of T cells (T helper (Th) 1, Th17) and humoral immunity (Dinarello 1996, Dinarello 2009, Lee et al., 2004, Miller et al., 2007, Nakae et al., 2001, Sutton et al., 2006, Wang et al., 1995, Weber et al., 2010).

IL-18, originally described as “IFNγ-inducing factor” (Nakamura et al., 1993) is constitutively expressed as pre-form in many cell types including endothelial and epithelial cells, keratinocytes, monocytes, macrophages, DCs and neutrophils (Bakele et al., 2014, Dinarello 2018). IL-18 does not activate COX2, but induces chemokine production and adhesion molecule expression (Dinarello 2018). In synergy with IL-12 or IL-15, which upregulate expression of the IL-18 receptor β-chain, IL-18 drives IFNγ secretion from T cells and NK cells (Okamura et al., 1998,

Yoshimoto et al., 1998) and induces Th1 and Th2 cell differentiation depending on the presence of co-stimulatory cytokines (Nakanishi 2018).

Aberrant IFNγ signalling plays an important role in the pathogenesis of hemophagocytic lymphohistiocytosis (HLH), a life-threatening clinical syndrome caused by overactivation of macrophages, NK cells and cytotoxic T cells, which results in an auto-amplification loop and highly elevated levels of proinflammatory cytokines (hypercytokinemia), hemophagocytosis, cytopenia, high fever, hepatosplenomegaly and potentially severe organ damage (Crayne et al., 2019, Janka et al., 2013, Mosser et al., 2008). Familial (primary) HLH and acquired (secondary) HLH are discriminated, which distinguishes the underlying cause of HLH due to a genetic defect or as a secondary result of pathogenic infections, malignancies, sepsis, drugs and inflammatory diseases, respectively (Janka et al., 2013, Novick et al., 2001, Takada et al., 2001). As a subclassification of secondary HLH, macrophage activation syndrome (MAS) describes HLH in patients suffering from autoinflammatory, autoimmune or rheumatological disorders, such as systemic juvenile idiopathic arthritis (sJIA), adult-onset Still's disease (AOSD), systemic lupus erythematosus (SLE), Kawasaki disease or NLRC4-associated autoinflammatory disease (NLRC4-AID, chapter 4.1.1) (Crayne et al., 2019, Janka 2012). In patients with familial HLH, impaired cytolytic activity of NK cells and cytotoxic T cells occurs as a result of genetic mutations affecting trafficking and release of cytotoxic granules (Morimoto et al., 2016, Perez et al., 1984). Consequently, pathogens and infected cells are not efficiently cleared and proinflammatory stimulation persists and drives aberrant IFNγ, TNF, IL-1, IL-6, IL-2, IL-12 release and immune system hyperactivation (Jordan et al., 2004, Takada et al., 2001).

A better understanding of the molecular mechanisms driving MAS has only recently been gained. In 2001, Takada et al. described significantly elevated IL-18 serum levels in HLH patients and determined a correlation with IFNγ levels and disease activity (Takada et al., 2001). Notably, a later study demonstrated the importance to discriminate between concentrations of free and total IL-18, since the latter may be partially or completely bound by IL-18BP and therefore biologically inactive (Novick et al., 2001). Investigating levels of total and free IL-

18 and IL-18BP in the serum of patients during active disease of MAS, familial HLH and infection-associated HLH (IA-HLH), findings from a recent study suggested that although total IL-18 and IL-18BP are significantly increased in all conditions, serum elevation of free IL-18 is a distinguishing feature specifically associated with MAS but not familial HLH (Weiss et al., 2018). Furthermore, additional normalization of total IL-18 to CXCL9, an IFNγ-induced monokine, which was significantly elevated in MAS, IA-HLH and familial HLH, further improved the distinction to familial HLH and allowed for discrimination between MAS and IA-HLH, suggesting IL-18 as a driving cytokine in MAS (Weiss et al., 2018). Given that in healthy individuals, baseline serum levels of IL-18BP exceed levels of IL-18 by at least 20-fold and IFNγ induces IL-18BP expression to sequester IL-18 and antagonize inflammation in a negative feedback mechanism (Novick et al., 2001, Paulukat et al., 2001), it has been suggested that the balance between total IL-18 and its endogenous inhibitor IL-18BP determines levels of free IL-18 and therefore disease activity (Weiss et al., 2018). Chronic elevation of total IL-18 and IL-18BP in MAS patients and experimental evidence from transgenic mice constitutively expressing free IL-18 (Il18tg mice) supports this hypothesis, since stimulation-induced MAS was more severe in Il18tg mice compared to wildtype (WT) animals (Weiss et al., 2018). Therefore, these findings establish a link between IL-18, IFNγ and MAS. Interestingly, MAS has been reported as a clinical symptom in some patients with GoF mutation in NLRC4 (chapter 4.1.1) (Canna et al., 2014, Liang et al., 2017, Moghaddas et al., 2018), but was not associated with overactivation of other inflammasomes, thus suggesting a distinct function in NLRC4-mediated pathologies.

1.3.3.3 Inflammasomopathies

GoF mutations in inflammasome-forming proteins NLRP1, NLRP3, NLRC4 and pyrin have been identified as genetic cause of monogenic inflammasome-associated AIDs, so called inflammasomopathies. Main molecular features of this disease group include uncontrolled cytokine release (IL-1β, IL-18) and pyroptotic cell death. The clinical spectrum of inflammasomopathies continues to expand and phenotypic heterogeneity associated with different mutations affecting the same gene is an interesting finding increasingly observed (Alehashemi et al., 2020). One example is the group of cryopyrin-associated periodic syndromes (CAPS), which combine pathologies associated with GoF mutations with NLRP3 (also called cryopyrin) and present as a spectrum of clinical phenotypes classified as familial cold autoinflammatory syndrome (FCAS) (Hoffman et al., 2001), Muckle-Wells syndrome (MWS) (Muckle 1979) and neonatal-onset multisystemic inflammatory disease (NOMID, also known as infantile neurological cutaneous articular syndrome (CINCA) (Aksentijevich et al., 2002). Clinically, the diseases manifest early in life (FCAS) or soon after birth (MWS, NOMID) with periodic fever attacks, skin rashes, arthralgia and headache. Additionally, the more severe clinical course of MWS and NOMID is often associated with sensorineural hearing loss, aseptic meningitis with mental retardation as well as joint malformations (Welzel et al., 2021). Interestingly, in FCAS patients, inflammatory episodes are triggered by cold exposure and last for ~24 hours (hrs), whereas this is less observed in MWS and NOMID patients, which often suffer from prolonged or persistent inflammation (Meier-Schiesser et al., 2021, Welzel et al., 2021).

Since AIDs associated with GoF mutations in NLRC4 are focus of this thesis, the molecular basis of NLRC4 inflammasome formation, signalling and its regulatory mechanisms are introduced below, before the clinical manifestations and genotypes of NLRC4-AIDs are summarized in chapter 4.1.1.

1.3.3.4 The NAIP/NLRC4 inflammasome

1.3.3.4.1 Importance of the NAIP/NLRC4 inflammasome

As previously mentioned (chapter 1.3.3), NLRC4 (also called ice-protease-activating factor (IPAF) (Poyet et al., 2001), caspase recruitment domain-containing protein 12 (CARD12) (Geddes et al., 2001) or CED-4-like protein (CLAN) (Damiano et al., 2001)) is composed of an N-terminal CARD domain, followed by a central NACHT domain (subdomains NBD, HD1, WHD, HD2) and a C-terminal LRR region (**Figure 1.2**) (Poyet et al., 2001).

NLRC4 is highly expressed in hematopoietic cells and gastrointestinal epithelial cells (Canna et al., 2014, Hu et al., 2010, Romberg et al., 2014, Sellin et al., 2014), and plays a well-established role in defence against several pathogens including *Listeria monocytogenes* (Wu et al., 2010), *Salmonella typhimurium* (Miao et al., 2010), *Pseudomonas aeruginosa* (Sutterwala et al., 2007), *Klebsiella pneumoniae* (Cai et al., 2012), *Burkholderia pseudomallei* (Ceballos-Olvera et al., 2011), *Legionella* species (Pereira et al., 2011), *Shigella flexneri* (Suzuki et al., 2007), *Escherichia coli* (Miao et al., 2010) and *Citrobacter rodentium* (Liu et al., 2012c). Interestingly, besides systemic infections, NLRC4 has been attributed a crucial role in the hematopoietic cell-independent immune response against enteric pathogens in mice, where NLRC4 expressed in IEC drives inflammation in response to *Salmonella* and *Citrobacter* infections (Nordlander et al., 2014, Rauch et al., 2017, Sellin et al., 2014).

Less-well established functions of NLRC4 have also been proposed, including a suggested role in mucosal immunity against *Candida albicans* infections in mice (Tomalka et al., 2011) as well as in the pathogenesis of ischemic brain injury (Denes et al., 2015) and sterile neuroinflammation (Freeman et al., 2017). Furthermore, a role in tumour biology is increasingly suggested, however study results are still controversial and no clear function has yet been established (Hu et al., 2010, Janowski et al., 2016, Kolb et al., 2016, Ohashi et al., 2019.

In the course of this thesis, proteins from human or mouse will be referred to by use of abbreviated prefixes, e.g. hNLRC4 or mNLRC4, respectively.

1.3.3.4.2 Ligand recognition by NAIPs

In contrast to other inflammasomes, the NLRC4 activation mechanism is relatively well understood and defines NLRC4 as a signalling adapter, rather than a direct sensor of ligands (**Figure 1.2**). This model is based on the initial observation by Zamboni et al., who showed the requirement of baculovirus inhibitor of apoptosis repeat (BIR)-containing 1e (Birc1e), also called mNAIP5, to induce caspase-1 activation and IL-1β secretion in murine macrophages infected with *L. pneumophila* and identified mNLRC4 as downstream adapter (Zamboni et al., 2006). Furthermore, co-immunoprecipitation studies in human embryonic kidney (HEK) 293 cells suggested direct interaction of mNAIP5 and mNLRC4 (Zamboni et al., 2006). In total, seven *Naip* genes exist in the mouse genome, whereas only one human *NAIP* is encoded *(*hNAIP) (Endrizzi et al., 2000).

In mice, ligand specificity of the mNAIP/mNLRC4 inflammasome was demonstrated to be determined by mNAIP paralogs, e.g. mNAIP1, mNAIP2, mNAIP5 and mNAIP6 (Kofoed et al., 2011). Performing paralog-specific small hairpin (sh) RNA-knockdown studies in primary BMDMs stimulated with various *Listeria* strains, Kofoed and Vance identified mNAIP2 as specific sensor for *Listeria* type three secretion system (T3SS) inner rod protein PrgJ, whereas mNAIP5 and mNAIP6 specifically detected flagellin (Kofoed et al., 2011), which was previously independently suggested by others (Ren et al., 2006, Zamboni et al., 2006).

Interestingly, the *Chromobacterium violaceum* T3SS needle protein CrpI was able to stimulate hNAIP/hNLRC4 inflammasome-mediated caspase-1 cleavage and pyroptosis in human U937 monocyte-derived macrophages, whereas cells did not respond to cytosolic *Legionella* flagellin or *Burkholderia* inner rod protein (BsaK) (Zhao et al., 2011). Yang and colleagues subsequently confirmed this finding and showed robust caspase-1 cleavage, cell death and IL-1β production in response to cytoplasmic exposure of needle toxins from *S. typhimurium* (PrgI) and *C. violaceum* (CrpI) in THP-1 and U937 cells (Yang et al., 2013). Furthermore, similar ligand specificity was demonstrated for the mouse ortholog mNAIP1, which was potently activated by needle proteins derived from *S. flexneri*

(MxiH) and enterohemorrhagic *E. coli* (EHEC, EprI) (Yang et al., 2013), as well as *S. typhimurium* (PrgI) (**Figure 1.2**) (Rayamajhi et al., 2013).

Importantly, in contrast to studies in immortalized monocytic human cell lines, flagellin from *Salmonella* and *L. pneumophila* activated hNAIP/hNLRC4 inflammasome signalling in primary human monocyte-derived macrophages (MDMs), which was explained by the identification of an alternative transcript variant, that showed 68 % amino acid (aa) sequence identity with mNAIP5 (full length hNAIP), whereas the isoform predominantly expressed in THP-1 and U937 cell lines was only 65 % identical to mNAIP5 and truncated (lack of nucleotides 3990-4160) (Kortmann et al., 2015). A subsequent study suggested binding of flagellin and T3SS rod and needle proteins to full length hNAIP in primary human MDMs (Reyes Ruiz et al., 2017). However, it remains unclear how several different ligands can be detected by one sensor or whether specific splice variants exist (Reyes Ruiz et al., 2017) and further studies as well as structural information would prove useful to address these questions.

The above mentioned T3SS represents a set of bacterial proteins spanning both membranes of Gram-negative pathogens. Although the term is sometimes used to refer to the bacterial injectisome complex as a whole, it more correctly describes the membrane-incorporated components that (1) contribute to the bacterial flagellum (flagellar T3SS) and (2) form the central machinery of the T3SS injectisome, which forms an extracellular needle to translocate effector proteins into host cells (Diepold et al., 2015). Thus, T3SS injectisomes contribute to the virulence of Gram-negative bacteria and although effector and needle proteins vary between bacterial species, structures and functions are conserved to some extent (Coburn et al., 2007, Wang et al., 2007). Therefore, specific binding of T3SS components and flagellin to NAIP paralogs allows recognition and NLRC4 inflammasome formation in response to a wide range of bacteria, although varying potencies have been observed between needle, flagellin or rod proteins derived from different pathogenic species (Yang et al., 2013, Zhao et al., 2011).

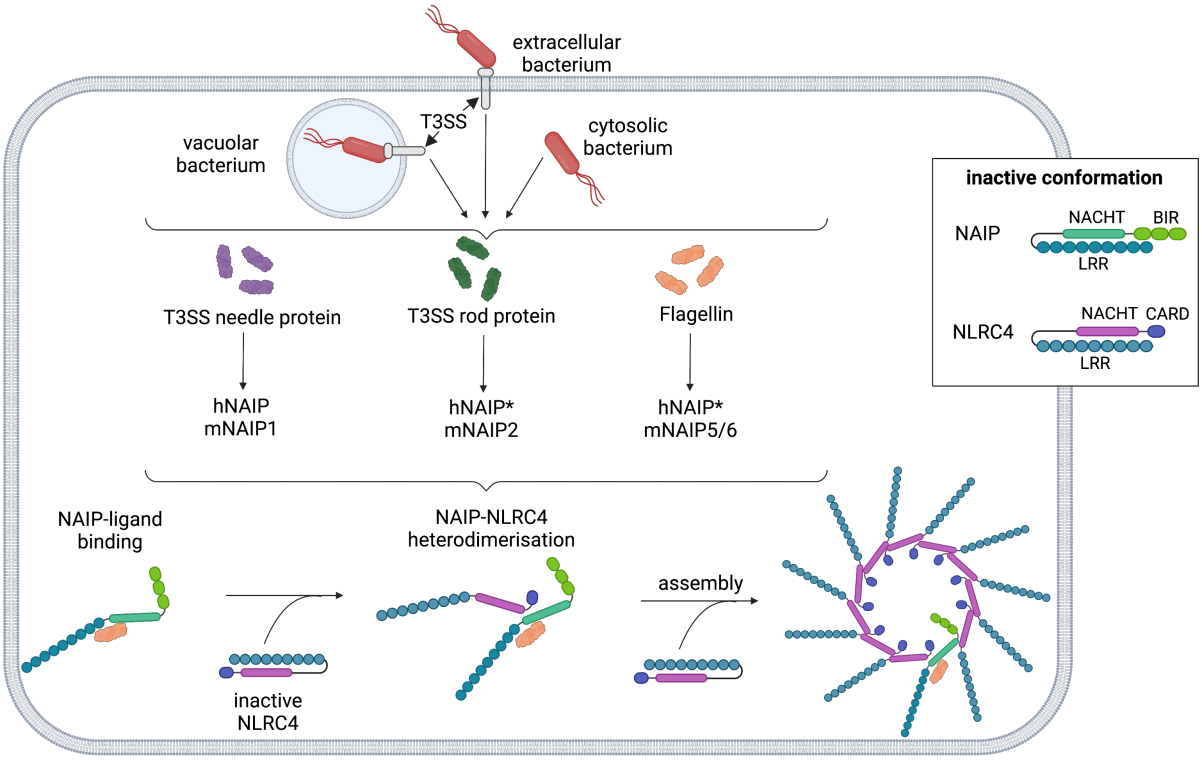

Figure 1.2 | Model of NAIP/NLRC4 inflammasome activation. NAIP and NLRC4 are cytoplasmic proteins, which adopt an inactive conformation. NAIP is characterized by three N-terminal BIR domains, a central NACHT and C-terminal LRR domain. NLRC4 possesses a similar domain structure, but contains an N-terminal CARD. NAIPs function as sensor proteins, which detect ligands from Gram-negative bacteria injected into the cell from the extracellular compartment, vacuoles or released from intracellular bacteria. In mice, mNAIP1, mNAIP2 and mNAIP5/6 have been identified to specifically bind type three secretion system (T3SS) needle, inner rod and flagellin, respectively. In humans, a single hNAIP has been suggested to detect all ligands and different transcript isoforms have also been reported (indicated by asterisk). Upon ligand binding, a conformational change in NAIP results in the active conformation, which recruits an inactive NLRC4 protein and subsequently induces structural changes that expose binding interfaces for NLRC4 self-assembly into a wheel-shaped inflammasome complex. NLR family apoptosis inhibitory protein, NAIP; NLR family CARD domain containing 4, NLRC4; baculovirus inhibitor of apoptosis protein repeat, BIR; caspase activation and recruitment domain, CARD; leucine-rich repeat, LRR; contained in NAIP, CIITA, HET-E, TP-1, NACHT. Figure modified from (Broz et al., 2016), created in BioRender.com.

1.3.3.4.3 NAIP/NLRC4 inflammasome effector mechanisms

In contrast to other PYD-containing NLRs, the N-terminal CARD domain of NLRC4 allows for direct recruitment of pro-caspase-1 via CARD-CARD homotypic interactions (**Figure 1.3 A**) (Poyet et al., 2001). However, interaction with ASC can still occur (Geddes et al., 2001, Proell et al., 2013), although its role is not well defined, but was suggested to enhance caspase-1 activation. Recent cryo-EM studies of the self-assembled ASC^{CARD} and $NLRC4^{CARD}$ filaments showed resemblance of their overall architecture and surface charge, which suggests that capase-1^{CARD} filament nucleation occurs unidirectional via comparable mechanisms from both ASC^{CARD} and $NLRC4^{CARD}$ seeds (Li et al., 2018d, Lu et al., 2016a). However, computational modelling of available structures suggested that direct caspase-1 nucleation by NAIP/NLRC4 oligomers may be rather inefficient due to spatial restrictions, if the inflammasome assembles into a helical structure as previously suggested (Li et al., 2018d). Thus, ASC filament formation and assembly of large specks was proposed to increase the nucleation seeds available for pro-caspase-1 recruitment, which may subsequently enhance downstream effects. Future studies aiming to elucidate the structure of an assembled NAIP/NLRC4 complex in association with ASC and caspase-1 will be required to validate this hypothesis (Lu et al., 2014).
Supporting the modulatory role of ASC, LPS-primed *Asc*$^{-/-}$ BMDMs transfected with flagellin show diminished IL-1β release as measured by ELISA, whereas cytokine release from *Nlrc4*$^{-/-}$ BMDMs was completely absent (Miao et al., 2006). Interestingly, in another study, macrophage cell death following infection with *S. typhimurium*, *P. aeruginosa* and *L. pneumophila* was found to be ASC-independent, whereas IL-1β release required ASC expression (**Figure 1.3 B**) (Broz et al., 2010a). Furthermore, although Chen et al. demonstrated that IL-1β secretion in BMDMs and neutrophils was partly dependent on ASC following *S. typhimurium* infection, only BMDMs underwent ASC-independent cell death, whereas pyroptosis of neutrophils was not observed (Chen et al., 2014b). Therefore, although further studies are required to elucidate the detailed function of ASC, these finding suggest a synergistic role in NAIP/NLRC4-mediated

cytokine maturation, whereas direct NAIP/NLRC4-induced caspase-1 activation can drive cell death with only limited cytokine release (**Figure 1.3 B**). Furthermore, uncoupling of caspase-1 effects may occur in some cell types downstream of NLRC4, which may partly be regulated by ASC.

Importantly, whereas most studies evaluated ASC function in murine cells in the context of infection, Moghaddas et al. showed that in NLRC4-deficient THP-1 cells reconstituted with the disease-causing GoF mutation NLRC4 W655C, ASC was not required for cell death induction, partially required for IL-1β secretion and completely required for IL-18 release (Moghaddas et al., 2018). However, when endogenous NLRC4 was stimulated with PrgI in THP-1 cells primed with TLR1/2 agonist Pam3CSK4, IL-1β and IL-18 cytokine release as well as cell death production were largely dependent on ASC expression. Therefore, these findings suggest distinct caspase-1 activation and regulatory mechanisms downstream of NLRC4 inflammasome induction by infection or GoF mutations in human cell lines, which require further investigation and may be the result of differential ASC-dependency or requirement of different levels of caspase-1 activity (Moghaddas et al., 2018).

1.3.3.4.4 Caspase-8-dependent NLRC4 effects

Caspase-8 is typically activated downstream of death receptors (e.g. TNF receptor, CD95) and induces apoptosis through caspase-3 cleavage (Boldin et al., 1996, Zhuang et al., 1999). Furthermore, caspase-8 functions as a regulator of NF-κB-mediated *IL1B* transcription and was suggested to directly cleave pro-IL-1β in certain contexts (Bossaller et al., 2012, Chen et al., 2015, DeLaney et al., 2019, Gringhuis et al., 2012). Since the first description of caspase-8 as a downstream effector of NLRC4, several studies have provided experimental evidence for the induction of apoptotic cell death and secondary necrosis via this pathway *in vitro*, that is distinct from caspase-1-mediated pyroptosis (Lee et al., 2018, Mascarenhas et al., 2017, Schneider et al., 2017). In the current model, ASC and caspase-8 interact via heterotypic interactions between the PYD of ASC

and the death effector domains (DED) of caspase-8 (**Figure 1.3 A**) (Vajjhala et al., 2015).

Initially, caspase-1-independent cell death by NLRC4-caspase-8 interaction was determined in the lung epithelial cell line A549 using overexpression systems (Kumar et al., 2010). During *S. typhimurium* infections in BMDMs, Man et al. showed recruitment of ASC, caspase-8 and caspase-1 into the same ASC speck, which was dependent on mNLRC4. Furthermore, in absence of caspase-1, ASC-caspase-8 speck formation was still observed which required the presence of ASC and NLRC4 (Man et al., 2013). In a later study using *L. pneumophila* infections, Mascarenhas et al. demonstrated the role of mNLRC4/ASC/caspase-8-dependent cell death induction, which reduced bacterial replication in BMDMs and mice lacking caspase-1 and caspase-11 (Mascarenhas et al., 2017). Interestingly, this study suggested that despite recruitment of caspase-8 to the caspase-1-containing inflammasome complex in WT macrophages (colocalization in 60 % of ASC specks), activation only occurred when caspase-1 or GSDMD were absent as measured by caspase-8 Glo assay (Mascarenhas et al., 2017). Subsequently, Lee et al. detected the catalytically active p18 subunit of caspase-8 in caspase-1/11-deficient primary BMDMs and to lesser extent in WT cells after flagellin stimulation, suggesting that both caspase-1 and caspase-8-dependent cell death events can occur simultaneously (Lee et al., 2018). Since IL-1β release and cytotoxicity in BMDMs expressing a mutant caspase-1 without enzymatic activity ($Casp1^{C284A/C284A}$) was unaltered when compared to *Casp1*$^{-/-}$ cells, this study suggested that caspase-1 and caspase-8 do not compete for NLRC4 binding. Therefore, it was proposed that the primary and secondary induction of pyroptosis and apoptosis, respectively, is more likely a result of differential kinetics, since pyroptosis is the more rapidly occurring event (Lee et al., 2018).

Pathogen-specific effects may play a role and require further investigations, however the current model suggests that in macrophages, NLRC4-ASC-caspase-8 interaction induces a secondary apoptotic pathway that mediates cell death predominantly in absence of caspase-1-dependent pyroptosis and therefore secures host protection if caspase-1-dependent pathway are inhibited

by bacterial evasion strategies. This model is in line with a recently proposed concept, that describes the sophisticated crosstalk between pyroptosis, apoptosis and necroptosis pathways and their complementary activation following NLRC4 inflammasome stimulation in macrophages and mice that inevitable drive cell and animal death (Doerflinger et al., 2020, Zhang et al., 2021). Combined, the genetic evidence from these studies suggests complementary activation of the following pathways: caspase-1-dependent pyroptosis, caspase-8-dependent apoptosis, caspase-1-mediated intrinsic apoptosis and receptor-interacting serine/threonine protein kinase 3 (RIPK3)-mediated necroptosis (**Figure 1.3 B**) (Doerflinger et al., 2020, Zhang et al., 2021).

Interestingly, in IEC, NLRC4 efficiently protects from enteric *Salmonella* infection via a distinct caspase-8-dependent mechanism, which was revealed in an elegant series of experiments using *Nlrc4*$^{-/-}$ mice with selective re-expression of mNLRC4 in LysM+ hematopoietic cells or IEC (Vill+) as well as intestinal organoid models (Rauch et al., 2017). NLRC4-specific stimulation with FlaTox (intracellular delivery of flagellin) demonstrated caspase-1 and GSDMD-dependent pyroptosis in IECs, which were subsequently expelled from the epithelial layer into the organoid lumen. Barrier integrity was maintained via actin rearrangement within neighbouring IECs, which subsequently closed the gap. Interestingly, cell expulsion occurred via ASC and caspase-8-dependent mechanisms, although caspase-1 was also sufficient but not essential to mediate this process. Furthermore, genetic deletion experiments demonstrated that caspase-1 and caspase-8 contribute to the release of prostaglandin E2 (PGE2), an eicosanoid, which can mediate vasodilation, fluid loss, diarrhea and leucocyte recruitment (Rauch et al., 2017). Enterocyte expulsion was independent of proinflammatory cytokines, but caspase-1-mediated IL-18 release from IECs was additionally observed (Rauch et al., 2017). Therefore, this study demonstrated that NLRC4 in IECs mediates coordinated caspase-1- and caspase-8-dependent functions to induce an immune response against intestinal infections.
Importantly, inflammatory lipid mediators PGE2 as well as thromboxane (TBX) and leukotriene B4 (LTB4) were previously reported to be released from resident

peritoneal macrophages following NLRC4 inflammasome activation in mice (von Moltke et al., 2012). In this study, rapid hypothermia occurred in a mNLRC4- and caspase-1-dependent manner.

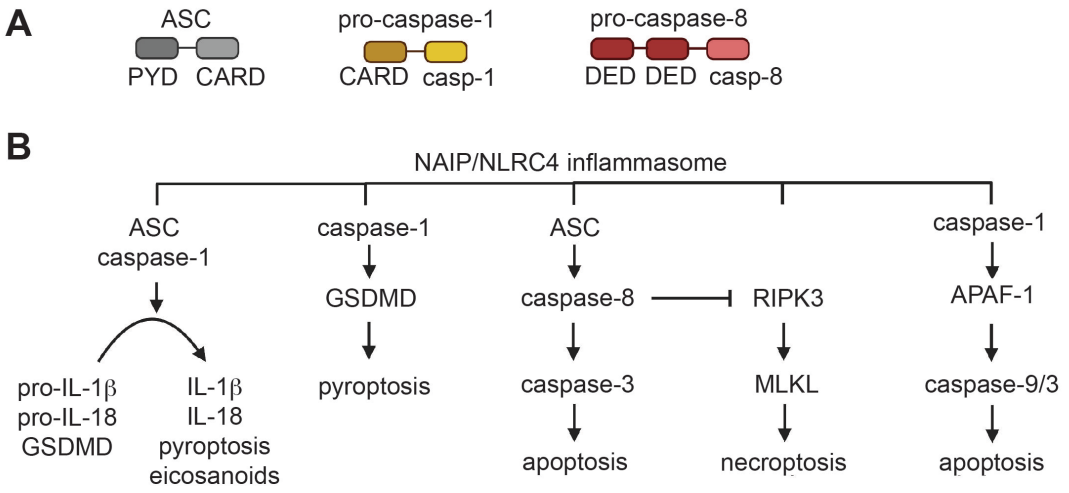

Figure 1.3 | Possible downstream pathways activated by the NAIP/NLRC4 inflammasome. A) Protein domains of NAIP/NLRC4 inflammasome-interacting adapter and effector proteins ASC, pro-caspase-1 and pro-caspase-8. Pyrin domain, PYD; caspase activation and recruitment domain, CARD; death effector domain, DED. **B)** The NAIP/NLRC4 inflammasome has been suggested to activate several downstream pathways. Interaction with ASC and caspase-1 induces cleavage of cytokine precursors (pro-IL-1β, pro-IL-18) and gasdermin D (GSDMD), leading to pyroptosis, cytokine and eicosanoid release. GSDMD-mediated pyroptosis was suggested to occur in absence of ASC following direct interaction between NLRC4 and caspase-1. Although pyroptosis acts as the default death pathway, apoptosis and necroptosis can alternatively be activated dependent on the crosstalk between cell death effectors. Suggested complementary death pathways are: ASC-dependent caspase-8 activation that drives caspase-3-mediated apoptosis; caspase-1-mediated intrinsic apoptosis induction via APAF-1, caspase-9 and caspase-3; RIPK3-mediated MLKL activation and necroptosis induction in absence of caspase-8 (Doerflinger et al., 2020, Zhang et al., 2021). Apoptosis-associated speck-like protein containing a CARD, ASC; apoptotic protease activating factor 1, APAF-1; receptor-interacting protein kinase 3, RIPK3; mixed lineage kinase domain-like, MLKL. Figure created with BioRender.com.

Mechanistically, Moltke and colleagues proposed that caspase-1 induces membrane pore formation, which allow for calcium influx and subsequent activation of the cytosolic phospholipase A2 (cPLA2), which synthesizes PGE2 and LTB4 prior to pyroptosis (**Figure 1.3 B**) (von Moltke et al., 2012). This function was not observed in BMDMs, most likely due to reduced transcription levels of synthesizing enzymes (*Cox1*, *Alox12/15* and *Alox5*), which further highlights the cell-type specific responses to NLRC4 activation (von Moltke et al., 2012).

Thus, although crucially important to prevent pathogen immune evasion and promote bacterial clearance during infection, activation of multiple effector functions downstream of NLRC4 likely collectively contributes to pathologies, if uncontrolled activation occurs (e.g. in NLRC4-AID) (Rauch et al., 2017, Zhang et al., 2021).

1.3.3.4.5 Interplay of NLRP3 and NLRC4

Due to their activation by different stimuli, the NLRP3 and NAIP/NLRC4 inflammasomes have been considered to form distinct inflammasome complexes, which share and compete for platform proteins. However interestingly, later studies showed that in situations when both NLRP3 and NAIP/NLRC4 are simultaneously stimulated, formation of a single inflammasome complex was observed (Broz et al., 2010b, Man et al., 2014a, Qu et al., 2016).

Interestingly, ASC specks in LPS-primed THP-1 macrophages infected with *S. typhimurium* featured a specific organization, where NLRC4 localized to an outer ring surrounding a circular arrangement of NLRP3 oligomers. Furthermore, caspase-1, caspase-8 and pro-IL-1β co-localized to these ASC specks (Man et al., 2014a).

Co-immunoprecipitation studies showed a physical interaction of NLRC4 and NLRP3 in LPS-primed and flagellin-transfected BMDMs, which suggests co-signalling of both molecules under these conditions. Overexpression studies in HEK293T cells showed that NLRP3 binding occurs via the NACHT domain of NLRC4 (Qu et al., 2016). Further pulldown experiments in phorbol myristate

acetate (PMA)-differentiated THP-1 cells infected with a strain of uropathogenic *E. coli* (UPEC, CFT073) co-precipitated NLRP3, NLRC4, NAIP and ASC (Verma et al., 2019), which suggests that this interaction does not specifically occur during *S. typhimurium* infections.

However, redundancy of NLRP3 and NLRC4 signalling during *S. typhimurium* infection has previously been suggested in BMDMs (Broz et al., 2010b) and a recent study identified *S. typhimurium* flagellin as a direct trigger for NLRP3 signalling in PMA-differentiated THP-1 cells (Gram et al., 2020). Flagellin-induced NLRP3 activation was independent of NAIP but dependent on reactive oxygen species (ROS) production and cathepsin activity in *NLRC4*$^{-/-}$ macrophage-like THP-1 cells. This study failed to determine whether a similar mechanism occurs in human MDMs, due to technical limitations such as the lack of genetic knockout (KO) cells or specific inhibitors for NLRC4 (Gram et al., 2020). It therefore remains questionable whether NLRP3 and NLRC4 only interact if they are simultaneously activated (e.g. during *S. typhimurium* infection) or whether mutual recruitment occurs if only one inflammasome is specifically stimulated.

However overall, these findings suggest that interaction and co-signalling of NLRP3 and NLRC4 may occur and that inflammasome complex formation may be a more flexible process than originally anticipated.

1.3.3.4.6 Regulation of the NLRC4 inflammasome

Inflammasomes play an essential role in innate immunity but also drive the development of inflammatory diseases, if dysregulated. Therefore, regulatory mechanisms are required to tightly control the balance between the immune response during infections while preventing host damage (Man et al., 2015).

Recently, IRF8 was identified as a transcriptional regulation of the NAIP/NLRC4 inflammasome, which was constitutively expressed in BMDMs. Genetic deletion of IRF8 resulted in reduced transcription of *Naip1, Naip2, Naip5, Naip6* and *Nlrc4* (Karki et al., 2018). NLRC4 inflammasome-mediated pro-caspase-1 cleavage, IL-18 release and cell death were significantly reduced in *Irf8*$^{-/-}$ BMDMs infected with *S. typhimurium*, *P. aeruginosa* or *B. thailandensis,* suggesting a crucial

requirement of functional IRF8 for optimal NLRC4 inflammasome activation (Karki et al., 2018). However, additional transcriptional regulators likely exist, since NAIP/NLRC4 inflammasome activity was not completely absent in *Irf8*$^{-/-}$ BMDMs (Karki et al., 2018). Small interfering RNA (siRNA)-mediated *IRF8* knockdown in human THP-1 cells reduced *NLRC4* baseline transcription, whereas this effect was not observed in U937 cells and human MDMs (Yashiro et al., 2021). However, siRNA-knockdown of PU.1, an Ets family transcription factor which increases IRF8-binding to DNA (Laricchia-Robbio et al., 2005) and was previously shown to control specific genes in macrophages in cooperation with IRF8 (Tamura et al., 2005), reduced *NLRC4* mRNA expression levels in U937 cells and MDMs (Yashiro et al., 2021). This effect was less pronounced for *NAIP* transcription, and both PU.1 and/or IRF8 controlled *NLRP3*, *PYCARD* (encoding ASC) and *CASP1* transcription in THP-1 cells in this study, suggesting a broad role in transcriptional regulation of inflammasomes. However, results obtained in other human cell models were inconsistent (Yashiro et al., 2021), and therefore the exact role of IRF8 and PU.1 requires further clarification. One suggested regulatory mechanism involves epigenetic regulator bromodomain-containing protein 4 (Brd4), which controlled IRF8/PU.1-mediated *Naip* transcription in BMDMs, but did not affect NLRP3 transcription or signalling (Dong et al., 2021).

On the post-translational level, only a few modifications of NLRC4 have been described, the role of which remains controversial.
Beside suppressor of gal1 (SUG1)-mediated NLRC4 ubiquitination, which has been suggested to promote caspase-8 activation (Kumar et al., 2010), one other PTM was proposed to regulate NLRC4 activity. Phosphorylation of residue serine 533 (S533), was the only phosphorylation site identified in a mass spectrometry analysis of BMDMs following stimulation with *S. typhimurium* (Qu et al., 2012). Between species, S533 is a conserved residue and located within the HD2 domain. When *Nlrc4*$^{-/-}$ BMDMs were reconstituted with NLRC4^{S533A}, an unphosphorylatable mutant, stimulation-induced caspase-1 activation, IL-1β secretion and pyroptosis were abrogated to the level of *Nlrc4*$^{-/-}$ BMDMs,

suggesting a critical role of phosphorylated S533 in NLRC4 inflammasome activation (Qu et al., 2012).

In two independent studies, protein kinase C isoform delta (PKCδ) (Qu et al., 2012) or leucine-rich repeat kinase 2 (LRRK2) (Liu et al., 2017b) were suggested as responsible kinases, however a consensus about the functional consequences of this PTM has not been reached.

Qu et al. observed autoactivation and cell death following reconstitution of BMDMs with the phosphomimetic NLRC4^{S533D} mutant (Qu et al., 2012), whereas findings from Matusiak et al. suggested S533 phosphorylation as a NAIP-independent priming event that was not sufficient to induce inflammasome signalling in flagellin-stimulated *Naip5*$^{-/-}$ BMDMs (Matusiak et al., 2015). In a study using BMDMs isolated from 3xFLAG-NLRC4$^{S533A/S533A}$ knock-in mice, phosphorylation was not essentially required for NLRC4 signalling and a compensatory mechanism through recruitment of NLRP3 and ASC was proposed (Qu et al., 2016). Importantly, S533 was phosphorylated in the reported crystal structure of inactive mNLRC4 (protein data bank (PDB):4KXF) which could suggest a stabilizing effect in the inactive state or indicate that although this phosphorylation is not sufficient to induce an open conformation, it may promote the release of the autoinhibited state subsequently to NAIP binding (Hu et al., 2013, Matusiak et al., 2015). Bypassing the potential artefacts associated with overexpression approaches or protein tags, Tenthorey et al., aimed to clarify the role using BMDMs from mice deficient in *Nlrc4*$^{-/-}$, or expressing phosphomimetic (NLRC4$^{S533D/S533D}$) or nonphosphorylatable (NLRC4$^{S533A/S533A}$) mutations introduced into the endogenous *Nlrc4* genomic locus (Tenthorey et al., 2020). Only a modest signalling deficiency of NLRC4$^{S533A/S533A}$ was identified when BMDMs were stimulated with low levels of cytoplasmic *L. pneumophila* flagellin or *S. typhimurium* (with or without P3CSK4 priming) (Tenthorey et al., 2020). Further, their results suggested that the S533 phosphorylation was not essential for NLRC4 activation at higher ligand concentrations and in *in vivo* infection experiments. No differences between WT NLRC4 and phosphomimetic NLRC4$^{S533D/S533D}$ indicated that phosphorylation of S533 in not sufficient to induce NLRC4 activation and a role of NLRP3 could not be determined (Tenthorey et al.,

2020). Therefore, the S533 phosphorylation may play a yet unidentified role and different genetic backgrounds of experimental mice, differences of microbiota, ligand source or dose-dependency effects could be a possible explanation for the differences observed in the previously performed studies (Tenthorey et al., 2020).

1.3.4 DNA sensors

DNA sensors play a crucial role in the immune defence against viral infections. Several DNA sensors have been proposed, although the best investigated and supposably predominantly activated pathway involves cyclic guanosine monophosphate (GMP)-adenosine monophosphate (AMP)-synthase (cGAS) and the immune adapter stimulator of interferon genes (STING) (Motwani et al., 2019).

The previously mentioned inflammasome-forming protein AIM2 and interferon-inducible protein 16 (IFI16) are classified as AIM2-like receptors (ALR) (Unterholzner et al., 2010). AIM2 possesses a N-terminal pyrin domain (PYD) and one C-terminal interferon-inducible nature and nuclear localization domain 200 (HIN-200), which mediates sequence-independent dsDNA binding and subsequent oligomerization and inflammasome formation with ASC (Bürckstümmer et al., 2009, Fernandes-Alnemri et al., 2009, Hornung et al., 2009, Jin et al., 2012). Interestingly, no GoF mutations in this gene have so far been associated with a monogenic AID. As a potential reason, the requirement of dsDNA binding for inflammasome assembly and an additional scaffold function for oligomerization has been suggested (Lugrin et al., 2018).

In contrast, IFI16 does not form inflammasomes and was identified as cytosolic DNA sensor upstream of the STING/TANK-binding kinase 1 (TBK1)/IRF3 pathway that mediates IFNα/β induction (Unterholzner et al., 2010).

Other less well investigated cytoplasmic DNA sensors are DNA-dependent activator of IRFs (DAI, also known as Z-DNA-binding protein (ZBP1)) and RNA polymerase III (Ablasser et al., 2009, Chiu et al., 2009, Takaoka et al., 2007). However, pathogen detection via these pathways is limited due to the cell type-specific expression of DAI and the mechanism of RNA polymerase III signalling,

which requires DNA-to-RNA transcription for subsequent RIG-I activation and has been suggested to be limited to AT-rich DNA molecules (Ablasser et al., 2009, Chiu et al., 2009, Lippmann et al., 2008). Furthermore, the DExD/H-box helicase DDX41 (Zhang et al., 2011) was suggested to act as sensor of bacterial c-di-GMP and form a complex with STING to induce an immune response (Parvatiyar et al., 2012).

1.3.4.1 Type I IFN pathway and interferonopathies

Recognition of nucleic acids released from pathogens represents a major strategy for innate immune system activation, which occurs through several sensors (chapter 1.3). However, given the evolutionarily conserved structure of nucleic acids and their immunogenic potential, dysregulation of RNA and DNA sensing pathways and recognition of self-DNA are often associated with AIDs. Downstream of nucleic acid sensing, TLR7, TLR8, TLR9 activate transcription factor IRF7 to induce type I IFN transcription. TLR3, TLR4, RIG-I, MDA5 and the cGAS-STING signalling pathways converge on the level of TBK1 activation, which phosphorylates IRF3 and induces its nuclear translocation (**Figure 1.4**) (Liu et al., 2015b). Synergistic DNA binding of transcription factors IRF3, IRF7 with NF-κB and activating transcription factor (ATF)-2/c-Jun forms the “enhanceosome” and results in maximal type I IFN transcription (*IFNB1, IFNA1* genes) (Ford et al., 2010). In humans, the family of type I IFNs comprises IFNα (12 functional subtypes), IFNβ, IFNκ, IFNω and IFNε, which signal through the common IFNα-receptor (IFNAR) (López de Padilla et al., 2016, Uzé et al., 2007). IFNAR is composed of two subunits IFNAR1 and IFNAR2, that are expressed by most cell types (Negrotto et al., 2011, Owczarek et al., 1997, Uzé et al., 2007). Mechanistically, high-affinity ligand binding occurs via IFNAR2 interaction, whereas the IFNAR1 subunit is essentially required for downstream signalling (Arduini et al., 1999, Cohen et al., 1995, López de Padilla et al., 2016). The best studied family members are IFNα and IFNβ and whereas IFNα is predominantly secreted by leucocytes, most cell types including fibroblasts produce IFNβ (Ivashkiv et al., 2014, Li et al., 2018b, Reis et al., 1989).

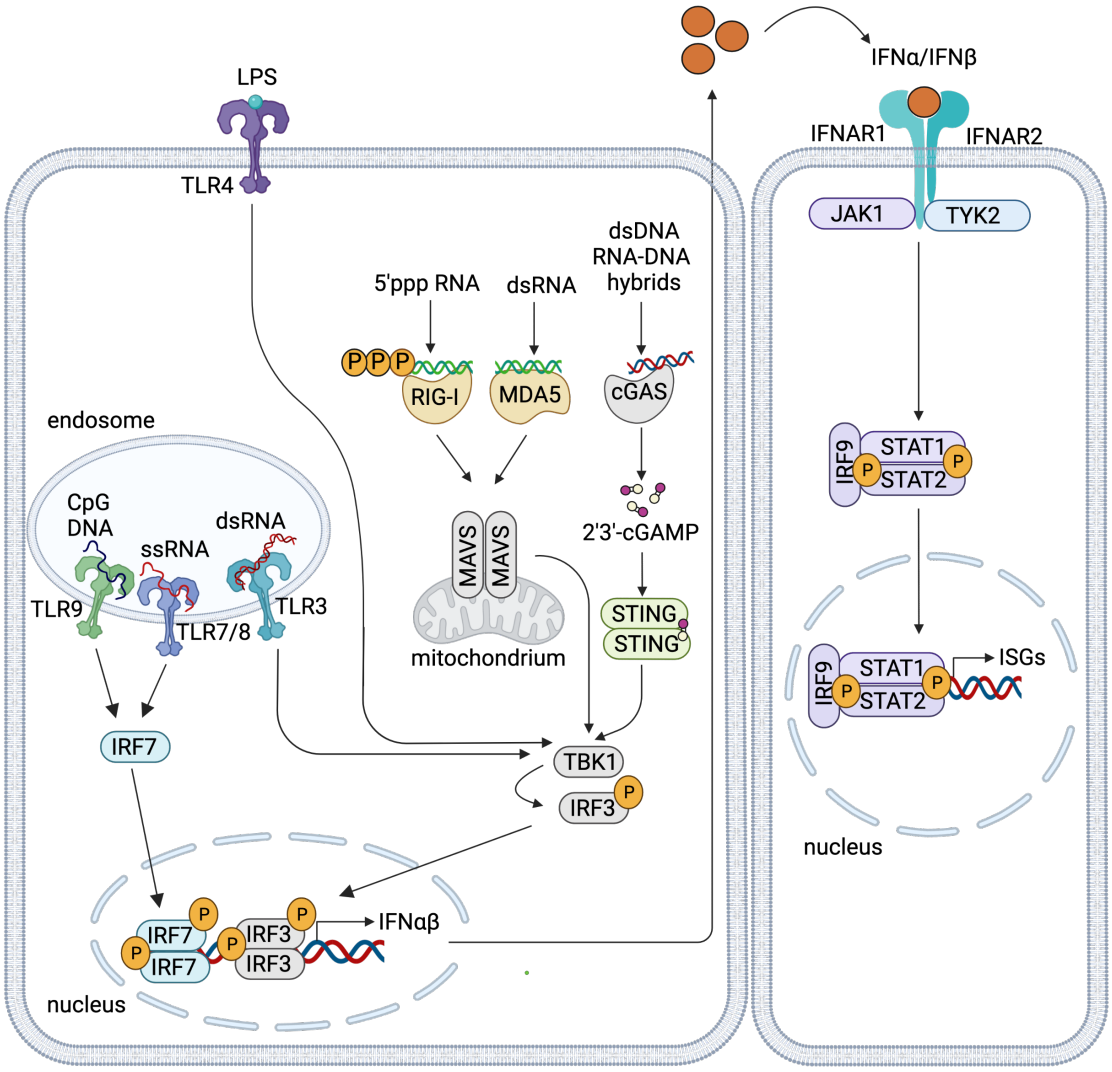

Figure 1.4 | Simplified scheme of type I IFN pathway induction. Type I IFNs (αβ) are induced downstream of cytosolic nucleic acid sensors RIG-I, MDA5, cGAS-STING and following activation of endosomal TLRs 3, 7, 8, 9 and surface-exposed TLR4. Transcription factors IRF7 and IRF3 are phosphorylated and dimerize to induce type I IFN transcription. Upon secretion, type I IFNs signal in a paracrine and autocrine manner via binding to the IFNα receptor (IFNAR). Signal transduction through activation of the JAK/STAT pathway induces the transcription of interferon-stimulated genes (ISGs). 2'3'-cyclic GMP-AMP, 2'3'-cGAMP; mitochondrial antiviral signalling protein, MAVS; melanoma differentiation-associated protein 5, MDA5; retinoic acid-inducible gene-I, RIG-I; cyclic GMP-AMP-synthase, cGAS; stimulator of interferon genes, STING; signal transducer and activator of transcription, STAT; Janus kinase, JAK; tyrosine kinase, TYK; interferon regulatory factor, IRF; TANK-binding kinase 1, TBK1; lipopolysaccharide, LPS; ss, single-stranded; ds, double-stranded; 5'-triphosphorylated RNA, 5'-ppp RNA; cytosine-phosphate-guanine-containing DNA; CpG DNA. Figure created with BioRender.com.

After ligand binding, signal transduction occurs via cytoplasmic tyrosine kinase 2 (TYK2) and Janus kinase 1 (JAK1), which active transcription factors signal transducer and activator of transcription (STAT) through a cascade of phosphorylation events (**Figure 1.4**) (López de Padilla et al., 2016). Heterodimerization of STAT1/STAT2 enables binding of IRF9 to form the IFN-stimulated gene factor 3 (ISGF3), that binds IFN-stimulated response elements (ISREs) leading to the transcription of thousands of IFN-stimulated genes (ISGs) (**Figure 1.4**) (Aaronson et al., 2002, López de Padilla et al., 2016, Mowen et al., 1998). The protein products of ISGs activate multiple antiviral and immunomodulatory effects aiming to limit the spread of the infectious pathogen, enhance antigen presentation and cytokine production in innate immune cells and activate the adaptive immune system (Ivashkiv et al., 2014).

Therefore, the type I IFN pathway induces a potent and versatile immune response to fight host infection (McNab et al., 2015). Recent years have also demonstrated the immunogenic potential of self-nucleic acids in the context of defective degradation pathways or mislocalization. These findings have shaped our understanding of the negative regulatory pathways that prevent type I IFN production by host antigens during homeostasis. Genetic defects in proteins involved in those control pathways result in overactivation of immune signalling and trigger severe autoinflammatory diseases, classified as type I interferonopathies (Crow 2011).

Over the past 10 years, the discovery of numerous novel gene mutations causing type I IFN-driven diseases have demonstrated a broad phenotypic spectrum and identified the immunomodulatory function of several proteins including three-primer repair exonuclease 1 *(*TREX1*)* (Crow et al., 2006a), ribonuclease H2 (RNaseH2) (Crow et al., 2006b), sterile alpha motif domain and HD domain-containing protein 1 (SAMHD1) (White et al., 2017), DNA polymerase subunit alpha 1 (POLA1) (Starokadomskyy et al., 2016), mitochondrial ATPase family AAA domain-containing protein 3A (ATAD3A) (Lepelley et al., 2021), ataxia telangiectasia mutated (ATM) and ARTEMIS (encoded by *DCLRE1C)* (Gul et al., 2018)*,* adenosine deaminase acting on RNA 1 (ADAR1) (Rice et al., 2012).

Due to the number of interferonopathies discovered (mutations in 38 different genes to date (Crow et al., 2021)), the pathomechanism and clinical manifestation will only be described in more detail for STING-associated vasculopathy with onset in infancy (SAVI) (chapter 1.3.4.3.3), due to the phenotypic similarities to COPA syndrome, which is a main focus of this thesis (chapter 3). However, first the cGAS-STING pathway, its activation mechanism, signalling and effector functions are introduced in the following sections.

1.3.4.2 DNA sensor cGAS

In 2013, cGAS (also known as male abnormal 21 domain containing-1 (MB21D1)) was identified as central cytosolic dsDNA sensor able to synthesize the second messenger 2'3'-cyclic GMP-AMP (2'3-'cGAMP) (Sun et al., 2013, Wu et al., 2013). cGAS was originally identified as sensor of dsDNA released from (retro-) viruses and bacteria including herpes simplex virus1 (HSV-1), vaccinia virus, human immunodeficiency virus (HIV), cytomegalovirus (CMV), *Listeria monocytogenes*, *Mycobacterium tuberculosis* and *Chlamydia trachomatis* (Hopfner et al., 2020). Furthermore, cGAS was shown to detect genomic DNA from parasites, e.g. *Plasmodium* (Hahn et al., 2018) and was activated by some RNA viruses, e.g. dengue virus or porcine reproductive and respiratory syndrome virus (PRRSV), which occurred secondary to virus-mediated release of mitochondrial host DNA (Sun et al., 2017, Xu et al., 2021).

Indeed, cGAS can also detect host mitochondrial and genomic DNA and strict compartmentalization was thought to prevent cGAS activation by endogenous ligands (Hopfner et al., 2020). Numerous breakthrough discoveries over the past years have challenged this dogma and contributed to a vast increase in our understanding of the complexity of cGAS localization, regulation and function.

The following section aims to summarize the structural basis of cGAS activation, key concepts and findings from recently published studies relevant to the understanding of the pathway and question investigated in chapter 3 of this thesis.

Cellular cGAS exists in an inactive state within nuclear and cytoplasmic compartments and associated with the cell membrane (Barnett et al., 2019, Gentili et al., 2019, Jiang et al., 2019, Liu et al., 2018a, Orzalli et al., 2015, Volkman et al., 2019). In this conformation, the catalytic site is structurally absent, and only forms following global conformational rearrangement induced by dsDNA binding (Civril et al., 2013, Gao et al., 2013a, Kranzusch et al., 2013, Li et al., 2013b). dsDNA binding occurs in a sequence-independent manner via electrostatic interactions and hydrogen bonding. Highly conserved positively charged amino acids located opposite to the catalytic domain of cGAS interact with the negatively charged DNA phosphate-sugar backbone of both DNA strands (Civril et al., 2013). Additionally required for DNA binding and stabilization of the cGAS-DNA complex is the “Zinc (Zn)-thumb” or ”Zn-ribbon”, a structurally conserved loop formed by histidine and cysteine residues which coordinate a zinc cation (Du et al., 2018). In this DNA-bound active conformation, a catalytic magnesium cation, guanosine triphosphate (GTP) and adenosine triphosphate (ATP) are bound in the catalytic centre (Civril et al., 2013), which results in synthesis of 2’3’-cGAMP, the high affinity ligand for STING (chapter 1.3.4.3) (Ablasser et al., 2013, Diner et al., 2013, Gao et al., 2013a).

Importantly, fluorescence anisotropy experiments confirmed preferred cGAS binding of dsDNA (dissociation constant (K_d)~87.6 nM) and markedly reduced binding affinity to ssDNA (K_d~1.5 μM). Whereas ssDNA was able to weakly stimulate cGAS activity, 2’3’-cGAMP was not synthesized in the presence of RNA ligands (Kranzusch et al., 2013).

dsDNA binding triggers cGAS dimerization that stabilizes the active conformation and results in a 2:2 cGAS:dsDNA complex, where both cGAS protomers interact with both DNA molecules through two binding sites (site A and B) (Civril et al., 2013, Li et al., 2013b). In this conformation, dsDNA strands of at least 16-18 base pairs (bp) length are able to accommodate cGAS dimer binding (Hopfner et al., 2020, Li et al., 2013b, Zhang et al., 2014). However, human cGAS requires dsDNA strands above >45 bp length (>2 helical DNA turns) to mount a substantial immune response at physiological concentrations, which was shown to depend on a ladder-like assembly of cGAS dimers along the same stimulatory dsDNA

strand (Andreeva et al., 2017). Furthermore, identification of an additional DNA binding site C provided the molecular basis for clustering between multiple dsDNA strands and higher order cGAS-dsDNA condensate formation (Xie et al., 2019). This process has also been described as cGAS-DNA phase separation, where liquid-like-droplets form membraneless organelles for local and temporary enrichment of proteins and reactants required for cGAS-mediated 2’3’-cGAMP production (Du et al., 2018). Furthermore, phase-separated droplets prevented TREX1-mediated DNA degradation, providing resistance to negative regulatory mechanisms, which were suggested to further boost the immune response (Zhou et al., 2021). The amplitude of cGAS-DNA phase separation as well as droplet dynamics/fluidity was substantially increased in presence of the N-terminal domain and largely dependent on the availability of zinc cations (Du et al., 2018, Zhou et al., 2021). Future studies are required to elucidate the key regulatory mechanisms of cGAS-DNA phase separation, however involvement of protein cofactors, such as the stress kinase protein kinase R (PKR) and double-stranded nucleic acid helicase G3BP1 (stress granule assembly factor 1), has previously been suggested, which may link cGAS activation to cellular stress response pathways (Hu et al., 2019).

Of note, human cGAS is able to bind shorter dsDNA (20 bp), however, robust activation and signalling requires presence at high concentrations (of both cGAS and DNA) (Andreeva et al., 2017). Interestingly, length-dependency in less pronounced in murine cGAS due to residue variation in the DNA binding site A (Zhou et al., 2018b).

Considering compartmentalization as protective mechanism to prevent activation by self-DNA, cGAS was originally anticipated to predominantly localize within the cytosol (Sun et al., 2013, Wu et al., 2013). However, recent evidence suggests that a considerable proportion of cGAS associates with chromosomal DNA following nuclear membrane disassembly in mitotic cells or resides within the nucleus during the steady state (Gentili et al., 2019, Guey et al., 2020, Jiang et al., 2019, Orzalli et al., 2015, Volkman et al., 2019, Yang et al., 2017, Zierhut et al., 2020). Therefore, spatial separation does not provide the only mechanism to silence cGAS upon self-DNA exposure. Instead, cGAS was shown to bind

nucleosomes with higher affinity than naked DNA via distinct histone-interacting residues as well as residues within DNA binding site B (Gentili et al., 2019, Volkman et al., 2019). Interestingly, chromatin tethering retained cGAS in a conformational state where histone-interactions sterically hindered the DNA-binding sites, thus preventing continuous activation by genomic host DNA (de Oliveira Mann et al., 2021, Zierhut et al., 2019).

Another layer of regulation is provided via barrier-to-autointegration factor 1 (BAF), which was found to compete with nuclear cGAS for DNA binding, thereby preventing its activation. siRNA-mediated knockdown experiments in different cell types showed that absence of BAF triggered spontaneous cGAS activation upon nuclear localization (e.g. in mitotic cells) (Guey et al., 2020).

Furthermore, cGAS was shown to be phosphorylated (at residue S305 in human cGAS) during mitosis by the kinase CDK1-cyclin B complex, which inhibited its catalytic activity. Once mitosis was completed, dephosphorylation was catalysed by type I phosphatase PP1, which suggests this PTM as an additional regulatory mechanism during cell division (Zhong et al., 2020).

Physiologically, nuclear localization of cGAS may be required for nuclear sensing of viral DNA, which in the case of HIV-2 has been shown to require additional presentation of the viral capsid protein via host factor NONO (non-POU domain-containing octamer binding protein) (Lahaye et al., 2018).

Despite antiviral signalling and recognition of DAMPs, a tumour-promoting function of cGAS was suggested, as it was shown to suppress homologous recombination, a crucial mechanism involved in DNA damage repair (Jiang et al., 2019, Liu et al., 2018a). Additionally, cGAS was found to induce signalling following rupture of chromatin or genomic-DNA-containing micronuclei, which are nuclear envelope-enclosed structures formed following DNA damage during aberrant mitosis, replication or DNA repair, thus linking genomic instability to immune system activation (Gluck et al., 2017, Harding et al., 2017, Mackenzie et al., 2017). Interestingly, recent findings suggests that micronuclei contain nuclear cGAS, therefore envelope rupture may not be necessary to prompt cGAS activation (Jiang et al., 2019). However, the mechanisms by which cGAS discriminates between micronuclear “damaged” DNA and intact chromosomal

DNA within the nucleus remain elusive and present an important direction of future research.

Furthermore, cGAS was suggested to be required for cellular senescence induction in response to DNA damaging agents, radiation and following recognition of cytosolic chromatin (Gluck et al., 2017, Yang et al., 2017). Particularly interesting in this context is the inflammatory phenotype associated with senescence-induced cytokine/chemokine secretion as part of the senescence-associated secretory phenotype (SASP), providing a link between cGAS activation, inflammation and senescence-associated age-related diseases (Coppé et al., 2010, Kaur et al., 2020, Yang et al., 2017).

Therefore, beside antiviral signalling, cGAS functions in diverse cellular processes and complex mechanisms exist to regulate pathway activity and self-DNA discrimination. Regulation may be cell-type specific and take place on multiple levels, including subcellular localization, cGAS expression levels, dependence on shape and length of the DNA ligand, PTMs, presence of cofactors and interacting proteins (Hopfner et al., 2020). Although our understanding of cGAS has vastly increased since its discovery, involvement in unexpected processes leaves many questions unanswered, including the regulatory mechanisms that fine-tune cGAS signalling in the nucleus and within phase separated droplets, which require further studies.

1.3.4.3 The STING pathway

The innate immune receptor and adapter protein STING (also known as MITA, MPYS and ERIS) is activated downstream of multiple intracellular nucleotide sensors including cGAS, IFI16, and DDX41 (Hansen et al., 2014, Ishikawa et al., 2009, Jin et al., 2008, Orzalli et al., 2015, Sun et al., 2009, Zhang et al., 2011, Zhong et al., 2008). Uncontrolled activation of STING due to GoF mutations has been shown to cause severe autoinflammatory disease (SAVI, chapter 1.3.4.3.3) (Ahn et al., 2014, Ahn et al., 2012, Gall et al., 2012, Liu et al., 2014b). Thus, to prevent pathway hyperactivity, tight regulation of STING is required. The following sections aim to introduce molecular features of STING, the STING

signalling pathway, effector functions and regulatory mechanisms relevant to the research question investigated in this thesis (chapter 3).

Whereas the role and mechanisms of IFI16- and DDX41-mediated STING activation is less well understood, numerous structural and functional studies have contributed to a more detailed understanding of STING activation by 2'3'-cGAMP, which represents the endogenous high-affinity ligand for STING downstream of cGAS signalling (Sun et al., 2013, Wu et al., 2013, Zhang et al., 2013). Additionally, STING does not only represent an "immune adapter" but also acts as a direct sensor of bacterial cyclic dinucleotide (CDN) ligands (cyclic di-AMP, cyclic di-GMP), due to structural similarities to endogenous 2'3'-cGAMP (Burdette et al., 2011, Zhang et al., 2013).

At rest, inactive STING homodimers localize to the endoplasmic reticulum (ER) membrane and ligand-induced ER exit and translocation to ER-Golgi-intermediate compartment (ERGIC) and the Golgi apparatus is required to induce several independent downstream pathways (Dobbs et al., 2015), including antiviral and proinflammatory signalling via activation of transcription factors IRF3 and NF-κB (Abe et al., 2014, Tanaka et al., 2012), MAPK pathway activation (Abe et al., 2014, Cavlar et al., 2013), autophagy (Gui et al., 2019), cellular senescence (Gluck et al., 2017, Li et al., 2018c), cell death (Gulen et al., 2017, Liu et al., 2018b) and lysosomal degradation (Gonugunta et al., 2017). Some STING-induced functions are well understood, e.g. IRF3 signalling, however other cellular response pathways require further investigation to identify involved signalling molecules and their regulation. Furthermore, it remains largely unclear how different STING functions are balanced and whether cell type-specific and context-dependent regulatory mechanisms exist *in vivo*.

1.3.4.3.1 STING trafficking

Trafficking of ER-resident STING represents the prerequisite for signalling (Dobbs et al., 2015) and occurs via coat protein complex II (COPII)-vesicles, similarly to other Golgi-directed protein cargo (Gui et al., 2019, Ran et al., 2019, Sun et al., 2018). The mechanistic details of COPII vesicle formation and

anterograde ER-to-Golgi protein transport in general are further described in chapter 1.4.1.1.

Co-immunoprecipitation experiments following transient transfection and cGAMP treatment in HEK293T cells showed increased binding of STING to COPII subunit SEC24 isoform C (Gui et al., 2019). Vice versa, *IFNB1* transcription was abrogated in foreskin fibroblasts (BJ cells) lacking COPII-initiating protein secretion associated Ras related GTPase (SAR) 1A or SEC24C in siRNA knockdown experiments (Gui et al., 2019), highlighting the crucial role of anterograde trafficking events for STING-induced type I IFN signalling. Furthermore, in a complementary study, siRNA-mediated knockdown of SAR1 and several other COPII subunits (SEC13, SEC23 and SEC31) reduced *IFNB1* transcription following HSV-1 infection in human foreskin fibroblasts (Ran et al., 2019). Additionally, Sun et al. identified isoform-specific binding and established that only SAR1B (but not SAR1A), SEC23B (but not SEC23A) and SEC24C (but not SEC24A) co-immunoprecipitated with STING, however not all known isoforms of COPII subunit proteins were tested (Sun et al., 2018).

Although the regulatory processes that control COPII vesicle loading and ER exit of activated STING require further investigation, several proteins have been proposed to positively regulate this process including adapter protein YIP family 5 (YIPF5) (Ran et al., 2019), inactive rhomboid protein 2 (iRHOM2) (Luo et al., 2016), translocon-associated protein β (TRAPβ) (Ishikawa et al., 2008), transmembrane emp24 protein transport domain-containing 2 (TMED2, p24 family protein) (Sun et al., 2018), sorting nexin-8 (SNX8) (Wei et al., 2018) and the ubiquitin regulatory X domain-containing protein 3B (UBXN3B) (Yang et al., 2018).

As a negative regulator, the ER-resident calcium sensor stromal interaction molecule 1 (STIM1) was suggested to associate with STING and anchor it within the ER membrane, since Golgi localization and IFN signalling of SAVI STING mutants was suppressed upon STIM1 overexpression in HEK293T cells (Srikanth et al., 2019). STIM1 regulates replenishment of intracellular calcium stores (e.g. ER) through store-operated calcium entry (SOCE) and ORAI1 channels at the plasma membrane, however STING trafficking remained normal

after *Orai1* depletion in mouse embryonic fibroblasts (MEFs), which suggested uncoupling of both STIM1 functions (Srikanth et al., 2019). Notably, an independent study reported reduced STING translocation and signalling when intracellular calcium levels were altered with calcium chelator BAPTA-AM (depletion) and ionophore ionomycin (elevation) (Kwon et al., 2018). Whether STIM1-dependent regulation of STING translocation is the underlying mechanisms in this context, requires further investigation.

The identification of STING ER exit protein (STEEP, CXorf56) suggested mechanistic insights into ER exit regulation via STEEP-mediated recruitment of phosphatidylinositol 3-kinase (PI3K) VPS34 (vacuolar protein sorting-associated protein 34) (Zhang et al., 2020). Subsequent generation and accumulation of negatively charged phosphatidylinositol 3-phosphate (PI3P) induced ER membrane curvature, which promoted COPII vesicle budding and STING translocation (Zhang et al., 2020). Congruently, STEEP-deficiency resulted in impaired STING signalling in THP-1 cells, HeLa cells and fibroblasts and selectively abolished STING translocation, whereas general anterograde transport remained intact. In line, SAVI STING mutants showed strongly increased STEEP binding in HEK293T overexpression systems (Zhang et al., 2020).

1.3.4.3.2 STING effector functions

Structural information of the STING dimer in complex with its activating ligand and downstream signalling molecules has largely shaped our understanding of the IRF3 activation pathway. STING is a transmembrane protein containing four N-terminal transmembrane domains (TMD), followed by a connector helix (CH) and connector loop (CL), the C-terminal cytoplasmic ligand-binding domain (LBD) and a C-terminal tail (CTT). When inactive, STING forms a butterfly-shaped dimer and resides within ER membranes (**Figure 1.5 A, B**) (Shang et al., 2019, Shang et al., 2012).

Modular binding and signalling motifs within STING, which are partly located within the CTT region, differ between distinct evolutionary lineages and determine

downstream STING effector functions, activation of inflammatory pathways and the magnitude of the response (de Oliveira Mann et al., 2019). All subsequently mentioned amino acid residues refer to the position in human proteins, if not indicated otherwise.

In vertebrate species, the CTT encodes the conserved TBK1-binding motif (residues 369–377), which mediates binding-induced TBK1 dimerization (**Figure 1.5 A**) (Zhang et al., 2019). TBK1 activation additionally relies on phosphorylation of residue S172 in its kinase activation loop, accessibility of which is sterically hindered in the STING-bound TBK1 dimer. Therefore, higher-order oligomerization has been suggested to be required for S172 *trans*-autophosphorylation by neighbouring TBK1 molecules (Larabi et al., 2013, Shu et al., 2013, Tu et al., 2013, Zhang et al., 2019). In line, *in vitro* co-immunoprecipitation and imaging experiments showed that in absence of cGAMP, STING and TBK1 constitutively interact, which suggests preformation of sterically silenced tetrameric STING-TBK1 dimer-dimer complexes at the ER membrane (Zhang et al., 2019). This is in contrast to a study by Zhang et al., who suggested that TBK1 recruitment occurs subsequent to ER exit, during ER-to-Golgi-translocation or at *trans*-Golgi compartments (Zhang et al., 2020). However, co-immunoprecipitation experiments performed in reconstituted STING-deficient MEFs showed weak interaction between TBK1 and STING at baseline, which was further enhanced following STING activation and might reflect STING/TBK1 tetramer preformation at the ER and subsequent oligomerization and enrichment at perinuclear compartments (Ogawa et al., 2018) (**Figure 1.5 C**).

Ligand binding occurs at a 2:1 stoichiometry (STING:ligand) (Burdette et al., 2011, Shang et al., 2012) and induces folding of both STING protomers to encapsulate the bound ligand (Shang et al., 2019). Furthermore, LBDs of both STING monomers undergo a 180° rotation whereas the TMDs maintain their position, which induces unwinding of both CLs into a parallel orientation (Shang et al., 2019). This conformational change stabilizes the STING dimer structure (Gao et al., 2013b, Huang et al., 2012, Shang et al., 2012), releases the CTT (Yin et al., 2012) and exposes lateral binding sites for subsequent oligomerization so

called “side-by-side” packing of STING dimers (Shang et al., 2019), which is thought to be the prerequisite for TBK1 *trans*-autophosphorylation and signalling (Zhang et al., 2019).

However, a crystal structure of STING bound to its bacterial ligand cyclic di-GMP demonstrated a rather open conformation, which suggests that alternative conformational changes can induce STING activation, since the functionality of this complex was confirmed by STING-dependent IRF3 phosphorylation in cyclic di-GMP-stimulated U937 cells (Ergun et al., 2019). Therefore, this data suggested that ligand-mediated dimer closure is not necessarily required for STING signalling, however induces higher potency STING activation (Ergun et al., 2019).

STING oligomerization/polymerization is further stabilized by disulfide bridge formation between cysteine (C) 148 residues of neighbouring dimers, which was suggested to occur at ER membranes (Ergun et al., 2019). In this oligomeric assembly, an active TBK1 protomer phosphorylates the adjacently located STING at residue S366 (Shang et al., 2019, Zhang et al., 2019), which contributes to the CTT-located pLxIS^{366} motif (x denotes any residue) and forms a docking site for IRF3 via the positively charged phospho-binding domain (**Figure 1.5 C**) (Liu et al., 2015b). The resulting spatial proximity is the prerequisite for TBK1-mediated IRF3 phosphorylation (Liu et al., 2015b, Zhao et al., 2019). Phosphorylated IRF3 then dissociates, dimerizes and translocates into the nucleus to activate type I and III IFN transcription (Liu et al., 2015b, Tanaka et al., 2012) (**Figure 1.5 C**). Although STING/TBK1 oligomerization was suggested to initiate at ER membranes, several studies used trafficking inhibitors and established STING translocation to perinuclear compartments (ERGIC and Golgi) as crucial step for IRF3 signalling (Dobbs et al., 2015, Stempel et al., 2019). This suggests the fulfilment of certain requirements that are only met at these compartments (Dobbs et al., 2015, Ishikawa et al., 2009, Konno et al., 2013). One possible explanation is the palmitoylation of STING cysteine residues in position 88 and 91 (C88/C91) mediated through Golgi-resident palmitoyltransferases (DHHC proteins 3, 7 and 15), which was suggested to promote further STING-TBK1 clustering and oligomerization at *trans*-Golgi lipid rafts to allow efficient

IRF3 activation (**Figure 1.5 C**) (Mukai et al., 2016). Importantly, palmitoylation inhibitor 2-bromopalmitate (2-BP) or the covalent inhibitor H-151, which directly targets C91, sufficiently suppressed STING-mediated IFN signalling induced by DNA stimulation and autoactive SAVI STING mutants, which suggested the essential requirement of this PTM for the IFN response (Haag et al., 2018, Mukai et al., 2016).

The detailed mechanisms of NF-κB activation downstream of STING are less well understood and somewhat controversial (**Figure 1.5 C)**. Based on original studies, the concept that TBK1 activates both IRF3 and NF-κB signalling downstream of STING was widely accepted (Abe et al., 2014, Pomerantz et al., 1999). However, later studies showed STING-mediated NF-κB activation independent of the TBK1-binding motif encoded within the CTT in a STING ortholog from *D. melanogaster* and a truncated hSTING splice variant, suggesting alternative mechanisms (Chen et al., 2014a, Martin et al., 2018). In contrast, in the serum of mice expressing a STING$^{\Delta CTT}$ mutant, no TNFα was detected following injection with STING agonist and *IFNB1* transcription was abrogated in BMDMs from these mice, which implies requirement of TBK1 for NF-κB activation and IFN signalling in mice (Yamashiro et al., 2020). Interestingly, a recent study identified redundancy of TBK1 and its homolog inhibitor of NF-κB (IκB) kinase (IKK) epsilon (IKKε) for STING-induced NF-κB signalling in myeloid cells from human and mice (Balka et al., 2020). Only simultaneous deletion of TBK1 and IKKε abrogated proinflammatory signalling, whereas TBK1 was largely responsible for IRF3-induced type I IFN activation (Balka et al., 2020). Here, NF-κB activation was suggested to occur via the canonical pathway involving transforming growth factor beta-activated kinase (TAK1) and IKKβ, whereas TNF receptor associated factor (TRAF) 6 was dispensable (Balka et al., 2020). In contrast, a previous study identified STING-mediated NF-κB signalling through TRAF6 and TBK1 in MEFs (Abe et al., 2014), suggesting that multiple pathways or cell-type specific differences may exist.

A cGAS-independent pathway of non-canonical STING-mediated NF-κB activation was shown to be induced following DNA damage in human

keratinocytes (Dunphy et al., 2018). Here, dsDNA breaks sensed by ataxia telangiectasia mutated (ATM) and poly ADP-ribose polymerase 1 (PARP-1) activated DNA sensor IFI16, which further promoted TRAF6-dependent K63-linked ubiquitination of STING and predominant NF-κB activation (Dunphy et al., 2018).

Importantly, although STING trafficking to perinuclear compartments is a crucial requirement for IRF3 signalling, NF-κB activation is sustained in cells treated with brefeldin A, a microbial toxin that inhibits COPII-mediated ER-to-Golgi transport (Ran et al., 2019, Lippincott-Schwartz et al., 1990). This is in line with other studies, showing normal NF-κB signalling with trafficking-defect STING mutants K224R and K288R (ubiquitination of these lysine (K) residues is required for trafficking), whereas IRF3-induced signalling was largely impaired in MEF-reconstitution assays (Ni et al., 2017, Stempel et al., 2019). Similarly, inhibition of STING trafficking with the murine CMV protein m152 ablated IRF3 activation, whereas NF-κB signalling remained intact (Stempel et al., 2019). In conclusion, these findings suggest that STING-induced NF-κB activation does not require inter-compartment translocation (**Figure 1.5 C**) (Dunphy et al., 2018) and highlights the differential regulatory mechanisms involved in STING-induced IRF3 and NF-κB signalling. Thus, many open questions regarding the site of NF-κB activation, involved signalling pathways and regulatory mechanisms remain unanswered and require further investigation.

Importantly, a recent study identified a TRAF6 recruitment sequence in the CTT of zebrafish STING, which largely promoted NF-κB signalling (de Oliveira Mann et al., 2019). Since human STING lacks this motif, the molecular mechanisms or binding site for TRAF6 remain elusive today, but provides an explanation for the primarily type I IFN-driven STING response in vertebrate species (de Oliveira Mann et al., 2019). Evolutionary differences between the protein domains and CTT-containing conserved binding motifs of vertebrate and fish STING are interesting and emphasize the diverse roles of this signalling pathway and multiple functions, that allowed the development of innate immune signalling

tailored to selection pressures in specific environmental niches, favouring either type I IFN or proinflammatory signalling (Stempel et al., 2019).

STING-mediated autophagy induction has been suggested as a strategy to clear cytosolic DNA (foreign and endogenous) and pathogens and is believed to be the evolutionarily oldest STING function, since it is also conserved in the non-vertebrate species *N. vectensis* (sea anemone) and amphibia such as *X. tropicalis* (western clawed frog), which lack the CTT (Gui et al., 2019, Watson et al., 2012). Overexpression and stimulation of STING$^{N.vectensis}$, STING$^{X.tropicalis}$ and CTT-truncated hSTING in HEK293T cells induced microtubule-associated protein 1A/1B light chain 3 (LC3)-II conversion, which is a commonly used readout for autophagosome formation (Gui et al., 2019). This process strictly relied on trafficking of STING-containing vesicles to the ERGIC, but was independent of TBK1 activation, since the CTT was absent (Gui et al., 2019). Liu et al. performed similar experiments using transiently transfected HeLa cells and confirmed STING-mediated autophagy induction via TBK1- and IRF3-independent mechanisms. Furthermore, a direct LC3 interaction through LC3-interacting regions (LIR motifs) located upstream the CTT in STING was suggested (Liu et al., 2019). Gui et al., specifically identified residues 330-334 of hSTING, with L333 and R334 being essentially required for autophagy induction (Gui et al., 2019) (**Figure 1.5 A**).

Subsequently, an independent study investigated functional consequences of STING$^{\Delta CTT}$ or the nonphosphorylatable mutant STING^{S365A} (equivalent to S366 in hSTING) endogenously expressed in mice in the context of HSV-1 infection (Yamashiro et al., 2020). Interestingly, STING$^{\Delta CTT}$ expression resulted in viral susceptibility similar to mice deficient in STING (Goldenticket (STING$^{gt/gt}$ mice)) or TBK1 (*Tbk1*$^{-/-}$/*Tnfr1*$^{-/-}$ due to embryonic lethality of *Tbk1*$^{-/-}$). In contrast, mice lacking IRF3 (*Irf3*$^{-/-}$) or expressing STING^{S365A} were partially resistant and able to clear the infection, although delayed to WT mice. Although the mechanistic basis for this observation was not extensively investigated, quantification of cGAMP-induced LC3-II conversion in primary macrophages derived from STING$^{\Delta CTT}$ or STING^{S365A} mice suggested that autophagy induction required presence of the CTT and occurred via TBK1-dependent mechanisms but was independent of

IRF3, STING S365 phosphorylation and type I IFNs (Yamashiro et al., 2020). Importantly, autophagy maturation was previously shown to require TBK1 (Pilli et al., 2012). Therefore, the role and function of TBK1 in STING-mediated autophagy induction remains to be investigated *in vivo*. Potential differences to *in vitro* generated knowledge and species-specific effects may play an additional role and may be the reason for the observed differences.

STING-mediated autophagosome formation appears distinct from canonical autophagosome biogenesis and occurred independent of serine/threonine kinase Unc-51-like kinase (ULK) and the PI3K VPS34-beclin kinase complex. Instead, dependency on WD repeat domain phosphoinositide-interacting protein 2 (WIPI2) and autophagy protein 5 (ATG5) was observed (Gui et al., 2019, Liu et al., 2019). Subsequent fusion of autophagosomes with Ras-related protein Rab7-positive lysosomes targets enclosed pathogens, DNA as well as STING for degradation, therefore providing a negative self-regulatory mechanism to terminate STING signalling (Gui et al., 2019, Liu et al., 2019). Similarly, STING was reported to undergo lysosomal degradation following Golgi exit downstream of TBK1/IRF3 pathway activation, which was found to be dependent on a motif encoded within residues 281-297 (trafficking-mediated degradation motif) (**Figure 1.5 A**) (Gonugunta et al., 2017).

Furthermore, a recent study elucidated a novel mechanism that negatively regulates excessive STING activation prior to signalling events. Based on *in vitro* experiments using recombinant protein and high-resolution imaging in different cell lines, STING was reported to undergo liquid-liquid phase separation and form “puzzle-like” biocondensates (STING phase separator) at ER membranes **(Figure 1.5 C**) (Yu et al., 2021). These gel-like condensates consisted of highly organized 2’3’-cGAMP-STING-TBK1 complexes and were suggested to function as “sponges” that trap excess 2’3’-cGAMP in a threshold-dependent manner. Thus, spatial separation of 2’3’-cGAMP/STING/TBK1 from IRF3 provides a negative regulatory mechanism to prevent aberrant immune signalling upon long-term stimulation (Yu et al., 2021). Interestingly, condensate formation required STING dimerization (residues 153-173 in hSTING) and a disordered region (residues 309-342 in hSTING) (**Figure 1.5 A**), and was diminished in cells

overexpressing autoactive STING mutants, which could therefore provide an explanation for constitutive STING signalling in some SAVI patients (Yu et al., 2021).

Importantly, cell type-specific effects of STING signalling may also play an important role and significantly contribute to the clinical phenotypes observed in SAVI. One example is the observation that STING activation primarily induces proapoptotic signalling in T lymphocytes, which further depended on the magnitude of STING activation and its expression level (Gulen et al., 2017). Using knock-in mice expressing SAVI mSTING$^{N153S/+}$ (N154S in hSTING) and Jurkat T cell lines reconstituted with hSTING^{N154S}, Wu et al. identified a link to ER stress, which primed T cells for apoptosis upon activation and found the “unfolded protein response (UPR)-motif” (aa 322-343) to be crucially important to mediate this IRF3-independent function (**Figure 1.5 A**) (Wu et al., 2019). The proposed model suggests that STING activation and ER exit disrupt ER calcium homeostasis, which synergistically increased T cell activation-induced ER stress and facilitated T cell apoptosis (following CD3/CD28 activation). *In vitro*, pharmacological inhibition of ER stress was able to reduce T cell death (Wu et al., 2019).

Therefore, although discoveries over the last decade significantly improved our understanding of several aspects of the cGAS-STING pathway, many old and emerging questions remain unanswered. Future studies are required to elucidate regulation mechanisms, PTMs and interacting proteins that act in concert to fine-tune STING signalling. The cGAS-STING pathway is not only crucial to mediate immune defence against infections but also increasingly implicated in the pathology of sterile inflammatory diseases. Therefore, an in-depth understanding of pathways activated in disease-relevant cell types provides a promising opportunity to determine targets for successful therapeutic intervention.

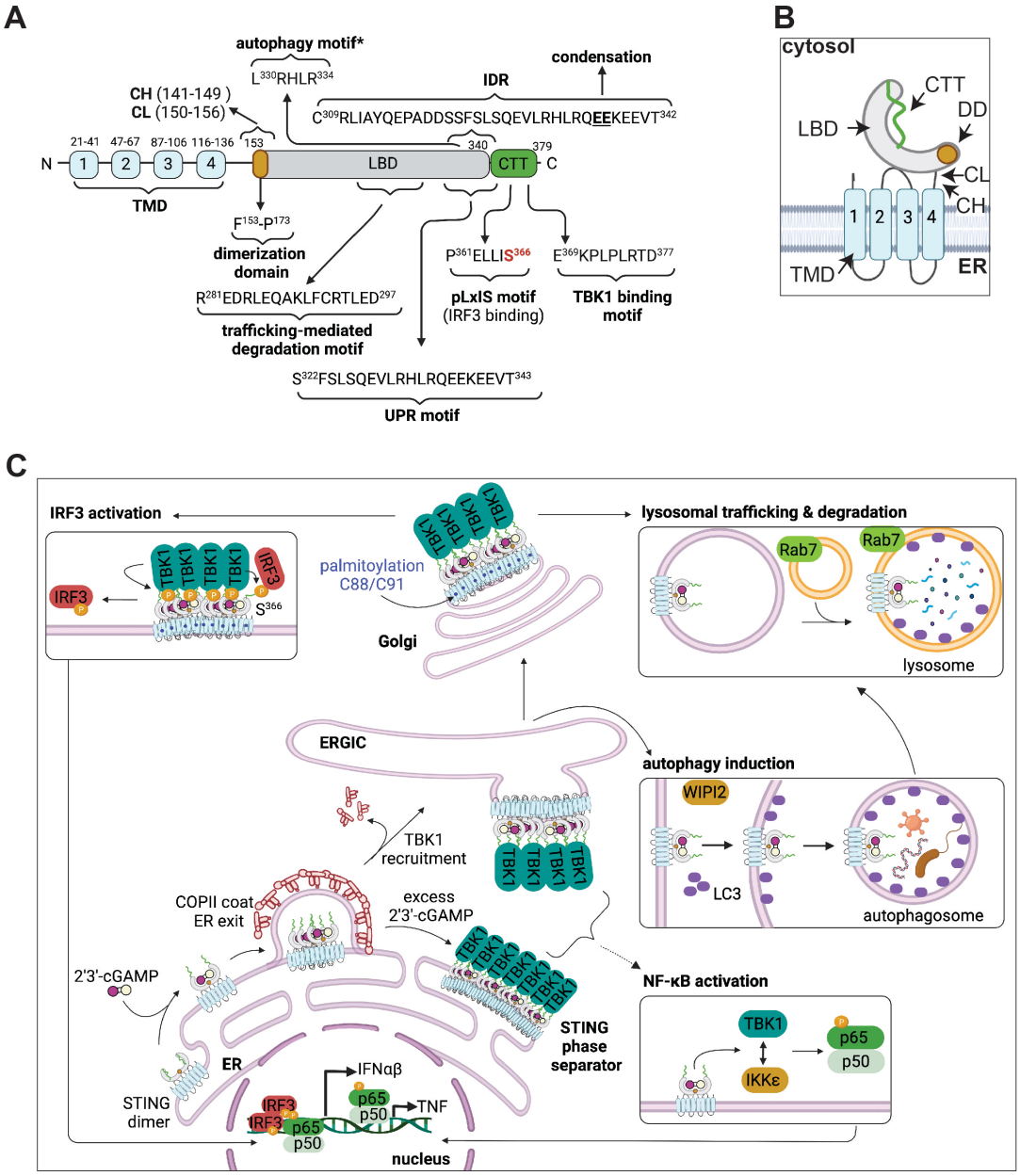

Figure 1.5 | Protein domains, signalling motifs and effector functions of STING. A) Schematic hSTING protein domain structure showing transmembrane domains (TMD) 1-4, dimerization domain (DD), connector helix (CH), connector loop (CL), ligand-binding domain (LBD) and the C-terminal tail (CTT) based on previously published domain borders (Shang et al., 2019, Wu et al., 2014). Indicated amino acids and residue position of conserved binding motifs refer to the hSTING amino acid sequence (Uniprot Q86WV6). Within the intrinsically disordered region (IDR), residues E336 and E337 (bold, underlined) are confirmed to be required for STING condensation and phase separation (Yu et al., 2021). Other shown binding motifs are indicated based on previously published studies: TBK1 binding motif (Zhang et al., 2019), pLxIS^{366} (x, any residue) contains the STING phosphorylation site S366 (red, bold) (Liu et al., 2015b), trafficking-mediated degradation motif mediates signalling-independent

STING sorting into endolysosomes (Gonugunta et al., 2017), unfolded protein response (UPR) motif (Wu et al., 2018) and residues for autophagy induction as suggested by Gui et al. (Gui et al., 2019). *contribution of multiple LC3-interaction regions (LIR) upstream the CTT have been proposed by Liu et al. (Liu et al., 2019). **B)** Schematic model of the three-dimensional arrangement of protein domains in monomeric inactive STING. Notably, STING resides as inactive dimer within the endoplasmic reticulum (ER) membrane (not shown). **C)** Simplified schematics of the STING signalling pathway and downstream effector functions. Inactive dimeric STING at the ER membrane undergoes conformational changes upon 2'3'-cGAMP binding which induce oligomerization, CTT exposure and ER exit via coat protein complex II (COPII)-dependent mechanisms. STING-mediated TBK1 recruitment occurs either at ER membranes or during vesicular transport towards the ER-and-Golgi-intermediate compartment (ERGIC). The ERGIC represents an intermediate signalling platform, where two distinct STING effector pathways diverge. One fraction of STING-containing vesicular membranes serves as source for autophagosome formation via WIPI2 and LC3 aiming to degrade invading pathogens, cytoplasmic DNA and STING itself. Eventually, autophagosomes fuse with Rab7-positive lysosomes for terminal degradation of their content. Trafficking-mediated lysosomal degradation of STING is also initiated off *trans*-Golgi compartments and represents a negative regulatory mechanism to terminate signalling. Another fraction of STING-containing vesicles at the ERGIC continues to traffic towards the Golgi, where Golgi-resident enzymes palmitoylate STING cysteine (C) resides in position 88 and 91 to promote 2'3'-cGAMP/STING/TBK1 clustering at the *trans*-Golgi. Polymerization promotes TBK1-mediated phosphorylation of STING residue S366 which creates an IRF3 docking site (pLxIS^{366} motif). Spatial proximity allows for TBK1-mediated IRF3 phosphorylation, which induces dimerization, nuclear translocation and type I IFN transcription. Activation of transcription factor NF-κB (p65, p50) likely occurs via TBK1- and IKKε-redundant mechanisms and induces transcription of proinflammatory cytokines and enhances type I IFN transcription following nuclear translocation. However, the mechanistic details and the cellular compartment of this process remain unclear. Since ER-to-Golgi translocation of STING represents the rate-limiting step of the signalling cascade, excess 2'3'-cGAMP-STING-TBK1 complexes were recently suggested to condensate in "puzzle-like" structures at the ER membrane and undergo liquid-liquid phase separation (STING phase separator formation), which prevents spatial proximity to IRF3 and thus limits the STING-mediated immune response. WD repeat domain phosphoinositide-interacting protein 2, WIPI2; microtubule-associated protein 1A/1B light chain 3, LC3. Figure created with BioRender.com.

1.3.4.3.3 STING-associated vasculopathy with onset in infancy

SAVI is classified as an interferonopathy and caused by familial or *de novo* GoF mutations in immune sensor and adapter protein STING, which results in ligand-independent constitutive signalling (Liu et al., 2014b). Since the initial description of the disease by Liu et al. in 2014, several SAVI-associated mutations have been identified, which map to conserved residues within domains required for ligand binding (G166), dimerization/polymerization (e.g., C206, G207, R281, R284) or within the connector loop/helix region (V147, F153, N154, V155) (Dai et al., 2020, Lin et al., 2021, Shang et al., 2019). Interestingly, a recent report identified the first SAVI-associated variant H72N located within the linker region between TMD2 and TMD3, which was identified in a family with three affected members with milder disease (Lin et al., 2021).

In general, the clinical phenotypes associated with SAVI are variable, however patients typically present during early childhood (median presentation age 3 months (Dai et al., 2020)) with skin abnormalities and/or respiratory symptoms (e.g. cough, tachypnea, dyspnea) and delayed development. Systemic inflammation, fever and peripheral vasculopathy causing skin lesions with pustular or blistering painful rashes on extremities and face, perforation of the nasal septum, loss of nails or amputation of extremities have been described. Pulmonary inflammation and interstitial lung disease (ILD) commonly develop in patients with a mild to severe clinical course, that may prompt lung transplantation or cause lethality in individual cases (Jeremiah et al., 2014, Konno et al., 2018, Omoyinmi et al., 2015, Picard et al., 2016, Tang et al., 2020b). Joint involvement or inflammation affecting the brain, kidneys or muscles are less commonly observed. Furthermore, T cell cytopenia and/or (transiently) elevated levels of autoantibodies were associated with SAVI in some patients (Dai et al., 2020, Jeremiah et al., 2014, Liu et al., 2014b, Picard et al., 2016, Saldanha et al., 2018, Tang et al., 2020b).

Patient blood analysis showed elevated ISGs transcription levels and *in vitro* experiments with patient-derived PBMCs demonstrated increased transcription of *IFNB1* and STAT1 phosphorylation at baseline, which remained largely unchanged upon further stimulation with exogenous STING ligand cGAMP (Liu

et al., 2014b). Analysis of the *IFNB1* reporter activity in transiently transfected HEK293T cells, which lack endogenous STING, revealed maximal pathway activation with SAVI STING mutants N154S, V155M, V147L, whereas WT STING or empty vector transfected cells had limited background activation. Thus, the GoF phenotype of the discovered mutations was established (Liu et al., 2014b) and independently confirmed in subsequent case reports (Jeremiah et al., 2014, Melki et al., 2017, Saldanha et al., 2018).

On a molecular level, STING GoF mutants were shown to stabilize dimerization and spontaneously undergo ER-to-Golgi translocation in absence of specific ligands, thus causing constitutive signalling and a predominant type I IFN-response (Jeremiah et al., 2014).

Treatment with systemic corticosteroids partially improved clinical symptoms in some patients, however broad immunosuppression, biologics and disease-modifying antirheumatic drugs (DMARDs) generally showed limited effect (Wang et al., 2021b). Importantly, Liu et al., provided *in vitro* evidence that JAK inhibitor treatment may be beneficial for SAVI patient outcome, since it successfully blocked baseline STAT1 phosphorylation in T and B cells derived from two SAVI patients (Liu et al., 2014b). Indeed, the majority of reported SAVI patients successfully responded to JAK inhibitors ruxolitinib (JAK1/2 inhibitor), baricitinib (JAK1/2 inhibitor) or tofacitinib (JAK1/3 inhibitor) (Frémond et al., 2021b, Rodero et al., 2016, Saldanha et al., 2018, Volpi et al., 2019), however poor responders or relapsing disease has also been reported in other cases (Tang et al., 2020b, Wang et al., 2021b). This emphasizes the important role of type I IFN-independent effects in SAVI pathology, since genetic deletion of *Irf3* in a mouse model with heterozygous expression of a SAVI-associated patient mutation N153S (equivalent to N154S in hSTING) did not ablate lung inflammation and T cell cytopenia, suggesting that STING-mediated NF-κB signalling or other effector functions may contribute to disease pathology despite a potential impact of species-specific differences in this study (Warner et al., 2017).

Furthermore, early diagnosis and therapy initiation were found to be crucial for long-term improvement of the clinical phenotype (Frémond et al., 2021b, Saldanha et al., 2018, Volpi et al., 2019) and the higher susceptibility for viral

infections represents an important side effect of JAK inhibitor treatment (Volpi et al., 2019).
Although elevated type I IFN levels are a common feature shared between all classified interferonopathies and some clinical manifestations overlap, crucial differences can also be observed. For example, the majority of IFN-driven diseases present with dominant skin and neurological involvement, the latter of which being rarely reported in SAVI (Crow et al., 2021). Instead, SAVI and COPA syndrome, a newly identified autoinflammatory disease caused by mutations in coatomer I subunit alpha (COPA) (chapter 3.1.1), present with lung inflammation, which is not commonly observed in other interferonopathies (Crow et al., 2021). The phenotypic overlap prompted the hypothesis, that pathology in COPA syndrome patients may be caused by dysregulated STING signalling, and experimental evidence for this is presented in chapter 3 of this thesis.

However, phenotypic variabilities between interferonopathies are likely contributed to by function and expression patterns of the mutant proteins and their interaction partners, which thus may determine the disease-causing cell types and susceptibility to type I IFN inhibition.
Furthermore, important to consider is the fact that besides IFN signalling, mutant proteins may also be involved in other signalling pathways that could be simultaneously activated and determine a distinct pathogenesis and therapy susceptibility. Mutations in proteasome subunit proteins or COPA, associated with PRAAS (proteasome-associated autoinflammatory syndrome) or COPA syndrome respectively, represent good examples, where immune activation through ER stress and UPR signalling (chapter 1.4) may contribute to the clinical phenotypes (Brehm et al., 2015, Ebstein et al., 2019, Liu et al., 2012a, Watkin et al., 2015).

1.4 The secretory pathway

In chapter 3 of this thesis, the molecular mechanisms driving aberrant type I IFN signalling in COPA syndrome are investigated. This immune disorder is caused by defective vesicular trafficking due to loss of function (LoF) mutations in COPA, the alpha subunit of coat protein complex I (COPI, coatomer), which mediates retrograde protein trafficking within the secretory pathway (Watkin et al., 2015). Therefore, this section introduces intracellular trafficking pathways and the molecular mechanisms involved in COPI function, to better understand the disease pathogenesis.

The secretory pathway is formed by a tightly controlled membrane network composed of ER, ERGIC, the Golgi apparatus and vesicles that transport proteins in between those compartments (**Figure 1.6**) (Martínez-Menárguez et al., 1999, Palade 1975). Mediating transport of proteins and lipids towards their cellular destination, the secretory pathway plays a crucial role in maintaining structural integrity and functional organization of cells and acts as a quality control mechanism for newly synthesized proteins (Harter C. 2002).

Around 30 % of all gene products in eukaryotic organisms enter the secretory pathway and are therefore targeted to the ER during or after protein translation (Aviram et al., 2017). Upon ER entry through the translocon pore, the oligosaccharyltransferase (OST) complex adds N-linked oligosaccharides to nascent unfolded proteins as the first instance of PTM, which influences protein folding, stability, solubility and resistance to proteases (Helenius et al., 2001, Kelleher et al., 2005). Furthermore, binding by ER-resident chaperone proteins such as binding immunoglobulin protein (BiP) prevents aggregation of polypeptide chains and aids correct protein folding (Alberts B 2002). The oxidative chemical environment within the ER lumen also facilitates the formation of disulfide bonds between cysteine residues that stabilize tertiary and quaternary structures (Tu et al., 2004).

Two quality control mechanisms have been reported to control correct protein assembly: ER-associated degradation (ERAD) and the UPR. ERAD selectively

targets misfolded proteins from the ER lumen and mediates their re-translocation into cytosolic compartments, where they are ubiquitinated and degraded via the ubiquitin proteasomal degradation pathway (Vembar et al., 2008). Accumulation of unfolded or misfolded proteins overwhelms the ER folding capacity, results in ER stress and triggers the UPR, which initiates several downstream pathways via ER stress sensors inositol-requiring protein 1 (IRE1), protein kinase R-like ER kinase (PERK) and activating transcription factor 6 (ATF6). The subsequently induced transcriptional and non-transcriptional responses aim to maintain cell survival and enhance protein folding for example through transient inhibition of global protein translation, promotion of ERAD and autophagy to clear unfolded proteins and enhanced synthesis of chaperones. However if persistent, apoptotic cell death is triggered (Hetz 2012).

Due to the polarization of the ER compartment, readily folded and modified proteins concentrate at the ribosome-free smooth ER in dedicated areas termed ER exit sites (ERES) (Bannykh et al., 1996). Here, on protruding membrane tubules, protein cargo is encapsulated into vesicles, via COPII-dependent processes (**Figure 1.6**), which induce anterograde ER-to-Golgi trafficking (Barlowe et al., 1994). Passing the ERGIC, which represents a tubulovesicular membrane cluster, vesicular transport is continued towards the *cis-Golgi* (Bannykh et al., 1997, Hauri et al., 1992). It is still debated whether the ERGIC forms a transient or permanent compartment. Based on experimental evidence from several studies, the currently accepted model suggests a more transient character, where ERGIC membranes arise from ERES via COPII-vesicles and gradually mature into *cis*-Golgi membranes while moving towards the cellular localization of *cis*-Golgi stacks (Mironov et al., 2003, Saraste et al., 2018). Fusion of COPI-vesicles, which mediate retrograde Golgi-to-ER transport as well as intra-Golgi transport delivers *cis*-Golgi membranes to the ERGIC, thereby altering its protein and membrane composition that allows for dynamic maturation into *cis*-Golgi cisternae (Letourneur et al., 1994, Orci et al., 1997, Saraste et al., 2018). However, as originally suggested by George Palade, vesicle shuttling, mediated by COPII and COPI complexes (chapter 1.4.1), is still considered to play a crucial role in transporting cargo proteins between ER and Golgi and

vesicle fusion has been suggested to additionally mediate ERGIC membrane maturation (Bonifacino et al., 2003, Palade 1975).

The Golgi apparatus (Golgi 1989) represents the central compartment of the secretory pathway and mediates protein trafficking, sorting and modification of post-translational glycosylation patterns (Pfeffer 2010). Organized as polarized stacked cisternae (elongated membranes), the *cis*-Golgi (early Golgi) receives proteins from ER and ERGIC via COP vesicle fusion, which travel through consecutive medial-cisternae and exit from the *trans*-Golgi network (late Golgi) towards their destination compartments (cell surface, endosomes, lysosomes) (Rothman et al., 1996).

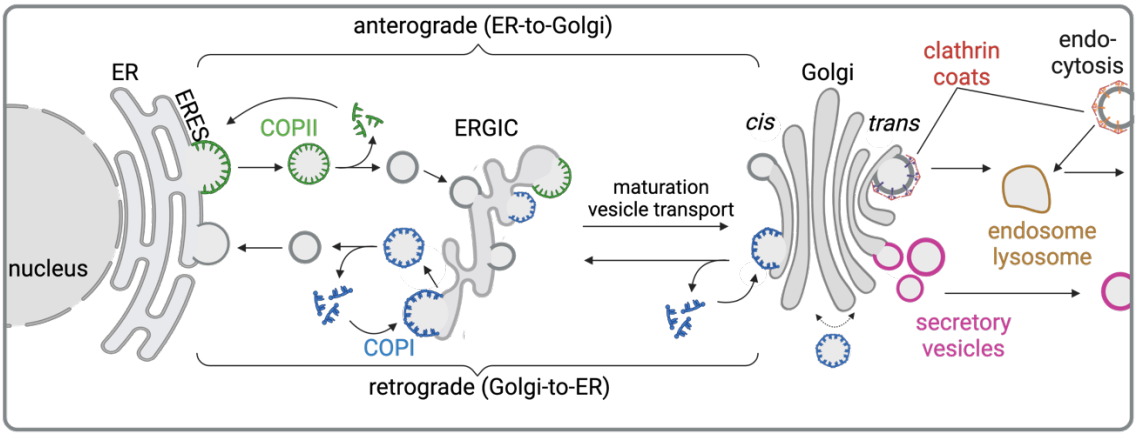

Figure 1.6 | Schematic illustration of the secretory pathway. Proteins are synthesized and secreted through the secretory pathway, which is composed of the endoplasmic reticulum (ER), the ER-Golgi-intermediate compartment (ERGIC), the Golgi apparatus and vesicles that mediate protein transport between the main organelles. Coat protein complex (COP) II vesicles (green) mediate anterograde ER-to-Golgi transport, COPI vesicles (blue) mediate retrograde Golgi-to-ER transport and intra-Golgi trafficking. COPI- and COPII-mediated vesicular transport and cisternal maturation was suggested to mediate ERGIC-to-*cis*-Golgi protein translocation. Clathrin-coated vesicles (red) are assembled at the *trans*-Golgi compartment and recruit cargo via adapter protein 1 (AP1) for direction towards the endosomal-lysosomal system. Other secretory cargo is recruited into vesicles (pink) for regulated secretion and stored until a signal triggers plasma membrane fusion and content release. Via AP2, clathrin-coated vesicles additionally mediate endocytosis at the plasma membrane. Figure created with BioRender.com.

Individual cisternal sub-compartments (*cis, medial, trans*) comprise a distinct set of enzymes including glycosyltransferases, glycosidases and nucleotide sugar transporters, which mediate multiple subsequent reactions to modify PTMs on traversing proteins and lipids tailored to their function (Stanley 2011).
In vertebrates, the Golgi assembles into a dynamic set of interconnected cisternae that present as a condensed ribbon structure (during interphase) (Gosavi et al., 2018, Wei et al., 2017).
At the *trans*-Golgi membrane, newly synthesized proteins interact with adapter proteins (AP) that mediate sorting into clathrin-coated vesicles for transport towards endosomes and lysosomes. Additionally, clathrin-coated vesicles mediate the classical endocytosis pathway at the plasma membrane (Kirchhausen et al., 2014). In specialized cells, large amounts of secreted proteins are sorted into secretory vesicles and stored in secretory granules until environmental signals are sensed that trigger exocytosis and content release into the extracellular space e.g. digestive enzymes, hormones, neurotransmitters (**Figure 1.6)** (Alberts B 2002).

1.4.1 Vesicular trafficking pathways

COPI, COPII and clathrin-coated carrier vesicles can be distinguished by structural and functional differences of vesicle-forming coat proteins as well as by their membrane compartment of origin (Hughson 2010). In general, coat proteins function to induce vesicle formation and recruit cargo proteins. Distinct peptide motif sequences presented by the cargo protein itself or trafficking adapters allows specific cargo loading, which is further introduced below with a focus on COPII and COPI vesicles (chapter 1.4.1.1 and 1.4.1.2). Vesicle formation and budding from the donor membrane follows a defined set of sequential interactions of coat-forming and regulatory proteins. Subsequently, coat proteins are released and recycled while vesicles translocate and fuse at their respective target membranes (Kirchhausen 2000).
Essential for the distribution of intracellular proteins within the early secretory pathway is the bidirectional transport between the ER, ERGIC and Golgi through

COPI and COPII vesicles. As previously mentioned, the widely established model defines COPII coats as mediators of the anterograde Golgi-bound transport route, whereas the COPI coat is involved in retrograde trafficking from Golgi to ER compartments and trafficking within the Golgi, thus contributing to cisternal maturation and cargo shuttling (Barlowe et al., 1994, Glick et al., 2009, Letourneur et al., 1994, Orci et al., 1997, Rabouille et al., 2005). Therefore, both coat protein complexes are essentially required to maintain proteostasis and organellar homeostasis in all cells.

1.4.1.1 COPII vesicles

The COPII coat is conserved throughout eukaryotic evolution and initial studies in *S. cerevisiae* have described subunits SEC13, SEC31, SEC23, SEC24 and the small GTPase SAR1 as essential components for COPII vesicle formation (Barlowe et al., 1994, Kaiser et al., 1990).

COPII complex assembly occurs as a sequential process, initiated by membrane-bound guanosine nucleotide exchange factor SEC12, which catalyses GDP-to-GTP exchange of small GTPase SAR1, a step that was suggested to induce a conformational change and exposure of a hydrophobic surface to mediate SAR1-GTP phospholipid binding (Bi et al., 2002, Goldberg 1998, Huang et al., 2001). Importantly, phospholipid composition and fluidity of synthetic liposomes used for experimental COPII assembly assays was shown to strongly influence COPII coat formation, therefore providing the molecular basis for targeted assembly at ER membranes (Matsuoka et al., 1998). After SAR1-GTP binding, the inner coat composed of SEC23 and SEC24 is recruited from the cytoplasm and forms a pre-budding complex with SAR1-GTP. SEC24 engages with cargo proteins, whereas SEC23 acts as GTPase-activating protein that stimulates SAR1-GTP hydrolysis activity and aids membrane curvature induction (Bi et al., 2002, Lee et al., 2005). As the final step, the SEC13/SEC31 complex is recruited to form an outer coat for structural stabilization and further drives membrane deformation (Stagg et al., 2006). GTP-hydrolysis by SAR1 induces vesicle budding and coat disassembly into the cytosol (Barlowe 2020, Barlowe et al., 1994). Interestingly, recent findings

by Shomron et al. challenge this well-established model and suggest COPII coat proteins as stationary molecules that mediate cargo enrichment and vesicle loading at ERES and remain bound to the ER-ERES membrane when vesicles are released (Shomron et al., 2021).

Noteworthy, in mammalian species paralogs/isoforms of most COPII subunits exist, which suggests functional differences and perhaps cargo specificity associated with distinct coat subsets, although some paralogs may be functionally redundant (Zanetti et al., 2012). Four isoforms of SEC24 (A, B, C, D) contain several distinct binding sites, which allow for interaction with a broad range of protein cargo and adapters (e.g. ERGIC-52, p24 family proteins/TMED). Trafficking adapters encode COPI- and COPII-specific binding motifs within a short cytosol-exposed C-terminus, which allows for their circulation within the early secretory pathway. Via the luminal domain, p24 family members bind cargo proteins and thus function as coat adapters for proteins without self-encoded trafficking motifs (Dominguez et al., 1998, Fiedler et al., 1996, Schimmöller et al., 1995).

The exact mechanisms of how cargo selectivity for thousands of different proteins is realized remains incompletely understood. Co-existence of two mechanisms/models has been suggested: (1) the cargo capture model (specific binding to coat receptors), and (2) the bulk flow model, which suggests receptor-independent cargo loading of protein-containing fluid into the budding vesicles, while ER-resident (e.g. chaperones, enzymes) or misfolded proteins are actively retained through interaction with ER structures (Thor et al., 2009, Wieland et al., 1987). However, unspecific bulk flow cannot be entirely prevented and cells have developed compensatory mechanisms to retrieve ER-resident proteins through retrograde COPI-mediated transport (Kuehn et al., 1998).

1.4.1.2 COPI vesicles

During retrograde transport, besides retrieval of ER-resident chaperones and trafficking adapters, COPI also returns misassembled protein complexes from the *cis*-Golgi and therefore contributes to organellar homeostasis and protein quality

control within the secretory pathway (Beck et al., 2009). Initial knowledge about the COPI complex was generated through studies in *S. cerevisiae,* which identified seven subunits COP1/SEC33/RET1, SEC26, SEC27, SEC21, RET2, SEC28, REC3 that correspond to subunits identified in mammalian cells: α-, β-, β'-, γ-, δ, ε- and ξ-COP (**Figure 1.7**) (encoded by *COPA*, *COPB1*, *COPB2*, *COPG*, *COPD*, *COPE* and *COPZ* genes) (Barlowe et al., 2013, Duden et al., 1991, Faulstich et al., 1996, Hara-Kuge et al., 1994, Harrison-Lavoie et al., 1993, Kuge et al., 1993, Serafini et al., 1991, Stenbeck et al., 1993, Waters et al., 1991). All protein subunits are subsequently referred to as COPA, COPB1, COPB2, COPG, COPD, COPE and COPZ.

Similar to COPII, the COPI complex can structurally be divided into two subcomplexes, the outer layer B-complex (COPA, COPB2, COPE) and the inner layer F-complex (COPB1, COPG, COPD, COPZ) (Beck et al., 2009).

COPI vesicle formation is initiated via activation of the cytoplasmic small GTPase ADP-ribosylation factor 1 (ARF1) (Orci et al., 1993), which in its GDP-bound state binds the cytoplasmic tail of p24 family proteins at the Golgi membrane (Contreras et al., 2004, Gommel et al., 2001). GDP-to-GTP exchange is mediated via Golgi-specific brefeldin A-resistance guanine nucleotide exchange factor 1 (GBF1), which induces a conformational change that exposes a N-terminal amphipathic helix that anchors into the *cis*-Golgi membrane (Chardin et al., 1996, Niu et al., 2005, Zhao et al., 2002). Subsequently, the cytosolic COPI coat is recruited as a pre-formed complex (containing both B and F subcomplexes) and binding occurs between ARF1-GTP and coatomer subunits COPB1, COPG, COPD and COPE (**Figure 1.7**) (Hara-Kuge et al., 1994, Dodonova et al., 2017, Eugster et al., 2000, Sun et al., 2007, Zhao et al., 1999, Zhao et al., 1997). Then, p24 adapter protein binding by COPG (through recognitions of a specific dimeric diphenylalanine (FF)-dibasic (BB) motif FFxxBB; x denotes any residue) and ARF1 dimerization induce conformational changes that promote coat polymerization and initiate membrane curvature (Beck et al., 2008, Béthune et al., 2006, Langer et al., 2008, Reinhard et al., 1999). Continued COPI coat polymerization eventually induces vesicle budding, which may occur autonomously, however regulatory factors have been identified although

mechanistic details remain unclear (Arakel et al., 2018). COPI release (uncoating) requires GTP-hydrolysis stimulated by ARF1-GTPase activating proteins (ARF1-GAPs) and is considered the prerequisite for vesicle fusion at the destination membrane (**Figure 1.7**) (Presley et al., 2002).

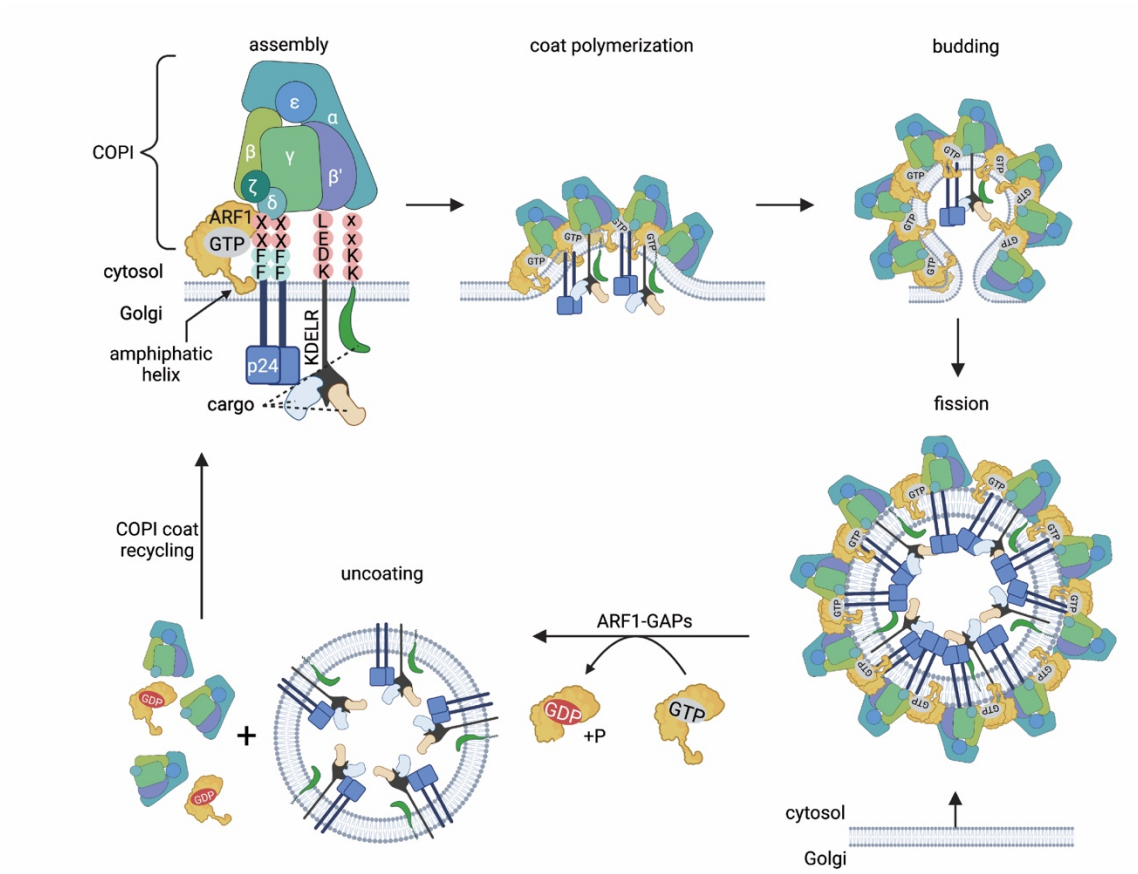

Figure 1.7 | COPI vesicle biogenesis at *cis*-Golgi membranes. Upon GDP-to-GTP exchange on small GTPase ARF1, a conformational change exposes the N-terminal amphiphatic helix and anchors ARF1-GTP into the *cis*-Golgi membrane. The pre-assembled heptameric COPI coat complex (α, β, ε, β', γ, δ, ζ) is recruited to the membrane and interacts with ARF1-GTP. γ-COP (COPG) binds p24 family protein dimers via a dimeric diphenylalanine-dibasic motif (FFxxBB, abbreviated FFxx in figure). Specific dilysine (KKxx) recognition motifs encoded at the C-terminal cytoplasmic tail of cargo or adapter proteins are recognized by COPI subunits α, β' and soluble proteins are bound via KDEL receptors (KDELR). Dimerization of ARF1 promotes membrane curvature and coat polymerization, which ultimately induce vesicle budding. ARF1-GAPs stimulate GTP-hydrolysis which releases ARF1-GDP and the freed COPI coat into the cytosol, where it is recycled. Figure adapted from (Beck et al., 2009). GTPase-activating protein, GAP; ADP-ribosylation factor 1, ARF1. Figure created with BioRender.com.

Vesicle recognition at the target compartment is mediated via organelle-specific vesicle tethers either through direct interaction with the coat or other factors, such as soluble N-ethylmaleimide-sensitive factor attachment protein receptors (SNAREs) and Rab GTPases (Arakel et al., 2018, Zink et al., 2009). Thus, it has been speculated that uncoating may be incomplete and remaining coat proteins may in part be required for vesicle identification and fusion with the destined target compartment (Arakel et al., 2018).

Cargo recruitment into COPI vesicles occurs via recognition of specific binding motifs by different subunits. Best characterized is the C-terminal dilysine motif (KKxx, K(x)Kxx, with x representing any amino acid) which binds to the WD40 β-propeller domains of COPA and COPB2 (**Figure 1.7**) (Cosson et al., 1994, Eugster et al., 2000). Interestingly, binding strength and therefore trafficking efficiency is determined by the surrounding residues encoded in position x and the motif's proximity to the membrane (Vincent et al., 1998, Zerangue et al., 2001). Furthermore, studies in HeLa cell showed that optimal ER retention required the presence of lysine residues in position -3 and -4 or -3 and -5 relative to the C-terminus, however presence of one or two lysines at various positions within the last 6 C-terminal amino acids retained the COPI-trafficking ability to some extent (Jackson et al., 1990).

Soluble ER-resident proteins involved in protein folding, modification and assembly (including chaperones) possess a C-terminal KDEL sequence that functions as ER-retention signal (amino acid sequence motif: lysine (K), aspartate (D), glutamate (E), leucine (L)) (**Figure 1.7**) (Munro et al., 1987). However, since studies in yeast and monkey fibroblasts showed that KDEL-tagged proteins can undergo PTM by Golgi enzymes (Dean et al., 1990, Pelham 1988), COPI-mediated transport is essential for their retrieval to the ER during the steady state. Soluble proteins lack a cytoplasmic tail and therefore bind the KDEL receptor (KDELR), which resides within the lumen of *cis*-Golgi and ERGIC compartments and functions as an adapter for COPI-vesicle loading (Dean et al., 1990, Lewis et al., 1990). KDELR binding is pH-dependent and allows for ligand-receptor-association within Golgi compartments (low pH) and release upon arrival at the ER (higher pH) (Wilson et al., 1993). Variants of the KDEL signal also exist, which

are distinctly bound by three different KDELR isoforms in humans, providing a mechanism for trafficking specificity (Raykhel et al., 2007).
Quality control of multimeric protein assembly is mediated via recognition of a diarginine motif ([ΦΨR]RxR, Φ being an aromatic residue, Ψ being a bulky hydrophobic residues, x denotes any residue) by COPB1 and COPD (Michelsen et al., 2005). In contrast to the dilysine motif, the diarginine motif is not necessarily located within the C-terminal tail, and has been identified along cytosolic-exposed protein regions (Beck et al., 2009). Mechanistically, it was proposed that whereas motif exposure in unassembled protein complexes mediates ER retention, steric masking upon complex formation allows ER export (Michelsen et al., 2005).

How COPI vesicles regulate bidirectional transport from Golgi-to-ER and within Golgi compartments, remains unclear. The discovery of subunit paralogs γ1 (COPG1), γ2 (COPG2) and ζ1 (COPZ1), ζ2 (COPZ2) in higher eukaryote lineages lead to the hypothesis of specialized functions or perhaps direction-specific COPI complex isotypes (Blagitko et al., 1999, Futatsumori et al., 2000). Indeed, subsequent studies using human and rat liver cell lines and mouse liver lysates identified presence of a single subunit paralog per heptameric complex and determined the stochastic ratio of coatomer isotypes from rat liver cytosols with 2:1:1 of COPI complex isotypes containing γ1ζ1 [COPG1/COPZ1] : γ2ζ1 [COPG2/COPZ1] : γ1ζ2 [COPG1/COPZ2], whereas γ2ζ2 [COPG2/COPZ2] was observed at lower frequency (<5%) (Wegmann et al., 2004). Localization studies revealed spatial segregation of COPG paralogs, with COPG1 and COPG2 being predominantly enriched in *cis*-Golgi or *trans*-Golgi compartments, respectively (Moelleken et al., 2007), which was hypothesized to reflect functional heterogeneity and specific roles. Based on cellular localization, COPG1 was proposed to be more likely involved in mediating retrograde transport between Golgi and ER while COPG2 may serve the intra-Golgi transport route (Moelleken et al., 2007). Functional differences could be exerted through interaction with locally distinct ARF isoforms or other co-factors including GAPs or tethers. However, so far specific functions have not be identified, and redundancy has been suggested, since proteomic profiling of vesicle content derived from HeLa,

HepG2 cells and murine macrophages did not reveal differences of the vesicular content in a SILAC-based mass spectrometry approach (Adolf et al., 2019, Futatsumori et al., 2000). Interestingly, *Copg1* and *Copg2* paralogs are differentially expressed in mouse embryonic stem cells (mESC) during neuronal differentiation and *in vitro* studies using pluripotent p19 cells identified an essential role of *Copg1* for neurite growth, which was paralog-specific (Jain Goyal et al., 2020).

From an evolutionary perspective, paralog-specific functions for COPI subunits may exist and may vary dependent on isoform expression, cellular differentiation state or the cell type investigated but could provide functional heterogeneity similar to the SEC24 paralogs which diversify the repertoire of cargos trafficked by COPII (Adolf et al., 2019).

1.5 Aims of this thesis

Great advances in sequencing technologies during the last decade have resulted in the identification of an increasing number of monogenic AID-associated genotypes. Investigating the disease-driving pathomechanisms does not only allow for identification of potential drug targets, but also improves our understanding of innate immune signalling and the controlling regulatory mechanisms. As part of this thesis two different AIDs, COPA syndrome and homozygous NLRC4-AID, were investigated aiming to elucidate the molecular dysfunctions associated with the identified patient mutations.

In 2015, Watkin and colleagues initially described COPA syndrome, a novel autoinflammatory and autoimmune disease (Watkin et al., 2015). Involved in retrograde Golgi-to-ER transport, COPA LoF mutations were shown to possess reduced cargo-binding affinity and ultimately increase ER stress and proinflammatory signalling, which was suggested to be the main mechanism driving pathology in these patients (Watkin et al., 2015). However, subsequent studies demonstrated a profound type I IFN signature, which raised questions regarding additional dysregulation of an – at the time – unknown innate immune pathway. Identification of the involved immune sensor and elucidation of the regulatory role of retrograde trafficking represent one aim of this thesis (chapter 3).

Previously reported cases of NLRC4-AID, a rare monogenic disorder, have been exclusively associated with heterozygous GoF mutations in inflammasome adapter protein NLRC4 (Canna et al., 2014, Romberg et al., 2014). This thesis presents the first description of a NLRC4-AID patient carrying a novel homozygous mutation, the pathogenic potential of which was investigated using cell-based (chapter 4) as well as structural and biophysical (chapter 5) approaches.

The specific aims of this thesis were:

1. Identification of the innate immune pathway dysregulation that is driving aberrant type I IFN signalling in COPA syndrome

2. Case description and *in vitro* validation of the pathogenic potential associated with the first described homozygous mutation in NLRC4 (A160T), which was identified in a patient with inflammatory flares and immune dysregulation

3. Biochemical, biophysical and structural characterization of NLRC4 A160T

The results of the experimental work targeting these aims are presented in chapter 3, 4 and 5, followed by an overall discussion (chapter 6) highlighting remaining questions and therapeutic opportunities.

2 Materials and Methods

2.1 Cell culture

Used cell lines were obtained from sources listed in **Table 1**. HEK293, HEK293T, HeLa cells and murine immortalized bone marrow-derived macrophages (iBMDM) were cultured in DMEM (Gibco) supplemented with 100 U/ml Penicillin/100 µg/ml Streptomycin (Sigma-Aldrich) and 10 % Fetal Bovine Serum (FBS, Sigma-Aldrich) in a humidified incubator at 37 °C and 10 % CO_2. Human monocytic THP-1 cells and the clonal cGAS$^{-/-}$ THP-1 cell line (Mankan et al., 2014) were maintained in RPMI-1640 (made inhouse, RPMI 1640 powder (Life Technologies), 23.8 mM sodium bicarbonate ($NaHCO_3$) (Merck), 1 mM sodium pyruvate ($C_3H_3NaO_3$) (Sigma-Aldrich) supplemented with 10 % FBS and 100 U/ml Penicillin/100 µg/ml Streptomycin at 37 °C and 5 % CO_2. All cell lines were regularly tested for contamination with mycoplasma using polymerase chain reaction (PCR)-based detection methods and cultures were maintained at subconfluent densities. All cell line-related work was performed in a class 2 laminar flow biosafety cabinet under sterile working conditions. Experiments requiring lenti/retroviral transduction were performed in S2 facilities (chapter 2.5).

Table 1 | Mammalian cell lines. Red fluorescent protein, RFP; blue fluorescent protein, BFP; apoptosis-associated speck-like protein containing a CARD, ASC.

Cell line	Source
HEK293	CellBank Australia (code 85120602)
HEK293T	CellBank Australia (code 12022001)
HEK293T ASC-RFP	described in (Cardona Gloria et al., 2018)
HEK293T ASC-BFP	kind gift from E. Latz, Institute of Innate Immunity, Medical faculty, University of Bonn
Flp-In™ 293 T-REx™	Thermo Fisher Scientific, Cat. No. R78007
THP-1 (WT)	ATCC TIB-202
THP-1 cGAS$^{-/-}$	described in (Mankan et al., 2014)
iBMDMs	described in (De Nardo et al., 2018a)
HeLa	Curie Institute, Paris (kind gift from P. Gleeson, Department of Biochemistry and Molecular Biology, University of Melbourne)

2.2 Primers

All primers and single guide (sg) RNAs were purchased from Metabion International AG (Germany) or Integrated DNA Technologies (Singapore).

Table 2 | PCR amplification primers. The listed primers were used for molecular cloning of *Sf*9 cell expression constructs for recombinant protein production (chapter 2.4.1.1), mammalian expression constructs for overexpression studies (chapter 2.4.1.1) and amplification of *NLRC4* from genomic DNA and mRNA transcripts to validate THP-1 cell clones generated in chapter 2.5.1.2. Numbers in brackets indicate amino acids (aa) residues amplified. Some primers encode *Bam*HI (5') and *Eco*RI (3') restriction enzyme recognition sites to enable subcloning into target plasmids (chapter 2.4.2). Deletion, Δ; full length, fl.

Primer	F/R	Sequence (5' → 3')
hNLRC4 fl (aa 1-1024)	F	CGCGGATCCATGAACTTCATCAAGGACAAC
	R	CGGAATTCAAGCGGTTACTAGTTTAAAAGC
hNLRC4$^{\Delta CARD}$ (aa 92-1024)	F	CGCGGATCCCAGACATCAGAAGGAGAC
	R	CGGAATTCAAGCGGTTACTAGTTTAAAAGC
hNLRC4$^{\Delta CARD/\Delta Loop}$ (aa 92-1024, Δ 622-644)	F	CCCAGCAGGGCTGTATCT
	R	CATAGCTCCCCCATAAAAGTC
mNlrc4 fl (aa 1-1024)	F	CGCGGATCCATGAACTTTATAAGGAACAAC
	R	CGGAATTCAAGCAGTCACTAGTTTAAAGGTGC
mNlrc4$^{\Delta CARD}$ (aa 90-1024)	F	CGCGGATCCATGTCTTATCAGGTCACAGAAG
	R	CGGAATTCAAGCAGTCACTAGTTTAAAGGTGC
*hNLRC4*_genomic DNA	F	GTAAAGGATGCTGGGGAAAG
	R	CAGGCCTTCAGCTAGTTTTATA
*hNLRC4*_ cDNA	F	GGACAAAGTCTTTTTCATCAGACATC
	R	CAGGCCTTCAGCTAGTTTTATA
PrgI (fl)	F	CGCGGATCCATGGCAACACCTTGGTCAGGCTATC
	R	CGGAATTCAACGGAAGTTCTGAATAATGGCAGCATC
hNAIP (fl)	F	GCGGATCCATGGCCACCCAGCAGAAAGC
	R	CGGAATTCATTTCTGAATGATTGGAGAGAACG

Table 3 | Mutagenesis primers. F, forward; R, reverse.

Target gene & mutation	F/R	Sequence (5' → 3')	Muta-genesis method
hCOPA (R233H)	F	AGTGAAGATCTGGCACATGAATGAATCAAAGGC	Quik Change, Agilent
	R	GCCTTTGATTCATTCATGTGCCAGATCTTCACT	
hCOPA (E241K)	F	TCAAAGGCATGGAAGGTTGATACCTGC	
	R	GCAGGTATCAACCTTCCATGCCTTTGA	
hNLRC4 EcoRI site 1	F	TGGCTACAATGAGTTCAAGCCCC	(Liu et al., 2008)
	R	TCAAGAAGGAAAAGAACCCTC	
hNLRC4 EcoRI site 2	F	CTGGAAGCAGGAGTTCAGGACTC	
	R	TTGAAGAACAAAGATACAGCC	
hNLRC4 A160T_A	F	CTCCTGCAGACTCTTCAGAGCCC	Quik Change, Agilent
	R	GGGCTCTGAAGAGTCTGCAGGAG	
hNLRC4 A160T_B	F	GCAGACTCTTCAGAGCCCCTGCATCATTGAAGGGGAATCTGG	(Liu et al., 2008)
	R	GCTCTGAAGAGTCTGCAGGAGGCCATTCAGGGTCAGC	
hNLRC4 S171F_A	F	TTGCCTTTGCCAAATTCCCCTTCAATGATGCAGGGG (Moghaddas et al., 2018)	Quik Change, Agilent
	R	CCCCTGCATCATTGAAGGGGAATTTGGCAAAGGCAA (Moghaddas et al., 2018)	
hNLRC4 S171F_B	F	GGAATTTGGCAAAGGCAAGTCCACTCTGCTGC	(Liu et al., 2008)
	R	CCTTTGCCAAATTCCCCTTCAATGATGCAGGGGC	
mNlrc4 EcoRI site 1	F	GATGGTTACAATGAGTTCCATCCCCAGAAC	Quik Change, Agilent
	R	GTTCTGGGGATGGAACTCATTGTAACCATC	
mNlrc4 EcoRI site 2	F	CAGGAGTTCCAAGCTCACACCCAAACCATGC	(Liu et al., 2008)
	R	GCTTGGAACTCCTGTCTGCCCATCTGAATTGC	
mNlrc4 EcoRI site 3	F	CAGGAGTTCAAGACTCTAGAGGTCACACTCCGAG	(Liu et al., 2008)
	R	GAGTCTTGAACTCCTGCTTCCAGTTGAAGAACAAAGACAC	
mNlrc4 A160T	F	CTCGAGACTCTGAAGAGCCCCTGCCTGATTGAAG	(Liu et al., 2008)
	R	CTTCAGAGTCTCGAGCAGGCTGCCCAAAGTCAG	

*hNAIP_* EcoRI site	F	GAACATTTTGTCAATTCCTGGGTCCAGAG AGAATTACC	(Liu et al., 2008)
	R	GGAATTGACAAAATGTTCTCCCGTTATGT CAACAAATCC	

Table 4 | Sequencing primers. F, forward; R, reverse.

Target gene/primer name	Sequence (5' → 3')
hCOPA	AAGACTTGGTAGTATCAGCCAGCCTGG
*hNLRC4*_1	GGAGACTTGGACGATTTGGC
*hNLRC4*_2	CAACTCCTGGATATACCTG
*hNLRC4*_3	CACAGGTGGAATCCACATG
*hNLRC4*_4	CACCAATGGCAGATTCTCAG
*mNlrc4*_1	CTGGGTGAAGATATCGAC
*mNlrc4*_2	CATTGTCACCACCACC
*mNlrc4*_3	CATTGGACTTCGTGAAGTTGG
hNAIP	GCTGAGAGGAGGTAAAATGAG
U6_F	ACCAAGGTCGGGCAGGAAGA
CMV_F	CGCAAATGGGCGGTAGGCGTG
pACEBac1_F	TACTGTTTTCGTAACAGTTTTG
pACEBac1_R	CATTTTATGTTTCAGGTTCAGG
FgH1t_sgRNA	CAGACATACAAACTAAAGAAT
EGFP_F	CAACGAGAAGCGCGATC

Table 5 | qRT-PCR primers. All primers refer to human genes.

Target gene	F/R	Sequence (5' → 3')
ACTIN	F	GCGAGAAGATGACCCAGATC
	R	CCAGTGGTACGGCCAGAGG
COPA	F	ACTGGCAATCTAGAACCTGTG
	R	GACCAGAAATATCCCAAACGC
TNF	F	TCTCTCAGCTCCACGCCATT
	R	CCCAGGCAGTCAGATCATCTTC
IFNA1	F	GCCTCGCCCTTTGCTTTACT
	R	CTGTGGGTCTCAGGGAGATCA
IFNB1	F	TGTCGCCTACTACCTGTTGTGC
	R	AACTGCAACCTTTCGAAGCC
ISG15	F	TCCTGGTGAGGAATAACAAGGG
	R	GTCAGCCAGAACAGGTCGTC
IFIT1	F	ATCCACAAGACAGAATAGCCAG
	R	CCAGACTATCCTTGACCTGATG
MX1	F	GTTTCCGAAGTGGACATCGCA
	R	CTGCACAGGTTGTTCTCAGC
USP18	F	CCTGAGGCAAATCTGTCAGTC
	R	CGAACACCTGAATCAAGGAGTTA
IL6	F	TCAATATTAGAGTCTCAACCCCCA
	R	GAAGGCGCTTGTGGAGAAGG

IL8	F	CTGGCCGTGGCTCTCTTG
	R	CCTTGGCAAAACTGCACCTT
COPG2	F	CCTAAGCCAGCCTTGAGATATG
	R	GTCCAGATTGCAGGCAGTAA
SURF4	F	GGTCTTGCTGGTTCTGATGT
	R	CCCACGATGTTCTGGACAATA
IL1B	F	AATCTGTACCTGTCCTGCGTGTT
	R	TGGGTAATTTTTGGGATCTACACTCT
NLRC4	F	CATCATTTGCTGCGAGAAGGTGG
	R	CGTCCAAGTCTCCTTCTGATGTCTG

2.3 Buffers

Table 6 | List of buffers used in this study. Sodium dodecyl sulphate-polyacrylamide gel electrophoresis, SDS-PAGE; adenosine diphosphate, ADP; size exclusion chromatography, SEC; anion exchange chromatography, AIEX.

Buffer	Components
1% NP-40 buffer	1% NP-40, 10 % glycerol, 20 mM Tris-HCl (pH 7.5), 150 mM NaCl, 1 mM ethylene glycol tetraacetic acid (EGTA)
1xRIPA buffer	20 mM Tris-HCl (pH 7.3), 150 mM NaCl, 5 mM EDTA, 1 % Triton X-100, 0.5 % sodium deoxycholate, 0.1 % SDS, 10 % glycerol
4x Laemmli buffer	240 mM Tris-HCl (pH 6.8), 40 % glycerol (v/v), 8 % SDS (w/v), 0.04 % bromophenol-blue, 5 % β-mercaptoethanol, 40 % glycerol, pH 6.8
SDS-PAGE separation gel buffer	1.5 M Tris-HCl, 0.4 % (w/v) SDS, pH 8.8
SDS-PAGE stacking gel buffer	0.5 M Tris-HCl, 0.4 % (w/v) SDS, pH 6.8
10x SDS-PAGE running buffer	0.25 M Tris, 1.94 M glycin, 1% SDS (w/v), pH 8.3
10x wet transfer buffer	200 mM Tris, 1.5 M glycine, pH 8.1-8.5
1x wet transfer buffer	1x wet transfer buffer, 20 % methanol, H_2O
1x TAE buffer	40 mM Tris, 20 mM acetic acid, 1 mM EDTA sodium salt dihydrate
PBND buffer	50 mM KCl, 10 mM Tris-HCl (pH 8.3), 2.5 mM $MgCl_2$, 0.1 mg/ml gelatin, 0.45% (v/v) NP-40, 0.45 % (v/v) Tween 20
Coomassie stain	40 % ethanol (v/v), 10 % acetic acid (v/v), 0.1 % Coomassie R250 (w/v)
Coomassie destain	10 % ethanol (v/v), 5 % acetic acid (v/v)
10x TBS	0.5 M Tris, 1.5 M NaCl, pH 8.0
1 mg/ml DNaseI	20 mM Tris-HCl (pH 7.5), 50 % (w/v) glycerol, 1 mg/ml DNase I

Purification of recombinant hNLRC4 truncations	
hNLRC4 lysis buffer	25 mM Tris-HCl, 150 mM NaCl, 10 mM imidazole, 5 mM β-mercaptoethanol, 1 mM ADP, 10 mM $MgCl_2$, pH 8.0
hNLRC4 wash buffer	25 mM Tris-HCl, 150 mM NaCl, 30 mM imidazole, 5 mM β-mercaptoethanol, 1 mM ADP, 10 mM $MgCl_2$, pH 8.0
hNLRC4 elution buffer	25 mM Tris-HCl, 150 mM NaCl, 250 mM imidazole, 5 mM β-mercaptoethanol, 1 mM ADP, 10 mM $MgCl_2$, pH 8.0
hNLRC4 SEC buffer	20 mM HEPES, 0.5 mM TCEP, 100 mM NaCl, 1 mM ADP, 10 mM $MgCl_2$, pH 8.0
Purification of recombinant mNLRC4 truncations	
mNLRC4 lysis buffer	25 mM Tris-HCl, 150 mM NaCl, 10 mM imidazole, 5 mM β-mercaptoethanol, pH 8.0
mNLRC4 wash buffer	25 mM Tris-HCl, 150 mM NaCl,30 mM imidazole, 5 mM β-mercaptoethanol, pH 8.0
mNLRC4 elution buffer	25 mM Tris-HCl, 150 mM NaCl, 250 mM imidazole, 5 mM β-mercaptoethanol, pH 8.0
mNLRC4 SEC buffer	20 mM HEPES, 0.5 mM TCEP, 100 mM NaCl, pH 8.0
Anion exchange chromatography hNLRC4 and mNLRC4	
AIEX buffer A (no salt)	25 mM Tris-HCl, 5 mM β-mercaptoethanol, pH 8.0
AIEX buffer B (high salt)	25 mM Tris-HCl, 5 mM β-mercaptoethanol, 1 M NaCl, pH 8.0

2.4 Molecular biology methods

2.4.1 Polymerase chain reaction

2.4.1.1 Target gene amplification for subcloning

Prior to subcloning, mutagenesis PCR was performed to mutate *Eco*RI recognition sites encoded in the coding sequence of *hNLRC4, mNlrc4* and *hNAIP* (chapter 2.4.1.2). PCR using the Q5 Polymerase (New England Biolabs, NEB) or Phusion®High-Fidelity DNA Polymerase (NEB) was performed to amplify human and mouse NLRC4, hNAIP, and the *S. typhimurium* needle toxin PrgI coding sequences for subcloning into the pcDNA3.1 mammalian expression plasmid or pACEBac1 backbone for expression in *Sf*9 cells. The pRP-HA-mCitrine-hIPAF plasmid (encoding hNLRC4, kind gift from R. Stahl, AG Latz, Institute of Innate

Immunity, Medical faculty, University of Bonn) and the mscv2.2-mNLRC4 plasmid (kind gift from R. Vance, Addgene plasmid # 60199) (Kofoed et al., 2011) were used as templates for the amplification of the human and mouse NLRC4 coding sequence, respectively. Furthermore, the pEXPR-NAIP-HA plasmid (kind gift from F. Schmidt, Institute of Innate Immunity, University of Bonn) and pET28a-His-MBP-TEV-PrgI plasmid served as template for hNAIP and PrgI amplification and subcloning, respectively. Elongation times and annealing temperatures were adjusted according to the manufacturer's recommendations and calculated using the NEB Tm Calculator online tool (https://tmcalculator.neb.com/#!/main). CARD-deleted hNLRC4 (hNLRC4$^{\Delta CARD}$, aa 92-1024) and mNLRC4 (mNLRC4$^{\Delta CARD}$, aa 90-1024) were amplified by use of specific primers (**Table 2**) and simultaneous PCR-mediated attachment of *Bam*HI (5') and *Eco*RI (3') restriction enzyme recognition sites for subcloning (encoded in primer sequence). The LRR-resident loop (aa 622-644) was deleted using the Q5 Site-Directed Mutagenesis kit (Cat. No. E0554S, NEB) to generate the hNLRC4$^{\Delta CARD/\ \Delta Loop}$ (aa 90-1024, Δ622-644) construct using specific primers (**Table 2**).

2.4.1.2 Mutagenesis PCR

Prior to subcloning of *hNLRC4*, *mNlrc4* or *hNAIP* (fl) into pACEBac1 and pcDNA3.1 backbones via *Eco*RI and *Bam*HI restriction enzyme recognition sites, silent mutagenesis of sequence-encoded *Eco*RI recognition sites was performed (*hNLRC4*: c.756A>G, c.1974A>G, *mNlrc4*: c.756A>G, c.1059A>G, c.1974G>A, *hNAIP*: c.765G>C) using the previously published site-directed plasmid mutagenesis protocol by Liu and colleagues (Liu et al., 2008). Using the same protocol, pACEBac1-6xHis-SUMO-TEV-hNLRC4$^{\Delta CARD}$ and hNLRC4$^{\Delta CARD/\ \Delta Loop}$, pACEBac1-6xHis-GFP-TEV-hNLRC4$^{\Delta CARD}$ and hNLRC4$^{\Delta CARD/\ \Delta Loop}$, pACEBac1-6xHis-SUMO-TEV-mNlrc4$^{\Delta CARD}$ and pcDNA5/FRT/TO NLRC4-SH with C-terminal Strep2-HA (SH)-tag (kind gift from F. Schmidt, Institute of Innate Immunity, University of Bonn) were mutated to introduce p.A160T (c.478G>A) and p.S171F (c.512C>T) mutations, respectively.

Introduction of hNLRC4 p.A160T (c.478G>A) and p.S171F (c.512C>T) mutations into the pEF-BOS-mCitrine-hNLRC4 plasmid was performed using the QuikChange II site-directed mutagenesis kit (Agilent technologies) following the manufacturer's recommendations. Similarly, this method was used to generate plasmids encoding COPA syndrome patient mutations c.721G>A (p.E241K) and c.698G>A (p.R233H) (Watkin et al., 2015). As template, the pCMV6Entry-COPA-myc-DDK plasmid (Origene, kind gift from A. Shum, Department of Medicine, University of California San Francisco) was used. All mutagenesis primers are listed in **Table 3**.

2.4.2 Molecular cloning

Amplified PCR products were separated based on DNA fragment length during agarose gel electrophoresis. Therefore, PCR samples were mixed with 6x DNA gel loading dye (Cat. No. B7024S, NEB) and run on 1-2 % agarose gels supplemented with UV-excitable DNA-binding dye (SYBR safe (Cat. No. S33102, Invitrogen) or peqGREEN (Cat. No. 732-3196, PeqLab, VWR)) in 1x TAE buffer (**Table 6**). As molecular weight size markers 100 bp-DNA Ladder extended (Cat. No. T835.1, Carl Roth) or GeneRuler 1 kilobase (kb) Plus DNA Ladder (Cat. No. SM1331, Thermo Fisher Scientific) were used. Separated bands were visualized using the ChemiDoc Touch Imaging System (BioRad). DNA fragments required for downstream cloning applications were extracted and purified using the ExtractMe DNA Clean-Up & Gel-Out-Kit (Cat. No. EM26.1, Blirt) following the manufacturer's instructions.

Subsequently, restriction digests of the amplified insert and target plasmid (pACEBac1-6xHis-SUMO-TEV, pACEBac1-6xHis-GFP-TEV, pcDNA3.1-3xHA, pcDNA3.1-3xFLAG, pcDNA3.1-myc) were performed to generated compatible overhangs (sticky ends). The reaction mix containing *Bam*HI-HF and *Eco*RI-HF restriction enzymes (Cat. No. R3136, R3101, NEB) was prepared following the manufacturer's recommendations. After 2 hours (hrs) incubation at 37 °C, digested products were purified using the ExtractMe DNA Clean-Up & Gel-Out-Kit (EM26.1,Blirt) to remove residual buffer and cleaved nucleotides. Digested

target plasmid and insert were ligated at a 1:3 ratio, which was calculated based on fragment size and concentration using the online tool NEBio Ligation calculator (https://nebiocalculator.neb.com/#!/ligation, NEB). The ligation reaction was performed using the T4 DNA ligase (Cat. No. M0202, NEB) following the manufacturer's protocol. After overnight incubation at 16 °C, the ligation mix was transformed into 50 µl of chemically competent *E. coli* strains DH10β, DH5α or Stbl3. After initial incubation on ice for 10-15 minutes (min), cells were heat shocked for 42 seconds at 42 °C, resuspended in 800 µl antibiotic-free Luria Bertani (LB) medium (Carl Roth) and incubated for 1 hr at 37 °C and 800 revolutions per minute (rpm). Cells were plated on agar plates containing appropriate selection antibiotics, e.g. ampicillin (100 µg/ml, Sigma-Aldrich), kanamycin (50 µg/ml, Sigma-Aldrich) or spectinomycine (50 µg/ml, Sigma-Aldrich) and incubated overnight at 37 °C. On the next day, colonies were picked and incubated in 4 ml antibiotic-containing LB medium overnight, before DNA was isolated using the ExtractMe Plasmid Mini Kit (Cat. No. EM01.1, Blirt) or Wizard™ PlusSV Miniprep Purification System (Cat. No. A1460, Promega). Sanger sequencing was performed (see chapter 2.4.3) and correct bacterial clones were further amplified in 100-300 ml antibiotics-containing LB medium overnight for DNA isolation using the NucleoBond Xtra Midi Kit for transfection-grade plasmid DNA (Cat. No. 740410.50, Machery-Nagel), GeneJET Plasmid Maxiprep Kit (Cat. No., K0492, Thermo Fisher Scientific) or PureLink HiPure Plasmid MaxiPrep Kit (Cat. No. K210006, Thermo Fisher Scientific) following the manufacturer's instructions. Concentration of purified DNA was measured at 260 nm absorbance using a NanoDrop spectrophotometer (Thermo Fisher Scientific). Purity was assessed using the 260/280 nm and 260/230 nm ratio.

The pcDNA5/FRT/TO hNLRC4-SH plasmids (used in chapter 2.5.2) encoding NLRC4 WT, A160T or S171F were cloned using the pENTR223-hNLRC4 plasmid and pDEST MCS-SH gateway destination vector and LR Clonase II enzyme mix (Cat. No. 11791-020, Invitrogen) following the manufacturer recommendations (plasmids and reagents were kindly provided by F. Schmidt, Institute of Innate Immunity, University of Bonn).

Used for CRISPR/Cas9 gene editing of THP-1 cells to introduce the NLRC4 A160T mutation on genomic level (chapter 2.5.1.2), the EF1alpha-Cas9-2A-EGFP/U6 plasmid (kind gift from T. Zillinger, Institute of Clinical Chemistry and Clinical Pharmacology, University of Bonn) was linearized using *Smi*I (*Swa*I, Cat. No. ER1241, Thermo Fisher Scientific) restriction enzyme digest following the manufacturer's instructions. The 20 nucleotide *NLRC4*-targeting sgRNA (see sequence below and **Table 11**) was designed manually based on the localization of the protospacer adjacent motif (PAM) proximal to the genomic site to be modified. Off-targets were analysed using the IDT CRISPR-Cas9 guide RNA design checker online tool (Integrated DNA Technologies). To generate the full length CRISPR-oligo, the NLRC4-specific sgRNA (underlined) was flanked by 5' and 3' bridging sequences resulting in a total of 60 nucleotide (5'-TGGAAAGGACGAAACACC –GACCCTGAATGGCCTCCTGC– GTTTTAGAGCTAGAAATAGCA-3'). Bridging sequences provided complementary overhangs for the subsequent NEBuilder DNA assembly reaction (**Table 7**), which was performed to ligate the *NLRC4*-specific sgRNA into the *Smi*I-digested EF1alpha-Cas9-2A-EGFP/U6 plasmid followed by 1 hr incubation at 50 °C. Transformation into chemically competent *E. coli* Stbl3 bacteria and DNA amplification (Miniprep, Maxiprep) were performed following the procedure described above. For Sanger sequencing, the U6 forward primer was used (**Table 4**).

Table 7 | NEBuilder DNA assembly reaction.

Reagent	Volume
*Smi*I-linearized EF1alpha-Cas9-2A-EGFP/U6 plasmid	1 µl (~ 30 ng)
Single strand sgRNA (5 µmol)	0.5 µl
Water	1.5 µl
2x NEBuilder HiFi DNA assembly mix (Cat. No. E2621, NEB)	2.5 µl

To generate CRISPR/Cas9 knockout cell lines (chapter 2.5.1.1), sgRNAs were annealed and cloned into FgH1t_UTG (with GFP reporter) and _UTC (with CFP reporter) plasmids (kind gift from M. Herold, Addgene plasmids #70183, #85551) (Aubrey et al., 2015), which were linearized by *Bsm*BI (Cat. No. R0739, NEB)

restriction digest following the manufacturer's recommendations. sgRNA forward and reverse oligos were annealed using the reaction mixture and temperature protocol described in **Table 8** and **Table 9**. Following ligation with T4 DNA ligase (Cat. No. M0202, NEB), subsequent transformation and DNA purification steps were performed according to the previously described procedures. sgRNA sequences are listed in **Table 10**.

Table 8 | sgRNA annealing reaction for subcloning into FgH1t plasmids.

Reagent	Volume
forward oligo (100 µM)	3 µl
reverse oligo (100 µM)	3 µl
3 M NaCl	0.5 µl
1 M $MgCl_2$	2 µl
1 M TRIS pH 7.5	2 µl
1xTE buffer	9.6 µl

Table 9 | Temperature gradient for sgRNA annealing reaction.

Temperature	Time
95 °C	5 min
gradual (0.1 °C/sec)	
70 °C	20 min
gradual (0.1 °C/sec)	
40 °C	20 min
gradual (0.1 °C/sec)	
25 °C	20 min
gradual (0.1 °C/sec)	
4 °C	hold

2.4.3 Sanger sequencing

Sanger sequences was performed by external services (Microsynth AG, Göttingen, Germany or the Australian Genome Research Facility (AGRF), Melbourne, Australia) using the listed sequencing primers (**Table 4).** Sanger sequencing aimed to identify the bacterial clones containing plasmids encoding the desired insert or point mutation and to confirm sequences of genomic DNA and *NLRC4* mRNA transcripts in THP-1 monoclonal cell lines (see 2.5.1.2). Samples were prepared according to the recommendations of the service

provider and analysis performed using ApE v2.0.61 and Snapgene 5.2.4 software.

2.5 Generation of stable cell lines

2.5.1 CRISPR/Cas9 gene editing

2.5.1.1 CRISPR/Cas9-mediated knockout cell line generation

COPA-, COPG1-, COPG2-, COPD-, COPE-deficient as well as MAVS$^{-/-}$, PKR$^{-/-}$, UNC93B1$^{-/-}$, NLRP3$^{-/-}$, STING$^{-/-}$ and SURF4$^{-/-}$ cells lines were generated using site-specific genetic editing via the clustered regularly interspaced short palindromic repeats (CRISPR)/Cas9 system as previously described (Baker et al., 2018). Third generation lentivirus was generated in HEK293T cells following the detailed protocol by Baker et al. using LipoFectMax™ Transfection Reagent (Cat. No. FP311, Sapphire Bioscience). Lentiviral transduction was performed to stably reconstitute the Cas9 endonuclease from *S.pyogenes* using the FU-Cas9-mCherry plasmid (kind gift from M. Herold, Addgene plasmid #70182) (Aubrey et al., 2015) or lentiCRISPR v2 Cas9 (kind gift from F. Zhang, Addgene plasmid # 52961) (Sanjana et al., 2014, Shalem et al., 2014) in WT THP-1 or HeLa cells, respectively, via spin inoculation (3 hrs, 2200 rpm, 32 °C) (**Figure 2.1**). Successfully transduced THP-1 or HeLa cells were sorted for medium mCherry expression levels by fluorescence-activated cell sorting (FACS) or selected by puromycin treatment (1 µg/ml), respectively (**Figure 2.1 A**). Subsequently, stably Cas9-expressing THP-1 or HeLa cell lines were used as control cells in all experiments and are referred to as parental cell line throughout this thesis. Using the same method (Baker et al., 2018), lentivirus containing the previously cloned (chapter 2.4.2) doxycycline (Dox)-inducible FgH1t-UTG (GFP-tagged) or FgH1t-UTC (CFP-tagged) plasmid encoding target-specific sgRNAs **(Table 10)** was generated and used to transduce parental THP-1 and HeLa cell lines via spin inoculation (3 hrs, 2200 rpm, 32 °C). Two days post transduction, the cells were sorted for the medium CFP- or GFP-positive population (**Figure 2.1 A**). Gene deletion was induced by treatment with Dox (1 µg/ml) for 72 hrs followed by an optional 24 hrs resting period in Dox-free complete growth medium depending on

the downstream application, before experiments were performed (**Figure 2.1 B**). Protein or gene deletion was assessed by western blotting (chapter 2.11) or quantitative Real-Time PCR (qRT-PCR, chapter 2.12).

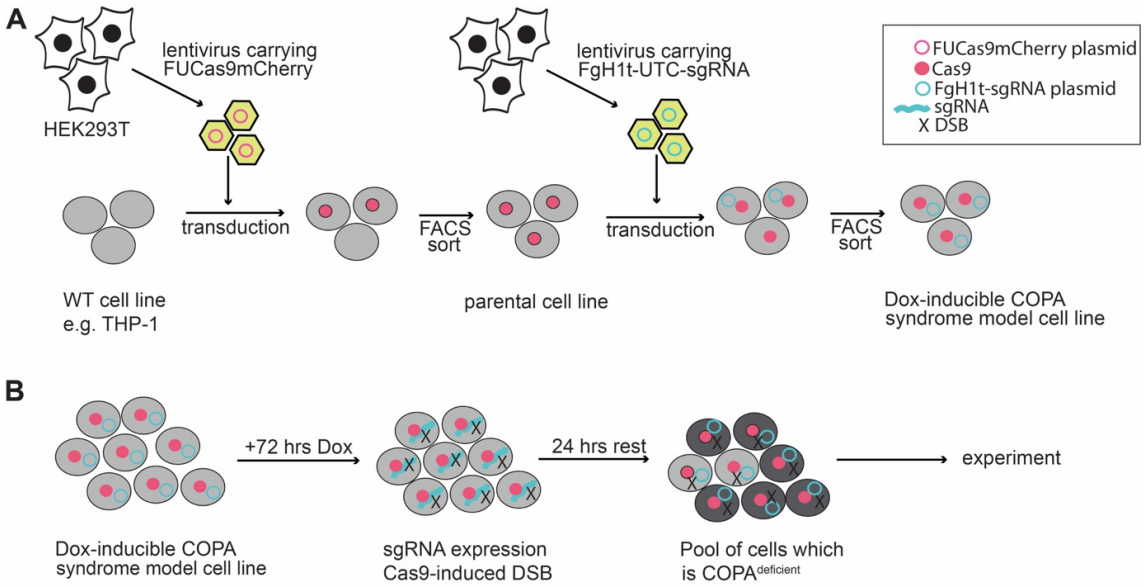

Figure 2.1 | Workflow to generate knockout cell lines using CRISPR/Cas9 gene editing technology. The generation of COPA syndrome model cell lines in THP-1 cells using fluorescent protein-tagged plasmids is shown. **A)** Lentivirus was generated by transient co-transfection of third generation lentiviral packaging plasmids (pVSVg, pMDL and pRES-REV (Baker et al., 2018)) and FU-Cas9-mCherry plasmid into HEK293T cells. Lentivirus particle-containing supernatant was harvested and used to transduce THP-1 WT cells by spin inoculation. FACS sorting selected a homogenous cell population expressing medium mCherry levels (parental cell line, constitutive Cas9 and mCherry expression). Subsequently, parental cell lines were transduced with lentiviral particles carrying the FgH1t-UTC plasmid encoding target gene-specific single guide (sg) RNAs controlled under a doxycycline (Dox)-inducible promoter together with a fluorescent tag (CFP, constitutively expressed). FACS sorting for the medium CFP-positive population resulted in a homogenous cell population, referred to as COPA syndrome model cell line. **B)** Prior to every experiment, Dox treatment (72 hrs, 1 µg/ml) induced sgRNA-guided Cas9-mediated double strand breaks (DSB), resulting in *COPA* gene deletion and generation of a heterogeneous pool of COPA^{deficient} cells (dark grey). A 24 hrs resting period was performed prior to some experiments depending on the downstream application.

Table 10 | Single guide RNAs for CRISPR/Cas9-mediated gene editing. sgRNAs targeting human genes were designed using the CHOPCHOP online tool (https://chopchop.cbu.uib.no/) (Labun et al., 2019, Montague et al., 2014).

Target gene	sgRNA sequence (5'→3')
COPA (sgRNA1)	TAGATTGCCAGTTCCACACT
COPA (sgRNA2)	AATTCGAGACCAAGAGCGCG
COPA (sgRNA3)	ACATCCGATTCCACCGCACC
STING	AGAGCACACTCTCCGGTACC
NLRP3	TCCCGCTGGACCATCCTCGGCATG
MAVS	AGTACTTCATTGCGGCACTG
PKR	TAATACATACCGTCAGAAGC
COPG1	TGGTCAAGTAGCACATCCGA
COPG2	GGAAAAGAAGATGTATACCG
SURF4 (sgRNA 1)	TCAGACAGAGGCGCGCCACG
SURF4 (sgRNA 2)	AGTCGCGCTGCTCGCTCCAC
UNC93B1	GGGCGTGCTCAAGAACGTGC

2.5.1.2 Generation of monoclonal NLRC4 A160T-encoding THP-1 cell lines via CRISPR/Cas9-mediated homology-directed repair

THP-1 WT cells were transiently electroporated (Neon Transfection system, Thermo Fisher Scientific; 1250 V, 50 ms, 1 pulse, $5x10^5$ THP-1 WT cells, 100 µl tips) to deliver 10 µg of EF1alpha-Cas9-2A-EGFP/U6 plasmid-encoding a sgRNA targeting *hNLRC4* together with the oligo repair template (2.5 µM) encoding two missense mutations within the *NLRC4* coding sequence: 1) nucleotide exchange c.468C>T (silent mutation on protein level) to introduce a *Bsa*I recognition site and 2) the patient mutation of interest, c.478G>A which encodes NLRC4 A160T (**Figure 4.7,** sequences in **Table 11)**. FACS sorting for EGFP-positive cells was performed 18 hrs after electroporation. Sorted cells were culture for 1 week as pool and used to generated monoclonal cell lines by limiting dilution (in 96-well plates, round bottom). After 4-6 weeks, visible colonies appeared and total DNA from single cell clones was isolated by Proteinase K lysis (200 µg/ml) in PBND buffer (**Table 6**) and 1 hr incubation at 55 °C, followed by heat inactivation for 10 min at 95 °C. A subsequent PCR reaction (total 25 µl) was performed to amplify the genomic *NLRC4* locus using the DreamTaq polymerase (Cat. No. EP0705, Thermo Fisher Scientific). 10 µl of the amplification product were subjected to *Bsa*I-HFv2 (Cat. No. R3733, NEB) enzymatic digest following the

manufacturer's recommendations to screen for successful oligo repair template integration as analysed by agarose gel electrophoresis (chapter 2.4.2) The remaining PCR product of clones showing the expected band pattern following *Bsa*I digest was enzymatically purified with rSAP (Cat. No. M0371, NEB) and Exo1 (Cat. No. M0568, NEB) digest and submitted for Sanger sequencing to confirm genotypes on genomic level (chapter 2.4.3).

Sequences of active h*NLRC4* mRNA transcripts were confirmed by Sanger sequencing after RNA isolation and cDNA transcription (chapter 2.12), which then served as template for h*NLRC4*-specific PCR with exon-spanning primers and the product of this reaction was subsequently sequenced. Primers used for PCR amplification and sequencing are listed in **Table 2** and **Table 4**, respectively.

Table 11 | Oligonucleotide sequences used for CRISPR/Cas9-mediated site-directed mutagenesis in THP-1 cells. Within the oligo repair template modified nucleotides to introduce *Bsa*I restriction enzyme recognition site (c.468C>T underlined and bold) and c.478G>A mutation encoding p.A160T (italic and bold) are highlighted.

	Sequence (5'→3')
hNLRC4-specific sgRNA sequence	GACCCTGAATGGCCTCCTGC
oligo repair template	GACCAACACCATCACCGCGTGGAGCAGC TGACCCTGAATGG**T**CTCCTGCAG***A***CTCTT CAGAGCCCCTGCATCATTGAAGGGGAAT CTGGC

2.5.2 Generation of Flp-In 293 T-REx cell lines stably expressing ASC-EGFP and hNLRC4.

Unmodified Flp-In 293 T-REx cells (control cell line) were maintained in complete growth medium supplemented with 4 µg/ml blasticidin (InvivoGen) and 50 µg/ml zeocin (InvivoGen). Stable ASC-EGFP-expressing monoclonal Flp-In 293 T-REx were generated via lentiviral transduction (Cardona Gloria et al., 2018). For lentivirus generation, HEK293T cells were seeded (6-well plate format) to reach 70 % confluency on the next day. Prior to transfection, the medium was replaced to antibiotic-free DMEM/2% FBS. Second generation lentiviral plasmids psPax2 (0.65 µg) and pMD2.G (0.35 µg) were co-transfected with pRRL pUbC ASC-

EGFP-Puro (1.5 µg, kind gift from F. Schmidt, Institute for Innate Immunity, University of Bonn) using polyethylenimine (PEI) Max (1 mg/ml, Polysciences) cellular transfection reagent at a DNA (µg) to PEI (µl) ratio of 1:1 and OptiMEM (Thermo Fisher Scientific). After 6 hrs incubation, the medium was replaced with complete growth medium and virus-containing supernatant harvested 48 hrs later. Subsequently, Flp-In 293 T-REx cells were inoculated with 250 µl filtered (0.45 µm) viral supernatant in presence of 10 µg/ml polybrene (Sigma-Aldrich) using a 24-well plate format. The cells were incubated overnight and transferred into a 10 cm dish. One day later, puromycin selection was initiated (1 µg/ml, InvivoGen) and cells continuously cultured until visible cell colonies appeared. Multiple single colonies were picked and cultured to confluence. Following screening of activation-induced versus baseline ASC specking by flow cytometry (see chapter 2.9), the clone with the lowest background ASC speck assembly was selected to generate isogenic human NLRC4-expressing Flp-In 293 T-REx-ASC-EGFP cells lines using the Flp-In system following the manufacturer's instructions (Thermo Fisher Scientific). Expression of human NLRC4 with C-terminal Strep2-HA (SH) tag was induced by Dox treatment (1 µg/ml, Sigma-Aldrich) for periods as indicated in respective figure legends. The cells were maintained in complete growth medium (chapter 2.1) with addition of 4 µg/ml blasticidin (InvivoGen), 50 µg/ml hygromycin B (InvivoGen), 1 µg/ml puromycin (InvivoGen).

2.5.3 Generation of stable STING-GFP-expressing HEK293T and HeLa cell lines

Stable STING-GFP expressing HEK293T, HeLa cell lines (parental (Cas9) and COPA^{deficient} (expressing Cas9+Dox-inducible sgRNA1 targeting *COPA* sgRNA1) were generated following the retroviral-based reconstitution method published by Pokatayey and Yan (Pokatayev and Yan, 2017). Briefly, retrovirus-particles were generated by co-transfection of pMRX-STING-GFP (6 µg, kind gift from N. Yan, Department of Immunology and Department of Microbiology, University of Texas), VSVg (4 µg) and gagpol (6 µg) plasmids into one 10 cm dish of HEK293T

cells using LipoFectMax TM Transfection Reagent (Cat. No. FP311, Sapphire Bioscience). Filtered (0.45 µm) supernatant was then used to infect HEK293T or HeLa cell lines in presence of polybrene (8 µg/ml), which were subsequently sorted for the low GFP-expressing population via FACS.

2.5.4 Reconstitution of the monoclonal cGAS$^{-/-}$ THP-1 cell line with GFP-FLAG-cGAS

Following the previously described method (Baker et al., 2018), lentiviral reconstitution of THP-1 cell lines (cGAS$^{-/-}$ parental and cGAS$^{-/-}$/COPA^{deficient}) with third generation lentivirus particles encoding pTRIP-CMV-GFP-FLAG-cGAS (gift from N. Manel, Addgene plasmid #86675) (Raab et al., 2016) was performed. Therefore, 1x10^{6} cells were incubated with 1ml virus-containing supernatant and polybrene (8 µg/ml) and centrifuged for 3 hrs at 2200 rpm and 32 °C. Following 24 hrs incubation, the cells were washed in 1x phosphate buffered saline (PBS) and resuspended in full growth medium supplemented with STING inhibitor H-151 (2.5 µM, Life Chemicals) in order to reduce cell death associated with cGAS-STING pathway overactivation. After 24 hrs incubation, cells were subjected to FACS sorting for the low GFP-expressing population and grown to confluence under standard culture conditions (chapter 2.1).

2.5.5 Fluorescence-activated cell sorting for cell line generation

Sterile FACS sorting of cell lines generated in chapter 2.5.1.1, chapter 2.5.3 and chapter 2.5.4 was performed by staff of the Walter and Eliza Hall Institute flow cytometry core facility (Melbourne, Australia). Depending on the experimental requirements and instrument availability, the BD FACSAria W (lasers: 375 nm, 405 nm, 488 nm, 561 nm and 640 nm), BD FACSAria C (lasers: 375 nm, 405 nm, 488 nm, 640 nm) or BD FACSAria Fusion (lasers: 405 nm, 488 nm, 561 nm and 640 nm) (BD Bioscience) were used.

Sterile FACS sorting of GFP-expressing THP-1 cells following electroporation in chapter 2.5.1.2 was performed by staff in the flow cytometry core facility of the Medical Faculty at the University of Bonn using the BD FACSAria III (laser: 375 nm, 405 nm, 488 nm, 561 nm and 640 nm; BD Bioscience).
Prior to sorting, cells were resuspended in sterile 1xPBS/2% FBS and kept on ice. Cells were sorted into 10 ml tubes containing 1 ml complete growth medium supplemented with 20 % total FBS using the 100 µm nozzle. Subsequently, the sorted homogenous cell population was centrifuged, resuspended in pre-warmed complete growth medium and cultured to confluence.

2.6 Patient samples

2.6.1 Genetic investigations

Informed consent from the patient presented in chapter 4.2.1, healthy parents and the brother was obtained for genetic investigations. Genomic DNA of study subjects was sequenced at the Laboratory of Genetics and Genomics of Rare Diseases “Giannina Gaslini” Institute (Genoa, Italy) for the analysis of selected genes (Papa et al., 2020). Next generation sequencing (NGS) was performed, using an Ampliseq design coupled with Ion PGM™ parallel sequencing (Thermo Fisher Scientific) and demonstrated the presence of a homozygous variant in the *NLRC4* gene that had only been reported as heterozygous genotype in the healthy population (Genome Aggregation Database (GnomAD)). The variant was confirmed and segregated by Sanger sequencing. Within the analysed panel of target genes (Papa et al., 2020), only one other heterozygous variant was identified in the *IL1RN* gene, resulting in a synonymous mutation (c.345C>T, p.D115=).

2.6.2 Peripheral blood mononuclear cell isolation and differentiation

Informed consent (ethical review board of Institute Giannina Gaslini-Genoa-Italy N. BIOL 6/5/04) was obtained from two healthy control (HC) donors and one

COPA syndrome patient (previously reported Volpi et al., 2018) prior to human blood sample collection and PBMC isolation for STING inhibitor treatment (method see chapter 2.7.3; **Figure 3.6**).

Following informed written consent, peripheral blood for serum cytokine analysis (**Figure 4.2 G**) was collected from 21 unrelated healthy donors (HCs, 11 male/10 females; 35.4 ± 13.4 years) and the here presented patient (chapter 4.2.1), proceeding from the metropolitan area of São Paulo (SP, Brazil).

For inflammasome stimulation experiments using MDMs (**Figure 4.4**), 20 ml peripheral blood was collected from 3 HCs (1 male/2 females; 24.7 ± 23.3 years) for PBMC isolation using Ficoll-Paque density gradient centrifugation (GE Healthcare). Monocytes were separated from other PBMCs by adhesion in 96-well culture plates ($0.8x10^6$ PBMCs/well) (Corning). After 2 hrs, non-adherent cells (mainly lymphocytes) were removed by washing 3 times with PBS (Sigma-Aldrich), while adherent cells (mainly monocytes) were cultured in RPMI-1640 (Gibco, Thermo Fisher Scientific) supplemented with 10 % FBS (Gibco, Thermo Fisher Scientific at 37 °C in 5 % CO_2. To obtain MDMs, monocytes were cultured in RPMI-1640/10 % FBS with 25 ng/ml monocyte colony stimulating factor (M-CSF; PeproTech) at 37 °C in 5 % CO_2 for 5 days.

2.7 *In vitro* stimulation experiments

2.7.1 Inflammasome stimulation in monocyte-derived macrophages

MDMs (isolation described in 2.6.2) were challenged with 1 µg/ml LPS (*E. coli* strain O111:B4; Sigma-Aldrich, St. Louis, MO) for 4 hrs with subsequent addition of 1 mM ATP (Sigma-Aldrich, St. Louis, MO) for 15 min or cytoplasmic delivery of 5 µg/ml flagellin from *S. typhimurium* (FLA, InvivoGen, San Diego, CA) in DOTAP liposomes (6 µg DOTAP (Roche)/1 µg FLA) for 2 hrs before supernatants were collected. Long-term stimulation was performed with 1 µg/ml LPS or 5 µg/ml FLA for 24 hrs.

2.7.2 Inflammasome pathway stimulation in THP-1 cell lines

To stimulate NLRC4 inflammasome signalling in monoclonal THP-1 cell lines (generated as described in chapter 2.5.1.2), $0.5x10^5$ cells were seeded in a 96-well plate format (flat bottom). Simultaneously, TLR1/2 agonist Pam3CSK4 (P3C, 100 ng/ml) (InvivoGen) and 1 µl retroviral supernatant of pMXsIG_PrgI_GFP (plasmid was a kind gift from E. Miao, Department of Immunology, Duke University School of Medicine, method following Miao et al., 2010) were added in presence of polybrene (8 µg/ml) followed by spin inoculation (2200 rpm, 32 °C, 1 hr). Cells and supernatants were analysed after 24 hrs incubation (37 °C, 5 % CO_2). The NLRP3 inflammasome was stimulated with 10 µM nigericin (InvivoGen) for 1 hr after 3 hrs priming with P3C (100 ng/ml) using $0.5x10^5$ cells/well (96-well flat bottom plate format).

To readout inflammasome formation, supernatants were collected for quantification of released cytokines by ELISA (chapter 2.8). Cell death was analysed by flow cytometry following propidium iodide (PI) staining (1 µg/ml, Sigma-Aldrich) of cells using the LSRFortessa (BD Bioscience) and the gating strategy shown below (**Figure 2.2**). The percentage of PI-positive cells represents dead cells as percentage of the total single cell population (singlets), analysed in FlowJo 10.7.1 software.

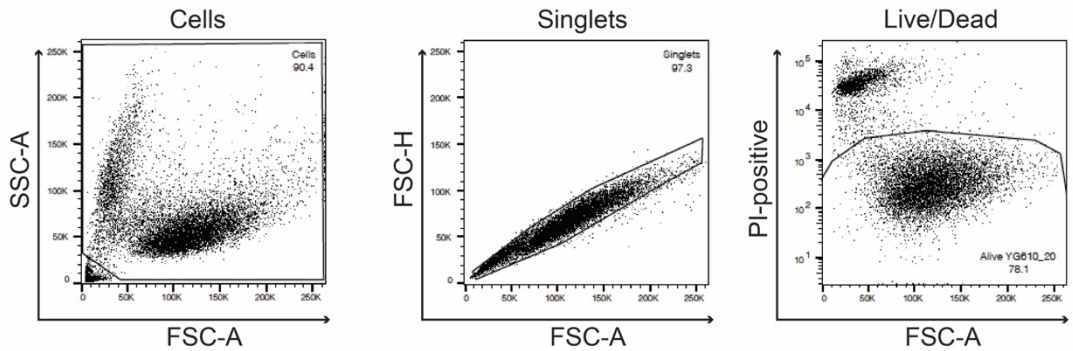

Figure 2.2 | Gating strategy for cell death analysis by flow cytometry. To analyse cell death after inflammasome stimulation, THP-1 cells were stained with propidium iodide (PI, 1 µg/ml) for 20 min on ice in 1xPBS/2% FBS, washed and analysed using the LSRFortessa flow cytometer. The percentage of dead cells (PI-positive, gated for as Boolean“NOT-alive” gate) was identified using the here depicted gating strategy. Forward scatter, FSC; side scatter, SSC; area, A; height, H.

2.7.3 STING inhibitor treatment of COPA syndrome patient PBMCs.

Ex vivo, PBMCs isolated from a COPA syndrome patient and 2 HCs (chapter 2.6.2) were treated with STING inhibitor H-151 (5 µM, Life Chemicals) at 37 °C for 4 hrs. Cells were fixed with pre-warmed fixation buffer (BioLegend) at 37 °C for 15 min and permeabilized with pre-chilled True-Phos™ perm buffer (BioLegend) for 1 hr at –20 °C. Cells were then stained with CD3-APC mAb (SK7, BD Biosciences), CD14-FITC mAb (M5E2, BD Biosciences) and phospho-TBK1/NAK (Ser172) (D52C2, Cell Signaling Technology), XP Rabbit mAb-PE (Cell Signaling Technology) or Rabbit mAb IgG XP Isotype Control-PE (DA1E, Cell Signaling Technology) at room temperature (RT) for 30 min. Samples were analysed using the FACSCanto A (BD Biosciences) flow cytometer and data analysis performed in FlowJo 10.7.1 software. The monocyte population was firstly identified based on cell size and granularity and subsequently confirmed by gating for the CD14-positive/CD3-negative subpopulation. Data for phosphorylated TBK1 (pTBK1) is presented as histogram showing mean fluorescence intensity (MFI) for the CD14-expressing monocyte population. Quantification **(Figure 3.6)** shows fold change of MFI (representing pTBK1) after H-151 treatment and was calculated using this formula:

$$fold\ change\ (pTBK1) = {MFI^{H-151} - MFI^{isotype\ ctrl}}/{MFI^{untreated} - MFI^{isotype\ ctrl}}$$

2.7.4 cGAS/STING activator and inhibitor treatment in THP-1 and HeLa cell lines.

THP-1 cells were stimulated with activators of the cGAS-STING pathway, e.g. HT-DNA (DNA sodium salt from herring testes, 2 µg/ml, transfected (Sigma-Aldrich)), poly (dA:dT) (1 µg/ml, transfected (InvivoGen) or cyclic di-AMP analogue 2'3'-c-di-AM(PS)$_2$ (Rp,Rp) (c-di-AM(PS)$_2$ in figure legend; 20 µM, InvivoGen). Transfections were performed using Lipofectamine 2000 transfection reagent (Life Technologies) and OptiMEM (Invitrogen) according to the manufacturer's instructions.

STING inhibitor studies were performed during Dox-induced sgRNA-mediated target gene deletion. Therefore, THP-1 cells were seeded at $8x10^4$ cells/well in 2 ml complete growth medium and cultured in presence of Dox (1 µg/ml, 6-well plate format) for 34 hrs. Then, STING inhibitor H-151 (2.5 µM, Life Chemicals) or DMSO (Vehicle control, Veh ctrl) was added and allowed to incubate for 11 hrs. Subsequently, cells were washed and incubation continued without inhibitor in complete growth medium (+Dox) until 72 hrs time point was reached.

To assess induction of spontaneous STING signalling following cytosolic phospholipase A2 alpha (cPLA2α) inhibition in iBMDMs, $2x10^5$ cells were seeded in 400 µl complete DMEM (24-well plate format) and incubated with arachidonyl trifluoromethyl ketone (AACOCF3, 10 or 20 µM, Sapphire Bioscience) or DMSO for 6 hrs. To confirm inhibitor functionality at the used concentrations, inducible nitric oxide synthase (iNOS) expression levels were investigated after overnight priming with IFNγ (50 ng/ml, 485-MI R&D Systems), followed by addition of AACOCF3 (10 or 20 µM, Sapphire Bioscience) or DMSO for 30 min before stimulation with LPS (25 ng/ml, LPS-SM Ultrapure, # tlrl-smlps, InvivoGen) for 6 hrs. Immunoblot analysis was performed as described in chapter 2.11.

2.8 Cytokine measurements by ELISA

Experimental supernatants (generated as described in 2.7.1 and 2.7.2) were immediately used or stored at -20 °C prior to ELISA analysis. IL-1β (Biolegend, Cat. No. 557953), total IL-18 (R&D Systems, Cat. No. DY318-05), TNF (R&D Systems, Cat No. DY210-05) and IL-8 (BD Bioscience, Cat. No. 555244) were measured in cell-free culture supernatants of THP-1 cells and MDMs according to the manufacturer's protocol.

To analyse protein levels of CXCL10 and IFNβ, THP-1 cells were seeded at $1.5x10^5$ cells per well into a 96-well plate (flat bottom) after 48 hrs after Dox addition. 24 hrs later, culture supernatants were collected to perform CXCL10/IP10 (Human CXCL10/IP-10 Quantikine ELISA Kit, Cat. No. DIP100, R&D Systems,) and IFNβ (VeriKine-HS Human IFN Beta Serum ELISA Kit, Cat.

No. 41415, PBL Bioscience) ELISAs following the manufacturer's recommendations.

Released IFNλ was measured following stimulation of the cGAS-STING pathway in THP-1 cells. Therefore, cells were cultured for 72 hrs in presence of Dox before being reseeded at $0.5x10^5$ cells/well into a 96-well plate (flat bottom). After 24 hrs stimulation with cGAS-STING pathway activators as described above (chapter 2.7.4), cell-free supernatants were collected to measure the IFNλ concentration using the IL-29/IL-28B ELISA (IFN-lamda 1/3) DuoSet ELISA, Cat. No. DY1598B, R&D Systems) according to the manufacturer's instructions.

To quantify the 2'3'-cGAMP concentration at baseline or following cGAS activation (chapter 2.7.4), $1x10^6$ or $0.5x10^6$ cells were lysed in 50 µl pre-cooled Thermo M-PER mammalian protein extraction reagent (Cat. No. 78503, Thermo Fisher Scientific), respectively. Lysis was performed for 10 min at 4 ºC with subsequent centrifugation for 15 min at top speed and 4 ºC. Samples were analysed using the 2'3'-cGAMP ELISA Kit (Cat. No. 501700, Cayman Chemical) following the manufacturer's instructions.

2.9 Time of flight inflammasome evaluation

To assess inflammasome activation, flow cytometry analysis by time of flight inflammasome evaluation (TOFIE) was performed (Sester et al., 2016, Sester et al., 2015). Throughout this study different ASC-expressing cell lines were used including HEK293T ASC-RFP cells (**Figure 4.5**), HEK293T ASC-BFP cells (**Figure 5.7**) and Flp-In 293 T-REx ASC-EGFP cells (**Figure 4.6** and **Figure 4.10**). All experiments were performed in technical duplicates. Cells were seeded into 24-well plates (500 µl medium/well) one day prior transfection or target gene induction to reach 70 % confluence on the day of the experiment. Transient transfection was performed with Lipofectamine 2000 transfection reagent (Life Technologies) and OptiMEM (Thermo Fisher Scientific) according to the manufacturer's instructions. Transfected DNA amounts were kept consistent between all wells in one experiment, using EV plasmid DNA. HEK293T ASC-RFP cells were transiently transfected with 50 ng of mCitrine-tagged pEF-BOS-

hNLRC4 WT, A160T, S171F, backbone alone (empty vector, EV) or 25 ng of each WT+A160T to mimic a heterozygous carrier. HEK293T ASC-BFP cells were transfected with 250 ng pcDNA3.1-3xHA-mNLRC4 WT or A160T plasmid DNA alone or co-transfected with pRP-mNAIP1-mCherry (kind gift from Rainer Stahl, AG Latz, Institute of Innate Immunity, University of Bonn) in absence or presence of pcDNA3.1-myc-PrgI (100 ng per construct).

In Flp-In 293 T-REx ASC-EGFP cell lines (generated in chapter 2.5.2), NLRC4 expression was induced by Dox treatment (1 µg/ml) for indicated times and inflammasome formation triggered by transient transfection of 250 ng pcDNA3.1-3xFLAG-hNAIP and pcDNA3.1-myc-PrgI. The c-FLAG pcDNA3.1 plasmid (kind gift from S. Smale, Addgene plasmid # 20011) (Sanjabi et al., 2005) was used as EV control for experiments performed in HEK293T ASC-BFP and Flp-In 293 T-REx ASC-EGFP cell lines. Flow cytometry using the FACSCanto (BD Bioscience) or LSRFortessa (BD Bioscience) to quantify ASC speck formation was performed 15 hrs to 27 hrs after transfection or Dox induction as indicated in the respective figure legends. Analysis was performed with FlowJo 10.7.1 software using the gating strategy shown in **Figure 2.3** (Sester et al., 2015).

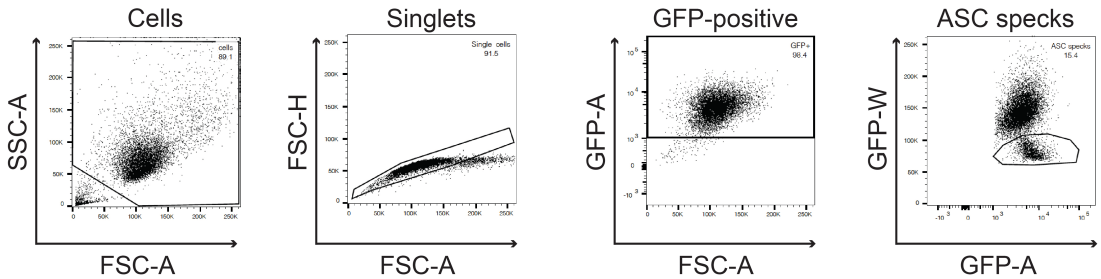

Figure 2.3 | Gating strategy for ASC speck quantification by flow cytometry. Representative FACS plots of Flp-In 293 T-REx ASC-EGFP cells expressing the autoactivating mutant NLRC4 S171F are shown following 27 hrs treatment with Dox (1 µg/ml). In this experiment, speck formation was quantified as percentage of the parental population (ASC-EGFP-positive cells) using the depicted gating strategy. Forward scatter, FSC; side scatter, SSC; area, A; height, H; width, W.

If a fluorescent-tagged plasmid was transfected, e.g. mCitrine-tagged pEF-BOS-hNLRC4 and pRP-mNAIP1-mCherry, only fluorescence-expressing cells were

included in the ASC speck analysis. In this case, gates were individually adjusted for the not mCitrine/mCherry-expressing control plasmids (EV) in these experiments.

2.10 Transient transfection of HEK293 and HEK293T cells for STING and COPA co-expression.

For overexpression studies, HEK293, HEK293T or HEK293T-STING-GFP cells were initially seeded at $2.5x10^5$ or $2x10^5$ cells/well in a 6-well plate format one day before transfection to allow cell attachment. Transient transfection of 0.5-1 µg total DNA was performed as stated in the figure or corresponding figure legend. Transient transfection of all plasmids including the pCMV6-Entry-COPA-myc-DDK plasmid (Origene, kind gift from A.Shum, Department of Medicine, University of California San Francisco) expressing COPA WT or mutants E241K and R233H (generated in chapter 2.4.1.2), pTRIP-CMV-GFP-FLAG-cGAS, pEF-BOS-mCitrine-STING and pEF-BOS-FLAG EV control (kindly provided by V.Hornung, LMU Munich), was performed using Lipofectamine 2000 transfection reagent (Life Technologies) following the manufacturer's instructions. If not stated otherwise, cells were routinely lysed for immunoblot analysis after 24 hrs incubation. Transfected DNA amounts were kept consistent between all wells in one experiment, using EV plasmid DNA.

2.11 Western blotting

To extract cytosolic proteins, $0.5–1x10^6$ cells were lysed in 1 % NP-40 buffer (**Table 6**) complemented with cOmplete^{TM} Protease Inhibitor Cocktail (Roche Biochemicals, Cat. No. 11697498001,) and 1 mM phenylmethylsulfonyl fluoride (PMSF, Carl Roth). After 30 min incubation on ice, the cell lysates were clarified by centrifugation for 15 min at 14000 x*g* and 4 °C. The cleared supernatant was mixed with 4x Laemmli buffer (**Table 6**).

To analyse cytosolic, nuclear, membrane-bound or phosphorylated proteins, cells were lysed in 1xRIPA buffer (**Table 6**) supplemented with cOmplete^{TM} Protease

Inhibitor Cocktail, 1 mM PMSF as well as phosphatase inhibitors (5 mM sodium fluoride (NaF), 10 mM sodium pyrophosphate (NaPPi), 1 mM sodium orthovanadate (Na_3VO_4)) and incubated for 30 min on ice. Using Pierce centrifuge columns (Thermo Fisher Scientific), protein lysates were purified of DNA and subsequently mixed with 4x Laemmli buffer.
Before loading onto SDS-PAGE gels, samples were incubated at 95 °C for 5 min. Size-based protein separation was achieved by use of 4-12 % SDS-PAGE gels (Novex) and MES-running buffer (Thermo Fisher Scientific) or self-made 12 % or 15 % SDS-PAGE gels and 1x SDS-PAGE running buffer (**Table 6**, **Table 12**). As molecular weight (MW) markers, Precision Plus Protein Kaleidoscope Prestained Protein Standard (Cat. No. 1610375, BioRad), Precision Plus Protein All Blue Prestained Protein Standard (Cat. No. 1610373, BioRad) or PageRuler Plus Prestained Protein Ladder (Cat. No. 26619, Thermo Fisher Scientific) were used.

Table 12 | Recipe for self-made SDS-PAGE gels.

	Stacking gel	Separation gel	
Reagent	5 %	12 %	15 %
H_2O	1.8 ml	3.375 ml	2.325 ml
Rotiphorese Gel 30 (Carl Roth)	0.45 ml	4.2 ml	5.25 ml
Stacking gel buffer (**Table 6**)	0.35 ml	–	–
Separation gel buffer (**Table 6**)	–	2.925 ml	2.925 ml
10 % APS	26.5 µl	117.75 µl	117.75 µl
TEMED (Merck)	2.65 µl	3.525 µl	3.525 µl

Proteins were then transferred onto a PVDF membrane (Immobilon®-P Transfer Membrane, Millipore) via wet transfer and blocked in 5 % skim milk/Tris-buffered saline (TBST) for 1 hr at RT. Membranes were probed with primary antibody diluted in 5 % skim milk/TBST or 5 % Bovine Serum Albumin (BSA)/TBST overnight at 4 °C. Used antibodies are listed in **Table 13**. On the next day, membranes were incubated with species-specific secondary antibodies for 1 hr at RT (1:10000, sheep-anti-mouse IgG-HRP (Cat. No. NXA931) or donkey-anti-rabbit IgG-HRP (Cat. No. NA934), GE Healthcare). For development, Immobilon Forte Western horseradish peroxidase (HRP) Substrate (Cat. No. WBLUF0500, Millipore) and the ChemiDoc Touch Imaging System (BioRad) were used.

Table 13 | List of antibodies, dilutions and dilution buffer used for immunoblot analysis.

Antibody	Cat. No.	Supplier	Dilution	Dilution buffer
anti-COPA clone H-3	sc-398099	Santa Cruz Biotechnology	1:1000	PBST/5 % skim milk
anti-COPD clone E-12	sc-515549	Santa Cruz Biotechnology	1:1000	PBST/5 % skim milk
anti-COPE clone A-4	sc-133195	Santa Cruz Biotechnology	1:1000	PBST/5 % skim milk
anti-COPG1 clone A-10	sc-393977	Santa Cruz Biotechnology	1:1000	PBST/5 % skim milk
anti-phospho-STAT1 Tyr701 clone 58D6	#9167	Cell Signaling Technology	1:1000	TBST/3 % BSA
anti-phospho-TBK1 Ser172 clone D52C2	#5483	Cell Signaling Technology	1:1000	TBST/3 % BSA
anti-phospho-IRF3 Ser386	ab76493	Abcam	1:500	TBST/3 % BSA
anti-STING clone D2P2F	#13647	Cell Signaling Technology	1:1000	TBST/5 % skim milk
anti-STAT1 clone D1K9Y	#14994	Cell Signaling Technology	1:1000	TBST/5 % skim milk
anti-TBK1/NAK	#3013	Cell Signaling Technology	1:1000	TBST/5 % skim milk
anti-cGAS, D1D3G	#15102	Cell Signaling Technology	1:1000	TBST/3 % BSA
anti-GFP	#A-11122	Life Technologies	1:1000	TBST/5 % skim milk
Anti-iNOS/NOS type II	#610329	BD Bioscience	1:1000	PBST/5 % skim milk
anti-Actin-HRP clone C4,	sc-47778	Santa Cruz Biotechnology	1:1000	PBST/5 % skim milk
anti-NLRC4 (D5Y8E)	#12421	Cell Signaling Technology	1:1000	TBST/3 % BSA
anti-FLAG M2-peroxidase (HRP) antibody	A8592	Sigma-Aldrich	1:5000	PBST/5 % skim milk
anti-HA tag clone GT423	SAB2702196	Sigma-Aldrich	1:1000	PBST/5 % skim milk

2.12 RNA isolation and quantitative Real-Time PCR

For all experiments in chapter 3, RNA was isolated using the ISOLATE II RNA Mini Kit (Cat. No. BIO-52073, Bioline) following the manufacturer's guidelines. The Superscript III Reverse Transcriptase (Cat. No. 18080085, Life Technologies) and oligo (dT) 15 primer (Cat. No. C110B-C, Promega) were used to reverse transcribe 1 µg of total RNA. Quantitative Real-Time PCR (qRT-PCR) was performed using 2x SYBR Green/ROX qPCR Master Mix (Cat. No. K0253, Thermo Fisher Scientific) and the ViiA 7 Real-time PCR system (Thermo Fisher Scientific).

The analysis of relative hNLRC4 mRNA transcript levels in monoclonal THP-1 cell lines in chapter 4.2.3.2 was performed by lysis of cells with RLT lysis buffer (Cat. No. 158904, Qiagen). RNA was isolated using EconoSpin columns (Cat. No. 1920-250, Epoche Life Science) with on-column DNA digest (DNaseI, Cat. No. EN0521, Thermo Fisher Scientic) following the manufacturer's instructions. Depending on the experiment, 300 to 500 ng RNA was reverse transcribed into cDNA using the ReverseAid Transcriptase (Cat. No. EP0442, Thermo Fisher Scientific,) according to the manufacturer's recommendations. Subsequently qRT-PCR analysis was performed using my-Budget 5x Eva Green QPCR-Mix II (Cat. No. 80-5800200, Bio-Budget Technologies GmbH) and the ViiA 7 Real-time PCR system (Thermo Fisher Scientific).qRT-PCR Primers used in this thesis are listed in **Table 5.** Samples were run in duplicates, normalized to housekeeper gene *ACTIN* and analysed using the ΔΔCt method. Data are presented as fold change relative to vehicle control or parental cell line as indicated in the figure.

2.13 Immunofluorescence microscopy

Glass coverslips (18 mm x 18 mm, thickness 1½, Zeiss) were sterilised in 80 % ethanol, 2x washed in PBS and placed in 6-well plates. After 72 hrs of Dox treatment, HeLa cells were seeded at $3x10^5$ cells/well in 2 ml complete growth medium and left to attach for 4-6 hrs. Following treatment with HT-DNA (2 µg/ml, transfected) for 2 hrs, cells were washed in 1xPBS and fixed in 2 ml ice cold

methanol for 15 min at -20°C when stained for endogenous STING. Staining for ER (KDEL) and Golgi (GM130) integrity was performed after fixation with 4 % paraformaldehyde for 15 min at RT (Cat. No. 15710, Electron Microscopy Sciences). The cells were thoroughly washed 3x in 1xPBS and blocked (5 % normal goat serum, 0.3 % Triton X-100, 1xPBS) for 1 hr at RT. Primary antibodies were diluted in antibody dilution buffer (1 % BSA, 0.3 % Triton X-100, 1xPBS) and incubated overnight at 4°C in a wet chamber using the following dilutions: anti-COPA (1:100, Santa Cruz Biotechnology, clone H-3, Cat. No. sc-398099), anti-COPG (1:100, Cat. No. 12393-I-AP, ProteinTech), anti-COPD (1:100, Cat. No. GTX630562, GeneTex), anti-GM130-AF647 (1:500, Cat. No. ab195303, Abcam), anti-STING (1:100, Cell Signaling Technology, clone D2P2F, Cat. No. #13647), anti-KDEL (1:200, clone 10C3, Cat. No. ab12223, Abcam (**Figure 3.5 C**) and anti-KDEL-AF568 (1:500, Cat. No. ab203421, Abcam (**Figure 3.9 A**). After 3 washes with 1xPBS, secondary antibodies (anti-rabbit-AF647, anti-mouse-AF488 (BD Biosciences)) were diluted (1:1000) in antibody diluent and incubated for 1 hr at RT in the dark. Considering the host species of antibodies used for co-staining experiments, sequential or simultaneous staining was performed. Cover slips were washed 3x in 1xPBS and mounted onto microscopy slides using Fluoromount-G with DAPI (Cat. No. 00-4959-52, Thermo Fisher Scientific). Z-stack images were acquired using the Leica SP8 Microscope (**Figure 3.5** and **Suppl. Figure 2**), the Zeiss 880 Airyscan Microscope (**Figure 3.4 F**) or the OMX-SR system (GE Healthcare) using immersion oil with an index of refraction of 1.518 and an Olympus PlanApo oil immersion objective lens with 60x/1.42 NA (**Figure 3.9 A**). Microscopical images were analysed with Fiji software version 2.1.0 and are presented as maximum intensity projections. Quantification analysis (**Figure 3.9 A**) was performed using Fiji software by creation of surface for KDEL and GM130 and subsequent calculation of spatial overlay resulting in the percentage of KDEL signal inside the Golgi.

2.14 Mass spectrometry

2.14.1 Immunoprecipitation of mCitrine-STING for quantitative proteomics analysis by mass spectrometry

This experiment was performed by Dr. Dominic De Nardo (Inflammation Division, WEHI, Melbourne, Australia). Immunoprecipitation (IP) experiments were performed as previously described (De Nardo et al., 2018b). Briefly, $3x10^6$ HEK293T cells were seeded in 10 cm culture dishes. The following morning cells were transiently transfected with 10 µg of either pEF-BOS EV control or pEF-BOS-mCitrine-hSTING plasmid DNA, performed in triplicates. After 48 hrs cells were lysed in 750 µl 1 % NP-40 buffer supplemented with 10 mM NaPPi, 5 mM NaF, 1 mM Na_3VO_4, 1 mM PMSF and 1x cOmplete™ Protease Inhibitor Cocktail (Cat. No. 11697498001, Roche Biochemicals). Whole cell lysates were clarified by centrifugation at 17000 x*g* for 10 min at 4 °C. For each IP sample, 1 µg of mouse IgG2A monoclonal GFP antibody (Thermo Fisher Scientific, [E36] A-11120) was crosslinked to 50 µl of Protein A Dynabeads® (Thermo Fisher Scientific, 10002D) using 5 mM BS^3 (Thermo Fisher Scientific) and incubated for 30 min at RT. The crosslinking reaction was quenched by adding 1 M Tris-HCl [pH 7.4]. Antibody-crosslinked Protein A Dynabeads® were thoroughly washed before 50 µl was then added to each IP sample and incubated on a rotator at 4 °C for 2 hrs. Beads were then washed 4x with 1 % NP-40 buffer using a DynaMag-2 magnetic holder (Thermo Fisher Scientific) before proteins were eluted with 0.5 % SDS in PBS. Further sample preparation and mass spectrometry (MS) analysis was performed by Dr. Laura Dagley from the Advanced Technology and Biology Division at WEHI (Melbourne, Australia). Eluted protein material was subjected to trypsin digestion using the FASP method as previously described (Delconte et al., 2016, Kedzierski et al., 2017, Wisniewski et al., 2009). Peptides were lyophilised using CentriVap (Labconco) prior to reconstitution in 60 µl 0.1 % formic acid/2 % acetonitrile. Peptide mixtures (2 µl) were separated by reverse-phase chromatography on a C18 fused silica column (I.D. 75 µm, O.D. 360 µm x 25 cm length) packed into an emitter tip (IonOpticks),

using nano-flow high-performance liquid chromatography (HPLC) (M-class, Waters). The HPLC was coupled to an Impact II UHR-QqTOF mass spectrometer (Bruker) using a CaptiveSpray source and nanoBooster at 0.20 Bar using acetonitrile. Peptides were loaded directly onto the column at a constant flow rate of 400 nl/min with 0.1 % formic acid in MilliQ water and eluted with a 90 min linear gradient from 2 to 34 % buffer B (99.9 % acetonitrile and 0.1 % formic acid). Mass spectra were acquired in a data-dependent manner including an automatic switch between MS and MS/MS scans using a 1.5 second duty cycle and 4 Hz MS1 spectra rate, followed by MS/MS scans at 8-20 Hz dependent on precursor intensity for the remainder of the cycle. MS spectra were acquired between a mass range of 200–2000 m/z. Peptide fragmentation was performed using collision-induced dissociation. Raw files consisting of high-resolution MS/MS spectra were processed with MaxQuant (version 1.6.6.0) for feature detection and protein identification using the Andromeda search engine (Cox et al., 2011) as previously described (Rautela et al., 2019). Extracted peak lists were searched against the reviewed *H. sapiens* (UniProt, March 2019) database as well as a separate reverse decoy database to empirically assess the false discovery rate (FDR) using strict trypsin specificity, allowing up to 2 missed cleavages. LFQ quantification was selected, with a minimum ratio count of 2. PSM and protein identifications were filtered using a target-decoy approach at an FDR of 1 %. Only unique and razor peptides were considered for quantification with intensity values present in at least 2 out of 3 replicates per group.

Statistical analyses were performed using LFQAnalyst (Shah et al., 2020) (https://bioinformatics.erc.monash.edu/apps/LFQ-Analyst/) whereby the LFQ intensity values were used for protein quantification. Missing values were replaced by values drawn from a normal distribution of 1.8 standard deviations and a width of 0.3 for each sample (Perseus-type). Protein-wise linear models combined with empirical Bayes statistics were used for differential expression analysis using Bioconductor package Limma whereby the adjusted *P*-value cutoff was set at 0.05 and log2 fold change cutoff set at 1. The Benjamini-Hochberg (BH) method of FDR correction was used. The MS proteomics data have been

deposited to the ProteomeXchange Consortium via the PRIDE partner repository (Perez-Riverol et al., 2019) with the dataset identifier PXD023135.

2.14.2 Mass spectrometry of recombinant *Sf*9 cell protein

Finger print mass spectrometry was performed to investigate PTMs on residue A160 or T160 in recombinant WT and mutant hNLRC4 protein truncations purified from *Sf*9 cells. Therefore, recombinant hNLRC4 WT and A160T ΔCARD and ΔCARD/ΔLoop protein produced in *Sf*9 cells (chapter 5.2.4) was separated by SDS-PAGE (chapter 2.16.13) and gels stained with freshly prepared Coomassie staining solution (**Table 6**). Bands representing recombinant protein were cut and submitted to the analytical mass spectrometry facility at the Georg-August-Universität Göttingen/Max Planck Institute for Biophysical Chemistry in collaboration with Monika Raabe, Annika Reinelt and Prof. Henning Urlaub. Protein samples were processed as described by Shevchenko et al. (Shevchenko et al., 1996). Peptides were then analysed by nano-HPLC coupled with Q-Exactive HF mass spectrometer (Thermo Fisher Scientific) using a linear gradient (5–90% buffer B (80% acetonitrile and 0.08% formic acid)) at a flow rate of 300 nl/min over a total gradient time of 58 min. The MS data were aquired by scanning the precursors in mass range from 350 to 1600 m/z at a resolution of 60000 at m/z 200. Top 20 precursor ions were chosen for MS2 by using data-dependent acquisition (DDA) mode at a resolution of 15000 at m/z 200 with maximum IT of 50 ms. Data analysis and search was performed against the amino acid sequence of recombinant protein truncations (WT (Uniprot:Q9NPP4) and mutant hNLRC4) using MaxQuant Software (1.6.5.0) and Scaffold (5.0.0.).

2.15 Statistical analysis

Unless otherwise stated in the figure legends, data are presented as mean of independent biological replicates ± SEM (standard error of the mean). Using GraphPad Prism 8 software, statistical comparison was made either by unpaired

Student's t-test, ratio paired Student's t-test, one-way or two-way ANOVA with subsequent multiple comparison testing as stated in the figure legends. *P*-values are indicated by numbers or as * $P<0.05$, ** $P<0.01$, *** $P<0.001$, **** $P<0.0001$.

2.16 Biochemical, biophysical and structural biology methods

2.16.1 Transformation and isolation of bacmid DNA

Baculovirus shuttle vectors (bacmids) are large plasmids encoding the baculovirus genome and serve as a rapid and efficient tool for the generation of recombinant baculovirus for large scale protein expression in insect cells. The main components of this expression system include the bacterial host strain *E. coli* DH10 MultiBac^{Turbo}, containing an improved baculovirus genome engineered to reduce virus-dependent cell lysis and maintain integrity of cellular compartments during protein production. Using electroporation (1700V, 1 pulse, Eporator Eppendorf) or heat shock (42 °C, 42 seconds) 25-50 µl of electrocompetent or chemically competent DH10 MultiBac^{Turbo} cells were transformed with 100 ng of the acceptor plasmid (pACEBac1) encoding the gene of interest under a polyhedrin (polh) promoter flanked by DNA elements required for Tn7 transposition (Tn7L, Tn7R) and a gentamicin resistance gene. DH10 MultiBac^{Turbo} cells additionally contain a helper plasmid encoding the Tn7 transposase that mediates transposition of the gene of interest from the pACEBac1 vector to the bacmid-encoded mini Tn7 attachment site which leads to the generation of the recombinant bacmid (Leusch et al., 1995, Mehalko et al., 2016). Transformed cells were recovered by incubation at 37 °C for 2-3 hrs after addition of 800 µl antibiotic-free LB medium. Subsequently, cells were plated on agar plates containing ampicillin (100 µg/ml, Sigma-Aldrich), kanamycin (50 µg/ml), tetracycline (10 µg/ml, Sigma-Aldrich), gentamycin (10 µg/ml, Sigma-Aldrich) as well as isopropyl-β-D-thiogalacto-pyranoside (IPTG, 40 µg/ml, Carl Roth) and BluoGal (100 µg/ml, Cat. No. B2904, Sigma-Aldrich) and incubated at 37 °C for 1-2 days. Colonies containing bacmid with the successfully integrated gene of interest are identified by blue-white screening, as Tn7 transposition

disrupts the LacZα subunit-coding sequence. LacZ encodes the enzyme β-galactosidase, which hydrolyses its substrate BluoGal resulting in formation of blue-coloured colonies after LacZ induction by IPTG. Consequently, bacterial clones carrying the inserted DNA appeared white.

White colonies were picked and incubated overnight in 4 ml LB medium (supplemented with ampicillin, tetracycline, kanamycin, gentamycin at the concentrations mentioned above) in a shaking incubator at 37 °C. Due to the large size, bacmid DNA was purified by isopropanol precipitation rather than using DNA-binding columns to avoid shear degradation. Therefore, bacteria were harvested and lysed using resuspension, lysis and neutralization buffers from the ExtractMe Plasmid Mini Kit (Cat. No. EM01.1, Blirt) following the manufacturer's instructions. Lysates were cleared by two subsequent centrifugation steps at 14000 rpm at 4 °C for 5 min. Supernatants were then transferred into a new tube containing 800 µl cold isopropanol (-20 °C) and centrifuged for 30 min at 14000 rpm and 4 °C. After two wash steps in 750 µl 70 % ethanol (-20 °C) and centrifugation for 10 min at 14000 rpm and 4 °C, pellets were dried at RT and resuspended in 20 µl nuclease-free water. Bacmid DNA was stored at 4 °C or immediately used for transfection of *Sf*9 cells.

2.16.2 *Sf*9 cell culture

*Sf*9 insect cells are derived from *Spodoptera frugiperda* pupal ovarian tissue and a widely used cell line for insect cell-based recombinant protein expression. As a significant advantage over bacterial- and yeast-based expression systems, insect cells possess some of the PTM pathways described for mammalian cells (N- and O-linked glycosylation, phosphorylation, acylation, palmitoylation) and are capable to assemble multisubunit protein complexes (Berger et al., 2004, de Carvalho et al., 1996, Klenk 1996, van Oers et al., 2015). Therefore, insect cells offer a large scale and high yield expression systems to produce recombinant protein with mammalian-like PTMs providing increased immunogenic similarity and functionality to mammalian proteins (van Oers et al., 2015). Although especially with regard to large scale manufacturing *Sf*9 cells offer many

advantages over mammalian expression systems (lower cost, less energy consumption, higher yield, lower safety requirements), however, crucial species-specific differences persist and limit the ability to produce authentic human recombinant protein using insect cell lines. Limitations include availability of required co-factors, or some specialized PTMs that can alter protein function and folding, which might be more or less relevant depending on the protein of interest and the research question investigated and therefore need to be considered individually (van Oers et al., 2015).

*Sf*9 cells were cultured in serum-free Sf-900™ SFM III culture medium (Cat. No. 12658019, Thermo Fisher Scientific) using reusable Erlenmeyer glass flasks in a shaking incubator at 27 °C and 80 rpm. In contrast to mammalian cell lines, no CO_2 supplementation is required and cells were cultured in antibiotic-free conditions. Cells were sub-cultured every three days and maintained at densities between 0.3– 5x10^6 cells/ml. Cell numbers, size and viability were monitored using an automatic cell counter (EVE™, NanoEnTek Inc) analysing 10 ul cell suspension after mixing with 0.4 % trypan blue staining solution (Cat. No. 15250061, Gibco, Thermo Fisher Scientific). Viability between 90-99 % and cell size of 10-12 µm was normally observed for healthy uninfected cells, whereas baculovirus-infected cells were larger (13-15 µm) and often showed reduced viability (60-80 %).

2.16.3 Transfection of *Sf*9 cells

*Sf*9 cells are naturally susceptible to baculovirus infections. Therefore, bacmid DNA containing the gene of interest was generated (chapter 2.16.1) and used to produce recombinant baculovirus as delivery system for heterologous recombinant protein expression in *Sf*9 cells. 0.35x10^6 *Sf*9 cells/ml were seeded into 6-well plates (2 ml/well) and incubated for 30 min at 27 °C (without shaking) to allow attachment. The transfection mix containing 1 µg purified bacmid DNA, 5 µl TransIT-LT1 transfection reagent (Cat. No. MIR2304, Mirus Bio) in 190 µl *Sf*9 cell culture medium was incubated for 20 min at RT and then transferred onto cells. After 72 hrs to 96 hrs incubation at 27 °C (without shaking), virus-containing

supernatant (termed V_0) was harvested, filtered (0.45 µm) to remove residual cell debris and directly used for further virus amplification (chapter 2.16.4) or stored at 4 °C.

2.16.4 Amplification of baculovirus (V_1 and V_2) in *Sf*9 cells

To generate high baculovirus titer for efficient infection of *Sf*9 cells and large-scale protein production, 2 ml of V_0 were used to infect 15 ml *Sf*9 cells seeded at a density of 0.6×10^6 cells/ml in an Erlenmeyer glass flask. Cells were cultured in suspension for 3 consecutive days and harvested by centrifugation at 2000 rpm for 5 min. Cleared supernatant (V_1) was filtered (0.45 µm) and stored at 4 °C or directly used to continue virus amplification. In a second step, 1 % (v/v) of V_1 was used to infect 50 ml *Sf*9 cells at a density of 1×10^6 cells/ml and incubated for 4 days in a shaking incubator at 27 °C and 80 rpm. Virus-containing supernatant was harvested as previously described and yielded the viral stock V_2, that was used to infect cells for protein expression (chapter 2.16.5). V_2 was stored at 4°C for a maximum of 5 days.

2.16.5 Protein expression in *Sf*9 cells

The protein expression and purification conditions used in this study were adapted from Hu et al. (Hu et al., 2013). 0.5 to 2 liters *Sf*9 cell culture volume were used at a cell density of 2.5×10^6 cells/ml, infected with 1 % (v/v) of V_2 and incubated in a shaking incubator at 27 °C for 48 hrs. Upon harvest, cell viability was typically reduced to 70 % viable cells and cell size was increased to 13-14 µm. The cell suspension was centrifuged for 20 min at 2000 rpm and 10 °C (Avanti J-26S XP centrifuge, Beckman Coulter) and the supernatant discarded. The pellet was washed in 1x PBS, transferred into a 50 ml Falcon tube, centrifuged for 20 min at 2000 rpm and 4 °C and snap-frozen in liquid nitrogen for storage at -80 °C or directly lysed for subsequent protein purification (chapter 2.16.6).

2.16.6 *Sf*9 cell lysis and sonication

All steps of the purification process were performed on ice and using pre-cooled equipment and solutions. *Sf*9 cell pellets were resuspended in 3-5 ml cold lysis buffer (**Table 6**; supplemented with 1 mM PMSF, 1 µg/ml DNase) per 1 g of *Sf*9 cell pellet and incubated on a magnetic stirrer at 4 °C until completely resuspended. Subsequently, cells were lysed by sonication on ice (amplitude 30 %, 5 min alternating between 5 sec pulse and 5 sec pause) and lysates cleared by centrifugation at 25000 rpm for 45 min at 10 °C (Avanti J-26S XP centrifuge, JA 25.50 rotor, Beckman Coulter). The cleared supernatant was filtered (0.45 µm) to remove residual cellular debris and used for subsequent affinity chromatography purification (see 2.16.7). 10 µl samples of supernatant and pellet were taken for analysis by SDS-PAGE and Coomassie staining.

2.16.7 Affinity chromatography

To separate the protein of interest from other proteins, nucleic acids and metabolites present in the whole cell lysate, it was expressed as fusion protein tagged with a N-terminal 6xHistidine (6xHis)-affinity tag. Gravity-flow affinity chromatography using HisPur™ Ni-NTA Resin (Cat. No. 88222, Thermo Fisher Scientific) was performed to specifically enrich His-tagged proteins on an immobilized resin, while unspecific binders were washed away during subsequent wash steps. In detail, clarified lysates were mixed with lysis-buffer-equilibrated HisPur™ Ni-NTA Resin and incubated for 1-2 hrs at 4 °C on a tube roller. Subsequently, the mixture was applied to an empty gravity-flow column and flow-through collected. The resin was washed 3x with at least two resin-bed volumes of wash buffer (**Table 6**). The His-tagged protein was eluted in 4 consecutive elution steps using 2 resin-bed volumes of elution buffer with 3 min incubation. Flow-through, wash and elution fractions were collected and a 10 µl sample analysed by SDS-PAGE. All elution fractions were pooled and concentrated before proteolytic cleavage of the affinity tag was performed (chapter 2.16.10).

2.16.8 Concentration of recombinant protein

Amicon Ultra Centrifugal Filter Units (Merck Millipore) were used to increase the protein concentration by centrifugation-mediated ultrafiltration. Depending on the MW of the recombinant protein, a filter unit with smaller pore size was selected, which allowed smaller proteins and buffer to pass through the membrane during centrifugation, but retained larger proteins, including the protein of interest. Centrifugation at 4 °C and 4000 rpm was performed until protein concentration or the volume required for downstream applications were reached.

2.16.9 Measurement of protein concentration

Protein concentrations were determined by measurement of absorbance at 280 nm using a NanoDrop spectrophotometer (Thermo Fisher Scientific) under consideration of MW and extinction coefficient of the protein of interest. Both parameters were determined using the Expasy ProtParam tool (https://web.expasy.org/protparam/) based on the amino acid sequence of the recombinant protein. Absorbance at 260 nm was monitored as a measure for nucleic acid contamination.

2.16.10 Tobacco Etch Virus protease digestion

Although affinity tags are valuable tools during protein expression and purification, they may influence functionality and behaviour of the purified recombinant protein in downstream applications. Therefore, a Tobacco Etch Virus (TEV) protease cleavage site (amino acid sequence: ENLYFQGS (Nam et al., 2020)) was engineered between the N-terminal 6xHis-SUMO-tag or 6xHis-GFP-tag and the protein of interest. Self-made TEV protease was used at 1 mg/100 mg protein solution and incubated overnight at 4 °C. TEV cleavage was performed after Ni-NTA affinity chromatography while the protein was dissolved in affinity chromatography elution buffer (**Table 6**).

2.16.11 Anion exchange chromatography

During ion exchange chromatography, proteins are separated based on differences in net surface charge and subsequent reversible binding to the oppositely charged column resin, which is determined by the protein-specific isoelectric point (pI) and the pH of the surrounding buffer. Here, anion exchange chromatography (AIEX) was performed using the HiTrap QXL column (5 ml, GE Healthcare) attached to a fast protein liquid chromatography (FPLC) Äkta Pure system (GE Healthcare) with buffers A (no salt) and B (high salt) listed in **Table 6.** The column was equilibrated using both buffers before the first run. Prior to sample loading, protein was concentrated to a maximal volume of 500 µl and subsequently diluted with 4.5 ml AIEX buffer A. The diluted protein sample (5 ml) was then loaded onto the column via capillary loop injection using the 5 ml loop. AIEX was performed in two steps at a flow rate of 2 ml/min: initial 16 column volumes (CV) linear elution gradient with 0-50 % of high salt buffer B addition, followed by 50-100 % buffer B addition over 4 CV. Elution fractions were collected in 2 ml fractions and subsequently analysed by SDS-PAGE (10 µl sample per fraction). AIEX was routinely performed to purify mNLRC4 truncations prior to SEC (chapter 5.2.3). Due to yield limitations, AIEX was not part of the standard purification protocol to purify recombinant hNLRC4 (chapter 5.2.4).

2.16.12 Size exclusion chromatography

Size exclusion chromatography (SEC) was performed to separate the purified recombinant protein according to size following affinity chromatography, TEV digest (for hNLRC4) or subsequent of AIEX (for mNLRC4). Methodically, the protein sample is applied to a column containing a porous matrix. Proteins larger than the beads elute first, as they are unable to diffuse into pores, whereas smaller proteins penetrate the pores to varying degrees based on their size, which results in a size-specific elution profile. This separation method is solely based on the size of the molecules and does not require binding or interaction with the column matrix. The concentrated protein solution was loaded onto a

Superdex (SD) 200 column of different sizes (Cytiva, column sizes: 10/300 Increase or 16/600 pg HiLoad) connected to an FPLC Äkta Pure System (GE Healthcare). The column was equilibrated with 1.2 CV of SEC buffer (**Table 6**). Depending on the column format, the protein sample was applied using a 500 µl or 5 ml loop connected to the FPLC system performing an isocratic elution over 1.2 CV. Elution fractions were collected in volumes between 0.1-2 ml, samples (10 µl) of which were subsequently analysed by SDS-PAGE based on the recorded elution profile.

Fractions containing the protein of interest at high purity were pooled, concentrated as described earlier (chapter 2.16.8) and snap-frozen in liquid nitrogen before stored at -80°C.

2.16.13 SDS-PAGE and Coomassie blue staining

Sodium dodecyl sulphate-polyacrylamide gel electrophoresis (SDS-PAGE) was performed to separate purified proteins according to MW and monitor samples for purity along all steps of protein purification. In this procedure, proteins are denatured by addition of SDS-containing Laemmli buffer (**Table 6**) and a subsequent boiling step (95 °C, 5 min). Samples were loaded onto self-made 12 % or 15 % SDS-PAGE gels and electrophoresis performed using constant current at 40 milliampere (mA). Subsequently, SDS-PAGE gels were covered in Coomassie staining solution (**Table 6**) and brought to boil in a microwave, followed by 10 to 20 min incubation on a shaking incubator. Afterwards, the solution was exchanged to destain solution (**Table 6**), repeatedly brought to boil and incubated for 10-20 min until protein bands were clearly visible. Gels were documented using the ChemiDoc Touch Imaging System (BioRad).

2.16.14 Protein crystallization

Protein crystallization screens were setup using purified recombinant hNLRC4$^{\Delta CARD}$ and hNLRC4$^{\Delta CARD/\Delta Loop}$ of WT and A160T mutant protein at concentrations ranging between 3-5 mg/ml in SEC buffer containing 20 mM HEPES, 100 mM NaCl, 1 mM ADP, 10 mM $MgCl_2$, 0.5 mM TCEP (pH 8.0) (**Table 6**). Several Molecular Dimensions crystallization screens including Morpheus (Cat. No. MD1-46), PACT Premier™ (Cat. No. MD1-29), ProPlex™ (Cat. No. MD1.38) and JCSG Plus™ (Cat. No. MD1-37) were setup using equal amounts of well solution and protein (0.1-0.2 nl) by hanging-drop vapor-diffusion method at different temperatures (4 °C, 10 °C, 15 °C, 20 °C). For setup, MRC2 well polystyrene crystallization plates (Cat. No. CPL-153L, Jena Bioscience) were pipetted manually or using the Crystal Gryphon LCP pipetting robot (Art Robbins Instruments). Crystal formation was monitored using the Formulatrix RI-1000. Potentially promising protein crystals were picked, cryopreserved and analysed at a synchroton radiation source.

2.16.15 Thermal shift assays

Nano differential scanning fluorimetry (NanoDSF) determines protein stability by measuring fluorescence of intrinsic aromatic amino acid residue tryptophan at 350 nm and 330 nm during thermal protein unfolding events (Alexander et al., 2014). Under native conditions, tryptophan residues are packed inside the hydrophobic core of the protein, however increasing temperature progressively induces protein denaturation and exposes tryptophane residues to the surface. The fluorescence signal intensity at both wavelengths is recorded and used to calculate the 350 nm/330 nm ratio. Mathematical transformation into the first derivative of the ratio curve reveals the maximal point of the curve, which indicates the melting Temperature Tm (inflection point) of the protein under the tested conditions. NanoDSF measurements in this thesis were performed using the using the Prometheus NT.48 nanoDSF device and PR.ThermControl software (NanoTemper Technologies).

2.16.15.1 Thermal stability in presence of ADP/ATP

To identify a potential effect of the hNLRC4 A160T mutation on protein folding and thermal stability, nanoDSF measurements were performed.
Recombinant hNLRC4$^{\Delta CARD}$ and hNLRC4$^{\Delta CARD/\Delta Loop}$ truncations were purified as described above and stored at -80 °C in SEC buffer (containing 1 mM ADP, **Table 6**). Prior to the experiment, proteins were thawed on ice. To remove excess ADP, which was supplemented during the purification process, a buffer exchange to 20 mM HEPES, 100 mM NaCl, 10 mM $MgCl_2$, 0.5 mM TCEP (pH 8.0) was performed using ZeBa spin desalting columns (7K MWCO, Cat. No. 89882, Thermo Fisher Scientific) according to the manufacturer's instructions. Thermal stability of recombinant protein (10 µM) was assessed at baseline and in presence of 500x molar excess of ADP or ATP (5 mM, Sigma-Aldrich) after 30 min incubation at RT. 10 ul protein sample was loaded per capillary (Prometheus NT.48 Capillaries, Cat. No. PR-C002, NanoTemper) and thermal unfolding was induced using a gradual temperature ramp ranging from 20–95 °C (1.5 °C/min). Fluorescence emission was measured at 350 nm and 330 nm and analysed using the PR.ThermControl Software (NanoTemper). Data are presented as emission ratio [Em_{350nm}/Em_{330nm}] and first derivative thereof. Different batches of recombinant protein were used for replicate experiments.

2.16.15.2 Buffer screen

To identify optimal buffer conditions for purification of hNLRC4, conformational stability of WT hNLRC4$^{\Delta CARD}$ and hNLRC4$^{\Delta CARD/\Delta Loop}$ was assessed by nanoDSF measurements in presence of different buffers and additives. Therefore, 0.5 µl protein (10 µM) was incubated with 9.5 µl buffer/additive for 30 min at RT and analysed using a 20–95 °C temperature ramp (1.5 °C/min). Different NaCl concentrations (50 mM, 100 mM, 150 mM, 200 mM, 300 mM, 500 mM) and the following buffers (at different pH) and additives were tested and compared to protein-specific Tm when dissolved in standard SEC buffer (**Table 6**): 1x PBS (pH 6.0, 6.5, 7.0, 7.5, 8.0), 50 mM MOPS (pH 6.5, 7.0, 7.5, 8.0), 50 mM MES (pH

6.0, 6.5), 50 mM HEPES (pH 7.0, 7.5, 8.0), 50 mM Citrate (pH 4, 6, 6.5), 50 mM Tris-HCl (pH 7.0, 7.5, 8.0, 9.0), 50 mM CAPS (pH 10.0), 50 mM Acetate (pH 5.0), 50 mM glycine (pH 3.0), 1 % CHAPS, 1 % NP-40, 0.1 % Triton-X-100, 5 % and 10 % glycerol, 50 % glucose, 200 mM $CaCl_2$, 50 mM $ZnCl_2$, 1 M $LiSO_4$, 100 mM $CuSO_4$, 100 mM $NiSO_4$, 100 mM $MgCl_2$, 50 mM EDTA, 0.5 M L-Arginine.

2.17 Phylogenetic analysis

A Clustal W alignment of NLRC4 amino acid sequences from selected species was performed to construct a phylogenetic tree comparing 1058 aa positions using the Maximum Likelihood method and the JTT matrix-based model (Jones et al., 1992) with bootstrap analysis (100 repeats). Sequence alignment and phylogenetic tree construction were performed using the MegaX software (version 10.2.6) (Felsenstein 1985, Kumar et al., 2018, Stecher et al., 2020).
The following Uniprot database accession numbers were used for the Clustal W alignment: *M. musculus* (mouse: Q3UP24), *H. sapiens* (human: Q9NPP4), *R. norvegicus* (rat: F1M649), *B. taurus* (cattle: F1MHT9), *X. tropicalis* (western clawed frog: F6R2G2), *P. troglodytes* (chimpanzee: A0A2J8L1X5), *F. catus* (cat: M3W537), *O. aries* (sheep: W5PLT9), *M. mulatta* (rhesus macaque: F7DWV6), *G. gorilla* (gorilla: G3QJV1), *P. anubis* (olive baboon): A0A096NWZ9, *M. lucifugus* (little brown bat): G1PV27, *E. caballus* (horse: F7CBZ7), *C. hircu*s (goat: A0A452EBW5), *D. leucas* (beluga whale: A0A2Y9N554).

3 Aberrant STING signalling causes innate immune system activation in COPA syndrome

3.1 Introduction

3.1.1 COPA syndrome

COPA syndrome is a recently discovered novel rare Mendelian monogenic disease presenting with features of autoinflammation and autoimmunity (Watkin et al., 2015), which was classified as autoinflammatory disorder by the International Union of Immunological Societies (Bousfiha et al., 2018). Using an alternative terminology, it is also known as Autoimmune Interstitial Lung, Joint and Kidney disease (AIKLJK) (Patwardhan et al., 2019).

Since the first description of COPA syndrome in 2015, 25 families have been reported worldwide **(Suppl. Table 1)** (Watkin et al., 2015, Boulisfane-El Khalifi et al., 2019, Fremond et al., 2020, Guan et al., 2021, Jensson et al., 2017, Kato et al., 2021, Krutzke et al., 2019, Mallea et al., 2020, Noorelahi et al., 2018, Taveira-DaSilva et al., 2019, Thaivalappil et al., 2021, Volpi et al., 2018, Lepelley et al., 2020, Patwardhan et al., 2019, Prenzel et al., 2020, Psarianos et al., 2021).

The coatomer alpha subunit (COPA) is encoded on chromosome 1 location 1q23.2 (Chow et al., 1996). Interestingly, across all known COPA syndrome patients, a total of only 14 LoF missense mutations have been identified, almost all within exon 8 and 9 of the *COPA* gene, which translates into a highly conserved 14 amino acid stretch (aa 230-243) (**Figure 3.1 A, B**). Two recent case reports described the first mutations outside this region, H199R, which maps to exon 7, and R281W in exon 9, adjacent to the previously identified mutation hotspot (Guan et al., 2021, Prenzel et al., 2020). All mutations lie within the functionally important and conserved WD40 domain of COPA, which is composed of repeated 40 amino acid-long motifs terminating in tryptophan (W) and aspartate (D), that assemble into a circular structure and mediate protein-protein interactions (**Figure 3.1 C**)**.** COPA is ubiquitously expressed in all cell types and if tested, expression levels of identified mutants were not altered (Watkin et al., 2015).

As previously mentioned, COPA recognizes dilysine motifs for packing into COPI vesicles for retrograde transport from Golgi to ER or trafficking within Golgi compartments (chapter 1.4.1.2)**.** COPA mutants have impaired binding efficiency to cargo proteins, therefore causing defective retrograde transport through dominant-negative effects (Watkin et al., 2015). As a consequence, ER stress, UPR, NF-κB pathway activation and Th17 cell-mediated autoimmunity were initially suggested pathomechanisms (Thaivalappil et al., 2021, Watkin et al., 2015), which have already been linked to lung disease and autoimmunity in other studies (Hasnain et al., 2012, Tanjore et al., 2012, Todd et al., 2008).

Clinically, the majority of patients present in early childhood (<five years of age) with symptoms including fever, arthralgia, arthritis, shortness of breath, cough, tachypnea that develop into inflammatory polyarticular arthritis, flares of diffuse alveolar hemorrhage (DAH) and/or ILD. During an uncontrolled and severe clinical course, lung disease can progress into fibrosis and end-stage pulmonary failure and require transplantation. Development of autoantibodies (anti-nuclear (ANA), anti-neutrophil cytoplasmic (ANCA), rheumatoid factor (RF)) has also been reported for a large number of patients (**Suppl. Table 1**). Less frequently, anti-cyclic citrullinated peptide (CPP) antibodies were detected, which may be associated with bone destructions observed in some patients (Frémond et al., 2021a, Taveira-DaSilva et al., 2019, Volpi et al., 2018, Watkin et al., 2015).

Kidney pathology, including impaired renal function, immunoglobulin (Ig) A nephropathy or lupus-like nephritis were reported in individual cases, two of which required kidney transplantation (**Suppl. Table 1**) (Boulisfane-El Khalifi et al., 2019, Guan et al., 2021, Mallea et al., 2020, Patwardhan et al., 2019, Watkin et al., 2015). However, the clinical presentation is highly variable between patients and differs with regard to severity of symptoms and organ involvement and cases of adult onset have also been reported (**Suppl. Table 1**) (Boulisfane-El Khalifi et al., 2019, Jensson et al., 2017, Kato et al., 2021, Mallea et al., 2020, Taveira-DaSilva et al., 2019).

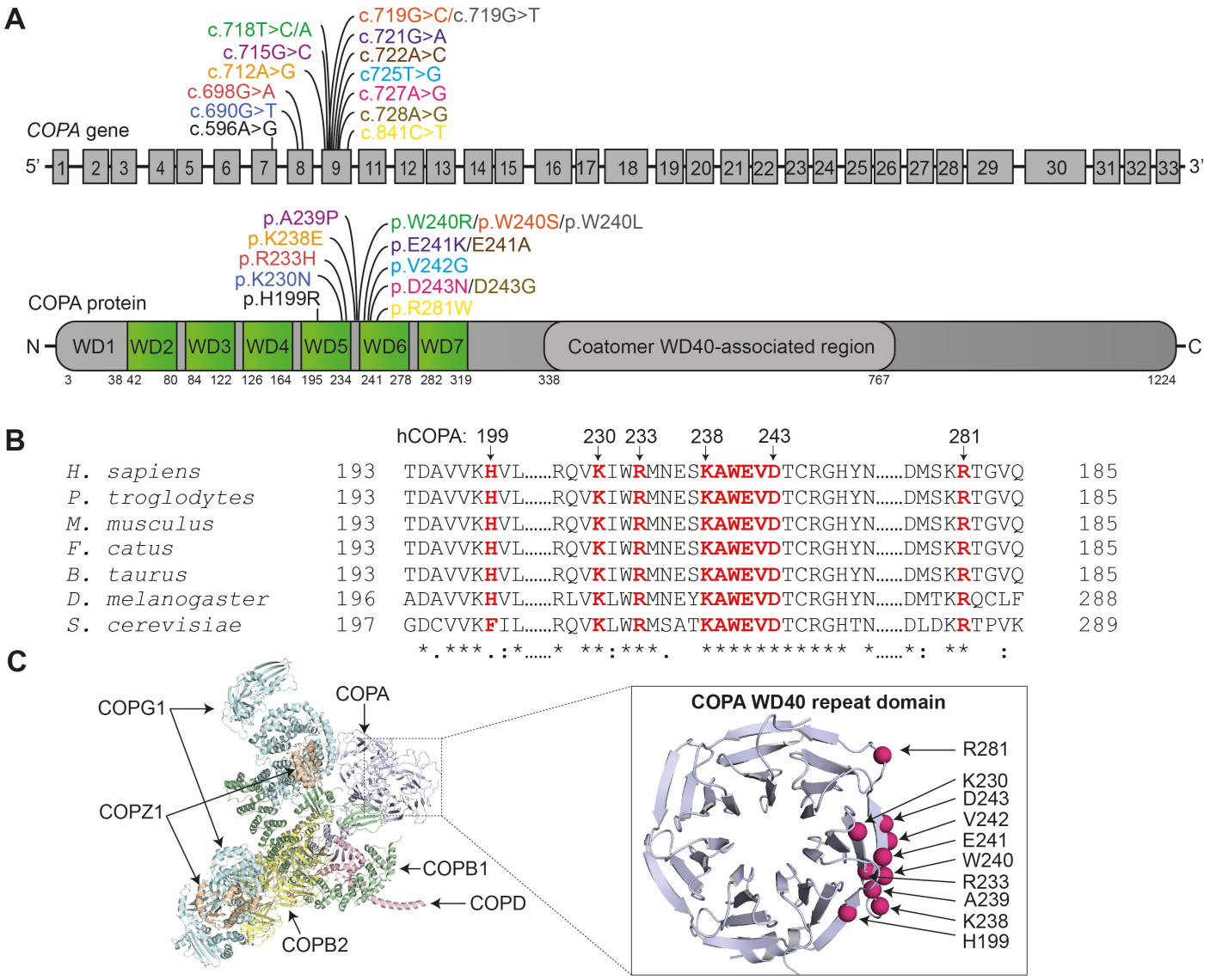
A
c.718T>C/A
c.715G>C
c.712A>G
c.698G>A
c.690G>T
c.596A>G
c.719G>C/c.719G>T
c.721G>A
c.722A>C
c725T>G
c.727A>G
c.728A>G
c.841C>T
COPA gene
5'
3'
p.A239P
p.K238E
p.R233H
p.K230N
p.H199R
p.W240R/p.W240S/p.W240L
p.E241K/E241A
p.V242G
p.D243N/D243G
p.R281W
COPA protein
N
C
WD1
WD2
WD3
WD4
WD5
WD6
WD7
Coatomer WD40-associated region
3 38 42 80 84 122 126 164 195 234 241 278 282 319 338 767 1224
B
hCOPA: 199 230 233 238 243 281
H. sapiens 193 TDAVVKHVL.....RQVKIWRMNESKAWEVDTCRGHYN.....DMSKRTGVQ 185
P. troglodytes 193 TDAVVKHVL.....RQVKIWRMNESKAWEVDTCRGHYN.....DMSKRTGVQ 185
M. musculus 193 TDAVVKHVL.....RQVKIWRMNESKAWEVDTCRGHYN.....DMSKRTGVQ 185
F. catus 193 TDAVVKHVL.....RQVKIWRMNESKAWEVDTCRGHYN.....DMSKRTGVQ 185
B. taurus 193 TDAVVKHVL.....RQVKIWRMNESKAWEVDTCRGHYN.....DMSKRTGVQ 185
D. melanogaster 196 ADAVVKHVL.....RLVKLWRMNEYKAWEVDTCRGHYN.....DMTKRQCLF 288
S. cerevisiae 197 GDCVVKFIL.....RQVKLWRMSATKAWEVDTCRGHTN.....DLDKRTPVK 289
*.***.:*.....* **:***. ********** *.....*: ** :
C
COPG1
COPA
COPZ1
COPB1
COPD
COPB2
COPA WD40 repeat domain
R281
K230
D243
V242
E241
W240
R233
A239
K238
H199

Figure 3.1 | Heterozygous missense mutations causative of COPA syndrome. Mutation-affected residues are highly conserved between species and located within the WD40 repeat domain**. A**) Schematic illustration of reported COPA mutations and their localization within the *COPA* gene and COPA protein. Exons (boxed numbers, top panel) and functional domains within the COPA protein are indicated (lower panel). **B**) Clustal Omega multiple sequence alignment of COPA amino acid sequences from indicated species. Residues affected by missense mutations are highlighted (red, bold) and numbered according to the human reference sequence. Sequences were obtained from Uniprot: *H. sapiens* (human, P53621), *S. cerevisiae* (yeast, P53622), *M. musculus* (mouse, Q8CIE6), *B. taurus* (cattle, Q27954), *P. troglodytes* (chimpanzee, H2Q0E3), *D. melanogaster* (fruit fly, Q9W0B8), *F. catus* (cat, M3W182). **C**) Ribbon structure presentation of the assembled COPI complex (PDB: 5ZNR, without COPE) and the COPA WD40 repeat domain (PDB: 6PBG) showing the location of residues affected by mutations (pink spheres). Figure adapted from Lepelley et al., 2020.

Atypical less commonly observed features in some patients include kidney and liver cysts, recurrent respiratory infections, malignancies, growth retardation, MAS, skin manifestation or neurological phenotypes, which expand the phenotypic spectrum of COPA syndrome (Brennan et al., 2017, Fremond et al., 2020, Jensson et al., 2017, Kato et al., 2021, Psarianos et al., 2021, Taveira-DaSilva et al., 2019, Thaivalappil et al., 2021, Watkin et al., 2015). Recently, the A239P mutation was linked to a clinical phenotype including interstitial pneumonitis and persistent transaminitis, which was not previously reported (Thaivalappil et al., 2021). Transaminases, including alanine aminotransferase (ALT) and aspartate aminotransferase (AST), are enzymes required for amino acid synthesis in the liver and therefore released into the blood stream upon hepatocellular damage, which can occur as a consequence of a range of different conditions (Oh et al., 2017). Extensive clinical evaluation was not able to establish a link to autoinflammatory or autoimmune dysregulation in the reported patient, however a liver biopsy identified nonspecific patches of intraparenchymal neutrophils (Thaivalappil et al., 2021).

In an unrelated patient carrying the same COPA mutation, ALT levels were only transiently and mildly elevated (Psarianos et al., 2021). As per clinical definition, mildly elevated transaminase levels are within five times the upper limit of the

reference range, which was estimated to occur in 10 % of the US population. Less than 5 % of these patients were diagnosed with liver disease, whereas the majority of individuals remained asymptomatic (Oh et al., 2017). Levels of ALT and AST measured for the index patients reported by Thaivalappil and colleagues varied between normal and 10-fold increased levels (Thaivalappil et al., 2021). Therefore, it remains unclear whether the liver-prone phenotype potentially associated with the A239P mutation is co-incidental, due to a yet unidentified autoimmune process, or a direct result of exacerbated ER stress on hepatocytes, which would further highlight the heterogeneous clinical presentation of COPA syndrome (Psarianos et al., 2021, Thaivalappil et al., 2021).
Despite the increasing number of COPA syndrome patient case reports since the first description in 2015, the phenotypic heterogeneity and the non-specific clinical manifestation impede the diagnosis of this disease. Sequencing-based genetic analysis of the patient and (if available) family members is required to identify familial or *de novo COPA* gene mutations. Future identification and analysis of more COPA syndrome patients will yield a better understanding of the clinical presentation and will be essential to stratify diagnostic procedures and therapies to improve early intervention and delay disease progression.

To date, a genotype-phenotype correlation in COPA syndrome could not be established (Taveira-DaSilva et al., 2019). The most commonly observed R233H mutation was found in eight families (**Suppl. Table 1**). All patients developed lung disease, but inflammation of joint and kidneys was observed to various degrees (Boulisfane-El Khalifi et al., 2019, Fremond et al., 2020, Krutzke et al., 2019, Taveira-DaSilva et al., 2019, Volpi et al., 2018, Watkin et al., 2015).
The E241K variant has only been identified in two families with severe lung disease, however no reports of inflammatory kidney disease exist to date (Jensson et al., 2017, Watkin et al., 2015). Remarkably, lung and joint involvement without kidney phenotype was also reported for another family with two affected patients carrying a different mutation of the same residue (E241A) (Patwardhan et al., 2019). However, since the renal phenotype might develop later in life, no conclusion about a possible correlation can be drawn and long-

term follow up of COPA syndrome patients is required. Although speculative, liver involvement has only been reported for the above-described A239P mutation and might be a phenotype specifically associated with mutations of this particular residue (Psarianos et al., 2021, Thaivalappil et al., 2021).
The majority of COPA syndrome patients are of Caucasian ethnic decent, but case reports of Asian and one African-American patient exist, which therefore does not indicate the contribution of a specific genetic background to disease development (Noorelahi et al., 2018, Watkin et al., 2015).

The disease is characterized by incomplete penetrance, leaving some individuals unaffected, despite carrying the mutation (Watkin et al., 2015). Consideration of 67 reported mutation carriers to date, including 53 affected patients and 14 asymptomatic individuals, reveals a clinical penetrance of 84.4 % and 74.3 % in female and male individuals, respectively (**Suppl. Table 1**). Therefore, other genetic variants, epigenetic differences and/or environmental risk factors such as infections or stress may influence disease onset and phenotypic variability. Overall, a female predominance to develop the disease appears to exist (Patwardhan et al., 2019).

Varying immunological features have been identified in patients, but are not consistently reported in the literature. In the initial study, Watkin and colleagues found elevated transcript levels of proinflammatory cytokines *IL1B*, *IL6* and *IL23 (IL23p19, IL12p40)* in B cell-derived lymphoblastoid cell lines (BLCLs) from two patients, likely as the consequence of ER stress-driven NF-κB signalling (Watkin et al., 2015). Since the cytokine milieu during CD4+ T cell activation is crucial for cell fate decisions during the development of specialized Th cell lineages (Li et al., 2020a) and increased CD4+ T cell lymphocyte infiltrates were found in patient lungs, subpopulations were analysed in this study. Patient PBMCs showed reduced levels of peripheral Th1 cells and increased levels of Th17 cells, the latter being implicated in autoimmunity (Brucklacher-Waldert et al., 2017, Leipe et al., 2010). Normally, Th17 differentiation additionally depends on transforming growth factor β (TGFβ) signalling, transcripts of which were not elevated in patient

BLCLs. However, ER stress activated transcription factor X-box binding protein 1 (XBP1) has been shown to directly promote Th17 differentiation in an inflammatory environment, despite the absence of TGFβ (Brucklacher-Waldert et al., 2017), supporting the hypothesis of an ER stress driven pathology (Watkin et al., 2015).

Subsequently, Volpi and colleagues were the first to describe elevated transcription levels of type I IFNs and ISGs in the peripheral blood of COPA syndrome patients, suggesting a role of type I IFN signalling and dysregulated innate immune system activation in disease pathogenesis (Volpi et al., 2018). An increasing number of subsequent case studies supported their findings and interestingly, mildly elevated IFNα serum levels were reported in asymptomatic mutation carriers (Lepelley et al., 2020).

Furthermore as previously mentioned, some clinical features of COPA syndrome, such as systemic inflammation, ILD, or renal immunopathology overlap with symptoms observed in SAVI and SLE, two type I IFN-driven inflammatory diseases (Boulisfane-El Khalifi et al., 2019). Therefore, although not yet officially classified as type I interferonopathy (d'Angelo et al., 2021), dysregulation of this pathway has become the focus in the field, since targeted inhibition might implement an opportunity for more effective treatment of COPA syndrome patients (see below).

3.1.2 Current treatment

The initial treatment strategy was based on long-term immunosuppression using a combination of systemic corticosteroids with mycophenolic acid, hydroxychloroquine or other steroid-sparing agents including anti-CD20 monoclonal antibody rituximab, TNF blocker etanercept, azathioprine or methotrexate to only name the most commonly used (**Suppl. Table 1**) (Guan et al., 2021, Tsui et al., 2018). Although effective in controlling some disease symptoms, progressive decline of pulmonary function was still observed in most patients (Jensson et al., 2017, Kato et al., 2021, Mallea et al., 2020, Tsui et al., 2018).

The lung pathology in COPA syndrome was initially suggested to be mainly driven by T cell-mediated autoimmunity following ER stress (Watkin et al., 2015) and inhibition of ER stress-induced T cell proliferation with mammalian target of rapamycin (mTOR) inhibitor sirolimus was successfully used to improve clinical symptoms of two COPA syndrome patients, who presented at young age (7.5 years, 3 months) with a pulmonary phenotype and additional joint pain or proteinuria, respectively (Guan et al., 2021, Kato et al., 2012). To avoid severe adverse effects during the course of the study, both patients were regularly monitored for systemic sirolimus concentration and inflammatory markers. Remarkably, long-term sirolimus treatment (1 year) resulted in reduced serum levels of IL-6 and decreased the peripheral blood type I IFN signature (Guan et al., 2021).

In another approach towards a more targeted therapy, three independent studies demonstrated the therapeutic benefit of JAK1/2 inhibition (baricitinib, ruxolitinib) or JAK1 inhibition (upadacitinib) in COPA syndrome patients (Fremond et al., 2020, Kato et al., 2021, Krutzke et al., 2019).

However, the innate immune sensor driving type I IFN signalling as well as the molecular mechanisms underlying COPA syndrome pathogenesis remained unclear and were therefore investigated in this thesis.

The data presented in the following chapter are currently in revision following peer review by Nature Communications. A preprint of this work was published on bioRxiv on 9th July 2020.

Of note, during the course of this thesis, several studies were published that independently confirmed some of the here presented results using different experimental models. Findings from these studies are included in the discussion in chapter 3.3.

3.2 Results

3.2.1 Generation of cellular model systems for COPA syndrome

Aiming to study the protein function of COPA in the context of innate immune signalling, we used CRISPR/Cas9 genome editing to delete COPA in human monocytic THP-1 and epithelial HeLa cell lines. This approach was based on the assumption that the reduced target protein binding efficiency of LoF mutations identified in COPA syndrome patients can be mimicked by reduction of WT COPA protein levels. Using sgRNAs targeting exon 5 (sgRNA 1), exon 1 (sgRNA 2), exon 7 (sgRNA 3) of the human *COPA* gene under a doxycycline (Dox)-inducible promoter, we generated three COPA-deficient THP-1 cells lines. The reduction of COPA protein levels coincided with spontaneous phosphorylation of STAT1 (pSTAT1), the transcription factor downstream of type I and III IFN signalling (**Figure 3.2 A**). Using this experimental approach, complete deletion of COPA could not be achieved long-term, because COPA is essential for cell survival (Sudo et al., 2010). To circumvent this, we used Dox-induced COPA deletion prior to every experiment and proceeded to use the THP-1 cell line with sgRNA 1 (subsequently termed COPA^{deficient}) as it demonstrated the greatest reduction in COPA levels and concomitantly increased pSTAT1 signal (**Figure 3.2 A**).
Similar to the previously reported elevation of proinflammatory cytokine transcripts and type I IFN signature in COPA syndrome patient PBMCs (Volpi et al., 2018, Watkin et al., 2015), qRT-PCR analysis of the generated COPA^{deficient} THP-1 cells revealed increased mRNA expression levels of proinflammatory cytokines (*TNF* and *IL6*), type I IFN subtypes *IFNA1* and *IFNB1* as well as ISGs including *ISG15*, *IFIT1* and *MX1* (**Figure 3.2 B**). Detailed analysis of inflammatory cytokine transcription kinetics at several time points during Dox-induced COPA deletion revealed sequential onset of TNF and type I IFN signalling (**Figure 3.2 C**), which may indicate subsequent activation of distinct inflammatory pathways. Furthermore, increased protein levels of IFNβ and the IFN-induced chemokine CXCL10 (Buttmann et al., 2004, Buttmann et al., 2007) were measured by ELISA in supernatants from COPA^{deficient} THP-1 cells (**Figure 3.2 D**).

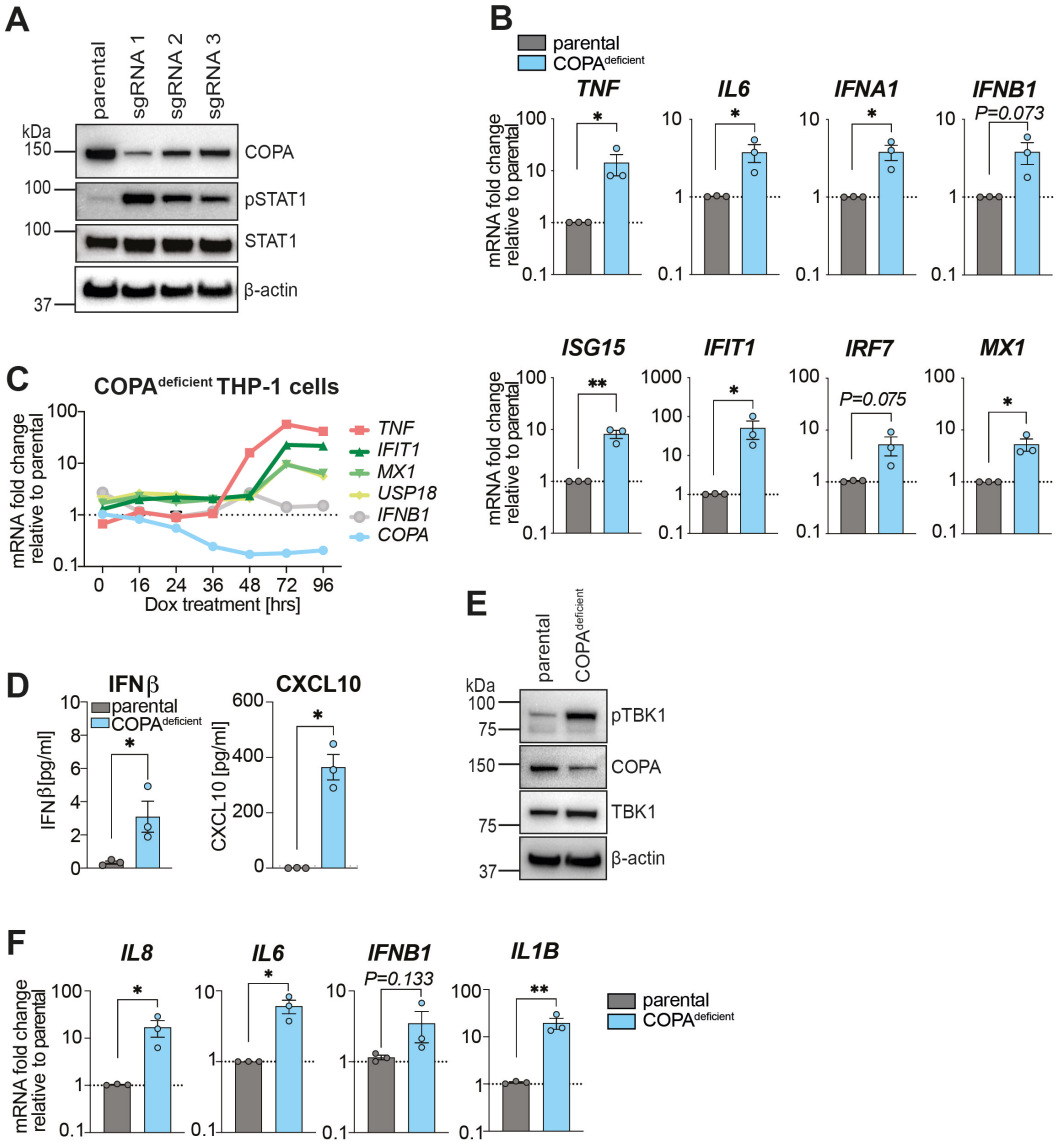

Figure 3.2 | Cell line models of COPA syndrome. A) CRISPR/Cas9-mediated generation of COPA-deficient THP-1 cell lines using three single guide (sg) RNAs targeting *COPA* exon 5 (sgRNA 1), exon 1 (sgRNA 2) or exon 7 (sgRNA 3). Baseline protein expression was analysed by immunoblot (after 72 hrs Dox+24 hrs rest). **B)** qRT-PCR analysis of transcription levels in COPA^{deficient} THP-1 cells (sgRNA 1). Data are mean ± SEM from n=3 replicate experiments presented as fold change to the parental control cell line (THP-1 Cas9). **C)** Representative qRT-PCR transcription kinetics of COPA^{deficient} THP-1 cells during Dox-induced *COPA* deletion. Technical duplicates are shown and error bars represent SD, n=3. **D)** ELISA analysis of baseline IFNβ and CXCL10 released from THP-1 cells. Data are mean ± SEM pooled from n=3 experiments. **E)** Immunoblotting in COPA^{deficient} HeLa cells generated by CRISPR/Cas9 targeting of *COPA* with sgRNA 1. **F)** qRT-PCR analysis of cells generated in E). Data are presented as described in B). Statistical analysis in B, D, F using ratio paired Student's t-test. *P*-values are indicated by numbers or as * $P<0.05$, ** $P<0.01$.

In order to independently confirm these findings in a different cell line, we used the same experimental approach and sgRNA 1 to delete COPA in epithelial HeLa cells (**Figure 3.2 E**). Similar to THP-1 cells, the reduction of COPA protein levels in HeLa cells resulted in increased transcription of proinflammatory cytokines and type I IFN (**Figure 3.2 F**), as well as elevated baseline phosphorylation of TBK1 (pTBK1), which is activated downstream of several PRRs (chapter 1.3.4.1) (Liu et al., 2015b, Liu et al., 2017a). Although silencing of the cGAS-STING pathway due to immortalisation with viral oncogenes in HeLa cells has been reported (Lau et al., 2015), we confirmed pathway activity in this particular cell line used here by stimulation with synthetic DNA analogues (**Suppl. Figure 1**). Therefore, we have successfully generated COPA^{deficient} THP-1 and HeLa cell lines that model inflammatory manifestations observed in COPA syndrome patients and present a useful tool to investigate the molecular mechanisms underlying this disease.

3.2.2 Inflammatory signalling in COPA syndrome model cell lines is driven by STING pathway overactivation

To identify the innate immune sensor that is driving the inflammatory response in our *in vitro* model of COPA syndrome, we used a hypothesis-driven approach and genetically co-deleted several candidate innate immune receptors in COPA^{deficient} THP-1 cells (**Figure 3.3**).

The inflammasome sensor NLRP3 was shown to be activated by numerous diverse stimuli, ranging from infections to cellular organelle dysfunction (reviewed in (Kelley et al., 2019)). Furthermore, aberrant NLRP3 activation is implicated in the autoinflammation observed in CAPS patients, as well as pathologies of other immune-mediated disorders including neurodegeneration, autoimmunity and metabolic syndrome (Li et al., 2020b, Pirzada et al., 2020). Interestingly, a recent report showed *trans*-Golgi network dispersal in response to multiple NLRP3 stimuli, which was suggested to serve as platform for NLRP3 aggregation and signalling (Chen et al., 2018). Since we observed spontaneous Golgi fragmentation in COPA^{deficient} HeLa cells (**Suppl. Figure 2**), we hypothesized these fragments as site of spontaneous NLRP3 activation following disturbed

cellular homeostasis. However, upon co-deletion of COPA and NLRP3, inflammatory signalling persisted (**Figure 3.3 A**).

The rationale behind investigating the involvement of cytoplasmic dsRNA sensor PKR was based on its function as eukaryotic translation initiation factor 2 alpha (eIF2α) kinase. Besides PKR, three other kinases namely PERK, heme-regulated inhibitor (HRI) and general control nonderepressible (GCN2), have been identified to downregulate protein translation by eIF2α phosphorylation in response to different stimuli, such as viral infections, ER stress, heme deficiency and nutritional stress, respectively (Donnelly et al., 2013). As previously suggested, retrograde transport deficiency induces ER stress (Watkin et al., 2015), which we also observed in our *in vitro* model (data not shown). Since PKR is the only eIF2α kinase that is known to induce type I IFN signalling (Balachandran et al., 2000), we excluded its involvement in COPA syndrome disease pathology (**Figure 3.3 B**).

RIG-I and MDA5 are two cytoplasmic RNA sensors, that mediate proinflammatory and type I IFN signalling in response to viral infections (chapter 1.3.2) (Kato et al., 2011). Through genetic deletion of their shared adapter protein MAVS in COPA^{deficient} THP-1 cells we were able to rule out inflammatory signalling via this pathway, which could have been the consequence of protein mislocalization caused by secretory pathway disturbances (**Figure 3.3 C**).

Based on its cellular localization, we investigated the ER-resident chaperone Unc93 homolog B1 (UNC93B1) (**Figure 3.3 D**), which is essential for the stability and signalling of nucleic acid sensing endosomal TLRs (TLR3, 7, 8, 9) and cell surface TLR5 (Huh et al., 2014, Pelka et al., 2018, Tabeta et al., 2006). Interestingly, studies in human and mice suggested a regulatory role of UNC93B1 in balancing TLR7 and TLR9 signalling, which leads to aberrant TLR7 activation and immune disease, if dysregulated (Fukui et al., 2009, Fukui et al., 2011, Lee et al., 2013, Pelka et al., 2018). However, co-deletion of any of the above-described immune receptors was not able to ameliorate the inflammatory phenotype in COPA^{deficient} THP-1 cells (**Figure 3.3**).

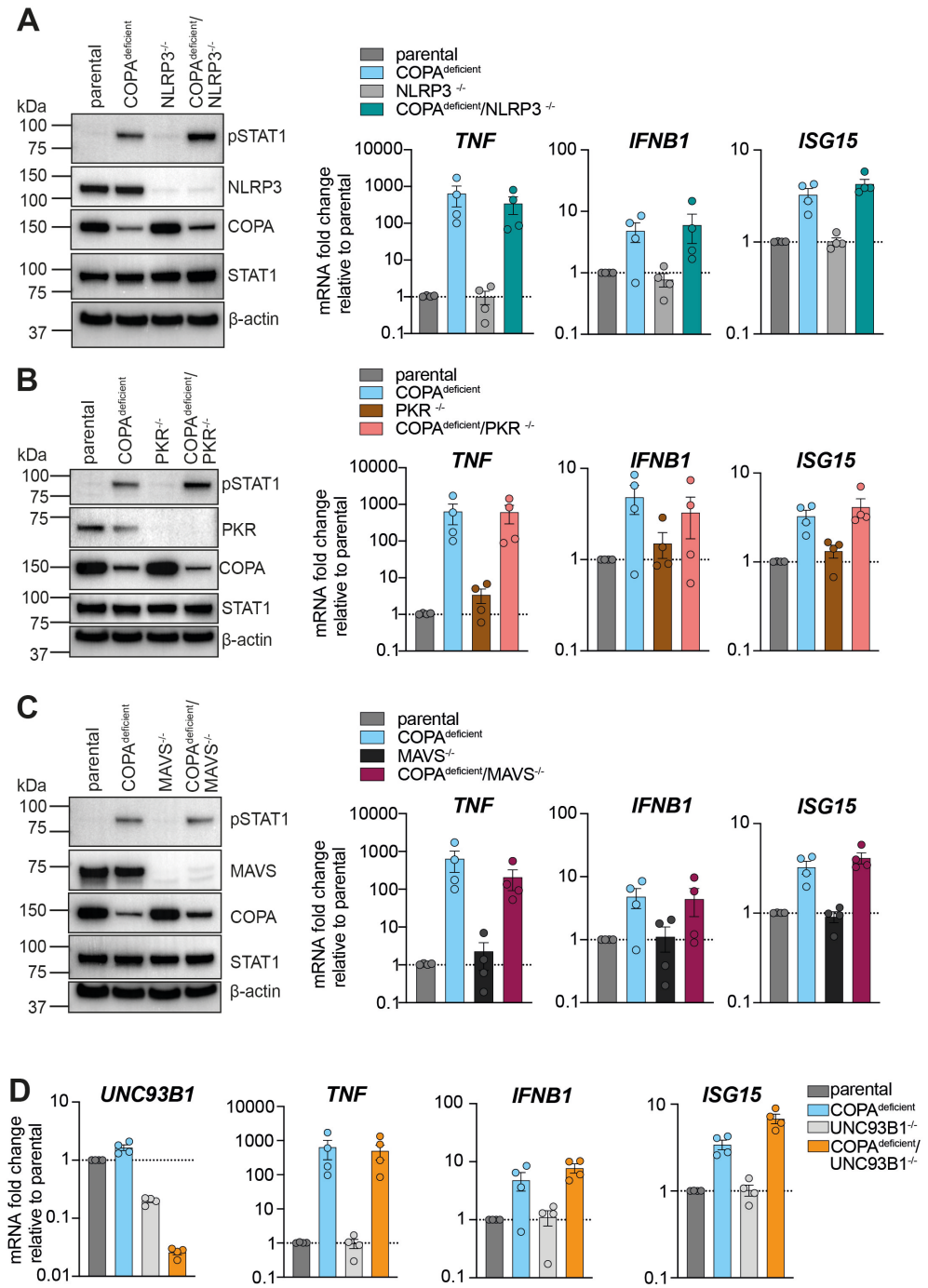

Figure 3.3 | Inflammatory signalling associated with COPA-deficiency is not mediated through NLRP3-, PKR-, MAVS or UNC93B1-dependent pathways. The effect of CRISPR/Cas9-mediated genetic co-deletion of NLRP3 (**A**), PKR (**B**), MAVS (**C**) or UNC93B1 (**D**) in COPA^{deficient} THP-1 cells was assessed by immunoblot analysis of phosphorylated STAT1 (pSTAT1) and qRT-PCR analysis of *TNF*, *IFNB1* and *ISG15* transcription at baseline. Data are presented as mean ± SEM from n=4 independent experiments. Due to the lack of a specific antibody, deletion of UNC93B1 was confirmed via transcript analysis by qRT-PCR (D).

Another candidate immune sensor was STING, which triggers inflammation downstream of multiple cytoplasmic nucleic acid sensors including cGAS (Ablasser et al., 2013, Sun et al., 2013, Wu et al., 2013). As previously described (chapter 1.3.4.3), inactive STING localizes on the ER membrane and requires COPII-mediated anterograde trafficking to translocate to Golgi compartments upon activation (Gui et al., 2019, Ogawa et al., 2018, Ran et al., 2019, Sun et al., 2018). Although COPA is not part of the COPII complex, all compartments of the secretory pathway form a tightly regulated and interdependent network within the cell (Szul et al., 2011). Therefore, we hypothesized that reduced functionality of COPA-mediated retrograde transport might potentially interfere with STING trafficking and cause aberrant signalling. In line with this, we identified COPA as a potential interaction partner for STING in an unbiased mass spectrometry-based quantitative proteomics experiment, where we analysed protein lysates from HEK293T cells following pulldown of overexpressed mCitrine (mCit)-tagged human STING (**Figure 3.4 A**). Furthermore, this screen identified surfeit locus protein 4 (SURF4) as a potential STING interactor, which was recently shown to act as adapter protein mediating STING-COPA interaction for subsequent retrograde trafficking (Deng et al., 2020b, Mukai et al., 2021). Additionally, other known STING-interacting proteins were found to be enriched in STING pulldowns, including TBK1. Although not significant, other COPI/COPII subunit proteins and ER- and Golgi-resident proteins were identified, highlighting the importance of the secretory pathway for STING regulation (see chapter 2.14.1 for data reposition). Interestingly, transmembrane protein 214 (TMEM214), involved in ER stress-induced caspase-4 activation and induction of apoptosis (Li et al., 2013a), was highly enriched in STING pulldowns, however a functional link to STING has not yet been described in the literature and was not further investigated in this thesis.

CRISPR/Cas9-mediated genetic deletion of STING ameliorated the spontaneous pSTAT1 signal (**Figure 3.4 B**) as well as inflammatory gene expression in COPA^{deficient} THP-1 cells (**Figure 3.4 C**). Interestingly, TNF transcription levels remained high after STING deletion and are likely the result of NF-κB pathway activation following ER stress, as previously suggested (Watkin et al., 2015).

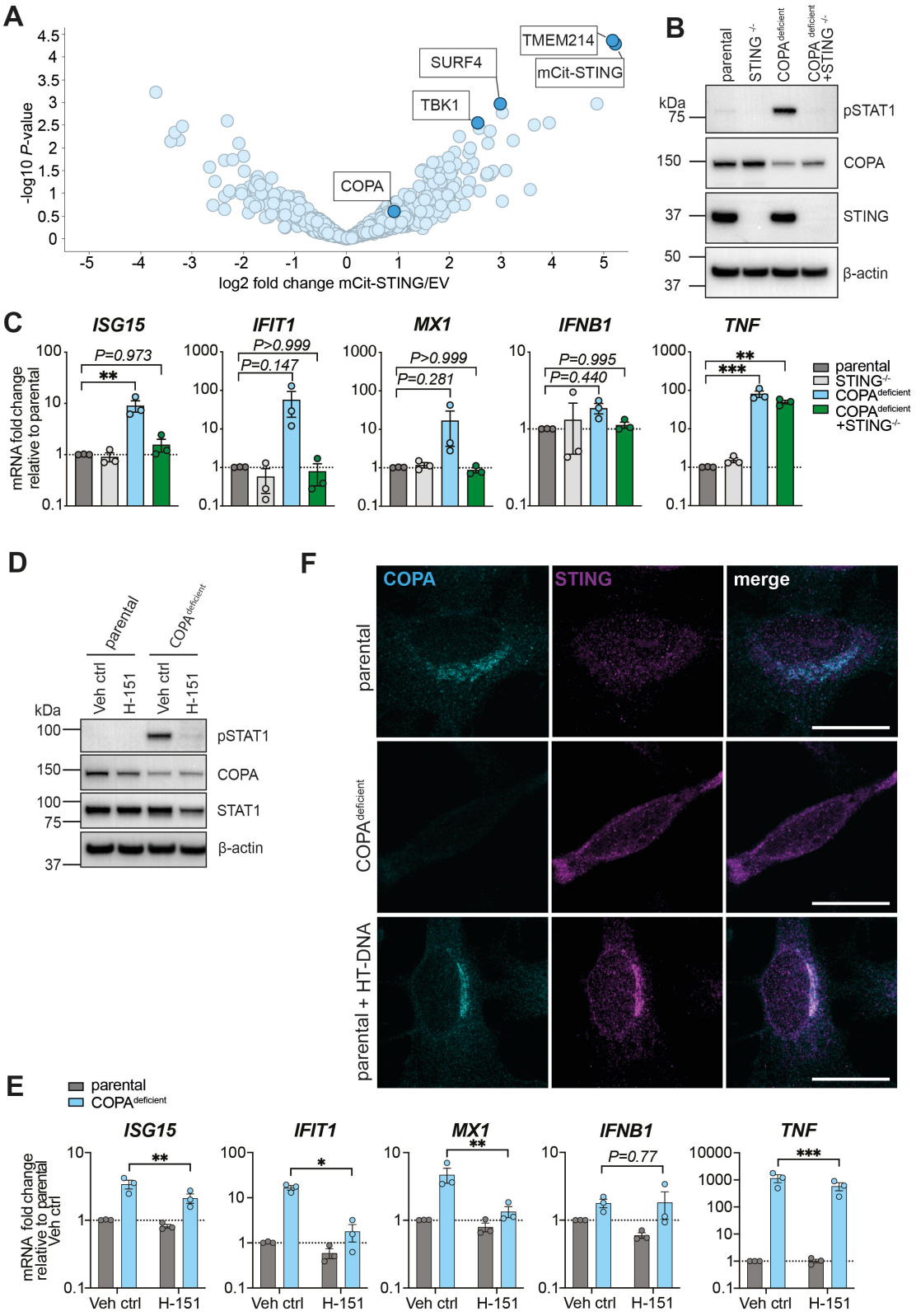

Figure 3.4 | Inflammation induced by COPA-deficiency is STING-dependent. A) Volcano plot representing the log2 protein ratios of potential STING-interacting proteins identified by mass spectrometry-based quantitative proteomics after transient overexpression of mCitrine (mCit)-tagged STING and pulldown in

HEK293T cells relative to empty vector (EV) control (n=3 independent pulldowns). **B)** Representative western blot of THP-1 cells of indicated genotypes after 72 hrs Dox treatment. Representative result of n=3. **C)** qRT-PCR analysis of transcription levels in THP-1 cells at baseline (72 hrs Dox). Data are means ± SEM of 3 independent experiments. Statistical significance was assessed by one-way ANOVA and Dunnett's multiple comparison test. **D)** Representative western blot of parental and COPA^{deficient} THP-1 cells after treatment with STING inhibitor H-151 (2.5 µM) or vehicle control (Veh ctrl). Representative result of n=3. **E)** Analysis of proinflammatory gene and ISG transcription in THP-1 cells treated as in D). Data are shown as mean ± SEM from 3 independent experiments. Statistical analysis by two-tailed ratio paired Student's t-test comparing control and H-151 treatment individually for each cell line. **F)** Super-resolution IF microscopy of parental and COPA^{deficient} HeLa cells stained for COPA (cyan) and endogenous STING (magenta). Parental cells transfected with HT-DNA (2 µg/ml, 2 hrs) show typical puncta formation which represents STING accumulation at Golgi compartments and indicates STING activation. Representative experiment shown of n=3; scale bar represents 20 µm. *P*-values are indicated by numbers or as * $P<0.05$, ** $P<0.01$, *** $P<0.001$.

We independently confirmed this result by genetic deletion of STING in COPA^{deficient} HeLa cells, which ameliorated baseline proinflammatory and type I IFN transcription and the pTBK1 signal (**Suppl. Figure 3**). Furthermore, in the context of potential pharmaceutical intervention, treatment of COPA^{deficient} THP-1 cells with the small molecule STING inhibitor H-151 was able to markedly reduce baseline STAT1 phosphorylation (**Figure 3.4 D**) and type I IFN-mediated gene transcription (**Figure 3.4 E**), thus indicating a possible targeted treatment for COPA syndrome patients.

ER-to-Golgi translocation of STING is a prerequisite for interaction with downstream signalling molecules (Dobbs et al., 2015, Ishikawa et al., 2009, Saitoh et al., 2009). We therefore aimed to investigate the cellular localization of STING in COPA-deficiency and performed immunofluorescence (IF) staining of endogenous STING in HeLa cells (**Figure 3.4 F**). As positive control, parental HeLa cells were stimulated with HT-DNA, a dsDNA molecule to activate cGAS-induced STING ER-to-Golgi translocation which can be observed as puncta formation (**Figure 3.4 F**). However, in COPA^{deficient} HeLa cells without further stimulation, puncta formation of endogenous STING was not as clear and rather

suggested formation of multiple smaller size specks distributed throughout the cytoplasm (**Figure 3.4 F**).

Since the overall signal of stained endogenous STING was quite weak, we stably overexpressed STING-GFP in these cell lines via retroviral transduction. Parental cells showed diffuse cytoplasmic distribution of STING-GFP when untreated and formation of puncta that co-localized with *cis*-Golgi marker GM130 following HT-DNA transfection (**Figure 3.5**). In COPA^{deficient} cells, multiple STING-GFP speckles were observed, which largely co-localized with GM130 (**Figure 3.5 A, B**). Co-localization with ER marker KDEL was not different when compared to parental cells (**Figure 3.5 C**). Considering that loss of COPA is associated with Golgi dispersal (Razi et al., 2009) (**Suppl. Figure 2**) and spontaneously accumulated STING-GFP co-localized with Golgi but not ER markers, these preliminary experiments suggest that STING signalling occurs due to spontaneous accumulation at the dispersed Golgi in this *in vitro* model of COPA syndrome.

Overall, these results suggest that spontaneous STING activation is driving the inflammatory response in COPA syndrome model THP-1 and HeLa cell lines, which is likely the result of STING accumulation at dispersed Golgi fragments.

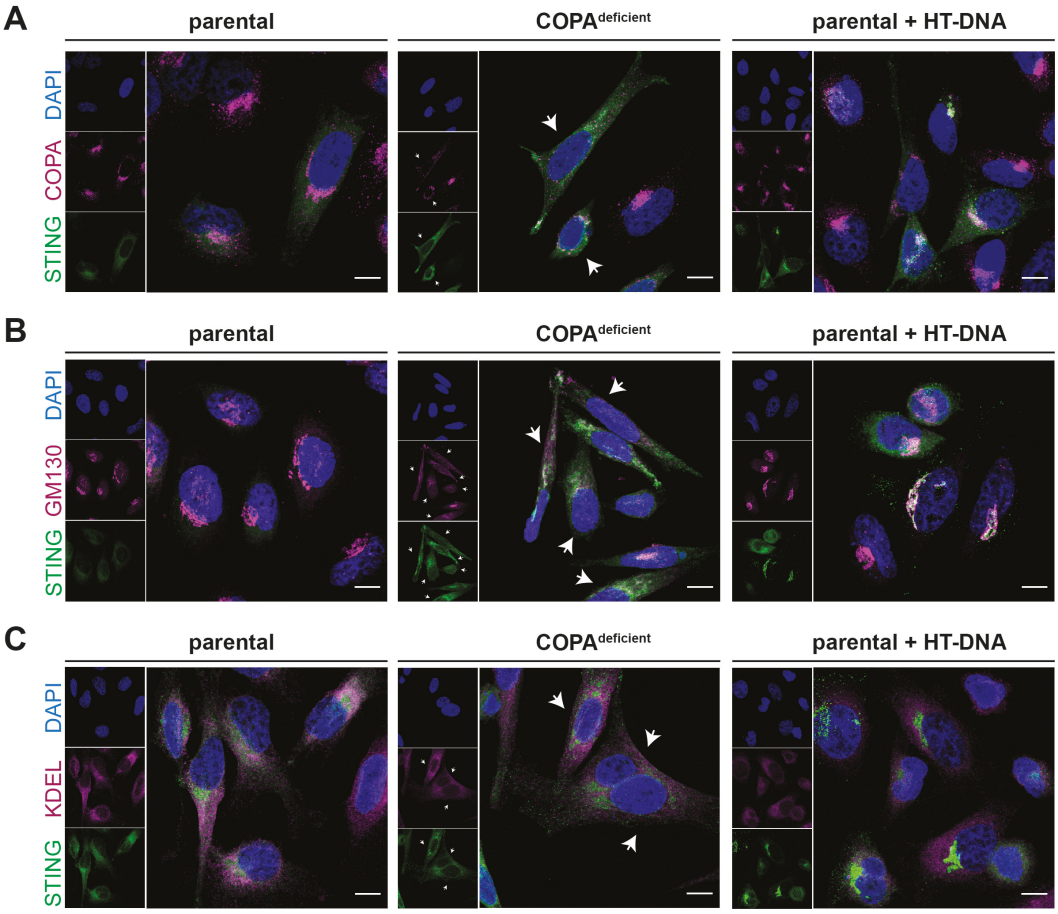

Figure 3.5 | STING-GFP co-localizes with the dispersed Golgi in COPA^{deficient} HeLa cells. Parental and COPA^{deficient} HeLa cells stably expressing STING-GFP were Dox-treated for 72 hrs, fixed and stained for COPA (**A**), *cis*-Golgi marker GM130 (**B**) or ER marker KDEL (**C**). Localization of activated STING-GFP (green) in parental HeLa cells transfected with HT-DNA (2 µg/ml, 2 hrs) resulted in STING-GFP accumulation at the Golgi, which is shown as positive control. Representative images; n=1; scale bar represents 10 µm; white arrows indicate COPA^{deficient} cells.

3.2.3 Mutations in COPA drive STING-dependent inflammation

In order to validate our findings in patient samples, we analysed PBMCs from a COPA syndrome patient carrying the c.698G>A (R233H) mutation with clinical presentation of severe polyarticular arthritis and lung disease (Volpi et al., 2018). At the time of sample collection, the patient was treated with prednisone and rituximab. *Ex vivo* flow cytometry analysis revealed elevated levels of pTBK1,

particularly in CD14-expressing monocytes (**Figure 3.6 A, B**). Treatment with STING inhibitor H-151 was able to ameliorate baseline TBK1 phosphorylation as shown in representative histograms and quantified as fold change of pTBK1 levels after H-151 treatment, thereby suggesting basal STING activation in patient PBMCs (**Figure 3.6 C, D**). Further experimental repeats would be desirable to confirm this result.

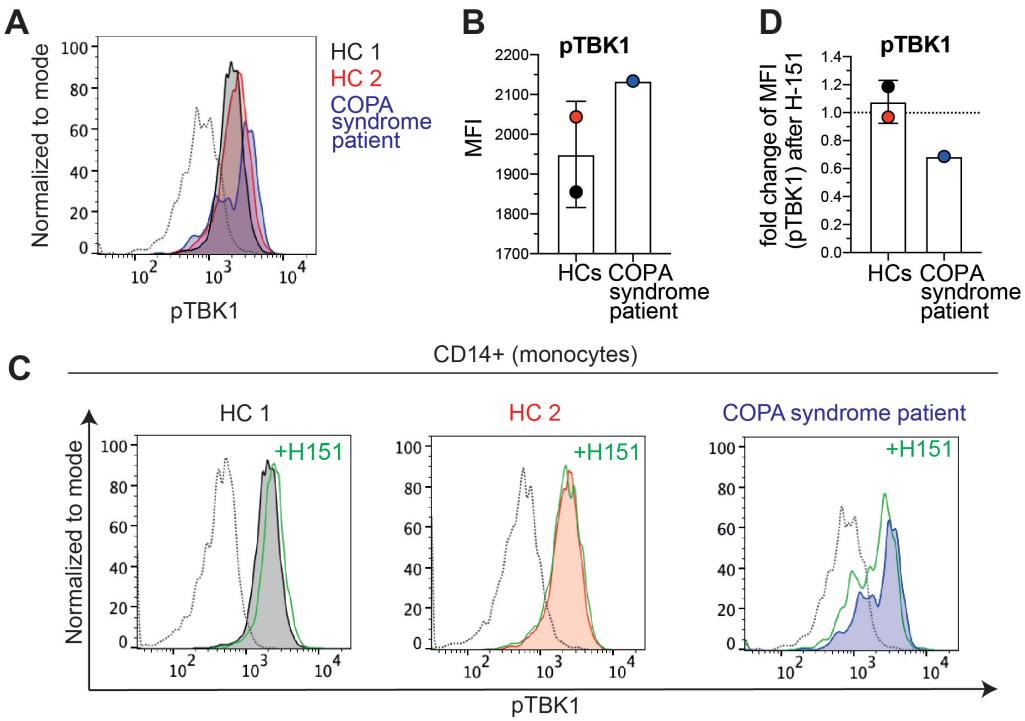

Figure 3.6 | STING inhibitor treatment ameliorates baseline TBK1 phosphorylation in COPA syndrome patient monocytes. *Ex vivo* flow cytometry analysis of phosphorylated TBK1 (pTBK1) in the monocytic subpopulation (CD14-positive, CD3-negative) isolated from COPA syndrome patient PBMCs carrying the R233H mutation (blue) and 2 healthy individuals (HCs: black, red). **A)** Analysis of pTBK1 levels without further stimulation. Histogram shows data of a representative experiment, dotted line indicates the isotype control. **B)** Column graph shows baseline pTBK1 signal quantified as mean fluorescence intensity (MFI) of the experiment shown in A). Error bar represents SD, n=1. **C)** pTBK1 signal before and after treatment with STING inhibitor H-151 (5 µM) for 4 hours (green line). Dotted line represents isotype control. n=1 **D)** Quantification of data shown in C). Bar graph represents fold change in pTBK1 MFI following H-151 treatment relative to the untreated control. Error bar represents SD.

To further study inflammation in the context of COPA syndrome patient mutations, we generated overexpression plasmids encoding the previously published LoF mutations E241K and R233H (Watkin et al., 2015).

Initially, we overexpressed these constructs in HEK293T cells, which lack detectable levels of endogenous STING (**Suppl. Figure 4**) (Reus et al., 2020, Sun et al., 2013). Phosphorylation of TBK1 and IRF3 was only observed when myc-tagged COPA mutant plasmids were co-expressed with mCit-tagged STING (**Figure 3.7 A**). However, in this system, STING is transiently overexpressed at high levels. This results in strong baseline activation of WT STING alone, observed by above background pTBK1 and pIRF3 signals (**Figure 3.7 A**). This is likely caused by spontaneous dimerization-induced Golgi translocation and subsequent pathway activation (Ergun et al., 2019), which is a commonly observed disadvantage of this experimental setup. STING signalling was slightly elevated by co-expression with WT COPA. Rather than a specific effect of WT COPA, this observation could be the result of high-level protein translation following co-transfection, that overwhelms ER folding and retrograde transport capacities and subsequently causes STING retention at the Golgi, which could promote signalling. Interestingly, when co-expressed with COPA mutants, STING activation was markedly increased (**Figure 3.7 A**). This indeed suggested that impaired retrograde trafficking prevents Golgi-to-ER retrieval and promotes STING accumulation at the Golgi compartment which results in increased signalling.

To bypass the disadvantages associated with transient overexpression, we tested a more physiological setting with lower, stable expression of STING-GFP incorporated via lentiviral transduction of HEK293T cells and subsequent FACS sorting for low expression close to endogenous level. Surprisingly, under these conditions, transient overexpression of COPA mutants E241K and R233H was not able to drive inflammation above EV control and COPA WT levels (**Figure 3.7 B**).

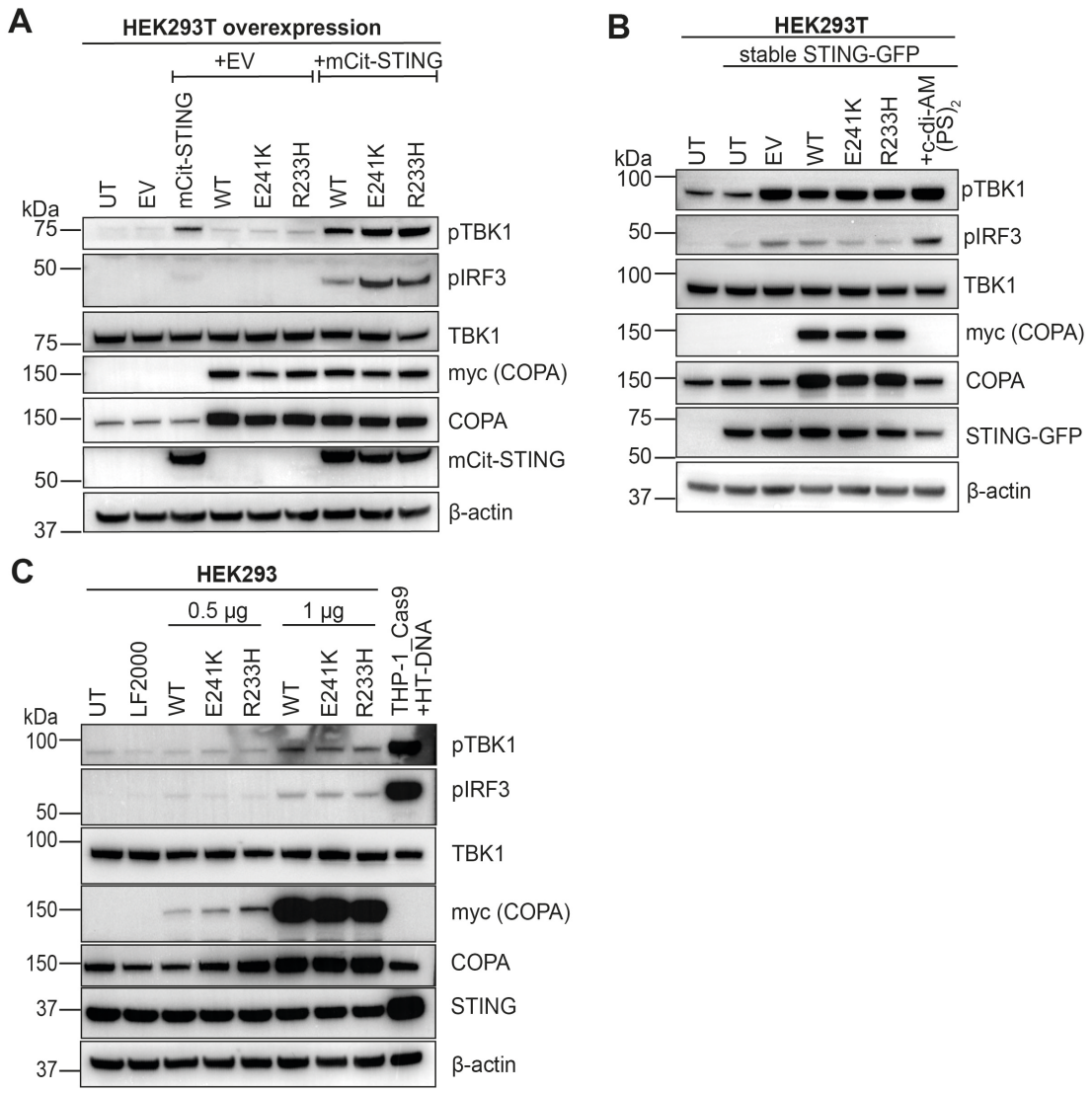

Figure 3.7 | Mutations in COPA trigger STING-dependent inflammation. A) Western blot analysis of HEK293T cells following co-overexpression of mCitrine-tagged (mCit)-STING and myc-tagged COPA WT and mutants E241K and R233H (0.5 µg DNA per construct) 24 hrs after transfection. Representative result of n=3. **B)** Immunoblot analysis of stably STING-GFP-expressing HEK293T cells 24 hrs after transient transfection with 0.5 µg plasmid DNA encoding myc-tagged COPA WT or mutants. Untransfected cells stimulated with c-di-AM$(PS)_2$ (20 µM, 2 hrs) are shown as control for ligand-mediated STING activation (last lane). Lane 1 shows HEK293T WT cells as non-transduced control. Representative result of n=3 experiments. **C)** HEK293 cells (express endogenous STING) were transiently transfected with myc-tagged COPA WT or mutants (0.5 µg and 1 µg DNA/well) and harvested for western blot analysis after 24 hrs. As positive control, cell lysate of parental THP-1 cells (THP-1_Cas9) stimulated with HT-DNA (2 µg/ml, 2 hrs) was loaded. Representative experiment of n=3 independent repeats. Lipofectamine 2000, LF2000; empty vector, EV; untreated, untransfected, UT; wildtype, WT.

In order to independently confirm this finding, we transiently transfected COPA WT, E241K and R233H using two different plasmid concentrations in HEK293 cells, which express endogenous STING at levels comparable to HeLa cells (**Suppl. Figure 4**). Again, in this system, overexpression of COPA mutants was not able to induce IRF3 phosphorylation over WT control levels (**Figure 3.7 C**). Importantly, these experiments suggest that inflammation driven by COPA mutations in HEK239T cells only occurs when STING is overexpressed. However, with endogenous levels of STING expression, as in HEK293 cells or HEK293T cells stably expressing STING-GFP, overexpressed COPA mutations cannot induce spontaneous signalling, likely because an essential player of the COPA syndrome pathology is lacking in these cell lines. Given that all the downstream machinery required for STING signalling appears to be intact in HEK293T cells (**Figure 3.7 A, B**) we wondered if the missing part of the pathway was actually upstream, specifically the cytoplasmic DNA sensor cGAS, since it is not endogenously expressed in HEK293T or HEK293 cell lines (**Suppl. Figure 4**).

3.2.4 Inflammatory signalling in COPA^{deficient} THP-1 cells is cGAS-dependent

In order to investigate the involvement of cGAS in COPA syndrome pathology, CRISPR/Cas9 gene editing was employed to delete COPA in a monoclonal cGAS KO (cGAS$^{-/-}$) THP-1 cell line (Mankan et al., 2014). Lack of cGAS completely abolished spontaneous phosphorylation of STAT1, which was re-established upon reconstitution with GFP-tagged cGAS via lentiviral transduction (**Figure 3.8 A**). Similarly, transcription levels of proinflammatory cytokines and ISGs were ameliorated in COPA^{deficient} cells when cGAS was deleted (**Figure 3.8 B**). Interestingly, co-deleted COPA^{deficient}/cGAS$^{-/-}$ THP-1 cells showed stronger reduction in *TNF* gene transcription compared to STING-deleted COPA^{deficient} THP-1 cells (**Figure 3.4 C**). One potential reason could be the monoclonal origin of the used cGAS$^{-/-}$ cell line, which completely lacks cGAS expression (Mankan et al., 2014), whereas the STING$^{-/-}$ THP-1 cells are a mixed population of

CRISPR/Cas9-deleted cells, with some residual STING being expressed. However, clonal cGAS deletion was still not able to fully reverse *TNF* transcription to baseline levels, which supports the involvement of ER stress as additional NF-κB activating pathway (Watkin et al., 2015).

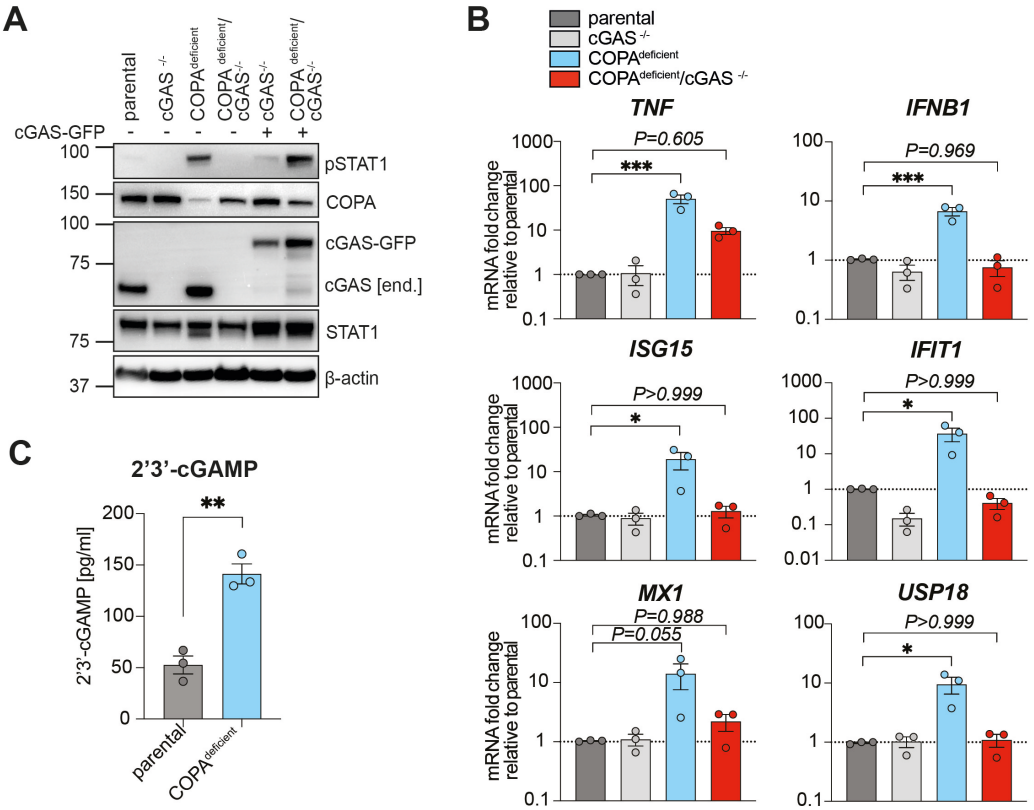

Figure 3.8 | Inflammatory signalling in COPA^{deficient} THP-1 cells requires cGAS. A) Immunoblot analysis of parental and monoclonal cGAS$^{-/-}$ THP-1 cells following deletion of COPA and reconstitution with cGAS-GFP via lentiviral transduction. CRISPR/Cas9-mediated gene deletion was induced with Dox for 72 hrs. A representative experiment is shown (n=2). Endogenous, end. **B)** qRT-PCR analysis of baseline ISGs and proinflammatory gene transcription in THP-1 cells with indicated genotypes. Data are mean ± SEM from 3 independent experiments. Statistical significance was assessed by one-way ANOVA with Dunnett's multiple comparison test. **C)** Baseline analysis of 2'3'-cGAMP levels in cell lysates of parental and COPA^{deficient} THP-1 cells by ELISA. Data are shown as mean ± SEM from 3 independent experiments. Statistical testing by unpaired Student's t-test. *P*-values are indicated by numbers or as * *P*<0.05, ** *P*<0.01, *** *P*<0.001.

Recently, the role of SURF4 as the adapter protein that mediates packaging of STING into COPI vesicles was established (Deng et al., 2020b, Mukai et al., 2021). In support of this, our mass spectrometry analysis identified SURF4 as an interactor of STING after overexpression in HEK293T cells (**Figure 3.4 A**). Assuming that lack of SURF4 specifically blocks Golgi-to-ER trafficking of STING and other SURF4 target proteins, we found increased phosphorylation of STAT1 and elevated transcription of ISGs following genetic deletion of SURF4 in THP-1 WT cells (**Suppl. Figure 5**, preliminary data). This phenotype was ablated in cGAS$^{-/-}$/SURF4$^{-/-}$ THP-1 cells (**Suppl. Figure 5**, preliminary data), further supporting the requirement of cGAS as the initial driver for STING accumulation at the Golgi and subsequent inflammatory signalling in COPA syndrome.

To further confirm cGAS activation, we analysed cytoplasmic levels of cGAS-produced second messenger 2'3'-cGAMP by ELISA. Surprisingly, 2'3'-cGAMP levels in COPA^{deficient} THP-1 cells were significantly elevated over parental controls (**Figure 3.8 C**). This result suggests cGAS activation above tonic levels in COPA-deficiency, however whether this is the primary defect driving COPA syndrome pathology remains to be validated in COPA mutant-expressing cells.

Together, this data demonstrates that cGAS is required for inflammatory signalling driven by COPA-deficiency in THP-1 cells, and that the second messenger 2'3'-cGAMP is elevated in these cells, indicating increased cGAS activity.

3.2.5 Spontaneous cGAS-STING signalling is activated by general deficiency in COPI-mediated retrograde transport

As previously described, besides COPA, the COPI complex consists of six other subunits similarly involved in functional retrograde trafficking (**Figure 1.7**) (Beck et al., 2009). Here, we sought to determine whether activation of the cGAS-STING signalling pathway is uniquely linked to a loss of COPA function, or whether disruption of the retrograde trafficking route in general results in inflammation via this pathway. Therefore, we selected COPI subunits COPG1 and COPD, which are part of the F-subcomplex and COPE, which similarly to

COPA belongs to the B-subcomplex (see chapter 1.4.1.2). Using the CRISPR/Cas9 technology we deleted these subunits in HeLa and THP-1 cells.
To confirm that retrograde transport is indeed impaired upon silencing of the selected COPI subunits, we used IF super-resolution microscopy and investigated localization and intensity of KDEL staining in COPI subunit-deficient HeLa cells (**Figure 3.9 A**). As previously mentioned, the amino acid sequence KDEL is an ER-specific retention signal encoded on the C-terminus of soluble ER-resident proteins that undergo Golgi-to-ER retrieval through COPI-mediated retrograde transport (chapter 1.4.1.2) (Munro et al., 1987). We therefore hypothesized that impaired retrograde transport would result in accumulation of KDEL signal within Golgi compartments. Overall, COPI subunit-deficient cells showed increased KDEL signal intensity compared to parental controls (**Figure 3.9 A**), which is likely the consequence of increased expression of KDEL-tagged ER chaperones following ER stress and activation of UPR pathways. Indeed, when compared to parental cells with intact retrograde transport, a significant shift in KDEL localization towards Golgi compartments was observed in COPA^{deficient}, COPG1^{deficient} and COPD^{deficient} HeLa cells (**Figure 3.9 A**). Quantification of this result is shown as the area ratio of KDEL signal overlaying with *cis*-Golgi marker GM130 divided by the total area of KDEL staining per cell (**Figure 3.9 A**). These results indicate that genetic deletion of COPA, COPG1 or COPD results in impaired retrograde trafficking, which is similar to the functional defect described for COPA mutants (Watkin et al., 2015). COPE^{deficient} cells were not analysed in this experiment, since they did not show an inflammatory phenotype (**Figure 3.9 B, C**). This observation is further discussed below.
Immunoblotting confirmed that unless intentionally deleted, only minor variability was observed for COPA, COPG1 and COPD protein expression levels across COPI subunit-deficient THP-1 cell lines (**Figure 3.9 B**). Therefore, despite deletion of selected subunits, expression levels of tested residual COPI proteins remained largely stable, suggesting that destabilization or complete co-depletion of subunits does not occur. As one exception, COPE expression levels were markedly reduced in COPA^{deficient} cells (**Figure 3.7 B**).

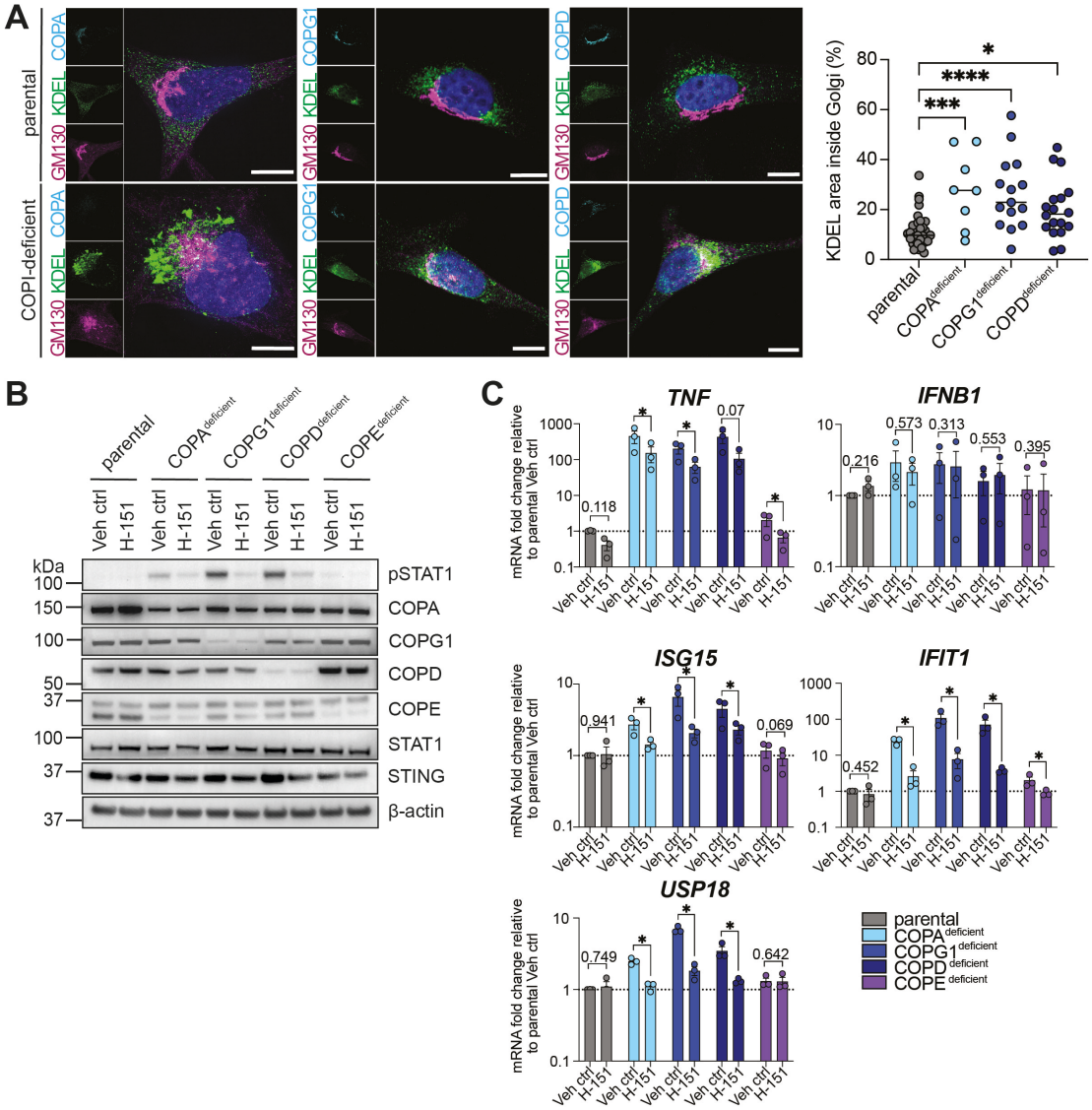

Figure 3.9 | cGAS-STING pathway activation is caused by general deficiency in COPI-mediated retrograde trafficking. A) Representative IF images of HeLa cell lines presented as maximum intensity projection. Parental cells (top) or cells CRISPR/Cas9-deleted for COPA (bottom left), COPG1 (bottom middle) or COPD (bottom right) were co-stained for KDEL (green), GM130 (magenta), the indicated COPI subunit (cyan) and DAPI (blue). The bar chart represents co-localized KDEL and GM130 signal quantified as % of KDEL area inside *cis*-Golgi. Each dot represents one cell and parental cells stained for different subunits were combined for quantification analysis. Statistical testing by one-way ANOVA and Dunnett's multiple comparison test, line at median. Scale bar 10 µm. **B)** Representative immunoblot analysis of THP-1 cells of indicated genotypes following treatment with STING inhibitor H-151 (2.5 µM), n=3 **C)** qRT-PCR analysis of THP-1 cells treated as described in B). Data are shown as mean ± SEM from n=3 independent experiments. Two-tailed ratio paired Student's t-test compared Veh ctrl and H-151 treatment individually for each cell line. *P*-values are indicated by numbers or as * *P*<0.05, *** *P*<0.001, **** *P*<0.0001.

In yeast, COPE was shown to be non-essential for functional retrograde transport, but its role as a structural component to stabilize COPA at higher temperatures has been described (Duden et al., 1998). Since COPE expression levels are dependent on COPA binding and coatomer integration (Eugster et al., 2000), co-depletion of both proteins in COPA^{deficient} cells is not surprising, however this was not observed when COPE was intentionally deleted. This indicates that COPE is not required for COPA stability and functional retrograde transport in human cells under the culture conditions used in this study. In line with this, only deficiency in COPI complex proteins COPA, COPG1 and COPD but not COPE resulted in spontaneous inflammatory signalling (**Figure 3.9 B, C**). In order to determine whether the inflammatory phenotype can be ameliorated by inhibition of cGAS-STING signalling, COPI subunit-deficient THP-1 cells were treated with STING inhibitor H-151. Immunoblot as well as qRT-PCR analysis showed reduction of STAT1 phosphorylation and decreased transcription of proinflammatory genes and ISGs after inhibitor treatment, respectively (**Figure 3.9 B, C**). These data demonstrate that indeed, the cGAS-STING pathway is activated upon deletion of different COPI subunit proteins and therefore a general defect in retrograde transport sufficiently induces inflammatory signalling. Consequently, aberrant STING signalling is unlikely to be the unique result of reduced COPA function.

3.2.6 Retrograde transport deficiency impairs DNA-induced cGAS signalling

To further elucidate the involvement of retrograde transport in cGAS-STING pathway regulation, we sought to investigate inflammatory signalling upon cGAS stimulation with transfected DNA (HT-DNA and poly (dA:dT)) and analysed cytoplasmic 2’3’-cGAMP production in THP-1 cells. Surprisingly, after stimulation, lower 2’3’-cGAMP levels were detected in cells lacking COPA, suggesting reduced cGAS activation following targeted stimulation (**Figure 3.10 A**). In order to independently confirm this result, three different COPA-deficient THP-1 cell lines (shown in **Figure 3.2** A) were stimulated with cGAS and STING ligands and

analysed for levels of IFNλ production, a type III IFN which is similarly activated to type I IFN upon PRR stimulation (Ank et al., 2006, Zhou et al., 2018a) (**Figure 3.10 B**). In line with the previous result, all tested COPA-deficient cell lines were less responsive to cGAS stimulation when compared to parental controls. Yet interestingly, direct STING stimulation by a cGAMP analogue was not impaired and comparable across all cell lines (**Figure 3.10 B**). A similar result was observed for COPG1^{deficient} THP-1 cells (**Figure 3.10 C**), which suggests a break point in the pathway, further highlighting the essential role of intact retrograde transport for functional cellular defence in response to foreign DNA.

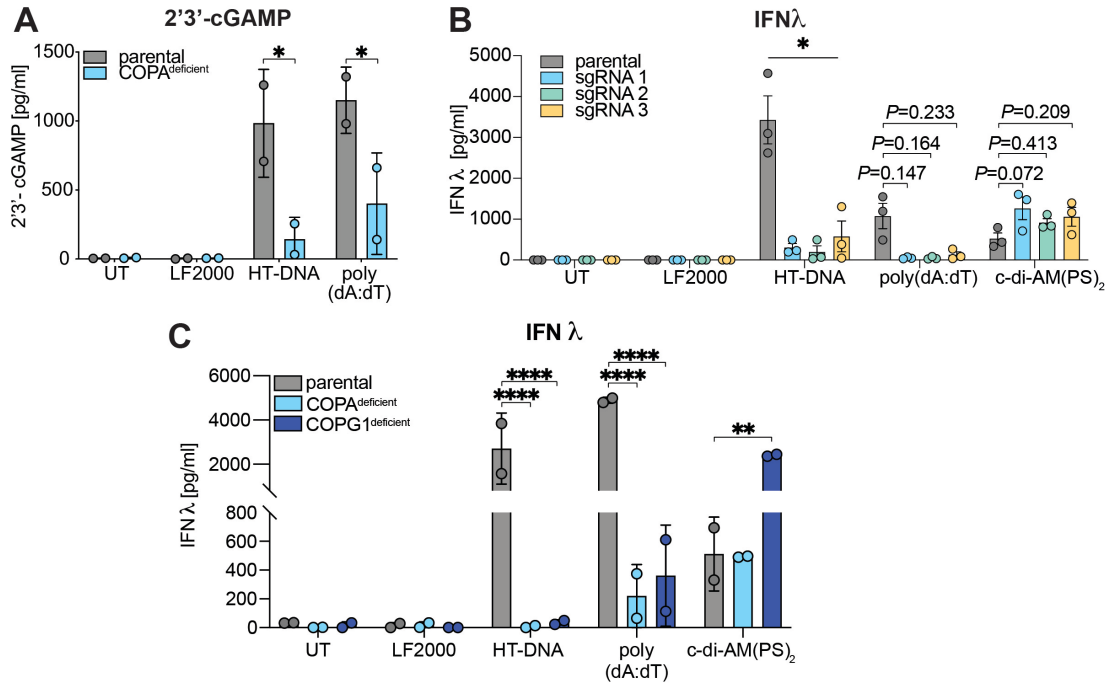

Figure 3.10 | DNA-induced cGAS signalling is impaired in COPA^{deficient} and COPG1^{deficient} THP-1 cells. THP-1 cell lines of indicated genotypes were stimulated with cGAS activators HT-DNA (2 µg/ml) and poly (dA:dT) (1 µg/ml) (**A, B, C**) and STING activator c-di-AM(PS)$_2$ (20 µM) (**B, C**) and analysed after 24 hrs. **A)** 2'3'-cGAMP levels in cell lysates measured by ELISA (n=2 experiments, error bars represent SD). **B)** Supernatants of COPA-deficient THP-1 cell lines generated in Figure 3.2 A were analysed for IFNλ by ELISA (n=3, error bars indicate SEM). **C)** ELISA analysis of IFNλ levels in supernatants of THP-1 cells (n=2, error bars indicate SD). A-C) Statistical analysis by two-way ANOVA and Sidak (A) or Dunnett's (B, C) multiple comparison test using parental cells as comparator group individually for each stimulus. *P*-values are indicated by numbers or as * *P*<0.05, ** *P*<0.01, **** *P*<0.0001. Lipofectamine 2000, LF2000.

3.2.7 Retrograde trafficking between Golgi and ER is the transport direction underlying STING mislocalization in COPI-deficiency

Besides retrieval of proteins from the Golgi to ER, the COPI complex is also required for trafficking within Golgi compartments (Letourneur et al., 1994, Martínez-Menárguez et al., 1999, Pellett et al., 2013, Popoff et al., 2011, Rothman et al., 1996). Disruption of which of these transport directions causes defective STING regulation in COPA syndrome has not yet been experimentally examined.

Within cells, trafficking of cargo proteins via different COPI transport routes may be regulated through multiple COPI complex isotypes, containing different sets of COPG and COPZ paralog combinations (Blagitko et al., 1999, Futatsumori et al., 2000, Wegmann et al., 2004). However as previously mentioned, whether functional heterogeneity exists has not yet been conclusively determined. Based on the spatial segregation and predominant enrichment at *cis*- or *trans*-Golgi compartments, respectively, COPG1-containing COPI coat vesicles were suggested to be more likely involved in mediating retrograde transport between Golgi and ER, while COPG2 may predominantly serve intra-Golgi transport (chapter 1.4.1.2) (Moelleken et al., 2007). Taking advantage of this proposed localization-dependent and perhaps functional distinction, we used CRISPR/Cas9 gene editing to specifically delete COPG1 or COPG2 in THP-1 cells to determine functional consequences for STING activation. Deletion efficiency was confirmed by immunoblotting for COPG1 and *COPG2* transcript analysis by qRT-PCR due to the lack of a specific antibody (**Figure 3.11 A, B**). Interestingly, only deletion of COPG1 resulted in spontaneous phosphorylation of STAT1 and inflammatory gene transcription, whereas this was not observed in COPG2^{deficient} cells (**Figure 3.11 A, C**). Our previous result showed amelioration of inflammatory signalling in COPG1^{deficient} cells by treatment with STING inhibitor H-151 (**Figure 3.9 B, C**), indicating STING pathway activation in COPG1^{deficient} THP-1 cells due to defective retrograde transport, whereas deletion of COPG2, potentially implicated in intra-Golgi transport, had no effect.

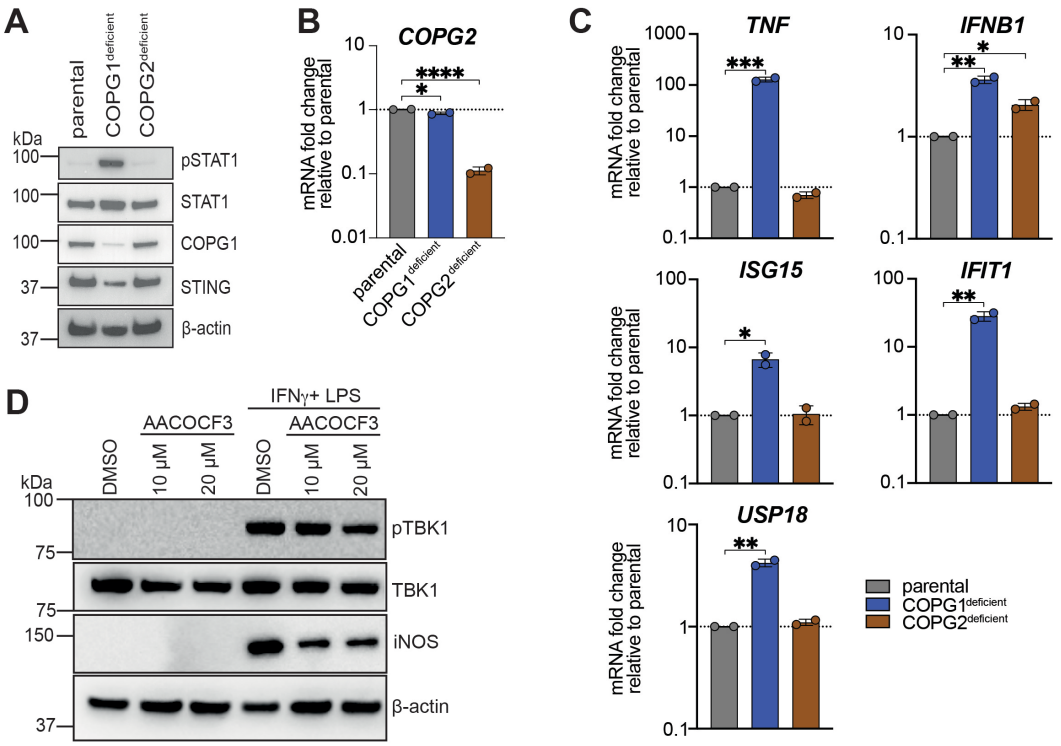

Figure 3.11 | Targeted inhibition of anterograde intra-Golgi transport does not activate spontaneous STING signalling. A) Representative immunoblot analysis of baseline signalling in THP-1 cells after targeted CRISPR/Cas9-mediated deletion of COPG1 or COPG2 paralogs. n=2. **B)** qRT-PCR analysis of *COPG2* transcription in cell lines used in A). n=2, error bars represent SD. **C)** qRT-PCR analysis of baseline inflammatory cytokine transcripts in COPG1- and COPG2-depleted THP-1 cells. Data were pooled from n=2 independent experiments, error bars represent SD. **D)** Representative western blot analysis of iBMDMs after treatment with cPLA2α inhibitor AACOCF3. Inhibitor activity was analysed by its effect on iNOS expression levels following IFNγ priming (50 ng/ml, overnight) and LPS stimulation (25 ng/ml, 6 hrs) in absence or presence of AACOCF3 (30 min pre-incubation). A representative experiment of n=3 is shown. B-C) Statistical analysis by one-way ANOVA with Dunnett's multiple comparison test. * $P<0.05$, ** $P<0.01$, *** $P<0.001$, **** $P<0.0001$.

However, given that functional redundancy between COPG1 and COPG2 has been proposed (Adolf et al., 2019), this result was not conclusive.

Therefore, in an alternative approach, we specifically blocked intra-Golgi trafficking by pharmacological inhibition of the calcium-dependent cytosolic phospholipase A2 alpha (cPLA2α) (San Pietro et al., 2009). cPLA2α is required for the formation of intercisternal tubules that connect Golgi stacks and are essential for intra-Golgi transport (de Figueiredo et al., 1999, de Figueiredo et al.,

1998, San Pietro et al., 2009). Treatment of iBMDMs with cPLA2α inhibitor arachidonyl trifluoromethyl ketone (AACOCF3) did not result in spontaneous phosphorylation of TBK1, indicating that defective intra-Golgi trafficking does not sufficiently activate spontaneous STING signalling. Since cPLA2α was shown to be involved in regulating iNOS (Chuang et al., 2015), we confirmed AACOCF3 activity by evaluating expression levels of iNOS in response to IFNγ and LPS stimulation. Pre-treatment with cPLA2α inhibitor reduced iNOS levels (**Figure 3.11 D**), thereby validating inhibitor functionality at the used concentrations (Ng et al., 2017, Paloschi et al., 2020).

Additionally, COPI-mediated formation of early endosome has been shown to play a role in autophagy induction (Razi et al., 2009). Importantly, functional autophagy and lysosomal degradation pathways are required for termination of STING signalling (Gonugunta et al., 2017, Gui et al., 2019, Liu et al., 2019). Therefore, a possible defect in those pathways caused by COPA-deficiency was excluded by monitoring STING expression levels during Dox-induced COPA depletion for 72 hrs in THP-1 cells. Progressive loss of COPA did not coincide with robust accumulation of STING in the here shown experiment and independent repeats, suggesting normal functionality of STING degradation pathways (**Figure 3.12**).

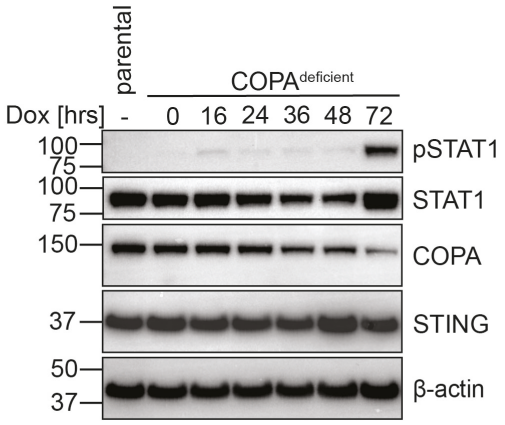

Figure 3.12 | Loss of COPA does not alter STING expression levels. Western blot analysis of STING expression levels in THP-1 cells during Dox treatment when COPA protein levels gradually declined. A representative result of n=3 independent experiments is shown.

Together, these findings suggest that although COPA mediates multiple transport directions within the secretory pathway, the disease-causing mechanism in COPA-deficiency likely relies on reduced Golgi-to-ER retrieval of the immune sensor protein STING.

Collectively, our results demonstrate that aberrant STING signalling in cell lines lacking COPA is the result of defective retrograde trafficking which impairs steady-state Golgi-to-ER retrieval of STING and causes subsequent accumulation at Golgi compartments. Spontaneous inflammation was dependent on upstream dsDNA detector cGAS in THP-1 cell lines, which suggests the requirement of a STING-activating stimulus to induce pathogenicity. However interestingly, cGAS no longer responds sufficiently to cytoplasmic DNA stimulation, suggesting a break in the cGAS-STING signalling axis due to COPA-deficiency. The finding that deletion of other COPI subunits, such as COPG1 and COPD, impart a similar cellular phenotype, suggests that immune-mediated disorders associated with mutations in other COPI subunit proteins may exist.

3.3 Discussion

In this study, we generated model cell lines that recapitulate the type I IFN signature observed in PBMCs from COPA syndrome patients (Volpi et al., 2018) and show that type I IFN signalling can be ablated by genetic deletion and pharmacological inhibition of STING and its upstream regulator cGAS. Interestingly, the clinical phenotype of COPA syndrome partially overlaps with symptoms reported in SAVI, including severe systemic inflammation, interstitial lung disease, arthritis, early onset in life and a predominant constitutive type I IFN gene activation (Clarke et al. 2020, Frémond et al., 2021b, Lepelley et al., 2020, Liu et al., 2014b). For SAVI, multiple case reports identified GoF mutations in STING, causing spontaneous dimerization and therefore constitutive STING pathway activation (Keskitalo et al., 2019, Melki et al., 2017, Saldanha et al., 2018). However, STING activation in COPA syndrome is likely less pronounced, since activated (phosphorylated) STING could not be detected in model cell lines and patient PBMCs (data not shown). Similarly, Kato et al. described absence of baseline pSTING and pTBK1 signals in bone marrow-derived dendritic cells (BMDCs) from phenotypic COPA syndrome patient mutation-expressing mice ($COPA^{V242G/wt}$) (Kato et al., 2021). In patients, this is supported by measurements of plasma or serum IFNα levels, which were found to be higher in SAVI patients when directly compared to patients with COPA syndrome (Lepelley et al., 2020). However interestingly, in co-localization studies we found that endogenous STING and reconstituted STING-GFP in $COPA^{deficient}$ HeLa cells spontaneously accumulated in multiple small specks scattered throughout the cytosol, which partially co-localized with dispersed Golgi fragments in preliminary experiments. Partial Golgi dispersal and redistribution has previously been observed in COPA-deficient cell lines (Razi et al., 2009) and also occurred after secretory pathway inhibition by treatment with brefeldin A, a small GTPase inhibitor that prevents initiation of COPI and II vesicle formation (Wortzel et al., 2017). STING signalling in COPA-depleted HeLa cells therefore likely occurs from smaller Golgi fragments, rather than an intact Golgi complex. In line with our data, spontaneous Golgi accumulation of STING in cell lines overexpressing COPA mutants and

COPA syndrome patient cells has recently been confirmed by independent studies (Deng et al., 2020b, Lepelley et al., 2020, Mukai et al., 2021), except in BMDCs from COPA$^{V242G/wt}$ mice, where pronounced and more rapid STING localization to the Golgi only occurred after STING stimulation (Kato et al., 2021). Since Golgi dispersal was not observed in the complementary studies (Deng et al., 2020b, Lepelley et al., 2020, Mukai et al., 2021), this is likely a distinct feature of the COPA-deletion model system. Importantly, ligand-stimulated STING activation is retained in our COPA^{deficient} cells, suggesting that Golgi fragmentation does not impair STING signalling (Uhlorn et al., 2020).

In contrast to SAVI, where STING is spontaneously active, we have demonstrated that aberrant type I IFN signalling in THP-1 cells lacking COPA and COPA-STING-adapter protein SURF4 requires upstream activation by cGAS, which normally protects cells from infections by sensing foreign DNA in the cytoplasm. This is in line with a previous study, which observed cGAS-dependence of the ISG signature in THP-1 cells after short hairpin (sh) RNA-mediated COPA knockdown and proposed tonic cGAS activation by low levels of cytoplasmic mitochondrial or genomic DNA as activator of STING translocation during the steady-state (Lepelley et al., 2020). However, cGAS-dependence appears to be a species- or cell-type specific effect, since overactive STING signalling was retained in cGAS-deficient MEFs stably expressing COPA mutants (Deng et al., 2020b, Mukai et al., 2021).

Our data indicate that retrograde trafficking by COPI retrieves STING from the Golgi to prevent signalling as a key mechanism of negative regulation during homeostatic conditions. Following activation, STING binding to SURF4 and COPA is reduced (Mukai et al., 2021), which results in accumulation at the Golgi and allows for interaction with downstream signalling molecules. Since LoF mutations in COPA reduce the COPI cargo-binding efficiency, steady-state Golgi-to-ER retrieval of the SURF4-STING complex is impaired and lowers the threshold for STING accumulation and signalling (Deng et al., 2020b, Kato et al., 2021, Lepelley et al., 2020, Mukai et al., 2021). This proposed mechanism is supported by the relatively high incomplete penetrance of clinical symptoms in individuals carrying COPA mutations (20-25 % (**Suppl. Table 1**) (Frémond et al.,

2021a)), indicating the requirement of additional triggers or environmental factors to disrupt the balance of homeostatic STING circulation and induce disease onset. Although not yet identified, contributing co-factors could be infections or additional predisposing mutations in genes regulating ER stress pathways or encoding other molecules involved in inflammatory signalling via cGAS-STING.

Furthermore, we observed increased levels of 2'3'-cGAMP in COPA^{deficient} THP-1 cells indicative of cGAS activation. This could be a secondary consequence of altered cellular homeostasis, such as disrupted mitochondrial integrity or prolonged ER stress in COPA-deficiency (Bravo et al., 2012, Bravo et al., 2011, Wang et al., 2011). Further validation of this finding in model systems expressing COPA mutants is required to fully exclude the possibility of Cas9-mediated cGAS activation in the here used experimental system (Pépin et al., 2016). cGAS activation as the primary consequence of COPA-deficiency seems less likely, since we and others showed that overexpression of COPA mutants in MEFs or HEK293T cells induced aberrant STING signalling independent of cGAS (Deng et al., 2020b, Lepelley et al., 2020, Mukai et al., 2021). This demonstrates that the main pathway defect is caused by STING accumulation at the Golgi. Importantly, based on these results, an activating stimulus appears to be required and provided either by overexpression of STING or baseline cGAS signalling (Lepelley et al., 2020). However, as previously mentioned, species-specific differences in the case of murine cell lines cannot be excluded (Deng et al., 2020b, Lepelley et al., 2020, Mukai et al., 2021).
Nevertheless, secondary activation of cGAS could further aggravate inflammation in patients, since cGAS overactivation by self-DNA has now been implicated in several inflammatory and autoimmune pathologies (Zhou et al., 2020). For example, Aicardi-Goutières syndrome and familial chilblain lupus are caused by mutations in *TREX1*, *RNaseH2* or *SAMHD1* that result in accumulation of genomic self-DNA in the cytoplasm via different mechanisms and therefore trigger cGAS-dependent spontaneous type I IFN signalling (Crow et al., 2006a, Fye et al., 2011, Kretschmer et al., 2015, Reijns et al., 2012). However, we do not yet know if genomic DNA is the activating ligand for cGAS in COPA syndrome.

Another possibility is that cGAS activation could be the result of leakage of mitochondrial DNA into the cytoplasm (Li et al., 2018c, Rongvaux et al., 2014). Within cells, ER and mitochondria form a structural and functional interactive network and both organelles exchange metabolites, signalling molecules and ions through so called mitochondrial-associated membranes (MAM) (Kornmann et al., 2009, Malhotra et al., 2011, Vance 1990). COPA-deficiency-induced alterations in ER and Golgi homeostasis may therefore impair mitochondrial integrity, leading to release of mitochondrial DNA and subsequent cGAS activation.

Intriguingly, cGAS has also been shown to undergo phase separation, which is described as droplet-like compartment formation for subsequent signalling (Du et al., 2018). It is believed that this phenomenon is highly dependent on the availability of ions, such as zinc cations, which are mainly stored in mitochondria and the ER (Lu et al., 2016b, Du et al., 2018, Singh et al., 2020). Therefore, it may be possible that increased ER stress activated by COPI-deficiency could result in uncontrolled release of zinc cations into the cytoplasm, which may facilitate the phase separation of cGAS and induce subsequent signalling (Du et al., 2018). Currently, the mechanism for cGAS activation in COPA syndrome requires further investigation.

In our study we show that the cGAS-STING pathway is activated upon deletion of different COPI subunit proteins COPA, COPG1 and COPD, whereas deficiency of COPE does not induce inflammatory signalling. Therefore, one could speculate that there may be other interferonopathies associated with defective retrograde transport caused by reduced function of COPI subunits other than COPA, that have not yet been described. Interestingly, LoF mutations in COPB2 (COPβ') or COPD (COPδ, encoded by *ARCN1* gene) are linked to diseases associated with skeletal developmental defects and microcephalus formation (DiStasio et al., 2017, Izumi et al., 2016). Given the manifestation of these conditions, an underlying type I IFN signature may be present but undocumented. However, similar to COPA syndrome, numerous other factors could be involved to

determine whether a particular COPI-deficiency results in a more pronounced developmental or inflammatory pathology.

A recent study identified a primary immunodeficiency disease associated with a novel homozygous LoF mutation in COPG1 (K652E) in five siblings presenting with recurrent bacterial and viral respiratory infections, T cell lymphopenia and dysregulated B cell function (Bainter et al., 2021). Impaired retrograde trafficking of KDELR-bound proteins and subsequently increased ER stress in activated B and T cells was identified as the underlying disease-causing mechanism. Treatment with the chemical chaperon tauroursodeoxycholic acid (TUDCA), an ER stress relieving agent, was able to reverse the B and T cell dysfunction in COPG1^{K652E} mice upon exposure to pet store mice (which models daily challenges of the human immune system). However, IL-6 serum levels remained elevated (Bainter et al., 2021), which may suggest additional activation of an ER stress-independent inflammatory pathway. In our *in vitro model,* CRISPR/Cas9-mediated deletion of COPG1 resulted in spontaneous STING signalling. However, since levels of type I IFN and ISGs were not measured in patients carrying the COPG1 K652E mutation and the clinical presentation does not overlap with symptoms of COPA syndrome, no conclusion about the contribution of a STING-driven pathology can be drawn.

Interestingly, we demonstrated that deficiency of COPA and COPG1 subunits results in strongly reduced cGAS activation following stimulation with synthetic DNA ligands, whereas direct STING stimulation is not impaired. This suggests defective innate immune defence mechanisms upon lost function of COPA and COPG1, which could perhaps contribute to immunodeficiency of COPG1 K652E patients. Although profound immunodeficiency has not been reported in COPA syndrome patients, recurrent respiratory and opportunistic infections were reported in individual cases (Jensson et al., 2017, Kato et al., 2021, Taveira-DaSilva et al., 2019, Watkin et al., 2015).

Since immune deficiency due to loss of cGAS-STING signalling is not described in the literature, it is not clear what pathology, if any, we should expect to see associated with COPI-mediated diseases.

The underlying cause of impaired stimulation-induced cGAS signalling in COPA^{deficient} and COPG1^{deficient} THP-1 cells remains elusive and is somewhat contradictory to elevated 2'3'-cGAMP baseline levels in COPA^{deficient} THP-1 cells. However, since dsDNA-induced second messenger production in parental control cells was ~10-fold higher compared to baseline levels in cells lacking COPA, cGAS activation may remain functional to some extent.

Secretory pathway defects may impact cGAS signalling on multiple levels, for example through insufficient PTMs, mislocalization of cGAS itself or essential regulatory proteins perhaps associated with phase separation. Recently, beside cytoplasmic compartments, the localization of cGAS within the nucleus has been established in various cell types, suggesting localization-dependent distinct functions (Gentili et al., 2019, Lahaye et al., 2018, Liu et al., 2018a, Orzalli et al., 2015, Sun et al., 2021, Volkman et al., 2019, Yang et al., 2017). Whereas nuclear cGAS has reduced enzymatic activity (Gentili et al., 2019, Sun et al., 2013) and may predominantly serve to control genomic DNA-related processes (Liu et al., 2018a), cytoplasmic cGAS localization was shown to be essential for its function as sensor of foreign DNA (Sun et al., 2021). Cytosolic shuttling is mediated through the N-terminal nuclear export signal (NES) L^{169}EKLKL^{174}, which is recognized by chromosome region maintenance 1 (CRM1, also known as Exportin-1 or XPO1) following stimulation with exogenous DNA (Gentili et al., 2019, Sun et al., 2021). Although neither cGAS nor CRM1 contain a C-terminal dilysine motif, COPI pathway deficiency could have a yet unknown direct or indirect impact on nucleocytoplasmic trafficking of cGAS, thereby limiting the inflammatory response following cytoplasmic DNA delivery.

Furthermore, a recent study redefines the localization of resting cGAS to the plasma membrane, where electrostatic interactions mediate binding to membrane lipids (Barnett et al., 2019). Interestingly, N-terminal cGAS truncations were unable to bind membranes, mislocalized within the cytoplasm, were spontaneously activated by cytosolic self-DNA and more responsive to drug-induced endogenous DNA damage. In contrast, type I IFN induction in response to viral infection was reduced compared to membrane-bound cGAS (Barnett et al., 2019).

Therefore, these examples demonstrate the importance of steady-state cGAS localization and the associated regulatory potential to prevent self-reactivity while enabling responsiveness to foreign DNA. Thus, further studies will be required to examine the subcellular localization of cGAS in COPI-deficient cells.
Although the previously discussed points are speculative and the mechanism remains unclear, the fact that dsDNA-stimulated cGAS signalling is largely impaired in the here used cell lines with defective retrograde transport remains a striking observation and hints towards an impactful role of COPI trafficking in cGAS pathway regulation. However as mentioned above, the physiological relevance in context of COPA syndrome patient mutations remains to be evaluated.

The involvement of STING in COPA syndrome has recently been further confirmed *in vivo*, using mouse models with heterozygous germline expression of COPA syndrome patient mutations E241K or V242G (COPA$^{E241K/wt}$ (Deng et al., 2020a, Deng et al., 2020b) and COPA$^{V242G/wt}$ (Kato et al., 2021)), which recapitulate the inflammatory lung phenotype observed in patients including lymphocyte infiltration and follicle formation. Whereas the lung phenotype was more pronounced in aged mice, signs of arthritis or kidney disease did not develop spontaneously in these models. Importantly, genetic deletion or pharmacological inhibition of STING completely abolished the ISG signature in murine-derived cells and genetic STING ablation was also able to recover embryonic lethality of homozygous COPA$^{E241K/E241K}$ mice when cross-bred with STING$^{gt/gt}$ animals (Deng et al., 2020b, Kato et al., 2021). Despite the phenotypic and clinical similarities observed in both mouse models, immunological phenotyping revealed increased levels of Th17 cells in COPA$^{E241K/wt}$ mice, which resembled findings in COPA syndrome patients carrying the E241K mutation (Deng et al., 2020a, Deng et al., 2020b, Watkin et al., 2015). However, this was not consistent in COPA$^{V242G/wt}$ mice (Kato et al., 2021). Furthermore, the functional evaluation revealed that COPA V242G to STING binding was not impaired in co-immunoprecipitation experiments, which is in contrast to reduced STING or SURF4 binding observed for other COPA mutants and the general

reduction in dilysine motif binding efficiency that was previously reported (Deng et al., 2020b, Kato et al., 2021, Lepelley et al., 2020, Mukai et al., 2021, Watkin et al., 2015). Nevertheless, inhibitor studies confirmed that inflammatory signalling in COPA$^{V242G/wt}$ mice-derived splenocytes was dependent on STING (Kato et al., 2021). Therefore, despite the adjacent location of E241K and V242G within the WD40 domain, the molecular consequences of certain COPA syndrome patient mutations may differ, which could be reflected in variability of phenotypic presentation and clinical manifestation.

Since functional retrograde trafficking is crucially important to maintain cellular homeostasis, deficiency of this pathway likely results in several molecular consequences leading to a complex disease pathology. To our knowledge today, the pathomechanisms in COPA syndrome include dysregulated type I IFN signalling, ER stress activation and T cell-mediated lung disease (Deng et al., 2020a, Kato et al., 2021, Lepelley et al., 2020, Mukai et al., 2021, Watkin et al., 2015). However, other yet unidentified pathways may be dysregulated and perhaps cell-type specific, thus contributing to variable disease onset, experienced symptoms and severity of the clinical course.

Notably, type I IFN production following stimulation of RNA sensor RIG-I and nucleic acid sensing TLR7 and TLR9 was impaired in COPA$^{V242G/wt}$ BMDCs (Kato et al., 2021). Furthermore in our hands, CRISPR/Cas9-mediated deletion of COPA in the human lymphoblastoid T cell line CEM and lung epithelial A549 cells revealed mildly increased type I IFN signalling, that appeared to occur via STING-independent pathways (data not shown). Although these findings require further experimental validation, they may suggest a possible link between retrograde trafficking deficiency and dysregulated RNA sensing pathways. In line with this, COPI vesicles and in particular subunits COPA and COPB have been suggested to interact with RNA and mediate long distance inter-compartmental trafficking in dendrites of neuronal cells (Todd et al., 2013) and yeast (Trautwein et al., 2004).

Involvement of STING-independent pathways is further supported by the phenotypic differences between SAVI and COPA syndrome. Although ILD is a predominant clinical manifestation of both diseases, DAH is commonly reported in COPA syndrome patients but only one recent case study reported this condition associated with SAVI (Tang et al., 2020b). Furthermore, cutaneous vasculopathy is a typical feature of SAVI, while skin manifestation is rarely reported in COPA syndrome (Guan et al., 2021, Jensson et al., 2017, Liu et al., 2014b). Although different protein expression levels and strength of aberrant STING signalling in disease-causing cell types may provide a possible explanation for the observed phenotypic differences, additional pathways activated by COPA-deficiency may additionally contribute.

Recently, the novel COPA variant, I164V, was described. Despite its location within the WD40 repeat domain, COPA I164V does not impair dilysine motif binding but rather acts as dominant variant with tumour-suppressing potential (Song et al., 2021). In contrast to COPA syndrome-causing mutations, which occur on genomic level, the I164V mutation results from adenosine (A)–to–inosine (I) dsRNA editing mediated by ADAR2 (Chan et al., 2014, Song et al., 2021). Mechanistically, edited COPA I164V was shown to be less stable and undergo proteasomal degradation more rapidly compared to WT COPA. COPA I164V-expressing cells expressed lower levels of caveolin-1 (CAV1), a protein implicated in PI3K/AKT/mTOR pathway activation and cell proliferation (Yang et al., 2016). Thus, during homeostasis, ADAR2-mediated editing of COPA maintains the balance between growth-promoting WT COPA and COPA I164V (35-50% of transcripts), which functions as tumour suppressor. Analysis of several cancer tissues revealed absence of COPA I164V due to ADAR2-deficiency, associated with more aggressive tumour growth and poor prognosis (Song et al., 2021). Similarly, other COPI subunits, including COPB2 and COPZ2 have been reported as oncogenes associated with several cancers (Feng et al., 2021, Shtutman et al., 2011).

In general, these findings suggest a link between increased COPI function and cancer development. Although renal, lung and thyroid carcinomas have been

reported in individual COPA syndrome patients, this was mostly associated with advanced patient age (Kato et al., 2021, Taveira-DaSilva et al., 2019). A tumour-promoting potential of LoF mutations in COPA can therefore likely be excluded.

Identification of the innate immune pathway underlying aberrant type I IFN signalling in COPA syndrome is particularly exciting in the context of pharmacological intervention. Originally, COPA syndrome patients have been treated with various combinations of immunosuppressive drugs including steroids, DMARDs, nonsteroidal anti-inflammatory drugs (NSAIDs) and biologics, which were only able to partially control the disease (Boulisfane-El Khalifi et al., 2019, Brennan et al., 2017, Fremond et al., 2020, Jensson et al., 2017, Noorelahi et al., 2018, Taveira-DaSilva et al., 2019, Tsui et al., 2018, Volpi et al., 2018, Watkin et al., 2015). For seven reported patients the severely progressing ILD and DAH resulted in end-stage pulmonary failure prompting lung transplantation and one additional patient has been reported as a listed candidate (Jensson et al., 2017, Mallea et al., 2020, Tsui et al., 2018, Watkin et al., 2015, Kato et al., 2021, Lepelley et al., 2020). Five patients underwent satisfying recovery at the time of case report publication, whereas two patients deceased due to post-transplant infections or respiratory failure (Kato et al., 2021). Importantly, *post mortem* biopsy analysis of the transplanted lung from the latter patient showed pathological findings similar to COPA-related ILD, which raises concerns regarding disease relapse (Kato et al., 2021). This is in congruence with data from *in vivo* models showing that the inflammatory cytokine milieu within the thymus of COPA$^{E241K/+}$ mice impairs negative selection of developing T cells, which results in T cell-mediated lung inflammation (Deng et al., 2020a). Therefore, long-term follow-up studies of COPA syndrome patients following lung transplantation are crucially important to establish an effective treatment strategy, aiming to maintain graft survival and prevent infections and relapse of T cell-mediated ILD. Further, early diagnosis and therapeutic intervention are crucial to prevent detrimental irreversible lung damage during young age.
Importantly, inhibition of type I IFN signalling by JAK inhibitors baricitinib and ruxolitinib has successfully improved disease and lung pathology in SAVI patients

(Balci et al., 2020, Frémond et al., 2016, Sanchez et al., 2018, Volpi et al., 2019), although transient or poor responders have also been reported (Tang et al., 2020b, Volpi et al., 2019). Similarly, JAK inhibitors ruxolitinib, baricitinib and upadacitinib successfully reduced the type I IFN signature and joint inflammation in COPA syndrome patients, with limited improvement of lung function leading to DAH relapse and fibrosis progression in one reported case (Fremond et al., 2020, Kato et al., 2021, Krutzke et al., 2019).

Although the factors that determine JAK inhibitor efficacy in SAVI and COPA syndrome patients remain unclear, type I IFN-independent and cell-type specific functions of STING should be considered. In T cells, STING disturbs calcium homeostasis, which increases the susceptibility to activation-induced ER stress and apoptosis (Wu et al., 2019). Furthermore, STING activation triggers autophagy (Gui et al., 2019), proinflammatory signalling through NF-κB and MAPK activation (Abe et al., 2014) as well as lysosomal trafficking and cell death (Gaidt et al., 2017). Future studies are required to elucidate the contribution of these pathways to STING-mediated pathologies, however it is likely that links exist.

Therefore, our study and complementary results from Deng et al. (Deng et al., 2020b) provide hope that targeting the STING pathway directly, for example with a STING inhibitor such as H-151, may be more specific and powerful to simultaneously block multiple STING effector functions. Compared to JAK inhibitor treatment, this approach may provide increased therapeutic benefit to control STING-mediated symptoms in COPA syndrome.

4 Recessive *NLRC4*-autoinflammatory disease reveals an ulcerative colitis locus

4.1 Introduction

4.1.1 NLRC4 inflammasomopathies

Classified as inflammasomopathies, autoinflammatory diseases caused by overactivation of NLRC4 signalling (NLRC4-AID) typically present very early in life with a broad spectrum of clinical manifestations and varying severity (Duncan et al., 2018).

Despite the first description of NLRC4 in 2001 (Geddes et al., 2001, Poyet et al., 2001), an autoinflammatory syndrome caused by GoF mutations in this gene was first reported in 2014 and originally described as a syndrome of enterocolitis and autoinflammation associated with mutation in *NLRC4* (SCAN4) or NLRC4 macrophage activation syndrome (NLRC4-MAS) with or without enterocolitis (Canna et al., 2014, Romberg et al., 2014).

To date, the literature reports 19 unrelated families with 47 NLRC4-AID patients harbouring one of 12 missense mutations or a 93 bp deletion in *NLRC4*, which affect highly conserved amino acid residues within the nucleotide-binding domain (NBD), helical domain 1 (HD1), winged helix domain (WHD) or leucine-rich repeat domain (LRR) (**Figure 4.1**, **Suppl. Table 2**). Due to the observed spectrum of clinical symptoms, NLRC4-AIDs are classified into four groups of phenotypes which include familial cold autoinflammatory syndrome (FCAS4), neonatal-onset multisystem inflammatory disease (NOMID), NLRC4-MAS and autoinflammation with infantile enterocolitis (AIFEC); with NOMID, NLRC4-MAS and AIFEC being associated with a more severe clinical course (Wang et al., 2021a, Barsalou et al., 2018, Bracaglia et al., 2015, Canna et al., 2017, Canna et al., 2014, Goddard 2017, Jeskey et al., 2020, Kashiwagi et al., 2008, Kawasaki et al., 2017, Kitamura et al., 2014, Liang et al., 2017, Moghaddas et al., 2018, Romberg et al., 2014, Siahanidou et al., 2019, Volker-Touw et al., 2017).

Importantly, extremely elevated serum levels of IL-18 are commonly observed in NLRC4-AID patients, which were found to remain high between inflammatory

flares and during currently used methods of therapeutic intervention (Canna et al., 2014, Romberg et al., 2014). Interestingly, this represents a special hallmark of MAS and NLRC4-AID, since only moderately elevated IL-18 levels are observed in other inflammasomopathies, such as those caused by NLRP3 mutations (in CAPS) (Almeida de Jesus et al., 2013, Weiss et al., 2018). Furthermore, although inflammatory flares in both CAPS and NLRC4-AID are associated with an elevation of systemic inflammation markers C-reactive protein (CRP) and erythrocyte sedimentation rate (ESR) in patient blood, other immunological and laboratory features differ. NLRC4-MAS coincides with an increase of lactate dehydrogenase (LDH) and ferritin, which are used as clinical markers of tissue damage (Kell et al., 2014, Sepulveda 2019), as well as reduced thrombocyte and leucocyte counts. In contrast, in CAPS patients, LDH and ferritin are mostly normal or only slightly elevated, whereas thrombocytosis and leucocytosis are commonly observed (Alehashemi et al., 2020), thus suggesting differences in disease pathogeneses. Furthermore, a gastrointestinal pathology with varying severity is often reported for NLRC4-AID patients but does not represent a typical feature of NLRP3-driven inflammasomopathies (Alehashemi et al., 2020).

Suppl. Table 2 summarizes previously published NLRC4-AID case reports highlighting the disease-causing mutation, diagnosis, symptoms, therapeutic intervention, clinical outcome and experimental techniques used to validate the pathogenic potential associated with the identified missense mutation. The following more detailed description aims to introduce the overall phenotypic presentation and highlights specific findings in individual cases as well as results from *in vitro* and *in vivo* validation experiments. Structural consequences induced by the identified missense mutations are further discussed in chapter 5.1.5.

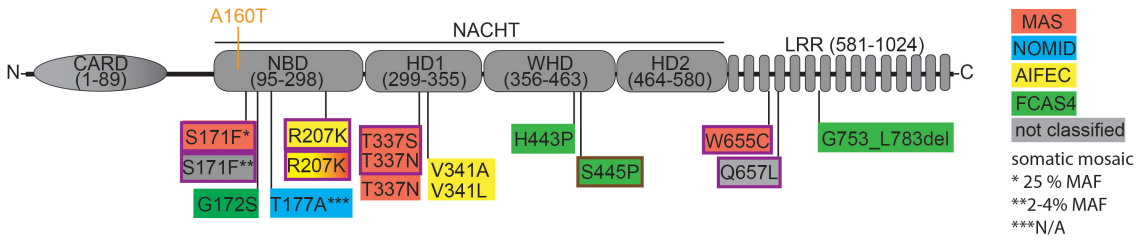

Figure 4.1 | Clinical diagnosis of NLRC4-AID and localization of gain of function mutations within NLRC4 protein domains. The indicated clinical diagnoses are adopted from respective case reports or following the clinical classification by Wang et al. (Wang et al., 2021a): macrophage activation syndrome (MAS; red), autoinflammation with infantile enterocolitis (AIFEC, yellow), familial cold autoinflammatory syndrome 4 (FCAS4, green) and neonatal-onset multisystem inflammatory disease (NOMID, blue). The purple outline indicates additional gastrointestinal pathology, such as intestinal inflammation, abdominal pain or diarrhea in patients with non-AIFEC diagnosis. Gradient colour for R207K indicates no clear diagnosis in this patient who presented with vasoplegic syndrome, systemic and early gastrointestinal inflammation and some laboratory features of MAS (Bardet et al., 2021). Grey colour indicates mutations in patients without distinct clinical diagnosis presenting with inflammatory flares affecting the skin, joints and/or gastrointestinal symptoms including the first case of late-onset NLRC4-AID (S171F**) (Chear et al., 2020, Ionescu et al., 2021). Within the family carrying the S445P mutation (brown outline), out of 13 affected individuals without gastrointestinal symptoms, two patients developed late-onset enterocolitis (ulcerative colitis, inflammatory bowel disease) (Volker-Touw et al., 2017). The novel homozygous mutation NLRC4 A160T reported in this thesis (chapter 4.2.1) is shown in orange. Asterisks indicate somatic mosaic mutations with reported mutant allele frequencies (MAF). Not available, N/A. Numbers refer to amino acid residues in hNLRC4 (Uniprot: Q9NPP4). Protein domain borders are indicated according to Hu et al. 2013.

FCAS, also termed familial cold urticaria was originally associated with mutations in *NLRP3* and *NLRP12*, characterized by autosomal dominant inheritance and recurrent episodes of cold-induced fever, rash, arthralgia, myalgia, nausea and conjunctivitis and additional sensorineural hearing loss in some cases. Presenting early in life, episodes typically occur within a few hours after cold exposure and resolve within one day (Jéru et al., 2008, Hoffman et al., 2001, Nakanishi et al., 2017). Interestingly, a similar phenotypic presentation was later described in patients carrying mutations in *NLRC4*, termed FCAS4 (*NLRP3/NLRP12* mutations were absent) (Jeskey et al., 2020, Volker-Touw et

al., 2017). To date, the literature reports four families with FCAS4, all caused by inherited NLRC4 GoF mutations (H443P, S445P, G172S, G753_L783del) (**Figure 4.1**) (Kitamura et al., 2014, Wang et al., 2021a, Jeskey et al., 2020, Volker-Touw et al., 2017). Of these missense mutations, H443P and S445P localize within the WHD of NLRC4 and were inherited across several generations affecting 13 family members of the respective kindreds (Kitamura et al., 2014, Volker-Touw et al., 2017). *In vitro* studies validating NLRC4 H443P showed spontaneous oligomerization, caspase-1 and IL-1β cleavage in HEK293T cells following transient co-expression with pro-caspase-1 and pro-IL-1β-encoding plasmids, which confirmed the GoF phenotype (Kitamura et al., 2014). Furthermore, patient-derived PBMCs stimulated with NLRC4-specific trigger PrgI or exposed to 32 °C temperature released elevated levels of IL-1β. Pathogenicity was further confirmed in transgenic mice with heterozygous expression of HA-tagged mNLRC4^{H443P}, which spontaneously developed dermatitis, severe arthritis, splenomegaly and bone erosion. The inflammatory phenotype was further triggered by cold exposure, however this was not essentially required for disease onset (Kitamura et al., 2014). Injection of neutralizing antibodies targeting immune cell activation markers or inflammatory cytokines identified IL-1β and infiltrating neutrophils as crucial drivers of the inflammatory response. Levels of IL-18 were not reported in this *in vivo* study (Kitamura et al., 2014).

In the family members carrying the NLRC4 S445P mutation, most patients developed arthralgia and conjunctivitis. Interestingly, distinct skin phenotypes were observed in adult and paediatric patients, described as erythematous nodes (with or without urticarial patches) or isolated urticarial rash, respectively (Volker-Touw et al., 2017). Besides cold-induced, episodes were also triggered by emotional stress or infections in some patients (Volker-Touw et al., 2017). Although unusual for FCAS4, additional gastrointestinal symptoms were observed in two patients of this family, who developed late-age onset ulcerative colitis (UC) or inflammatory bowel disease (IBD), respectively. However due to the late onset it remains unclear whether these are directly linked to the NLRC4 mutation (Volker-Touw et al., 2017).

The classical FCAS4 phenotype was further expanded by a recent case report of a patient who presented with longer lasting inflammatory episodes (three to six days), persistent facial skin rash and chronic ulcers, which were exacerbated during cold exposure (Jeskey et al., 2020). Interestingly, genomic analysis revealed a 93 bp in-frame deletion (c.2258_2350del; p.G753_L783del) in exon 5 within the LRR domain, which was observed in both affected family members, who presented with similar symptoms (Jeskey et al., 2020). Additionally, the index patient from this study and another FCAS4 patient carrying the NLRC4 S445P mutation (Volker-Touw et al., 2017) experienced sensorineural hearing loss, which is a typical feature of NLRP3-driven inflammasomopathies as mentioned above (Goldbach-Mansky et al., 2006).
The recently identified G172S mutation mapped to the NBD of NLRC4 and caused FCAS4-like symptoms in a mother and her son. Both individuals presented with mild systemic inflammation including fever, arthralgia and recurrent skin rashes, however disease onset following cold exposure was only reported for the mother (Wang et al., 2021a).
If measured and reported, IL-18 serum levels were elevated in FCAS4 patients (Volker-Touw et al., 2017, Wang et al., 2021a).

Originally, NOMID described the most severe form of CAPS (Prieur et al., 1987), however one case study identified a patient with somatic mosaic heterozygous GoF mutation in NLRC4, T177A, which was diagnosed as NOMID based on a similar clinical manifestation (**Figure 4.1**). The patient presented with the typically observed face morphology (saddle nose, frontal bossing), fever, skin and joint inflammation as well as sensorineural hearing loss, aseptic meningitis and mental retardation. MAS was not reported, however serum levels of IL-18 remained consistently elevated, even when symptoms were successfully controlled by treatment with recombinant IL-1 receptor antagonist anakinra (Kashiwagi et al., 2008, Kawasaki et al., 2017, Kawashima et al., 2007). To date, this remains the only report of a NLRC4 mutation associated with a classical phenotypic presentation of NOMID.

Both NLRC4-MAS and AIFEC are characterized by a more severe clinical course, which frequently requires hospitalization during inflammatory episodes and may have fatal consequences (Barsalou et al., 2018, Bracaglia et al., 2015, Canna et al., 2017, Canna et al., 2014, Goddard 2017, Liang et al., 2017, Moghaddas et al., 2018, Romberg et al., 2014, Siahanidou et al., 2019). Both conditions are caused by overactivation of macrophages, NK cells and cytotoxic T cells that lead to profound IL-1β-, IL-18- and IFNγ-mediated hyperinflammation, which is clinically diagnosed as MAS (chapter 1.3.3.2) (Canna et al., 2017, Canna et al., 2014, Romberg et al., 2014). NLRC4-MAS does not typically present with gastrointestinal pathology, whereas infantile secretory diarrhea, abdominal pain, intestinal inflammatory infiltrates and enterocolitis are commonly observed in AIFEC patients and represent a hallmark to discriminate both manifestations. Several NLRC4-MAS patients have been reported with additional signs of gastrointestinal inflammation, however laboratory tests, clinical examinations and biopsies of the GIT are typically performed to confirm the diagnosis of AIFEC (Canna et al., 2017, Canna et al., 2014, Romberg et al., 2014). NLRC4-MAS and AIFEC patients develop symptoms very early in life (between days to months of age), in fact one patient with MAS and enterocolitis carrying the S171F mutation developed disease *in utero* (Liang et al., 2017). Stringent and early therapeutic intervention using immunomodulatory therapy is required, however four reported patients succumbed to the severe clinical course of the disease at very young age (Liang et al., 2017, Moghaddas et al., 2018, Romberg et al., 2014).

To date, MAS and AIFEC are the most reported phenotypes associated with NLRC4 overactivation, caused by GoF mutations within different functional domains (**Figure 4.1**). One of the first reports of AIFEC identified the V341A mutation within the HD1 in three affected family members (Romberg et al., 2014). The index case in this study developed symptoms 10 days after birth and succumbed at day 23 due to severe alveolar hemorrhage. A similar symptomatic presentation was also reported for the five year old half-brother and the 43 year old father, who are still alive. Interestingly, although the father developed symptoms early in life and required frequent hospitalization, the gastrointestinal manifestation resolved by one year of age. During later life, he presented with a

more pronounced inflammatory phenotype affecting skin, joints and respiratory abilities. Inflammatory episodes were frequently triggered by physical and emotional stress (Romberg et al., 2014). Remarkably, despite carrying the same mutation, individuals in this family experienced variable clinical presentations and outcomes, emphasizing the heterogeneity of NLRC4-associated autoinflammation. Pathogenicity of NLRC4 V341A was confirmed *in vitro*, showing increased pro-caspase-1 cleavage and ASC speck formation in HEK293 overexpression assays as well as increased IL-1β, IL-18 release and cell death after LPS priming of patient-derived macrophages (Romberg et al., 2014).
At the same time, Canna et al. independently described a seven year old patient with recurrent periodic fevers, autoinflammation, mild gastrointestinal symptoms, skin rash and splenomegaly who first developed symptoms at six months of age caused by the heterozygous *de novo* T337S mutation in *NLRC4* (Canna et al., 2014). *In vitro* experiments using patient-derived monocytes or MDMs showed increased cell death and elevated levels of released IL-18 at baseline. Increased cytokine release and pyroptosis following stimulation with LPS and flagellin confirmed NLRC4 inflammasome hyperactivation (Canna et al., 2014). Inflammatory episodes were well controlled after treatment with anakinra was initiated, despite remaining high levels of IL-1β and IL-18 (Canna et al., 2014).
Affecting the C-terminal LRR, the W655C mutation was described in two unrelated patients with very early-onset MAS (11 days or 18 months of age) and extremely high levels of serum IL-18 with gastrointestinal symptoms including abdominal pain, secretory diarrhea, and mortality due to the severity of their condition (Moghaddas et al., 2018). *In vitro* evaluation of monocytic THP-1 cells reconstituted with NLRC4 W655C showed increased cytokine release and cell death production following priming with TLR1/2 agonist Pam3CSK4, which occurred in a caspase-1-dependent manner and suggested constitutive NLRC4 activation (Moghaddas et al., 2018).

In addition to the above-described cases identified with *NLRC4* germline mutations, three patients with mosaic somatic mutations have been reported (Ionescu et al., 2021, Kawasaki et al., 2017, Liang et al., 2017), which originate

from *de novo* mutations during postzygotic development. Whether the mutation occurs early or late during postzygotic stages determines the extent of affected cell lineages and defines subsequent organ distribution (Freed et al., 2014). Depending on the tissue distribution of the mutant allele, organ involvement, clinical presentation and disease outcome may differ.

Interestingly, somatic mosaicism of the same mutation in NLRC4, S171F, was identified in a patient with neonatal-onset presentation of MAS and enterocolitis (Liang et al., 2017) and the first described patient of late-onset NLRC4-AID, who initially developed clinical symptoms at age 47 (Ionescu et al., 2021). A very severe clinical course of MAS was observed in the child with *in utero*-onset (Liang et al., 2017), manifesting as ascites, anemia and fetal thrombotic vasculopathy of the placenta, the latter most likely being the consequence of the inflammatory cytokine environment (Liang et al., 2017). Disease progression continued after birth and the patient deceased after 60 days due to respiratory failure, acidosis and hyperkalemia. *Post mortem* analysis identified fibrotic changes in several organs including liver and pancreas, chronic bowel injury with necrotizing enterocolitis-like pattern indicating severe organ inflammation. In patient blood, the mutant allele was detected at a frequency of 25 %, however organ distribution was not fully assessed and IL-1β and IL-18 levels were not measured (Liang et al., 2017).

In the previously overall healthy patient with late-age disease onset, recurrent episodes of fever and systemic inflammation developed at age 47 years and occurred every six to eight weeks for two to three days without skin manifestation. Increasing flare frequency was subsequently observed (at age 53 years), which was initially well controlled by anakinra treatment, however progressed (55 years of age) towards increased flare frequency, myalgia, arthralgia, gastrointestinal symptoms, inflammation and anemia. MAS was not reported and elevation of anakinra dose normalized inflammation (Ionescu et al., 2021). Repeated genetic analysis of peripheral blood revealed the somatic mosaic mutation NLRC4 S171F at a mutant allele frequency between 2-4 %. Serum IL-18 levels remained consistently high during anti-IL-1β treatment. The *in vitro* analysis of patient PBMCs showed elevated baseline IL-18 release, which was not significantly

increased following NLRC4 stimulation, suggesting stimulus-independent maximal activation. However, stimulation of NLRP3 or NLRC4 *in vitro* only triggered low IL-1β release from patient PBMCs. Additionally, LPS priming failed to induce *IL1B* transcription, although *IL6* transcription was normal (Ionescu et al., 2021). Given the responsiveness to anakinra treatment, the deficiency to secrete IL-1β was surprising and explained by methodological differences compared to *ex vivo* stimulation experiments in previous studies (use of PBMCs and shorter stimulation time) (Ionescu et al., 2021).

The differences regarding clinical course and disease onset between both patients carrying the S171F mutation are striking and likely the result of different mutant allele frequency and differentially affected cell lineages.

The second known somatic mosaic mutation NLRC4 T177A was identified in the above-described patient with phenotypical presentation of NOMID (Kawasaki et al., 2017). Somatic mosaicism was discovered experimentally when Kawasaki and colleagues aimed to generate an *in vitro* disease model and derived induced pluripotent stem cell (iPSC) lines from patient fibroblasts (Kawasaki et al., 2017). Functional analysis of IL-1β release following LPS priming revealed phenotypic heterogeneity between monocytes derived from multiple iPSC clones, which could be separated into two groups: WT response or overactive inflammasome signalling. Whole exome sequencing confirmed presence of the NLRC4 T177A mutation only in cell lines with GoF phenotype, which was experimentally demonstrated by caspase-1- and NLRC4-dependent cytokine release after LPS stimulation (Kashiwagi et al., 2008, Kawasaki et al., 2017, Kawashima et al., 2007).

Therefore, these examples illustrate the challenges of diagnosing NLRC4-AID due to the heterogeneity of clinical manifestations. Diagnosis relies on the measurement of clinical inflammatory markers, serum cytokine analysis and genetic sequencing. Importantly, since the recent description of the first case of late-onset NLRC4-AID (Ionescu et al., 2021), this diagnosis should be considered independent of the age of the presenting patient.

4.1.2 Genotype-phenotype correlation

Based on the above description of identified mutations and associated clinical manifestations (**Figure 4.1**, **Suppl. Table 2**), a clear genotype-phenotype correlation has not yet been established and further studies are required to understand functional consequences of NLRC4 mutations on the molecular level (Liang et al., 2017). However interestingly, the only two described mutations within the WHD were associated with the milder FCAS4 phenotype (Kitamura et al., 2014, Volker-Touw et al., 2017), which may suggest mild NLRC4 activation following structural changes in this domain. In contrast, mutations in NBD, HD1 and LRR caused predominantly severe clinical courses. Within the LRR, two unrelated patients carrying the W655C mutation succumbed due to the severity of NLRC4-MAS and gastrointestinal symptoms very early in life, which may indicate a particularly severe disease progression upon disturbance of this domain, as previously suggested (Moghaddas et al., 2018). However, a patient carrying the Q657L mutations in a nearby residue experienced a less severe clinical course and was alive at age 7, although due to the proximity of both mutated residues a similar disease-causing mechanism of action was suggested (Chear et al., 2020).

An additional level of heterogeneity is implicated by the previously mentioned family of FCAS4 patients, where the NLRC4 S445P mutation caused distinct skin phenotypes in paediatric and adult patients and varying efficacy of anakinra treatment was observed (Volker-Touw et al., 2017).

Similarly, within one family, the V341A mutation caused AIFEC in three male family members, however disease outcomes largely differed, with two surviving individuals aged 7 and 46 years and one patient who succumbed to the disease at 23 days of life (Romberg et al., 2014).

Based on these examples, the disease phenotype and severity associated with mutations in NLRC4 cannot necessarily be predicted according to the affected functional domain. Further understanding of NLRC4 inflammasome biology and distinct molecular pathways is required to elucidate a possible genotype-phenotype correlation. Additional contribution of environmental factors or genetic

variants may further determine the time of disease onset, phenotypic presentation and clinical outcome in NLRC4-AID patients.

4.1.3 Current treatment

The previously published case reports highlight the phenotypic diversity, which is associated with challenges to treat NLRC4-mediated diseases. Whereas in some patients with FCAS4, symptoms spontaneously resolved without treatment or were manageable with NSAIDs or corticosteroids, other patients experienced severe and life-threatening clinical courses and required hospitalization, intensive care and therapeutic intervention with immunosuppressive drugs and biologics (**Suppl. Table 2**). Blockade of IL-1β signalling with anakinra (IL-1 receptor antagonist), canakinumab (anti-IL-1β monoclonal antibody) and rilonacept (soluble IL-1β and IL-1α decoy receptor) has proven as a highly effective treatment of inflammasomopathies caused by NLRP3 mutations (Gillespie et al., 2010, Kullenberg et al., 2016, Yokota et al., 2017). However, in NLRC4-AID, the response to anakinra treatment is variable and limited, especially in patients with early disease onset and severe clinical course involving gastrointestinal symptoms and MAS (Canna et al., 2017, Moghaddas et al., 2018) (**Suppl. Table 2**). These differences are largely attributed to the important role and contribution of IL-18 signalling to NLRC4-AID pathology, which is emphasized by dramatically elevated serum levels that are absent in CAPS patients (**Suppl. Table 2**) (Weiss et al., 2018). Pro-IL-18 is broadly expressed in myeloid and epithelial cells and a correlation between MAS, persistent elevation of total serum IL-18, IL-18BP and highly elevated levels of biologically active free IL-18 during disease activity was described, suggesting that IL-18 could be the predominantly disease-driving cytokine in NLRC4-AID, at least in some patients (Weiss et al., 2018).
Therefore, neutralization of free IL-18 by treatment with recombinant human IL-18 binding protein (rhIL-18BP) (tradekinig-α, A2 Biotherapeutics) has been suggested as a promising treatment strategy for NLRC4-driven AIDs (Canna et al., 2017). The evaluation of this drug is currently ongoing in phase 3 clinical trials

(see below), but compassionate use in one AIFEC patient successfully controlled disease symptoms, after anakinra treatment alone had no effect (Canna et al., 2017). A second study reports rhIL-18BP treatment of a patient with NLRC4-MAS and severe gastrointestinal phenotype presenting 11 days after birth. The patient was unresponsive to anakinra, but rhIL-18BP treatment improved some clinical parameters, however long-term effects could not be assessed because treatment was terminated due to the severity of the disease and end-organ damage following wishes of the patient's family (Moghaddas et al., 2018). This case emphasizes that efficacy of rhIL-18BP treatment likely depends on the duration and severity of the illness prior to therapy initiation.

RhIL-18BP tradekinig-α is currently trialled for NLRC4-MAS, XIAP-deficiency (NCT03113760, phase 3 ongoing) and AOSD (NCT02398435, phase 2 completed), which are diseases that commonly present with elevation of serum IL-18 levels and do not yet have a potent standard of care (Colafrancesco et al., 2012, Wada et al., 2014). Targeting the same pathway, a recombinant humanized monoclonal anti-IL-18 antibody (GSK1070806, GlaxoSmithKline) is being evaluated for several other conditions including IBD (NCT01035645, phase 1, completed), type 2 diabetes mellitus (NCT01648153, phase 2, completed) and Crohn's disease (NCT03681067, phase 1 and 2, completed), since *in vivo* evidence supports the important role of IL-18-driven proinflammatory signalling in IBD and type 2 diabetes (Thorand et al., 2005, Williams et al., 2019). Inhibition of this pathway may therefore provide a promising strategy for the treatment of both rare autoinflammatory conditions as well as more common chronic intestinal or metabolic disorders.

Additionally, alternative therapeutic approaches targeting signalling pathways downstream of IL-18 have been trialled in NLRC4-AID patients with promising results. Bracaglia and colleagues report a patient who developed NLRC4-MAS 20 days after birth (Bracaglia et al., 2015). Combination treatment of broad immunosuppression and anti-human IFNγ–neutralizing monoclonal antibody emapalumab resulted in progressive improvement of all symptoms and full recovery at 4.5 months. Interestingly, despite clinical recovery, serum levels of

IL-18 and IFNγ remained elevated, indicating that NLRC4 autoactivation persisted (Bracaglia et al., 2015).

Combination therapy with anakinra and mTOR inhibitor rapamycin was able to significantly improve clinical parameters and symptoms in one patient with MAS and enterocolitis and additionally reduced IL-18 plasma levels (Barsalou et al., 2018). In this study, the positive effect of rapamycin was suggested to be attributable to prevention of IL-18-mediated activation of NK cells and T cell differentiation by mTOR inhibition (Almutairi et al., 2019, Chi 2012). Furthermore, *in vitro* analysis of patient-derived MDMs stimulated with LPS and NLRP3 or NLRC4 activators showed reduced cytokine release and caspase-1 activity in presence of rapamycin. This additional direct inhibitory effect on inflammasome signalling requires further investigation but was proposed to be the result of autophagy (Barsalou et al., 2018), which was previously shown to reduce NLRP3-mediated cytokine release in macrophages (Ko et al., 2017).

These reports highlight alternative approaches targeting downstream effects of IL-18 to prevent exacerbated systemic inflammation, which proved efficient in combination with immunosuppressants or anti-IL-1β therapy.

Hematopoietic stem cell transplantation (HSCT) was established as the only curative treatment for primary HLH, which resembles MAS regarding clinical disease course and immunological characteristics as previously mentioned (chapter 1.3.3.2) (Bergsten et al., 2017, Trottestam et al., 2011). Although not peer-reviewed or published, a conference presentation at the 2017 Annual Meeting of the Clinical Immunology Society reported an early-onset patient carrying the NLRC4 GoF mutation R207K, who presented with HLH-like syndrome classified as AIFEC by Wang et al. (Wang et al., 2021a). The clinical manifestation included fever, thrombocytopenia, coagulopathy, enteropathy, renal and respiratory failure, which was treated with bone marrow transplantation at 4 months of age (conference presentation (Goddard 2017)). Successful recovery allowed termination of anakinra treatment, however the long-term outcome was not reported and therefore the therapeutic benefit remains unclear to date and requires further studies (Goddard 2017). Notably, since experimental evidence from murine studies suggests a significant contribution of NLRC4-

mediated release of IL-18 and eicosanoids from IEC or tissue-resident peritoneal macrophages (Rauch et al., 2017, von Moltke et al., 2012, Weiss et al., 2018), HSCT may only represent a partial cure of the myeloid cell-driven inflammation in NLRC4-AID patients.
These case reports highlight that the clinical outcome of patients with a severe clinical course largely depends on rapid diagnosis. Assessment of IL-18 levels could serve as biomarker and together with genetic sequencing prompt the diagnosis of NLRC4-AID. Although no standard treatment currently exists, early therapeutic intervention by targeted inhibition of inflammation-mediating cytokine pathways has shown promising results in individual cases and appears crucial to prevent severe organ damage in NLRC4-MAS and AIFEC patients (Romberg et al., 2017).

In contrast to the previously reported heterozygous genotypes associated with NLRC4-AID, we here report the autoinflammatory phenotype of a patient identified with the first homozygous mutation in NLRC4 (A160T) and validate the pathogenic potential of this mutation *in vitro* using cell-based assays (chapter 4). Furthermore, mutation-induced consequences on the protein structure and biophysical behaviour were investigated using recombinant protein approaches (chapter 5).

Results presented in chapter 4 (except **Figure 4.10**) have been published in the Journal of Clinical Immunology (Steiner et al., 2021).

In this chapter, all annotations refer to human NLRC4 (hNLRC4) unless indicated otherwise.

4.2 Results

4.2.1 Case presentation

A 62 year old Brazilian female patient was evaluated for recurrent episodes of systemic inflammation since six months of age. Episodes were characterized by recurrent low-grade fever, chills, oral ulceration, uveitis, arthralgia (sometimes arthritis), myalgia and abdominal pain followed by diarrhea with mucus and variable erythematous macular rash. Several inflammatory episodes were triggered by gastrointestinal and urinary tract infections, mainly caused by *E. coli* or both *E. coli* and *Klebsiella*, respectively. The flares lasted from seven to ten days and occurred on average three to four times per year, but more than ten flares a year could be observed. Episodes of fever correlated with elevation of acute phase markers in the patient's serum, including CRP, serum amyloid A (SAA) and ESR, indicating inflammation (**Figure 4.2 A-C**). A whole-body PET-CT scan realized during one of the flares while the patient suffered from abdominal pain and diarrhea (in 2016) depicted heterogeneous and diffuse bowel glycolytic activity (**Figure 4.2 D**).

Colon biopsies were performed and showed unspecific lymphocyte infiltration. However, ulcers, abscesses or clear signs of inflammation could not be observed during regular macroscopical examinations. Fecal calprotectin levels, a commonly used marker to monitor neutrophil migration into gastrointestinal tissue (Pathirana et al., 2018), measured 1293 mg/kg before anti-IL-1β therapy was started, which was above normal range (<50 mg/kg) and indicated gastrointestinal inflammation. Serum IgG was decreased, while IgA and IgM levels were low but within reference ranges (**Figure 4.2 E**). Flow cytometry analysis of total lymphocytes collected when the patient was not in flare showed decreased levels of B cells (CD19+: patient 1.6% vs. reference 11%), as well as low B memory cells (CD27+: patient 21.6% vs. reference >27%) and elevated double negative T cells (CD4-/CD8-/TCR αβ: patient 2.1% vs. reference < 1.7%) (data not shown). ANA testing fluctuated between negative (1:80) and positive (1:320) values (data not shown).

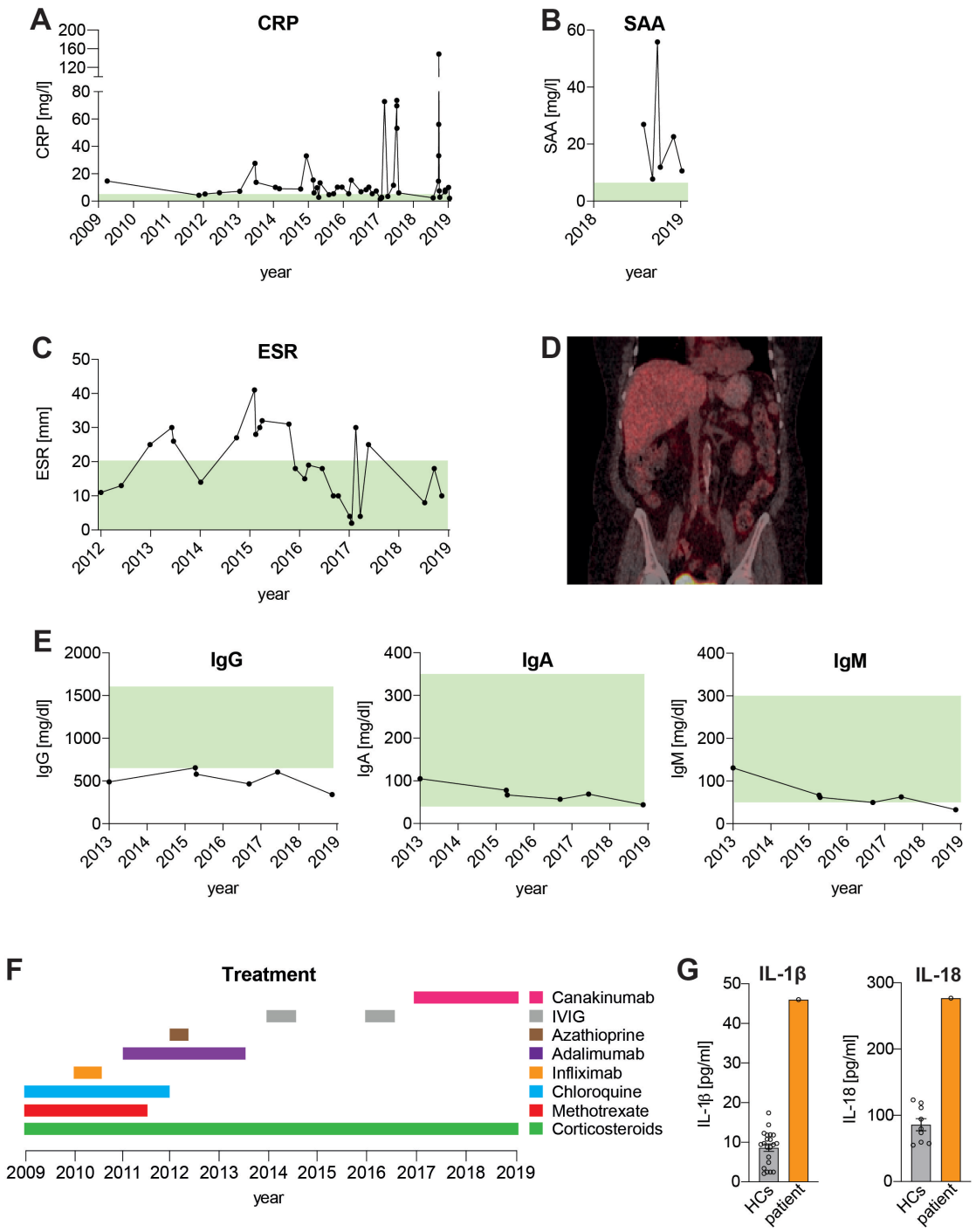

Figure 4.2 | Biochemical analysis of patient samples, treatment timeline and serum cytokine levels. A-C) Patient blood analysis of clinical inflammation markers over the indicated time period measuring **A)** C-reactive protein (CRP, normal range (green): <5 mg/l), **B)** serum amyloid A (SAA, normal range (green): <6.4 mg/l) and **C)** erythrocyte sedimentation rate (ESR, normal range (green): <20 mm). **D)** Whole-body PET-CT scan performed during an inflammatory episode in 2016. **E)** Measurement of serum levels of IgG (normal range (green): 650-1600 mg/dl), IgA (normal range (green): 40-350 mg/dl) and

IgM (normal range (green): 50-300 mg/dl) over several years. **F)** Timeline for immunomodulatory treatments. Chloroquine: 400 mg daily, no effect. Methotrexate: 20 mg weekly, no effect. Azathioprine: 50 mg daily, stopped after concomitant viral infection was observed. Infliximab: 400 mg every 2 months, no effect. Adalimumab: 40 mg every 2 weeks, no effect. IVIG: 40 g every month, no effect. Canakinumab: 4 mg/kg every month, persistent flares but less severe in symptoms and allowed corticosteroid taper. Corticosteroids: until 2017 the patient had prescription of 60 mg for short periods (2-3 days but sometimes to 10 days) and then stopped. Since 2017, 60 mg daily of prednisone was started after a severe flare but canakinumab allowed tapering the dose of Corticosteroids to 10 mg daily. **G)** ELISA analysis of patient serum cytokine levels (IL-1β and IL-18) performed in 2018 while on anti-IL-1β treatment (canakinumab); healthy controls, HCs.

The patient had a long history of corticosteroid use on demand and did not achieve control of clinical symptoms using any DMARDs including azathioprine, chloroquine, methotrexate, anti-TNF therapies (adalimumab, infliximab) or intravenous immunoglobulin (IVIG). Since 2017, due to the frequency and severity of flares, high doses of corticosteroids were prescribed and somewhat effective in controlling disease (**Figure 4.2 F**). Perhaps associated with prolonged use of corticosteroids the patient developed diabetes, hypertension and dyslipidaemia. As the patient had a decrease in renal function, a kidney biopsy was performed and negative congo red staining ruled out renal amyloidosis (data not shown). Because anakinra is not available in Brazil, therapy with anti-IL-1β monoclonal antibody canakinumab was started and able to partially control the symptoms, which resulted in reduced number of flares, diminished hospitalization, allowance for corticosteroid dose reduction and an overall improved quality of life, but inflammatory flares still occurred.

Serum levels of IL-18 remained moderately elevated in the patient (mean 276.80 pg/ml) compared to healthy controls (HCs) (mean 85.82 pg/ml) while on canakinumab treatment. Similarly, a slight increase in serum IL-1β levels persisted (mean 46 pg/ml, healthy controls: mean 8.62 pg/ml), which provided the first evidence towards an inflammasomopathy (**Figure 4.2 G**). However, at the time of serum collection for cytokine measurements, the patient had already received continuous canakinumab treatment for 8 months (1 injection of 4 mg/kg

per month). Serum was collected just before another dose of canakinumab was injected. Since no patient data on cytokine serum levels prior to canakinumab treatment are available and canakinumab binding to circulating IL-1β has been reported to prolong cytokine half-life (Lachmann et al., 2009), the interpretation of serum IL-1β levels remains indicative. Nonetheless, elevated serum IL-18 levels, that are independent of canakinumab treatment suggested an inflammasome-mediated disease.

Analysis of a target gene panel (Papa et al., 2020) and subsequent next generation sequencing identified a homozygous mutation in exon 4 of the *NLRC4* gene (NM_021209), c.478G>A encoding the A160T variant. Familial genetic segregation analysis using standard Sanger sequencing identified the healthy father, mother and brother to be heterozygous carriers of the mutant allele (**Figure 4.3 A, B)**. Parents were non-consanguineous, with the father and mother of German or Syrian ancestry, respectively. The estimated allele frequency in the general population is 0.00081 and there are no reported healthy homozygotes in the Genome Aggregation Database (GnomAD). Alignment of NLRC4 amino acid sequences of different species identified alanine (A) in position 160 as a conserved residue in human, non-human primates (except gorilla) and rodents. Interestingly, in ungulate species and cats, the wildtype sequence encodes a threonine (T) in this position (Clustal Omega alignment (Madeira et al., 2019)) (**Figure 4.3 C**).

An in-depth analysis of the structural consequences associated with the A160T substitution is described in Chapter 5.2.

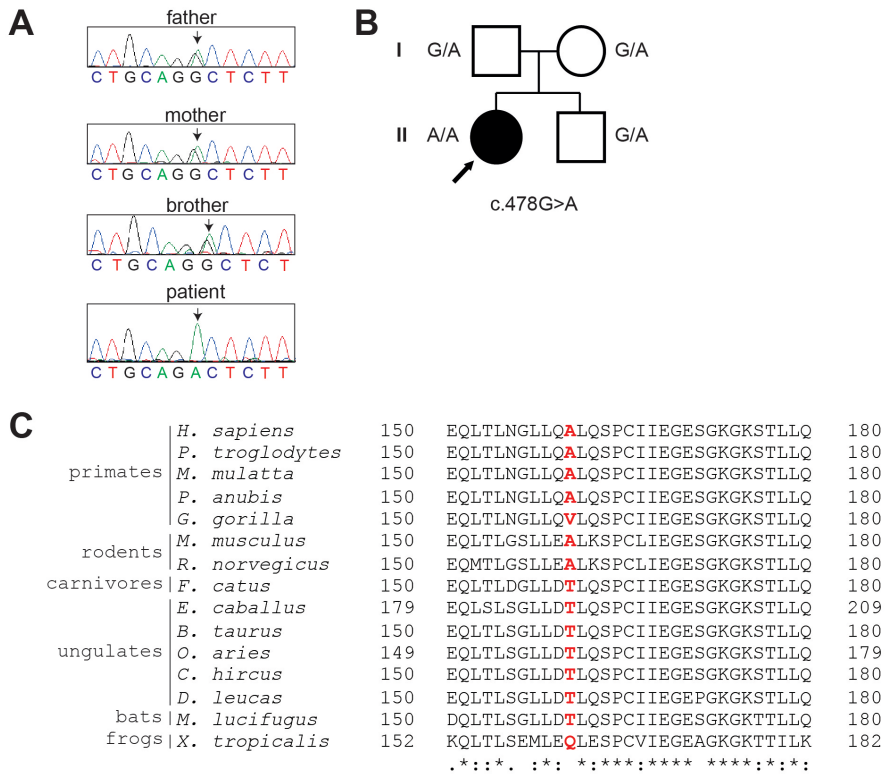

Figure 4.3 | Genetic sequencing identified a homozygous mutation in *NLRC4* affecting the conserved residue p.A160. A) Sanger sequencing confirmed the c.478 G>A transition (indicated by arrow) in exon 4 of the *NLRC4* gene, encoding the amino acid substitution p.A160T. Sequencing chromatograms show homozygous or heterozygous genotypes for the patient and healthy family members, respectively. **B)** Family pedigree with indicated genotypes. Circle represents female subject, square represents male subject, solid form represents affected individual. **C)** Clustal Omega multiple sequence alignment of the NLRC4 amino acid sequence from indicated species. The amino acid residue corresponding to position 160 in hNLRC4 is highlighted in bold red. Full length NLRC4 amino acid sequences were obtained from UniProt (*M. musculus* (mouse: Q3UP24), *H. sapiens* (human: Q9NPP4), *R. norvegicus* (rat: F1M649), *B. taurus* (cattle: F1MHT9), *X. tropicalis* (western clawed frog: F6R2G2), *P. troglodytes* (chimpanzee: A0A2J8L1X5), *F. catus* (cat: M3W537), *O. aries* (sheep: W5PLT9), *M. mulatta* (rhesus macaque: F7DWV6), *G. gorilla* (gorilla: G3QJV1), *P. anubis* (olive baboon: A0A096NWZ9), *M. lucifugus* (little brown bat: G1PV27), *E. caballus* (horse: F7CBZ7), *C. hircus* (goat: A0A452EBW5), *D. leucas* (beluga whale: A0A2Y9N554).

4.2.2 Patient MDMs show increased inflammasome signalling *in vitro*

In order to investigate the disease-causing potential of the NLRC4 A160T mutation *in vitro*, peripheral blood from the patient and HC individuals was collected to isolate the monocyte cell population. Subsequent to differentiation into MDMs, cells were primed with TLR4 agonist LPS and stimulated with ATP or transfected flagellin to activate NLRP3 and NLRC4 inflammasome formation, respectively (**Figure 4.4**). Unstimulated patient MDMs secreted slightly more IL-18 and treatment with cytoplasmic flagellin (DOTAP/FLA) alone did reveal some differences in IL-1β and IL-18 release, suggesting increased baseline and ligand-induced activity of NLRC4 A160T in patient cells without LPS priming (**Figure 4.4 A**). However, substantially elevated IL-1β and IL-18 levels were observed in patient MDMs upon LPS priming and activation of both investigated inflammasomes, with the most pronounced difference in IL-18 released following stimulation of NLRC4 in primed cells (LPS+DOTAP/FLA) (**Figure 4.4 A**). TNF levels, measured as inflammasome-independent priming control, were comparable in most tested condition. Notably, only in the LPS alone treated control, patient MDMs produced slightly more TNF than the HC donor cells **(Figure 4.4 B)**, which may indicate uneven cell numbers in this particular condition that could be in part accountable for the observed increase in IL-1β and IL-18 release in patient MDMs treated with LPS **(Figure 4.4 A).** Interestingly, we found that longer-term (24 hrs) stimulation with LPS did not alter IL-18 production, but 24 hrs flagellin (FLA, extracellular) showed an increase in IL-18 release for the patient MDMs, which may suggest internalization of FLA and an increased response of NLRC4 A160T at later time points.

Overall, these results suggested NLRC4 A160T autoactivation to some extent, and that environment, infection or other triggers are able to exaggerate responses due to NLRC4 A160T, which is consistent with flares of disease experienced by the patient. Furthermore, patient-derived MDMs appeared to be more responsive to NLRP3-specific stimuli (LPS+ATP), which is an interesting observation. Increased responsiveness to short-term LPS stimulation (4 hrs) may suggest LPS

internalization and non-canonical NLRP3 inflammasome activation, however future experiments are required to evaluate the involvement of NLRP3 signalling.

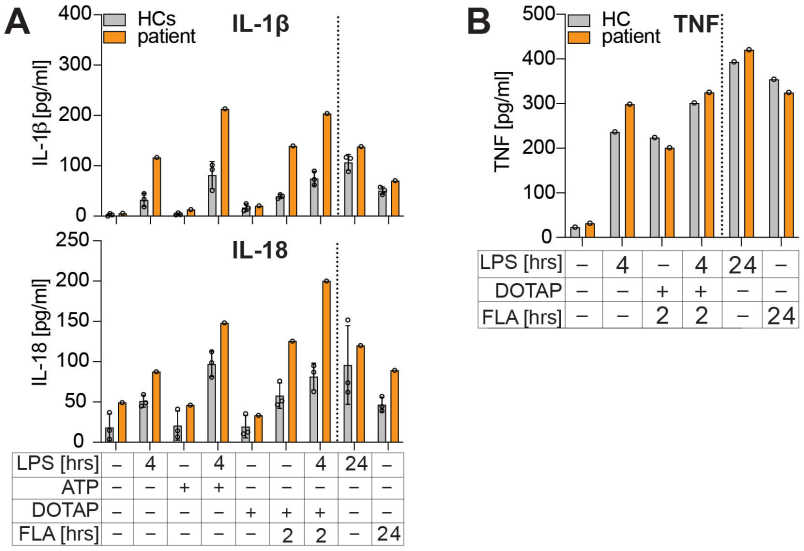

Figure 4.4 | Inflammasome-related cytokine secretion is increased in patient MDMs. A) Monocyte-derived macrophages (MDMs) from the patient and healthy donors (HCs, n=3) were challenged with LPS (1 µg/ml) or *S. typhimurium* flagellin (FLA, 5 µg/ml) for indicated time periods and stimulated with ATP (1 mM, 15 min) or transfected FLA in DOTAP liposomes (2 hours (hrs)). Supernatants were analysed for IL-1β and IL-18 by ELISA. Error bars represent SD. n=1 **B)** ELISA quantification of TNF levels for a subset of conditions shown in A). MDMs from the patient and one HC are shown. n=1.

4.2.3 *In vitro* validation confirms the pathogenicity of NLRC4 A160T in immortalized human cell lines

4.2.3.1 NLRC4 A160T results in increased ASC speck formation

As an *in vitro* readout for inflammasome assembly and activation on a single cell level, the time of flight inflammasome evaluation (TOFIE) assay was performed, which observes the cellular relocalization of inflammasome adapter protein ASC (Sester et al., 2015). In the resting state, ASC is diffusely distributed within the cytoplasm and forms distinct puncta following inflammasome sensor activation,

which reflects recruitment into the inflammasome complex, referred to as ASC speck (Martinon et al., 2002). When ASC is directly linked to a fluorescent tag, speck formation can be observed microscopically or quantified by flow cytometry based on a shift in the width-to-area ratio of the fluorescence signal (Sester et al., 2016, Sester et al., 2015). This experimental setup has previously been used to confirm the disease-causing potential of other autoactivating mutations in NLRC4 (Ionescu et al., 2021, Moghaddas et al., 2018). HEK293T cells stably expressing ASC linked to red fluorescent protein (ASC-RFP) were transiently transfected with mCitrine-tagged NLRC4 WT or A160T-encoding plasmids, which resulted in increased ASC speck formation by NLRC4 A160T, suggesting spontaneous inflammasome assembly (**Figure 4.5 A**). To resemble a heterozygous carrier, WT and A160T NLRC4 were co-transfected at a 50:50 ratio, which resulted in slightly elevated ASC speck formation compared to WT NLRC4. The previously described dominant autoactivating mutation NLRC4 S171F (Ionescu et al., 2021, Liang et al., 2017) resulted in stronger inflammasome activation than A160T, which is recessively inherited in this case (**Figure 4.5 A**).

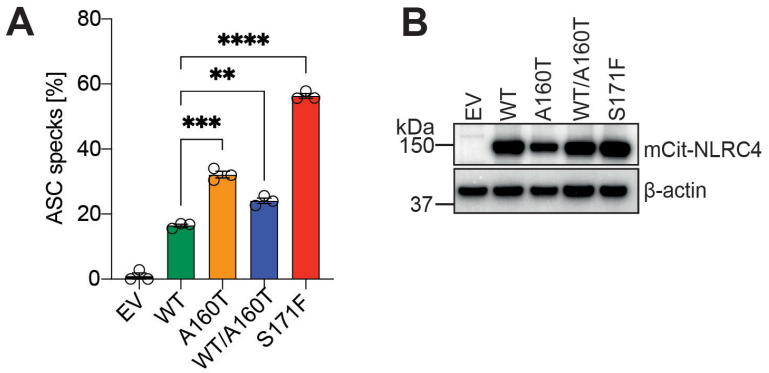

Figure 4.5 | Time of flight inflammasome analysis in HEK293T ASC-RFP cells after transient transfection. A) HEK293T ASC-RFP cells were transiently transfected with empty vector (EV), mCitrine (mCit)-tagged hNLRC4 WT, A160T, WT/A160T (heterozygous) or S171F (total 50 ng DNA/500 µl). ASC speck formation was quantified by flow cytometry after 15 hrs incubation. Data are presented as mean ± SEM from 3 independent experiments. Statistical testing by Student's t-test. **B)** Western blot analysis of HEK293T ASC-RFP cells in A) shown as a representative result of 3 independent experiments. ** $P<0.01$; *** $P<0.001$; **** $P<0.0001$.

Protein levels of NLRC4 WT, WT/A160T and S171F were comparable following overexpression in this assay, but slightly reduced for NLRC4 A160T (**Figure 4.5 B**). This finding was consistent between experimental repeats, which may suggest that in some circumstances this mutant is less stable and degraded more rapidly.

To independently confirm these results, Flp-In 293 T-REx cell lines stably expressing ASC tagged with enhanced green fluorescent protein (ASC-EGFP) and NLRC4 WT, A160T or S171F were generated. Site-specific genomic integration of a single copy of NLRC4 under a Dox-inducible promoter yielded a highly controlled and consistent experimental system (**Figure 4.6 A**). Importantly, western blot analysis confirmed similar NLRC4 expression levels between different cell lines (**Figure 4.6 B**), which leads us to speculate that reduced A160T stability might only occur when expressed above endogenous levels (**Figure 4.5 B**). When NLRC4 expression in the Flp-In 293 T-REx ASC-EGFP system was induced by Dox treatment, ASC speck formation was spontaneously initiated by the autoactive NLRC4 S171F mutant, but not by A160T or WT NLRC4 (**Figure 4.6 C**). Interestingly, upon NLRC4 inflammasome stimulation by transient co-transfection of plasmids encoding sensor protein hNAIP and *S. typhimurium* T3SS needle protein PrgI, ASC speck formation by NLRC4 A160T was significantly increased over WT levels (**Figure 4.6 D**). However in this experiment, protein expression levels of NLRC4 A160T were slightly below WT levels (**Figure 4.6 E**). This was attributable to a small difference in mRNA transcript expression in this case (qRT-PCR data not shown), rather than intrinsic defects in protein stability and may result in slight underestimation of the effect caused by NLRC4 A160T.

Overall, these data suggest that NLRC4 A160T induces spontaneous inflammasome assembly above WT levels when overexpressed. This effect was dose-dependent and less pronounced but still significant when NLRC4 WT and A160T were co-expressed to mimic a heterozygous carrier. However, in the context of more endogenous expression levels in Flp-In 293 T-REx cell lines, NLRC4 A160T was not autoactive and only induced above WT ASC speck formation in a ligand-dependent manner.

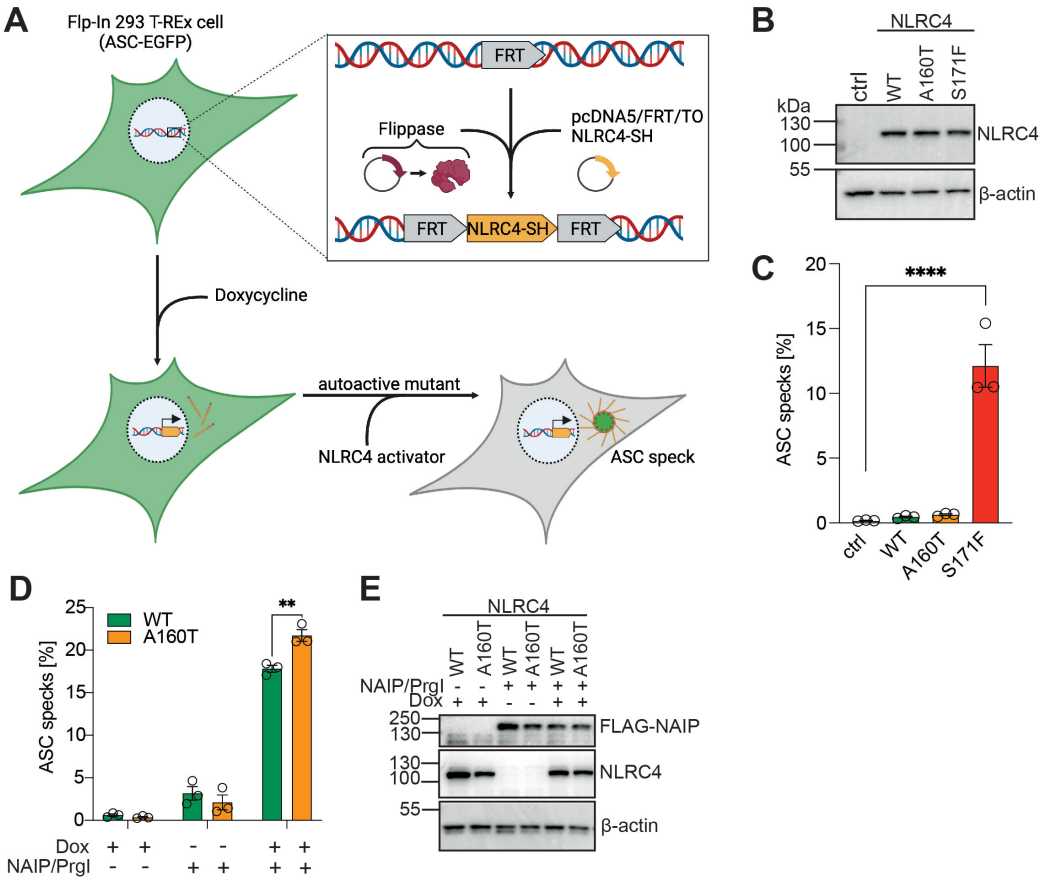

Figure 4.6 | ASC speck formation in Flp-In 293 T-REx ASC-EGFP cell lines with monogenic NLRC4 expression. A) Schematic diagram showing the generation of stable Flp-In 293 T-REx ASC-EGFP cell lines with isogenic expression of NLRC4 WT, A160T or S171F. Transient co-transfection of the Flippase recombinase-expressing plasmid (pOG44) and an expression plasmid encoding the Strep2-HA (SH)-tagged human *NLRC4* gene (pcDNA5/FRT/TO NLRC4-SH) flanked by Flippase recognition sites (FRT) generated stable isogenic cell lines. In this system, doxycycline (Dox) treatment induces NLRC4-SH transcription and subsequent ASC specking by autoactivating NLRC4 mutants or WT NLRC4 following stimulation. Figure created with BioRender.com. **B)** Western blot analysis of NLRC4 expression levels in cell lines generated in A) after 27 hrs Dox treatment showing a representative result of n=3. **C)** Baseline ASC speck formation of cell lines shown in B) analysed by flow cytometry after 27 hrs Dox treatment. Control (ctrl) cells did not contain an NLRC4 insert. Data pooled from n=3 independent experiments shown as mean ± SEM. Statistical significance was assessed by one-way ANOVA and Dunnett's multiple comparison test. **D)** Flow cytometry analysis of ASC speck formation in cell lines generated in A) following Dox induction and transient transfection with FLAG-hNAIP and myc-PrgI (250 ng DNA/500 µl, 16 hrs). Data are presented as mean ± SEM, pooled from n=3 independent experiments. Statistical significance was assessed by two-way ANOVA with Šidák's multiple comparison test. **E)** Representative western blot of D), n=1. ** $P<0.01$; **** $P<0.0001$.

4.2.3.2 Genome editing of THP-1 cells to express NLRC4 A160T

We next sought to investigate the effect of NLRC4 A160T in a human monocyte-like cell line with endogenous expression of proteins relevant for inflammasome activation and cytokine release. However, hematopoietic cell types are difficult to transfect with lipid-based DNA delivery methods and prone to proinflammatory pathway activation and cell death upon detection of cytoplasmic DNA by various PRRs (Baker et al., 2018). The use of a lentiviral/retroviral system, where plasmid DNA-carrying viral particles deliver DNA into target cells and mediate its genomic integration, overcomes these hurdles (Baker et al., 2018), and yields a valuable tool to produce stable cell lines with long-term expression of a particular gene of interest. However, the genomic integration site varies dependent on the preferences of the delivering virus and can lie within active transcription units or near transcription start sites, which harbours the risk of insertional mutagenesis and may alter the regulation of endogenous cellular genes (Ciuffi 2016, Demeulemeester et al., 2015, Lewinski et al., 2006). Furthermore, the concentration and quality of the generated plasmid-delivering virus particles used for cell infection in combination with viral transduction rates determine the number of integrated transgene copies per cell. A previous study showed that a linear correlation between the multiplicity of infection (MOI, which indicates the number of virions added per host cell), the number of transduced cells and gene integration exists until the maximal transduction capacity is reached. Afterwards, further increase of the MOI only increased the transgene copy number per cell, whereas the number of transduced cells did not further improve (Kustikova et al., 2003). Both quality and MOI of virus-containing supernatants can vary between independent preparations (e.g. WT and mutant) and may therefore result in variable transgene expression on the individual cell level, which is difficult to determine and impacts comparability. Furthermore, genomic integration of multiple transgene copies per cell controlled under an exogenous promoter generates a rather artificial system, which may pose challenges in discovering mild disease phenotypes, of course depending on the functional context.

To circumvent these effects, direct modification and nucleotide substitution in the host cell genome can be undertaken via site-directed mutagenesis that employs

CRISPR/Cas9-mediated generation of DNA double strand breaks (DSBs) and homology-directed repair (HDR) (Biot-Pelletier et al., 2016). Within the cell, CRISPR/Cas9-induced DSBs are resolved via two main mechanisms, non-homologous end joining (NHEJ) or HDR and decisions of which pathway is undertaken depend on several factors including cell cycle phase, expression of regulatory proteins, structure of generated DNA ends at the break site and availability of a repair template (Symington et al., 2011). Therefore, both pathways occur at different rates in individual cells and cell types. In general, NHEJ is the predominantly activated pathway, initiated upon recognition of various DNA end structures, which quickly repairs lesions via direct ligation of broken ends. The error-prone nature of this mechanism often generates gene KOs as a consequence of frameshift mutations following random insertion and deletion of nucleotides (indels) (reviewed in (Gu et al., 2008)). In contrast, HDR requires an intact homologous sequence as template to repair the break aiming to recover genetic information that was potentially lost (Liang et al., 1998). Therefore, HDR represents the desired mechanism for precise genome editing, realized via addition of a homologous oligo repair template encoding the nucleotide exchange of interest (Biot-Pelletier et al., 2016, Jasin et al., 2013). Maintaining endogenous transcriptional regulation and protein expression levels highlight the ultimate advantages of this approach which are beneficial to investigate the effects of a potentially disease-causing mutation *in vitro*.

In the case of NLRC4 A160T, the clinical features presented by the patient together with the data generated from ASC speck inflammasome formation assays (chapter 4.2.3.1), suggested a rather mild pathogenic effect. Therefore, generating a human disease model using CRISPR/Cas9-mediated HDR and site directed mutagenesis to introduce A160T into the THP-1 cell genome while maintaining endogenous gene regulation and expression levels seemed a rational approach, despite the low efficiency of this method, that has previously been reported (Carroll 2014, Harrison et al., 2014, Lin et al., 2016).

Details of the methodology used are described in chapter 2.5.1.2. In brief, WT THP-1 cells were electroporated to increase cellular membrane permeability and deliver plasmid DNA encoding GFP, Cas9 and the NLRC4-specific sgRNA

together with a single strand oligo repair template. The 45 bp long oligo repair template encoded for the c.478G>A nucleotide exchange (encodes NLRC4 A160T) flanked by homology arms of symmetric length upstream and downstream of the DNA cut site (**Figure 4.7 A**). Simultaneously, this mutation disrupted the protospacer adjacent motif (PAM) site which avoids Cas9-mediated DSB within the integrated HDR template. Additionally, a silent point mutation (c.468C>T) was introduced to generate a *BsaI* restriction enzyme recognition site (5'-GGTCTC-3') to facilitate the detection of successfully integrated oligo repair templates by PCR and diagnostic restriction digest during the subsequent screening process of single cell clones (see below).

Following electroporation and FACS sorting for the GFP-positive cell population, cells were subsequently cultured as pool for one week to allow recovery. Then, single cell clones were generated by limiting dilution. Upon formation of visible colonies after four to six weeks, genomic DNA was isolated from all single cell clones and screened for presence of the oligo repair template using NLRC4-specific PCR amplification (yielding 637 bp) followed by *BsaI* restriction digest (**Figure 4.7 B**). Screening of over 1000 clones identified 16 clones that showed the expected band pattern after *BsaI* digest (homozygous and heterozygous). However, subsequent Sanger sequencing yielded only one clone carrying the correctly edited sequence on one allele, whereas the second allele encoded the WT sequence with -1 bp frameshift mutation inducing a premature termination codon. The resulting heterozygous A160T/KO genotype was observed as a double band after *BsaI* digest, reflecting the uncut WT allele (637 bp) and the cut DNA fragments (317 bp + 320 bp) generated from the A160T-encoding edited allele (**Figure 4.7 B**). As control cell line, a WT/KO clone with one intact WT allele and 1 bp deletion on the second allele was chosen. Furthermore, a NLRC4 KO/KO cell line was selected with homozygous 143 bp deletion resulting in a premature stop codon at residue position 166 with subsequent nonsense-mediated decay of mRNA transcripts. The reduced amplicon size prior to *BsaI* digest in the KO/KO cell line is indicative of the deletion (**Figure 4.7 B**).

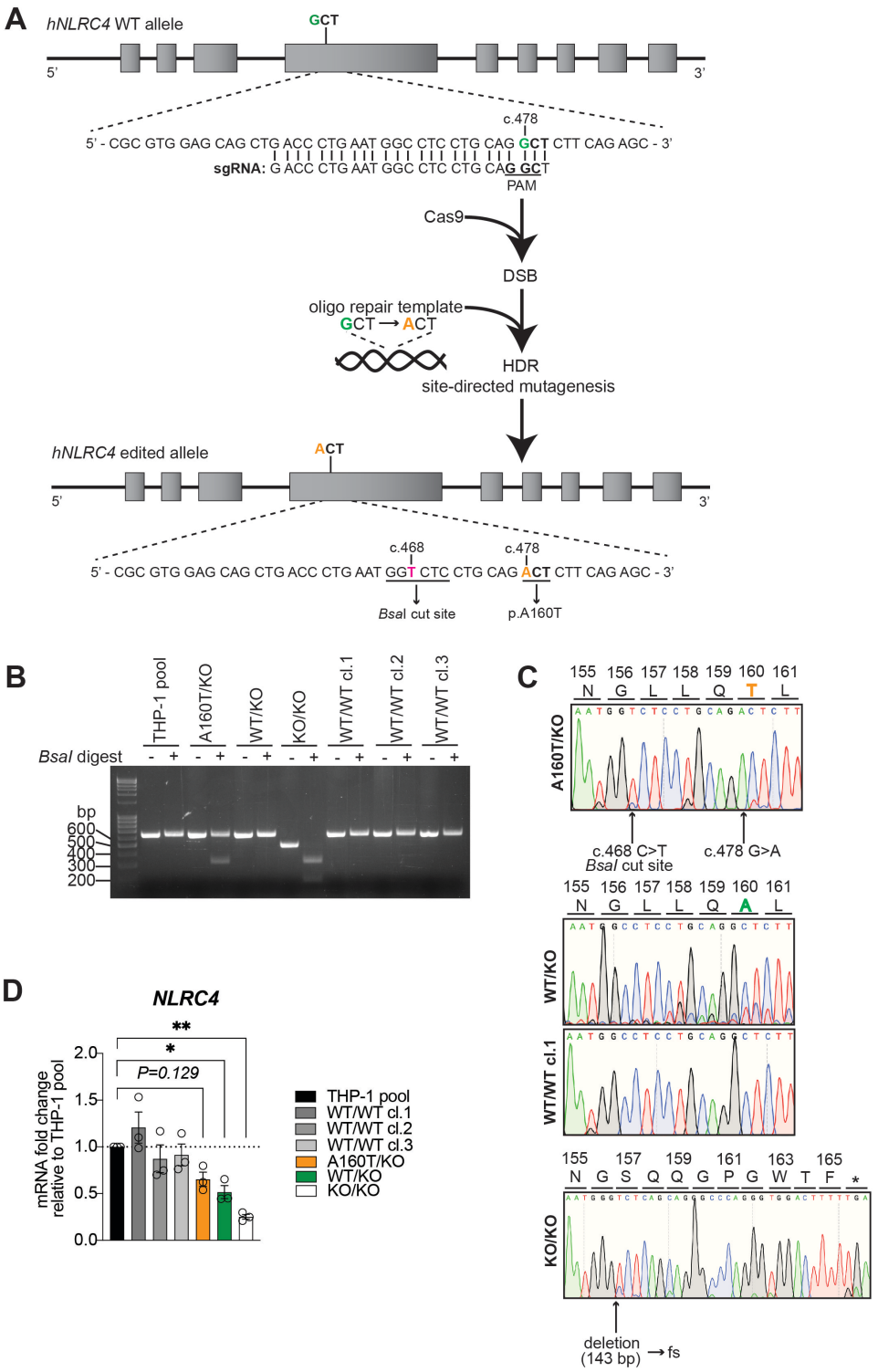

Figure 4.7 | Generation and validation of monoclonal THP-1 cell lines. A) CRISPR/Cas9-mediated homology-directed repair (HDR) was employed to introduce the A160T mutation (encoded by c.478G>A) on genomic level in WT THP-1 cells. Binding site within exon 4, reverse PAM site (underlined, bold) and sequence of the used single guide (sg) RNA are shown. The WT sequence c.478G is highlighted in green (bold) and was edited to c.478A (orange) encoded

in the DNA repair template. Additionally, a silent mutation at c.468C>T was introduced to generate a *Bsa*I restriction enzyme recognition site, which was subsequently used to screen monoclonal cell lines for repair template integration. **B)** Representative agarose gel showing the *NLRC4*-specific PCR amplification product (637 bp) before and after *Bsa*I digest for selected cell lines (genotypes indicated). Only cell lines with successfully integrated oligo repair template are sensitive to *Bsa*I digest (fragment size:317 bp + 320 bp). **C)** Sanger sequencing following RNA isolation, cDNA synthesis and *NLRC4*-specific PCR confirmed presence of c.478G>A (A160T) and c.468C>T mutations in the actively transcribed *NLRC4* mRNA transcript in THP-1 cell clone A160T/KO. WT/KO and WT/WT clone 1 are shown as representative reference for the WT sequence. Amino acid position and corresponding residues are indicated. A homozygous 143 bp deletion was detected in the KO/KO cell line, inducing a frameshift (fs) and premature stop codon at position 166. **D)** qRT-PCR analysis of *NLRC4* mRNA transcript levels in THP-1 cell clones with indicated genotypes shown as mean ± SEM pooled from n=3 independent experiments. *P*-values were calculated using one-way ANOVA and Dunnett's multiple comparison test using the THP-1 cell pool as comparator group. * $P<0.05$; ** $P<0.01$. double-strand breaks, DSB; clone, cl.

Interestingly, restriction enzyme digest resulted in two smaller DNA fragments, which suggested random DNA repair-mediated generation of a *BsaI* recognition site (**Figure 4.7 B**). The complete KO phenotype of this cell line was also confirmed in the NLRC4 stimulation assay, where the KO/KO cell line did not respond (**Figure 4.8**). Further, three clonal cell lines with two functional NLRC4 WT alleles (WT/WT cl.1-3) and the original WT THP-1 cell pool were used as control cell lines in all assays to monitor for inter-clonal variability.

Presence of the mutation in the actively transcribed *NLRC4* mRNA transcript of A160T/KO cells was confirmed by Sanger sequencing following RNA isolation, cDNA synthesis and NLRC4-specific PCR (**Figure 4.7 C**). The sequencing chromatogram showed single peaks for both introduced mutations, the silent c.468C>T mutation (*BsaI* cut site) and the desired c.478G>A mutation encoding NLRC4 A160T, indicating complete absence of WT transcripts, which therefore confirmed the A160T/KO genotype. The correct *NLRC4* WT sequence was detected in transcripts of the WT/KO cell line and all WT/WT clones (**Figure 4.7 C,** data not shown). qRT-PCR analysis of relative *NLRC4* transcription levels compared to the THP-1 cell pool confirmed around 50 % reduction of transcription

levels in cell lines expressing one functional *NLRC4* allele, e.g. A160T/KO and WT/KO, whereas WT/WT cl. 1-3 showed levels similar to the pooled population (**Figure 4.7 D**). Based on the similar genotype and comparable transcription levels of *NLRC4*, the WT/KO cell line was used as direct comparator group for A160T/KO cells in all subsequent stimulation assays.

4.2.3.3 Increased cytokine release and cell death caused by NLRC4 A160T is ligand-dependent in THP-1 cells

To investigate the effect of the A160T mutation in THP-1 cells, we stimulated the NAIP/NLRC4 inflammasome in the above generated cell lines (chapter 4.2.3.2). As previously described, inflammasome activation requires two signals: signal 1 (priming) to induce NF-κB-mediated transcription of inflammasome machinery and signal 2 which represents the actual inflammasome-specific stimulus (chapter 1.3.3.1). To provide both signals, monoclonal THP-1 cells were primed with TLR1/2 agonist Pam3CSK4 (P3C) and stimulated with retrovirus expressing *S. typhimurium* PrgI needle protein. Cell death induction and cytokine (IL-1β and IL-18) release were used as experimental readouts for inflammasome activation (**Figure 4.8**). The KO/KO clone did not respond to NLRC4 stimulation, confirming the specificity of the used stimulus. Overall, NLRC4 signalling appeared comparable between WT/WT clones and the THP-1 pooled population, with a few exceptions: IL-1β release was increased in WT/WT cl. 3 and all WT/WT clones (cl. 1-3) were more susceptible to cell death than the THP-1 pool.
Interestingly, when compared to the WT/KO cell line, NLRC4 A160T-expressing cells (A160T/KO) showed enhanced inflammasome signalling when treated with P3C and PrgI, as observed by significantly elevated release of IL-1β (**Figure 4.8 A**), IL-18 (**Figure 4.8 B**) and increased cell death production (**Figure 4.8 C**). Spontaneous signalling after P3C priming alone was not observed, indicating that A160T does not cause NLRC4 autoactivation and requires a NLRC4-specific stimulus to elicit pathogenicity. To exclude a differential response due to variability in P3C-induced priming, levels of released IL-8, an inflammasome-independent NF-κB-induced cytokine, were quantified (**Figure 4.8 D**). A small

increase in IL-8 release by A160T/KO cells was observed in response to P3C priming alone, however this was not consistent in the PrgI-treated samples. Therefore, these results suggest that priming in the P3C + PrgI-treated cells was overall similar and increased cytokine release and cell death observed in A160T/KO cells was a direct consequence of more pronounced NLRC4 activation and signalling.

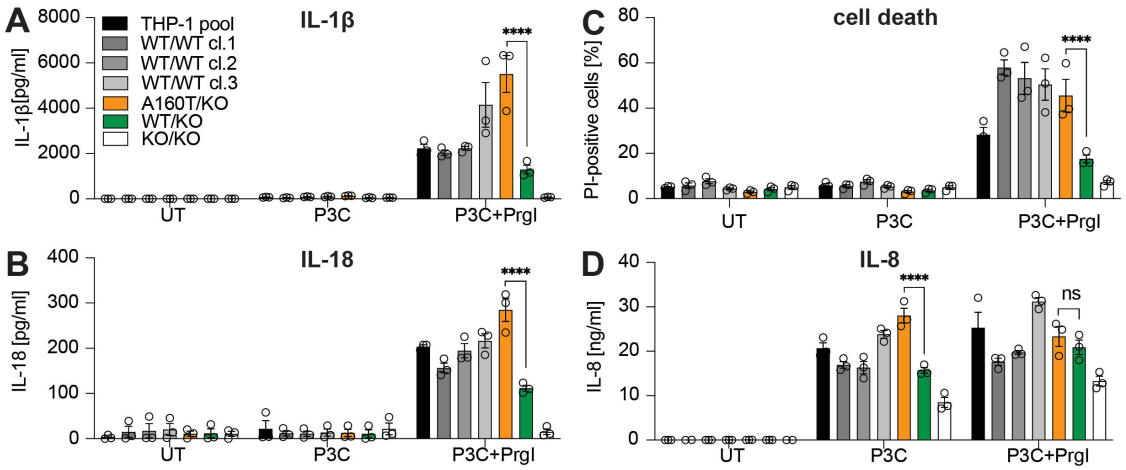

Figure 4.8 | NLRC4 inflammasome stimulation in monoclonal THP-1 cell lines. Monoclonal THP-1 cell lines of indicated genotypes were analysed for release of IL-1β (**A**) and IL-18 (**B**), cell death production (**C**) and IL-8 secretion (**D**) after 24 hrs treatment with Pam3CSK4 (P3C, 100 ng/ml) and PrgI (1 µl retroviral supernatant) by ELISA (cytokines) or flow cytometry of propidium iodide (PI)-positive cells (cell death). Data were pooled from n=3 independent experiments and are shown as mean ± SEM. Statistical testing by two-way ANOVA with Tukey's multiple comparison test was performed. For greater clarity only statistical significances relevant for the study results are indicated. **** $P<0.0001$, not significant, ns.

However, it should be noted that whereas a pool of cells is characterized by genetic, epigenetic and phenotypic heterogeneity, a single cell-derived clonal cell line does not capture this diversity (Giuliano et al., 2019). Therefore, ideally the analysis of multiple single cell clones with the same genotype is required before definite conclusions about an observed phenotype can be drawn. In the case of NLRC4 A160T, we were not able to generate multiple single cell clones carrying

this mutation. However, the concern that clonality of A160T/KO and WT/KO cell lines is associated with fundamental differences in regulation or expression of inflammasome pathway-related proteins remains valid.

To address this question and exclude such differences, we sought to activate the NLRP3 inflammasome, since the majority of inflammasome machinery is shared between NLRC4 and NLRP3. In this experiment, comparable levels of released cytokines and cell death in all cell lines were expected. NLRP3 was stimulated by P3C priming with subsequent addition of nigericin, a microbial toxin which induces potassium efflux, triggering the key event of NLRP3 activation (Muñoz-Planillo et al., 2013). In this experiment, cell death production was comparable across all cell lines, whereas released cytokine levels showed higher variability (**Figure 4.9 A-C**). The A160T/KO clone released more IL-1β and IL-18 compared to the WT/KO control clone, however, levels were similar to WT/WT cl.1 in the case of IL-1β and the THP-1 cell pool in the case of IL-18 release (**Figure 4.9 A-C**). This data suggested that there are likely some clonal differences between the A160T/KO and WT/KO cell lines, however the extent of the observed difference was substantially lower after NLRP3 stimulation. Whereas NLRP3-stimulated A160T/KO cells released 2.6-fold more IL-1β and 1.4-fold more IL-18 than WT/KO cells, IL-1β and IL-18 levels were 4.3-fold and 2.5-fold increased in A160T/KO cells after NLRC4 stimulation (**Figure 4.8**, **Figure 4.9**).

Together these findings suggest that NLRC4 A160T enhances stimulus-dependent NLRC4 signalling in THP-1 cells. However, the effect observed in the here generated monoclonal THP-1 cell line A160T/KO is likely not solely caused by the mutation. Additional contributing factors specific to this clonal cell line may include differences in NF-κB-mediated priming events or could be related to processes involved in cytokine activation, since cytokine release was also elevated in control experiments when NLRP3 was stimulated. Nonetheless, based on the extent of the observed difference, these results provide evidence for the pathogenicity of NLRC4 A160T, although confirmation of this result with additional cell clones is desirable.

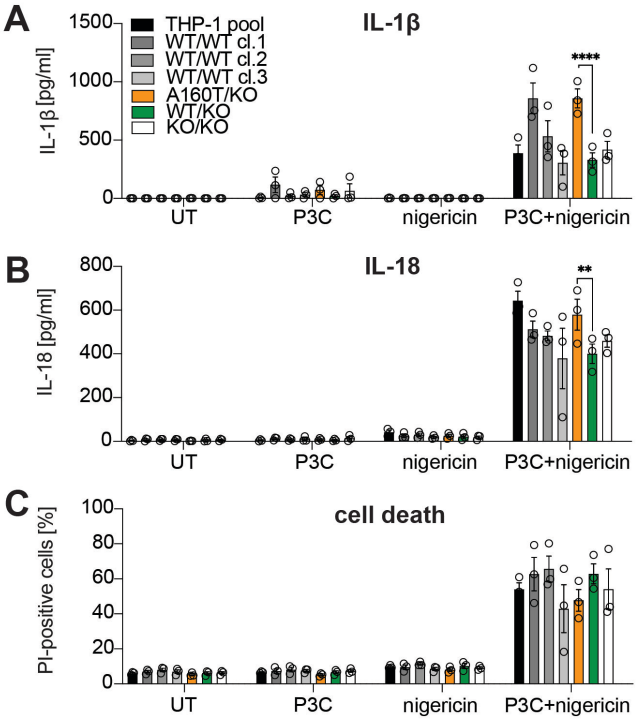

Figure 4.9 | NLRP3 signalling in monoclonal THP-1 cell lines. Assessment of IL-1β (**A**), IL-18 (**B**) release and cell death (**C**) following NLRP3 stimulation by ELISA or flow cytometry measuring propidium iodide (PI)-positive cells, respectively. THP-1 cell clones were primed with Pam3CSK4 (P3C, 100 ng/ml) for 3 hrs with subsequent nigericin treatment (10 µM, 1 hr). Data were pooled from n=3 independent experiments and are shown as mean ± SEM. Statistical testing by two-way ANOVA and Tukey's multiple comparison test. For greater clarity only statistical significances relevant for the study results are indicated. *P*-values: ***P*<0.01, ****P*<0.0001.

4.2.3.4 The A160T mutation does not synergistically enhance spontaneous inflammasome formation of autoactive NLRC4 S171F

So far, our results suggested ligand-induced increased signalling by NLRC4 A160T, whereas spontaneous inflammasome activation was not observed in Flp-In 293 T-REx cells (**Figure 4.6**) or P3C-primed A160T/KO THP-1 cells without NLRC4 stimulation (**Figure 4.8**).

This is in contrast to previously described heterozygous GoF mutations in NLRC4, which spontaneously induce inflammasome signalling *in vitro* in a ligand-independent manner (Barsalou et al., 2018, Canna et al., 2014, Kitamura et al.,

2014, Moghaddas et al., 2018, Romberg et al., 2014, Wang et al., 2021a). Mechanistically, it has been suggested that these mutations interrupt the autoinhibited conformation of NLRC4, which promotes spontaneous inflammasome assembly (further discussed in chapter 5.1.5). Therefore, ligand-dependency of the A160T mutant suggests a distinct molecular mechanism, which impacts the ligand-induced activation process and perhaps increases binding affinities between NAIP and NLRC4 or between NLRC4 monomers, thereby facilitating inflammasome oligomerization. Next, we were wondering whether this effect specifically occurs following ligand-stimulation or could enhance signalling of an autoactive mutant. To address this question, we analysed ASC speck formation in Flp-In 293 T-REx ASC-EGFP cells stably expressing NLRC4 S171F or the A160T/S171F double mutant. Since a potential difference in the kinetics of NLRC4 oligomerization was expected, ASC speck formation was monitored over a time course of 10 hrs where Dox treatment induced NLRC4 expression without additional stimulation (**Figure 4.10 A**). Interestingly, a difference was not observed which indicated that the conformational change mediated by the S171F mutation results in maximal NLRC4 oligomerization that could not be further enhanced by A160T. Western blot analysis showed comparable NLRC4 expression levels in the used cell lines (**Figure 4.10 B**).

Additional stimulation through co-transfection of plasmids encoding NAIP and PrgI increased ASC speck formation by NLRC4 S171F and double mutant NLRC4 A160T/S171F to similar extents (data not shown). These results indicate that in the context of the autoactivating mutation S171F, A160T does not further enhance inflammasome formation in presence and absence of a specific ligand. This suggests that the conformational change induced by S171F and subsequent NLRC4 autoactivation bypasses the effect that is mediated through the A160T exchange in WT NLRC4 in its active conformation.

Since the previously described NLRC4 GoF mutations are associated with a broad spectrum of clinical manifestations, the underlying molecular mechanisms driving pathogenesis may differ depending on the mutational change, leaving the possibility that A160T may exhibit synergistic effects in the context of some but

not all NLRC4-AID-causing mutations. Addressing this question in future studies could be valuable to understand the molecular mechanism by which A160T elicits pathogenicity.

Whether ligand-induced and GoF mutation-mediated NLRC4 signalling occur via similar downstream pathways remains elusive today but provides an interesting discussion point for the observation that A160T enhanced NLRC4 signalling in a stimulation-dependent manner but not in context of the autoactivating mutation S171F.

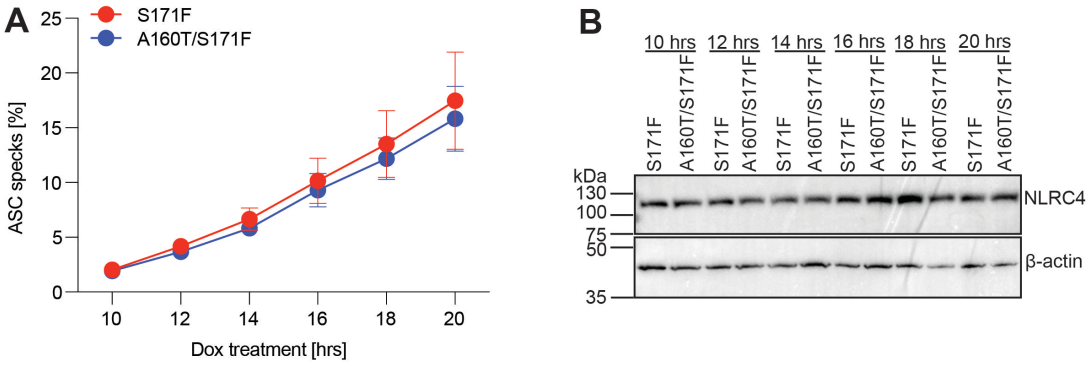

Figure 4.10 | Kinetics of ASC speck formation by autoactive NLRC4 S171F and double mutant A160T/S171F. ASC speck formation was assessed in Flp-In 293 T-REx ASC-EGFP cells stably expressing Doxycycline (Dox)-inducible autoactive mutant NLRC4 S171F or the double mutant A160T/S171F. **A)** Ligand-independent spontaneous inflammasome formation was assessed as ASC speck formation quantified by flow cytometry. Time points refer to hours (hrs) post Dox induction. Data are pooled from n=3 independent experiments and presented as mean ± SEM. **B)** Representative western blot analysis of NLRC4 expression levels in the whole cell lysate of cells analysed in A), n=1.

4.2.4 Heterozygous NLRC4 A160T allele carriers are at increased risk to develop ulcerative colitis

The NLRC4 inflammasome is a crucial player of intestinal immune defence and induces release of the proinflammatory cytokines IL-1β and IL-18 in response to microbial invaders (Romberg et al., 2017). Unlike pro-IL-1β, which is a NF-κB-induced cytokine, the IL-18 precursor protein is constitutively expressed in

various cell types, including IEC and was previously shown to be involved in intestinal inflammation (Pizarro et al., 1999).

The umbrella term IBD describes a group of autoimmune diseases, comprised of the most common subtypes Crohn's diseases and ulcerative colitis (UC), which are characterized by chronic inflammation of the GIT driven by the presence of commensal bacteria. The exact cause of IBD remains unknown, however aberrant intestinal immune system activation as well as defects in the epithelial barrier function play an important role (Jostins et al., 2012, Podolsky 2002). Whereas Crohn's disease is characterized by inflammation that can affect the lining of the entire digestive tract from the mucosa to deeper layers, inflammation in UC is more restricted to the mucosa of the large intestine including parts of rectum and colon (Fakhoury et al., 2014, Podolsky 2002). Several factors have been suggested to contribute to the development of IBD including environmental influences such as infections and diet as well as genetic susceptibility (Hou et al., 2011, Lidar et al., 2009, Shoda et al., 1996). To date genome-wide association studies (GWAS) have identified more than 200 genetic loci associated with an increased risk for the development of IBD (Jostins et al., 2012, Liu et al., 2015a). Interestingly, many of the identified IBD loci have also been implicated in immune-mediated diseases (Jostins et al., 2012). Of note, clinical studies correlated the severity of IBD with increased levels of IL-18 (Pizarro et al., 1999).

Since the NLRC4 A160T allele occurs at an estimated allele frequency of 0.00081 in the general population (GnomAD) and previously reported patients with GoF mutations in NLRC4 showed high serum levels of circulating IL-18 and severe intestinal inflammation and enterocolitis (Canna et al., 2014, Moghaddas et al., 2018, Romberg et al., 2014), we aimed to investigate the genome-wide association of the NLRC4 A160T allele with IBD.

As a resource, the IBD Exomes Browser (Broad Institute) was used, which presents data from a meta-analysis association study in IBD patients and control subjects from three population cohorts, namely European (Ashkenazi-Jewish), non-Finnish European and European (Finnish), wherein the heterozygous NLRC4 A160T allele was observed at frequencies of 0.088 %, 0.18 % and 0.23 %, respectively.

In this analysis, the NLRC4 A160T allele was significantly enriched in UC patients compared to healthy controls with an odds ratio (OR) of 2.546 ((95% confidence interval (CI) 1.778-3.644), *P*=0.01305), which indicates that carriers of this allele have a 2.5-fold increased risk to develop UC (**Table 14**). Of note, the correlation between NLRC4 A160T and Crohn's disease was less clear (OR=1.62 (95% CI 1.119-2.346), *P*=0.2615) (data taken from IBD Exomes Browser, Cambridge, MA http://ibd.broadinstitute.org, accessed October 2018), suggesting this locus as a risk factor predominantly for the development of UC.

In general, the identification IBD-associated genetic variants allows for the description of risk factors and genetic susceptibility loci associated with the development of this disease and provides a promising strategy for the identification of drug targets and diagnostic markers. Enrichment of NLRC4 A160T in UC patients therefore holds promise that targeted inhibition of NLRC4 signalling and downstream proinflammatory cytokines may provide a therapeutic opportunity for these patients.

Table 14 | Association of *NLRC4* (c.478G>A, p.A160T) with ulcerative colitis in the genome across different populations. Data accessed from IBD Exomes Browser, Cambridge, MA http://ibd.broadinstitute.org, accessed October 2018. ulcerative colitis, UC; odds ratio, OR.

Population	Homozygous Reference	Heterozygous Alternate	UC Allele Frequency	non-UC Allele Frequency	OR [95% Interval]	*P*-value
European (Ashkenazi-Jewish)	5680	5	0.0007184	0.0003292	1.035	0.9749
Non-Finnish European	7726	14	0.001161	0.000361	2.862	0.1707
European (Finnish)	11453	26	0.003589	0.001159	4.125	0.0392
Total					**2.546 [1.778, 3.644]**	**0.01305**

In summary, *NLRC4* (c.478G>A, p.A160T) is likely to be the first identified recessive mutation in this gene causing a monogenic disease characterised by autoinflammation and immune dysregulation. This allele is pathogenic *in vitro* and enhances stimulus-dependent NLRC4 signalling, however with reduced strength compared to dominant NLRC4 mutations and results in a modest increase in IL-18 *in vivo*. Nevertheless, heterozygous carriers of NLRC4 A160T are at increased risk of developing UC.

4.3 Discussion

Here we describe the first patient diagnosed with an autoinflammatory disease caused by a recessive mutation in *NLRC4* (c.478G>A, p.A160T). Clinically, the patient presented with early-onset recurrent episodes of systemic inflammation, characterized by fever, arthralgia, abdominal pain and diarrhea who is alive at age 62 years and currently treated with corticosteroids and canakinumab. Overall, the disease manifestation in this patient was milder compared to previously reported cases of AIFEC or NLRC4-MAS caused by heterozygous NLRC4 GoF mutations. The difference in the clinical course severity is also reflected in serum levels of the proinflammatory cytokine IL-18, which were extremely elevated in previously reported patients (total IL-18: ~10^3-10^5 pg/ml), compared to modestly elevated levels in the here described patient (total IL-18: 276.8 pg/ml) (Barsalou et al., 2018, Bracaglia et al., 2015, Canna et al., 2017, Canna et al., 2014, Chear et al., 2020, Kawasaki et al., 2017, Moghaddas et al., 2018, Romberg et al., 2014, Siahanidou et al., 2019, Volker-Touw et al., 2017, Wang et al., 2021a).

Importantly, our study measured serum levels of total IL-18, which includes both free IL-18 and IL-18 bound to IL-18BP, the latter being neutralized and biologically inactive (Novick et al., 1999). Based on this, elevated serum IL-18 levels in the here described patient demonstrate increased NLRC4 pathway activity, however no conclusions about the extent of IL-18-mediated signalling can be drawn, since accurate levels of free IL-18 were not determined.

As previously mentioned, the dramatic elevation of IL-18 levels is a special hallmark of NLRC4-AID (Weiss et al., 2018). In CAPS, GoF mutations in NLRP3 appear to drive disease pathology mainly through aberrant IL-1β release, since clinical symptoms in the majority of CAPS patients are efficiently controlled with IL-1β signalling inhibitors such as anakinra, canakinumab or rilonacept (Hoffman et al., 2008, Kullenberg et al., 2016, Lachmann et al., 2009). In contrast, especially in NLRC4-AID patients with very early disease onset and severe clinical course involving MAS and enterocolitis, IL-1β inhibition was less effective and targeted antagonism of IL-18 signalling with rhIL-18BP or an anti-IFNγ monoclonal antibody showed promising results, highlighting the importance of

these cytokines as crucial drivers for NLRC4-AID pathogenesis (Bracaglia et al., 2015, Canna et al., 2017, Moghaddas et al., 2018).

In line, the here reported patient with homozygous NLRC4 A160T mutation showed a partial response to canakinumab treatment, which resulted in reduced number of flares, diminished hospitalization and an improved quality of life, however inflammatory episodes still occurred on a regular basis. Since inhibitory drugs targeting IL-18 are still undergoing clinical trials and have not yet been approved (chapter 4.1.3), emergency compassionate use of rhIL-18BP was considered and requested for this patient, however declined by the developing pharmaceutical company.

Together these case reports illustrate a vast potential associated with a combination therapy blocking both IL-1β and IL-18 signalling, which may represent the most efficient strategy to treat NLRC4-AID patients.

Interestingly, all previously reported cases of NLRC4-AID were caused by heterozygous GoF mutations affecting highly conserved residues located within different functional domains of NLRC4, which were predicted to impair NLRC4 autoinhibition and induce ligand-independent inflammasome signalling (further discussed in chapter 5.1.5). Experimental evidence to support this hypothesis is limited to cell-based *in vitro* assays using patient-derived cells or overexpression/reconstitution models as well as a limited number of *in vivo* transgenic mouse models (Kitamura et al., 2014, Weiss et al., 2018). However, structural studies analysing NLRC4 proteins carrying disease-causing mutations are lacking to date, but required to elucidate the true structural impact of these mutations. If, as suggested, GoF mutation-induced conformational changes collectively converge to promote the open conformation of NLRC4, the observation of variable disease manifestations and clinical course severity is surprising. A potentially underlying genotype-phenotype correlation is not yet well understood, which in turn reflects the complex NLRC4 inflammasome biology. Pathway regulation occurs at multiple levels, including transcriptional regulation, PTMs, variability of interacting inflammasome adapters and effectors (caspase-1, caspase-8, ASC, and perhaps NLRP3) and downstream activated pathways (cell death, cytokine release, eicosanoid production), a multifactorial interplay of

which may provide the molecular foundation for diversity of NLRC4-AID-induced phenotypes. Additional contribution of environmental triggers, genetic background and tissue-dependent variable expression patterns of regulatory proteins may further influence disease pathology and determine the clinical manifestation. Interesting in this context, a single-nucleotide polymorphism (SNP) within the NLRC4 5'-untranslated region was identified by GWAS and correlated with reduced serum levels of IL-18. Functionally, differences in NLRC4 isoform usage and PU.1 transcription factor binding were suggested to alter NLRC4 expression levels and affect IL-18 production (Zeller et al., 2015). Therefore, SNPs within *NLRC4*, other pathway-related genes or *IL18* may result in a susceptible genetic background and could promote the development of distinct NLRC4-AID phenotypes (He et al., 2010).

In contrast to the previously described heterozygous NLRC4 autoactivating mutations, the here presented experimental evidence suggests a different mechanism of action for NLRC4 A160T. Pathogenicity of this mutation was ligand-dependent in Flp-In 293 T-REx and THP-1 cell assays, where NLRC4 A160T was monogenic or endogenously expressed, respectively. Only when overexpressed in HEK293T cells, A160T mediated increased inflammasome formation without an additional ligand, however this is likely the result of high expression levels and subsequent spontaneous oligomerization. In this experiment, western blot analysis consistently showed reduced expression levels of homozygously expressed A160T following transient transfection (**Figure 4.5 B**). This may either suggest reduced stability of the mutant protein or increased cell death induction, the latter being commonly observed in reconstitution assays with NLRC4 GoF mutations. However, the possibility of cell death is unlikely, since HEK293T cells lack endogenous expression of caspase-1 (Agostini et al., 2004), the microscopic examination did not reveal signs of cell death and the expression levels of the β-actin loading control only showed minimal variation between samples. Since equal expression levels of NLRC4 WT and A160T were observed in Dox-induced FlpIn-293 T-REx cells (**Figure 4.6 B**), we suggest that perhaps the plasmid DNA, specifically used for transient transfection of HEK293T cells in this experiment (**Figure 4.5**) might have been of lower quality. Therefore,

reduced expression levels of NLRC4 A160T may result in an underestimation of the effect in this assay.

Temperature-induced pathogenicity of NLRC4 A160T was not observed in *in vitro* experiments (data not shown) and cold-induced inflammatory flares were not reported by the patient, which therefore likely excludes a mechanism of action similar to mutations associated with FCAS4.

Ligand-dependency of A160T pathogenicity is in line with the co-occurrence of several inflammatory episodes with gastrointestinal and urinary tract infections in the patient. As causative pathogens *E. coli* and *Klebsiella* were detected in most cases, however a detailed analysis of *Klebsiella* species was not part of the clinical diagnostic procedure. These pathogens are classified as Gram-negative bacteria and belong to the family of Enterobacteriaceae which are generally rod-shaped. It is well established that *E. coli* possess flagella to ensure motility and enteropathogenic strains (EPEC, EHEC) contain a T3SS, thus providing NAIP/NLRC4 inflammasome-specific ligands (Berg 2003, Fox et al., 2020, Slater et al., 2018). In contrast, *Klebsiella* species were originally considered non-motile, however emerging evidence now suggests presence of flagella under certain conditions, as shown for one *K. pneumoniae* strain isolated from a paediatric patient (Carabarin-Lima et al., 2016). Furthermore, *K. pneumoniae* has been shown to trigger NLRC4 in human MDMs and mice after intratracheal delivery (Cai et al., 2012), and although less frequently than *E. coli*, *K. pneumoniae* has been identified as causative pathogen in urinary tract infections (Cristea et al., 2017, Faoagali 1975, Fihn 2003, Gupta et al., 2001). However, *K. pneumoniae* is typically non-flagellated and does not encode T3SS proteins, therefore the ligand that activates NAIP is unclear but could be flagellin as mentioned above (Cai et al., 2012, Carabarin-Lima et al., 2016, Fouts et al., 2008).

In contrast to the well-defined activating ligands of the NAIP/NLRC4 inflammasome, a wide spectrum of stimuli was shown to activate NLRP3, and an interaction of both inflammasome proteins within the same signalling complex has been described during *S. typhimurium* infections of murine macrophages, when triggers for both inflammasomes were presented (Man et al., 2014a, Qu et al., 2016). Additionally, a recent study suggested that canonical NLRP3

inflammasomes can form directly in response to flagellin from *S. typhimurium* and *B. subtilis* in PMA-differentiated THP-1 cells deficient for NLRC4, which was dependent on ROS production and/or cathepsin B activity (Gram et al., 2020).
Therefore, although speculative, it is possible that NLRP3 signalling plays an additional role in the pathogenesis of the here described patient, perhaps dependent on the infectious trigger. In line with this hypothesis, patient MDMs and clonal THP-1 (A160T/KO) cells showed higher cytokine release than control cells when treated with NLRP3-specific stimuli. Interestingly, increased NLRP3 signalling following stimulation with LPS and ATP was also reported in PBMC-derived macrophages from a previously described NLRC4-MAS patient (Canna et al., 2014). Therefore, future studies are required to investigate the involvement of NLRP3 in the context of NLRC4 GoF mutation-induced inflammasome activation.
In clonal THP-1 cells carrying the A160T mutation (A160T/KO genotype), increased NLRP3 activity following TLR1/2-priming and nigericin stimulation was only apparent on the level of cytokine release, whereas cell death induction was comparable to control cells. Therefore, synergistic effects of NLRC4 A160T and NLRP3 may be confined to cytokine-processing pathways. However, the observed near-maximum levels of induced cell death combined with the limitations of an end point assay complicate the interpretation of this result. Dose-dependency studies with NLRP3-specific ligands or real-time observation of cell death induction kinetics are required before conclusions can be drawn.
Important to consider in this context is the variability associated with the analysis of single cell-derived clonal cell lines, which is a major disadvantage of the here used experimental THP-1 cell system. Despite the speculative effect of NLRC4 A160T on NLRP3 activation, all other clonal THP-1 cell lines were expected to respond similarly to NLRP3 stimulation, since this pathway was not genetically modified. However, levels of released IL-1β and IL-18 varied largely following NLRP3 activation, whereas cell death induction was more homogenous. Most noticeable was the increase in IL-1β release from WT/WT cl.1 and A160T/KO cell lines, whereas the THP-1 cell pool and A160T/KO cells released more IL-18, although this difference was less pronounced compared to all other clonal cell

lines. Furthermore, some variability was observed when the NF-κB-induced but inflammasome-independent cytokine IL-8 was measured to compare priming efficiencies in the NLRC4-stimulation assay. This variability can be explained by the previously described genetic, epigenetic and phenotypic heterogeneity of single cells and consequently single cell-derived clonal cell lines (Giuliano et al., 2019, Tian et al., 2020, Velazquez-Villarreal et al., 2020). Variable genetic background and epigenetic regulation could alter the magnitude of the biological effect induced by a mutation of interest. Bulk RNA-sequencing experiments could be performed to identify such variability. However, this approach is costly and correlating gene expression profiles to translated protein levels and pathway activation is influenced by multiple other factors. Therefore, ideally multiple single cell clones with the desired genotype should be analysed before concluding about an observed mutation-specific phenotype. In this study, we were only able to generate one THP-1 cell line carrying the A160T mutation via site-directed mutagenesis using CRISPR/Cas9-mediated genome editing and HDR. Although 15 other clonal cell lines with repair template integration were detected through PCR and restriction digest screening, Sanger sequencing of the genomic *NLRC4* locus identified additional frameshift mutations, which highlights the previously reported low efficiency of this methodical approach (Carroll 2014, Harrison et al., 2014, Lin et al., 2016). Although without success, aiming to improve the HDR efficiency in our experiment we used SCR7, an inhibitor of DNA Ligase IV (LIG4) which ligates compatible DNA ends, to block NHEJ and channel DNA repair towards HDR (Hu et al., 2018). Multiple other approaches to indirectly and directly increase HDR efficiency have been described. These include genetic modification and overexpression of key HDR proteins (Vispé et al., 1998), synchronization of HDR-permissive cell cycle phases (Lin et al., 2014, Maurissen et al., 2020) or improved design and delivery of the DNA repair template (nuclear localization (Han et al., 2020), tethering to Cas9-guide RNA-nucleoprotein complex (Aird et al., 2018), use of chromatin-associated template DNA (Cruz-Becerra et al., 2020)). The most promising strategies involve the use of small molecules for targeted inhibition or enhancement of key proteins driving NHEJ or HDR, respectively, due to their time efficient and reversible mode of action,

concentration-dependent control of toxicity and applicability to cell lines (reviewed in (Bischoff et al., 2020)). Using these compounds could prove useful to generate additional THP-1 cell lines with genomic expression of NLRC4 A160T via CRISPR/Cas9 and HDR for further evaluation of the mutation-associated pathogenicity. A direct comparison of heterozygous and homozygous A160T genotypes in THP-1 cell assays would also be desirable to elucidate dose-dependency effects and experimentally characterize the pathological implications for heterozygous allele carriers.

Alternatively, other more efficient strategies of precise genome editing could be trialled. Recently described advancements of CRISPR/Cas9-based technologies include base editing and prime editing, which both induce genomic point mutations without DSB (Anzalone et al., 2019, Nishida et al., 2016). Prime editing employs a single prime editing guide RNA (pegRNA), which specifies the target site and encodes an edit-containing RNA template, that is used in combination with a Cas9 nickase-reverse transcriptase fusion protein (Anzalone et al., 2019). After pegRNA-mediated guidance to the target site, the Cas9 nickase cuts only the non-complementary DNA strand upstream the PAM site. This exposes a 3' OH group where binding of the RNA template (second part of the pegRNA) serves as primer for the reverse transcriptase activity of the fusion protein to copy the sequence of the editing template. The extended new 3'flap then replaces the original unedited 5'flap, which is in turn degraded by a cellular nuclease FEN1 (flap endonuclease 1). Simultaneous introduction of a silent mutation to modify the PAM site sequence prevents repeated editing. Mismatch repair resolves the heteroduplex DNA conformation if only one strand was edited. Avoidance of DSB (induced by conventional CRISPR/Cas9) limits the use of error-prone DNA repair pathways and therefore reduces the risk of random indels, prevents frameshift mutations and thereby maintains functionality of the edited gene (Scholefield et al., 2021). Additional advantages are that in contrast to HDR, which only occurs in dividing cells, prime editing can occur in any phase of the cell cycle and off-target effects are uncommon. Therefore, this method represents a promising strategy for the generation of *in vitro* systems to model disease-causing variants and has already been used in a variety of studies (Gao et al., 2021, Anzalone et

al., 2019, Geurts et al., 2020, Liu et al., 2020, Rousseau et al., 2020, Sürün et al., 2020).

Although ligand-dependency of NLRC4 A160T-mediated inflammasome activation was experimentally determined in our study, numerous questions remain unanswered and require further investigation.

Studying cytokine release and cell death in mutant THP-1 cells in absence of NAIP, caspase-1, caspase-8, ASC or NLRP3 will reveal further insights into the upstream requirements and downstream effects mediated by the A160T mutation and answer the question regarding a possible involvement of NLRP3. Furthermore, using primary cells or iPSCs derived from patient cells may be advantageous to identify the mechanism of action of NLRC4 A160T, since expression levels of inflammasome-forming proteins and occurrence of NAIP splice variants may be distinctly different between primary and immortalized cells (Gram et al., 2020, Kawasaki et al., 2017, Kortmann et al., 2015).

Similarly, the role of NAIP/NLRC4 inflammasome effector proteins has not yet been assessed for most of the NLRC4 GoF mutations, but could reveal interesting insights into NLRC4 signalling pathways and the associated disease phenotypes. Only Moghaddas and colleagues have investigated the *in vitro* effects of the NLRC4 W655C mutation in THP-1 cells genetically deleted for ASC, caspase-1 and caspase-8, and observed differential effects on cytokine release and cell death (Moghaddas et al., 2018). In this assay, NLRC4 W655C-mediated IL-18 release was completely dependent on both caspase-1 and ASC, whereas complete and partial dependence of IL-1β on caspase-1 or ASC was observed, respectively. Interestingly, only caspase-1 deletion was able to significantly reduce but not completely abrogate cell death, whereas ASC did not contribute. Genetic deletion of caspase-8 or pharmacological inhibition of NLRP3 did not affect downstream effects of NLRC4 W655C. In contrast, caspase-8-deficient NLRC4 WT cells stimulated with NLRC4-specific triggers showed reduced IL-18 release and cell death. These findings result in further questions regarding differential signalling of NLRC4 when activated by GoF mutations or NAIP-specific ligands (Moghaddas et al., 2018).

Furthermore, the activation of multiple cell death pathways mediated through NLRC4 interaction with caspase-1 or ASC-caspase-8 has been reported (Doerflinger et al., 2020, Lee et al., 2018, Zhang et al., 2021), which evidences various molecular functions associated with NLRC4 activation, that require complex regulatory mechanisms. Interestingly, caspase-1 protease activity was shown to suppress activation of the NLRC4/ASC/caspase-8 apoptosis pathway, which adds another layer of regulation mediated by mutual interaction of inflammasome effectors (Van Opdenbosch et al., 2017). Importantly, in caspase-1-deficient cells, NLRC4 activation induced caspase-8-dependent apoptosis without proinflammatory cytokine release (Van Opdenbosch et al., 2017). Therefore, understanding the interaction and regulatory mechanisms involved in the diverse NLRC4 pathways, will improve our understanding of disease-associated phenotypes and may allow for a more personalized and targeted therapy of NLRC4-associated pathological conditions.

Hypotheses regarding a potential mechanism of action of NLRC4 A160T remain speculative. However, the stimulation-induced phenotype suggest that T160 may facilitate the interaction between ligand-bound NAIP and NLRC4 or NLRC4 monomers, thereby promoting inflammasome nucleation and oligomerization. A comprehensive analysis of potential structural impacts associated with the A160T mutation is provided in chapter 5.2.

Importantly, in contrast to alanine, threonine residues are commonly phosphorylated by cellular kinases, which modifies chemical properties and the structural conformation of proteins and represents an important PTM able to diversify protein functions and coordinate signalling networks (Wang et al., 2014). In contrast to other proteins, which are often heavily phosphorylated on multiple residues for functional regulation, mass spectrometry analysis of NLRC4 stimulated with *S. typhimurium* in BMDMs only identified one phosphorylated residue, S533 (Qu et al., 2012). Although several studies aimed to clarify the functional consequences of this PTM, its requirement and role during the process of NLRC4 inflammasome activation and signalling remains inconclusive, especially since phosphorylated S533 was present in the autoinhibited crystal

structure of mNLRC4 (Hu et al., 2013) and contradictory results have been obtained in different studies (chapter 1.3.3.4.6) (Qu et al., 2016, Qu et al., 2012, Tenthorey et al., 2020). The possibility that T160 could present an additional phosphorylation site with regulatory potential is further evaluated and discussed in chapter 5.2.6.

Noteworthy is the observation that A160 is a conserved residue in humans, most non-human primates and rodent species, whereas NLRC4 of cats and ungulate species encodes for a threonine in position 160 in the WT sequence. The evolutionary relationship and possible functional implications of this observation are further discussed in chapter 5.2.1. Studying NLRC4 signalling in bovine or feline macrophages could therefore provide an interesting opportunity to reveal functional characteristics specific to NLRC4 T160, which may have been lost during evolutionary development (further discussed in chapter 5.3).

The finding that not only homozygous expression of NLRC4 A160T but also heterozygous co-expression with NLRC4 WT was able to drive increased ASC speck formation in HEK293T cells is of great relevance, given the heterozygous occurrence of the A160T allele in the general population (allele frequency 0.0008, GnomAD). Mechanistically, based on the orchestration of conformational changes that drive NLRC4 self-oligomerization, expression of a certain ratio of autoactive NLRC4 mutants is anticipated to sufficiently facilitate inflammasome nucleation, which subsequently engages WT protein and explains the autosomal-dominant effect of NLRC4-AID-associated GoF mutations (Hu et al., 2015, Zhang et al., 2015). A similar mechanism could be proposed for heterozygous NLRC4 A160T, however, ligand-dependency differentiates both scenarios.

Interesting in this context is the significant enrichment of the heterozygous NLRC4 A160T allele in UC patients, given the constitutive expression of NLRC4 and pro-IL-18 in intestinal cells (Nordlander et al., 2014, Pizarro et al., 1999, Sellin et al., 2014), the enterocolitis phenotype observed in AIFEC patients together with gastrointestinal symptoms and modestly elevated IL-18 levels in the here described patient. Meta-analysis association data from the IBD Exomes Browser identified a 2.5-fold increased risk for heterozygous NLRC4 A160T allele carriers

to develop UC (**Table 14**), therefore suggesting this allele as a potential susceptibility locus associated with this disease.

Despite being heterozygous allele carriers, parents and brother of the here reported patient were healthy and did not experience UC-related symptoms, which emphasizes the role of additional genetic or environmental co-factors and the multifactorial nature of this disease.

Furthermore, it is important to consider that genetic heterogeneity varies between different populations and the identification of a genetic risk locus is greatly affected by allele frequency and the effect size (Liu et al., 2015a), and therefore requires large studies within different populations before definite conclusions can be drawn. Further studies to evaluate functional and genetic aspects of NLRC4 A160T in UC patients are therefore desirable to validate the here described observations. In this context, analysis of serum IL-18 levels in heterozygous allele carriers could be very informative, especially with regard to whether UC development can be predicted or the disease course monitored.

Based on the IBD Exomes Browser data, A160T was the variant with highest risk to develop UC within the *NLRC4* gene. Other genetic variants with comparable ORs have been reported in various inflammatory pathway-related molecules, such as NLRP7 and NOD2. NLRP7 (S361L) was found in association with a 4.79-fold increased risk for UC development (OR=4.79, *P*=0.0039) and a 3.17-fold increased risk for Crohn's disease development (OR=3.17, *P*=0.037), which was identified by whole exome sequencing of ten families with multiple cases of IBD (Onoufriadis et al., 2018).

NOD2 was the first susceptibility gene identified for IBD, which shows particular strong association with Crohn's disease (Hugot et al., 2001, Ogura et al., 2001c), however some NOD2 variants are suggested risk factors for UC development, for example NOD2 (R38M): OR=2.904, *P*=0.03291 (IBD Exomes Browser). NOD2, which is mainly expressed in monocytes, macrophages but also in IECs (Hisamatsu et al., 2003, Negroni et al., 2018, Ogura et al., 2001b), induces apoptosis and proinflammatory signalling through NF-κB and MAPK pathways in response to cytoplasmic detection of MDP, a bacterial peptidoglycan (Magalhaes et al., 2011). Mutations in this gene disrupt the intestinal epithelial barrier due to

reduced defence against microbial invaders, which can cause chronic intestinal inflammation (Hugot et al., 2001, Ogura et al., 2001c, Philpott et al., 2014). Interestingly, for NOD2 and Crohn's disease, a gene dosage effect was described and suggested a positive correlation between the number of mutations in NOD2 with age of onset, affected tissues and severity of the disease (Lesage et al., 2002). Therefore, NOD2 is only one example of how PRRs maintain intestinal immune system homeostasis and drive aberrant inflammation if dysregulated.

So far, a role of NLRC4 in IBD has not yet been clearly defined. One study identified NLRC4 expression in IECs as essential player to defeat intestinal colonization of *C. rodentium*, an enteropathogen associated with inflammation and diarrhea that may be implicated in the development of IBD if colonization is not appropriately controlled (Mundy et al., 2005, Nordlander et al., 2014). Several animal studies investigated a link between NLRC4 and chronic intestinal inflammation using a mouse model of chemically induced colitis, where dextran sodium sulfate (DSS) treatment injures the gut epithelial layer and causes intestinal inflammation driven by the gut-colonizing bacteria (Allen et al., 2010, Carvalho et al., 2012, Hu et al., 2010). However, these studies obtained different results. Whereas Hu and colleagues found no difference in DSS-induced colitis in *Nlrc4*$^{-/-}$ mice and controls (Hu et al., 2010), mNLRC4 had protective effects in a similar study performed by Allen and colleagues (Allen et al., 2010). This was in line with a later study where Carvalho and colleagues observed more severe colitis, reduced IL-18 release and increased death in *Nlrc4*$^{-/-}$ mice after DSS treatment and suggested that mNLRC4-mediated IL-18 release plays an important role in colitis protection (Carvalho et al., 2012). One proposed reason for the different data obtained in the above-described studies is the microbiome variability between mouse strains from different institutions, which may have great impact on colitis development if mNLRC4-deficiency impairs the barrier function of IECs (Ringel-Scaia et al., 2016).

Although the exact link between NLRC4 and colitis remains unclear, elevated IL-18 levels have been shown in association with intestinal inflammation (Chikano et al., 2000, Sivakumar et al., 2002) and IBD (Ludwiczek et al., 2005). Additionally, homeostatic IL-18 signalling seems crucially important and

contributes to the immune-mediated aspect of the intestinal barrier, which does not cause host damage (Hayes et al., 2018). The NLRP6 inflammasome was shown to largely contribute to this pathway and prevent intestinal colonization with IBD-inducing bacteria (Elinav et al., 2011, Kempster et al., 2011, Levy et al., 2015, Seregin et al., 2017).

The here described finding, that the NLRC4 A160T mutation is increasingly associated with UC contributes evidence towards an important role of NAIP/NLRC4 signalling as potential source of elevated IL-18 in IBD. Therefore, targeted inhibition of extensive IL-18 signalling provides a promising therapeutic opportunity, not only for patients suffering from NLRC4-AID, but also in IBD (Mokry et al., 2019).

Interestingly, in light of the corona virus disease 2019 (COVID-19) pandemic, the term COVID-MAS was coined, which describes the uncontrolled cytokine release in late stage COVID-19 patients, caused by infection with the coronavirus-2 (SARS-CoV-2) pathogen, which shows similarities to NLRC4-MAS (McGonagle et al., 2020, Satış et al., 2021). Besides other inflammatory markers, serum IL-18 levels were remarkably elevated in COVID-19 patients and correlated with disease severity in a study of 58 cases (Satış et al., 2021). Aberrant macrophage activation and cytokine storm were observed and associated with acute respiratory distress syndrome, organ failure and high morbidity (Tufan et al., 2020). Inhibiting IL-1β with anakinra in combination with immunosuppressive and antiviral drugs significantly improved the clinical outcome of COVID-19 patients with severe disease progression, as identified in a retrospective study (Cavalli et al., 2020). However, clinical evidence suggests an important contribution of IL-18-mediated downstream effects, such as IFNγ induction, activation of Th1 cells, NK cells and macrophages to the COVID-19 pathogenesis, therefore suggesting targeted inhibition of IL-18 signalling as promising treatment strategy in these patients (Satış et al., 2021).

Although cell-based *in vitro* assays provide great potential to study biological effects and pathogenic potential of genetic variants, understanding how a missense mutation impacts structure and chemical properties of a protein is

equally elucidating with regard to alterations of protein function. Therefore, chapter 5 continues the investigation of NLRC4 A160T from a structural, biochemical and biophysical perspective, aiming to identify the molecular mechanisms through which NLRC4 A160T elicits pathogenicity.

5 Structural and biophysical characterization of NLRC4 A160T

5.1 Introduction

5.1.1 ATPases associated with diverse cellular activities

Protein function requires a correct three-dimensional (3D) conformation and the presence of functional motifs, which are often evolutionarily conserved. Therefore, classification of proteins according to structural similarities and amino acid sequence homology aids their functional characterization (Nishikawa et al., 1983). In this context, all NLR proteins are classified as P-loop NTPases based on the presence of the highly conserved NACHT domain, which possesses a nucleoside-triphosphatase (NTPase) activity and is important for protein function (Leipe et al., 2004). P-loop NTPases contain a 200-250 amino acid long ATP binding domain (AAA domain), which encodes two conserved amino acid sequence motifs, namely the Walker A motif (phosphate-binding, (P)-loop) and Walker B motif, residues of which coordinate nucleotide binding and hydrolysis, respectively (Snider et al., 2008, Walker et al., 1982). Structurally, the conformation of the P-loop domain is characterized by a typical three-layer $\alpha\beta\alpha$ sandwich of repeating β-loop-α units, where β-strands are arranged in parallel orientation and surrounded by α-helices (Milner-White et al., 1991).

Throughout evolution, P-loop NTPases diversified into two distinct subgroups, which are classified based on the structural arrangement of the P-loop-surrounding β sheets: 1) the kinase-GTPase (KG) family, where P-loop and the Walker B motif-containing strand are adjacent to each other and 2) the additional strand catalytic E (ASCE) family, which contain an additional strand between P-loop and the Walker B strand (Leipe et al., 2003, Leipe et al., 2004, Leipe et al., 2002). In ASCE proteins, the functional module contains β-sheets that follow a characteristic arrangement as $\beta5-\beta1-\beta4-\beta3-\beta2$ topology and contains an additional conserved catalytic glutamate residue within the Walker B motif, which further specifies this group (**Figure 5.1**) (Leipe et al., 2003, Snider et al., 2008).

Within ASCE proteins, NLRs are subclassified within the group of ATPases associated with diverse cellular activities (AAA+ ATPases), which contains a great variety of proteins implicated in various functions including membrane fusion, proteolysis, protein folding, DNA replication, transcriptional regulation and cell division processes (Ammelburg et al., 2006). Sequence similarity to animal apoptosis-regulating proteins such as *C. elegans* cell death protein 4 (CED4) and apoptotic protease activating factor 1 (APAF-1) resulted in further subclassification of NLRs as signal transduction ATPases with numerous domains (STAND) ATPases (Leipe et al., 2004).

In this protein family, the central ATPase activity module is referred to as core nucleotide-binding oligomerization (NOD) module (NACHT domain), formed by nucleotide-binding domain (NBD), helical domain 1 (HD1) and winged helix domain (WHD) (Inohara et al., 2001) (**Figure 5.1**). All NLRs additionally contain the helical domain 2 (HD2) as part of this module (Maharana et al., 2018, Sandall et al., 2020).

Distinct functional motifs and structural features of STAND family proteins include the conserved hhGRExE sequence (h denotes hydrophobic residue, x denotes any residue) upstream of the Walker A motif. Additionally, a GxP motif (GxP module) is located within the HD1, which forms a helical bundle (**Figure 5.1**) (Leipe et al., 2004). Although the glycine (G) residue is lacking in NLRs, proline (P) is highly conserved (consensus sequence PhhCW in NLRs, h denotes hydrophobic residue) and interacts with the adenine moiety of the bound nucleotide (Maharana et al., 2018, Sandall et al., 2020). More conserved between family members of P-loop NTPases in general is the eight amino acid long Walker A motif (consensus sequence GxxxxGK[S/T], x denotes any residue) which forms a flexible loop between strand β1 and helix α1 (**Figure 5.1**) (Walker et al., 1982). The conserved lysine (K) residue in this motif is critically important to coordinate nucleotide binding through interaction of its positively charged side chains with $\beta-$ and $\gamma-$phosphates of the bound nucleotide (Saraste et al., 1990, Wendler et al., 2012). The hydroxyl group of the polar serine (S) or threonine (T) encoded at the end of the Walker A motif participates in coordination of the magnesium cation (Miller et al., 2016, Saraste et al., 1990).

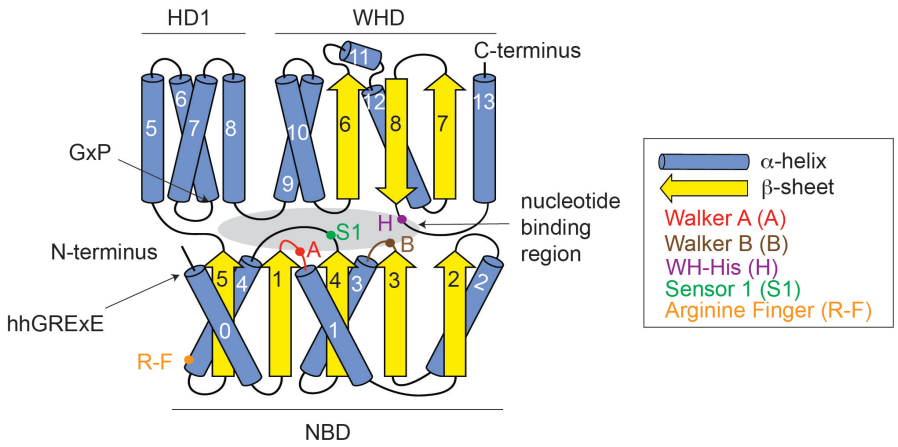

Figure 5.1 | Topology diagram of the conserved STAND ATPase NOD module. Schematic localization of conserved motifs within β-strands (arrow-heads on C-terminal side) and α–helices (cylinder) of the STAND ATPase core, which is organized as β5–β1–β4–β3–β2 topology. The nucleotide binding region is indicated (grey oval). h, denotes hydrophobic amino acids; x, denotes any amino acid; nucleotide-binding oligomerization module, NOD; nucleotide-binding domain, NBD; helical domain 1, HD1; winged helix domain, WHD; signal transduction ATPases with numerous domains, STAND. Figure modified from Danot et al. (Danot et al., 2009).

Located on strand β3, the Walker B motif mediates ATP hydrolysis and consists of two conserved acidic residues (consensus sequence: hhhh[DE], h denotes hydrophobic residue), which coordinate the catalytical magnesium ion towards the ATP-β-γ-phosphate moiety and arranges a water molecule for the nucleophilic attack (**Figure 5.1**) (Leipe et al., 2004, Walker et al., 1982). Importantly, the Walker B motif is not required for ATP binding (Hanson et al., 2005). Furthermore, NLR proteins possess a modified Walker B motif, which lacks the typical glutamate (E) and is characterized by presence of an additional DE motif two residues downstream (hhhhDxxDE) (Proell et al., 2008). The conserved glutamate (E) of the Walker B motif can rotate between positions that allow or prohibit the nucleophilic water attack. This transition is regulated by the "glutamate switch" residues (conserved asparagine, N) located on the adjacent β-strand, which upon binding of the ligand/target changes its orientation and switches the Walker B glutamate between the active and inactive conformation and thus controls the ATPase activity of the protein (Zhang et al., 2008).

β-strand 4 is located between β1 and β3 and contains a conserved C-terminal polar residue which corresponds to sensor 1, a conserved motif in AAA+ superfamily proteins (Iyer et al., 2004). Sensor 1 was suggested to “sense” the γ-phosphate and assists the Walker B motif residue in coordination of the attacking water molecule (**Figure 5.1**) (Wendler et al., 2012).

Moreover, AAA+ ATPases contain characteristic arginine fingers located at the end of the α4-helix, which are a single or multiple conserved arginine residues (R) located proximal to the γ-phosphate in the ATP-bound state, which promote ATP hydrolysis (Ogura et al., 2004) (**Figure 5.1**). The sensor 2 motif is formed by conserved arginine (R) or lysine (K) residues located just before the β5-strand (Proell et al., 2008). However, this feature is missing in most members of the STAND family, which instead possess a conserved histidine (H) at the beginning of the last helix within the WHD (WH-His) (**Figure 5.1**). Functionally, WH-His acts as replacement of sensor 2 by contributing hydrogen bonds to coordinate phosphate moieties of the bound nucleotide (Ogura et al., 2004, Proell et al., 2008). Importantly, sensor 1, sensor 2 and arginine fingers are not conserved between all members of the AAA+ ATPase family (Wendler et al., 2012).

Structurally, the adenine moiety of the nucleotide is localized between NBD and HD1 and the phosphate groups interact with the P-loop, specifically the Walker A-containing β-strand (**Figure 5.1**) (Neuwald et al., 1999).

5.1.2 Self-assembly of STAND ATPases

In general, ATPases function to generate energy for biological processes, such as conformational change, complex formation, transport and degradation of proteins (Ogura et al., 2001a). As part of this process, AAA+ ATPases form wheel-shaped oligomeric complexes, a structural prerequisite for the enzymatic activity and signalling to occur (Hanson et al., 2005, Ogura et al., 2001a). Most commonly observed are hexamer arrangements, which suggests high stability of this conformation (Ogura et al., 2001a). However, pentamer to octamer symmetries have also been described as well as helical and double ring

formations. Interestingly, the underlying stoichiometry is flexible, since mixed populations of ring-like complexes containing variable numbers of monomers were observed for several members of this class (reviewed in (Sysoeva 2017)).
Generally for STAND family proteins, a relatively low ATP conversion rate of ~0.1/min for *E. coli* maltose regulon (MalT) (Marquenet et al., 2007) and 1/min for AfsR, a regulatory transcription factor in *Streptomyces coelicolor* (Lee et al., 2002), have been detected, whereas some STAND proteins do not show detectable ATPase activity or lack the required structural motifs (Danot et al., 2009). Notably, the majority of STAND ATPases was identified to preferentially bind ATP, whereas GTP-binding was observed for CIITA, the transcription regulator of MHC class II gene expression (Harton et al., 1999).
In STAND ATPases, the NACHT domain is linked to C-terminal and N-terminal functional domains to mediate specific downstream signalling events (Danot et al., 2009). The C-terminus is the typical localization of a sensor domain and various domains with repeated motifs, such as WD40, LRR and TPR (tetratricopeptide repeat)-like domains have been identified (Danot et al., 2009). N- or C-terminally located effector domains determine protein function and mediate protein-protein interactions (CARD, TIR, coiled-coil and PYD), nucleic acid binding (LuxR- and OmpR-type or TROVE domains) or enzymatic activity (adenylate cyclase kinase) (Danot et al., 2009).
The mechanistic details of STAND ATPase oligomerization and signalling are not completely understood. However, combined experimental evidence from studies of various STAND family members from different species, including MalT (Danot 2015), CED4 (Yan et al., 2005), APAF-1 (Yu et al., 2005, Riedl et al., 2005), NLRs (Hu et al., 2013, Tanabe et al., 2004, Tenthorey et al., 2014) and plant R proteins (Bernoux et al., 2016, Slootweg et al., 2013) suggested mechanistical similarities, which may be partly conserved between all STAND ATPase members containing characteristic signalling motifs (Danot et al., 2009). These similarities prompted the proposal of an “assembly model”, in which NACHT ATPases act as molecular switches, that exist in an inactive long-lived adenosine diphosphate (ADP)-bound monomeric state (autoinhibited, “off” state) (**Figure 5.2**). As previously mentioned (chapter 1.3.3.1), in the case of NLRs, two signals are required to induce full

activation and oligomerization (“on” state). Signal one, referred to as the priming signal, is believed to open the autoinhibited conformation to enable ADP-to-ATP exchange, followed by ligand/inducer binding (signal 2), which initiates self-assembly. Active oligomeric ring-like complexes then function as signalling hubs that recruit downstream signalling molecules via effector domains (**Figure 5.2**) (Danot et al., 2009).

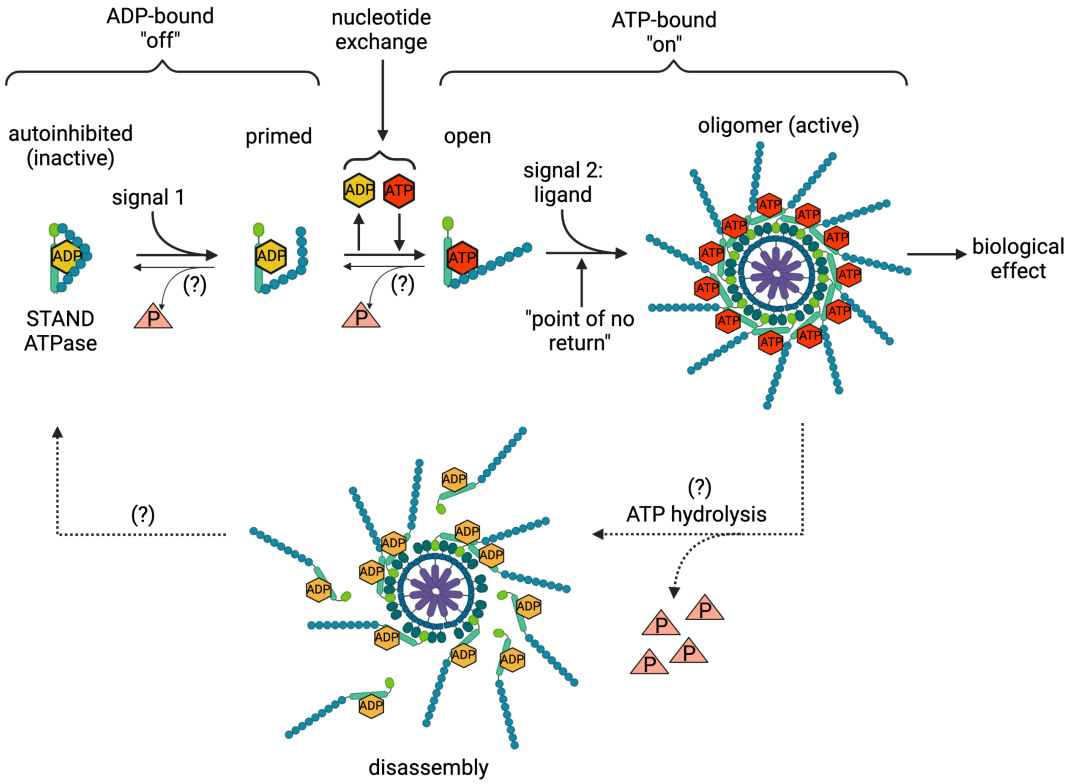

Figure 5.2 | Self-assembly of STAND ATPases. Binary switch model adapted from Danot et al., 2009. STAND ATPases exist in an ADP-bound inactive state characterized by a closed conformation (“off”). Full activation and oligomerization require two signals. In the case of NLRs, the initial priming signal renders the conformation more susceptible for nucleotide exchange to ATP. If signal 2 is detected while in this conformation, self-assembly occurs, which is believed to follow the “point of no return” principle for some proteins. The explicit function of ATP hydrolysis remains to be determined, but may revert ATP-bound monomers into the autoinhibited conformation when a specific ligand (signal 2) is lacking. In some cases, ATP hydrolysis may mediate disassembly of the active oligomeric complex and terminate signalling. Signal transduction ATPases with numerous domains, STAND. Figure created with BioRender.com.

Importantly, the role of ATP hydrolysis during self-assembly and signalling events remains controversial. Whereas *in vitro* studies of MalT using a non-hydrolysable ATP analogue or ATPase-deficient mutants suggested the requirement of ATP binding but not hydrolysis during self-assembly (Richet et al., 1989, Schreiber et al., 1999, Marquenet et al., 2007), ATP hydrolysis was required for cytochrome c-induced APAF-1 apoptosome formation (Hu et al., 1999, Kim et al., 2005) and mutations impairing ATPase activity in plant R protein I-2 resulted in constitutive activation (Tameling et al., 2006). Therefore, the role and timing of ATP hydrolysis remains unclear and might differ between individual STAND ATPase family members. For NLRs, ATP hydrolysis may retrieve the inactive conformation in absence of signal 2, as a negative regulatory mechanism to reset ATP-bound monomers. This suggestion is supported by the relatively low ATPase activity, which only provides limited energy to mediate conformational reorganization (Hu et al., 2013, Reubold et al., 2009). Alternatively, hydrolysis-induced conformational changes may induce disassembly of the active signalling complex and reset oligomers to the inactive monomeric conformation (**Figure 5.2**) (Marquenet et al., 2007). Therefore, although the functional consequences require further investigation, modulation of ATP binding and hydrolysis by regulatory molecules can control STAND ATPase function. In case of MalT, negative regulators were found to stabilize the ADP-bound inactivate conformation (Joly et al., 2004, Joly et al., 2002, Marquenet et al., 2007), whereas the inducer maltotriose promoted ADP-to-ATP exchange (Marquenet et al., 2007). However, the regulation of STAND ATPases is likely more complex than this model suggests and specific differences between various family members may exist (Danot et al., 2009). On a structural level, distinct conformational features define both the ADP-bound resting state as well as the ATP-bound active state, which is explained in more detail for NLRC4 in chapter 5.1.4. Further studies investigating structural and biochemical characteristics of STAND ATPases are required to reveal the mechanistic details of their activation, however these studies are challenging due to the large protein size and self-oligomerization abilities of members in this protein class, which impedes

purification of full length recombinant monomeric protein (Danot et al., 2009, Ye et al., 2008).

5.1.3 ATP-dependence and activation mechanism of NLRs

As mentioned above, the role, kinetics and molecular consequences of ATP hydrolysis in NLR proteins have not yet been fully elucidated and only limited insights from well-studied NLRs including NLRP1, NLRP3, NLRP7 and NLRP12 exist (Sandall et al., 2020). Based on *in silico* analysis and modelling, similarities of NACHT domain structural features between all NLRP family proteins (NLRP1-14) suggest a similar mode of nucleotide binding and ATP-dependent activation (Maharana et al., 2018). To illustrate one example, domain localization and interactions of nucleotide-binding residues contributing to the Walker A (G^{169}ESGKGKS^{176}), Walker B (L^{244}FLLDGYNE^{252}), PhhCW (P^{338}LFVV) and WH-His (FFH^{443}) motifs are shown for mNLRC4 in **Figure 5.3 A**. Similar to NLRP4, NLRP9 and NLRP13, NLRC4 lacks the sensor 1 motif (Proell et al., 2008, Sandall et al., 2020).

For most NLRs, functional ATP hydrolysis has not yet been experimentally confirmed (Sandall et al., 2020). Whereas the Walker A motif is largely conserved within the NLR family, sequence variability within other NACHT domain motifs involved in ATPase activity and structural reorganization may suggest variability of NLR activation mechanisms, e.g. differences in nucleotide exchange-induced conformational change, enzymatic activity, activation kinetics and effector function (MacDonald et al., 2013, Sandall et al., 2020).

For example, the role of ATP hydrolysis during NLRP1 inflammasome activation remains controversial with experimental results suggesting ATP hydrolysis as a requirement for inflammasome-mediated caspase-1 activation (Faustin et al., 2007), whereas in a later study ATP hydrolysis activity was completely absent (Martino et al., 2016).

In contrast, NLRP3 has been more extensively investigated and the requirement of a functional NACHT domain for ATP binding and hydrolysis in inflammasome assembly and signalling was established using recombinant protein and *in vitro*

reconstitution assays (Duncan et al., 2007, Mortimer et al., 2016, Shim et al., 2017). Importantly, spontaneous IL-1β release by disease-causing NLRP3 GoF mutations (A439V (Sobolewska et al., 2016) or R260W (Neven et al., 2004)) was abrogated when the Walker A motif was dysfunctional (mutation of G231, K232, T233 to alanine (A)) emphasizing the essential role of nucleotide binding for inflammasome assembly (Duncan et al., 2007). Additional pathway regulation occurs through PTMs of amino acid residues proximal to or within the NACHT domain, such as phosphorylation of serine residues S198 and S295 (Mortimer et al., 2016, Song et al., 2017, Zhang et al., 2017), which may alter the protein conformation and thereby influence functional features like ATP binding and hydrolysis activity (Mortimer et al., 2016, Sandall et al., 2019, Song et al., 2017). Interestingly, whereas autophagy-mediated NLRP3 degradation was shown to take several hours (Yan et al., 2015), S295 phosphorylation by protein kinase A (PKA) rapidly terminated NLRP3 signalling via reduction of its ATPase function, thereby presenting a more efficient way of negative regulation (Mortimer et al., 2016, Sokolowska et al., 2015). This suggests that ATP hydrolysis is an essential requirement for NLRP3 inflammasome complex formation and signalling (Mortimer et al., 2016). This is further supported by the identification of several anti-inflammatory compounds able to specifically inhibit NLRP3 signalling via reduction of the ATPase activity (Cocco et al., 2016, Juliana et al., 2010, Shim et al., 2017). The commonly used NLRP3 inhibitor MCC950 (CRID3), a sulfonylurea derivative, was suggested to bind residues within the Walker B motif, block ATP hydrolysis and promote a conformational change towards the closed state (Coll et al., 2019, Tapia-Abellán et al., 2019). Importantly, recent structural information further clarifies MCC950 sulfonylurea group interaction with Walker A motif residues (preprint Hochheiser et al., 2021). In line, the inability of disease-causing NLRP3 mutations (A439V and R260W) to bypass the ATP binding requirement highlight its functional importance and confirm the nucleotide-binding site as a promising target for therapeutic inhibition, which could prove useful for the treatment of many NLRP3-associated diseases (Duncan et al., 2007).

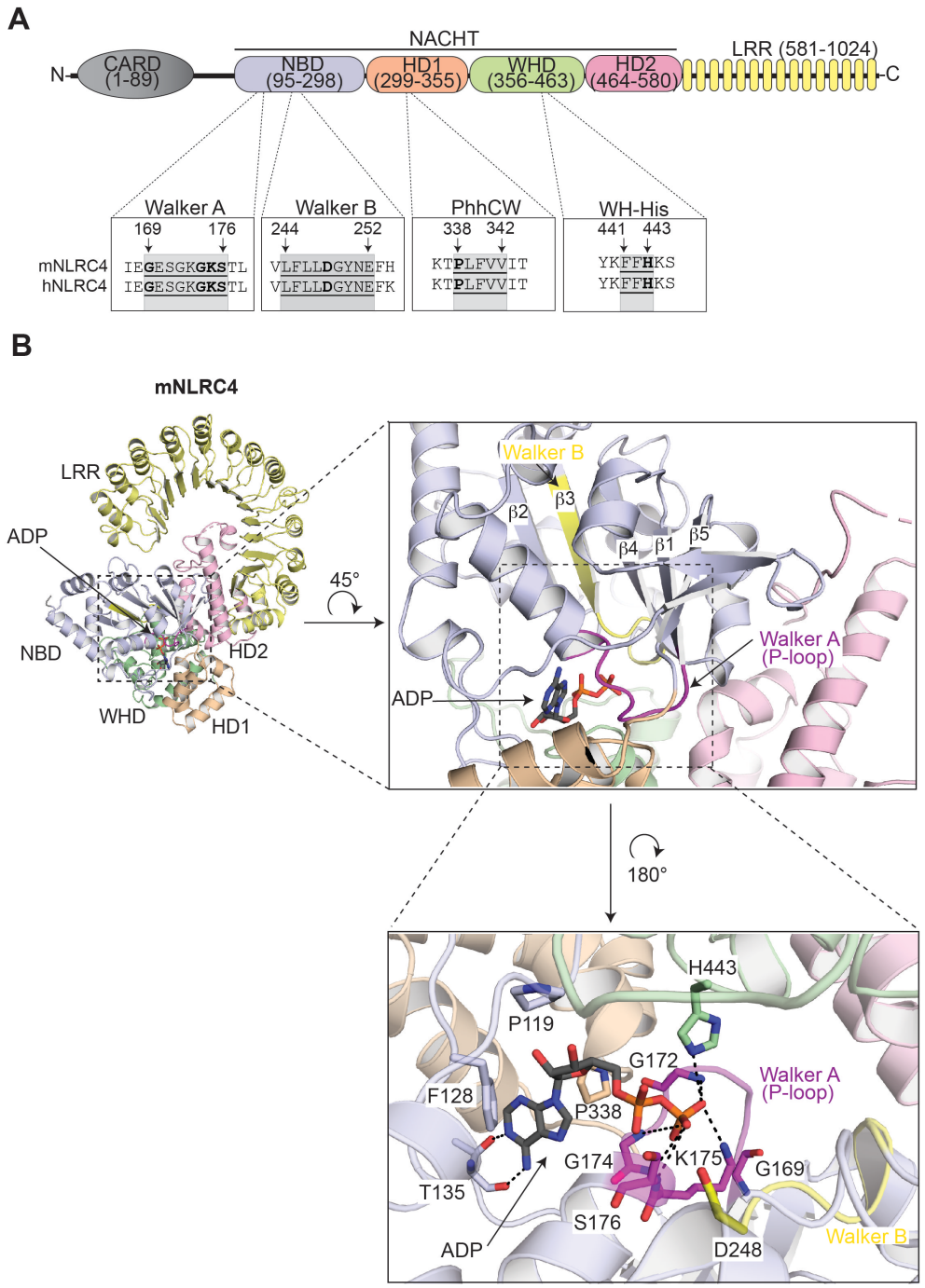

Figure 5.3 | Primary domain structure and key functional motifs of NLRC4. Primary protein domain structure of mNLRC4 with indicated amino acid residue boundaries as described by Hu et al. (Hu et al., 2013). Domain-localization and sequence of conserved ATP binding/hydrolysis motifs (grey boxes) are shown for human (h) and mouse (m) NLRC4. Amino acids directly interacting with bound ADP (bold) are shown as determined by Maharana et al. based on alignment of NLRP1-14, NOD1, NOD2 and NLRC4 (Maharana et al., 2018). **B)** Ribbon representation of mNLRC4 (PDB:4KXF) showing the nucleotide-binding pocket (core β-strands 1-5) and detailed interaction of ADP

with highly conserved residues (described in A) within the Walker A (P-loop, purple) and Walker B motif (yellow), indicated by dotted black lines. Nucleotide binding occurs through Walker A residues, whereas Walker B residue D248 coordinates the magnesium cation and the water molecule during the nucleophilic attack (ATP hydrolysis). NBD residue T135 stabilizes the adenine moiety via two hydrogen bonds. P338, as part of the PhhCW motif, directly stabilizes the adenine moiety. WHD residue H443 forms a hydrogen bond with the β-phosphate of ADP. P119 and F128 additionally stabilize the adenine moiety. Figure modified from Hu et al., 2013. ADP (dark grey) and amino acids in stick presentation are coloured by element: blue: nitrogen, red: oxygen, orange: phosphorus. Caspase activation and recruitment domain, CARD; nucleotide-binding domain, NBD; helical domain 1, HD1; winged helix domain, WHD; helical domain 2, HD2; leucine-rich repeat, LRR; contained in NAIP, CIITA, HET-E, TP1, NACHT.

In vitro experiments determined the ATPase activity of full length mNLRC4 with a hydrolysis rate of 3.24±0.24 ATP molecules per 1 mNLRC4 per hour (Hu et al., 2013). A similarly low hydrolysis activity of 4.33±0.13 was observed for APAF-1 in the monomeric autoinhibited conformation (Reubold et al., 2009). Therefore, although the role of hydrolysis in NLRC4 inflammasome formation is not yet fully understood, the low hydrolysis rate may suggest a negative regulatory function. Thus, ATP to ADP conversion may return the inactive conformation if potent ligands remain absent. Importantly, the Walker A mutant mNLRC4^{K175R} abolished spontaneous oligomerization of NLRC4ΔLRR (Kofoed et al., 2011) and was found to be rapidly degraded when overexpressed (Halff et al., 2012). Therefore, although the detailed mechanistic regulation remains elusive, nucleotide binding and perhaps hydrolysis play essential roles in NLRC4 inflammasome regulation. The regulatory and signalling mechanisms of most other NLR family proteins are poorly characterized and require future experimental investigation in order to increase our understanding of inflammasome immunology, which will be key to the development of therapies for inflammasome-driven diseases.

5.1.4 Structural insights into NAIP/NLRC4 inflammasome formation

The structural conformation of mNLRC4 is well investigated, both in the inactive and activated state, the latter in complex with ligand-bound mNAIP. In fact, the NAIP/NLRC4 inflammasome represents a prototypical inflammasome complex, which has significantly contributed to the broad understanding of inflammasome formation and signalling in general.

Hu et al. used X-ray crystallography to solve the structure of monomeric mNLRC4 deleted of the N-terminal CARD domain (aa 1-89, ΔCARD) and a flexible loop (aa 622-644, ΔLoop) within the LRR at 3.2 Å resolution (referred to as $mNLRC4^{\Delta CARD/\Delta Loop}$), which revealed the autoinhibited conformation (PDB:4KXF; Hu et al., 2013). Interestingly, although protein purification and crystallization procedures were performed in absence of exogenously added nucleotides, inactive $mNLRC4^{\Delta CARD/\Delta Loop}$ crystallized in an ADP-bound state, suggesting increased conformational stability (Hu et al., 2013). In this autoinhibited conformation NBD, HD1 and WHD residues interact with the bound ADP nucleotide. Specifically, the previously mentioned Walker A motif residues (G169, G174, K175, S176) form five hydrogen bonds with the phosphate groups of ADP and together with two hydrogen bonds between NBD residue T135 and adenine atoms N1 and N6 stabilize the inactive structure (**Figure 5.3 B**). This interaction does not occur with guanine, therefore providing the foundation for adenine-specificity and ADP/ATP binding. Hydrogen bond interaction between residue H443 (in WHD) and the β-phosphate group is critically important to further stabilize the inactive state (**Figure 5.3 B**) (Hu et al., 2013).

The C-terminal LRR domain of NLRC4 is formed by 15 repeats of a structural unit containing a leucine-rich β-strand and a subsequent α-helix. In contrast to the original assumption, the LRR does not function as a sensor domain (Tenthorey et al., 2017), but plays an essential role in autoinhibition, which was confirmed in HEK293T reconstitution assays, where LRR-truncated mNLRC4 caused ligand-independent constitutive caspase-1-mediated pro-IL-1β cleavage, which was further enhanced upon additional deletion of the HD2 domain (Hu et al., 2013). In the inactive conformation, the LRR is distantly located from the nucleotide-

binding site, HD1 and WHD, but interacts with HD2 and NBD residues to occlude the NBD via hydrogen bond formation (Hu et al., 2013).

The function of the HD2 is less well defined, however the above-mentioned deletion experiments indicate a role in autoinhibition. This is supported by structural findings that suggest HD2 residue interaction with the α8-helix of the NBD, a conserved structure important for oligomer formation and activation. Therefore, in the autoinhibited state, HD2-NBD interactions occlude the α8-helix (Hu et al., 2013).

The active conformation of the NAIP/NLRC4 inflammasome was initially investigated by negative stain EM studies of co-expressed mNAIP5, mNLRC4 and flagellin, which revealed a disk-like structure consisting of 11 or 12 protomers mostly present as stacked pairs (Halff et al., 2012). In a follow-up cryo-ET study (PDB:5AJ2, 40 Å resolution), the flagellin/mNAIP5/mNLRC4 inflammasome assembled into a heterogenous mixture of right- and left-handed continuous helices of variable lengths (at least 1 to 2 turns or more). In this study, detailed analysis of the averaged right-handed multimer revealed 11.65 protomers per turn (Diebolder et al., 2015).

Subsequently, Zhang et al. (PDB:3JBL, 4.7 Å resolution) and Hu et al. elucidated the stoichiometry of the PrgJ-mNAIP2-mNLRC4$^{\Delta CARD}$ inflammasome, which formed 10- to 12-bladed discs consisting of one PrgJ-bound mNAIP2 and 9 to 11 mNLRC4$^{\Delta CARD}$ protomers (Hu et al., 2015, Zhang et al., 2015). A similar stoichiometry was observed for inflammasome complexes containing full length mNLRC4 (Hu et al., 2015). Superposition and subsequent refinement analysis revealed the highest resolution (4.7 Å) for the 11-mer complex, however natural occurrence of heterogeneously arranged inflammasome complexes cannot be excluded. Overall, the inflammasome disc appeared as a dome-shaped ring with an inner hole, surrounded by an inner (containing NBD, HD1 and WHD) and outer ring (containing HD2 and LRR). On the level of individual NLRC4 protomers, the active state is characterized by extensive conformational changes, specifically, the ~90° rotation of WHD-HD2-LRR away from the NBD-HD1 module (Hu et al., 2015, Zhang et al., 2015). The hinge region is formed by helix α14, which locates between HD1 and WHD domains (Zhang et al., 2015). However, whether opening

of WHD-NBD-HD1 interactions, that determine the ADP-bound inactive state, is associated with nucleotide exchange to ATP remains unclear, due to the lack of electron density in this experiment (Zhang et al., 2015).

Modelling and superposition analysis of the mNAIP2$^{\Delta BIR}$-mNLRC4$^{\Delta CARD}$ interaction interfaces revealed the presence of distinctly charged, oppositely located A (donor) and B (acceptor) surfaces in mNAIP2 and mNLRC4, suggesting directional oligomerization. Two main interfaces exist, which are largely formed by NBD (large patch) and LRR (small patch) residues via hydrophobic, polar and charged interactions (Zhang et al., 2015). Based on the calculated electrostatic surface potential, this model suggests specific binding between the basic mNAIP2-A surface and the acidic mNLRC4-B surface. The mNLRC4-A surface is located on the opposite side and largely basic to mediate B-site binding of the following mNLRC4 molecule (Zhang et al., 2015). Notably, similar mNLRC4 B-site residues provide the acceptor surface for both mNAIP2 and mNLRC4 A-site interactions. Compatibility of mNLRC4-B and -A surfaces represents the pre-requisite for NAIP-independent oligomerization of hyperactive NLRC4 mutants causing AID (Duncan et al., 2018, Tenthorey et al., 2017, Zhang et al., 2015). Interestingly, in this model the mNAIP2-B surface was found to be incompatible with either mNLRC4-A or mNAIP2-A surfaces, which identifies the mNAIP2-A site as unique nucleation surface and explains the presence of a single NAIP molecule per complex and the inability of NAIP to self-assemble inflammasomes (Hu et al., 2015, Tenthorey et al., 2017, Zhang et al., 2015). Importantly, this finding raises questions regarding the NAIP/NLRC4 inflammasome disc closure, and may suggest that the natural conformation of this inflammasome is more likely a helical structure as observed by Diebolder and colleagues (Diebolder et al., 2015). In line with this, cryo-EM studies of the flagellin-mNAIP5-mNLRC4 inflammasome found the majority of discs assembled into open rings (PDB:6B5B, 5.2 Å resolution) (Tenthorey et al., 2017), also described as “split washer-like” structure (Matyszewski et al., 2018).

A common observation in all studies was the heterogeneity of inflammasome complex constitution (10 to 12 protomers) and conformational arrangement (single or double discs, disc or short helices), which hinders the generation of

definite structural information, even with different approaches. High resolution cryo-EM data generation relies on averaging of individual particles, which is limited with increasing sample heterogeneity. X-ray crystallography requires a highly homogenous protein sample to allow protein crystal formation and structure determination. Therefore, no definite conclusion about the molecular structure of the NAIP/NLRC4 inflammasome can yet be drawn. To some extent, the observed heterogeneity may be the result of experimental artefacts, such as use of truncated proteins, expression systems or concentration-dependent aggregation. However, inflammasome complex formation might be a more flexible process than originally anticipated and may vary depending on the inducing ligand or NAIP protein, leaving the possibility that structural variability of NAIP/NLRC4 inflammasomes naturally occurs. The existence of a potential correlation between inflammasome structure and induced downstream effects could be an interesting avenue for future studies.

Interestingly, two recently published cryo-EM data sets of the human NLRC4^{CARD} domain filament showed assembly into a left-handed helix with 3.6 protomer subunits per turn, suggesting that oligomers containing four NLRC4^{CARD} protomers could sufficiently nucleate caspase-1^{CARD} filament formation (Li et al., 2018d, Matyszewski et al., 2018). However, a Monte Carlo simulation demonstrated that 10 or 11 NLRC4 proteins potentiate the likelihood for tetrameric base assembly by NLRC4^{CARD} domains to above 80 %, which is not sufficiently achieved with only four NLRC4 protomers (5%) (Matyszewski et al., 2018). Therefore, these studies further support the flexible nature of inflammasome formation, that may additionally determine signalling strength and efficiency of downstream effector activation.

Overall, the resolution of these protein structures ranges from 3.2 Å to 40 Å. Therefore, high resolution information is still lacking and the partial use of recombinant protein truncations leaves some open questions regarding amino acid side chain interactions and the conformation of the full length protein. Furthermore, all structural studies investigated mNLRC4 and despite high amino acid sequence identity and expected structural resemblance, structural

information of hNLRC4 is desirable to aid understanding of mutation-induced conformational changes and pharmacological inhibitor development.

5.1.5 Structural impact of disease-causing gain of function mutations in NLRC4

Conformational stability of a protein largely relies on the interaction of amino acid side chains, which is mediated through their unique chemical characteristics. Therefore, residue substitution can severely impact protein folding and lead to conformational and functional consequences (Teng et al., 2010).

As mentioned above, the autoinhibited conformation of NLRC4 relies on tight interaction between NBD, HD1 and WHD domains, which is stabilized by ADP binding. Additional extensive binding interfaces between HD2-LRR, NBD-LRR and HD2-NBD further support the inactive state through interaction between previously identified highly conserved amino acid residues (Hu et al., 2013). Therefore, mutations in critical residues can directly destabilize the inactive conformation and result in loss of autoinhibition that drives spontaneous NLRC4 oligomerization, constitutive inflammasome signalling and NLRC4-AID (chapter 4.1.1). Indeed, although the structural consequences of previously described hNLRC4 GoF functions have not yet been experimentally determined, the majority of mutations were predicted to cause conformational changes that disrupt the inactive conformation, based on the analysis of side chain interactions using available structural data of mNLRC4.

Interestingly, disease-associated mutations have not yet been identified within the HD2 or CARD, which indicates limited or lacking contribution of these domains towards NLRC4 autoinhibition. In line with this, the X-ray structure of inactive mNLRC4 was determined using a recombinant CARD-truncated protein ($mNLRC4^{\Delta CARD/\Delta Loop}$) (PDB:4KXF, Hu et al., 2013). In the case of HD2, only single residues may function as negative regulators of NLRC4 oligomerization through steric masking of the α8-helix within the NBD (chapter 5.1.4) (Hu et al., 2013). However, HD2 residues do not directly impact nucleotide binding and hydrolysis and missense mutations in this domain are perhaps associated with a lower

disease-causing potential and have therefore not yet been associated with a diagnosis of NLRC4-AID.

Several missense mutations located within the NBD affect highly conserved residues within or adjacent to the Walker A motif, e.g. S171F, G172S, T177A, R207K) (Goddard 2017, Kawasaki et al., 2017, Liang et al., 2017, Wang et al., 2021a) (**Figure 5.4 A, E**). The WT residue G172 forms a stabilizing hydrogen bond with the bound ADP molecule, which is interrupted by exchange from hydrophobic glycine to hydrophilic serine (G172S) in this position. Steric hindrance likely disturbs the interaction of S172 with HD1 domain residue L339, which consequently destabilizes NBD and WHD interactions (Wang et al., 2021a). Similarly, the S171F mutation maps to a highly conserved residue and likely disturbs the ADP binding interface by replacement of a hydrophilic serine with the significantly larger and hydrophobic amino acid phenylalanine (F) (Liang et al., 2017). Furthermore, this mutation may negatively impact side chain interactions of adjacently located residues (G170 and G172) with HD1 residue T337, which was suggested to destabilize the autoinhibited conformation (Wen et al., 2021). Additionally, based on the *in silico* 3D structural analysis using Prosa2003 modelling, Ionescu et al. proposed that the more favourable conformation adopted by NLRC4 S171F may resemble the active structure (Ionescu et al., 2021). The T177A mutation was suggested to disturb hydrogen bond formation with the ADP molecule (Kawasaki et al., 2017). Interestingly, the R207 residue (S207 in mNLRC4) is less conserved between species and located downstream of the Walker A motif. Due to its more distant localization, structural consequences of the R207K mutation are less predictable, however may result in destabilization of WHD-NBD interactions and therefore promote opening of the NLRC4 inactive conformation (Bardet et al., 2021, Goddard 2017).

Within the HD1, mutations affecting two highly conserved residues T337S/N (Bardet et al., 2021, Bracaglia et al., 2015, Canna et al., 2014) and V341A/L (Barsalou et al., 2018, Canna et al., 2017, Romberg et al., 2014, Siahanidou et al., 2019) were identified in NLRC4-MAS and AIFEC patients (**Figure 5.4 B, E**). Notable is their localization just outside and within the α12-helix, which is positioned in close proximity to the ADP binding site. Therefore, mutation-induced

conformational changes may result in increased helix flexibility and destabilize the NBD interface leading to a more open conformation and ligand-independent NLRC4 activation (Romberg et al., 2014).

Within the WHD, the H443P mutation interrupts the hydrogen bond formation between WH-His residue H443 and the β-phosphate group of ADP (**Figure 4.5 C, E**) (Kitamura et al., 2014). Furthermore, residues T337, S341 and H443 are located within the “hinge region” where WHD-HD2-LRR rotation results in the transition between the inactive and active conformation (Zhang et al., 2015). Mutation of these residues therefore likely alters interactions within the hinge region that may promote unfolding into the active state (Zhang et al., 2015).

The W655C mutation within the LRR was shown to promote NLRC4 oligomerization by creating a LRR-LRR interface, which is not engaged during physiological ligand-mediated NLRC4 WT activation (Moghaddas et al., 2018). The adjacent Q657L mutation was proposed to act via a similar mechanism, although no functional studies or structural modelling was performed (Chear et al., 2020). The reported 93 bp in-frame deletion (G753_L783del) likely results in the loss of regulatory residues and could alter the secondary structure of the remaining LRR, which may impair its autoinhibitory function (**Figure 5.4 D, E**) (Jeskey et al., 2020).

Importantly, whereas the structural changes caused by some mutations result in constitutive NLRC4 signalling and persistent severe disease activity, other patients experience inflammatory flares only following cold exposure or in response to other environmental triggers (**Suppl. Table 2**). The reasons for this phenotypical diversity are not well understood and require further investigation.

However, structural changes induced by individual mutations may differ in the extent of autoactivation and could be associated with distinct molecular consequences, that may determine the clinical manifestation of the disease.

A

```
                                Walker A
H. sapiens        169 GESGKGKSTLLQRIAMLWGSGKCKALTKFKFVFFLRLSRA  208
P. troglodytes    169 GESGKGKSTLLQRIAMLWGSGKCKALTKFKFVFFLRLSRA  208
M. musculus       169 GESGKGKSTLLQRIAMLWASGGCRALKGFRLVFFIHLRSA  208
R. novegicus      169 GESGKGKSTLLQKIAMLWASGMCPALNQFKLVFFIRLSSA  208
B. taurus         169 GESGKGKSTLLQRIAMLWASGECQALTKFKLVFFLRLSRA  208
F. catus          169 GESGKGKSTLLQQIAMLWASGTCGALTKFKLVFFVRLSRA  208
                      ************:*****.** * **. *::***::*  *
```

B

```
                          PhhCW
H. sapiens        334 LMKTPLFVVITCAIQMGESEFHSHTQ  359
P. troglodytes    334 LMKTPLFVVITCAIQMGESEFHSHTQ  359
M. musculus       334 LMKTPLFVVITCAIQMGRQEFQAHTQ  359
R. norvegicus     334 LMRTPLFVVITCAIQMGSEEFQAHTQ  359
B. taurus         334 LMKTPLFVVITCAIQMGKSEFHSHTQ  359
F. catus          334 LMKTPLFVVITCVIQMGESKFHSYTQ  359
                      **:*********.**** .:*:::**
```

C

```
                         WH-His
                            ↓
H. sapiens        438 KYKFFHKSFQEYTAGRRLSSLLTSHE  480
P. troglodytes    438 KYKFFHKSFQEYTAGRRLSSLLTSHE  480
M. musculus       438 TYKFFHKSFQEYTAGRRLSSLLTSKE  480
R. norvegicus     438 TYKFFHKSFQEYTAGRRLSSLLKSRE  480
B. taurus         438 KYKFFHQSFQEYTAGRRLSSLLTSGE  480
F. catus          438 KYKFFHNSFQEYIAGRRLSSLLKSQE  480
                      .*****:***** *********.* *
```

D

```
                              660 751
                               ↓   ↓
H. sapiens        652 FFNWKQEFR…LPGGLTDSLGNLKNLTKLIMDNIKMNEEDAIKLAE  785
P. troglodytes    652 FFNWKQEFR…LPGGLTDSLGNLKNLTKLIMDNIKMNEEDAIKLAE  785
M. musculus       652 FFNWKQEFK…LPGGLIDSLGNLKNLERLILDDIRMNEEDAKNLAE  785
R. norvegicus     651 FFNWMQKFK…LPGGLADSLGNLKNLLKLILDDIRLNEEDAKSLAE  784
B. taurus         645 FFNWKQEFK…LPGGLTDNLGNLKNLMKLILDNIQMNEEDALKLAE  778
F. catus          651 FFNWKQEFK…LPGGLTDSLGNLKNLMKLILYNIKMNEEDAIKLAE  784
                      **** *:*: ***** *.******* :**: :*::***** .***
```

E

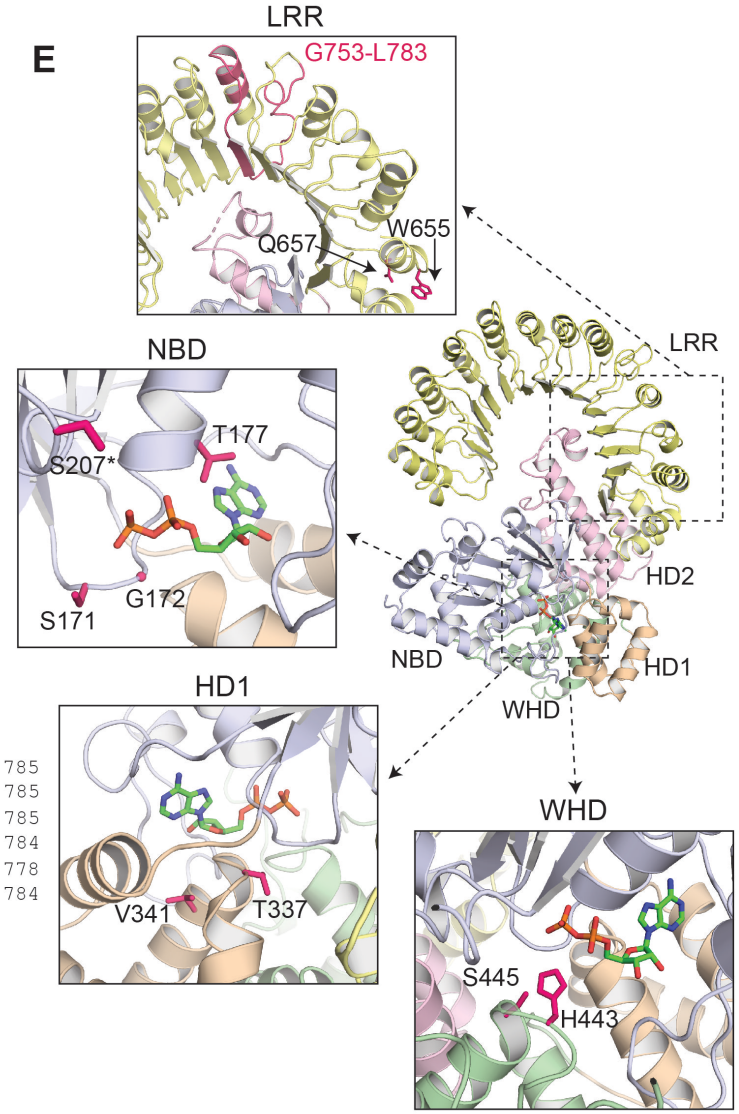

Figure 5.4 | Reported NLRC4-AID associated gain of function mutations affect highly conserved residues proximal to the nucleotide-binding site and within the LRR. A-D) Clustal Omega alignment of NLRC4 amino acid sequences from multiple species indicating conserved motifs (Walker A, PhhCW, WH-His). Previously described residues affected by gain of function mutations associated with NLRC4-AID within the NBD (**A**), HD1 (**B**), WHD (**C**) and LRR (**D**) are shown (red bold). Numbers indicate amino acid residue position. **E)** Cartoon representation showing the localization of in A-D highlighted residues within the inactive ADP-bound structure of mNLRC4$^{\Delta CARD/\Delta Loop}$ (PDB:4KXF). Amino acid side chains (pink) are shown in stick presentation. ADP is coloured in green highlighting different elements: blue: nitrogen, red: oxygen, orange: phosphorus. *indicates murine residue S207 as equivalent to R207 in hNLRC4. Nucleotide-binding domain (NBD): light blue, helical domain 1 (HD1): wheat, winged helix domain (WHD): green, helical domain 2 (HD2): pink, leucine-rich repeat domain (LRR): yellow. Amino acid sequences were retrieved from the Uniprot database: *M. musculus* (mouse: Q3UP24), *H. sapiens* (human: Q9NPP4), *R. norvegicus* (rat: F1M649), *P. troglodytes* (chimpanzee: A0A2J8L1X5), *F. catus* (cat: M3W537), *B. taurus* (cattle: F1MHT9).

In chapter 5 of this thesis, the evolutionary relationships between NLRC4 from different species are described, followed by *in silico* analysis of the potential conformational consequences caused by the NLRC4 A160T mutation based on currently available protein structures of murine NLRC4. Furthermore, since structural information on human NLRC4 is lacking to date, we aimed to generate high purity recombinant hNLRC4 truncations for X-ray crystallography as well as biochemical and biophysical characterization of the conformational impacts associated with the A160T mutation.

The data presented in chapter 5 is unpublished and has not been submitted for publication.

5.2 Results

5.2.1 Evolutionary relationship of NLRC4 proteins from different species

The in **Figure 4.3 C** shown amino acid sequence alignment of NLRC4 from different species revealed conservation of A160 between human, non-human primates (except gorillas (V160)) and rodents (mice, rat), whereas ungulate species and cats encoded T160 in their wildtype sequence. Given that previous cases of NLRC4-AID were caused by mutations in highly conserved residues, this observation was surprising and prompted the analysis of the evolutionary relationship between these species and their inflammasome development.

Innate immunity in general comprises the most conserved immune defence mechanisms, that to some extent occur in all species (Suckale et al., 2005). However, inter-species differences in protein sequences are commonly observed, which may reflect evolutionarily distinct function or regulation. One example represents the highly diverse family of mammalian AIM2-like receptors, which suggests that species-specific environmental challenges associated with habitats or host-pathogen interactions drive evolutionary development and functional divergence of immune pathway proteins, although redundancy also exists (Brunette et al., 2012). We therefore wondered, whether the phylogenetic development of species, confined to those used in the previously shown amino acid sequence alignment (**Figure 4.3 C**), would reflect the evolutionary development of NLRC4 proteins.

Using the NLRC4 amino acid sequence alignment, a phylogenetic tree was constructed using the Maximum Likelihood algorithm and MEGAX software (**Figure 5.5**). Bootstrap analysis of 100 repeats resulted in values between 93 to 100 for most nodes, whereas divergence between NLRC4 of human and gorilla, bats and ungulates as well as horse and cat were less well supported with values of 33, 38 or 45 respectively (**Figure 5.5**). Bootstrapping measures the consistency of the identified phylogenetic groups by multiple rounds of resampling that builds replicate alignments using partial sequences of the same original full length template (Efron 1979, Felsenstein 1985, Russo et al., 2018). Therefore, bootstrap values indicate the number of replicate analyses, which

result in this particular clade and are used as a measure of accuracy for the generated branches. Whereas values of 90 % and above indicate high confidence, lower values (commonly used cut off for moderate support <70 %) suggest that the identification of the depicted sister groups is less robust and should be interpreted with care (Hillis et al., 1993). However, for our analysis the overall evolutionary relationship between different phylogenetic orders was most relevant, which retrieved high bootstrap analysis values.

Interestingly, phylogenetic clustering of species encoding NLRC4 T160 (ungulates, bats, carnivores) was observed, whereas primates and rodents encoding NLRC4 A160 formed a separate clade (**Figure 5.5**).

Within the order of primates, gorilla NLRC4 is the most closely related to human NLRC4 despite the presence of valine (V) in position 160. Western clawed frog (*X. tropicalis*) NLRC4 encoding for Q160 formed the outgroup, with the highest divergence from NLRC4 of other species (**Figure 5.5**).

Importantly, the evolutionary relationship of NLRC4 proteins elucidated here is recapitulated in the species phylogeny, with primates and rodents grouped together in one clade, whereas bats, carnivores and ungulates formed a different cluster, as analysed by Tsagkogeorga et al. using data sets of both the coding sequence nucleotides and amino acids via Randomized Axelerated Maximum Likelihood (RAxML) analysis (see Figure 1 of (Tsagkogeorga et al., 2013)). This suggests that the NLRC4 protein evolution was not influenced by a distinct evolutionary event in one particular species and traces back to a common ancestral protein, although this assumption would need to be confirmed by determination of the phylogenetic relationship at the nucleotide level (Russo et al., 2018).

Although evolutionarily closely related, carnivores, ungulates (including the beluga whale) and bats distinctly differ regarding their predominant habitats (water, land, air), form of movement (swim, walk, fly) and nutritional requirements (carnivore, herbivore). Given that NLRC4 plays an important role in gastrointestinal immune defence, which is shaped by the host-microbiome interactions and perhaps diet-associated pathogen exposure (Wu et al., 2012, Zheng et al., 2020a), one could speculate that T160 may represent the primordial

sequence, whereas substitution to alanine could be a modification tailored to distinct functional requirements of primate and rodent NLRC4.

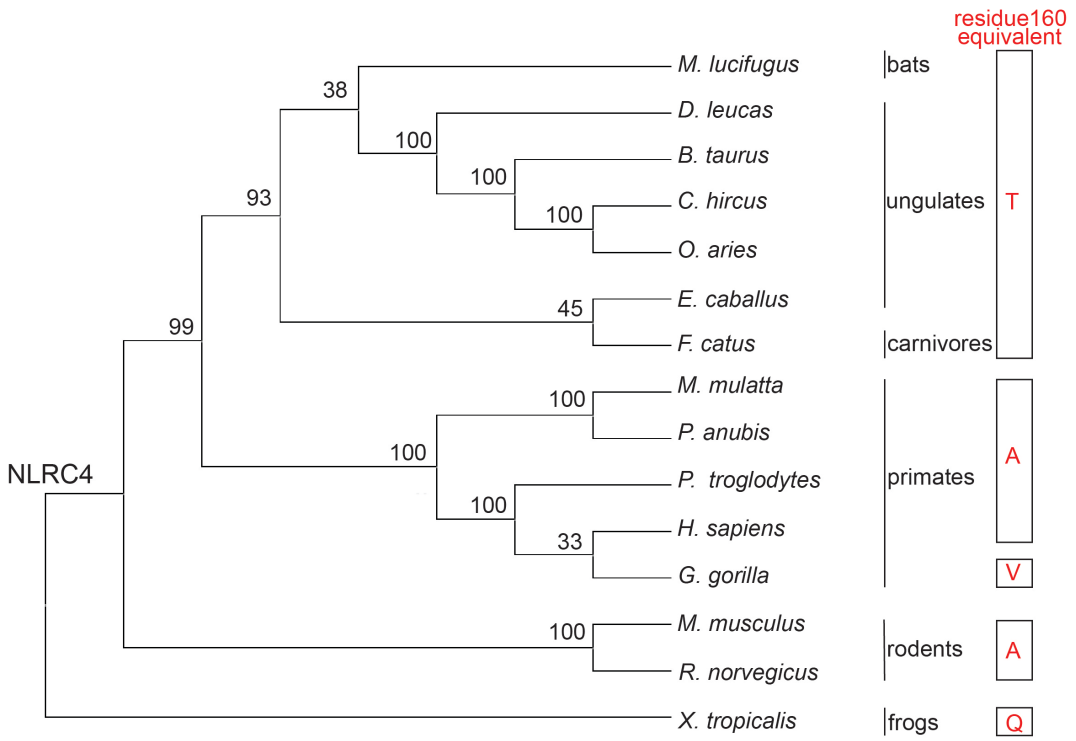

Figure 5.5 | Evolutionary relationship of NLRC4 proteins from different species. Cladogram showing the phylogenetic relationship of NLRC4 proteins from selected species. Affiliation to the phylogenetic order and amino acid residue located at the position equivalent to residue 160 in hNLRC4 is indicated (red) as per alignment shown in **Figure 4.3 C**. Full length NLRC4 amino acid sequences were obtained from UniProt (*M. musculus* (mouse: Q3UP24), *H. sapiens* (human: Q9NPP4), *R. norvegicus* (rat: F1M649), *B. taurus* (cattle: F1MHT9), *X. tropicalis* (western clawed frog: F6R2G2), *P. troglodytes* (chimpanzee: A0A2J8L1X5), *F. catus* (cat: M3W537), *O. aries* (sheep: W5PLT9), *M. mulatta* (rhesus macaque: F7DWV6), *G. gorilla* (gorilla: G3QJV1), *P. anubis* (olive baboon: A0A096NWZ9), *M. lucifugus* (little brown bat: G1PV27), *E. caballus* (horse: F7CBZ7), *C. hircus* (goat: A0A452EBW5), *D. leucas* (beluga whale: A0A2Y9N554)) and aligned using the Clustal W algorithm in MEGAX software. The cladogram was constructed using the Maximum Likelihood method and the JTT matrix-based model (Jones et al., 1992). Values of bootstrap analysis (100 repeats) indicate the percentage of trees in which the associated taxa clustered together. A total of 1058 amino acid residues were included in the final dataset used for phylogenetic tree construction in MEGAX software (version 10.2.6) (Kumar et al., 2018, Stecher et al., 2020).

5.2.2 Residue A160 is surface exposed and localizes proximal to the nucleotide-binding site

Alanine is a small amino acid with a single methyl group side chain, which mediates its non-polar and hydrophobic characteristics. Although only slightly larger with one additional methyl group, the threonine side chain contains a hydroxyl group which determines its hydrophilic and polar character. Therefore, whereas alanine is rather unreactive, threonine residues are often involved in hydrogen bond formation, which may have structural consequences under some circumstances. Furthermore, besides serine and tyrosine, threonine residues are commonly phosphorylated and can be modified by O-linked glycosylation, which renders the mutant residue T160 susceptible to PTMs, that may alter protein function (Walsh et al., 2005).

To investigate potential consequences of the A160T substitution on the structural level, we sought to analyse the localization of this residue in the 3D protein structure of NLRC4. However, experimentally determined structural information of hNLRC4 is not available to date. As previously described, A160 is a conserved residue between human and mouse and proteins from both species share 75 % identity on amino acid sequence level (Clustal Omega alignment tool (Madeira et al., 2019)). Therefore, we used the crystal structure of inactive ADP-bound mNLRC4$^{\Delta CARD/\Delta Loop}$ (PDB:4KXF, Hu et al., 2013), where residue A160 is accessible on the surface and localizes proximal to the β1-strand just upstream the Walker A motif (P-loop) (**Figure 5.6 A**). However, no direct interaction with ADP or residues of the nucleotide-binding pocket could be observed, which is in contrast to the previously described GoF mutations, where affected residues were mostly buried in the protein core with direct links to the nucleotide-binding site (**Figure 5.4 E**).

In general, side chain interactions with adjacently located residues depend on the fulfilment of spatial requirements and the presence of complementary charges, hydrophobic patches or hydrogen bond donor/acceptors to form ionic bonds, hydrophobic interactions (distance 3.3-4 Å) or hydrogen bonds (distance 2.7-3.3 Å), respectively (McRee 1999). In the case of A160, distance measurements

using the PyMOL software did not reveal obvious inter-residue interactions (data not shown). However, although perhaps less relevant for a surface-exposed residue, the 3.2 Å resolution of the available crystal structure only allows for limited conclusion about side chain interactions. Instead, a higher resolution would be preferable to fully resolve the orientation of smaller size side chains, which is essentially required to understand the full network of the surrounding residues and the resulting consequences of an amino acid exchange (Cohen et al., 2009).

We further confirmed these observations using the computational 3D structure prediction of full length hNLRC4 WT and A160T, generated using the AlphaFold 2 protein structure database (Jumper et al., 2021, Tunyasuvunakool et al., 2021). AlphaFold 2 is a recently published artificial intelligence system, which has been shown to predict both backbone and side chain orientation of structurally unknown proteins based on the primary amino acid sequence with near-experimental accuracy. In this approach, generation of a 3D structure model relies on multiple rounds of sequence alignments, model refinements as well as evolutionary similarities and homology to previously solved structures (Jumper et al., 2021, Tunyasuvunakool et al., 2021). Both in AlphaFold 2 generated models of WT and A160T NLRC4 appear as closed conformation (**Figure 5.6 B**), which resemble the experimentally determined crystal structure of inactive mNLRC4 (PDB:4KXF). The overlay of both models suggests overall structural conformity with slightly variable orientation of the N-terminal CARD domain and an LRR-resident loop (aa 629-642, absent in 4KXF mNLRC4$^{\Delta CARD/\Delta Loop}$). These differences are likely the result of the computational prediction due to the natural flexibility of the linker connecting the CARD and NBD and the disordered character of the LRR-resident loop. Consistent with the localization in the murine structure, residues A160 and T160 are solvent exposed and conformational changes of the nucleotide-binding pocket were not predicted, since all conserved motifs including the P-loop aligned in both models (**Figure 5.6 B**).

However, given that AlphaFold 2 was trained based on experimentally determined structures deposited into the PDB (Jumper et al., 2021), which includes the previously mentioned structural information on mNLRC4$^{\Delta CARD/\Delta Loop}$

(PDB:4KXF, Hu et al., 2013) (chapter 5.1.4), the resemblance of the predicted human model to the previously experimentally determined structure of inactive mNLRC4 is not surprising and restricts unbiased conclusions regarding the localization and interaction of residue A160 in hNLRC4. Furthermore, since AlphaFold 2 has not yet been validated to predict the effect of mutations, especially those with potential impact on protein folding and conformational stability (preprint (Pak et al., 2021)), interpretations about the potential effect of the A160T mutation are not conclusive.

However, since the *in vitro* validation of this mutation showed a robust functional phenotype only after ligand-dependent activation (chapter 4), structural changes may not impact the inactive conformation. Therefore, using the cryo-EM structure of flagellin-mNAIP5 assembled with two mNLRC4 molecules (Tenthorey et al., 2017), we investigated whether A160 contributes to interface formation between mNAIP5-mNLRC4 heterodimers or mNLRC4 homodimers in context of the previously identified A and B binding surfaces of mNLRC4 ((**Figure 5.6 C**), see chapter 5.1.4). However, we found that residue A160 does not contribute to the mNLRC4 A or B surface and is localized in spatial distance to the adjacent second mNLRC4 protomer, which does not suggest direct interaction. Furthermore, the mNAIP5-mNLRC4 interaction occurs on the site opposite to A160 localization, which indicates that a direct impact on this interface is unlikely (**Figure 5.6 C**).

Therefore, although a direct structural impact of the threonine substitution on nucleotide binding or NLRC4 conformation in the inactive or active state is not immediately obvious in the available structures, the localization proximal to the conserved Walker A motif is a meaningful observation and suggests that perhaps modified interactions with adjacent residues could result in indirect conformational changes. Therefore, experimental determination of high-resolution structural information for mutant hNLRC4 T160 would be useful to resolve detailed side chain interactions and investigate the conformational impact of this mutation.

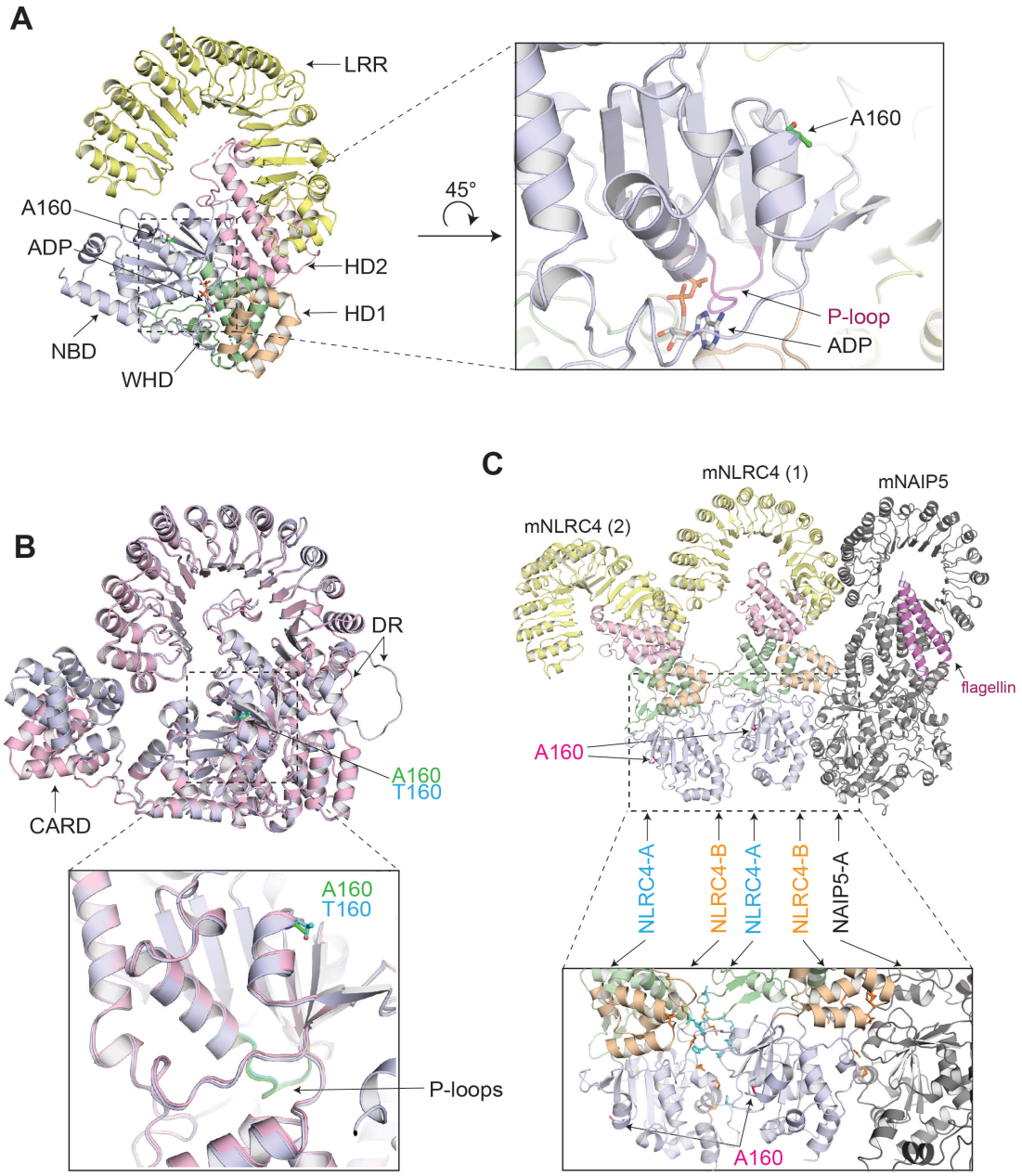

Figure 5.6 | Computational analysis of structural consequences of A160T. A) Ribbon representation of the crystal structure of inactive mNLRC4$^{\Delta CARD/\Delta Loop}$ (PDB:4KXF, resolution 3.2 Å) showing the localization of residue A160 (green) in stick presentation proximal to the highly conserved P-loop (magenta) and the bound ADP. Protein domains are colour-coded: nucleotide-binding domain (NBD): light blue; helical domain 1 (HD1): wheat; winged helix domain (WHD): green; helical domain 2 (HD2): pink; leucine-rich repeat domain (LRR): yellow. Amino acid side chains and ADP are coloured by element: blue: nitrogen, red: oxygen, orange: phosphorus. **B)** Overlay of the AlphaFold 2 predicted 3D structures of full length WT (light blue) and mutant (light pink) hNLRC4. Individual models were generated with AlphaFold 2 and overlayed using PyMOL software. P-loops and residue 160 in WT and mutant hNLRC4 A160T are highlighted in green or cyan, respectively. Side chains coloured by element as described in A).

C) Localization of A160 within the assembled flagellin-mNAIP5-mNLRC4$^{\Delta CARD}$ cryo-EM structure (PDB:6B5B, resolution 5.2 Å). Domains of two assembled activated mNLRC4$^{\Delta CARD}$ protomers (1 and 2) are coloured as described in A). mNAIP5 and flagellin are shown in grey and magenta, respectively. Previously described and opposingly charged basic A (cyan) and acidic B (orange) surfaces in mNLRC4 are indicated. Stick presentation highlights the localization of residue A160 (pink) and interface forming residues of mNLRC4-A (in cyan: H144, R145, H269, R285, H286, R288, H289, Q433, R434) and mNLRC4-B (in orange: P112, N116, E122, D123, D125, I127, L220, L313, M349, D368) as previously described (Zhang et al., 2015).

Solvent exposure of the mutant residue suggests a mechanism of action distinct from previously identified NLRC4-AID mutations and could reflect its milder phenotype and the necessity to have two alleles causing a Mendelian disease. Furthermore, the surface exposed localization raises the possibility that this residue may provide a target site for PTMs (see chapter 5.2.6).

5.2.3 Purification of recombinant mNLRC4$^{\Delta CARD}$ truncations

Since the crystal structure of mNLRC4$^{\Delta CARD/\Delta Loop}$ has been determined by Hu and colleagues (Hu et al., 2013) and human and mouse NLRC4 share high amino acid sequence identity with A160 being a conserved residue, we first sought to follow the established protocol to generate recombinant mNLRC4 to compare biochemical and biophysical characteristics and investigate the structural impact of the A160T mutation.

Expression construct design and purification conditions were therefore largely based on the previously published study, in which mNLRC4 truncations deleted of the N-terminal CARD domain (mNLRC4$^{\Delta CARD}$; Δ1-89 aa) were generated to prevent self-assembly and aggregation (Hu et al., 2013), which is a commonly observed issue during full length NLR protein purification (Danot et al., 2009, Ye et al., 2008). In these initial experiments we did not delete the LRR-resident loop (aa 622-644) to avoid structural or functional impairment.

mNLRC4$^{\Delta CARD}$ (aa 90-1024) was cloned into the pACEBac1 backbone and expressed as N-terminal 6xHis-SUMO-TEV-fusion protein in *Sf*9 cells (**Figure**

5.7 A). After Ni-NTA affinity purification and TEV cleavage to remove the 6xHis-SUMO tag, mNLRC4$^{\Delta CARD}$ was further purified by anion exchange chromatography (AIEX, data not shown) and size exclusion chromatography (SEC) (**Figure 5.7 B**). WT and mutant protein eluted as a single peak with retention volumes between 13.5-15.9 ml and 13.1-15.3 ml, respectively, which largely overlapped when purified on different days using the same equipment (**Figure 5.7 B**). The determined retention volumes corresponded to an apparent molecular weight (MW) range of 75 kDa to 158 kDa (based on the manufacturer's function test), and therefore suggest the presence of monomeric mNLRC4$^{\Delta CARD}$, which has a MW of 105 kDa when calculated based on the amino acid sequence. The SDS-PAGE analysis of representative elution fractions (**Figure 5.7 B**) and the final protein (**Figure 5.7 C**) confirmed the generation of highly pure protein. For the recombinant WT protein, **Figure 5.7 B** (left panel) shows one elution fraction representative of the central peak and several samples taken from the side fractions of the main peak, containing lower-concentrated protein. For mNLRC4$^{\Delta CARD}$ A160T, samples of elution fractions covering the entire peak were analysed (**Figure 5.7 B**, right panel). Overall, WT and mutant protein behaved similarly during the purification procedure, which yielded 585 µg and 865 µg recombinant protein from 500 ml *Sf*9 cell expression volume, respectively, in the here shown experiment. The slightly higher yield obtained for mNLRC4$^{\Delta CARD}$ A160T is most likely attributable to inter-experimental variability, since WT and mutant proteins were expressed and purified on different days using identical equipment and experimental procedures.

Structural analysis by Hu and colleagues identified mNLRC4$^{\Delta CARD/\Delta Loop}$ in an ADP-bound state, although ADP was not added during protein purification (Hu et al., 2013). We therefore wondered if ADP supplementation during the purification process would stabilize the recombinant protein and increase the final yield. However, addition of 1 mM ADP and 10 mM $MgCl_2$ to all purification buffers (except during AIEX) resulted in similar yield and suggested that ADP binding is saturated during protein translation and folding in *Sf*9 cells, which stably maintains the inactive conformation (data not shown).

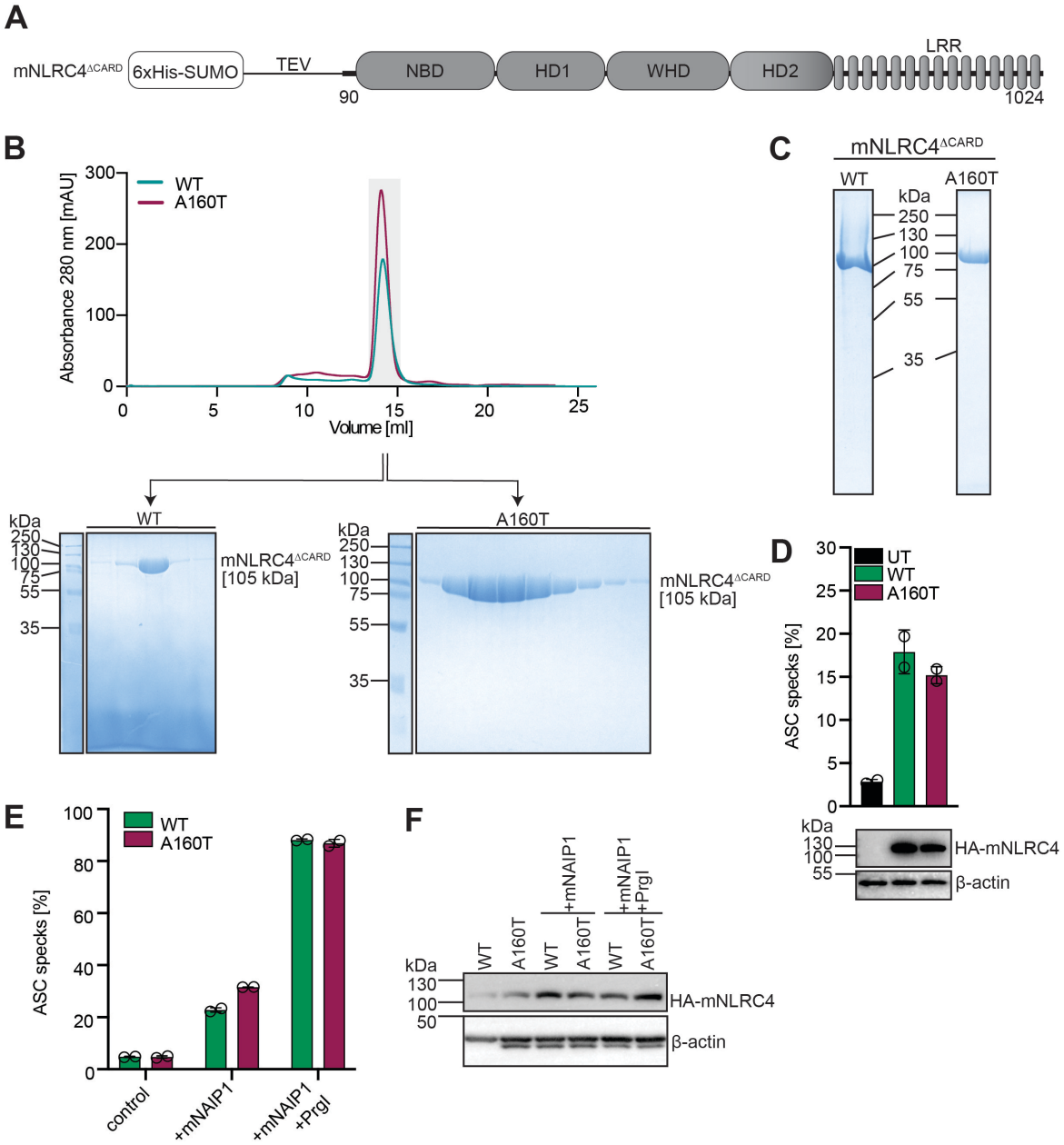

Figure 5.7 | Purification of recombinant mNLRC4$^{\Delta CARD}$ and functional analysis of A160T in mNLRC4. A) Schematic illustration of the *Sf*9 cell expression construct used to generate recombinant WT and A160T mNLRC4$^{\Delta CARD}$ (Δ1-89) protein. Construct design and domain boundaries are based on work from Hu and colleagues (Hu et al., 2013). The N-terminal 6xHis-SUMO-TEV-tag allowed for Ni-NTA affinity chromatography and was subsequently cleaved by TEV digest. Tobacco Etch Virus cleavage site, TEV. **B)** Overlay of preparative SEC elution profiles under standard purification conditions (20 mM HEPES, 100 mM NaCl, 0.5 mM TCEP, pH 8.0). mNLRC4$^{\Delta CARD}$ WT and mutant eluted in one dominant peak with retention volumes between 13.5-15.9 ml and 13.1-15.3 ml, respectively, characteristic for proteins with a MW ranging from 75 kDa to 158 kDa. Purifications were performed on different days using the same Superdex 200 (10/300 Increase) column at a flow rate of 0.75 ml/min.

Representative elution fractions were analysed via Coomassie-stained SDS-PAGE using 15 % or 12 % SDS-PAGE gels for WT or mutant, respectively. For the WT protein, one elution fraction from the peak centre and several fractions from the sides of the peak were analysed, whereas samples from elution fractions spanning the entire peak are shown for mNLRC4$^{\Delta CARD}$ A160T. **C)** Coomassie-stained SDS-PAGE gel of final concentrated purified protein after SEC in B). 4 µg protein per lane were loaded on 12 % (WT) or 15% (A160T) SDS-PAGE gels. **D)** Flow cytometry analysis of ASC speck formation following transient transfection of full length HA-mNLRC4 WT or A160T (250 ng DNA, 16 hrs) in HEK293T ASC-BFP cells. Expression levels were analysed by HA-tag-specific western blotting. Technical duplicates of one experiment are shown, error bars represent SD, n=1. Untreated empty-vector transfected control, UT. **E)** ASC speck formation of HA-mNLRC4 WT or A160T was analysed after co-transfection with empty vector (control), mNAIP1-mCherry and myc-PrgI (100 ng DNA per construct), quantified by flow cytometry after 16 hrs incubation. Technical duplicates of one experiment are shown, error bars represent SD, n=1. In all samples except empty vector-transfected controls, the applied gating strategy excluded mCherry-negative cells to only analyse speck formation in successfully transfected HEK293T ASC-BFP cells. **F)** Western blot analysis of mNLRC4 expression levels of cells used in E), assessed using a HA-tag specific antibody, n=1.

Before using the recombinant protein for crystallization experiments, we sought to determine whether the functional phenotype of the A160T mutation is reproducible in the murine system. The rationale therefore was that despite the high amino acid similarity between mouse and human NLRC4, inflammasome activation pathways in both species are fundamentally distinct. Whereas in mice, different mNAIP paralogs specifically recognize distinct stimuli, in human cells one hNAIP protein is activated by multiple ligands (see chapter 1.3.3.4.2). Given that *in vitro* validation of hNLRC4 A160T (chapter 4) revealed that the pathogenicity of this mutation is dependent on ligand-binding and therefore NAIP interaction, we wanted to confirm the functional phenotype in mNLRC4.

ASC speck assays were performed using HEK293T cells stably expressing blue fluorescent protein-tagged ASC (ASC-BFP). Transient transfection with full length mNLRC4 WT or A160T induced spontaneous ASC specking, which was slightly lower for A160T compared to WT levels, most likely due to reduced protein expression as analysed by western blot in this experiment (**Figure 5.7 D**, preliminary data). To mimic an activation stimulus, mNLRC4 was expressed at lower levels to reduce baseline activation and co-transfected with mNAIP1 or

mNAIP1+ PrgI. After activation, ASC speck formation induced by WT and mutant NLRC4 was comparable in this experiment and proteins were expressed at similar levels in stimulated conditions (**Figure 5.7 E, F**; preliminary data). However, mNLRC4 A160T co-expression with mNAIP1 alone resulted in slightly increased ASC speck formation over WT control cells, which could be of interest if consistently observed in future experimental repeats. Of note, this data is preliminary and lacks the investigation of a possible effect of mNLRC4 A160T in combination with ligand-bound mNAIP2 or mNAIP5/6. However, due to time limitations we focused on mNLRC4 A160T pathogenicity in context of PrgI-activated mNAIP1 to maintain consistency and comparability to human *in vitro* experiments (chapter 4).

According to this preliminary data, the phenotype of the A160T mutation may not be recapitulated in mNLRC4, which could suggest species-specific differences associated with the mode of ligand/NAIP binding that may taper or abolish the effect of the A160T mutation in mice.

Therefore, subsequent experiments focused on the purification of recombinant hNLRC4 for use in downstream applications.

5.2.4 Purification of recombinant hNLRC4$^{\Delta CARD}$ and hNLRC4$^{\Delta CARD/\Delta Loop}$

As a starting point to produce monomeric recombinant hNLRC4, we adapted the construct design from Hu and colleagues (Hu et al., 2013) with slightly adjusted domain borders to generate hNLRC4$^{\Delta CARD}$ (Δ1-91 aa) and hNLRC4$^{\Delta CARD/\Delta Loop}$ (Δ1-91 aa and Δ622-644 aa) truncations, since deleting the flexible loop between LRR-residues 622-644 proved to be the crucial step to generate high-diffracting protein crystals for structural determination in the previous study (Hu et al., 2013). Here, WT and A160T hNLRC4$^{\Delta CARD}$ and hNLRC4$^{\Delta CARD/\Delta Loop}$ were expressed as N-terminal 6xHis-SUMO-TEV-tagged fusion proteins using *Sf*9 cells (**Figure 5.8 A**). Initial experiments showed that addition of ADP (1 mM) and $MgCl_2$ (10 mM) during the purification procedure largely increased the final yield (data not shown), which was overall lower compared to previous purification of mNLRC4$^{\Delta CARD}$ (chapter 5.2.3). Following Ni-NTA affinity chromatography and TEV digest, WT and A160T hNLRC4$^{\Delta CARD}$ and hNLRC4$^{\Delta CARD/\Delta Loop}$ eluted as two peaks in preparative SEC experiments from the Superdex 200 (HiLoad SD200 16/600 pg) column (**Figure 5.8 B, C**). Based on the retention volume of 42.7-57.7 ml and 42.1-65.1 ml for hNLRC4$^{\Delta CARD}$ and hNLRC4$^{\Delta CARD/\Delta Loop}$, respectively, peak 1 eluted as void volume, which contains large protein aggregates that cannot be further size-separated by the resin. Coomassie-stained SDS-PAGE analysis of representative elution fractions confirmed the presence of hNLRC4 truncations and showed a variety of other different-sized proteins in peak 1, which is often observed after His-tag affinity chromatography (**Figure 5.8 B, C**). Peak 2 protein eluted between 68.7-76.7 ml and 70.1-79.1 ml for hNLRC4$^{\Delta CARD}$ and hNLRC4$^{\Delta CARD/\Delta Loop}$, respectively, which corresponds to an apparent MW between 60-160 kDa (based on manufacturer's function test). The peak 2 elution fractions contained highly purified protein, which likely represents monomeric hNLRC4$^{\Delta CARD}$ and hNLRC4$^{\Delta CARD/\Delta Loop}$ with calculated MWs of 105 kDa and 102 kDa, respectively (**Figure 5.8 B, C**). Preparative SEC elution profiles of all proteins were comparable, although peak 2 was slightly shifted towards a higher retention volume for both WT and A160T hNLRC4$^{\Delta CARD/\Delta Loop}$, which is reflective of their smaller MW (**Figure 5.8 B, C**).

A sequential workflow of Ni-NTA affinity purification, TEV-mediated affinity tag cleavage and SEC yielded protein with >90 % estimated purity (**Figure 5.8 D**), which was subsequently used for extensive crystallization screens, however without success. Since protein crystallization relies heavily on the homogeneity of the protein molecules within the used sample (Edavettal et al., 2012), in following purifications AIEX chromatography was performed as additional purification step prior to SEC. As a result, the protein purity was improved, reflected by disappearance of peak 1 from the SEC elution chromatogram (data not shown) and reduction of residual protein contaminants in the final SDS-PAGE analysis (**Figure 5.8 E**). Using this protocol, purification of 2 liters *Sf*9 cell expression volume yielded 440 µg WT hNLRC4$^{\Delta CARD}$, 310 µg mutant hNLRC4$^{\Delta CARD}$, 120 µg WT hNLRC4$^{\Delta CARD/\Delta Loop}$ and 360 µg mutant hNLRC4$^{\Delta CARD/\Delta Loop}$ for the representative experiment shown in **Figure 5.8 E**. This yield was markedly lower than yields obtained when mNLRC4$^{\Delta CARD}$ was purified (chapter 5.2.3) and limited the feasibility of biochemical assays for protein characterization.

Several approaches to improve the purification protocol towards higher yields, e.g. substitution of the N-terminal tag to His-GFP-TEV, were not successful (data not shown). Furthermore, since multiple factors influence stability of recombinant proteins, a nano differential scanning fluorimetry (nanoDSF) screen was performed to identify optimal purification buffer conditions. The tested parameters included salt concentration, buffer substance, different pH or supplements (listed in method section 2.16.15.2), however none of the tested combinations resulted in largely improved thermal stability (data not shown).

Therefore, given the low yields from recombinant hNLRC4 purifications, further crystallization trials were not feasible as they require high amounts of concentrated pure protein to optimize numerous crystallization conditions. Instead, we performed thermal stability assays to determine the impact of the A160T mutation on conformational stability of the here purified hNLRC4 truncations (chapter 5.2.5).

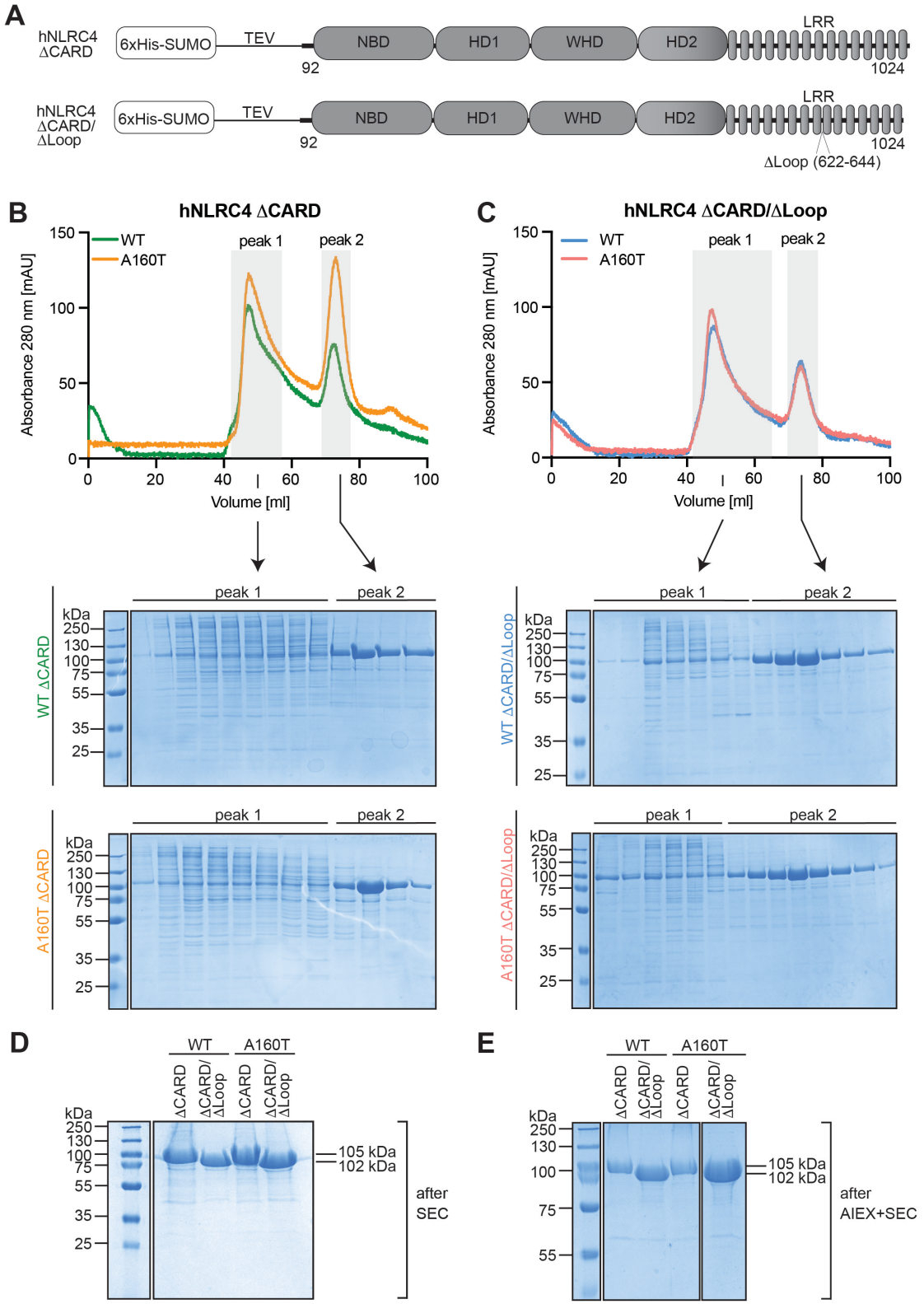

Figure 5.8 | Purification of WT and A160T hNLRC4$^{\Delta CARD}$ and hNLRC4$^{\Delta CARD/\Delta Loop}$. A) Outline of *Sf*9 cell expression constructs used for the production of recombinant hNLRC4$^{\Delta CARD}$ (Δ1-91 aa) and hNLRC4$^{\Delta CARD/\Delta Loop}$ (Δ1-91 and Δ622-644 aa) truncations. Protein truncations were fused to a N-terminal 6xHis-SUMO-

tag containing a subsequent TEV protease cleavage site. **B)** Overlay of preparative SEC chromatograms of WT and mutant (A160T) NLRC4$^{\Delta CARD}$ after Ni-NTA affinity chromatography and TEV cleavage. SEC was performed using the Superdex 200 (HiLoad SD200 16/600 pg) column at a flow rate of 0.8 ml/min using SEC buffer supplemented with ADP (20 mM HEPES, 100 mM NaCl, 0.5 mM TCEP, 1 mM ADP, 10 mM $MgCl_2$, pH 8.0). Proteins shown in the elution profile overlay were purified on the same day using the identical column and procedures. WT and mutant proteins eluted as peak 1 and 2, with retention volumes between 42.7-57.7 ml and 68.7-76.7 ml, respectively. Whereas peak 1 eluted close to the void volume, peak 2 corresponded to an apparent MW of 60-160 kDa. Coomassie-stained SDS-PAGE covers the range of both peaks as indicated. **C)** Purification and analysis of WT and mutant NLRC4$^{\Delta CARD/\Delta Loop}$ as described in B). Peak 1 protein eluted between 42.1-65.1 ml (void) and peak 2 protein between 70.1-79.1 ml, corresponding to an apparent MW of 60-160 kDa. **D)** Coomassie-stained SDS-PAGE analysis of final peak 2 protein (after SEC, elution fraction pooling and concentration) of NLRC4$^{\Delta CARD}$ (105 kDa) and NLRC4$^{\Delta CARD/\ \Delta Loop}$ (102 kDa) purified in B) and C), respectively. Per lane, 8 µg protein were loaded. **E)** Coomassie-stained SDS-PAGE analysis of final protein after SEC using the in B) described protocol. Purity of recombinant protein was increased through preceding anion exchange (AIEX) chromatography. Each lane contained a calculated volume equal to 4 µg of protein. Samples were run on the same 12 % SDS-PAGE gel and not relevant lanes were cropped out.

5.2.5 Thermal stability is not altered by the NLRC4 A160T mutation

NanoDSF is an analytical method used to determine the conformational stability of proteins based on the intrinsic fluorescence of tryptophan residues (**Figure 5.9 A**) (Alexander et al., 2014). In the native state, hydrophobic amino acids (including tryptophan) are buried in the protein core. Exposure to an increasing linear temperature gradient causes gradual protein unfolding and solvent exposure of core residues, leading to a red shift in the detected intrinsic fluorescence spectrum, presented as ratio of emitted light (Em) at wavelengths 350 nm and 330 nm. Mathematical conversion of the fluorescence ratio curve into the first derivate determines the inflection point of the ratio curve as melting temperature (Tm), which corresponds to the temperature at which 50% of proteins are unfolded. Thus, the Tm reflects the conformational stability of a protein, which can be influenced by the surrounding chemicals or ligand binding. Furthermore, in some cases amino acid substitutions have the potential to impact

protein folding and the 3D protein structure, resulting in a conformational stability distinct from the WT protein, which is reflected in a Tm shift (**Figure 5.9 A**).

To interrogate this question in the case of the A160T mutation, thermal unfolding of recombinant WT and mutant hNLRC4$^{\Delta CARD}$ and hNLRC4$^{\Delta CARD/\Delta Loop}$ was measured in presence of a temperature gradient ranging from 25-95 °C (results shown between 25-70 °C). Unfolding characteristics did not differ between WT and A160T hNLRC4 as shown in the representative fluorescence intensity ratio curve and its first derivative, which determined very similar Tm values of ~48 °C or ~47.3 °C for WT and mutant hNLRC4$^{\Delta CARD}$ and hNLRC4$^{\Delta CARD/\Delta Loop}$ truncations, respectively (**Figure 5.9 B, C**).

Since ADP was shown to stabilizes the inactive conformation of mNLRC4 (Hu et al., 2013) and nucleotide exchange to ATP promotes self-assembly of STAND ATPases, which NLRs are classified as (chapter 5.1.1) (Leipe et al., 2004), we sought to investigate the thermal stability of WT and mutant NLRC4 in presence of both nucleotides (**Figure 5.9 D**). Interestingly, neither incubation with 50x molar excess ADP nor ATP significantly altered the thermal stability of WT or mutant hNLRC4, indicating that under the here used experimental conditions, the inactive conformation of hNLRC4 $^{\Delta CARD}$ and hNLRC4 $^{\Delta CARD/\Delta Loop}$ is highly stable and not affected by the A160T mutation.

Interestingly, the Tm of the ΔCARD/ΔLoop truncated proteins was consistently lower compared to the ΔCARD truncations across all tested conditions, indicating that deletion of the Loop slightly reduces conformational stability.

Overall, these experiments showed that under the tested conditions and in an autoinhibited conformation, the A160T mutation does not impact the thermal stability of the analysed hNLRC4 truncations. In this experiment, addition of excess ATP did not induce a detectable conformational change in WT or mutant NLRC4, however it remains unclear whether ATP was unable to bind the nucleotide-binding site or whether successful ATP binding had no effect. Based on these results and results from our previously described *in vitro* assays (chapter 4) further studies with a focus on NLRC4 A160T in the context of activation will be required to understand the molecular consequences of this mutation.

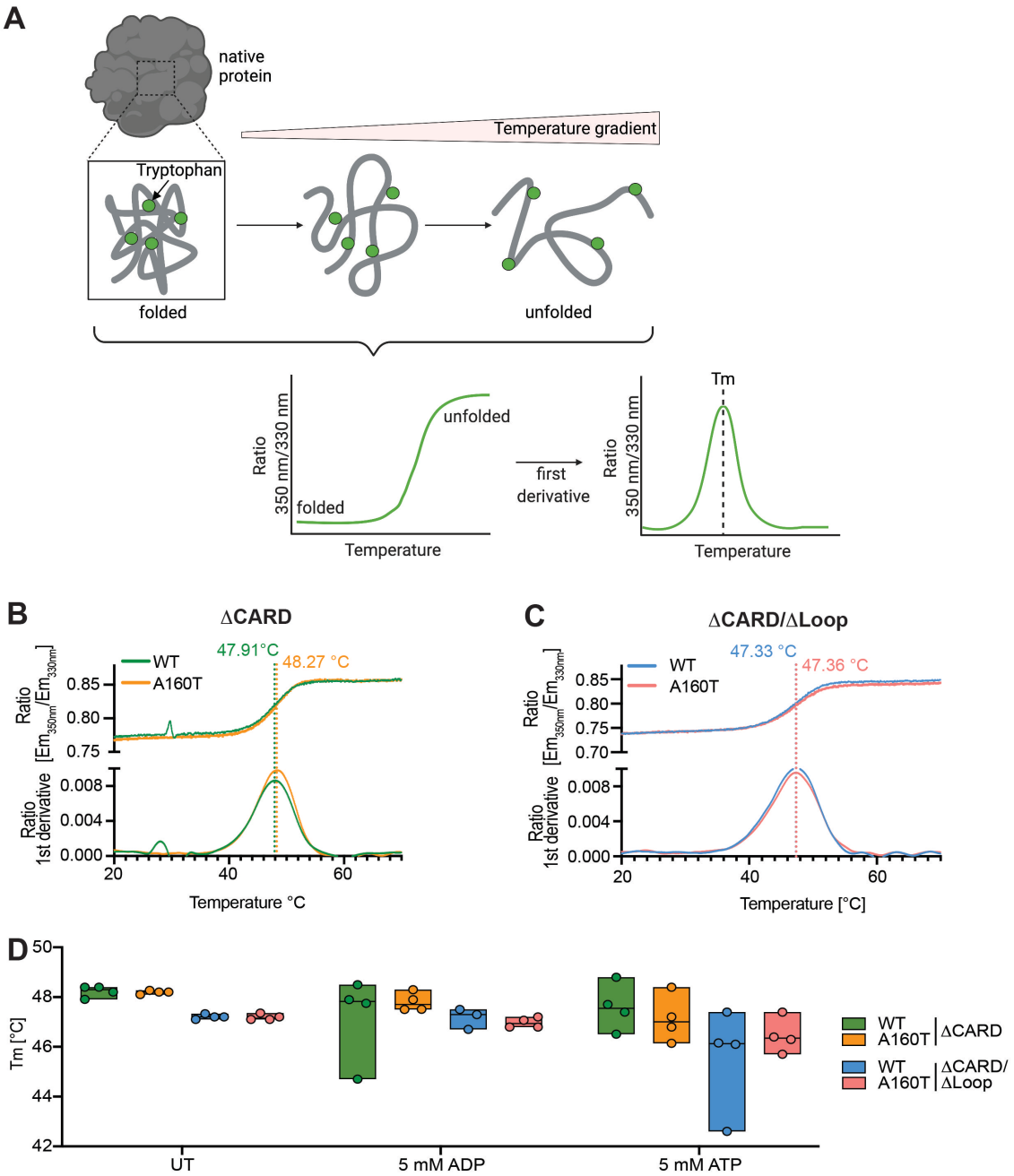

Figure 5.9 | Thermal stability of hNLRC4. A) Simplified principle of nano differential scanning fluorimetry (nanoDSF), which monitors the intrinsic protein fluorescence based on tryptophan residues at 350 nm and 330 nm wavelengths. In the native protein state, hydrophobic amino acids are buried within the core of the protein structure. Increasing temperatures induce gradual protein unfolding which results in solvent exposure of tryptophan residues, that is detected as a shift in the fluorescence ratio. Transforming the ratio curve into the first derivation results in a peak-shaped curve, where the maximum value corresponds to the melting temperature (Tm), which describes the temperature when 50 % of the protein is unfolded and can therefore be used as an indicator of conformational stability. **B)** Representative melting curves and corresponding first derivate

shown as overlay for WT (green) and mutant (A160T, orange) hNLRC4$^{\Delta CARD}$ (10 µM). The dotted lines and numbers specify the calculated Tm after exposure to a temperature gradient ranging from 25 to 95 °C (results for 25-70 °C are shown) using a ramp of 1.5 °C/min. This assay was performed under standard reaction conditions (20 mM HEPES, 100 mM NaCl, 0.5 mM TCEP, pH 8.0). **C)** Representative experiment to compare Tm of WT (blue) and A160T (red) hNLRC4$^{\Delta CARD/\Delta Loop}$ under conditions described in B). **D)** Thermal stability of recombinant WT and mutant hNLRC4$^{\Delta CARD}$ and hNLRC4$^{\Delta CARD/\Delta Loop}$ (10 µM) was assessed after 30 min incubation (at room temperature) with ADP or ATP (5 mM, 50x molar excess) using experimental conditions as described in B). Data are pooled from at least n=3 independent experiments, lines indicate median.

5.2.6 Evaluation of residue T160 as potential phosphorylation site

Protein function is frequently regulated by a wide range of PTMs, with phosphorylation events being especially important during signal transduction (Roskoski 2012). Depending on the modified functional group, O- and N-phosphorylation is discriminated (Ardito et al., 2017, Roskoski 2012). Most frequently, protein kinases covalently attach a phosphoryl group (PO_3^{2-}) to the nucleophilic hydroxyl (-OH) group present in the side chains of three amino acids: serine, threonine and tyrosine residues, which results in O-phosphorylation (Ardito et al., 2017, Mann et al., 2002). N-phosphorylation of histidine and aspartate side chains is commonly observed in bacterial and fungal two-component signal transduction systems (Barrett et al., 1998, Rodrigue et al., 2000). Phosphate binding introduces a hydrophilic polar group, which can alter side chain interactions and induce a local or global structural change to the protein conformation (Xin et al., 2012). The reverse process, dephosphorylation, is catalysed by phosphatases (Cohen 2002).

The functional consequences of the interplay between phosphorylation and dephosphorylation reactions are diverse and regulate protein activity as well as the formation of protein complexes and signalling networks, as some proteins specifically recognize phospho-motifs through conserved domain structures. In most cases, proteins are modified by multiple different types of PTMs with varying chemical consequences, which attached to different residues are able to

counteract or synergize each other's function (Csizmok et al., 2018). Therefore, PTMs provide a highly complex mechanism to regulate protein function and activity (Csizmok et al., 2018).

PTM by phosphorylation is a commonly observed theme in regulation of inflammasome protein activity. For example, multiple phosphorylated residues in NLRP3 have been identified with functional consequences ranging from inflammasome activation to inhibition via different mechanisms (reviewed in (Sandall et al., 2019)).

For NLRC4, residue S533 has been determined as a phosphorylation site, however the regulatory role remains controversial (chapter 1.3.3.4.6) (Matusiak et al., 2015, Qu et al., 2012, Raghawan et al., 2017, Tenthorey et al., 2020).

Given the surface exposure of T160 in mutant NLRC4 and exchange of an unreactive alanine to the phosphorylatable amino acid threonine, we considered the possibility of post-translational phosphorylation. As previously mentioned, in the amino acid sequence of hNLRC4, T160 localizes 9 residues upstream the Walker A motif (G169, G174, K175, S176) (**Figure 5.10 A**), which is essentially required for ATP binding of AAA+ ATPases (chapter 5.1.1). Interestingly, in NLRP3, phosphorylation of residue S198, which localizes 28 residues upstream the Walker A motif (G226, G231, K232, T233) (**Figure 5.10 A**), has been shown to promote NLRP3 inflammasome assembly (Song et al., 2017). Extensive analysis in human and mouse cell lines as well as *in vivo* models identified phosphorylation of S198 (S194 in mice) as a LPS-mediated and transcription-independent priming mechanism, which was essentially required for signalling of ligand-activated WT NLRP3 as well as the autoactive CAPS-associated mutant NLRP3 T346M. Mechanistically, S198 was phosphorylated by MAPK c-Jun N-terminal kinase 1 (JNK1), which is activated downstream of TLR signalling via MyD88- or TRIF-dependent pathways that occurs rapidly after receptor stimulation (Song et al., 2017).

We therefore hypothesized that the A160T mutation in NLRC4 may generate an off-target threonine phosphorylation site similar to S198 in NLRP3, which – if phosphorylated – may promote inflammasome assembly.

To investigate amino acid sequence and structural similarities between NLRP3 and NLRC4 in the region of interest, we performed a sequence alignment (**Figure 5.10 A**) and a structural superposition analysis (**Figure 5.10 B**). On amino acid sequence level, hNLRP3 and hNLRC4 share 21.45 % sequence identity (Clustal Omega alignment (Madeira et al., 2019)) and show accurate sequence alignment of the conserved Walker A motifs (**Figure 5.10 A**). Upstream of this motif, where the NLRP3 S198 phosphorylation site is located, e.g. between hNLRP3 residues K192-Q225, and hNLRC4 residues N155-E168 the amino acid sequences are less conserved. As a result, inconsistent alignments were obtained with different algorithms (Clustal Omega vs NCBI Blast protein), in none of which hNLRP3 residue S198 was directly aligned to hNLRC4 residue A160 or T160 (**Figure 5.10 A**) and data not shown). However, more meaningful is the comparative analysis of the residue localization within the 3D structure of the protein. Therefore, using the PyMOL software, full length hNLRP3 (PDB:7PZC, preprint (Hochheiser et al., 2021)) was aligned to the NBD-HD1 (residues P164-R351) of mNLRC4 $T160^{\Delta CARD/\Delta Loop}$ (PDB:4KXF, computational mutagenesis of A160 to T160), since these domains are structurally most conserved between both proteins and contain conserved regulatory motifs on amino acid sequence level. Subsequent structural superposition analysis revealed surface exposure and proximal localization of mNLRC4 T160 and hNLRP3 S198 (**Figure 5.10 B**). Distance measurements of 16 Å further support spatial proximity and suggest that phosphorylation of T160 in hNLRC4 could mediate functional consequences similar to S198 phosphorylation in NLRP3.

Interestingly, based on the amino acid sequence, the NetPhos 3.1 server online tool predicted T160 in hNLRC4 as a potential phosphorylation site of protein kinase C (PKC) (Blom et al., 2004).

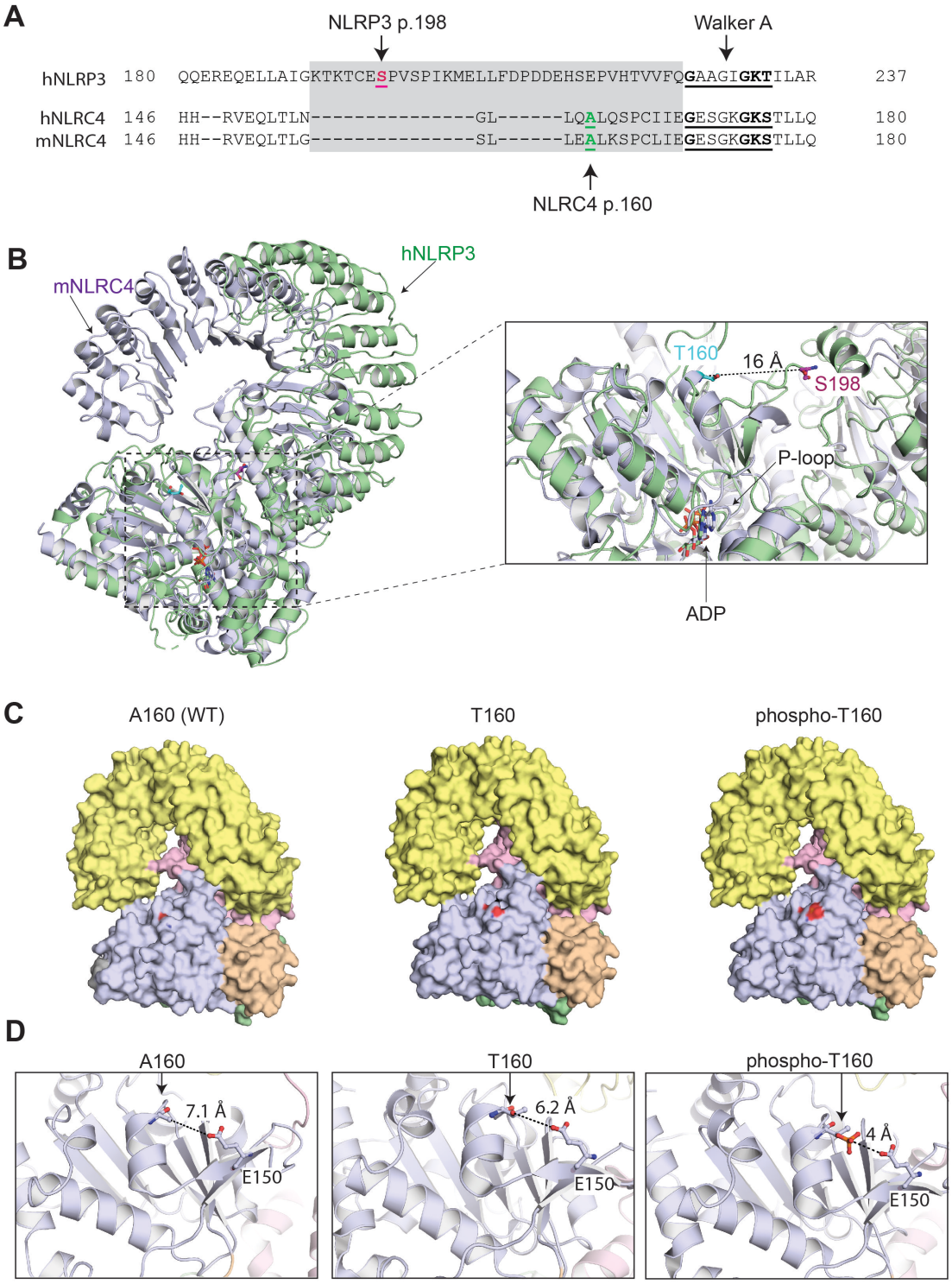

Figure 5.10 | T160 may represent an off-target phosphorylation site. A) Clustal Omega sequence alignment of hNLRP3 (Uniprot: Q96P20) and mouse (m) and human (h) NLRC4 WT amino acid sequences (Uniprot: Q3UP24, Q9NPP4). The highly conserved Walker A motif (underlined, bold residues), phosphorylation site S198 in NLRP3 (magenta, bold) and NLRC4 residue A160 (green, bold) are highlighted. Grey box indicates residues K192-Q225 (hNLRP3) and N155-E168 (hNLRC4), which are less conserved between both proteins.

residue position, p. **B)** Structural superposition analysis of full length hNLRP3 (green, PDB:7PZC) aligned to NBD-HD1 (residues P164-R351) of mNLRC4 T160 (purple, PDB:4KXF, computational mutagenesis to T160). Distance between alpha C atoms of hNLRP3 S198 (magenta) and mNLRC4 T160 (cyan) measured 16 Å (PyMOL software). The P-loops and bound ADP are indicated by arrows. **C)** Electrostatic surface representation of residue 160 in mNLRC4 (PDB:4KXF) WT (A160), mutant (T160) and T160 after *in silico* phosphorylation using the Pytms plugin and PyMOL software. Negative surface charge is indicated in red and protein domains are colour-coded: nucleotide-binding domain (NBD): light blue; helical domain 1 (HD1): wheat; winged helix domain (WHD): green; helical domain 2 (HD2): pink; leucine-rich repeat domain (LRR): yellow. **D)** Stick presentation of residue A160/T160 and glutamate (E) 150 in mNLRC4 (PDB:4KXF) showing the distance (dotted black line) between functional groups measured using the PyMOL software. Side chain atoms are coloured by element: blue: nitrogen, red: oxygen, orange: phosphorus. Angstrom, Å.

As an initial attempt to investigate this hypothesis experimentally, we used a mass spectrometry approach, since PTMs increase the MW of amino acids (Mann et al., 2003). Specifically in the case of phosphorylation, an addition of 80 Da can be observed (Mann et al., 2003). *Sf*9 cell-purified monomeric recombinant WT and mutant hNLRC4$^{\Delta CARD}$ and hNLRC4$^{\Delta CARD/\Delta Loop}$ protein was enzymatically digested with trypsin and subjected to peptide mass fingerprint analysis (in collaboration with Prof. Henning Urlaub, Max Planck Institute, Goettingen). The determined mass-to-charge ratios of detected peptides were analysed using the MaxQuant software and compared to the expected peptide masses based on the amino acid sequence of WT and mutant hNLRC4 (T160 modification based on WT sequence Uniprot: Q9NPP4). The overall coverage in this experiment reached 92-94 % for the analysed proteins. Based on the calculated difference between expected and detected masses, PTMs were identified. This experiment revealed several serine residues consistently phosphorylated in all samples, including the previously described S533 and two additional sites (S457, S536; data not shown). However, phosphorylation of T160 was not detected (data not shown). Further, oxidation of methionine was frequently observed in all samples affecting the same residues (data not shown). Although this PTM has been implicated in functional consequences and

pathologic conditions (Brot et al., 1991), it is a commonly observed artefact of electrospray ionization (Morand et al., 1993) and was therefore not further investigated.

We further performed a computational analysis of the potential structural consequences associated with phosphorylated T160. *In silico* mutagenesis and residue phosphorylation was conducted using the PyMOL software. This analysis revealed a more pronounced negative surface charge as a result of the T160 mutation, which was further enhanced after computational phosphate addition (**Figure 5.10 C**). Additionally, modelling of phospho-T160 suggests surface expansion, which may have the potential to generate or interrupt a so far unknown binding interface (**Figure 5.10 C**). Although the detailed analysis and distance measurements of nearby amino acid side chain interactions did not identify obvious structural clashes, phosphate addition increased the proximity between threonine 160 and the negatively charged glutamate (E) 150 from 6.2 Å to 4.0 Å (**Figure 5.10 D**), which may result in structural consequences.

Since this hypothesis remains speculative to date, future studies will be required to identify whether T160 is phosphorylated in human cell lines and elucidate the functional importance of this PTM as well as the resulting conformational consequences, that may facilitate NLRC4 activation.

5.3 Discussion

Besides functional analyses using *in vitro* cell-based assays, *in silico* prediction of structural consequences has proven powerful to gain insights into the disease-causing mechanisms of previously reported mutations in *hNLRC4* (Liang et al., 2017, Moghaddas et al., 2018, Romberg et al., 2014).

Using the available structural information on mNLRC4 and the AlphaFold 2 predictions of the human protein structure, residue A160 was identified as solvent exposed and located proximal to the nucleotide-binding site upstream the Walker A motif. This localization is distinct from previously reported NLRC4 GoF mutations, which mostly affected residues directly involved in nucleotide binding or inter-domain interactions. Therefore, the distinct localization together with our *in vitro* data showing ligand-dependent overactivation instead of spontaneous signalling and the relatively mild clinical manifestation (chapter 4.2.1) suggest a mechanism of action that does not directly interrupt NLRC4 autoinhibition.

Structurally, the consequences induced by the A160T mutation may be rather subtle or indirect, and therefore difficult to predict via *in silico* analysis. Furthermore, between all available structures of NLRC4, the autoinhibited conformation was solved at the highest resolution of 3.2 Å, which did not allow for definite conclusions about the side chain interactions and hampered the detailed analysis of structural consequences of the threonine exchange. Therefore, this chapter aimed to generate high-resolution structural information of NLRC4 and characterize the biochemical and biophysical properties of the A160T mutant.

Murine and human NLRC4 truncations were recombinantly expressed using a baculovirus expression system. Interestingly, despite the high sequence identity, proteins of both species showed distinctly different preparative SEC elution profiles. Whereas the murine protein eluted as single peak equivalent to the molecular mass of monomeric NLRC4, two peaks were observed for the human protein, which corresponded to larger size aggregates (predominant peak 1, eluted in void volume) and the monomeric protein (peak 2). Notably, the underlying reason for the observed difference may partly be attributable to differences in the oligomerization behaviour of NLRC4 proteins from both species

as well as differences in the performed purification protocol. Whereas the murine protein was purified using AIEX chromatography and SEC, the AIEX step was omitted during purification of the human protein, in order to increase the purification yield. Therefore, SEC elution chromatograms of mouse and human protein are not directly comparable. However, although the data for AIEX chromatography were not shown, mNLRC4$^{\Delta CARD}$ did appear as one predominant peak during both AIEX chromatography and subsequent SEC, suggesting reduced self-aggregation compared to hNLRC4 truncations, which eluted as two peaks during AIEX or SEC. If AIEX chromatography and SEC were consecutively performed during purification of hNLRC4 truncations, aggregates (peak1) were largely removed in the SEC elution profile which resulted in a single peak similar to mNLRC4, although the yield was drastically reduced.

Whereas the presence of ADP and $MgCl_2$ during the purification procedure had no effect in the case of the murine protein, ADP and $MgCl_2$ addition stabilized monomeric hNLRC4 and increased the final yield to some extent. Optimisation of the used domain borders, purification tags or use of an insect cell-specific codon-optimized hNLRC4 sequence may be beneficial to further increase the yield of recombinant hNLRC4 in the baculovirus expression system.

Limited solubility and increased aggregation of hNLRC4 compared to the murine ortholog was consistently observed, although the reasoning for these species-specific differences remains unclear, especially in light of 75 % amino acid sequence identity. However, difficulties to produce high quality monomeric hNLRC4 may be reflected in the availability of structural information, which only exists for the murine protein (Diebolder et al., 2015, Halff et al., 2012, Hu et al., 2013, Tenthorey et al., 2014, Zhang et al., 2015). Furthermore, previous studies using recombinant hNLRC4 in biochemical assays or negative stain EM stated difficulties, such as protein aggregation and low yield (Halff et al., 2012).

Similarly, the crystal structure of ADP-bound rabbit NOD2 has been solved (Maekawa et al., 2016), whereas structural information of hNOD2 does not currently exist and may be indicative of similar aggregation-related issues and a potential species-specific effect.

In general, spontaneous oligomerization is a frequently encountered problem when purifying proteins with oligomerization domains (Faustin et al., 2007, Makoni et al., 2021, Zhang et al., 2015). Therefore, instead of a baculovirus expression system, a mammalian cell system might be better suited to enable more complex PTMs, which may have significant impact on protein stability and reduce spontaneous aggregation (Makoni et al., 2021). Furthermore, aggregation of inflammasome proteins was reported to occur in a concentration-dependent manner (Makoni et al., 2021), which highlights the challenging balance between large-scale recombinant protein production and maintaining the conformational integrity of the purified protein. Along these lines, Halff and colleagues were able to purify hNLRC4 from HEK293E cells, however observed spontaneous polymerization at concentrations above 1 mg/ml (Halff et al., 2012).

Therefore, although *in vitro* studies with recombinant protein represent a very valuable experimental approach, feasibility of downstream analytics and structural studies require large quantities of homogenous pure protein and are often limited by the low yield of recombinant protein production. Therefore, further optimization of the protein expression system and purification conditions is required before crystallization trials with hNLRC4 A160T can be continued. Although recombinant production of monomeric mNLRC4 A160T resulted in higher yields, preliminary functional analysis raised concerns about the presence of the disease-causing phenotype in the murine protein. Thus, further studies are necessary to investigate a potential effect of mNLRC4 A160T in concert with mNAIP2 and mNAIP5/6.

Notably, for both human and murine NLRC4, WT and the A160T mutant eluted with similar retention volumes during preparative SEC. This suggests that the A160T mutation adopts a conformation similar to the WT protein and is unlikely to induce a global conformational change that releases NLRC4 autoinhibition, since spontaneously assembled larger size inflammasome complexes would elute at lower volumes (or within the void volume). Although determination of the precise MW of a possible protein complex can only be obtained with analytic SEC experiments or SEC-coupled with multi angle light scattering (MALS),

comparable elution profiles from preparative SEC experiments provide initial evidence that both WT and NLRC4 A160T adopt an inactive conformation.
Consistently, A160T did not alter the conformational stability of NLRC4 in thermal shift assays, regardless of ADP or ATP nucleotide addition.
Therefore, although the biochemical and biophysical characterization was not extensive, these results complement the findings from cellular *in vitro* assays (chapter 4) and suggest that the A160T exchange does not impact NLRC4 conformation and function when the protein is in the inactivated state. However, the conformational consequences of NLRC4 A160T in the activated state require further investigation.
Functionally, WT NLRC4 activation relies on binding of ligand-activated NAIP to induce a conformational change and inflammasome assembly. Based on computational analysis, residue A160 does not contribute to NLRC4-homodimer interfaces or localizes near the NLRC4-NAIP-heterodimer binding surface. However, structural changes may indirectly increase NAIP-to-NLRC4 or NLRC4-to-NLRC4 binding affinities. Consequently, this may facilitate activation-induced inflammasome formation or decrease the threshold for NLRC4 self-assembly. Initial co-immunoprecipitation experiments in HEK293T cells did not identify such differences (data not shown). However, technical limitations of the downstream analysis by western blotting, such as signal saturation and semi-quantitative analysis, may not provide the required sensitivity to identify potentially subtle differences. Rather, a highly sensitive approach, such as surface plasmon resonance (SPR) binding analysis (Hu et al., 2017), will be useful to determine NLRC4 and NAIP binding affinities of WT and mutant NLRC4 to investigate this hypothesis experimentally. Further, assessing the kinetics of inflammasome assembly by fluorescence polarization will be valuable to confirm the functional consequence of altered binding affinities (Sborgi et al., 2018, Zhang et al., 2015).
Interestingly, a similar mechanism of action has been proposed for a heterozygous CAPS-associated mutation located within the PYD of NLRP3 (c.92A>T, p.D31V) (Hu et al., 2017). Here, the amino acid exchange altered the surface charge leading to enhanced interaction of mutant NLRP3 with the PYD of adapter protein ASC (Hu et al., 2017).

In contrast, consequences for protein interactions induced by the NLRC4 A160T mutation are less predictable, since this residue does not directly contribute to an identified interaction interface or a functionally required motif.

As an alternative hypothesis, we investigated the possibility of mutant residue T160 as an off-target phosphorylation site, based on the similarities to NLRP3 residue S198. Both residues are surface exposed, similarly localized upstream the Walker A motif and NLRP3 S198 phosphorylation by JNK1 was shown to be essentially required for NLRP3 self-assembly (Song et al., 2017). Mechanistically for NLRP3, the S198 phosphorylating kinase JNK1 is activated in a transcription-independent priming step through TLR receptor signalling. Following S198 phosphorylation, deubiquitination of NLRP3 occurs, which results in rapid NLRP3 activation (10-30 min) (Juliana et al., 2012, Song et al., 2017). Fast activation of NLRP3 is thought to complement the transcription-mediated priming events, which need more time but are required for long-lasting and strong inflammasome signalling (Bauernfeind et al., 2009, Song et al., 2017).
Interestingly, Song and colleagues observed NLRP3 S198 phosphorylation in murine BMDMs, primary human monocytes and monocytic cell lines (THP-1 and U937) following priming with LPS, Pam3CSK4, poly I:C or PMA differentiation, respectively as well as after overexpression in HEK293T cells (Song et al., 2017). Although not discussed in the respective study, perhaps endogenous expression of JNK1 in HEK293T cells (Su et al., 2016) is sufficient to spontaneously phosphorylate overexpressed NLRP3.
Similarly, we observed increased activation of NLRC4 A160T in Pam3CSK4-primed and PrgI-stimulated THP-1 cells and in HEK293T overexpression assays (chapter 4), suggesting that phosphorylation events similar to those described for NLRP3 could cause more rapid activation of mutant NLRC4 and therefore result in increased cytokine release and ASC speck formation.
Prediction of structural changes induced by the phosphorylation is challenging, since this information is not encoded within the amino acid sequence but determined through local interaction of amino acid side chains. However, based on the structural information available and the current understanding of the

activation mechanism of other AAA+ ATPases or NLRs, addition of the negatively charged phosphoryl group within a surface-accessible loop may result in conformational changes, which render the nucleotide-binding site more accessible for ADP-to-ATP exchange and facilitate inflammasome activation.

A comparable structural theme characterizes the inactive state of MAP kinases where the active site is occluded by a T-loop (activation loop) and requires dual phosphorylation of T-loop residues threonine and tyrosine (TxY motif, x denotes any residue) to induce the catalytically active conformation (Davis 2000).

However, this hypothesis remains speculative at this point and further studies are required for experimental validation. Although phosphorylation of insect cell-expressed recombinant proteins has previously been reported (de Carvalho et al., 1996), whether the specific kinase that might be responsible for phosphorylating T160 is expressed in *Sf*9 cells or whether similar phosphorylation patterns exist, remains questionable. The phospho-proteomics analysis should therefore be repeated with recombinant protein purified from a human cell line and in presence of phosphatase inhibitors before definite conclusions about phosphorylation of T160 can be drawn. Further challenges are the heterogeneity of the sample, as only a small ratio of the analysed proteins may be phosphorylated, and the limited stability of threonine phosphorylations (Mann et al., 2003). Notably, in this experiment only monomeric peak 2 protein was analysed, however it is possible that phosphorylated protein may oligomerize and elute within peak 1, which will be included in future experiments. Here, we only performed the standard mass spectrometry experimental procedure, however, more sensitive approaches and enrichment techniques for phosphorylated proteins have been developed such as immobilized metal affinity chromatography (IMAC) (Brill et al., 2004), chemical replacement of phospho-S/T-residues with a biotin-tag (Oda et al., 2001) or selective isolation of phospho-peptides based on chemical modifications (Zhou et al., 2001).These approaches are especially relevant for analysis of phospho-proteins in cell lysates, which may be a more suitable experimental approach to identify the T160 phosphorylation and investigate its functional consequence in future experiments. Performance of

inflammasome activation assays with phosphomimetic mutants represents another useful experimental strategy.

Furthermore, identification of the phosphorylating kinase would be valuable as targeted inhibition could provide an alternative therapeutic opportunity for the here described patient (chapter 4.2.1). Kinase specificity is largely influenced by the amino acids adjacent to the phosphorylated residue (linear motif) (Pearson et al., 1991, Pinna et al., 1996), which create a structural interface (Blom et al., 2004). The typical sequence motif recognized by JNK1 contains residues serine or threonine directly followed by a conserved proline [consensus sequence: S/T]P) (Bogoyevitch et al., 2006), which indeed is present within the “activation loop” of NLRP3 encoded by $S^{198}PxS^{201}P$ (x denotes any residue; Hochheiser et al., 2021, Song et al., 2017). In contrast, the NLRC4 T160 mutation results in a T^{160}xxSP motif, in which T160 is less likely to be a substrate of JNK1. However, other kinase families have broader specificity, such as AGC kinases, which comprise protein kinases A, G and C (PKA, PKG and PKC) (Bradley et al., 2019). This is in congruence with the NetPhos 3.1 prediction, which suggested that PKC could potentially recognize and phosphorylate hNLRC4 T160 as an off-target. However importantly, kinase-substrate interactions are additionally determined by residues outside the linear recognition motif as well as the structural characteristics of the kinase domain (Shi et al., 2021), which limits the accuracy of *in silico* predictions (Ritz et al., 2009).

Despite the outlined similarities, one crucial difference exists. The NLRP3 S198 phosphorylation was shown to be essentially required for NLRP3 inflammasome formation and signalling (Song et al., 2017). In contrast, WT NLRC4 inflammasome formation does not require this modification, since A160 cannot be phosphorylated. This suggests that, if T160 acts via a similar mechanism, phosphorylation only facilitates NAIP/NLRC4 inflammasome formation and perhaps lowers the threshold of the activation process.

Particularly interesting in this context is the observation that T160 is broadly encoded in the WT sequence of the analysed members of ungulate and carnivore species. Therefore, considering the higher activity of NLRC4 T160, the

phylogenetic relationships identified in chapter 5.2.1 suggest evolutionary processes that required adaptation and attenuation of NLRC4 signalling in primates and rodents. Since NLRC4 is activated by bacterial ligands, co-evolution of host immune defence mechanisms and the microbiome could have contributed to this process (Dethlefsen et al., 2007).

Within primates, the presence of V160 in gorilla NLRC4 is an interesting observation. Amino acids alanine and valine possess similar chemical properties as both are classified as unpolar amino acids and – given the surface exposure of residue 160 – the structural consequences associated with an exchange to the slightly larger valine are challenging to predict. Valine does not contain any additional functional groups, therefore the biological consequences may only be evaluated experimentally. It is possible that within primates, A160 tolerates substitution to some extent without causing immune system overactivation. Alternatively, V160 in gorilla NLRC4 may reflect a specific adaptation to pathogenic challenges distinct for this species. To date, a comparative analysis of the immune response to NLRC4-specific stimuli in gorillas and other primate species has not yet been reported in the literature, but represents an interesting line of future research that may discover unique regulatory mechanisms and functions perhaps specific to V160 in gorilla NLRC4.

Interestingly, inter-species differences on the level of the NLRC4 inflammasome and effector caspases have been described in carnivore species (Digby et al., 2021, Eckhart et al., 2009). For example, dogs and other species of the Canidae family were suggested to be deficient for the NLRC4 inflammasome, since premature termination codons prevent *NLRC4* gene expression while *NAIP* genes are completely absent (Digby et al., 2021, Eckhart et al., 2009). In contrast, an intact *NLRC4* gene was detected within the cat genome (and other Felidae) which indicates integrity of this pathway in some carnivore species encoding NLRC4 T160 (Digby et al., 2021, Eckhart et al., 2009). Therefore, studying the molecular mechanisms of inflammasome formation in other species could prove valuable to understand the role and unique features of NLRC4 T160 inflammasome signalling. In this context, a recent study identified a caspase-1/caspase-4 fusion protein expressed in carnivore species, which is composed

of the N-terminal caspase-1 CARD domain and a C-terminal catalytic domain resembling that of murine caspase-11 (caspase -4 or -5 in human) (Devant et al., 2021, Digby et al., 2021, Eckhart et al., 2008). Therefore, cats and other species may have developed distinct regulatory mechanisms and effector protein networks in presence of functional NLRC4 T160, which may be specific to the T160 variant and coordinate its inflammatory response.

Selection pressure shaped by diet, habitat and microbial exposure may have contributed to the evolutionary processes and development of the WT NLRC4 A160 inflammasome in humans. Perhaps as a direct result of dietary differences between omnivore versus carnivore or herbivore species, the human GIT is exposed to a diverse set of commensal bacteria and enteropathogens, whereas a meat-rich diet is thought to be antimicrobial (Digby et al., 2021). Since NLRC4 is expressed in the gastrointestinal epithelium, evolutionary attenuation of NLRC4 inflammasome signalling may have been required to dampen the innate immune response and increase survival in a particular primate- and human-specific environmental niche. Alternatively, the availability of clean water to the majority of the western human population may have made a highly reactive gastrointestinal immune system dispensable and rather detrimental. Since humans and mice have co-existed over the past 15000 years (Weissbrod et al., 2017) and both species were exposed to similar environmental factors, co-evolution of NLRC4 A160 in these species may not be surprising. However, given the distinct environmental niche of primates, a shared early evolutionary event is conceivable, however the contributing factors remain unclear.

Nonetheless, studying the NLRC4 T160 inflammasome in other species may reveal interesting insights in regulatory mechanisms, protein interactors and functional consequences caused by this mutation. Further, it is possible that species-specific differences regarding inflammatory protein signalling networks exist, which may suggest inflammasome plasticity shaped by evolutionary processes. Therefore, NLRC4 T160 may only be overactive specifically in the context of human inflammasome networks.

Overall, the structural and biophysical analysis of the mechanism by which the A160T mutation increases NLRC4 activation was limited by difficulties in recombinant protein production. The desire to generate structural information for hNLRC4 remains valid, especially in light of pharmacological drug development. So far, one small molecule NLRC4 inhibitor, the benzoxazolone acetamide C77 has been described and validated *in vitro* (Sebastian-Valverde et al., 2021). Interestingly, the competitive inhibitor also reduced NLRP3- and NLRP7-mediated IL-1β release in primary microglia and was therefore suggested to bind the structurally conserved nucleotide-binding site of these proteins (Sebastian-Valverde et al., 2021). Combined inhibition of NLRC4 and NLRP3 inflammasome signalling may present a promising approach for diseases where both inflammasomes synergistically mediate inflammation, perhaps through indirect activation by released DAMPs or inflammatory feedback mechanisms, as for example observed in neuroinflammation (Saadi et al., 2020, Lin et al., 2020, Liu et al., 2014a, Soares et al., 2019).

Targeted specific inhibition of overactive NLRC4 signalling holds promising potential for treatment of NLRC4-AIDs, while other inflammasome pathways remain responsive to sustain the innate immune defence. This requires identification or development of compounds, which specifically block functionally important structures in NLRC4 that are less conserved to other inflammasome proteins. Specific disruption of LRR-LRR binding interfaces may present one possible approach, which would hinder NLRC4 oligomerization and prevent signalling. Especially interesting in this context is the identification of *NLRC4* gene mutations, such as A160T, which may prove useful to identify patients suffering from inherited or sporadic AIDs that would likely benefit from targeted NLRC4 inflammasome inhibition.

6 Overall Discussion

Studying molecular mechanisms underlying monogenic AIDs is valuable to investigate potential therapeutic targets and elucidate previously unknown mechanisms of immune system regulation.

In this context, one aim of this thesis was to identify the innate immune sensor driving previously reported aberrant type I IFN signalling in COPA syndrome patients (Volpi et al., 2018). Although COPA syndrome represents a complex inflammatory disease, encompassing features of both autoinflammation and autoimmunity that may partially result from ER stress (Watkin et al., 2015), we here demonstrate that the cGAS-STING pathway is the main driver of type I IFN production in COPA-deficient and COPA mutant-expressing cell lines (chapter 3). This is in line with other recently published studies, that independently confirmed the involvement of STING *in vitro* using patient-derived cells as well as cell line and mouse models (Deng et al., 2020a, Deng et al., 2020b, Kato et al., 2021, Lepelley et al., 2020, Mukai et al., 2021).

Since the original description of COPA syndrome in five unrelated families in 2015 (Watkin et al., 2015), 17 published case reports identified a total of 25 families with 67 mutation carriers and 53 symptomatic patients (**Suppl. Table 1**), which suggests that COPA syndrome might not be as rare as originally anticipated. However, this disease may often be misdiagnosed due to the relatively unspecific clinical manifestation involving isolated or combined inflammation of the lung, joints and/or kidney. Therefore, COPA syndrome is one example that emphasizes the importance of genetic screening if an AID is suspected. Based on knowledge from reported COPA syndrome patients, early diagnosis is crucially important to prevent irreversible lung and joint damage at young age, and longer-term studies using broad immunosuppression and/or JAK/STAT pathway inhibition are required to determine the efficacy of currently used treatment strategies.

Given the involvement of STING, it is conceivable that other STING effector functions (chapter 1.3.4.3.2) may contribute to the disease manifestation of COPA syndrome and may occur cell-type specific and dependent on STING

expression levels. One example represents the predominantly pro-apoptotic response following STING activation in T cells, a result of high STING expression levels and synergistic disruption of calcium homeostasis (Gulen et al., 2017, Wu et al., 2019). Furthermore, apart from type I IFN production (Liu et al., 2015b) and STING-mediated apoptosis (Gulen et al., 2017, Sze et al., 2013, Tang et al., 2016), STING induces NF-κB signalling (Abe et al., 2014), autophagy (Gui et al., 2019, Liu et al., 2019) and lysosomal degradation pathways (Gonugunta et al., 2017), however the regulatory mechanisms controlling these downstream functions are less well characterised. Therefore, future studies are required to investigate these functions in more detail and perhaps identify other not yet known effector mechanisms in less commonly investigated cell types, that could additionally contribute to manifestations of COPA syndrome and STING-associated diseases in general.

Importantly, together with *in vitro* data from Deng et al. (Deng et al., 2020b), our results demonstrate the therapeutic potential of direct STING inhibition (**Figure 3.6**), which may be able to simultaneously block several STING effector functions that are not necessarily inhibited using less targeted treatment, e.g. JAK/STAT inhibition. Although a STING inhibitor has not yet been clinically approved, an increasing number of cGAS-STING driven inflammatory conditions and neurodegenerative diseases have been identified (Chu et al., 2021, Nazmi et al., 2019, Sliter et al., 2018, Yu et al., 2020), which prompted several research efforts to develop inhibitory compounds targeting STING. At the moment, two predominant approaches involve targeted inhibition of ligand binding or blocking STING palmitoylation sites (C88 or C91) (Haag et al., 2018, Li et al., 2018a, Siu et al., 2019). Additionally, residues contributing to the STING polymerization interface have been suggested as potential drug targets (Ergun et al., 2019), however future study are required to investigate this approach and develop candidate compounds for clinical evaluation.

It is conceivable that complete control of COPA syndrome pathogenesis can only be achieved by simultaneous inhibition of STING and ER stress-induced UPR pathways. UPR signalling has been shown to drive inflammatory signalling through NF-κB (Martinon et al., 2010), and was implicated in lung fibrosis

(Dickens et al., 2019, Kropski et al., 2015). There are also associations with Th17 cell differentiation and autoinflammation (DeLay et al., 2009, Goodall et al., 2010), which together may make a significant contribution to the manifestation of COPA syndrome. Thus, further studies are required to delineate distinct molecular consequences of both pathways and determine if pathway specific inhibitors either alone or in combination could potentially be a treatment for patients.

Overall, our finding that defective retrograde trafficking results in aberrant STING signalling is quite surprising and significantly contributed to the current model of the STING signalling pathway and its regulatory mechanisms. Originally, STING was thought to reside anchored within the ER membrane and undergo ligand-mediated ER-to-Golgi translocation (Dobbs et al., 2015). However, COPA-deficiency has revealed that STING constitutively translocates between secretory pathway compartments (ER-Golgi-lysosome) during homeostasis (Chu et al., 2021, Lepelley et al., 2020). The observed cGAS-dependence together with structural requirements for STING dimerization and ER exit suggest that tonic shuttling is potentially the result of background levels of cytoplasmic self-DNA (Gao et al., 2013b, Shang et al., 2019, Zhang et al., 2019). Therefore, in the revised model, COPI-mediated retrograde transport and lysosomal degradation pathways represent negative regulatory mechanisms to prevent uncontrolled STING signalling during the steady state.

From an evolutionary perspective, STING trafficking is highly conserved and can be traced back to *N. vectensis*, an anemone species, where STING stimulation induces translocation and autophagy-mediated DNA degradation but not type I IFN signalling (Gui et al., 2019). When compared to other innate immune pathways, such as the rather linear transduction cascades downstream TLRs or RNA sensors RIG-I and MDA5, traversing the secretory pathway adds a higher level of complexity to the STING pathway. This higher complexity could be advantageous, as it presents multiple steps which might be perturbed by pathogens, triggering an immune response. For example, intracellular pathogens often co-opt cellular compartments (ER, Golgi, endosomes, mitochondria) and host protein machinery to facilitate their own replication (Kellermann et al., 2021).

Thus, surveillance for secretory pathway perturbances would present an elegant strategy to detect a broad range of infectious agents and bypass the requirement of conserved PAMPs. In this context, STING may function as a sensor of homeostasis-altering molecular processes (HAMPs) (Liston and Masters 2017) and monitor secretory pathway integrity. STING trafficking is well regulated by interaction with numerous accessory proteins (Chu et al., 2021). Thus, pathogen interference or genetic defects in trafficking co-factors are likely to disrupt STING flux, result in STING accumulation and induce subsequent signalling. Besides COPA syndrome, the neurodegenerative manifestation of Niemann-Pick disease, a lysosomal storage disorder, has recently been shown to be driven by such a defect (Chu et al., 2021). In this study, Niemann-Pick disease type C1 protein (NPC1) was identified as an adapter that tethers STING into lysosomes and promotes its degradation in post-Golgi compartments. Loss of NPC1 function was shown to cause cGAS-independent aberrant STING activation and neuroinflammation in *Npc1*$^{-/-}$ mice (Chu et al., 2021).

Another example represents C9orf72, which functions in a complex as GTPase-activating protein for ARF GTPases and is involved in lysosome formation (Su et al., 2020). Haploinsufficiency of C9orf72 is associated with amyotrophic lateral sclerosis (ALS) and frontotemporal degeneration (FTD) (Shi et al., 2018). Interestingly, *C9orf72*$^{-/-}$ BMDMs showed delayed STING degradation and increased type I IFN transcription following stimulation with cGAMP and a STING-dependent type I IFN signature was detected in PBMCs isolated from ALS patients carrying the C9orf72 repeat expansion (McCauley et al., 2020). As a result, LoF mutations in other secretory pathway regulators or STING trafficking adapters may be associated with STING-driven diseases and this is in line with our data showing that deficiency in other COPI subunits (COPG1, COPD) similarly activates STING (**Figure 3.9 B, C**).

Conversely, prolonging STING activation may have therapeutic benefit in certain disease contexts. Blockade of trafficking-induced STING degradation boosts type I IFN production and may have the potential to promote STING-mediated anti-tumour immunity (Gonugunta et al., 2017, Jiang et al., 2020). However, strategies to fine-tune this response require further investigation and balancing the strength

and duration of STING activation may be key to avoid STING-mediated tumour-promoting effects and immune system overactivation (Decout et al., 2021). Interestingly, recent studies further suggest STING activation in response to accumulated immunogenic self-glycans (Fermaintt et al., 2019), cholesterol reduction (York et al., 2015) and alterations in intracellular calcium levels (Kwon et al., 2018, Liu et al., 2012b). These findings increasingly position STING as sensor of ER homeostasis, due to the central role of this organelle in protein glycosylation, cholesterol synthesis and regulation of calcium homeostasis (Voeltz et al., 2002), which may link STING dysregulation to other pathologic conditions such as metabolic diseases (Oduro et al., 2021).

Several other molecular mechanisms are likely to prompt innate immune system activation following disturbance of structural and functional integrity of cellular organelles. One example represents the NLRP3 stimulus-induced structural reorganisation of the Golgi ribbon, which results in *trans*-Golgi network dispersal and exposure of phosphatidylinositol-4-phosphate for NLRP3 recruitment. *Trans*-Golgi reorganisation was suggested to occur upstream of NLRP3 inflammasome formation and caspase-1 activity in response to several distinct stimuli. Thus, NLRP3 appears to be specifically recruited to the morphologically disturbed Golgi (Chen et al., 2018). Since NLRP3 is activated by a broad range of PAMPs and DAMPs, *trans*-Golgi disassembly was proposed as an event commonly induced by most activating stimuli (Chen et al., 2018). Therefore, NLRP3 provides an excellent example how innate immunity has evolved to detect a broad range of threats through alteration of cellular homeostasis, rather than specific recognition of a defined set of PAMPs. Similarly, other NLRs, such as pyrin and NLRP1 are increasingly emerging as complex immune sensors, which can be activated through cytoskeletal alterations, cleavage by viral proteases or altered levels of oxidized thioredoxin, respectively, although further studies are required to understand the complex mechanisms involved in regulation and activation of these inflammasome sensors (Gao et al., 2016, Kile et al., 2007, Kim et al., 2015, Levinsohn et al., 2012, Tsu et al., 2021, Xu et al., 2014, Zhong et al., 2018) (preprint (Ball et al., 2021)).

In stark contrast, the NAIP/NLRC4 inflammasome in human and mice was shown to respond to a well-defined set of PAMPs released from some Gram-negative bacteria, namely flagellin, T3SS needle and inner rod proteins (chapter 1.3.3.4.2). Therefore, NAIPs can be considered as classical PRRs that recognize evolutionarily conserved molecular features distinctly expressed by pathogens. Although this strategy may seem disadvantageous due to the presumably narrow range of ligands, aberrant activation by self-antigens is prevented. Indeed, AIDs associated with the NAIP/NLRC4 inflammasome have only been reported to be genetically caused by heterozygous GoF mutations in *NLRC4* (Canna et al., 2014, Romberg et al., 2014). Early onset and the severe clinical manifestation of NLRC4-MAS and AIFEC demonstrate the potency of uncontrolled NLRC4 activation, that can have lethal consequences in some cases (Liang et al., 2017, Moghaddas et al., 2018, Romberg et al., 2014).

In chapter 4 of this thesis, the first patient with a homozygous mutation in *NLRC4*, NLRC4 A160T was described, who presented with moderately elevated serum levels of IL-18, recurrent episodes of inflammation and immune dysregulation with early childhood onset. Using cellular models, we provided *in vitro* evidence that the identified mutation is likely pathogenic and induces increased NLRC4 activation in a ligand-dependent manner (chapter 4). This is in line with the inflammatory episodes experienced by the patient, which were occasionally triggered by urinary and GIT infections with Gram-negative pathogens. Therefore, ligand-dependency, moderately increased serum levels of IL-18 and a relatively mild clinical manifestation set the NLRC4 A160T-mediated AID apart from previously described conditions and overall suggest a distinct mechanism of action, which requires further experimental studies (discussed in chapters 4.3). We subsequently employed complementary structural biology *in silico* approaches and thermal stability assays to identify possible conformational changes associated with T160, however the evaluation of CARD-truncated NLRC4 in the inactive conformation did not reveal differences when compared to the WT protein (chapter 5). Consistently, these results point towards a structural change or perhaps PTM specific to T160 that may be restricted to NLRC4 in its

active conformation. Mechanistically, T160 may alter the NLRC4 binding affinity to ligand-bound NAIP or between NLRC4 monomers and thus facilitate ligand-induced inflammasome assembly, however future experiments are required to test these hypotheses (discussed in chapter 5.3).

Although NLRC4-AID is a rare monogenic disorder, heterozygous occurrence of the A160T allele has been reported in the general population with the highest allele frequency of 0.001 in Europeans (total allele frequency 0.0008, GnomAD), and meta-analysis association data made available by the IBD Exomes Browser (**Table 14**) suggested this allele as potential risk locus for the development of UC. However, given that closely related heterozygous family members of the here reported index case were healthy and did not report any gastrointestinal symptoms, additional environmental and genetic co-factors are likely to contribute to disease onset and pathogenesis. Determining these co-factors that may enhance the pathogenic effect of NLRC4 A160T would be interesting, yet challenging to identify and require a relatively large cohort to provide informative results.

As previously discussed (chapter 4.3), genetic screening for the A160T variant and measurement of serum IL-18 levels (and IL-18BP) could provide a promising approach to determine a subset of UC patients that may benefit from targeted inhibition of IL-18. Indeed, IL-18 elevation has been implicated in the pathogenesis of IBD (Ludwiczek et al., 2005, Mokry et al., 2019), although the role of NLRC4 signalling in this disease context remains controversial (discussed in chapter 4.3).

The mechanisms of activation and assembly of the NAIP/NLRC4 inflammasome are well investigated, however numerous questions remain unsolved.

We do not know how different stimuli are recognized by hNAIP (Reyes Ruiz et al., 2017), which possesses the highest homology to mNAIP1 that specifically detects T3SS needle proteins (Yang et al., 2013). Thus, structural information would be valuable to gain insights into the presumably unique ligand-binding mechanisms of hNAIP. Furthermore, simultaneous occurrence of *Klebsiella* infections and inflammatory flares in the here reported patient may suggest this pathogen as an initiating trigger for NAIP/NLRC4 inflammasome activation.

However, the performed diagnostic procedure did not determine the specific species, which could provide insights into the nature of the NAIP-specific stimulus. Generally, as previously mentioned (chapter 4.3), *Klebsiella pneumoniae* is relatively well investigated and considered typically non-flagellated and non-T3SS-encoding, therefore the ligand that activates NAIP/NLRC4 signalling is unclear (Fouts et al., 2008). Co-infections with other pathogens or NLRP3 co-activation may therefore contribute to NLRC4 signalling in this context, however in-depth studies will be required to determine such interplay. Interestingly, this observation also raises the possibility of additional unidentified ligands of hNAIP, which may be specific to human cells, given that most original studies determined the ligand specificity of the NAIP/NLRC4 inflammasome in murine systems (Kofoed et al., 2011, Mariathasan et al., 2004, Miao et al., 2010). Furthermore, a link between NLRC4 and actin reorganization has been suggested in response to *S. typhimurium* infection (Man et al., 2014b), which would be interesting to further investigate in the context of HAMPs.

Another question evolves around the therapeutic effect of biologics to treat NLRP3- and NLRC4-mediated inflammasomopathies. Anti-IL-1β treatment has been shown to be highly efficient to treat symptoms of most CAPS patients (Koné-Paut et al., 2014) and achieves good responses in some NLRC4-AID patients (Canna et al., 2014, Ionescu et al., 2021, Siahanidou et al., 2019, Volker-Touw et al., 2017). However, in severe NLRC4-AID manifestations MAS and AIFEC, especially during inflammatory flare, inhibition of IL-1β had limited effects (Canna et al., 2017, Moghaddas et al., 2018). Furthermore, canakinumab treatment only partially controls disease in the here described patient and inflammatory episodes still occur (chapter 4.2.1). The factors that determine anti-IL-1β therapy efficacy in individual NLRC4-AID patients remain unclear but will be interesting to investigate, given that within one kindred carrying the same mutation responsiveness to anakinra varied (Volker-Touw et al., 2017).
Although NLRP3 and NLRC4 inflammasome hyperactivation similarly induces caspase-1-mediated cytokine maturation and pyroptosis, the central hallmark of NLRC4-AID is the high and consistent elevation of IL-18 serum levels, which is

not commonly observed in patients with GoF mutations in NLRP3, NLRP1 or pyrin and therefore highlights the important role of IL-18 in the distinct disease pathogenesis (Weiss et al., 2018). A potential explanation for this difference was recently suggested based on differential expression patterns of inflammasome-associated proteins and cytokine precursors in disease-causing immune and non-immune cells in mice. Whereas *Nlrp3* and *Il1b* transcript levels exceed *Nlrc4* and *Il18* in monocytes and neutrophils, gastrointestinal epithelial cells show higher *Il18 and Nlrc4* transcription (Weiss et al., 2018). Therefore, mutation-induced overactivation of NLRP3 results in a predominant IL-1β response, whereas in cell types with high NLRC4 expression, hyperactivation likely produces higher levels of mature IL-18. Indeed, experimental evidence from a mouse model expressing the NLRC4 GoF mutation NLRC4$^{T337S/T337S}$ suggested that chronically elevated IL-18 serum levels largely originate from NLRC4 activation in IECs rather than hematopoietic cells (Weiss et al., 2018). Cellular sources of IL-18 are difficult to determine in humans, however when MDMs from a NLRC4-MAS patient were analysed *ex vivo*, higher levels of IL-18 at baseline and after NLRP3 or NLRC4 stimulation were detected when compared to MDMs from healthy donors and a NOMID patient with NLRP3 GoF mutation (Canna et al., 2014). Therefore, together with murine studies these findings suggest that myeloid and epithelial cells are likely to contribute to NLRC4-driven IL-18 release in humans leading to extremely high serum levels.

Interestingly, literature review of previously reported NLRC4-AID cases shows that if measured, serum IL-18 levels were highly elevated even in patients responsive to anti-IL-1β therapy, which perhaps suggests threshold-dependency. However, it needs to be noted, that the minority of studies performed tests to discriminate between circulating total IL-18 (which may be inactivated by IL-18BP) and free IL-18. Potentially these measurements are therefore less informative values to draw conclusions about functional IL-18 and the magnitude of IL-18 signalling (Novick et al., 2001, Weiss et al., 2018).

Consistently high levels of IL-18 and IL-18BP during a four year observation period were reported in one NLRC4-MAS patients (Canna et al., 2014, Weiss et al., 2018). Given that clinical disease markers were maintained within normal

ranges during the majority of this time, the crucial role of IL-18BP to neutralize IL-18 and prevent disease flares becomes evident. Therefore, it is possible that the clinical phenotype caused by NLRC4 GoF mutations depends on both the strength of NLRC4 autoactivation as well as abundance, functionality and regulation of IL-18BP. If IL-18 levels are sufficiently antagonized, clinical symptoms may be predominantly IL-1β-mediated and efficiently treated with anti-IL-1β therapy. Therefore, genetic predisposition or environmental factors that interfere with this endogenous negative feedback loop may contribute to the disease phenotype, determine the severity of the clinical course and the response to IL-1β inhibition. IL-18 may therefore serve as a promising biomarker for diagnostic purposes, to predict therapy response and disease outcome and additionally represents a promising therapeutic target for NLRC4-MAS and AIFEC patients (Weiss et al., 2018).

Notably, besides cytokine release, murine studies showed that in certain cell types NLRC4 can induce eicosanoid release as well as pyroptotic and apoptotic cell death pathways depending on expression levels of inflammasome effector caspase-1, which may vary between cell types (Lee et al., 2018, Rauch et al., 2017, von Moltke et al., 2012). Therefore, multiple proinflammatory pathways are activated downstream of NLRC4, which may be most efficiently blocked by directly targeting its activation.

Investigating the underlying molecular basis for the variable clinical phenotypes associated with disease-causing NLRC4 mutations remains an interesting subject of future studies. Similarly, a large spectrum of inflammatory manifestations has been described for NLRP3-driven CAPS (Aksentijevich et al., 2007) and missense mutations in pyrin are associated with two distinct clinical presentations: FMF and pyrin-associated autoinflammation with neutrophilic dermatosis (PAAND) (Alghamdi 2017, Masters et al., 2016, Moghaddas et al., 2017, The French et al., 1997).

Due to the limited number of reported NLRC4-AID patients, a clear genotype-phenotype correlation for NLRC4-AID has not yet been established. However, one could hypothesize that depending on residue localization within functional

domains and the induced structural consequences, mutations may differentially impact the interaction with downstream effectors. Consistently, studies in A549 cells showed that NLRC4 H443P (located within the WHD) increasingly interacts with SUG1 and thus promotes caspase-8 dependent apoptosis, which was not observed for two other tested mutations localized within the HD1 (T337S and V341S) (Raghawan et al., 2017). To validate this hypothesis, another reported WHD-resident mutation, S445P, causative of familial FCAS4 in 13 patients could be investigated (Volker-Touw et al., 2017).

Although to date no other patients carrying the homozygous NLRC4 A160T mutation have been reported, the identification of these individuals, observation of their clinical manifestations and molecular disease-causing features will be valuable to confirm the pathogenicity associated with this genotype. Whether variable phenotypes develop in different patients will be an interesting question for future studies. Given the occurrence of heterozygous allele carriers in the general population, homozygous individuals are likely to exist and depending on the environmental challenges and genetic predisposition may develop an inflammatory disease. Therefore, the here reported index case and the presented *in vitro* data raise awareness of this likely pathogenic mutation and provide a molecular basis for future investigations.

7 Outlook

During past decades, several breakthrough discoveries have transformed the field of innate immunity. Starting from the original concept of pathogen detection via recognition of a defined set of PAMPs, emerging evidence increasingly established a number of innate immune sensors as detectors of self-antigens released from damaged host cells (DAMPs) and perturbation of cellular homeostasis (HAMPs). Furthermore, the originally proposed definition of AIDs as distinct monogenic disorders of innate immune system overactivation (McDermott et al., 1999) has been expanded towards integration of multifactorial conditions considering environmental and genetic co-factors and features of autoimmunity and immunodeficiency (Savic et al., 2020).

Studies of monogenic disorders similar to those presented in this thesis were fundamental to foster progress in understanding activating ligands, signalling pathways and regulatory mechanisms involved in PRR signalling.
Especially with regards to complex diseases such as COPA syndrome, understanding the interplay of involved pathogenic pathways and elucidating the molecular mechanisms underlying the incomplete penetrance will aid to further improve currently implemented treatment plans and may provide therapeutic benefit for other inflammatory diseases associated with trafficking defects.

Structural approaches possess a tremendous potential to understand the conformational and functional consequences of disease-causing mutations and provide valuable information for drug development. Structural information for human STING is available and several preclinical small molecule inhibitors targeting STING have been described in the literature. Given the increasing involvement of aberrant cGAS-STING signalling as key driver of several autoinflammatory, stress- and tissue damage-associated conditions, targeted inhibition of this pathway has broad therapeutical implications and future studies in the field are focussed on the development of drug candidates for clinical testing. Importantly, therapeutic efficacy of cGAS-STING inhibitors in the context

of neurodegenerative diseases additionally relies on the compounds ability to penetrate the blood brain barrier, which will have to be considered when clinical candidates are developed.

Although AlphaFold 2 predictions have significantly transformed the field and provide incredible advantage for drug development, assist experimental protein structure determination and foster research of proteins with yet unknown function, its potential to predict “unnatural” destabilizing conformations caused by missense mutations is limited (preprint (Pak et al., 2021)). Further limitations include prediction of multiple conformations of dynamic proteins, protein interactions in complexes and small molecule binding, where experimental methods provide higher accuracy.

In the context of SAVI, aberrant STING signalling occurs in a ligand-independent manner due to mutations proposed to mimic ligand binding or alter polymerization interfaces. The recent description of a novel SAVI variant located within a transmembrane-linker domain (Lin et al., 2021), raises questions regarding the structural consequences that induce STING autoactivation in this case. Thus, experimentally determined structural information of disease-causing STING mutants may provide interesting insight into conformational changes associated with spontaneous STING ER exit that may reveal yet unconsidered approaches to specifically inhibit STING.

Experimentally determined structural data on human NLRC4 WT or AID-causing mutants does not currently exist and is challenging to generate as demonstrated in this thesis. Nevertheless, given that the currently available therapies provide only limited control of NLRC4-driven diseases, future studies are required to develop inhibitors that specifically target NLRC4 and directly block its various proinflammatory downstream effects. However, we do acknowledge that NLRC4-driven diseases are rare pathologies and thus inhibitor development may not be profitable. Therefore, it is hoped that the rhIL-18BP that is currently undergoing clinical investigations will efficiently control NLRC4-AIDs and may provide therapeutic benefit to a broader range of conditions characterized by “high IL-18 states” (Alehashemi et al., 2020).

Despite the significant increase in knowledge over the past decades, studying the molecular consequences associated with genetic defects of AID patients remains an exciting field and together with greatly improved sequencing technologies provides promising future opportunities towards a better understanding of innate immunity.

References

Aaronson D. S. and Horvath C. M. A road map for those who don't know JAK-STAT. Science. 2002; 296: 1653-1655

Abe T. and Barber G. N. Cytosolic-DNA-mediated, STING-dependent proinflammatory gene induction necessitates canonical NF-κB activation through TBK1. J Virol. 2014; 88: 5328-5341

Ablasser A.,Bauernfeind F.,Hartmann G.,Latz E.,Fitzgerald K. A. and Hornung V. RIG-I-dependent sensing of poly(dA:dT) through the induction of an RNA polymerase III–transcribed RNA intermediate. Nature Immunology. 2009; 10: 1065-1072

Ablasser A.,Goldeck M.,Cavlar T.,Deimling T.,Witte G.,Röhl I.,Hopfner K. P.,Ludwig J. and Hornung V. cGAS produces a 2'-5'-linked cyclic dinucleotide second messenger that activates STING. Nature. 2013; 498: 380-384

Adolf F.,Herrmann A.,Hellwig A.,Beck R.,Brügger B. and Wieland F. T. Scission of COPI and COPII vesicles is independent of GTP hydrolysis. Traffic. 2013; 14: 922-932

Adolf F.,Rhiel M.,Hessling B.,Gao Q.,Hellwig A.,Béthune J. and Wieland F. T. Proteomic Profiling of Mammalian COPII and COPI Vesicles. Cell Rep. 2019; 26: 250-265.e255

Agostini L.,Martinon F.,Burns K.,McDermott M. F.,Hawkins P. N. and Tschopp J. NALP3 forms an IL-1beta-processing inflammasome with increased activity in Muckle-Wells autoinflammatory disorder. Immunity. 2004; 20: 319-325

Ahn J.,Ruiz P. and Barber G. N. Intrinsic self-DNA triggers inflammatory disease dependent on STING. J Immunol. 2014; 193: 4634-4642

Ahn J.,Gutman D.,Saijo S. and Barber G. N. STING manifests self DNA-dependent inflammatory disease. Proc Natl Acad Sci U S A. 2012; 109: 19386-19391

Aird E. J.,Lovendahl K. N.,St. Martin A.,Harris R. S. and Gordon W. R. Increasing Cas9-mediated homology-directed repair efficiency through covalent tethering of DNA repair template. Communications Biology. 2018; 1: 54

Akira S.,Uematsu S. and Takeuchi O. Pathogen recognition and innate immunity. Cell. 2006; 124: 783-801

Aksentijevich I.,Putnam C. D.,Remmers E. F.,Mueller J. L.,Le J.,Kolodner R. D.,Moak Z.,Chuang M.,Austin F.,Goldbach-Mansky R.,Hoffman H. M. and Kastner D. L. The clinical continuum of cryopyrinopathies: novel CIAS1 mutations in North American patients and a new cryopyrin model. Arthritis Rheum. 2007; 56: 1273-1285

Aksentijevich I.,Nowak M.,Mallah M.,Chae J. J.,Watford W. T.,Hofmann S. R.,Stein L.,Russo R.,Goldsmith D.,Dent P.,Rosenberg H. F.,Austin F.,Remmers E. F.,Balow J. E., Jr.,Rosenzweig S.,Komarow H.,Shoham N. G.,Wood G.,Jones J.,Mangra N.,Carrero H.,Adams B. S.,Moore T. L.,Schikler K.,Hoffman H.,Lovell D. J.,Lipnick R.,Barron K.,O'Shea J. J.,Kastner D. L. and Goldbach-Mansky R. De novo CIAS1 mutations, cytokine activation, and evidence for genetic heterogeneity in patients with neonatal-onset multisystem inflammatory disease (NOMID): a new member of the expanding family of pyrin-associated autoinflammatory diseases. Arthritis Rheum. 2002; 46: 3340-3348

Alberts B J. A., Lewis J (2002). Molecular Biology of the Cell. New York, Garland Science.

Alehashemi S. and Goldbach-Mansky R. Human Autoinflammatory Diseases Mediated by NLRP3-, Pyrin-, NLRP1-, and NLRC4-Inflammasome Dysregulation Updates on Diagnosis, Treatment, and the Respective Roles of IL-1 and IL-18. Frontiers in Immunology. 2020; 11:

Alexander C. G.,Wanner R.,Johnson C. M.,Breitsprecher D.,Winter G.,Duhr S.,Baaske P. and Ferguson N. Novel microscale approaches for easy, rapid determination of protein stability in academic and commercial settings. Biochim Biophys Acta. 2014; 1844: 2241-2250

Alghamdi M. Familial Mediterranean fever, review of the literature. Clin Rheumatol. 2017; 36: 1707-1713

Allen I. C.,TeKippe E. M.,Woodford R. M.,Uronis J. M.,Holl E. K.,Rogers A. B.,Herfarth H. H.,Jobin C. and Ting J. P. The NLRP3 inflammasome functions as a negative regulator of tumorigenesis during colitis-associated cancer. J Exp Med. 2010; 207: 1045-1056

Allen I. C.,Wilson J. E.,Schneider M.,Lich J. D.,Roberts R. A.,Arthur J. C.,Woodford R. M.,Davis B. K.,Uronis J. M.,Herfarth H. H.,Jobin C.,Rogers A. B. and Ting J. P. NLRP12 suppresses colon inflammation and tumorigenesis through the negative regulation of noncanonical NF-κB signaling. Immunity. 2012; 36: 742-754

Almeida de Jesus A. and Goldbach-Mansky R. Monogenic autoinflammatory diseases: concept and clinical manifestations. Clin Immunol. 2013; 147: 155-174

Almutairi S. M.,Ali A. K.,He W.,Yang D. S.,Ghorbani P.,Wang L.,Fullerton M. D. and Lee S. H. Interleukin-18 up-regulates amino acid transporters and facilitates amino acid-induced mTORC1 activation in natural killer cells. J Biol Chem. 2019; 294: 4644-4655

Ammelburg M.,Frickey T. and Lupas A. N. Classification of AAA+ proteins. J Struct Biol. 2006; 156: 2-11

Andreeva L.,Hiller B.,Kostrewa D.,Lässig C.,de Oliveira Mann C. C.,Jan Drexler D.,Maiser A.,Gaidt M.,Leonhardt H.,Hornung V. and Hopfner K. P. cGAS senses long and HMGB/TFAM-bound U-turn DNA by forming protein-DNA ladders. Nature. 2017; 549: 394-398

Andrei C.,Dazzi C.,Lotti L.,Torrisi M. R.,Chimini G. and Rubartelli A. The secretory route of the leaderless protein interleukin 1beta involves exocytosis of endolysosome-related vesicles. Mol Biol Cell. 1999; 10: 1463-1475

Ank N.,West H. and Paludan S. R. IFN-lambda: novel antiviral cytokines. J Interferon Cytokine Res. 2006; 26: 373-379

Anzalone A. V.,Randolph P. B.,Davis J. R.,Sousa A. A.,Koblan L. W.,Levy J. M.,Chen P. J.,Wilson C.,Newby G. A.,Raguram A. and Liu D. R. Search-and-replace genome editing without double-strand breaks or donor DNA. Nature. 2019; 576: 149-157

Arakel E. C. and Schwappach B. Formation of COPI-coated vesicles at a glance. J Cell Sci. 2018; 131:

Ardito F.,Giuliani M.,Perrone D.,Troiano G. and Lo Muzio L. The crucial role of protein phosphorylation in cell signaling and its use as targeted therapy (Review). Int J Mol Med. 2017; 40: 271-280

Arduini R. M.,Strauch K. L.,Runkel L. A.,Carlson M. M.,Hronowski X.,Foley S. F.,Young C. N.,Cheng W.,Hochman P. S. and Baker D. P. Characterization of a soluble ternary complex formed between human interferon-beta-1a and its receptor chains. Protein Sci. 1999; 8: 1867-1877

Aubrey B. J.,Kelly G. L.,Kueh A. J.,Brennan M. S.,O'Connor L.,Milla L.,Wilcox S.,Tai L.,Strasser A. and Herold M. J. An inducible lentiviral guide RNA platform enables the identification of tumor-essential genes and tumor-promoting mutations in vivo. Cell Rep. 2015; 10: 1422-1432

Aviram N. and Schuldiner M. Targeting and translocation of proteins to the endoplasmic reticulum at a glance. J Cell Sci. 2017; 130: 4079-4085

Bainter W.,Platt C. D.,Park S.-Y.,Stafstrom K.,Wallace J. G.,Peters Z. T.,Massaad M. J.,Becuwe M.,Salinas S. A.,Jones J.,Beaussant-Cohen S.,Jaber F.,Yang J.-S.,Walther T. C.,Orange J. S.,Rao C.,Rakoff-Nahoum S.,Tsokos M.,Naseem S. U. R.,Al-Tamemi S.,Chou J.,Hsu V. W. and Geha R. S. Combined immunodeficiency due to a mutation in the γ1 subunit of the coat protein I complex. The Journal of Clinical Investigation. 2021; 131:

Bakele M.,Joos M.,Burdi S.,Allgaier N.,Pöschel S.,Fehrenbacher B.,Schaller M.,Marcos V.,Kümmerle-Deschner J.,Rieber N.,Borregaard N.,Yazdi A.,Hector A. and Hartl D.

Localization and functionality of the inflammasome in neutrophils. J Biol Chem. 2014; 289: 5320-5329

Baker P. J. and Masters S. L. Generation of Genetic Knockouts in Myeloid Cell Lines Using a Lentiviral CRISPR/Cas9 System. Methods Mol Biol. 2018; 1714: 41-55

Balachandran S.,Roberts P. C.,Brown L. E.,Truong H.,Pattnaik A. K.,Archer D. R. and Barber G. N. Essential Role for the dsRNA-Dependent Protein Kinase PKR in Innate Immunity to Viral Infection. Immunity. 2000; 13: 129-141

Balci S.,Ekinci R. M. K.,de Jesus A. A.,Goldbach-Mansky R. and Yilmaz M. Baricitinib experience on STING-associated vasculopathy with onset in infancy: A representative case from Turkey. Clin Immunol. 2020; 212: 108273

Balka K. R.,Louis C.,Saunders T. L.,Smith A. M.,Calleja D. J.,D'Silva D. B.,Moghaddas F.,Tailler M.,Lawlor K. E.,Zhan Y.,Burns C. J.,Wicks I. P.,Miner J. J.,Kile B. T.,Masters S. L. and De Nardo D. TBK1 and IKKε Act Redundantly to Mediate STING-Induced NF-κB Responses in Myeloid Cells. Cell Reports. 2020; 31: 107492

Ball D. P.,Wang A. E.,Warren C. D.,Wang Q.,Griswold A. R.,Rao S. D. and Bachovchin D. A. Oxidized thioredoxin-1 restrains the NLRP1 inflammasome. bioRxiv. 2021; 2021.2009.2020.461118

Bannykh S. I. and Balch W. E. Membrane dynamics at the endoplasmic reticulum-Golgi interface. J Cell Biol. 1997; 138: 1-4

Bannykh S. I.,Rowe T. and Balch W. E. The organization of endoplasmic reticulum export complexes. J Cell Biol. 1996; 135: 19-35

Bardet J.,Laverdure N.,Fusaro M.,Picard C.,Garnier L.,Viel S.,Collardeau-Frachon S.,Guillebon J.-M. D.,Durieu I.,Casari-Thery C.,Mortamet G.,Laurent A. and Belot A. NLRC4 GOF Mutations, a Challenging Diagnosis from Neonatal Age to Adulthood. Journal of Clinical Medicine. 2021; 10: 4369

Barlowe C. Twenty-five years after coat protein complex II. Mol Biol Cell. 2020; 31: 3-6

Barlowe C.,Orci L.,Yeung T.,Hosobuchi M.,Hamamoto S.,Salama N.,Rexach M. F.,Ravazzola M.,Amherdt M. and Schekman R. COPII: a membrane coat formed by Sec proteins that drive vesicle budding from the endoplasmic reticulum. Cell. 1994; 77: 895-907

Barlowe C. K. and Miller E. A. Secretory Protein Biogenesis and Traffic in the Early Secretory Pathway. Genetics. 2013; 193: 383-410

Barnett K. C.,Coronas-Serna J. M.,Zhou W.,Ernandes M. J.,Cao A.,Kranzusch P. J. and Kagan J. C. Phosphoinositide Interactions Position cGAS at the Plasma Membrane to Ensure Efficient Distinction between Self- and Viral DNA. Cell. 2019; 176: 1432-1446.e1411

Baroja-Mazo A.,Martín-Sánchez F.,Gomez A. I.,Martínez C. M.,Amores-Iniesta J.,Compan V.,Barberà-Cremades M.,Yagüe J.,Ruiz-Ortiz E.,Antón J.,Buján S.,Couillin I.,Brough D.,Arostegui J. I. and Pelegrín P. The NLRP3 inflammasome is released as a particulate danger signal that amplifies the inflammatory response. Nat Immunol. 2014; 15: 738-748

Barrett J. F. and Hoch J. A. Two-component signal transduction as a target for microbial anti-infective therapy. Antimicrob Agents Chemother. 1998; 42: 1529-1536

Barsalou J.,Blincoe A.,Fernandez I.,Dal-Soglio D.,Marchitto L.,Selleri S.,Haddad E.,Benyoucef A. and Touzot F. Rapamycin as an Adjunctive Therapy for NLRC4 Associated Macrophage Activation Syndrome. Frontiers in Immunology. 2018; 9:

Bauernfeind F. G.,Horvath G.,Stutz A.,Alnemri E. S.,MacDonald K.,Speert D.,Fernandes-Alnemri T.,Wu J.,Monks B. G.,Fitzgerald K. A.,Hornung V. and Latz E. Cutting edge: NF-kappaB activating pattern recognition and cytokine receptors license NLRP3 inflammasome activation by regulating NLRP3 expression. J Immunol. 2009; 183: 787-791

Beck R.,Rawet M.,Wieland F. T. and Cassel D. The COPI system: molecular mechanisms and function. FEBS Lett. 2009; 583: 2701-2709

Beck R.,Sun Z.,Adolf F.,Rutz C.,Bassler J.,Wild K.,Sinning I.,Hurt E.,Brügger B.,Béthune J. and Wieland F. Membrane curvature induced by Arf1-GTP is essential for vesicle formation. Proc Natl Acad Sci U S A. 2008; 105: 11731-11736

Berg H. C. (2003). E. coli in motion, Springer-Verlag, New York.

Berger I.,Fitzgerald D. J. and Richmond T. J. Baculovirus expression system for heterologous multiprotein complexes. Nature Biotechnology. 2004; 22: 1583-1587

Bergsten E.,Horne A.,Aricó M.,Astigarraga I.,Egeler R. M.,Filipovich A. H.,Ishii E.,Janka G.,Ladisch S.,Lehmberg K.,McClain K. L.,Minkov M.,Montgomery S.,Nanduri V.,Rosso D. and Henter J. I. Confirmed efficacy of etoposide and dexamethasone in HLH treatment: long-term results of the cooperative HLH-2004 study. Blood. 2017; 130: 2728-2738

Bernoux M.,Burdett H.,Williams S. J.,Zhang X.,Chen C.,Newell K.,Lawrence G. J.,Kobe B.,Ellis J. G.,Anderson P. A. and Dodds P. N. Comparative Analysis of the Flax Immune Receptors L6 and L7 Suggests an Equilibrium-Based Switch Activation Model. The Plant Cell. 2016; 28: 146-159

Béthune J.,Kol M.,Hoffmann J.,Reckmann I.,Brügger B. and Wieland F. Coatomer, the coat protein of COPI transport vesicles, discriminates endoplasmic reticulum residents from p24 proteins. Mol Cell Biol. 2006; 26: 8011-8021

Bi X.,Corpina R. A. and Goldberg J. Structure of the Sec23/24–Sar1 pre-budding complex of the COPII vesicle coat. Nature. 2002; 419: 271-277

Biot-Pelletier D. and Martin V. J. J. Seamless site-directed mutagenesis of the Saccharomyces cerevisiae genome using CRISPR-Cas9. Journal of Biological Engineering. 2016; 10: 6

Bischoff N.,Wimberger S.,Maresca M. and Brakebusch C. Improving Precise CRISPR Genome Editing by Small Molecules: Is there a Magic Potion? Cells. 2020; 9:

Blagitko N.,Schulz U.,Schinzel A. A.,Ropers H. H. and Kalscheuer V. M. gamma2-COP, a novel imprinted gene on chromosome 7q32, defines a new imprinting cluster in the human genome. Hum Mol Genet. 1999; 8: 2387-2396

Blom N.,Sicheritz-Pontén T.,Gupta R.,Gammeltoft S. and Brunak S. Prediction of post-translational glycosylation and phosphorylation of proteins from the amino acid sequence. Proteomics. 2004; 4: 1633-1649

Bogoyevitch M. A. and Kobe B. Uses for JNK: the many and varied substrates of the c-Jun N-terminal kinases. Microbiol Mol Biol Rev. 2006; 70: 1061-1095

Boldin M. P.,Goncharov T. M.,Goltseve Y. V. and Wallach D. Involvement of MACH, a Novel MORT1/FADD-Interacting Protease, in Fas/APO-1- and TNF Receptor–Induced Cell Death. Cell. 1996; 85: 803-815

Bonifacino J. S. and Lippincott-Schwartz J. Coat proteins: shaping membrane transport. Nat Rev Mol Cell Biol. 2003; 4: 409-414

Bossaller L.,Chiang P. I.,Schmidt-Lauber C.,Ganesan S.,Kaiser W. J.,Rathinam V. A.,Mocarski E. S.,Subramanian D.,Green D. R.,Silverman N.,Fitzgerald K. A.,Marshak-Rothstein A. and Latz E. Cutting edge: FAS (CD95) mediates noncanonical IL-1β and IL-18 maturation via caspase-8 in an RIP3-independent manner. J Immunol. 2012; 189: 5508-5512

Boulisfane-El Khalifi S.,Viel S.,Lahoche A.,Fremond M. L.,Lopez J.,Lombard C.,Dubos F.,Reumaux H.,Gnemmi V.,Legendre M.,Crow Y. J.,Thumerelle C. and Belot A. COPA Syndrome as a Cause of Lupus Nephritis. Kidney Int Rep. 2019; 4: 1187-1189

Bousfiha A.,Jeddane L.,Picard C.,Ailal F.,Bobby Gaspar H.,Al-Herz W.,Chatila T.,Crow Y. J.,Cunningham-Rundles C.,Etzioni A.,Franco J. L.,Holland S. M.,Klein C.,Morio T.,Ochs H. D.,Oksenhendler E.,Puck J.,Tang M. L. K.,Tangye S. G.,Torgerson T. R.,Casanova J. L. and Sullivan K. E. The 2017 IUIS Phenotypic Classification for Primary Immunodeficiencies. J Clin Immunol. 2018; 38: 129-143

Bracaglia C.,Gatto A.,Pardeo M.,Lapeyre G.,Ferlin W.,Nelson R.,de Min C. and De Benedetti F. Anti interferon-gamma (IFNγ) monoclonal antibody treatment in a patient carrying an NLRC4 mutation and severe hemophagocytic lymphohistiocytosis. Pediatric Rheumatology Online Journal. 2015; 13: O68-O68

Bradley D. and Beltrao P. Evolution of protein kinase substrate recognition at the active site. PLoS Biol. 2019; 17: e3000341

Bravo R.,Gutierrez T.,Paredes F.,Gatica D.,Rodriguez A. E.,Pedrozo Z.,Chiong M.,Parra V.,Quest A. F.,Rothermel B. A. and Lavandero S. Endoplasmic reticulum: ER stress regulates mitochondrial bioenergetics. Int J Biochem Cell Biol. 2012; 44: 16-20

Bravo R.,Vicencio J. M.,Parra V.,Troncoso R.,Munoz J. P.,Bui M.,Quiroga C.,Rodriguez A. E.,Verdejo H. E.,Ferreira J.,Iglewski M.,Chiong M.,Simmen T.,Zorzano A.,Hill J. A.,Rothermel B. A.,Szabadkai G. and Lavandero S. Increased ER-mitochondrial coupling promotes mitochondrial respiration and bioenergetics during early phases of ER stress. J Cell Sci. 2011; 124: 2143-2152

Brehm A.,Liu Y.,Sheikh A.,Marrero B.,Omoyinmi E.,Zhou Q.,Montealegre G.,Biancotto A.,Reinhardt A.,Almeida de Jesus A.,Pelletier M.,Tsai W. L.,Remmers E. F.,Kardava L.,Hill S.,Kim H.,Lachmann H. J.,Megarbane A.,Chae J. J.,Brady J.,Castillo R. D.,Brown D.,Casano A. V.,Gao L.,Chapelle D.,Huang Y.,Stone D.,Chen Y.,Sotzny F.,Lee C. C.,Kastner D. L.,Torrelo A.,Zlotogorski A.,Moir S.,Gadina M.,McCoy P.,Wesley R.,Rother K. I.,Hildebrand P. W.,Brogan P.,Krüger E.,Aksentijevich I. and Goldbach-Mansky R. Additive loss-of-function proteasome subunit mutations in CANDLE/PRAAS patients promote type I IFN production. J Clin Invest. 2015; 125: 4196-4211

Brennan M.,McDougall C.,Walsh J.,Crow Y. J. and Davidson J. 013. COPA syndrome - a new condition to consider when features of polyarthritis and interstitial lung disease are present. Rheumatology. 2017; 56:

Brill L. M.,Salomon A. R.,Ficarro S. B.,Mukherji M.,Stettler-Gill M. and Peters E. C. Robust phosphoproteomic profiling of tyrosine phosphorylation sites from human T cells using immobilized metal affinity chromatography and tandem mass spectrometry. Anal Chem. 2004; 76: 2763-2772

Brot N. and Weissbach H. Biochemistry of methionine sulfoxide residues in proteins. Biofactors. 1991; 3: 91-96

Broz P. and Dixit V. M. Inflammasomes: mechanism of assembly, regulation and signalling. Nature Reviews Immunology. 2016; 16: 407-420

Broz P.,von Moltke J.,Jones J. W.,Vance R. E. and Monack D. M. Differential requirement for Caspase-1 autoproteolysis in pathogen-induced cell death and cytokine processing. Cell Host Microbe. 2010a; 8: 471-483

Broz P.,Newton K.,Lamkanfi M.,Mariathasan S.,Dixit V. M. and Monack D. M. Redundant roles for inflammasome receptors NLRP3 and NLRC4 in host defense against Salmonella. Journal of Experimental Medicine. 2010b; 207: 1745-1755

Brucklacher-Waldert V.,Ferreira C.,Stebegg M.,Fesneau O.,Innocentin S.,Marie J. C. and Veldhoen M. Cellular Stress in the Context of an Inflammatory Environment Supports TGF-β-Independent T Helper-17 Differentiation. Cell Rep. 2017; 19: 2357-2370

Brunette R. L.,Young J. M.,Whitley D. G.,Brodsky I. E.,Malik H. S. and Stetson D. B. Extensive evolutionary and functional diversity among mammalian AIM2-like receptors. J Exp Med. 2012; 209: 1969-1983

Bürckstümmer T.,Baumann C.,Blüml S.,Dixit E.,Dürnberger G.,Jahn H.,Planyavsky M.,Bilban M.,Colinge J.,Bennett K. L. and Superti-Furga G. An orthogonal proteomic-genomic screen identifies AIM2 as a cytoplasmic DNA sensor for the inflammasome. Nat Immunol. 2009; 10: 266-272

Burdette D. L.,Monroe K. M.,Sotelo-Troha K.,Iwig J. S.,Eckert B.,Hyodo M.,Hayakawa Y. and Vance R. E. STING is a direct innate immune sensor of cyclic di-GMP. Nature. 2011; 478: 515-518

Burrows P. D.,Suematsu S. and Watanabe T. Activation of self-reactive B cells and autoimmune diseases. Rev Immunogenet. 2000; 2: 38-51

Buttmann M.,Merzyn C. and Rieckmann P. Interferon-beta induces transient systemic IP-10/CXCL10 chemokine release in patients with multiple sclerosis. J Neuroimmunol. 2004; 156: 195-203

Buttmann M.,Berberich-Siebelt F.,Serfling E. and Rieckmann P. Interferon-beta is a potent inducer of interferon regulatory factor-1/2-dependent IP-10/CXCL10 expression in primary human endothelial cells. J Vasc Res. 2007; 44: 51-60

Cai S.,Batra S.,Wakamatsu N.,Pacher P. and Jeyaseelan S. NLRC4 inflammasome-mediated production of IL-1β modulates mucosal immunity in the lung against gram-negative bacterial infection. J Immunol. 2012; 188: 5623-5635

Canna S. W.,Girard C.,Malle L.,de Jesus A.,Romberg N.,Kelsen J.,Surrey L. F.,Russo P.,Sleight A.,Schiffrin E.,Gabay C.,Goldbach-Mansky R. and Behrens E. M. Life-threatening NLRC4-associated hyperinflammation successfully treated with IL-18 inhibition. J Allergy Clin Immunol. 2017; 139: 1698-1701

Canna S. W.,de Jesus A. A.,Gouni S.,Brooks S. R.,Marrero B.,Liu Y.,DiMattia M. A.,Zaal K. J.,Sanchez G. A.,Kim H.,Chapelle D.,Plass N.,Huang Y.,Villarino A. V.,Biancotto A.,Fleisher T. A.,Duncan J. A.,O'Shea J. J.,Benseler S.,Grom A.,Deng Z.,Laxer R. M. and Goldbach-Mansky R. An activating NLRC4 inflammasome mutation causes autoinflammation with recurrent macrophage activation syndrome. Nat Genet. 2014; 46: 1140-1146

Cano V.,Moranta D.,Llobet-Brossa E.,Bengoechea J. A. and Garmendia J. Klebsiella pneumoniae triggers a cytotoxic effect on airway epithelial cells. BMC Microbiol. 2009; 9: 156

Carabarin-Lima A.,León-Izurieta L.,Rocha-Gracia R. d. C.,Castañeda-Lucio M.,Torres C.,Gutiérrez-Cazarez Z.,González-Posos S.,Martínez de la Peña C. F.,Martinez-Laguna Y. and Lozano-Zarain P. First evidence of polar flagella in Klebsiella pneumoniae isolated from a patient with neonatal sepsis. Journal of Medical Microbiology. 2016; 65: 729-737

Cardona Gloria Y.,Latz E. and De Nardo D. Generation of Innate Immune Reporter Cells Using Retroviral Transduction. Methods Mol Biol. 2018; 1714: 97-117

Carroll D. Genome Engineering with Targetable Nucleases. Annual Review of Biochemistry. 2014; 83: 409-439

Carvalho F. A.,Nalbantoglu I.,Aitken J. D.,Uchiyama R.,Su Y.,Doho G. H.,Vijay-Kumar M. and Gewirtz A. T. Cytosolic flagellin receptor NLRC4 protects mice against mucosal and systemic challenges. Mucosal Immunol. 2012; 5: 288-298

Cavalli G.,De Luca G.,Campochiaro C.,Della-Torre E.,Ripa M.,Canetti D.,Oltolini C.,Castiglioni B.,Tassan Din C.,Boffini N.,Tomelleri A.,Farina N.,Ruggeri A.,Rovere-Querini P.,Di Lucca G.,Martinenghi S.,Scotti R.,Tresoldi M.,Ciceri F.,Landoni G.,Zangrillo A.,Scarpellini P. and Dagna L. Interleukin-1 blockade with high-dose anakinra in patients with COVID-19, acute respiratory distress syndrome, and hyperinflammation: a retrospective cohort study. Lancet Rheumatol. 2020; 2: e325-e331

Cavlar T.,Deimling T.,Ablasser A.,Hopfner K.-P. and Hornung V. Species-specific detection of the antiviral small-molecule compound CMA by STING. The EMBO Journal. 2013; 32: 1440-1450

Ceballos-Olvera I.,Sahoo M.,Miller M. A.,Del Barrio L. and Re F. Inflammasome-dependent pyroptosis and IL-18 protect against Burkholderia pseudomallei lung infection while IL-1β is deleterious. PLoS Pathog. 2011; 7: e1002452

Chamaillard M.,Hashimoto M.,Horie Y.,Masumoto J.,Qiu S.,Saab L.,Ogura Y.,Kawasaki A.,Fukase K.,Kusumoto S.,Valvano M. A.,Foster S. J.,Mak T. W.,Nuñez G. and Inohara N. An

essential role for NOD1 in host recognition of bacterial peptidoglycan containing diaminopimelic acid. Nat Immunol. 2003; 4: 702-707

Chan T. H.,Lin C. H.,Qi L.,Fei J.,Li Y.,Yong K. J.,Liu M.,Song Y.,Chow R. K.,Ng V. H.,Yuan Y. F.,Tenen D. G.,Guan X. Y. and Chen L. A disrupted RNA editing balance mediated by ADARs (Adenosine DeAminases that act on RNA) in human hepatocellular carcinoma. Gut. 2014; 63: 832-843

Chardin P.,Paris S.,Antonny B.,Robineau S.,Béraud-Dufour S.,Jackson C. L. and Chabre M. A human exchange factor for ARF contains Sec7- and pleckstrin-homology domains. Nature. 1996; 384: 481-484

Chear C. T.,Nallusamy R.,Canna S. W.,Chan K. C.,Baharin M. F.,Hishamshah M.,Ghani H.,Ripen A. M. and Mohamad S. B. A novel de novo NLRC4 mutation reinforces the likely pathogenicity of specific LRR domain mutation. Clin Immunol. 2020; 211: 108328

Chen H.,Pei R.,Zhu W.,Zeng R.,Wang Y.,Wang Y.,Lu M. and Chen X. An alternative splicing isoform of MITA antagonizes MITA-mediated induction of type I IFNs. J Immunol. 2014a; 192: 1162-1170

Chen J. and Chen Z. J. PtdIns4P on dispersed trans-Golgi network mediates NLRP3 inflammasome activation. Nature. 2018; 564: 71-76

Chen K. W.,Groß C. J.,Sotomayor F. V.,Stacey K. J.,Tschopp J.,Sweet M. J. and Schroder K. The neutrophil NLRC4 inflammasome selectively promotes IL-1β maturation without pyroptosis during acute Salmonella challenge. Cell Rep. 2014b; 8: 570-582

Chen M.,Xing Y.,Lu A.,Fang W.,Sun B.,Chen C.,Liao W. and Meng G. Internalized Cryptococcus neoformans Activates the Canonical Caspase-1 and the Noncanonical Caspase-8 Inflammasomes. The Journal of Immunology. 2015; 195: 4962-4972

Chi H. Regulation and function of mTOR signalling in T cell fate decisions. Nature Reviews Immunology. 2012; 12: 325-338

Chikano S.,Sawada K.,Shimoyama T.,Kashiwamura S. I.,Sugihara A.,Sekikawa K.,Terada N.,Nakanishi K. and Okamura H. IL-18 and IL-12 induce intestinal inflammation and fatty liver in mice in an IFN-gamma dependent manner. Gut. 2000; 47: 779-786

Chiu Y. H.,Macmillan J. B. and Chen Z. J. RNA polymerase III detects cytosolic DNA and induces type I interferons through the RIG-I pathway. Cell. 2009; 138: 576-591

Chow V. T. and Quek H. H. HEP-COP, a novel human gene whose product is highly homologous to the alpha-subunit of the yeast coatomer protein complex. Gene. 1996; 169: 223-227

Chu T.-T.,Tu X.,Yang K.,Wu J.,Repa J. J. and Yan N. Tonic prime-boost of STING signalling mediates Niemann–Pick disease type C. Nature. 2021; 596: 570-575

Chuang D. Y.,Simonyi A.,Kotzbauer P. T.,Gu Z. and Sun G. Y. Cytosolic phospholipase A2 plays a crucial role in ROS/NO signaling during microglial activation through the lipoxygenase pathway. Journal of Neuroinflammation. 2015; 12: 199

Ciuffi A. The benefits of integration. Clin Microbiol Infect. 2016; 22: 324-332

Civril F.,Deimling T.,de Oliveira Mann C. C.,Ablasser A.,Moldt M.,Witte G.,Hornung V. and Hopfner K. P. Structural mechanism of cytosolic DNA sensing by cGAS. Nature. 2013; 498: 332-337

Clarke S. L. N.,Robertson L.,Rice G. I.,Seabra L.,Hilliard T. N.,Crow Y. J. and Ramanan A. V. Type 1 interferonopathy presenting as juvenile idiopathic arthritis with interstitial lung disease: report of a new phenotype. Pediatric Rheumatology. 2020; 18: 37

Coburn B.,Sekirov I. and Finlay B. B. Type III secretion systems and disease. Clin Microbiol Rev. 2007; 20: 535-549

Cocco M.,Miglio G.,Giorgis M.,Garella D.,Marini E.,Costale A.,Regazzoni L.,Vistoli G.,Orioli M.,Massulaha-Ahmed R.,Détraz-Durieux I.,Groslambert M.,Py B. F. and Bertinaria M. Design,

Synthesis, and Evaluation of Acrylamide Derivatives as Direct NLRP3 Inflammasome Inhibitors. ChemMedChem. 2016; 11: 1790-1803

Cohen B.,Novick D.,Barak S. and Rubinstein M. Ligand-induced association of the type I interferon receptor components. Mol Cell Biol. 1995; 15: 4208-4214

Cohen I. R. Cell-mediated Autoimmunity: Antigen Reactive Lymphocytes recruit Specific Effector Lymphocytes. Nature New Biology. 1973; 242: 60-61

Cohen M.,Potapov V. and Schreiber G. Four distances between pairs of amino acids provide a precise description of their interaction. PLoS Comput Biol. 2009; 5: e1000470

Cohen P. The origins of protein phosphorylation. Nature Cell Biology. 2002; 4: E127-E130

Colafrancesco S.,Priori R.,Alessandri C.,Perricone C.,Pendolino M.,Picarelli G. and Valesini G. IL-18 Serum Level in Adult Onset Still's Disease: A Marker of Disease Activity. Int J Inflam. 2012; 2012: 156890

Coll R. C.,Hill J. R.,Day C. J.,Zamoshnikova A.,Boucher D.,Massey N. L.,Chitty J. L.,Fraser J. A.,Jennings M. P.,Robertson A. A. B. and Schroder K. MCC950 directly targets the NLRP3 ATP-hydrolysis motif for inflammasome inhibition. Nature Chemical Biology. 2019; 15: 556-559

Contreras I.,Ortiz-Zapater E. and Aniento F. Sorting signals in the cytosolic tail of membrane proteins involved in the interaction with plant ARF1 and coatomer. Plant J. 2004; 38: 685-698

Coppé J. P.,Desprez P. Y.,Krtolica A. and Campisi J. The senescence-associated secretory phenotype: the dark side of tumor suppression. Annu Rev Pathol. 2010; 5: 99-118

Cosson P. and Letourneur F. Coatomer interaction with di-lysine endoplasmic reticulum retention motifs. Science. 1994; 263: 1629-1631

Cox J.,Neuhauser N.,Michalski A.,Scheltema R. A.,Olsen J. V. and Mann M. Andromeda: a peptide search engine integrated into the MaxQuant environment. J Proteome Res. 2011; 10: 1794-1805

Crayne C. B.,Albeituni S.,Nichols K. E. and Cron R. Q. The Immunology of Macrophage Activation Syndrome. Frontiers in Immunology. 2019; 10:

Cristea O. M.,Avrămescu C. S.,Bălășoiu M.,Popescu F. D.,Popescu F. and Amzoiu M. O. Urinary tract infection with Klebsiella pneumoniae in Patients with Chronic Kidney Disease. Curr Health Sci J. 2017; 43: 137-148

Crow Y. J. Type I interferonopathies: a novel set of inborn errors of immunity. Ann N Y Acad Sci. 2011; 1238: 91-98

Crow Y. J. and Stetson D. B. The type I interferonopathies: 10 years on. Nature Reviews Immunology. 2021;

Crow Y. J.,Hayward B. E.,Parmar R.,Robins P.,Leitch A.,Ali M.,Black D. N.,van Bokhoven H.,Brunner H. G.,Hamel B. C.,Corry P. C.,Cowan F. M.,Frints S. G.,Klepper J.,Livingston J. H.,Lynch S. A.,Massey R. F.,Meritet J. F.,Michaud J. L.,Ponsot G.,Voit T.,Lebon P.,Bonthron D. T.,Jackson A. P.,Barnes D. E. and Lindahl T. Mutations in the gene encoding the 3′-5′ DNA exonuclease TREX1 cause Aicardi-Goutières syndrome at the AGS1 locus. Nature Genetics. 2006a; 38: 917-920

Crow Y. J.,Leitch A.,Hayward B. E.,Garner A.,Parmar R.,Griffith E.,Ali M.,Semple C.,Aicardi J.,Babul-Hirji R.,Baumann C.,Baxter P.,Bertini E.,Chandler K. E.,Chitayat D.,Cau D.,Déry C.,Fazzi E.,Goizet C.,King M. D.,Klepper J.,Lacombe D.,Lanzi G.,Lyall H.,Martínez-Frías M. L.,Mathieu M.,McKeown C.,Monier A.,Oade Y.,Quarrell O. W.,Rittey C. D.,Rogers R. C.,Sanchis A.,Stephenson J. B.,Tacke U.,Till M.,Tolmie J. L.,Tomlin P.,Voit T.,Weschke B.,Woods C. G.,Lebon P.,Bonthron D. T.,Ponting C. P. and Jackson A. P. Mutations in genes encoding ribonuclease H2 subunits cause Aicardi-Goutières syndrome and mimic congenital viral brain infection. Nat Genet. 2006b; 38: 910-916

Cruz-Becerra G. and Kadonaga J. T. Enhancement of homology-directed repair with chromatin donor templates in cells. Elife. 2020; 9:

Csizmok V. and Forman-Kay J. D. Complex regulatory mechanisms mediated by the interplay of multiple post-translational modifications. Curr Opin Struct Biol. 2018; 48: 58-67

d'Angelo D. M.,Di Filippo P.,Breda L. and Chiarelli F. Type I Interferonopathies in Children: An Overview. Frontiers in Pediatrics. 2021; 9:

Dai Y.,Liu X.,Zhao Z.,He J. and Yin Q. Stimulator of Interferon Genes-Associated Vasculopathy With Onset in Infancy: A Systematic Review of Case Reports. Front Pediatr. 2020; 8: 577918

Damiano J. S.,Stehlik C.,Pio F.,Godzik A. and Reed J. C. CLAN, a novel human CED-4-like gene. Genomics. 2001; 75: 77-83

Danot O. How 'arm-twisting' by the inducer triggers activation of the MalT transcription factor, a typical signal transduction ATPase with numerous domains (STAND). Nucleic Acids Res. 2015; 43: 3089-3099

Danot O.,Marquenet E.,Vidal-Ingigliardi D. and Richet E. Wheel of Life, Wheel of Death: A Mechanistic Insight into Signaling by STAND Proteins. Structure. 2009; 17: 172-182

Davis R. J. Signal transduction by the JNK group of MAP kinases. Cell. 2000; 103: 239-252

de Carvalho M. G. S.,McCormack A. L.,Olson E.,Ghomashchi F.,Gelb M. H.,Yates J. R., III and Leslie C. C. Identification of Phosphorylation Sites of Human 85-kDa Cytosolic Phospholipase A₂ Expressed in Insect Cells and Present in Human Monocytes (∗). Journal of Biological Chemistry. 1996; 271: 6987-6997

de Figueiredo P.,Polizotto R. S.,Drecktrah D. and Brown W. J. Membrane tubule-mediated reassembly and maintenance of the Golgi complex is disrupted by phospholipase A2 antagonists. Mol Biol Cell. 1999; 10: 1763-1782

de Figueiredo P.,Drecktrah D.,Katzenellenbogen J. A.,Strang M. and Brown W. J. Evidence that phospholipase A₂ activity is required for Golgi complex and trans Golgi network membrane tubulation. Proceedings of the National Academy of Sciences. 1998; 95: 8642-8647

De Nardo D.,Kalvakolanu D. V. and Latz E. (2018a). Immortalization of Murine Bone Marrow-Derived Macrophages. Macrophages: Methods and Protocols. G. Rousselet. New York, NY, Springer New York: 35-49.

De Nardo D.,Balka K. R.,Cardona Gloria Y.,Rao V. R.,Latz E. and Masters S. L. Interleukin-1 receptor-associated kinase 4 (IRAK4) plays a dual role in myddosome formation and Toll-like receptor signaling. J Biol Chem. 2018b; 293: 15195-15207

de Oliveira Mann C. C. and Hopfner K.-P. Nuclear cGAS: guard or prisoner? The EMBO Journal. 2021; 40: e108293

de Oliveira Mann C. C.,Orzalli M. H.,King D. S.,Kagan J. C.,Lee A. S. Y. and Kranzusch P. J. Modular Architecture of the STING C-Terminal Tail Allows Interferon and NF-κB Signaling Adaptation. Cell Reports. 2019; 27: 1165-1175.e1165

Dean N. and Pelham H. R. Recycling of proteins from the Golgi compartment to the ER in yeast. J Cell Biol. 1990; 111: 369-377

Decout A.,Katz J. D.,Venkatraman S. and Ablasser A. The cGAS–STING pathway as a therapeutic target in inflammatory diseases. Nature Reviews Immunology. 2021; 21: 548-569

DeLaney A. A.,Berry C. T.,Christian D. A.,Hart A.,Bjanes E.,Wynosky-Dolfi M. A.,Li X.,Tummers B.,Udalova I. A.,Chen Y. H.,Hershberg U.,Freedman B. D.,Hunter C. A. and Brodsky I. E. Caspase-8 promotes c-Rel–dependent inflammatory cytokine expression and resistance against Toxoplasma gondii. Proceedings of the National Academy of Sciences. 2019; 116: 11926-11935

DeLay M. L.,Turner M. J.,Klenk E. I.,Smith J. A.,Sowders D. P. and Colbert R. A. HLA-B27 misfolding and the unfolded protein response augment interleukin-23 production and are associated with Th17 activation in transgenic rats. Arthritis Rheum. 2009; 60: 2633-2643

Delconte R. B.,Kolesnik T. B.,Dagley L. F.,Rautela J.,Shi W.,Putz E. M.,Stannard K.,Zhang J. G.,Teh C.,Firth M.,Ushiki T.,Andoniou C. E.,Degli-Esposti M. A.,Sharp P. P.,Sanvitale C. E.,Infusini G.,Liau N. P.,Linossi E. M.,Burns C. J.,Carotta S.,Gray D. H.,Seillet C.,Hutchinson D. S.,Belz G. T.,Webb A. I.,Alexander W. S.,Li S. S.,Bullock A. N.,Babon J. J.,Smyth M. J.,Nicholson S. E. and Huntington N. D. CIS is a potent checkpoint in NK cell-mediated tumor immunity. Nat Immunol. 2016; 17: 816-824

Demeulemeester J.,De Rijck J.,Gijsbers R. and Debyser Z. Retroviral integration: Site matters: Mechanisms and consequences of retroviral integration site selection. Bioessays. 2015; 37: 1202-1214

Denes A.,Coutts G.,Lénárt N.,Cruickshank S. M.,Pelegrin P.,Skinner J.,Rothwell N.,Allan S. M. and Brough D. AIM2 and NLRC4 inflammasomes contribute with ASC to acute brain injury independently of NLRP3. Proceedings of the National Academy of Sciences. 2015; 112: 4050-4055

Deng Z.,Law C. S.,Ho F. O.,Wang K. M.,Jones K. D.,Shin J.-S. and Shum A. K. A Defect in Thymic Tolerance Causes T Cell–Mediated Autoimmunity in a Murine Model of COPA Syndrome. The Journal of Immunology. 2020a; ji2000028

Deng Z.,Chong Z.,Law C. S.,Mukai K.,Ho F. O.,Martinu T.,Backes B. J.,Eckalbar W. L.,Taguchi T. and Shum A. K. A defect in COPI-mediated transport of STING causes immune dysregulation in COPA syndrome. J Exp Med. 2020b; 217:

Dethlefsen L.,McFall-Ngai M. and Relman D. A. An ecological and evolutionary perspective on human–microbe mutualism and disease. Nature. 2007; 449: 811-818

Devant P.,Cao A. and Kagan J. C. Evolution-inspired redesign of the LPS receptor caspase-4 into an interleukin-1β–converting enzyme. Science Immunology. 2021; 6: eabh3567

Dick M. S.,Sborgi L.,Rühl S.,Hiller S. and Broz P. ASC filament formation serves as a signal amplification mechanism for inflammasomes. Nature Communications. 2016; 7: 11929

Dickens J. A.,Malzer E.,Chambers J. E. and Marciniak S. J. Pulmonary endoplasmic reticulum stress-scars, smoke, and suffocation. Febs j. 2019; 286: 322-341

Diebolder C. A.,Halff E. F.,Koster A. J.,Huizinga E. G. and Koning R. I. Cryoelectron Tomography of the NAIP5/NLRC4 Inflammasome: Implications for NLR Activation. Structure. 2015; 23: 2349-2357

Diepold A. and Armitage J. P. Type III secretion systems: the bacterial flagellum and the injectisome. Philos Trans R Soc Lond B Biol Sci. 2015; 370:

Digby Z.,Tourlomousis P.,Rooney J.,Boyle J. P.,Bibo-Verdugo B.,Pickering R. J.,Webster S. J.,Monie T. P.,Hopkins L. J.,Kayagaki N.,Salvesen G. S.,Warming S.,Weinert L. and Bryant C. E. Evolutionary loss of inflammasomes in the Carnivora and implications for the carriage of zoonotic infections. Cell Rep. 2021; 36: 109614

Dinarello C. A. Biologic basis for interleukin-1 in disease. Blood. 1996; 87: 2095-2147

Dinarello C. A. Immunological and Inflammatory Functions of the Interleukin-1 Family. Annu Rev Immunol. 2009; 27: 519-550

Dinarello C. A. Overview of the IL-1 family in innate inflammation and acquired immunity. Immunol Rev. 2018; 281: 8-27

Diner E. J.,Burdette D. L.,Wilson S. C.,Monroe K. M.,Kellenberger C. A.,Hyodo M.,Hayakawa Y.,Hammond M. C. and Vance R. E. The innate immune DNA sensor cGAS produces a noncanonical cyclic dinucleotide that activates human STING. Cell Rep. 2013; 3: 1355-1361

Ding J.,Wang K.,Liu W.,She Y.,Sun Q.,Shi J.,Sun H.,Wang D. C. and Shao F. Pore-forming activity and structural autoinhibition of the gasdermin family. Nature. 2016; 535: 111-116

DiStasio A.,Driver A.,Sund K.,Donlin M.,Muraleedharan R. M.,Pooya S.,Kline-Fath B.,Kaufman K. M.,Prows C. A.,Schorry E.,Dasgupta B. and Stottmann R. W. Copb2 is essential for embryogenesis and hypomorphic mutations cause human microcephaly. Hum Mol Genet. 2017; 26: 4836-4848

Dobbs N.,Burnaevskiy N.,Chen D.,Gonugunta V. K.,Alto N. M. and Yan N. STING Activation by Translocation from the ER Is Associated with Infection and Autoinflammatory Disease. Cell Host Microbe. 2015; 18: 157-168

Dodonova S. O.,Aderhold P.,Kopp J.,Ganeva I.,Röhling S.,Hagen W. J. H.,Sinning I.,Wieland F. and Briggs J. A. G. 9Å structure of the COPI coat reveals that the Arf1 GTPase occupies two contrasting molecular environments. Elife. 2017; 6:

Doerflinger M.,Deng Y.,Whitney P.,Salvamoser R.,Engel S.,Kueh A. J.,Tai L.,Bachem A.,Gressier E.,Geoghegan N. D.,Wilcox S.,Rogers K. L.,Garnham A. L.,Dengler M. A.,Bader S. M.,Ebert G.,Pearson J. S.,De Nardo D.,Wang N.,Yang C.,Pereira M.,Bryant C. E.,Strugnell R. A.,Vince J. E.,Pellegrini M.,Strasser A.,Bedoui S. and Herold M. J. Flexible Usage and Interconnectivity of Diverse Cell Death Pathways Protect against Intracellular Infection. Immunity. 2020; 53: 533-547.e537

Dominguez M.,Dejgaard K.,Füllekrug J.,Dahan S.,Fazel A.,Paccaud J. P.,Thomas D. Y.,Bergeron J. J. and Nilsson T. gp25L/emp24/p24 protein family members of the cis-Golgi network bind both COP I and II coatomer. J Cell Biol. 1998; 140: 751-765

Dong X.,Hu X.,Bao Y.,Li G.,Yang X.-d.,Slauch J. M. and Chen L.-F. Brd4 regulates NLRC4 inflammasome activation by facilitating IRF8-mediated transcription of Naips. Journal of Cell Biology. 2021; 220:

Donnelly N.,Gorman A. M.,Gupta S. and Samali A. The eIF2α kinases: their structures and functions. Cell Mol Life Sci. 2013; 70: 3493-3511

Du M. and Chen Z. J. DNA-induced liquid phase condensation of cGAS activates innate immune signaling. Science. 2018; 361: 704-709

Duden R.,Kajikawa L.,Wuestehube L. and Schekman R. ϵ-COP is a structural component of coatomer that functions to stabilize α-COP. The EMBO Journal. 1998; 17: 985-995

Duden R.,Griffiths G.,Frank R.,Argos P. and Kreis T. E. Beta-COP, a 110 kd protein associated with non-clathrin-coated vesicles and the Golgi complex, shows homology to beta-adaptin. Cell. 1991; 64: 649-665

Duncan J. A. and Canna S. W. The NLRC4 Inflammasome. Immunol Rev. 2018; 281: 115-123

Duncan J. A.,Bergstralh D. T.,Wang Y.,Willingham S. B.,Ye Z.,Zimmermann A. G. and Ting J. P. Cryopyrin/NALP3 binds ATP/dATP, is an ATPase, and requires ATP binding to mediate inflammatory signaling. Proc Natl Acad Sci U S A. 2007; 104: 8041-8046

Dunphy G.,Flannery S. M.,Almine J. F.,Connolly D. J.,Paulus C.,Jønsson K. L.,Jakobsen M. R.,Nevels M. M.,Bowie A. G. and Unterholzner L. Non-canonical Activation of the DNA Sensing Adaptor STING by ATM and IFI16 Mediates NF-κB Signaling after Nuclear DNA Damage. Mol Cell. 2018; 71: 745-760.e745

Ebstein F.,Poli Harlowe M. C.,Studencka-Turski M. and Krüger E. Contribution of the Unfolded Protein Response (UPR) to the Pathogenesis of Proteasome-Associated Autoinflammatory Syndromes (PRAAS). Frontiers in Immunology. 2019; 10:

Eckhart L.,Ballaun C.,Uthman A.,Gawlas S.,Buchberger M.,Fischer H. and Tschachler E. Duplication of the caspase-12 prodomain and inactivation of NLRC4/IPAF in the dog. Biochem Biophys Res Commun. 2009; 384: 226-230

Eckhart L.,Ballaun C.,Hermann M.,VandeBerg J. L.,Sipos W.,Uthman A.,Fischer H. and Tschachler E. Identification of novel mammalian caspases reveals an important role of gene loss in shaping the human caspase repertoire. Mol Biol Evol. 2008; 25: 831-841

Edavettal S. C.,Hunter M. J. and Swanson R. V. (2012). Genetic Construct Design and Recombinant Protein Expression for Structural Biology. Structure-Based Drug Discovery. L. W. Tari. Totowa, NJ, Humana Press: 29-47.

Efron B. Bootstrap Methods: Another Look at the Jackknife. The Annals of Statistics. 1979; 7: 1-26, 26

Elinav E.,Strowig T.,Kau A. L.,Henao-Mejia J.,Thaiss C. A.,Booth C. J.,Peaper D. R.,Bertin J.,Eisenbarth S. C.,Gordon J. I. and Flavell R. A. NLRP6 inflammasome regulates colonic microbial ecology and risk for colitis. Cell. 2011; 145: 745-757

Endrizzi M. G.,Hadinoto V.,Growney J. D.,Miller W. and Dietrich W. F. Genomic sequence analysis of the mouse Naip gene array. Genome Res. 2000; 10: 1095-1102

Ergun S. L.,Fernandez D.,Weiss T. M. and Li L. STING Polymer Structure Reveals Mechanisms for Activation, Hyperactivation, and Inhibition. Cell. 2019; 178: 290-301.e210

Eugster A.,Frigerio G.,Dale M. and Duden R. COP I domains required for coatomer integrity, and novel interactions with ARF and ARF-GAP. Embo j. 2000; 19: 3905-3917

Evavold C. L.,Ruan J.,Tan Y.,Xia S.,Wu H. and Kagan J. C. The Pore-Forming Protein Gasdermin D Regulates Interleukin-1 Secretion from Living Macrophages. Immunity. 2018; 48: 35-44.e36

Fakhoury M.,Negrulj R.,Mooranian A. and Al-Salami H. Inflammatory bowel disease: clinical aspects and treatments. J Inflamm Res. 2014; 7: 113-120

Faoagali J. L. Klebsiella urinary tract infection. N Z Med J. 1975; 81: 286-288

Faulstich D.,Auerbach S.,Orci L.,Ravazzola M.,Wegchingel S.,Lottspeich F.,Stenbeck G.,Harter C.,Wieland F. T. and Tschochner H. Architecture of coatomer: molecular characterization of delta-COP and protein interactions within the complex. J Cell Biol. 1996; 135: 53-61

Faustin B.,Lartigue L.,Bruey J. M.,Luciano F.,Sergienko E.,Bailly-Maitre B.,Volkmann N.,Hanein D.,Rouiller I. and Reed J. C. Reconstituted NALP1 inflammasome reveals two-step mechanism of caspase-1 activation. Mol Cell. 2007; 25: 713-724

Feldmeyer L.,Werner S.,French L. E. and Beer H. D. Interleukin-1, inflammasomes and the skin. Eur J Cell Biol. 2010; 89: 638-644

Felsenstein J. Confidence Limits on Phylogenies: An Approach Using the Bootstrap. Evolution. 1985; 39: 783-791

Feng Y.,Lei X.,Zhang L.,Wan H.,Pan H.,Wu J.,Zou M.,Zhu L. and Mi Y. COPB2: a transport protein with multifaceted roles in cancer development and progression. Clinical and Translational Oncology. 2021; 23: 2195-2205

Fermaintt C. S.,Sano K.,Liu Z.,Ishii N.,Seino J.,Dobbs N.,Suzuki T.,Fu Y.-X.,Lehrman M. A.,Matsuo I. and Yan N. A bioactive mammalian disaccharide associated with autoimmunity activates STING-TBK1-dependent immune response. Nature Communications. 2019; 10: 2377

Fernandes-Alnemri T.,Yu J. W.,Datta P.,Wu J. and Alnemri E. S. AIM2 activates the inflammasome and cell death in response to cytoplasmic DNA. Nature. 2009; 458: 509-513

Fiedler K.,Veit M.,Stamnes M. A. and Rothman J. E. Bimodal interaction of coatomer with the p24 family of putative cargo receptors. Science. 1996; 273: 1396-1399

Fihn S. D. Clinical practice. Acute uncomplicated urinary tract infection in women. N Engl J Med. 2003; 349: 259-266

Ford E. and Thanos D. The transcriptional code of human IFN-beta gene expression. Biochim Biophys Acta. 2010; 1799: 328-336

Fouts D. E.,Tyler H. L.,DeBoy R. T.,Daugherty S.,Ren Q.,Badger J. H.,Durkin A. S.,Huot H.,Shrivastava S.,Kothari S.,Dodson R. J.,Mohamoud Y.,Khouri H.,Roesch L. F.,Krogfelt K. A.,Struve C.,Triplett E. W. and Methé B. A. Complete genome sequence of the N2-fixing broad host range endophyte Klebsiella pneumoniae 342 and virulence predictions verified in mice. PLoS Genet. 2008; 4: e1000141

Fox S.,Goswami C.,Holden M.,Connolly J. P. R.,Mordue J.,O'Boyle N.,Roe A.,Connor M.,Leanord A. and Evans T. J. A highly conserved complete accessory Escherichia coli type III secretion system 2 is widespread in bloodstream isolates of the ST69 lineage. Scientific Reports. 2020; 10: 4135

Franchi L.,Warner N.,Viani K. and Nuñez G. Function of Nod-like receptors in microbial recognition and host defense. Immunol Rev. 2009; 227: 106-128

Franklin B. S.,Bossaller L.,De Nardo D.,Ratter J. M.,Stutz A.,Engels G.,Brenker C.,Nordhoff M.,Mirandola S. R.,Al-Amoudi A.,Mangan M. S.,Zimmer S.,Monks B. G.,Fricke M.,Schmidt R. E.,Espevik T.,Jones B.,Jarnicki A. G.,Hansbro P. M.,Busto P.,Marshak-Rothstein A.,Hornemann S.,Aguzzi A.,Kastenmüller W. and Latz E. The adaptor ASC has extracellular and 'prionoid' activities that propagate inflammation. Nature Immunology. 2014; 15: 727-737

Freed D.,Stevens E. L. and Pevsner J. Somatic mosaicism in the human genome. Genes (Basel). 2014; 5: 1064-1094

Freeman L.,Guo H.,David C. N.,Brickey W. J.,Jha S. and Ting J. P.-Y. NLR members NLRC4 and NLRP3 mediate sterile inflammasome activation in microglia and astrocytes. Journal of Experimental Medicine. 2017; 214: 1351-1370

Frémond M.-L. and Nathan N. COPA syndrome, 5 years after: Where are we? Joint Bone Spine. 2021a; 88: 105070

Fremond M. L.,Legendre M.,Fayon M.,Clement A.,Filhol-Blin E.,Richard N.,Berdah L.,Roullaud S.,Rice G. I.,Bondet V.,Duffy D.,Sileo C.,Ducou le Pointe H.,Begueret H.,Coulomb A.,Neven B.,Amselem S.,Crow Y. and Nathan N. Use of ruxolitinib in COPA syndrome manifesting as life-threatening alveolar haemorrhage. Thorax. 2020; 75: 92-95

Frémond M. L.,Rodero M. P.,Jeremiah N.,Belot A.,Jeziorski E.,Duffy D.,Bessis D.,Cros G.,Rice G. I.,Charbit B.,Hulin A.,Khoudour N.,Caballero C. M.,Bodemer C.,Fabre M.,Berteloot L.,Le Bourgeois M.,Reix P.,Walzer T.,Moshous D.,Blanche S.,Fischer A.,Bader-Meunier B.,Rieux-Laucat F.,Crow Y. J. and Neven B. Efficacy of the Janus kinase 1/2 inhibitor ruxolitinib in the treatment of vasculopathy associated with TMEM173-activating mutations in 3 children. J Allergy Clin Immunol. 2016; 138: 1752-1755

Frémond M. L.,Hadchouel A.,Berteloot L.,Melki I.,Bresson V.,Barnabei L.,Jeremiah N.,Belot A.,Bondet V.,Brocq O.,Chan D.,Dagher R.,Dubus J. C.,Duffy D.,Feuillet-Soummer S.,Fusaro M.,Gattorno M.,Insalaco A.,Jeziorski E.,Kitabayashi N.,Lopez-Corbeto M.,Mazingue F.,Morren M. A.,Rice G. I.,Rivière J. G.,Seabra L.,Sirvente J.,Soler-Palacin P.,Stremler-Le Bel N.,Thouvenin G.,Thumerelle C.,Van Aerde E.,Volpi S.,Willcocks S.,Wouters C.,Breton S.,Molina T.,Bader-Meunier B.,Moshous D.,Fischer A.,Blanche S.,Rieux-Laucat F.,Crow Y. J. and Neven B. Overview of STING-Associated Vasculopathy with Onset in Infancy (SAVI) Among 21 Patients. J Allergy Clin Immunol Pract. 2021b; 9: 803-818.e811

Fukui R.,Saitoh S.,Matsumoto F.,Kozuka-Hata H.,Oyama M.,Tabeta K.,Beutler B. and Miyake K. Unc93B1 biases Toll-like receptor responses to nucleic acid in dendritic cells toward DNA- but against RNA-sensing. J Exp Med. 2009; 206: 1339-1350

Fukui R.,Saitoh S.-I.,Kanno A.,Onji M.,Shibata T.,Ito A.,Onji M.,Matsumoto M.,Akira S.,Yoshida N. and Miyake K. Unc93B1 Restricts Systemic Lethal Inflammation by Orchestrating Toll-like Receptor 7 and 9 Trafficking. Immunity. 2011; 35: 69-81

Futatsumori M.,Kasai K.,Takatsu H.,Shin H. W. and Nakayama K. Identification and characterization of novel isoforms of COP I subunits. J Biochem. 2000; 128: 793-801

Fye J. M.,Orebaugh C. D.,Coffin S. R.,Hollis T. and Perrino F. W. Dominant mutation of the TREX1 exonuclease gene in lupus and Aicardi-Goutieres syndrome. J Biol Chem. 2011; 286: 32373-32382

Gaidt M. M.,Ebert T. S.,Chauhan D.,Ramshorn K.,Pinci F.,Zuber S.,O'Duill F.,Schmid-Burgk J. L.,Hoss F.,Buhmann R.,Wittmann G.,Latz E.,Subklewe M. and Hornung V. The DNA Inflammasome in Human Myeloid Cells Is Initiated by a STING-Cell Death Program Upstream of NLRP3. Cell. 2017; 171: 1110-1124.e1118

Gall A.,Treuting P.,Elkon K. B.,Loo Y. M.,Gale M., Jr.,Barber G. N. and Stetson D. B. Autoimmunity initiates in nonhematopoietic cells and progresses via lymphocytes in an interferon-dependent autoimmune disease. Immunity. 2012; 36: 120-131

Gao P.,Ascano M.,Wu Y.,Barchet W.,Gaffney B. L.,Zillinger T.,Serganov A. A.,Liu Y.,Jones R. A.,Hartmann G.,Tuschl T. and Patel D. J. Cyclic [G(2',5')pA(3',5')p] is the metazoan second messenger produced by DNA-activated cyclic GMP-AMP synthase. Cell. 2013a; 153: 1094-1107

Gao P.,Ascano M.,Zillinger T.,Wang W.,Dai P.,Serganov A. A.,Gaffney B. L.,Shuman S.,Jones R. A.,Deng L.,Hartmann G.,Barchet W.,Tuschl T. and Patel D. J. Structure-function analysis of STING activation by c[G(2',5')pA(3',5')p] and targeting by antiviral DMXAA. Cell. 2013b; 154: 748-762

Gao P.,Lyu Q.,Ghanam A. R.,Lazzarotto C. R.,Newby G. A.,Zhang W.,Choi M.,Slivano O. J.,Holden K.,Walker J. A.,Kadina A. P.,Munroe R. J.,Abratte C. M.,Schimenti J. C.,Liu D. R.,Tsai S. Q.,Long X. and Miano J. M. Prime editing in mice reveals the essentiality of a single base in driving tissue-specific gene expression. Genome Biology. 2021; 22: 83

Gao W.,Yang J.,Liu W.,Wang Y. and Shao F. Site-specific phosphorylation and microtubule dynamics control Pyrin inflammasome activation. Proc Natl Acad Sci U S A. 2016; 113: E4857-4866

Geddes B. J.,Wang L.,Huang W. J.,Lavellee M.,Manji G. A.,Brown M.,Jurman M.,Cao J.,Morgenstern J.,Merriam S.,Glucksmann M. A.,DiStefano P. S. and Bertin J. Human CARD12 is a novel CED4/Apaf-1 family member that induces apoptosis. Biochem Biophys Res Commun. 2001; 284: 77-82

Gentili M.,Lahaye X.,Nadalin F.,Nader G. P. F.,Puig Lombardi E.,Herve S.,De Silva N. S.,Rookhuizen D. C.,Zueva E.,Goudot C.,Maurin M.,Bochnakian A.,Amigorena S.,Piel M.,Fachinetti D.,Londoño-Vallejo A. and Manel N. The N-Terminal Domain of cGAS Determines Preferential Association with Centromeric DNA and Innate Immune Activation in the Nucleus. Cell Reports. 2019; 26: 2377-2393.e2313

Geurts M. H.,de Poel E.,Pleguezuelos-Manzano C.,Carrillo L.,Andersson-Rolf A.,Boretto M.,Beekman J. M. and Clevers H. Evaluating CRISPR-based Prime Editing for cancer modeling and CFTR repair in intestinal organoids. bioRxiv. 2020; 2020.2010.2005.325837

Gillespie J.,Mathews R. and McDermott M. F. Rilonacept in the management of cryopyrin-associated periodic syndromes (CAPS). J Inflamm Res. 2010; 3: 1-8

Girardin S. E.,Boneca I. G.,Viala J.,Chamaillard M.,Labigne A.,Thomas G.,Philpott D. J. and Sansonetti P. J. Nod2 is a general sensor of peptidoglycan through muramyl dipeptide (MDP) detection. J Biol Chem. 2003; 278: 8869-8872

Giuliano C. J.,Lin A.,Girish V. and Sheltzer J. M. Generating Single Cell–Derived Knockout Clones in Mammalian Cells with CRISPR/Cas9. Current Protocols in Molecular Biology. 2019; 128: e100

Glick B. S. and Nakano A. Membrane traffic within the Golgi apparatus. Annu Rev Cell Dev Biol. 2009; 25: 113-132

Gluck S.,Guey B.,Gulen M. F.,Wolter K.,Kang T. W.,Schmacke N. A.,Bridgeman A.,Rehwinkel J.,Zender L. and Ablasser A. Innate immune sensing of cytosolic chromatin fragments through cGAS promotes senescence. Nat Cell Biol. 2017; 19: 1061-1070

Goddard A. V. G. (2017). A Novel NLRC4 Mutation Treated With Bone Marrow Transplantation. Immune Deficiency & Dysregulation North American Conference, Seattle, Clinical Immunology Society.

Goldbach-Mansky R.,Dailey N. J.,Canna S. W.,Gelabert A.,Jones J.,Rubin B. I.,Kim H. J.,Brewer C.,Zalewski C.,Wiggs E.,Hill S.,Turner M. L.,Karp B. I.,Aksentijevich I.,Pucino F.,Penzak S. R.,Haverkamp M. H.,Stein L.,Adams B. S.,Moore T. L.,Fuhlbrigge R. C.,Shaham B.,Jarvis J. N.,O'Neil K.,Vehe R. K.,Beitz L. O.,Gardner G.,Hannan W. P.,Warren R. W.,Horn W.,Cole J. L.,Paul S. M.,Hawkins P. N.,Pham T. H.,Snyder C.,Wesley R. A.,Hoffmann S. C.,Holland S. M.,Butman J. A. and Kastner D. L. Neonatal-onset multisystem inflammatory disease responsive to interleukin-1beta inhibition. N Engl J Med. 2006; 355: 581-592

Goldberg J. Structural basis for activation of ARF GTPase: mechanisms of guanine nucleotide exchange and GTP-myristoyl switching. Cell. 1998; 95: 237-248

Golgi C. On the structure of the nerve cells of the spinal ganglia. 1898. J Microsc. 1989; 155: 9-14

Gommel D. U.,Memon A. R.,Heiss A.,Lottspeich F.,Pfannstiel J.,Lechner J.,Reinhard C.,Helms J. B.,Nickel W. and Wieland F. T. Recruitment to Golgi membranes of ADP-ribosylation factor 1 is mediated by the cytoplasmic domain of p23. Embo j. 2001; 20: 6751-6760

Gonugunta V. K.,Sakai T.,Pokatayev V.,Yang K.,Wu J.,Dobbs N. and Yan N. Trafficking-Mediated STING Degradation Requires Sorting to Acidified Endolysosomes and Can Be Targeted to Enhance Anti-tumor Response. Cell Rep. 2017; 21: 3234-3242

Goodall J. C.,Wu C.,Zhang Y.,McNeill L.,Ellis L.,Saudek V. and Gaston J. S. Endoplasmic reticulum stress-induced transcription factor, CHOP, is crucial for dendritic cell IL-23 expression. Proc Natl Acad Sci U S A. 2010; 107: 17698-17703

Gosavi P.,Houghton F. J.,McMillan P. J.,Hanssen E. and Gleeson P. A. The Golgi ribbon in mammalian cells negatively regulates autophagy by modulating mTOR activity. J Cell Sci. 2018; 131:

Gram A. M.,Wright J. A.,Pickering R. J.,Lam N. L.,Booty L. M.,Webster S. J. and Bryant C. E. Salmonella Flagellin Activates NAIP/NLRC4 and Canonical NLRP3 Inflammasomes in Human Macrophages. The Journal of Immunology. 2020; ji2000382

Gringhuis S. I.,Kaptein T. M.,Wevers B. A.,Theelen B.,van der Vlist M.,Boekhout T. and Geijtenbeek T. B. Dectin-1 is an extracellular pathogen sensor for the induction and processing of IL-1β via a noncanonical caspase-8 inflammasome. Nat Immunol. 2012; 13: 246-254

Gu J. and Lieber M. R. Mechanistic flexibility as a conserved theme across 3 billion years of nonhomologous DNA end-joining. Genes Dev. 2008; 22: 411-415

Guan Y.,Liu H.,Tang X.,Xu H.,Peng Y.,Zhou C. and Zhao S. Effective sirolimus treatment of 2 COPA syndrome patients. The Journal of Allergy and Clinical Immunology: In Practice. 2021; 9: 999-1001.e1001

Guey B.,Wischnewski M.,Decout A.,Makasheva K.,Kaynak M.,Sakar M. S.,Fierz B. and Ablasser A. BAF restricts cGAS on nuclear DNA to prevent innate immune activation. Science. 2020; 369: 823-828

Gui X.,Yang H.,Li T.,Tan X.,Shi P.,Li M.,Du F. and Chen Z. J. Autophagy induction via STING trafficking is a primordial function of the cGAS pathway. Nature. 2019; 567: 262-266

Gul E.,Sayar E. H.,Gungor B.,Eroglu F. K.,Surucu N.,Keles S.,Guner S. N.,Findik S.,Alpdundar E.,Ayanoglu I. C.,Kayaoglu B.,Geckin B. N.,Sanli H. A.,Kahraman T.,Yakicier C.,Muftuoglu M.,Oguz B.,Cagdas Ayvaz D. N.,Gursel I.,Ozen S.,Reisli I. and Gursel M. Type I IFN-related NETosis in ataxia telangiectasia and Artemis deficiency. J Allergy Clin Immunol. 2018; 142: 246-257

Gulen M. F.,Koch U.,Haag S. M.,Schuler F.,Apetoh L.,Villunger A.,Radtke F. and Ablasser A. Signalling strength determines proapoptotic functions of STING. Nature Communications. 2017; 8: 427

Guo H.,Callaway J. B. and Ting J. P. Inflammasomes: mechanism of action, role in disease, and therapeutics. Nat Med. 2015; 21: 677-687

Gupta K.,Hooton T. M. and Stamm W. E. Increasing antimicrobial resistance and the management of uncomplicated community-acquired urinary tract infections. Ann Intern Med. 2001; 135: 41-50

Haag S. M.,Gulen M. F.,Reymond L.,Gibelin A.,Abrami L.,Decout A.,Heymann M.,van der Goot F. G.,Turcatti G.,Behrendt R. and Ablasser A. Targeting STING with covalent small-molecule inhibitors. Nature. 2018; 559: 269-273

Hahn W. O.,Butler N. S.,Lindner S. E.,Akilesh H. M.,Sather D. N.,Kappe S. H.,Hamerman J. A.,Gale M., Jr.,Liles W. C. and Pepper M. cGAS-mediated control of blood-stage malaria promotes Plasmodium-specific germinal center responses. JCI Insight. 2018; 3:

Halff E. F.,Diebolder C. A.,Versteeg M.,Schouten A.,Brondijk T. H. C. and Huizinga E. G. Formation and Structure of a NAIP5-NLRC4 Inflammasome Induced by Direct Interactions with Conserved N- and C-terminal Regions of Flagellin*. Journal of Biological Chemistry. 2012; 287: 38460-38472

Han J. P.,Chang Y. J.,Song D. W.,Choi B. S.,Koo O. J.,Yi S. Y.,Park T. S. and Yeom S. C. High Homology-Directed Repair Using Mitosis Phase and Nucleus Localizing Signal. Int J Mol Sci. 2020; 21:

Hansen K.,Prabakaran T.,Laustsen A.,Jørgensen S. E.,Rahbæk S. H.,Jensen S. B.,Nielsen R.,Leber J. H.,Decker T.,Horan K. A.,Jakobsen M. R. and Paludan S. R. Listeria monocytogenes induces IFNβ expression through an IFI16-, cGAS- and STING-dependent pathway. The EMBO Journal. 2014; 33: 1654-1666

Hanson P. I. and Whiteheart S. W. AAA+ proteins: have engine, will work. Nature Reviews Molecular Cell Biology. 2005; 6: 519-529

Hara-Kuge S.,Kuge O.,Orci L.,Amherdt M.,Ravazzola M.,Wieland F. T. and Rothman J. E. En bloc incorporation of coatomer subunits during the assembly of COP-coated vesicles. J Cell Biol. 1994; 124: 883-892

Harding S. M.,Benci J. L.,Irianto J.,Discher D. E.,Minn A. J. and Greenberg R. A. Mitotic progression following DNA damage enables pattern recognition within micronuclei. Nature. 2017; 548: 466-470

Harrison M. M.,Jenkins B. V.,O'Connor-Giles K. M. and Wildonger J. A CRISPR view of development. Genes & Development. 2014; 28: 1859-1872

Harrison-Lavoie K. J.,Lewis V. A.,Hynes G. M.,Collison K. S.,Nutland E. and Willison K. R. A 102 kDa subunit of a Golgi-associated particle has homology to beta subunits of trimeric G proteins. Embo j. 1993; 12: 2847-2853

Harter C. R. C. (2002). The Secretory Pathway From History to the State of the Art. . Fusion of Biological Membranes and Related Problems. F. S. Hilderson H. Subcellular Biochemistry, Springer, Boston, MA. vol 34.

Hartmann G. Nucleic Acid Immunity. Adv Immunol. 2017; 133: 121-169

Harton J. A.,Cressman D. E.,Chin K. C.,Der C. J. and Ting J. P. GTP binding by class II transactivator: role in nuclear import. Science. 1999; 285: 1402-1405

Hasnain S. Z.,Lourie R.,Das I.,Chen A. C. and McGuckin M. A. The interplay between endoplasmic reticulum stress and inflammation. Immunol Cell Biol. 2012; 90: 260-270

Hauri H.-P. and Schweizer A. The endoplasmic reticulum—Golgi intermediate compartment. Current Opinion in Cell Biology. 1992; 4: 600-608

Hayes C. L.,Dong J.,Galipeau H. J.,Jury J.,McCarville J.,Huang X.,Wang X. Y.,Naidoo A.,Anbazhagan A. N.,Libertucci J.,Sheridan C.,Dudeja P. K.,Bowdish D. M. E.,Surette M. G. and Verdu E. F. Commensal microbiota induces colonic barrier structure and functions that contribute to homeostasis. Sci Rep. 2018; 8: 14184

He M.,Cornelis M. C.,Kraft P.,van Dam R. M.,Sun Q.,Laurie C. C.,Mirel D. B.,Chasman D. I.,Ridker P. M.,Hunter D. J.,Hu F. B. and Qi L. Genome-wide association study identifies variants at the IL18-BCO2 locus associated with interleukin-18 levels. Arterioscler Thromb Vasc Biol. 2010; 30: 885-890

Heilig R.,Dick M. S.,Sborgi L.,Meunier E.,Hiller S. and Broz P. The Gasdermin-D pore acts as a conduit for IL-1β secretion in mice. Eur J Immunol. 2018; 48: 584-592

Helenius A. and Aebi M. Intracellular functions of N-linked glycans. Science. 2001; 291: 2364-2369

Hetz C. The unfolded protein response: controlling cell fate decisions under ER stress and beyond. Nature Reviews Molecular Cell Biology. 2012; 13: 89-102

Hillis D. M. and Bull J. J. An Empirical Test of Bootstrapping as a Method for Assessing Confidence in Phylogenetic Analysis. Systematic Biology. 1993; 42: 182-192

Hisamatsu T.,Suzuki M.,Reinecker H. C.,Nadeau W. J.,McCormick B. A. and Podolsky D. K. CARD15/NOD2 functions as an antibacterial factor in human intestinal epithelial cells. Gastroenterology. 2003; 124: 993-1000

Hiscott J.,Marois J.,Garoufalis J.,D'Addario M.,Roulston A.,Kwan I.,Pepin N.,Lacoste J.,Nguyen H.,Bensi G. and et al., Characterization of a functional NF-kappa B site in the human interleukin 1 beta promoter: evidence for a positive autoregulatory loop. Mol Cell Biol. 1993; 13: 6231-6240

Hochheiser I.,Pilsl M.,Hagelueken G.,Moecking J.,Marleaux M.,Brinkschulte R.,Latz E.,Engel C. and Geyer M. (2021). Cryo-EM structure of the NLRP3 decamer bound to the cytokine release inhibitory drug CRID3, bioRxiv.

Hoffman H. M.,Mueller J. L.,Broide D. H.,Wanderer A. A. and Kolodner R. D. Mutation of a new gene encoding a putative pyrin-like protein causes familial cold autoinflammatory syndrome and Muckle–Wells syndrome. Nature Genetics. 2001; 29: 301-305

Hoffman H. M.,Throne M. L.,Amar N. J.,Sebai M.,Kivitz A. J.,Kavanaugh A.,Weinstein S. P.,Belomestnov P.,Yancopoulos G. D.,Stahl N. and Mellis S. J. Efficacy and safety of rilonacept (interleukin-1 Trap) in patients with cryopyrin-associated periodic syndromes: results from two sequential placebo-controlled studies. Arthritis Rheum. 2008; 58: 2443-2452

Hopfner K.-P. and Hornung V. Molecular mechanisms and cellular functions of cGAS–STING signalling. Nature Reviews Molecular Cell Biology. 2020; 21: 501-521

Hornung V.,Ablasser A.,Charrel-Dennis M.,Bauernfeind F.,Horvath G.,Caffrey D. R.,Latz E. and Fitzgerald K. A. AIM2 recognizes cytosolic dsDNA and forms a caspase-1-activating inflammasome with ASC. Nature. 2009; 458: 514-518

Hornung V.,Ellegast J.,Kim S.,Brzózka K.,Jung A.,Kato H.,Poeck H.,Akira S.,Conzelmann K. K.,Schlee M.,Endres S. and Hartmann G. 5'-Triphosphate RNA is the ligand for RIG-I. Science. 2006; 314: 994-997

Hou J. K.,Abraham B. and El-Serag H. Dietary intake and risk of developing inflammatory bowel disease: a systematic review of the literature. Am J Gastroenterol. 2011; 106: 563-573

Hu B.,Elinav E.,Huber S.,Booth C. J.,Strowig T.,Jin C.,Eisenbarth S. C. and Flavell R. A. Inflammation-induced tumorigenesis in the colon is regulated by caspase-1 and NLRC4. Proc Natl Acad Sci U S A. 2010; 107: 21635-21640

Hu J.,Zhu Y.,Zhang J. Z.,Zhang R. G. and Li H. M. A Novel Mutation in the Pyrin Domain of the NOD-like Receptor Family Pyrin Domain Containing Protein 3 in Muckle-Wells Syndrome. Chin Med J (Engl). 2017; 130: 586-593

Hu S.,Sun H.,Yin L.,Li J.,Mei S.,Xu F.,Wu C.,Liu X.,Zhao F.,Zhang D.,Huang Y.,Ren L.,Cen S.,Wang J.,Liang C. and Guo F. PKR-dependent cytosolic cGAS foci are necessary for intracellular DNA sensing. Sci Signal. 2019; 12:

Hu Y.,Benedict M. A.,Ding L. and Núñez G. Role of cytochrome c and dATP/ATP hydrolysis in Apaf-1-mediated caspase-9 activation and apoptosis. Embo j. 1999; 18: 3586-3595

Hu Z.,Shi Z.,Guo X.,Jiang B.,Wang G.,Luo D.,Chen Y. and Zhu Y.-S. Ligase IV inhibitor SCR7 enhances gene editing directed by CRISPR–Cas9 and ssODN in human cancer cells. Cell & Bioscience. 2018; 8: 12

Hu Z.,Zhou Q.,Zhang C.,Fan S.,Cheng W.,Zhao Y.,Shao F.,Wang H.-W.,Sui S.-F. and Chai J. Structural and biochemical basis for induced self-propagation of NLRC4. Science. 2015; 350: 399-404

Hu Z.,Yan C.,Liu P.,Huang Z.,Ma R.,Zhang C.,Wang R.,Zhang Y.,Martinon F.,Miao D.,Deng H.,Wang J.,Chang J. and Chai J. Crystal structure of NLRC4 reveals its autoinhibition mechanism. Science. 2013; 341: 172-175

Huang M.,Weissman J. T.,Beraud-Dufour S.,Luan P.,Wang C.,Chen W.,Aridor M.,Wilson I. A. and Balch W. E. Crystal structure of Sar1-GDP at 1.7 A resolution and the role of the NH2 terminus in ER export. J Cell Biol. 2001; 155: 937-948

Huang Y.-H.,Liu X.-Y.,Du X.-X.,Jiang Z.-F. and Su X.-D. (2012) The structural basis for the sensing and binding of cyclic di-GMP by STING. Nature structural & molecular biology 19, 728-730 DOI: 10.1038/nsmb.2333

Hughson F. M. Copy coats: COPI mimics clathrin and COPII. Cell. 2010; 142: 19-21

Hugot J. P.,Chamaillard M.,Zouali H.,Lesage S.,Cézard J. P.,Belaiche J.,Almer S.,Tysk C.,O'Morain C. A.,Gassull M.,Binder V.,Finkel Y.,Cortot A.,Modigliani R.,Laurent-Puig P.,Gower-Rousseau C.,Macry J.,Colombel J. F.,Sahbatou M. and Thomas G. Association of NOD2 leucine-rich repeat variants with susceptibility to Crohn's disease. Nature. 2001; 411: 599-603

Huh J. W.,Shibata T.,Hwang M.,Kwon E. H.,Jang M. S.,Fukui R.,Kanno A.,Jung D. J.,Jang M. H.,Miyake K. and Kim Y. M. UNC93B1 is essential for the plasma membrane localization and signaling of Toll-like receptor 5. Proc Natl Acad Sci U S A. 2014; 111: 7072-7077

Inohara N. and Nuñez G. The NOD: a signaling module that regulates apoptosis and host defense against pathogens. Oncogene. 2001; 20: 6473-6481

Ionescu D.,Peñín-Franch A.,Mensa-Vilaró A.,Castillo P.,Hurtado-Navarro L.,Molina-López C.,Romero-Chala S.,Plaza S.,Fabregat V.,Buján S.,Marques J.,Casals F.,Yagüe J.,Oliva B.,Fernández-Pereira L. M.,Pelegrín P. and Aróstegui J. I. First Description of Late-Onset Autoinflammatory Disease Due to Somatic NLRC4 Mosaicism. Arthritis Rheumatol. 2021;

Ishikawa H. and Barber G. N. STING is an endoplasmic reticulum adaptor that facilitates innate immune signalling. Nature. 2008; 455: 674-678

Ishikawa H.,Ma Z. and Barber G. N. STING regulates intracellular DNA-mediated, type I interferon-dependent innate immunity. Nature. 2009; 461: 788-792

Ivashkiv L. B. and Donlin L. T. Regulation of type I interferon responses. Nat Rev Immunol. 2014; 14: 36-49

Iyer L. M.,Leipe D. D.,Koonin E. V. and Aravind L. Evolutionary history and higher order classification of AAA+ ATPases. J Struct Biol. 2004; 146: 11-31

Izumi K.,Brett M.,Nishi E.,Drunat S.,Tan E. S.,Fujiki K.,Lebon S.,Cham B.,Masuda K.,Arakawa M.,Jacquinet A.,Yamazumi Y.,Chen S. T.,Verloes A.,Okada Y.,Katou Y.,Nakamura T.,Akiyama T.,Gressens P.,Foo R.,Passemard S.,Tan E. C.,El Ghouzzi V. and Shirahige K. ARCN1 Mutations Cause a Recognizable Craniofacial Syndrome Due to COPI-Mediated Transport Defects. Am J Hum Genet. 2016; 99: 451-459

Jackson M. R.,Nilsson T. and Peterson P. A. Identification of a consensus motif for retention of transmembrane proteins in the endoplasmic reticulum. Embo j. 1990; 9: 3153-3162

Jain Goyal M.,Zhao X.,Bozhinova M.,Andrade-López K.,de Heus C.,Schulze-Dramac S.,Müller-McNicoll M.,Klumperman J. and Béthune J. A paralog-specific role of COPI vesicles in the neuronal differentiation of mouse pluripotent cells. Life Sci Alliance. 2020; 3:

Janeway C. A., Jr. and Medzhitov R. Innate immune recognition. Annu Rev Immunol. 2002; 20: 197-216

Janka G. E. Familial and acquired hemophagocytic lymphohistiocytosis. Annu Rev Med. 2012; 63: 233-246

Janka G. E. and Lehmberg K. Hemophagocytic lymphohistiocytosis: pathogenesis and treatment. Hematology. 2013; 2013: 605-611

Janowski A. M.,Colegio O. R.,Hornick E. E.,McNiff J. M.,Martin M. D.,Badovinac V. P.,Norian L. A.,Zhang W.,Cassel S. L. and Sutterwala F. S. NLRC4 suppresses melanoma tumor progression independently of inflammasome activation. J Clin Invest. 2016; 126: 3917-3928

Jasin M. and Rothstein R. Repair of strand breaks by homologous recombination. Cold Spring Harb Perspect Biol. 2013; 5: a012740

Jensson B. O.,Hansdottir S.,Arnadottir G. A.,Sulem G.,Kristjansson R. P.,Oddsson A.,Benonisdottir S.,Jonsson H.,Helgason A.,Saemundsdottir J.,Magnusson O. T.,Masson G.,Thorisson G. A.,Jonasdottir A.,Jonasdottir A.,Sigurdsson A.,Jonsdottir I.,Petursdottir V.,Kristinsson J. R.,Gudbjartsson D. F.,Thorsteinsdottir U.,Arngrimsson R.,Sulem P.,Gudmundsson G. and Stefansson K. COPA syndrome in an Icelandic family caused by a recurrent missense mutation in COPA. BMC Med Genet. 2017; 18: 129

Jeremiah N.,Neven B.,Gentili M.,Callebaut I.,Maschalidi S.,Stolzenberg M. C.,Goudin N.,Frémond M. L.,Nitschke P.,Molina T. J.,Blanche S.,Picard C.,Rice G. I.,Crow Y. J.,Manel N.,Fischer A.,Bader-Meunier B. and Rieux-Laucat F. Inherited STING-activating mutation underlies a familial inflammatory syndrome with lupus-like manifestations. J Clin Invest. 2014; 124: 5516-5520

Jéru I.,Duquesnoy P.,Fernandes-Alnemri T.,Cochet E.,Yu J. W.,Lackmy-Port-Lis M.,Grimprel E.,Landman-Parker J.,Hentgen V.,Marlin S.,McElreavey K.,Sarkisian T.,Grateau G.,Alnemri E. S. and Amselem S. Mutations in NALP12 cause hereditary periodic fever syndromes. Proceedings of the National Academy of Sciences. 2008; 105: 1614-1619

Jeskey J.,Parida A.,Graven K. and Hostoffer R. Novel Gene Deletion in NLRC4 Expanding the Familial Cold Inflammatory Syndrome Phenotype. Allergy Rhinol (Providence). 2020; 11: 2152656720928062

Jiang H.,Xue X.,Panda S.,Kawale A.,Hooy R. M.,Liang F.,Sohn J.,Sung P. and Gekara N. O. Chromatin-bound cGAS is an inhibitor of DNA repair and hence accelerates genome destabilization and cell death. Embo j. 2019; 38: e102718

Jiang M.,Chen P.,Wang L.,Li W.,Chen B.,Liu Y.,Wang H.,Zhao S.,Ye L.,He Y. and Zhou C. cGAS-STING, an important pathway in cancer immunotherapy. Journal of Hematology & Oncology. 2020; 13: 81

Jin L.,Waterman P. M.,Jonscher K. R.,Short C. M.,Reisdorph N. A. and Cambier J. C. MPYS, a novel membrane tetraspanner, is associated with major histocompatibility complex class II and mediates transduction of apoptotic signals. Mol Cell Biol. 2008; 28: 5014-5026

Jin T.,Perry A.,Jiang J.,Smith P.,Curry James A.,Unterholzner L.,Jiang Z.,Horvath G.,Rathinam Vijay A.,Johnstone Ricky W.,Hornung V.,Latz E.,Bowie Andrew G.,Fitzgerald Katherine A. and Xiao T. S. Structures of the HIN Domain:DNA Complexes Reveal Ligand Binding and Activation Mechanisms of the AIM2 Inflammasome and IFI16 Receptor. Immunity. 2012; 36: 561-571

Joly N.,Böhm A.,Boos W. and Richet E. MalK, the ATP-binding cassette component of the Escherichia coli maltodextrin transporter, inhibits the transcriptional activator malt by antagonizing inducer binding. J Biol Chem. 2004; 279: 33123-33130

Joly N.,Danot O.,Schlegel A.,Boos W. and Richet E. The Aes protein directly controls the activity of MalT, the central transcriptional activator of the Escherichia coli maltose regulon. J Biol Chem. 2002; 277: 16606-16613

Jones D. T.,Taylor W. R. and Thornton J. M. The rapid generation of mutation data matrices from protein sequences. Comput Appl Biosci. 1992; 8: 275-282

Jordan M. B.,Hildeman D.,Kappler J. and Marrack P. An animal model of hemophagocytic lymphohistiocytosis (HLH): CD8+ T cells and interferon gamma are essential for the disorder. Blood. 2004; 104: 735-743

Jostins L.,Ripke S.,Weersma R. K.,Duerr R. H.,McGovern D. P.,Hui K. Y.,Lee J. C.,Schumm L. P.,Sharma Y.,Anderson C. A.,Essers J.,Mitrovic M.,Ning K.,Cleynen I.,Theatre E.,Spain S. L.,Raychaudhuri S.,Goyette P.,Wei Z.,Abraham C.,Achkar J. P.,Ahmad T.,Amininejad L.,Ananthakrishnan A. N.,Andersen V.,Andrews J. M.,Baidoo L.,Balschun T.,Bampton P. A.,Bitton A.,Boucher G.,Brand S.,Büning C.,Cohain A.,Cichon S.,D'Amato M.,De Jong D.,Devaney K. L.,Dubinsky M.,Edwards C.,Ellinghaus D.,Ferguson L. R.,Franchimont D.,Fransen K.,Gearry R.,Georges M.,Gieger C.,Glas J.,Haritunians T.,Hart A.,Hawkey C.,Hedl M.,Hu X.,Karlsen T. H.,Kupcinskas L.,Kugathasan S.,Latiano A.,Laukens D.,Lawrance I. C.,Lees C. W.,Louis E.,Mahy G.,Mansfield J.,Morgan A. R.,Mowat C.,Newman W.,Palmieri O.,Ponsioen C. Y.,Potocnik U.,Prescott N. J.,Regueiro M.,Rotter J. I.,Russell R. K.,Sanderson J. D.,Sans M.,Satsangi J.,Schreiber S.,Simms L. A.,Sventoraityte J.,Targan S. R.,Taylor K. D.,Tremelling M.,Verspaget H. W.,De Vos M.,Wijmenga C.,Wilson D. C.,Winkelmann J.,Xavier R. J.,Zeissig S.,Zhang B.,Zhang C. K.,Zhao H.,Silverberg M. S.,Annese V.,Hakonarson H.,Brant S. R.,Radford-Smith G.,Mathew C. G.,Rioux J. D.,Schadt E. E.,Daly M. J.,Franke A.,Parkes M.,Vermeire S.,Barrett J. C. and Cho J. H. Host-microbe interactions have shaped the genetic architecture of inflammatory bowel disease. Nature. 2012; 491: 119-124

Juliana C.,Fernandes-Alnemri T.,Kang S.,Farias A.,Qin F. and Alnemri E. S. Non-transcriptional Priming and Deubiquitination Regulate NLRP3 Inflammasome Activation*. Journal of Biological Chemistry. 2012; 287: 36617-36622

Juliana C.,Fernandes-Alnemri T.,Wu J.,Datta P.,Solorzano L.,Yu J. W.,Meng R.,Quong A. A.,Latz E.,Scott C. P. and Alnemri E. S. Anti-inflammatory compounds parthenolide and Bay 11-7082 are direct inhibitors of the inflammasome. J Biol Chem. 2010; 285: 9792-9802

Jumper J.,Evans R.,Pritzel A.,Green T.,Figurnov M.,Ronneberger O.,Tunyasuvunakool K.,Bates R.,Žídek A.,Potapenko A.,Bridgland A.,Meyer C.,Kohl S. A. A.,Ballard A. J.,Cowie A.,Romera-Paredes B.,Nikolov S.,Jain R.,Adler J.,Back T.,Petersen S.,Reiman D.,Clancy E.,Zielinski M.,Steinegger M.,Pacholska M.,Berghammer T.,Bodenstein S.,Silver D.,Vinyals O.,Senior A. W.,Kavukcuoglu K.,Kohli P. and Hassabis D. Highly accurate protein structure prediction with AlphaFold. Nature. 2021; 596: 583-589

Kaiser C. A. and Schekman R. Distinct sets of SEC genes govern transport vesicle formation and fusion early in the secretory pathway. Cell. 1990; 61: 723-733

Karki R.,Lee E.,Place D.,Samir P.,Mavuluri J.,Sharma B. R.,Balakrishnan A.,Malireddi R. K. S.,Geiger R.,Zhu Q.,Neale G. and Kanneganti T.-D. IRF8 Regulates Transcription of Naips for NLRC4 Inflammasome Activation. Cell. 2018; 173: 920-933.e913

Kashiwagi Y.,Kawashima H.,Nishimata S.,Nagao R.,Watanabe K.,Takekuma K. and Hoshika A. Extreme efficiency of anti-interleukin 1 agent (anakinra) in a Japanese case of CINCA syndrome. Clin Rheumatol. 2008; 27: 277-279

Kastner D. L.,Aksentijevich I. and Goldbach-Mansky R. Autoinflammatory disease reloaded: a clinical perspective. Cell. 2010; 140: 784-790

Kato H.,Takahasi K. and Fujita T. RIG-I-like receptors: cytoplasmic sensors for non-self RNA. Immunol Rev. 2011; 243: 91-98

Kato H.,Nakajima S.,Saito Y.,Takahashi S.,Katoh R. and Kitamura M. mTORC1 serves ER stress-triggered apoptosis via selective activation of the IRE1-JNK pathway. Cell Death Differ. 2012; 19: 310-320

Kato H.,Takeuchi O.,Mikamo-Satoh E.,Hirai R.,Kawai T.,Matsushita K.,Hiiragi A.,Dermody T. S.,Fujita T. and Akira S. Length-dependent recognition of double-stranded ribonucleic acids by retinoic acid-inducible gene-I and melanoma differentiation-associated gene 5. J Exp Med. 2008; 205: 1601-1610

Kato T.,Yamamoto M.,Honda Y.,Orimo T.,Sasaki I.,Murakami K.,Hemmi H.,Fukuda-Ohta Y.,Isono K.,Takayama S.,Nakamura H.,Otsuki Y.,Miyamoto T.,Takita J.,Yasumi T.,Nishikomori R.,Matsubayashi T.,Izawa K. and Kaisho T. Augmentation of STING-induced type I interferon production in COPA syndrome. Arthritis Rheumatol. 2021;

Kaur J. and Farr J. N. Cellular senescence in age-related disorders. Translational Research. 2020; 226: 96-104

Kawai T. and Akira S. The role of pattern-recognition receptors in innate immunity: update on Toll-like receptors. Nature Immunology. 2010; 11: 373-384

Kawai T.,Takahashi K.,Sato S.,Coban C.,Kumar H.,Kato H.,Ishii K. J.,Takeuchi O. and Akira S. IPS-1, an adaptor triggering RIG-I- and Mda5-mediated type I interferon induction. Nature Immunology. 2005; 6: 981-988

Kawasaki T. and Kawai T. Toll-Like Receptor Signaling Pathways. Frontiers in Immunology. 2014; 5:

Kawasaki Y.,Oda H.,Ito J.,Niwa A.,Tanaka T.,Hijikata A.,Seki R.,Nagahashi A.,Osawa M.,Asaka I.,Watanabe A.,Nishimata S.,Shirai T.,Kawashima H.,Ohara O.,Nakahata T.,Nishikomori R.,Heike T. and Saito M. K. Identification of a High-Frequency Somatic NLRC4 Mutation as a Cause of Autoinflammation by Pluripotent Cell-Based Phenotype Dissection. Arthritis Rheumatol. 2017; 69: 447-459

Kawashima H.,Sato A.,Nishimata S.,Yamada N.,Kashiwagi Y.,Watanabe K.,Takekuma K.,Hoshika A. and Ozawa T. A case report of neonatal onset multisystemic inflammatory disease in Japan treated with continuous hemodiafiltration and steroid pulse therapy. Ther Apher Dial. 2007; 11: 232-234

Kayagaki N.,Warming S.,Lamkanfi M.,Vande Walle L.,Louie S.,Dong J.,Newton K.,Qu Y.,Liu J.,Heldens S.,Zhang J.,Lee W. P.,Roose-Girma M. and Dixit V. M. Non-canonical inflammasome activation targets caspase-11. Nature. 2011; 479: 117-121

Kayagaki N.,Kornfeld O. S.,Lee B. L.,Stowe I. B.,O'Rourke K.,Li Q.,Sandoval W.,Yan D.,Kang J.,Xu M.,Zhang J.,Lee W. P.,McKenzie B. S.,Ulas G.,Payandeh J.,Roose-Girma M.,Modrusan Z.,Reja R.,Sagolla M.,Webster J. D.,Cho V.,Andrews T. D.,Morris L. X.,Miosge L. A.,Goodnow C. C.,Bertram E. M. and Dixit V. M. NINJ1 mediates plasma membrane rupture during lytic cell death. Nature. 2021; 591: 131-136

Kedzierski L.,Tate M. D.,Hsu A. C.,Kolesnik T. B.,Linossi E. M.,Dagley L.,Dong Z.,Freeman S.,Infusini G.,Starkey M. R.,Bird N. L.,Chatfield S. M.,Babon J. J.,Huntington N.,Belz G.,Webb A.,Wark P. A.,Nicola N. A.,Xu J.,Kedzierska K.,Hansbro P. M. and Nicholson S. E. Suppressor of cytokine signaling (SOCS)5 ameliorates influenza infection via inhibition of EGFR signaling. Elife. 2017; 6:

Kell D. B. and Pretorius E. Serum ferritin is an important inflammatory disease marker, as it is mainly a leakage product from damaged cells. Metallomics. 2014; 6: 748-773

Kelleher D. J. and Gilmore R. An evolving view of the eukaryotic oligosaccharyltransferase. Glycobiology. 2005; 16: 47R-62R

Kellermann M.,Scharte F. and Hensel M. Manipulation of Host Cell Organelles by Intracellular Pathogens. International Journal of Molecular Sciences. 2021; 22: 6484

Kelley N.,Jeltema D.,Duan Y. and He Y. The NLRP3 Inflammasome: An Overview of Mechanisms of Activation and Regulation. Int J Mol Sci. 2019; 20:

Kempster S. L.,Belteki G.,Forhead A. J.,Fowden A. L.,Catalano R. D.,Lam B. Y.,McFarlane I.,Charnock-Jones D. S. and Smith G. C. Developmental control of the Nlrp6 inflammasome

and a substrate, IL-18, in mammalian intestine. Am J Physiol Gastrointest Liver Physiol. 2011; 300: G253-263

Keskitalo S.,Haapaniemi E.,Einarsdottir E.,Rajamäki K.,Heikkilä H.,Ilander M.,Pöyhönen M.,Morgunova E.,Hokynar K.,Lagström S.,Kivirikko S.,Mustjoki S.,Eklund K.,Saarela J.,Kere J.,Seppänen M. R. J.,Ranki A.,Hannula-Jouppi K. and Varjosalo M. Novel TMEM173 Mutation and the Role of Disease Modifying Alleles. Frontiers in Immunology. 2019; 10:

Kile B. T.,Panopoulos A. D.,Stirzaker R. A.,Hacking D. F.,Tahtamouni L. H.,Willson T. A.,Mielke L. A.,Henley K. J.,Zhang J.-G.,Wicks I. P.,Stevenson W. S.,Nurden P.,Watowich S. S. and Justice M. J. Mutations in the cofilin partner Aip1/Wdr1 cause autoinflammatory disease and macrothrombocytopenia. Blood. 2007; 110: 2371-2380

Kim H.-E.,Du F.,Fang M. and Wang X. Formation of apoptosome is initiated by cytochrome c-induced dATP hydrolysis and subsequent nucleotide exchange on Apaf-1. Proceedings of the National Academy of Sciences of the United States of America. 2005; 102: 17545-17550

Kim M. L.,Chae J. J.,Park Y. H.,De Nardo D.,Stirzaker R. A.,Ko H. J.,Tye H.,Cengia L.,DiRago L.,Metcalf D.,Roberts A. W.,Kastner D. L.,Lew A. M.,Lyras D.,Kile B. T.,Croker B. A. and Masters S. L. Aberrant actin depolymerization triggers the pyrin inflammasome and autoinflammatory disease that is dependent on IL-18, not IL-1β. J Exp Med. 2015; 212: 927-938

Kirchhausen T. Three ways to make a vesicle. Nature Reviews Molecular Cell Biology. 2000; 1: 187-198

Kirchhausen T.,Owen D. and Harrison S. C. Molecular structure, function, and dynamics of clathrin-mediated membrane traffic. Cold Spring Harb Perspect Biol. 2014; 6: a016725

Kitamura A.,Sasaki Y.,Abe T.,Kano H. and Yasutomo K. An inherited mutation in NLRC4 causes autoinflammation in human and mice. J Exp Med. 2014; 211: 2385-2396

Klenk H.-D. Post-translational modifications in insect cells. Cytotechnology. 1996; 20: 139-144

Knodler L. A.,Crowley S. M.,Sham H. P.,Yang H.,Wrande M.,Ma C.,Ernst R. K.,Steele-Mortimer O.,Celli J. and Vallance B. A. Noncanonical inflammasome activation of caspase-4/caspase-11 mediates epithelial defenses against enteric bacterial pathogens. Cell Host Microbe. 2014; 16: 249-256

Ko J. H.,Yoon S. O.,Lee H. J. and Oh J. Y. Rapamycin regulates macrophage activation by inhibiting NLRP3 inflammasome-p38 MAPK-NFκB pathways in autophagy- and p62-dependent manners. Oncotarget. 2017; 8: 40817-40831

Kofoed E. M. and Vance R. E. Innate immune recognition of bacterial ligands by NAIPs determines inflammasome specificity. Nature. 2011; 477: 592-595

Kolb R.,Phan L.,Borcherding N.,Liu Y.,Yuan F.,Janowski A. M.,Xie Q.,Markan K. R.,Li W.,Potthoff M. J.,Fuentes-Mattei E.,Ellies L. G.,Knudson C. M.,Lee M. H.,Yeung S. J.,Cassel S. L.,Sutterwala F. S. and Zhang W. Obesity-associated NLRC4 inflammasome activation drives breast cancer progression. Nat Commun. 2016; 7: 13007

Koné-Paut I. and Galeotti C. Anakinra for cryopyrin-associated periodic syndrome. Expert Rev Clin Immunol. 2014; 10: 7-18

Konno H.,Konno K. and Barber G. N. Cyclic dinucleotides trigger ULK1 (ATG1) phosphorylation of STING to prevent sustained innate immune signaling. Cell. 2013; 155: 688-698

Konno H.,Chinn I. K.,Hong D.,Orange J. S.,Lupski J. R.,Mendoza A.,Pedroza L. A. and Barber G. N. Pro-inflammation Associated with a Gain-of-Function Mutation (R284S) in the Innate Immune Sensor STING. Cell Rep. 2018; 23: 1112-1123

Kornmann B.,Currie E.,Collins S. R.,Schuldiner M.,Nunnari J.,Weissman J. S. and Walter P. An ER-mitochondria tethering complex revealed by a synthetic biology screen. Science. 2009; 325: 477-481

Kortmann J.,Brubaker S. W. and Monack D. M. Cutting Edge: Inflammasome Activation in Primary Human Macrophages Is Dependent on Flagellin. The Journal of Immunology. 2015; 1403100

Kranzusch P. J.,Lee A. S.,Berger J. M. and Doudna J. A. Structure of human cGAS reveals a conserved family of second-messenger enzymes in innate immunity. Cell Rep. 2013; 3: 1362-1368

Kretschmer S.,Wolf C.,Konig N.,Staroske W.,Guck J.,Hausler M.,Luksch H.,Nguyen L. A.,Kim B.,Alexopoulou D.,Dahl A.,Rapp A.,Cardoso M. C.,Shevchenko A. and Lee-Kirsch M. A. SAMHD1 prevents autoimmunity by maintaining genome stability. Ann Rheum Dis. 2015; 74: e17

Kropski J. A.,Pritchett J. M.,Zoz D. F.,Crossno P. F.,Markin C.,Garnett E. T.,Degryse A. L.,Mitchell D. B.,Polosukhin V. V.,Rickman O. B.,Choi L.,Cheng D. S.,McConaha M. E.,Jones B. R.,Gleaves L. A.,McMahon F. B.,Worrell J. A.,Solus J. F.,Ware L. B.,Lee J. W.,Massion P. P.,Zaynagetdinov R.,White E. S.,Kurtis J. D.,Johnson J. E.,Groshong S. D.,Lancaster L. H.,Young L. R.,Steele M. P.,Phillips Iii J. A.,Cogan J. D.,Loyd J. E.,Lawson W. E. and Blackwell T. S. Extensive phenotyping of individuals at risk for familial interstitial pneumonia reveals clues to the pathogenesis of interstitial lung disease. Am J Respir Crit Care Med. 2015; 191: 417-426

Krutzke S.,Rietschel C. and Horneff G. Baricitinib in therapy of COPA syndrome in a 15-year-old girl. Eur J Rheumatol. 2019; 7: 1-4

Kuehn M. J.,Herrmann J. M. and Schekman R. COPII-cargo interactions direct protein sorting into ER-derived transport vesicles. Nature. 1998; 391: 187-190

Kuge O.,Hara-Kuge S.,Orci L.,Ravazzola M.,Amherdt M.,Tanigawa G.,Wieland F. T. and Rothman J. E. zeta-COP, a subunit of coatomer, is required for COP-coated vesicle assembly. J Cell Biol. 1993; 123: 1727-1734

Kullenberg T.,Löfqvist M.,Leinonen M.,Goldbach-Mansky R. and Olivecrona H. Long-term safety profile of anakinra in patients with severe cryopyrin-associated periodic syndromes. Rheumatology (Oxford). 2016; 55: 1499-1506

Kumar S.,Stecher G.,Li M.,Knyaz C. and Tamura K. MEGA X: Molecular Evolutionary Genetics Analysis across Computing Platforms. Mol Biol Evol. 2018; 35: 1547-1549

Kumar Y.,Radha V. and Swarup G. Interaction with Sug1 enables Ipaf ubiquitination leading to caspase 8 activation and cell death. Biochemical Journal. 2010; 427: 91-104

Kustikova O. S.,Wahlers A.,Kühlcke K.,Stähle B.,Zander A. R.,Baum C. and Fehse B. Dose finding with retroviral vectors: correlation of retroviral vector copy numbers in single cells with gene transfer efficiency in a cell population. Blood. 2003; 102: 3934-3937

Kwon D.,Sesaki H. and Kang S.-J. Intracellular calcium is a rheostat for the STING signaling pathway. Biochemical and Biophysical Research Communications. 2018; 500: 497-503

Labun K.,Montague T. G.,Krause M.,Torres Cleuren Y. N.,Tjeldnes H. and Valen E. CHOPCHOP v3: expanding the CRISPR web toolbox beyond genome editing. Nucleic Acids Research. 2019; 47: W171-W174

Lachmann H. J.,Kone-Paut I.,Kuemmerle-Deschner J. B.,Leslie K. S.,Hachulla E.,Quartier P.,Gitton X.,Widmer A.,Patel N. and Hawkins P. N. Use of canakinumab in the cryopyrin-associated periodic syndrome. N Engl J Med. 2009; 360: 2416-2425

Lahaye X.,Gentili M.,Silvin A.,Conrad C.,Picard L.,Jouve M.,Zueva E.,Maurin M.,Nadalin F.,Knott G. J.,Zhao B.,Du F.,Rio M.,Amiel J.,Fox A. H.,Li P.,Etienne L.,Bond C. S.,Colleaux L. and Manel N. NONO Detects the Nuclear HIV Capsid to Promote cGAS-Mediated Innate Immune Activation. Cell. 2018; 175: 488-501.e422

Lamkanfi M. and Dixit V. M. Mechanisms and functions of inflammasomes. Cell. 2014; 157: 1013-1022

Langer J. D.,Roth C. M.,Bethune J.,Stoops E. H.,Brugger B.,Herten D. P. and Wieland F. T. A conformational change in the alpha-subunit of coatomer induced by ligand binding to gamma-COP revealed by single-pair FRET. Traffic. 2008; 9: 597-607

Larabi A.,Devos J. M.,Ng S. L.,Nanao M. H.,Round A.,Maniatis T. and Panne D. Crystal structure and mechanism of activation of TANK-binding kinase 1. Cell Rep. 2013; 3: 734-746

Laricchia-Robbio L.,Tamura T.,Karpova T.,Sprague B. L.,McNally J. G. and Ozato K. Partner-regulated interaction of IFN regulatory factor 8 with chromatin visualized in live macrophages. Proceedings of the National Academy of Sciences of the United States of America. 2005; 102: 14368-14373

Lau L.,Gray E. E.,Brunette R. L. and Stetson D. B. DNA tumor virus oncogenes antagonize the cGAS-STING DNA-sensing pathway. Science. 2015; 350: 568-571

Lee B. L.,Moon J. E.,Shu J. H.,Yuan L.,Newman Z. R.,Schekman R. and Barton G. M. UNC93B1 mediates differential trafficking of endosomal TLRs. Elife. 2013; 2: e00291

Lee B. L.,Mirrashidi K. M.,Stowe I. B.,Kummerfeld S. K.,Watanabe C.,Haley B.,Cuellar T. L.,Reichelt M. and Kayagaki N. ASC- and caspase-8-dependent apoptotic pathway diverges from the NLRC4 inflammasome in macrophages. Scientific Reports. 2018; 8: 3788

Lee D. J.,Du F.,Chen S. W.,Nakasaki M.,Rana I.,Shih V. F. S.,Hoffmann A. and Jamora C. Regulation and Function of the Caspase-1 in an Inflammatory Microenvironment. J Invest Dermatol. 2015; 135: 2012-2020

Lee J. K.,Kim S. H.,Lewis E. C.,Azam T.,Reznikov L. L. and Dinarello C. A. Differences in signaling pathways by IL-1beta and IL-18. Proc Natl Acad Sci U S A. 2004; 101: 8815-8820

Lee M. C.,Orci L.,Hamamoto S.,Futai E.,Ravazzola M. and Schekman R. Sar1p N-terminal helix initiates membrane curvature and completes the fission of a COPII vesicle. Cell. 2005; 122: 605-617

Lee P. C.,Umeyama T. and Horinouchi S. afsS is a target of AfsR, a transcriptional factor with ATPase activity that globally controls secondary metabolism in Streptomyces coelicolor A3(2). Mol Microbiol. 2002; 43: 1413-1430

Leipe D. D.,Koonin E. V. and Aravind L. Evolution and classification of P-loop kinases and related proteins. J Mol Biol. 2003; 333: 781-815

Leipe D. D.,Koonin E. V. and Aravind L. STAND, a class of P-loop NTPases including animal and plant regulators of programmed cell death: multiple, complex domain architectures, unusual phyletic patterns, and evolution by horizontal gene transfer. J Mol Biol. 2004; 343: 1-28

Leipe D. D.,Wolf Y. I.,Koonin E. V. and Aravind L. Classification and evolution of P-loop GTPases and related ATPases. J Mol Biol. 2002; 317: 41-72

Leipe J.,Grunke M.,Dechant C.,Reindl C.,Kerzendorf U.,Schulze-Koops H. and Skapenko A. Role of Th17 cells in human autoimmune arthritis. Arthritis Rheum. 2010; 62: 2876-2885

Lepelley A.,Della Mina E.,Van Nieuwenhove E.,Waumans L.,Fraitag S.,Rice G. I.,Dhir A.,Frémond M. L.,Rodero M. P.,Seabra L.,Carter E.,Bodemer C.,Buhas D.,Callewaert B.,de Lonlay P.,De Somer L.,Dyment D. A.,Faes F.,Grove L.,Holden S.,Hully M.,Kurian M. A.,McMillan H. J.,Suetens K.,Tyynismaa H.,Chhun S.,Wai T.,Wouters C.,Bader-Meunier B. and Crow Y. J. Enhanced cGAS-STING-dependent interferon signaling associated with mutations in ATAD3A. J Exp Med. 2021; 218:

Lepelley A.,Martin-Niclós M. J.,Le Bihan M.,Marsh J. A.,Uggenti C.,Rice G. I.,Bondet V.,Duffy D.,Hertzog J.,Rehwinkel J.,Amselem S.,Boulisfane-El Khalifi S.,Brennan M.,Carter E.,Chatenoud L.,Chhun S.,Coulomb l'Hermine A.,Depp M.,Legendre M.,Mackenzie K. J.,Marey J.,McDougall C.,McKenzie K. J.,Molina T. J.,Neven B.,Seabra L.,Thumerelle C.,Wislez M.,Nathan N.,Manel N.,Crow Y. J. and Frémond M. L. Mutations in COPA lead to abnormal trafficking of STING to the Golgi and interferon signaling. J Exp Med. 2020; 217:

Lesage S.,Zouali H.,Cézard J. P.,Colombel J. F.,Belaiche J.,Almer S.,Tysk C.,O'Morain C.,Gassull M.,Binder V.,Finkel Y.,Modigliani R.,Gower-Rousseau C.,Macry J.,Merlin F.,Chamaillard M.,Jannot A. S.,Thomas G. and Hugot J. P. CARD15/NOD2 mutational analysis and genotype-phenotype correlation in 612 patients with inflammatory bowel disease. Am J Hum Genet. 2002; 70: 845-857

Letourneur F.,Gaynor E. C.,Hennecke S.,Démollière C.,Duden R.,Emr S. D.,Riezman H. and Cosson P. Coatomer is essential for retrieval of dilysine-tagged proteins to the endoplasmic reticulum. Cell. 1994; 79: 1199-1207

Leusch M. S.,Lee S. C. and Olins P. O. A novel host-vector system for direct selection of recombinant baculoviruses (bacmids) in Escherichia coli. Gene. 1995; 160: 191-194

Levinsohn J. L.,Newman Z. L.,Hellmich K. A.,Fattah R.,Getz M. A.,Liu S.,Sastalla I.,Leppla S. H. and Moayeri M. Anthrax lethal factor cleavage of Nlrp1 is required for activation of the inflammasome. PLoS Pathog. 2012; 8: e1002638

Levy M.,Thaiss C. A.,Zeevi D.,Dohnalová L.,Zilberman-Schapira G.,Mahdi J. A.,David E.,Savidor A.,Korem T.,Herzig Y.,Pevsner-Fischer M.,Shapiro H.,Christ A.,Harmelin A.,Halpern Z.,Latz E.,Flavell R. A.,Amit I.,Segal E. and Elinav E. Microbiota-Modulated Metabolites Shape the Intestinal Microenvironment by Regulating NLRP6 Inflammasome Signaling. Cell. 2015; 163: 1428-1443

Lewinski M. K.,Yamashita M.,Emerman M.,Ciuffi A.,Marshall H.,Crawford G.,Collins F.,Shinn P.,Leipzig J.,Hannenhalli S.,Berry C. C.,Ecker J. R. and Bushman F. D. Retroviral DNA integration: viral and cellular determinants of target-site selection. PLoS Pathog. 2006; 2: e60

Lewis M. J. and Pelham H. R. B. A human homologue of the yeast HDEL receptor. Nature. 1990; 348: 162-163

Li A.,Song N.-J.,Riesenberg B. P. and Li Z. The Emerging Roles of Endoplasmic Reticulum Stress in Balancing Immunity and Tolerance in Health and Diseases: Mechanisms and Opportunities. Frontiers in Immunology. 2020a; 10: 3154

Li C.,Wei J.,Li Y.,He X.,Zhou Q.,Yan J.,Zhang J.,Liu Y.,Liu Y. and Shu H. B. Transmembrane Protein 214 (TMEM214) mediates endoplasmic reticulum stress-induced caspase 4 enzyme activation and apoptosis. J Biol Chem. 2013a; 288: 17908-17917

Li S.,Hong Z.,Wang Z.,Li F.,Mei J.,Huang L.,Lou X.,Zhao S.,Song L.,Chen W.,Wang Q.,Liu H.,Cai Y.,Yu H.,Xu H.,Zeng G.,Wang Q.,Zhu J.,Liu X.,Tan N. and Wang C. The Cyclopeptide Astin C Specifically Inhibits the Innate Immune CDN Sensor STING. Cell Rep. 2018a; 25: 3405-3421.e3407

Li S. F.,Gong M. J.,Zhao F. R.,Shao J. J.,Xie Y. L.,Zhang Y. G. and Chang H. Y. Type I Interferons: Distinct Biological Activities and Current Applications for Viral Infection. Cell Physiol Biochem. 2018b; 51: 2377-2396

Li T. and Chen Z. J. The cGAS-cGAMP-STING pathway connects DNA damage to inflammation, senescence, and cancer. J Exp Med. 2018c; 215: 1287-1299

Li X.,Shu C.,Yi G.,Chaton C. T.,Shelton C. L.,Diao J.,Zuo X.,Kao C. C.,Herr A. B. and Li P. Cyclic GMP-AMP synthase is activated by double-stranded DNA-induced oligomerization. Immunity. 2013b; 39: 1019-1031

Li Y.,Fu T.-M.,Lu A.,Witt K.,Ruan J.,Shen C. and Wu H. Cryo-EM structures of ASC and NLRC4 CARD filaments reveal a unified mechanism of nucleation and activation of caspase-1. Proceedings of the National Academy of Sciences. 2018d; 115: 10845-10852

Li Z.,Guo J. and Bi L. Role of the NLRP3 inflammasome in autoimmune diseases. Biomedicine & Pharmacotherapy. 2020b; 130: 110542

Liang F.,Han M.,Romanienko P. J. and Jasin M. Homology-directed repair is a major double-strand break repair pathway in mammalian cells. Proceedings of the National Academy of Sciences. 1998; 95: 5172-5177

Liang J.,Alfano D. N.,Squires J. E.,Riley M. M.,Parks W. T.,Kofler J.,El-Gharbawy A.,Madan-Kheterpal S.,Acquaro R. and Picarsic J. Novel NLRC4 Mutation Causes a Syndrome of Perinatal Autoinflammation With Hemophagocytic Lymphohistiocytosis, Hepatosplenomegaly, Fetal Thrombotic Vasculopathy, and Congenital Anemia and Ascites. Pediatr Dev Pathol. 2017; 20: 498-505

Lidar M.,Langevitz P. and Shoenfeld Y. The role of infection in inflammatory bowel disease: initiation, exacerbation and protection. Isr Med Assoc J. 2009; 11: 558-563

Lin B.,Torreggiani S.,Kahle D.,Rumsey D. G.,Wright B. L.,Montes-Cano M. A.,Silveira L. F.,Alehashemi S.,Mitchell J.,Aue A. G.,Ji Z.,Jin T.,de Jesus A. A. and Goldbach-Mansky R. Case Report: Novel SAVI-Causing Variants in STING1 Expand the Clinical Disease Spectrum and Suggest a Refined Model of STING Activation. Frontiers in Immunology. 2021; 12:

Lin J. and Musunuru K. Genome engineering tools for building cellular models of disease. Febs j. 2016; 283: 3222-3231

Lin S. and Mei X. Role of NLRP3 Inflammasomes in Neuroinflammation Diseases. European Neurology. 2020; 83: 576-580

Lin S.,Staahl B. T.,Alla R. K. and Doudna J. A. Enhanced homology-directed human genome engineering by controlled timing of CRISPR/Cas9 delivery. Elife. 2014; 3: e04766

Lippincott-Schwartz J.,Donaldson J. G.,Schweizer A.,Berger E. G.,Hauri H.-P.,Yuan L. C. and Klausner R. D. Microtubule-dependent retrograde transport of proteins into the ER in the presence of brefeldin a suggests an ER recycling pathway. Cell. 1990; 60: 821-836

Lippmann J.,Rothenburg S.,Deigendesch N.,Eitel J.,Meixenberger K.,van Laak V.,Slevogt H.,N'Guessan P D.,Hippenstiel S.,Chakraborty T.,Flieger A.,Suttorp N. and Opitz B. IFNbeta responses induced by intracellular bacteria or cytosolic DNA in different human cells do not require ZBP1 (DLM-1/DAI). Cell Microbiol. 2008; 10: 2579-2588

Liston A. and Masters S. L. Homeostasis-altering molecular processes as mechanisms of inflammasome activation. Nat Rev Immunol. 2017; 17: 208-214

Liu D.,Wu H.,Wang C.,Li Y.,Tian H.,Siraj S.,Sehgal S. A.,Wang X.,Wang J.,Shang Y.,Jiang Z.,Liu L. and Chen Q. STING directly activates autophagy to tune the innate immune response. Cell Death & Differentiation. 2019; 26: 1735-1749

Liu H. and Naismith J. H. An efficient one-step site-directed deletion, insertion, single and multiple-site plasmid mutagenesis protocol. BMC Biotechnol. 2008; 8: 91

Liu H.,Zhang H.,Wu X.,Ma D.,Wu J.,Wang L.,Jiang Y.,Fei Y.,Zhu C.,Tan R.,Jungblut P.,Pei G.,Dorhoi A.,Yan Q.,Zhang F.,Zheng R.,Liu S.,Liang H.,Liu Z.,Yang H.,Chen J.,Wang P.,Tang T.,Peng W.,Hu Z.,Xu Z.,Huang X.,Wang J.,Li H.,Zhou Y.,Liu F.,Yan D.,Kaufmann S. H. E.,Chen C.,Mao Z. and Ge B. Nuclear cGAS suppresses DNA repair and promotes tumorigenesis. Nature. 2018a; 563: 131-136

Liu J. Z.,van Sommeren S.,Huang H.,Ng S. C.,Alberts R.,Takahashi A.,Ripke S.,Lee J. C.,Jostins L.,Shah T.,Abedian S.,Cheon J. H.,Cho J.,Dayani N. E.,Franke L.,Fuyuno Y.,Hart A.,Juyal R. C.,Juyal G.,Kim W. H.,Morris A. P.,Poustchi H.,Newman W. G.,Midha V.,Orchard T. R.,Vahedi H.,Sood A.,Sung J. Y.,Malekzadeh R.,Westra H. J.,Yamazaki K.,Yang S. K.,Barrett J. C.,Alizadeh B. Z.,Parkes M.,Bk T.,Daly M. J.,Kubo M.,Anderson C. A. and Weersma R. K. Association analyses identify 38 susceptibility loci for inflammatory bowel disease and highlight shared genetic risk across populations. Nat Genet. 2015a; 47: 979-986

Liu L. and Chan C. IPAF inflammasome is involved in interleukin-1β production from astrocytes, induced by palmitate; implications for Alzheimer's Disease. Neurobiol Aging. 2014a; 35: 309-321

Liu S. and Guan W. STING Signaling Promotes Apoptosis, Necrosis, and Cell Death: An Overview and Update. Mediators of Inflammation. 2018b; 2018: 1202797

Liu S.,Cai X.,Wu J.,Cong Q.,Chen X.,Li T.,Du F.,Ren J.,Wu Y. T.,Grishin N. V. and Chen Z. J. Phosphorylation of innate immune adaptor proteins MAVS, STING, and TRIF induces IRF3 activation. Science. 2015b; 347: aaa2630

Liu T.,Zhang L.,Joo D. and Sun S. C. NF-kappaB signaling in inflammation. Signal Transduct Target Ther. 2017a; 2:

Liu W.,Liu X. n.,Li Y.,Zhao J.,Liu Z.,Hu Z.,Wang Y.,Yao Y.,Miller A. W.,Su B.,Cookson M. R.,Li X. and Kang Z. LRRK2 promotes the activation of NLRC4 inflammasome during Salmonella Typhimurium infection. Journal of Experimental Medicine. 2017b; 214: 3051-3066

Liu X.,Zhang Z.,Ruan J.,Pan Y.,Magupalli V. G.,Wu H. and Lieberman J. Inflammasome-activated gasdermin D causes pyroptosis by forming membrane pores. Nature. 2016; 535: 153-158

Liu Y.,Li X.,He S.,Huang S.,Li C.,Chen Y.,Liu Z.,Huang X. and Wang X. Efficient generation of mouse models with the prime editing system. Cell Discovery. 2020; 6: 27

Liu Y.,Zhai H.,Alemayehu H.,Hopkins L. J.,Borgeaud A. C.,Heroven C.,Howe J. D.,Boulanger J.,Bryant C. E. and Modis Y. Cryo-electron tomography of ASC signalling sites in pyroptotic cells. bioRxiv. 2021; 2021.2009.2020.461078

Liu Y.,Ramot Y.,Torrelo A.,Paller A. S.,Si N.,Babay S.,Kim P. W.,Sheikh A.,Lee C. C.,Chen Y.,Vera A.,Zhang X.,Goldbach-Mansky R. and Zlotogorski A. Mutations in proteasome subunit β type 8 cause chronic atypical neutrophilic dermatosis with lipodystrophy and elevated temperature with evidence of genetic and phenotypic heterogeneity. Arthritis Rheum. 2012a; 64: 895-907

Liu Y.,Jesus A. A.,Marrero B.,Yang D.,Ramsey S. E.,Sanchez G. A. M.,Tenbrock K.,Wittkowski H.,Jones O. Y.,Kuehn H. S.,Lee C. R.,DiMattia M. A.,Cowen E. W.,Gonzalez B.,Palmer I.,DiGiovanna J. J.,Biancotto A.,Kim H.,Tsai W. L.,Trier A. M.,Huang Y.,Stone D. L.,Hill S.,Kim H. J.,St Hilaire C.,Gurprasad S.,Plass N.,Chapelle D.,Horkayne-Szakaly I.,Foell D.,Barysenka A.,Candotti F.,Holland S. M.,Hughes J. D.,Mehmet H.,Issekutz A. C.,Raffeld M.,McElwee J.,Fontana J. R.,Minniti C. P.,Moir S.,Kastner D. L.,Gadina M.,Steven A. C.,Wingfield P. T.,Brooks S. R.,Rosenzweig S. D.,Fleisher T. A.,Deng Z.,Boehm M.,Paller A. S. and Goldbach-Mansky R. Activated STING in a vascular and pulmonary syndrome. N Engl J Med. 2014b; 371: 507-518

Liu Y. P.,Zeng L.,Tian A.,Bomkamp A.,Rivera D.,Gutman D.,Barber G. N.,Olson J. K. and Smith J. A. Endoplasmic reticulum stress regulates the innate immunity critical transcription factor IRF3. J Immunol. 2012b; 189: 4630-4639

Liu Z.,Zaki M. H.,Vogel P.,Gurung P.,Finlay B. B.,Deng W.,Lamkanfi M. and Kanneganti T. D. Role of inflammasomes in host defense against Citrobacter rodentium infection. J Biol Chem. 2012c; 287: 16955-16964

López de Padilla C. M. and Niewold T. B. The type I interferons: Basic concepts and clinical relevance in immune-mediated inflammatory diseases. Gene. 2016; 576: 14-21

Lu A.,Magupalli V. G.,Ruan J.,Yin Q.,Atianand M. K.,Vos M. R.,Schröder G. F.,Fitzgerald K. A.,Wu H. and Egelman E. H. Unified polymerization mechanism for the assembly of ASC-dependent inflammasomes. Cell. 2014; 156: 1193-1206

Lu A.,Li Y.,Schmidt F. I.,Yin Q.,Chen S.,Fu T. M.,Tong A. B.,Ploegh H. L.,Mao Y. and Wu H. Molecular basis of caspase-1 polymerization and its inhibition by a new capping mechanism. Nat Struct Mol Biol. 2016a; 23: 416-425

Lu Q.,Haragopal H.,Slepchenko K. G.,Stork C. and Li Y. V. Intracellular zinc distribution in mitochondria, ER and the Golgi apparatus. Int J Physiol Pathophysiol Pharmacol. 2016b; 8: 35-43

Ludwiczek O.,Kaser A.,Novick D.,Dinarello C. A.,Rubinstein M. and Tilg H. Elevated systemic levels of free interleukin-18 (IL-18) in patients with Crohn's disease. Eur Cytokine Netw. 2005; 16: 27-33

Lugrin J. and Martinon F. The AIM2 inflammasome: Sensor of pathogens and cellular perturbations. Immunological Reviews. 2018; 281: 99-114

Luo W. W.,Li S.,Li C.,Lian H.,Yang Q.,Zhong B. and Shu H. B. iRhom2 is essential for innate immunity to DNA viruses by mediating trafficking and stability of the adaptor STING. Nat Immunol. 2016; 17: 1057-1066

MacDonald J. A.,Wijekoon C. P.,Liao K. C. and Muruve D. A. Biochemical and structural aspects of the ATP-binding domain in inflammasome-forming human NLRP proteins. IUBMB Life. 2013; 65: 851-862

Mackenzie K. J.,Carroll P.,Martin C. A.,Murina O.,Fluteau A.,Simpson D. J.,Olova N.,Sutcliffe H.,Rainger J. K.,Leitch A.,Osborn R. T.,Wheeler A. P.,Nowotny M.,Gilbert N.,Chandra T.,Reijns M. A. M. and Jackson A. P. cGAS surveillance of micronuclei links genome instability to innate immunity. Nature. 2017; 548: 461-465

Madeira F.,Park Y. m.,Lee J.,Buso N.,Gur T.,Madhusoodanan N.,Basutkar P.,Tivey A. R. N.,Potter S. C.,Finn R. D. and Lopez R. The EMBL-EBI search and sequence analysis tools APIs in 2019. Nucleic Acids Research. 2019; 47: W636-W641

Maekawa S.,Ohto U.,Shibata T.,Miyake K. and Shimizu T. Crystal structure of NOD2 and its implications in human disease. Nature Communications. 2016; 7: 11813

Magalhaes J. G.,Lee J.,Geddes K.,Rubino S.,Philpott D. J. and Girardin S. E. Essential role of Rip2 in the modulation of innate and adaptive immunity triggered by Nod1 and Nod2 ligands. Eur J Immunol. 2011; 41: 1445-1455

Maharana J.,Panda D. and De S. Deciphering the ATP-binding mechanism(s) in NLRP-NACHT 3D models using structural bioinformatics approaches. PLoS One. 2018; 13: e0209420

Makoni N. J.,Garrad E. C.,Redzic A. and Nichols M. R. Expression of NLRP3 inflammasome proteins in ExpiCHO-S mammalian cells reveals oligomerization properties that are highly sensitive to solution conditions. Biotechnology Progress. 2021; 37: e3153

Malhotra J. D. and Kaufman R. J. ER stress and its functional link to mitochondria: role in cell survival and death. Cold Spring Harb Perspect Biol. 2011; 3: a004424

Mallea J. M.,Kornafeld A.,Khoor A. and Erasmus D. B. Lung Transplantation in a Patient with COPA Syndrome. Case Rep Transplant. 2020; 2020: 3624795

Man S. M. and Kanneganti T. D. Regulation of inflammasome activation. Immunol Rev. 2015; 265: 6-21

Man S. M.,Tourlomousis P.,Hopkins L.,Monie T. P.,Fitzgerald K. A. and Bryant C. E. Salmonella Infection Induces Recruitment of Caspase-8 to the Inflammasome To Modulate IL-1β Production. The Journal of Immunology. 2013; 191: 5239-5246

Man S. M.,Hopkins L. J.,Nugent E.,Cox S.,Glück I. M.,Tourlomousis P.,Wright J. A.,Cicuta P.,Monie T. P. and Bryant C. E. Inflammasome activation causes dual recruitment of NLRC4 and NLRP3 to the same macromolecular complex. Proceedings of the National Academy of Sciences. 2014a; 111: 7403-7408

Man S. M.,Ekpenyong A.,Tourlomousis P.,Achouri S.,Cammarota E.,Hughes K.,Rizzo A.,Ng G.,Wright J. A.,Cicuta P.,Guck J. R. and Bryant C. E. Actin polymerization as a key innate immune effector mechanism to control Salmonella infection. Proceedings of the National Academy of Sciences. 2014b; 111: 17588-17593

Mankan A. K.,Schmidt T.,Chauhan D.,Goldeck M.,Höning K.,Gaidt M.,Kubarenko A. V.,Andreeva L.,Hopfner K. P. and Hornung V. Cytosolic RNA:DNA hybrids activate the cGAS-STING axis. Embo j. 2014; 33: 2937-2946

Mann M. and Jensen O. N. Proteomic analysis of post-translational modifications. Nat Biotechnol. 2003; 21: 255-261

Mann M.,Ong S. E.,Grønborg M.,Steen H.,Jensen O. N. and Pandey A. Analysis of protein phosphorylation using mass spectrometry: deciphering the phosphoproteome. Trends Biotechnol. 2002; 20: 261-268

Mariathasan S.,Newton K.,Monack D. M.,Vucic D.,French D. M.,Lee W. P.,Roose-Girma M.,Erickson S. and Dixit V. M. Differential activation of the inflammasome by caspase-1 adaptors ASC and Ipaf. Nature. 2004; 430: 213-218

Marquenet E. and Richet E. How integration of positive and negative regulatory signals by a STAND signaling protein depends on ATP hydrolysis. Mol Cell. 2007; 28: 187-199

Martin M.,Hiroyasu A.,Guzman R. M.,Roberts S. A. and Goodman A. G. Analysis of Drosophila STING Reveals an Evolutionarily Conserved Antimicrobial Function. Cell Rep. 2018; 23: 3537-3550.e3536

Martínez-Menárguez J. A.,Geuze H. J.,Slot J. W. and Klumperman J. Vesicular tubular clusters between the ER and Golgi mediate concentration of soluble secretory proteins by exclusion from COPI-coated vesicles. Cell. 1999; 98: 81-90

Martino L.,Holland L.,Christodoulou E.,Kunzelmann S.,Esposito D. and Rittinger K. The Biophysical Characterisation and SAXS Analysis of Human NLRP1 Uncover a New Level of Complexity of NLR Proteins. PLoS One. 2016; 11: e0164662

Martinon F.,Burns K. and Tschopp J. The inflammasome: a molecular platform triggering activation of inflammatory caspases and processing of proIL-beta. Mol Cell. 2002; 10: 417-426

Martinon F.,Chen X.,Lee A.-H. and Glimcher L. H. TLR activation of the transcription factor XBP1 regulates innate immune responses in macrophages. Nature Immunology. 2010; 11: 411-418

Mascarenhas D. P. A.,Cerqueira D. M.,Pereira M. S. F.,Castanheira F. V. S.,Fernandes T. D.,Manin G. Z.,Cunha L. D. and Zamboni D. S. Inhibition of caspase-1 or gasdermin-D enable caspase-8 activation in the Naip5/NLRC4/ASC inflammasome. PLoS Pathog. 2017; 13: e1006502

Masters S. L.,Lagou V.,Jéru I.,Baker P. J.,Van Eyck L.,Parry D. A.,Lawless D.,De Nardo D.,Garcia-Perez J. E.,Dagley L. F.,Holley C. L.,Dooley J.,Moghaddas F.,Pasciuto E.,Jeandel P. Y.,Sciot R.,Lyras D.,Webb A. I.,Nicholson S. E.,De Somer L.,van Nieuwenhove E.,Ruuth-Praz J.,Copin B.,Cochet E.,Medlej-Hashim M.,Megarbane A.,Schroder K.,Savic S.,Goris A.,Amselem S.,Wouters C. and Liston A. Familial autoinflammation with neutrophilic dermatosis reveals a regulatory mechanism of pyrin activation. Sci Transl Med. 2016; 8: 332ra345

Matsuoka K.,Orci L.,Amherdt M.,Bednarek S. Y.,Hamamoto S.,Schekman R. and Yeung T. COPII-coated vesicle formation reconstituted with purified coat proteins and chemically defined liposomes. Cell. 1998; 93: 263-275

Matusiak M.,Van Opdenbosch N.,Vande Walle L.,Sirard J.-C.,Kanneganti T.-D. and Lamkanfi M. Flagellin-induced NLRC4 phosphorylation primes the inflammasome for activation by NAIP5. Proceedings of the National Academy of Sciences. 2015; 112: 1541-1546

Matyszewski M.,Zheng W.,Lueck J.,Antiochos B.,Egelman E. H. and Sohn J. Cryo-EM structure of the NLRC4(CARD) filament provides insights into how symmetric and asymmetric supramolecular structures drive inflammasome assembly. J Biol Chem. 2018; 293: 20240-20248

Matzinger P. Tolerance, danger, and the extended family. Annu Rev Immunol. 1994; 12: 991-1045

Maurissen T. L. and Woltjen K. Synergistic gene editing in human iPS cells via cell cycle and DNA repair modulation. Nature Communications. 2020; 11: 2876

McCauley M. E.,O'Rourke J. G.,Yáñez A.,Markman J. L.,Ho R.,Wang X.,Chen S.,Lall D.,Jin M.,Muhammad A. K. M. G.,Bell S.,Landeros J.,Valencia V.,Harms M.,Arditi M.,Jefferies C. and

Baloh R. H. C9orf72 in myeloid cells suppresses STING-induced inflammation. Nature. 2020; 585: 96-101

McDermott M. F.,Aksentijevich I.,Galon J.,McDermott E. M.,Ogunkolade B. W.,Centola M.,Mansfield E.,Gadina M.,Karenko L.,Pettersson T.,McCarthy J.,Frucht D. M.,Aringer M.,Torosyan Y.,Teppo A. M.,Wilson M.,Karaarslan H. M.,Wan Y.,Todd I.,Wood G.,Schlimgen R.,Kumarajeewa T. R.,Cooper S. M.,Vella J. P.,Amos C. I.,Mulley J.,Quane K. A.,Molloy M. G.,Ranki A.,Powell R. J.,Hitman G. A.,O'Shea J. J. and Kastner D. L. Germline mutations in the extracellular domains of the 55 kDa TNF receptor, TNFR1, define a family of dominantly inherited autoinflammatory syndromes. Cell. 1999; 97: 133-144

McGonagle D. and McDermott M. F. A proposed classification of the immunological diseases. PLoS Med. 2006; 3: e297

McGonagle D.,Sharif K.,O'Regan A. and Bridgewood C. The Role of Cytokines including Interleukin-6 in COVID-19 induced Pneumonia and Macrophage Activation Syndrome-Like Disease. Autoimmun Rev. 2020; 19: 102537

McNab F.,Mayer-Barber K.,Sher A.,Wack A. and O'Garra A. Type I interferons in infectious disease. Nature Reviews Immunology. 2015; 15: 87-103

McRee D. E. (1999). 3 - COMPUTATIONAL TECHNIQUES. Practical Protein Crystallography (Second Edition). D. E. McRee. San Diego, Academic Press: 91-cp91.

Mehalko J. L. and Esposito D. Engineering the transposition-based baculovirus expression vector system for higher efficiency protein production from insect cells. J Biotechnol. 2016; 238: 1-8

Meier-Schiesser B. and French L. E. Autoinflammatory syndromes. JDDG: Journal der Deutschen Dermatologischen Gesellschaft. 2021; 19: 400-426

Melki I.,Rose Y.,Uggenti C.,Van Eyck L.,Frémond M. L.,Kitabayashi N.,Rice G. I.,Jenkinson E. M.,Boulai A.,Jeremiah N.,Gattorno M.,Volpi S.,Sacco O.,Terheggen-Lagro S. W. J.,Tiddens H.,Meyts I.,Morren M. A.,De Haes P.,Wouters C.,Legius E.,Corveleyn A.,Rieux-Laucat F.,Bodemer C.,Callebaut I.,Rodero M. P. and Crow Y. J. Disease-associated mutations identify a novel region in human STING necessary for the control of type I interferon signaling. J Allergy Clin Immunol. 2017; 140: 543-552.e545

Miao E. A.,Alpuche-Aranda C. M.,Dors M.,Clark A. E.,Bader M. W.,Miller S. I. and Aderem A. Cytoplasmic flagellin activates caspase-1 and secretion of interleukin 1β via Ipaf. Nature Immunology. 2006; 7: 569-575

Miao E. A.,Mao D. P.,Yudkovsky N.,Bonneau R.,Lorang C. G.,Warren S. E.,Leaf I. A. and Aderem A. Innate immune detection of the type III secretion apparatus through the NLRC4 inflammasome. Proc Natl Acad Sci U S A. 2010; 107: 3076-3080

Michelsen K.,Yuan H. and Schwappach B. Hide and run. Arginine-based endoplasmic-reticulum-sorting motifs in the assembly of heteromultimeric membrane proteins. EMBO Rep. 2005; 6: 717-722

Miller J. M. and Enemark E. J. Fundamental Characteristics of AAA+ Protein Family Structure and Function. Archaea. 2016; 2016: 9294307

Miller L. S.,Pietras E. M.,Uricchio L. H.,Hirano K.,Rao S.,Lin H.,O'Connell R. M.,Iwakura Y.,Cheung A. L.,Cheng G. and Modlin R. L. Inflammasome-Mediated Production of IL-1β Is Required for Neutrophil Recruitment against Staphylococcus aureus In Vivo. The Journal of Immunology. 2007; 179: 6933-6942

Milner-White E. J.,Coggins J. R. and Anton I. A. Evidence for an ancestral core structure in nucleotide-binding proteins with the type A motif. J Mol Biol. 1991; 221: 751-754

Mironov A. A.,Mironov A. A.,Beznoussenko G. V.,Trucco A.,Lupetti P.,Smith J. D.,Geerts W. J. C.,Koster A. J.,Burger K. N. J.,Martone M. E.,Deerinck T. J.,Ellisman M. H. and Luini A. ER-to-Golgi Carriers Arise through Direct En Bloc Protrusion and Multistage Maturation of Specialized ER Exit Domains. Dev Cell. 2003; 5: 583-594

Moelleken J.,Malsam J.,Betts M. J.,Movafeghi A.,Reckmann I.,Meissner I.,Hellwig A.,Russell R. B.,Sollner T.,Brugger B. and Wieland F. T. Differential localization of coatomer complex isoforms within the Golgi apparatus. Proc Natl Acad Sci U S A. 2007; 104: 4425-4430

Moghaddas F.,Llamas R.,De Nardo D.,Martinez-Banaclocha H.,Martinez-Garcia J. J.,Mesa-Del-Castillo P.,Baker P. J.,Gargallo V.,Mensa-Vilaro A.,Canna S.,Wicks I. P.,Pelegrin P.,Arostegui J. I. and Masters S. L. A novel Pyrin-Associated Autoinflammation with Neutrophilic Dermatosis mutation further defines 14-3-3 binding of pyrin and distinction to Familial Mediterranean Fever. Ann Rheum Dis. 2017; 76: 2085-2094

Moghaddas F.,Zeng P.,Zhang Y.,Schutzle H.,Brenner S.,Hofmann S. R.,Berner R.,Zhao Y.,Lu B.,Chen X.,Zhang L.,Cheng S.,Winkler S.,Lehmberg K.,Canna S. W.,Czabotar P. E.,Wicks I. P.,De Nardo D.,Hedrich C. M.,Zeng H. and Masters S. L. Autoinflammatory mutation in NLRC4 reveals a leucine-rich repeat (LRR)-LRR oligomerization interface. J Allergy Clin Immunol. 2018; 142: 1956-1967.e1956

Mokry L. E.,Zhou S.,Guo C.,Scott R. A.,Devey L.,Langenberg C.,Wareham N.,Waterworth D.,Cardon L.,Sanseau P.,Davey Smith G. and Richards J. B. Interleukin-18 as a drug repositioning opportunity for inflammatory bowel disease: A Mendelian randomization study. Scientific Reports. 2019; 9: 9386

Montague T. G.,Cruz J. M.,Gagnon J. A.,Church G. M. and Valen E. CHOPCHOP: a CRISPR/Cas9 and TALEN web tool for genome editing. Nucleic Acids Research. 2014; 42: W401-W407

Morand K.,Talbo G. and Mann M. Oxidation of peptides during electrospray ionization. Rapid Commun Mass Spectrom. 1993; 7: 738-743

Morimoto A.,Nakazawa Y. and Ishii E. Hemophagocytic lymphohistiocytosis: Pathogenesis, diagnosis, and management. Pediatrics International. 2016; 58: 817-825

Mortimer L.,Moreau F.,MacDonald J. A. and Chadee K. NLRP3 inflammasome inhibition is disrupted in a group of auto-inflammatory disease CAPS mutations. Nature Immunology. 2016; 17: 1176-1186

Mosser D. M. and Edwards J. P. Exploring the full spectrum of macrophage activation. Nat Rev Immunol. 2008; 8: 958-969

Motwani M.,Pesiridis S. and Fitzgerald K. A. DNA sensing by the cGAS–STING pathway in health and disease. Nature Reviews Genetics. 2019; 20: 657-674

Mowen K. and David M. Role of the STAT1-SH2 domain and STAT2 in the activation and nuclear translocation of STAT1. J Biol Chem. 1998; 273: 30073-30076

Muckle T. J. The 'Muckle-Wells' syndrome. Br J Dermatol. 1979; 100: 87-92

Mukai K.,Konno H.,Akiba T.,Uemura T.,Waguri S.,Kobayashi T.,Barber G. N.,Arai H. and Taguchi T. Activation of STING requires palmitoylation at the Golgi. Nature Communications. 2016; 7: 11932

Mukai K.,Ogawa E.,Uematsu R.,Kuchitsu Y.,Kiku F.,Uemura T.,Waguri S.,Suzuki T.,Dohmae N.,Arai H.,Shum A. K. and Taguchi T. Homeostatic regulation of STING by retrograde membrane traffic to the ER. Nature Communications. 2021; 12: 61

Mundy R.,MacDonald T. T.,Dougan G.,Frankel G. and Wiles S. Citrobacter rodentium of mice and man. Cell Microbiol. 2005; 7: 1697-1706

Muñoz-Planillo R.,Kuffa P.,Martínez-Colón G.,Smith B. L.,Rajendiran T. M. and Núñez G. K^+ efflux is the common trigger of NLRP3 inflammasome activation by bacterial toxins and particulate matter. Immunity. 2013; 38: 1142-1153

Munro S. and Pelham H. R. A C-terminal signal prevents secretion of luminal ER proteins. Cell. 1987; 48: 899-907

Murphy K., Travers, P., Walport, M., & Janeway, C. (2017). Janeway's immunobiology (9th edition.), Garland Science/Taylor & Francis Group, LLC.

Nakae S.,Asano M.,Horai R. and Iwakura Y. Interleukin-1 beta, but not interleukin-1 alpha, is required for T-cell-dependent antibody production. Immunology. 2001; 104: 402-409

Nakamura K.,Okamura H.,Nagata K.,Komatsu T. and Tamura T. Purification of a factor which provides a costimulatory signal for gamma interferon production. Infect Immun. 1993; 61: 64-70

Nakanishi H.,Kawashima Y.,Kurima K.,Chae J. J.,Ross A. M.,Pinto-Patarroyo G.,Patel S. K.,Muskett J. A.,Ratay J. S.,Chattaraj P.,Park Y. H.,Grevich S.,Brewer C. C.,Hoa M.,Kim H. J.,Butman J. A.,Broderick L.,Hoffman H. M.,Aksentijevich I.,Kastner D. L.,Goldbach-Mansky R. and Griffith A. J. NLRP3 mutation and cochlear autoinflammation cause syndromic and nonsyndromic hearing loss DFNA34 responsive to anakinra therapy. Proc Natl Acad Sci U S A. 2017; 114: E7766-e7775

Nakanishi K. Unique Action of Interleukin-18 on T Cells and Other Immune Cells. Front Immunol. 2018; 9: 763

Nam H.,Hwang B. J.,Choi D. Y.,Shin S. and Choi M. Tobacco etch virus (TEV) protease with multiple mutations to improve solubility and reduce self-cleavage exhibits enhanced enzymatic activity. FEBS Open Bio. 2020; 10: 619-626

Nazmi A.,Field R. H.,Griffin E. W.,Haugh O.,Hennessy E.,Cox D.,Reis R.,Tortorelli L.,Murray C. L.,Lopez-Rodriguez A. B.,Jin L.,Lavelle E. C.,Dunne A. and Cunningham C. Chronic neurodegeneration induces type I interferon synthesis via STING, shaping microglial phenotype and accelerating disease progression. Glia. 2019; 67: 1254-1276

Negroni A.,Pierdomenico M.,Cucchiara S. and Stronati L. NOD2 and inflammation: current insights. J Inflamm Res. 2018; 11: 49-60

Negrotto S.,C J. D. G.,Lapponi M. J.,Etulain J.,Rivadeneyra L.,Pozner R. G.,Gomez R. M. and Schattner M. Expression and functionality of type I interferon receptor in the megakaryocytic lineage. J Thromb Haemost. 2011; 9: 2477-2485

Neuwald A. F.,Aravind L.,Spouge J. L. and Koonin E. V. AAA+: A class of chaperone-like ATPases associated with the assembly, operation, and disassembly of protein complexes. Genome Res. 1999; 9: 27-43

Neven B.,Callebaut I.,Prieur A. M.,Feldmann J.,Bodemer C.,Lepore L.,Derfalvi B.,Benjaponpitak S.,Vesely R.,Sauvain M. J.,Oertle S.,Allen R.,Morgan G.,Borkhardt A.,Hill C.,Gardner-Medwin J.,Fischer A. and de Saint Basile G. Molecular basis of the spectral expression of CIAS1 mutations associated with phagocytic cell-mediated autoinflammatory disorders CINCA/NOMID, MWS, and FCU. Blood. 2004; 103: 2809-2815

Ng C. Y.,Kannan S.,Chen Y. J.,Tan F. C. K.,Ong W. Y.,Go M. L.,Verma C. S.,Low C.-M. and Lam Y. A New Generation of Arachidonic Acid Analogues as Potential Neurological Agent Targeting Cytosolic Phospholipase A2. Scientific Reports. 2017; 7: 13683

Ni G.,Konno H. and Barber G. N. Ubiquitination of STING at lysine 224 controls IRF3 activation. Sci Immunol. 2017; 2:

Nishida K.,Arazoe T.,Yachie N.,Banno S.,Kakimoto M.,Tabata M.,Mochizuki M.,Miyabe A.,Araki M.,Hara K. Y.,Shimatani Z. and Kondo A. Targeted nucleotide editing using hybrid prokaryotic and vertebrate adaptive immune systems. Science. 2016; 353:

Nishikawa K.,Kubota Y. and Ooi T. Classification of proteins into groups based on amino acid composition and other characters. I. Angular distribution. J Biochem. 1983; 94: 981-995

Niu T. K.,Pfeifer A. C.,Lippincott-Schwartz J. and Jackson C. L. Dynamics of GBF1, a Brefeldin A-sensitive Arf1 exchange factor at the Golgi. Mol Biol Cell. 2005; 16: 1213-1222

Noorelahi R.,Perez G. and Otero H. J. Imaging findings of Copa syndrome in a 12-year-old boy. Pediatr Radiol. 2018; 48: 279-282

Nordlander S.,Pott J. and Maloy K. J. NLRC4 expression in intestinal epithelial cells mediates protection against an enteric pathogen. Mucosal Immunology. 2014; 7: 775-785

Novick D.,Kim S. H.,Fantuzzi G.,Reznikov L. L.,Dinarello C. A. and Rubinstein M. Interleukin-18 binding protein: a novel modulator of the Th1 cytokine response. Immunity. 1999; 10: 127-136

Novick D.,Schwartsburd B.,Pinkus R.,Suissa D.,Belzer I.,Sthoeger Z.,Keane W. F.,Chvatchko Y.,Kim S. H.,Fantuzzi G.,Dinarello C. A. and Rubinstein M. A novel IL-18BP ELISA shows elevated serum IL-18BP in sepsis and extensive decrease of free IL-18. Cytokine. 2001; 14: 334-342

Oda Y.,Nagasu T. and Chait B. T. Enrichment analysis of phosphorylated proteins as a tool for probing the phosphoproteome. Nat Biotechnol. 2001; 19: 379-382

Oduro P. K.,Zheng X.,Wei J.,Yang Y.,Wang Y.,Zhang H.,Liu E.,Gao X.,Du M. and Wang Q. The cGAS–STING signaling in cardiovascular and metabolic diseases: Future novel target option for pharmacotherapy. Acta Pharmaceutica Sinica B. 2021;

Ogawa E.,Mukai K.,Saito K.,Arai H. and Taguchi T. The binding of TBK1 to STING requires exocytic membrane traffic from the ER. Biochemical and Biophysical Research Communications. 2018; 503: 138-145

Ogura T. and Wilkinson A. J. AAA+ superfamily ATPases: common structure--diverse function. Genes Cells. 2001a; 6: 575-597

Ogura T.,Whiteheart S. W. and Wilkinson A. J. Conserved arginine residues implicated in ATP hydrolysis, nucleotide-sensing, and inter-subunit interactions in AAA and AAA+ ATPases. Journal of Structural Biology. 2004; 146: 106-112

Ogura Y.,Inohara N.,Benito A.,Chen F. F.,Yamaoka S. and Nunez G. Nod2, a Nod1/Apaf-1 family member that is restricted to monocytes and activates NF-kappaB. J Biol Chem. 2001b; 276: 4812-4818

Ogura Y.,Bonen D. K.,Inohara N.,Nicolae D. L.,Chen F. F.,Ramos R.,Britton H.,Moran T.,Karaliuskas R.,Duerr R. H.,Achkar J. P.,Brant S. R.,Bayless T. M.,Kirschner B. S.,Hanauer S. B.,Nuñez G. and Cho J. H. A frameshift mutation in NOD2 associated with susceptibility to Crohn's disease. Nature. 2001c; 411: 603-606

Oh R. C.,Hustead T. R.,Ali S. M. and Pantsari M. W. Mildly Elevated Liver Transaminase Levels: Causes and Evaluation. Am Fam Physician. 2017; 96: 709-715

Ohashi K.,Wang Z.,Yang Y. M.,Billet S.,Tu W.,Pimienta M.,Cassel S. L.,Pandol S. J.,Lu S. C.,Sutterwala F. S.,Bhowmick N. and Seki E. NOD-like receptor C4 Inflammasome Regulates the Growth of Colon Cancer Liver Metastasis in NAFLD. Hepatology. 2019; 70: 1582-1599

Okamura H.,Kashiwamura S.-i.,Tsutsui H.,Yoshimoto T. and Nakanishi K. Regulation of interferon-γ production by IL-12 and IL-18. Current Opinion in Immunology. 1998; 10: 259-264

Omoyinmi E.,Melo Gomes S.,Nanthapisal S.,Woo P.,Standing A.,Eleftheriou D.,Klein N. and Brogan P. A. Stimulator of interferon genes-associated vasculitis of infancy. Arthritis Rheumatol. 2015; 67: 808

Onoufriadis A.,Stone K.,Katsiamides A.,Amar A.,Omar Y.,de Lange K. M.,Taylor K.,Barrett J. C.,Pollok R.,Hayee B.,Mansfield J. C.,Sanderson J. D.,Simpson M. A.,Mathew C. G. and Prescott N. J. Exome Sequencing and Genotyping Identify a Rare Variant in NLRP7 Gene Associated With Ulcerative Colitis. J Crohns Colitis. 2018; 12: 321-326

Orci L.,Palmer D. J.,Amherdt M. and Rothman J. E. Coated vesicle assembly in the Golgi requires only coatomer and ARF proteins from the cytosol. Nature. 1993; 364: 732-734

Orci L.,Stamnes M.,Ravazzola M.,Amherdt M.,Perrelet A.,Söllner T. H. and Rothman J. E. Bidirectional transport by distinct populations of COPI-coated vesicles. Cell. 1997; 90: 335-349

Orzalli M. H.,Broekema N. M.,Diner B. A.,Hancks D. C.,Elde N. C.,Cristea I. M. and Knipe D. M. cGAS-mediated stabilization of IFI16 promotes innate signaling during herpes simplex virus infection. Proceedings of the National Academy of Sciences. 2015; 112: E1773-E1781

Owczarek C. M.,Hwang S. Y.,Holland K. A.,Gulluyan L. M.,Tavaria M.,Weaver B.,Reich N. C.,Kola I. and Hertzog P. J. Cloning and characterization of soluble and transmembrane isoforms of a novel component of the murine type I interferon receptor, IFNAR 2. J Biol Chem. 1997; 272: 23865-23870

Pak M. A.,Markhieva K. A.,Novikova M. S.,Petrov D. S.,Vorobyev I. S.,Maksimova E. S.,Kondrashov F. A. and Ivankov D. N. Using AlphaFold to predict the impact of single mutations on protein stability and function. bioRxiv. 2021; 2021.2009.2019.460937

Palade G. Intracellular aspects of the process of protein synthesis. Science. 1975; 189: 347-358

Paloschi M. V.,Lopes J. A.,Boeno C. N.,Silva M. D. S.,Evangelista J. R.,Pontes A. S.,da Silva Setúbal S.,Rego C. M. A.,Néry N. M.,Ferreira e Ferreira A. A.,Pires W. L.,Felipin K. P.,Ferreira G. E. M.,Bozza P. T. and Zuliani J. P. Cytosolic phospholipase A2-α participates in lipid body formation and PGE2 release in human neutrophils stimulated with an l-amino acid oxidase from Calloselasma rhodostoma venom. Scientific Reports. 2020; 10: 10976

Papa R.,Rusmini M.,Volpi S.,Caorsi R.,Picco P.,Grossi A.,Caroli F.,Bovis F.,Musso V.,Obici L.,Castana C.,Ravelli A.,Van Gijn M. E.,Ceccherini I. and Gattorno M. Next generation sequencing panel in undifferentiated autoinflammatory diseases identifies patients with colchicine-responder recurrent fevers. Rheumatology (Oxford). 2020; 59: 344-360

Parvatiyar K.,Zhang Z.,Teles R. M.,Ouyang S.,Jiang Y.,Iyer S. S.,Zaver S. A.,Schenk M.,Zeng S.,Zhong W.,Liu Z. J.,Modlin R. L.,Liu Y. J. and Cheng G. The helicase DDX41 recognizes the bacterial secondary messengers cyclic di-GMP and cyclic di-AMP to activate a type I interferon immune response. Nat Immunol. 2012; 13: 1155-1161

Pathirana W. G. W.,Chubb S. P.,Gillett M. J. and Vasikaran S. D. Faecal Calprotectin. Clin Biochem Rev. 2018; 39: 77-90

Patwardhan A. and Spencer C. H. An unprecedented COPA gene mutation in two patients in the same family: comparative clinical analysis of newly reported patients with other known COPA gene mutations. Pediatr Rheumatol Online J. 2019; 17: 59

Paulukat J.,Bosmann M.,Nold M.,Garkisch S.,Kämpfer H.,Frank S.,Raedle J.,Zeuzem S.,Pfeilschifter J. and Mühl H. Expression and release of IL-18 binding protein in response to IFN-gamma. J Immunol. 2001; 167: 7038-7043

Pearson R. B. and Kemp B. E. Protein kinase phosphorylation site sequences and consensus specificity motifs: tabulations. Methods Enzymol. 1991; 200: 62-81

Pelham H. R. Evidence that luminal ER proteins are sorted from secreted proteins in a post-ER compartment. Embo j. 1988; 7: 913-918

Pelka K.,Bertheloot D.,Reimer E.,Phulphagar K.,Schmidt S. V.,Christ A.,Stahl R.,Watson N.,Miyake K.,Hacohen N.,Haas A.,Brinkmann M. M.,Marshak-Rothstein A.,Meissner F. and Latz E. The Chaperone UNC93B1 Regulates Toll-like Receptor Stability Independently of Endosomal TLR Transport. Immunity. 2018; 48: 911-922.e917

Pellett P. A.,Dietrich F.,Bewersdorf J.,Rothman J. E. and Lavieu G. Inter-Golgi transport mediated by COPI-containing vesicles carrying small cargoes. Elife. 2013; 2: e01296

Pépin G.,Ferrand J.,Höning K.,Jayasekara W. S.,Cain J. E.,Behlke M. A.,Gough D. J.,BR G. W.,Hornung V. and Gantier M. P. Cre-dependent DNA recombination activates a STING-dependent innate immune response. Nucleic Acids Res. 2016; 44: 5356-5364

Pereira M. S.,Marques G. G.,Dellama J. E. and Zamboni D. S. The Nlrc4 Inflammasome Contributes to Restriction of Pulmonary Infection by Flagellated Legionella spp. that Trigger Pyroptosis. Front Microbiol. 2011; 2: 33

Perez N.,Virelizier J. L.,Arenzana-Seisdedos F.,Fischer A. and Griscelli C. Impaired natural killer activity in lymphohistiocytosis syndrome. J Pediatr. 1984; 104: 569-573

Perez-Riverol Y.,Csordas A.,Bai J.,Bernal-Llinares M.,Hewapathirana S.,Kundu D. J.,Inuganti A.,Griss J.,Mayer G.,Eisenacher M.,Pérez E.,Uszkoreit J.,Pfeuffer J.,Sachsenberg T.,Yilmaz

S.,Tiwary S.,Cox J.,Audain E.,Walzer M.,Jarnuczak A. F.,Ternent T.,Brazma A. and Vizcaíno J. A. The PRIDE database and related tools and resources in 2019: improving support for quantification data. Nucleic Acids Res. 2019; 47: D442-d450

Pfeffer S. R. How the Golgi works: a cisternal progenitor model. Proceedings of the National Academy of Sciences of the United States of America. 2010; 107: 19614-19618

Philpott D. J.,Sorbara M. T.,Robertson S. J.,Croitoru K. and Girardin S. E. NOD proteins: regulators of inflammation in health and disease. Nat Rev Immunol. 2014; 14: 9-23

Picard C.,Thouvenin G.,Kannengiesser C.,Dubus J. C.,Jeremiah N.,Rieux-Laucat F.,Crestani B.,Belot A.,Thivolet-Béjui F.,Secq V.,Ménard C.,Reynaud-Gaubert M. and Reix P. Severe Pulmonary Fibrosis as the First Manifestation of Interferonopathy (TMEM173 Mutation). Chest. 2016; 150: e65-71

Pilli M.,Arko-Mensah J.,Ponpuak M.,Roberts E.,Master S.,Mandell M. A.,Dupont N.,Ornatowski W.,Jiang S.,Bradfute S. B.,Bruun J. A.,Hansen T. E.,Johansen T. and Deretic V. TBK-1 promotes autophagy-mediated antimicrobial defense by controlling autophagosome maturation. Immunity. 2012; 37: 223-234

Pinna L. A. and Ruzzene M. How do protein kinases recognize their substrates? Biochim Biophys Acta. 1996; 1314: 191-225

Pirzada R. H.,Javaid N. and Choi S. The Roles of the NLRP3 Inflammasome in Neurodegenerative and Metabolic Diseases and in Relevant Advanced Therapeutic Interventions. Genes (Basel). 2020; 11:

Pizarro T. T.,Michie M. H.,Bentz M.,Woraratanadharm J.,Smith M. F., Jr.,Foley E.,Moskaluk C. A.,Bickston S. J. and Cominelli F. IL-18, a novel immunoregulatory cytokine, is up-regulated in Crohn's disease: expression and localization in intestinal mucosal cells. J Immunol. 1999; 162: 6829-6835

Podolsky D. K. Inflammatory bowel disease. N Engl J Med. 2002; 347: 417-429

Pokatayev V. and Yan N. Methods of Assessing STING Activation and Trafficking. Methods Mol Biol. 2017; 1656: 167-174

Pokatayev V.,Yang K.,Tu X.,Dobbs N.,Wu J.,Kalb R. G. and Yan N. Homeostatic regulation of STING protein at the resting state by stabilizer TOLLIP. Nature Immunology. 2020; 21: 158-167

Pomerantz J. L. and Baltimore D. NF-kappaB activation by a signaling complex containing TRAF2, TANK and TBK1, a novel IKK-related kinase. Embo j. 1999; 18: 6694-6704

Popoff V.,Adolf F.,Brügger B. and Wieland F. COPI budding within the Golgi stack. Cold Spring Harb Perspect Biol. 2011; 3: a005231

Poyet J. L.,Srinivasula S. M.,Tnani M.,Razmara M.,Fernandes-Alnemri T. and Alnemri E. S. Identification of Ipaf, a human caspase-1-activating protein related to Apaf-1. J Biol Chem. 2001; 276: 28309-28313

Prenzel F.,Harfst J.,Schwerk N.,Ahrens F.,Rietschel E.,Schmitt-Grohé S.,Rubak S. M. L.,Poplawska K.,Baden W.,Vogel M.,Hollizeck S.,Ley-Zaporozhan J.,Brasch F.,Reu S.,Griese M. and Group L. F. K.-L.-R. S. Lymphocytic interstitial pneumonia and follicular bronchiolitis in children: A registry-based case series. Pediatric Pulmonology. 2020; 55: 909-917

Presley J. F.,Ward T. H.,Pfeifer A. C.,Siggia E. D.,Phair R. D. and Lippincott-Schwartz J. Dissection of COPI and Arf1 dynamics in vivo and role in Golgi membrane transport. Nature. 2002; 417: 187-193

Prieur A. M.,Griscelli C.,Lampert F.,Truckenbrodt H.,Guggenheim M. A.,Lovell D. J.,Pelkonnen P.,Chevrant-Breton J. and Ansell B. M. A chronic, infantile, neurological, cutaneous and articular (CINCA) syndrome. A specific entity analysed in 30 patients. Scand J Rheumatol Suppl. 1987; 66: 57-68

Proell M.,Riedl S. J.,Fritz J. H.,Rojas A. M. and Schwarzenbacher R. The Nod-like receptor (NLR) family: a tale of similarities and differences. PLoS One. 2008; 3: e2119

Proell M.,Gerlic M.,Mace P. D.,Reed J. C. and Riedl S. J. The CARD plays a critical role in ASC foci formation and inflammasome signalling. Biochem J. 2013; 449: 613-621

Psarianos P.,Kwan J. Y. Y.,Dell S.,Wee W. B.,Rey-McIntyre K.,Chen H.,Dissanayake D.,Laxer R. M.,Shum A.,Liu F. F. and Yip K. W. COPA Syndrome (Ala239Pro) Presenting with Isolated Follicular Bronchiolitis in Early Childhood: Case Report. J Clin Immunol. 2021;

Puren A. J.,Fantuzzi G. and Dinarello C. A. Gene expression, synthesis, and secretion of interleukin 18 and interleukin 1beta are differentially regulated in human blood mononuclear cells and mouse spleen cells. Proc Natl Acad Sci U S A. 1999; 96: 2256-2261

Py Bénédicte F.,Kim M.-S.,Vakifahmetoglu-Norberg H. and Yuan J. Deubiquitination of NLRP3 by BRCC3 Critically Regulates Inflammasome Activity. Mol Cell. 2013; 49: 331-338

Qiao Y.,Wang P.,Qi J.,Zhang L. and Gao C. TLR-induced NF-κB activation regulates NLRP3 expression in murine macrophages. FEBS Lett. 2012; 586: 1022-1026

Qu Y.,Misaghi S.,Newton K.,Maltzman A.,Izrael-Tomasevic A.,Arnott D. and Dixit V. M. NLRP3 recruitment by NLRC4 during Salmonella infection. J Exp Med. 2016; 213: 877-885

Qu Y.,Misaghi S.,Izrael-Tomasevic A.,Newton K.,Gilmour L. L.,Lamkanfi M.,Louie S.,Kayagaki N.,Liu J.,Kömüves L.,Cupp J. E.,Arnott D.,Monack D. and Dixit V. M. Phosphorylation of NLRC4 is critical for inflammasome activation. Nature. 2012; 490: 539-542

Raab M.,Gentili M.,de Belly H.,Thiam H. R.,Vargas P.,Jimenez A. J.,Lautenschlaeger F.,Voituriez R.,Lennon-Duménil A. M.,Manel N. and Piel M. ESCRT III repairs nuclear envelope ruptures during cell migration to limit DNA damage and cell death. Science. 2016; 352: 359-362

Rabouille C. and Klumperman J. Opinion: The maturing role of COPI vesicles in intra-Golgi transport. Nat Rev Mol Cell Biol. 2005; 6: 812-817

Raghawan A. K.,Sripada A.,Gopinath G.,Pushpanjali P.,Kumar Y.,Radha V. and Swarup G. A Disease-associated Mutant of NLRC4 Shows Enhanced Interaction with SUG1 Leading to Constitutive FADD-dependent Caspase-8 Activation and Cell Death. J Biol Chem. 2017; 292: 1218-1230

Ran Y.,Xiong M. G.,Xu Z. S.,Luo W. W.,Wang S. Y. and Wang Y. Y. YIPF5 Is Essential for Innate Immunity to DNA Virus and Facilitates COPII-Dependent STING Trafficking. J Immunol. 2019; 203: 1560-1570

Rathinam V. A. K.,Zhao Y. and Shao F. Innate immunity to intracellular LPS. Nat Immunol. 2019; 20: 527-533

Rauch I.,Deets K. A.,Ji D. X.,von Moltke J.,Tenthorey J. L.,Lee A. Y.,Philip N. H.,Ayres J. S.,Brodsky I. E.,Gronert K. and Vance R. E. NAIP-NLRC4 Inflammasomes Coordinate Intestinal Epithelial Cell Expulsion with Eicosanoid and IL-18 Release via Activation of Caspase-1 and -8. Immunity. 2017; 46: 649-659

Rautela J.,Dagley L. F.,de Oliveira C. C.,Schuster I. S.,Hediyeh-Zadeh S.,Delconte R. B.,Cursons J.,Hennessy R.,Hutchinson D. S.,Harrison C.,Kita B.,Vivier E.,Webb A. I.,Degli-Esposti M. A.,Davis M. J.,Huntington N. D. and Souza-Fonseca-Guimaraes F. Therapeutic blockade of activin-A improves NK cell function and antitumor immunity. Sci Signal. 2019; 12:

Rayamajhi M.,Zak D. E.,Chavarria-Smith J.,Vance R. E. and Miao E. A. Cutting Edge: Mouse NAIP1 Detects the Type III Secretion System Needle Protein. The Journal of Immunology. 2013; 191: 3986-3989

Raykhel I.,Alanen H.,Salo K.,Jurvansuu J.,Nguyen V. D.,Latva-Ranta M. and Ruddock L. A molecular specificity code for the three mammalian KDEL receptors. J Cell Biol. 2007; 179: 1193-1204

Razi M.,Chan E. Y. W. and Tooze S. A. Early endosomes and endosomal coatomer are required for autophagy. Journal of Cell Biology. 2009; 185: 305-321

Reijns M. A.,Rabe B.,Rigby R. E.,Mill P.,Astell K. R.,Lettice L. A.,Boyle S.,Leitch A.,Keighren M.,Kilanowski F.,Devenney P. S.,Sexton D.,Grimes G.,Holt I. J.,Hill R. E.,Taylor M. S.,Lawson K. A.,Dorin J. R. and Jackson A. P. Enzymatic removal of ribonucleotides from DNA is essential for mammalian genome integrity and development. Cell. 2012; 149: 1008-1022

Reinhard C.,Harter C.,Bremser M.,Brugger B.,Sohn K.,Helms J. B. and Wieland F. Receptor-induced polymerization of coatomer. Proc Natl Acad Sci U S A. 1999; 96: 1224-1228

Reis L. F.,Ho Lee T. and Vilcek J. Tumor necrosis factor acts synergistically with autocrine interferon-beta and increases interferon-beta mRNA levels in human fibroblasts. J Biol Chem. 1989; 264: 16351-16354

Ren T.,Zamboni D. S.,Roy C. R.,Dietrich W. F. and Vance R. E. Flagellin-deficient Legionella mutants evade caspase-1- and Naip5-mediated macrophage immunity. PLoS Pathog. 2006; 2: e18

Reubold T. F.,Wohlgemuth S. and Eschenburg S. A new model for the transition of APAF-1 from inactive monomer to caspase-activating apoptosome. J Biol Chem. 2009; 284: 32717-32724

Reus J. B.,Trivino-Soto G. S.,Wu L. I.,Kokott K. and Lim E. S. SV40 Large T Antigen Is Not Responsible for the Loss of STING in 293T Cells but Can Inhibit cGAS-STING Interferon Induction. Viruses. 2020; 12:

Reyes Ruiz V. M.,Ramirez J.,Naseer N.,Palacio N. M.,Siddarthan I. J.,Yan B. M.,Boyer M. A.,Pensinger D. A.,Sauer J.-D. and Shin S. Broad detection of bacterial type III secretion system and flagellin proteins by the human NAIP/NLRC4 inflammasome. Proceedings of the National Academy of Sciences. 2017; 114: 13242-13247

Rice G. I.,Kasher P. R.,Forte G. M.,Mannion N. M.,Greenwood S. M.,Szynkiewicz M.,Dickerson J. E.,Bhaskar S. S.,Zampini M.,Briggs T. A.,Jenkinson E. M.,Bacino C. A.,Battini R.,Bertini E.,Brogan P. A.,Brueton L. A.,Carpanelli M.,De Laet C.,de Lonlay P.,del Toro M.,Desguerre I.,Fazzi E.,Garcia-Cazorla A.,Heiberg A.,Kawaguchi M.,Kumar R.,Lin J. P.,Lourenco C. M.,Male A. M.,Marques W., Jr.,Mignot C.,Olivieri I.,Orcesi S.,Prabhakar P.,Rasmussen M.,Robinson R. A.,Rozenberg F.,Schmidt J. L.,Steindl K.,Tan T. Y.,van der Merwe W. G.,Vanderver A.,Vassallo G.,Wakeling E. L.,Wassmer E.,Whittaker E.,Livingston J. H.,Lebon P.,Suzuki T.,McLaughlin P. J.,Keegan L. P.,O'Connell M. A.,Lovell S. C. and Crow Y. J. Mutations in ADAR1 cause Aicardi-Goutières syndrome associated with a type I interferon signature. Nat Genet. 2012; 44: 1243-1248

Richet E. and Raibaud O. MalT, the regulatory protein of the Escherichia coli maltose system, is an ATP-dependent transcriptional activator. Embo j. 1989; 8: 981-987

Riedl S. J.,Li W.,Chao Y.,Schwarzenbacher R. and Shi Y. Structure of the apoptotic protease-activating factor 1 bound to ADP. Nature. 2005; 434: 926-933

Ringel-Scaia V. M.,McDaniel D. K. and Allen I. C. The Goldilocks Conundrum: NLR Inflammasome Modulation of Gastrointestinal Inflammation during Inflammatory Bowel Disease. Crit Rev Immunol. 2016; 36: 283-314

Ritz A.,Shakhnarovich G.,Salomon A. R. and Raphael B. J. Discovery of phosphorylation motif mixtures in phosphoproteomics data. Bioinformatics. 2009; 25: 14-21

Rodero M. P.,Frémond M. L.,Rice G. I.,Neven B. and Crow Y. J. JAK inhibition in STING-associated interferonopathy. Ann Rheum Dis. 2016; 75: e75

Rodrigue A.,Quentin Y.,Lazdunski A.,Méjean V. and Foglino M. Two-component systems in Pseudomonas aeruginosa: why so many? Trends Microbiol. 2000; 8: 498-504

Rodriguez K. R.,Bruns A. M. and Horvath C. M. MDA5 and LGP2: accomplices and antagonists of antiviral signal transduction. J Virol. 2014; 88: 8194-8200

Romberg N.,Vogel T. P. and Canna S. W. NLRC4 inflammasomopathies. Curr Opin Allergy Clin Immunol. 2017; 17: 398-404

Romberg N.,Al Moussawi K.,Nelson-Williams C.,Stiegler A. L.,Loring E.,Choi M.,Overton J.,Meffre E.,Khokha M. K.,Huttner A. J.,West B.,Podoltsev N. A.,Boggon T. J.,Kazmierczak B. I. and Lifton R. P. Mutation of NLRC4 causes a syndrome of enterocolitis and autoinflammation. Nat Genet. 2014; 46: 1135-1139

Rongvaux A.,Jackson R.,Harman C. C.,Li T.,West A. P.,de Zoete M. R.,Wu Y.,Yordy B.,Lakhani S. A.,Kuan C. Y.,Taniguchi T.,Shadel G. S.,Chen Z. J.,Iwasaki A. and Flavell R. A. Apoptotic caspases prevent the induction of type I interferons by mitochondrial DNA. Cell. 2014; 159: 1563-1577

Roskoski R. ERK1/2 MAP kinases: Structure, function, and regulation. Pharmacological Research. 2012; 66: 105-143

Rothman J. E. and Wieland F. T. Protein Sorting by Transport Vesicles. Science. 1996; 272: 227-234

Rousseau J.,Mbakam C. H.,Guyon A.,Tremblay G.,Begin F. G. and Tremblay J. P. Specific mutations in genes responsible for Alzheimer and for Duchenne Muscular Dystrophy introduced by Base editing and PRIME editing. bioRxiv. 2020; 2020.2007.2031.230565

Rubartelli A.,Cozzolino F.,Talio M. and Sitia R. A novel secretory pathway for interleukin-1 beta, a protein lacking a signal sequence. Embo j. 1990; 9: 1503-1510

Rühl S. and Broz P. Caspase-11 activates a canonical NLRP3 inflammasome by promoting K(+) efflux. Eur J Immunol. 2015; 45: 2927-2936

Rühl S.,Shkarina K.,Demarco B.,Heilig R.,Santos J. C. and Broz P. ESCRT-dependent membrane repair negatively regulates pyroptosis downstream of GSDMD activation. Science. 2018; 362: 956-960

Russo C. A. M. and Selvatti A. P. Bootstrap and Rogue Identification Tests for Phylogenetic Analyses. Mol Biol Evol. 2018; 35: 2327-2333

Saadi M.,Karkhah A.,Pourabdolhossein F.,Ataie A.,Monif M. and Nouri H. R. Involvement of NLRC4 inflammasome through caspase-1 and IL-1β augments neuroinflammation and contributes to memory impairment in an experimental model of Alzheimer's like disease. Brain Res Bull. 2020; 154: 81-90

Saito T. and Gale M., Jr. Differential recognition of double-stranded RNA by RIG-I-like receptors in antiviral immunity. The Journal of experimental medicine. 2008; 205: 1523-1527

Saitoh T.,Fujita N.,Hayashi T.,Takahara K.,Satoh T.,Lee H.,Matsunaga K.,Kageyama S.,Omori H.,Noda T.,Yamamoto N.,Kawai T.,Ishii K.,Takeuchi O.,Yoshimori T. and Akira S. Atg9a controls dsDNA-driven dynamic translocation of STING and the innate immune response. Proc Natl Acad Sci U S A. 2009; 106: 20842-20846

Saldanha R. G.,Balka K. R.,Davidson S.,Wainstein B. K.,Wong M.,Macintosh R.,Loo C. K. C.,Weber M. A.,Kamath V.,Moghaddas F.,De Nardo D.,Gray P. E. and Masters S. L. A Mutation Outside the Dimerization Domain Causing Atypical STING-Associated Vasculopathy With Onset in Infancy. Front Immunol. 2018; 9: 1535

San Pietro E.,Capestrano M.,Polishchuk E. V.,DiPentima A.,Trucco A.,Zizza P.,Mariggiò S.,Pulvirenti T.,Sallese M.,Tete S.,Mironov A. A.,Leslie C. C.,Corda D.,Luini A. and Polishchuk R. S. Group IV phospholipase A(2)alpha controls the formation of inter-cisternal continuities involved in intra-Golgi transport. PLoS Biol. 2009; 7: e1000194

Sanchez G. A. M.,Reinhardt A.,Ramsey S.,Wittkowski H.,Hashkes P. J.,Berkun Y.,Schalm S.,Murias S.,Dare J. A.,Brown D.,Stone D. L.,Gao L.,Klausmeier T.,Foell D.,de Jesus A. A.,Chapelle D. C.,Kim H.,Dill S.,Colbert R. A.,Failla L.,Kost B.,O'Brien M.,Reynolds J. C.,Folio L. R.,Calvo K. R.,Paul S. M.,Weir N.,Brofferio A.,Soldatos A.,Biancotto A.,Cowen E. W.,Digiovanna J. J.,Gadina M.,Lipton A. J.,Hadigan C.,Holland S. M.,Fontana J.,Alawad A. S.,Brown R. J.,Rother K. I.,Heller T.,Brooks K. M.,Kumar P.,Brooks S. R.,Waldman M.,Singh H. K.,Nickeleit V.,Silk M.,Prakash A.,Janes J. M.,Ozen S.,Wakim P. G.,Brogan P. A.,Macias

W. L. and Goldbach-Mansky R. JAK1/2 inhibition with baricitinib in the treatment of autoinflammatory interferonopathies. J Clin Invest. 2018; 128: 3041-3052

Sandall C. F. and MacDonald J. A. Effects of phosphorylation on the NLRP3 inflammasome. Arch Biochem Biophys. 2019; 670: 43-57

Sandall C. F.,Ziehr B. K. and MacDonald J. A. ATP-Binding and Hydrolysis in Inflammasome Activation. Molecules. 2020; 25:

Sanjabi S.,Williams K. J.,Saccani S.,Zhou L.,Hoffmann A.,Ghosh G.,Gerondakis S.,Natoli G. and Smale S. T. A c-Rel subdomain responsible for enhanced DNA-binding affinity and selective gene activation. Genes Dev. 2005; 19: 2138-2151

Sanjana N. E.,Shalem O. and Zhang F. Improved vectors and genome-wide libraries for CRISPR screening. Nat Methods. 2014; 11: 783-784

Saraste J. and Marie M. Intermediate compartment (IC): from pre-Golgi vacuoles to a semi-autonomous membrane system. Histochemistry and Cell Biology. 2018; 150: 407-430

Saraste M.,Sibbald P. R. and Wittinghofer A. The P-loop--a common motif in ATP- and GTP-binding proteins. Trends Biochem Sci. 1990; 15: 430-434

Satış H.,Özger H. S.,Aysert Yıldız P.,Hızel K.,Gulbahar Ö.,Erbaş G.,Aygencel G.,Guzel Tunccan O.,Öztürk M. A.,Dizbay M. and Tufan A. Prognostic value of interleukin-18 and its association with other inflammatory markers and disease severity in COVID-19. Cytokine. 2021; 137: 155302

Sauer J. D.,Sotelo-Troha K.,von Moltke J.,Monroe K. M.,Rae C. S.,Brubaker S. W.,Hyodo M.,Hayakawa Y.,Woodward J. J.,Portnoy D. A. and Vance R. E. The N-ethyl-N-nitrosourea-induced Goldenticket mouse mutant reveals an essential function of Sting in the in vivo interferon response to Listeria monocytogenes and cyclic dinucleotides. Infect Immun. 2011; 79: 688-694

Savic S.,Caseley E. A. and McDermott M. F. Moving towards a systems-based classification of innate immune-mediated diseases. Nature Reviews Rheumatology. 2020; 16: 222-237

Sborgi L.,Ude J.,Dick M. S.,Vesin J.,Chambon M.,Turcatti G.,Broz P. and Hiller S. Assay for high-throughput screening of inhibitors of the ASC-PYD inflammasome core filament. Cell Stress. 2018; 2: 82-90

Sborgi L.,Rühl S.,Mulvihill E.,Pipercevic J.,Heilig R.,Stahlberg H.,Farady C. J.,Müller D. J.,Broz P. and Hiller S. GSDMD membrane pore formation constitutes the mechanism of pyroptotic cell death. Embo j. 2016; 35: 1766-1778

Schimmöller F.,Singer-Krüger B.,Schröder S.,Krüger U.,Barlowe C. and Riezman H. The absence of Emp24p, a component of ER-derived COPII-coated vesicles, causes a defect in transport of selected proteins to the Golgi. Embo j. 1995; 14: 1329-1339

Schneider K. S.,Groß C. J.,Dreier R. F.,Saller B. S.,Mishra R.,Gorka O.,Heilig R.,Meunier E.,Dick M. S.,Ćiković T.,Sodenkamp J.,Médard G.,Naumann R.,Ruland J.,Kuster B.,Broz P. and Groß O. The Inflammasome Drives GSDMD-Independent Secondary Pyroptosis and IL-1 Release in the Absence of Caspase-1 Protease Activity. Cell Rep. 2017; 21: 3846-3859

Scholefield J. and Harrison P. T. Prime editing – an update on the field. Gene Therapy. 2021; 28: 396-401

Schreiber V. and Richet E. Self-association of the Escherichia coli transcription activator MalT in the presence of maltotriose and ATP. J Biol Chem. 1999; 274: 33220-33226

Schroder K. and Tschopp J. The Inflammasomes. Cell. 2010; 140: 821-832

Sebastian-Valverde M.,Wu H.,Al Rahim M.,Sanchez R.,Kumar K.,De Vita R. J. and Pasinetti G. M. Discovery and characterization of small-molecule inhibitors of NLRP3 and NLRC4 inflammasomes. Journal of Biological Chemistry. 2021; 296:

Sellin M. E.,Müller A. A.,Felmy B.,Dolowschiak T.,Diard M.,Tardivel A.,Maslowski K. M. and Hardt W. D. Epithelium-intrinsic NAIP/NLRC4 inflammasome drives infected enterocyte expulsion to restrict Salmonella replication in the intestinal mucosa. Cell Host Microbe. 2014; 16: 237-248

Sepulveda J. L. (2019). Chapter 9 - Challenges in routine clinical chemistry testing analysis of small molecules. Accurate Results in the Clinical Laboratory (Second Edition). A. Dasgupta&J. L. Sepulveda, Elsevier: 101-140.

Serafini T.,Stenbeck G.,Brecht A.,Lottspeich F.,Orci L.,Rothman J. E. and Wieland F. T. A coat subunit of Golgi-derived non-clathrin-coated vesicles with homology to the clathrin-coated vesicle coat protein beta-adaptin. Nature. 1991; 349: 215-220

Seregin S. S.,Golovchenko N.,Schaf B.,Chen J.,Pudlo N. A.,Mitchell J.,Baxter N. T.,Zhao L.,Schloss P. D.,Martens E. C.,Eaton K. A. and Chen G. Y. NLRP6 Protects Il10(-/-) Mice from Colitis by Limiting Colonization of Akkermansia muciniphila. Cell Rep. 2017; 19: 733-745

Sester D. P.,Zamoshnikova A.,Thygesen S. J.,Vajjhala P. R.,Cridland S. O.,Schroder K. and Stacey K. J. Assessment of Inflammasome Formation by Flow Cytometry. Curr Protoc Immunol. 2016; 114: 14.40.11-14.40.29

Sester D. P.,Thygesen S. J.,Sagulenko V.,Vajjhala P. R.,Cridland J. A.,Vitak N.,Chen K. W.,Osborne G. W.,Schroder K. and Stacey K. J. A novel flow cytometric method to assess inflammasome formation. J Immunol. 2015; 194: 455-462

Seth R. B.,Sun L.,Ea C. K. and Chen Z. J. Identification and characterization of MAVS, a mitochondrial antiviral signaling protein that activates NF-kappaB and IRF 3. Cell. 2005; 122: 669-682

Shah A. D.,Goode R. J. A.,Huang C.,Powell D. R. and Schittenhelm R. B. LFQ-Analyst: An Easy-To-Use Interactive Web Platform To Analyse and Visualize Label-Free Proteomics Data Preprocessed with MaxQuant. J Proteome Res. 2020; 19: 204-211

Shalem O.,Sanjana N. E.,Hartenian E.,Shi X.,Scott D. A.,Mikkelson T.,Heckl D.,Ebert B. L.,Root D. E.,Doench J. G. and Zhang F. Genome-scale CRISPR-Cas9 knockout screening in human cells. Science. 2014; 343: 84-87

Shang G.,Zhang C.,Chen Z. J.,Bai X. C. and Zhang X. Cryo-EM structures of STING reveal its mechanism of activation by cyclic GMP-AMP. Nature. 2019; 567: 389-393

Shang G.,Zhu D.,Li N.,Zhang J.,Zhu C.,Lu D.,Liu C.,Yu Q.,Zhao Y.,Xu S. and Gu L. Crystal structures of STING protein reveal basis for recognition of cyclic di-GMP. Nat Struct Mol Biol. 2012; 19: 725-727

Shevchenko A.,Jensen O. N.,Podtelejnikov A. V.,Sagliocco F.,Wilm M.,Vorm O.,Mortensen P.,Shevchenko A.,Boucherie H. and Mann M. Linking genome and proteome by mass spectrometry: large-scale identification of yeast proteins from two dimensional gels. Proc Natl Acad Sci U S A. 1996; 93: 14440-14445

Shi G.,Robles J. T.,Song C.,Salichos L.,Lou H. J.,Gerstein M. and Turk B. E. Proteome-wide screening for mitogen-activated protein kinase docking motifs and interactors. bioRxiv. 2021; 2021.2008.2020.457142

Shi J.,Zhao Y.,Wang Y.,Gao W.,Ding J.,Li P.,Hu L. and Shao F. Inflammatory caspases are innate immune receptors for intracellular LPS. Nature. 2014; 514: 187-192

Shi J.,Zhao Y.,Wang K.,Shi X.,Wang Y.,Huang H.,Zhuang Y.,Cai T.,Wang F. and Shao F. Cleavage of GSDMD by inflammatory caspases determines pyroptotic cell death. Nature. 2015; 526: 660-665

Shi Y.,Lin S.,Staats K. A.,Li Y.,Chang W. H.,Hung S. T.,Hendricks E.,Linares G. R.,Wang Y.,Son E. Y.,Wen X.,Kisler K.,Wilkinson B.,Menendez L.,Sugawara T.,Woolwine P.,Huang M.,Cowan M. J.,Ge B.,Koutsodendris N.,Sandor K. P.,Komberg J.,Vangoor V. R.,Senthilkumar K.,Hennes V.,Seah C.,Nelson A. R.,Cheng T. Y.,Lee S. J.,August P. R.,Chen J. A.,Wisniewski N.,Hanson-Smith V.,Belgard T. G.,Zhang A.,Coba M.,Grunseich C.,Ward M. E.,van den Berg L. H.,Pasterkamp R. J.,Trotti D.,Zlokovic B. V. and Ichida J. K. Haploinsufficiency leads to

neurodegeneration in C9ORF72 ALS/FTD human induced motor neurons. Nat Med. 2018; 24: 313-325

Shim D.-W.,Shin W.-Y.,Yu S.-H.,Kim B.-H.,Ye S.-K.,Koppula S.,Won H.-S.,Kang T.-B. and Lee K.-H. BOT-4-one attenuates NLRP3 inflammasome activation: NLRP3 alkylation leading to the regulation of its ATPase activity and ubiquitination. Scientific Reports. 2017; 7: 15020

Shoda R.,Matsueda K.,Yamato S. and Umeda N. Epidemiologic analysis of Crohn disease in Japan: increased dietary intake of n-6 polyunsaturated fatty acids and animal protein relates to the increased incidence of Crohn disease in Japan. Am J Clin Nutr. 1996; 63: 741-745

Shomron O.,Nevo-Yassaf I.,Aviad T.,Yaffe Y.,Zahavi E. E.,Dukhovny A.,Perlson E.,Brodsky I.,Yeheskel A.,Pasmanik-Chor M.,Mironov A.,Beznoussenko G. V.,Mironov A. A.,Sklan E. H.,Patterson G. H.,Yonemura Y.,Sannai M.,Kaether C. and Hirschberg K. COPII collar defines the boundary between ER and ER exit site and does not coat cargo containers. J Cell Biol. 2021; 220:

Shtutman M.,Baig M.,Levina E.,Hurteau G.,Lim C.-u.,Broude E.,Nikiforov M.,Harkins T. T.,Carmack C. S.,Ding Y.,Wieland F.,Buttyan R. and Roninson I. B. Tumor-specific silencing of COPZ2 gene encoding coatomer protein complex subunit ζ2 renders tumor cells dependent on its paralogous gene COPZ1. Proceedings of the National Academy of Sciences. 2011; 108: 12449-12454

Shu C.,Sankaran B.,Chaton C. T.,Herr A. B.,Mishra A.,Peng J. and Li P. Structural insights into the functions of TBK1 in innate antimicrobial immunity. Structure. 2013; 21: 1137-1148

Siahanidou T.,Nikaina E.,Kontogiorgou C.,Tzanoudaki M.,Stefanaki K.,Skiathitou A. V.,Petropoulou T. and Kanariou M. Autoinflammation with Infantile Enterocolitis Associated with Recurrent Perianal Abscesses. J Clin Immunol. 2019; 39: 237-240

Singh V.,Xu L.,Boyko S.,Surewicz K. and Surewicz W. K. Zinc promotes liquid–liquid phase separation of tau protein. Journal of Biological Chemistry. 2020; 295: 5850-5856

Siu T.,Altman M. D.,Baltus G. A.,Childers M.,Ellis J. M.,Gunaydin H.,Hatch H.,Ho T.,Jewell J.,Lacey B. M.,Lesburg C. A.,Pan B. S.,Sauvagnat B.,Schroeder G. K. and Xu S. Discovery of a Novel cGAMP Competitive Ligand of the Inactive Form of STING. ACS Med Chem Lett. 2019; 10: 92-97

Sivakumar P. V.,Westrich G. M.,Kanaly S.,Garka K.,Born T. L.,Derry J. M. J. and Viney J. L. Interleukin 18 is a primary mediator of the inflammation associated with dextran sulphate sodium induced colitis: blocking interleukin 18 attenuates intestinal damage. Gut. 2002; 50: 812-820

Slater S. L.,Sågfors A. M.,Pollard D. J.,Ruano-Gallego D. and Frankel G. The Type III Secretion System of Pathogenic Escherichia coli. Curr Top Microbiol Immunol. 2018; 416: 51-72

Sliter D. A.,Martinez J.,Hao L.,Chen X.,Sun N.,Fischer T. D.,Burman J. L.,Li Y.,Zhang Z.,Narendra D. P.,Cai H.,Borsche M.,Klein C. and Youle R. J. Parkin and PINK1 mitigate STING-induced inflammation. Nature. 2018; 561: 258-262

Slootweg E. J.,Spiridon L. N.,Roosien J.,Butterbach P.,Pomp R.,Westerhof L.,Wilbers R.,Bakker E.,Bakker J.,Petrescu A.-J.,Smant G. and Goverse A. Structural Determinants at the Interface of the ARC2 and Leucine-Rich Repeat Domains Control the Activation of the Plant Immune Receptors Rx1 and Gpa2 Plant Physiology. 2013; 162: 1510-1528

Snider J.,Thibault G. and Houry W. A. The AAA+ superfamily of functionally diverse proteins. Genome Biol. 2008; 9: 216

Soares J. L.,Oliveira E. M. and Pontillo A. Variants in NLRP3 and NLRC4 inflammasome associate with susceptibility and severity of multiple sclerosis. Mult Scler Relat Disord. 2019; 29: 26-34

Sobolewska B.,Angermair E.,Deuter C.,Doycheva D.,Kuemmerle-Deschner J. and Zierhut M. NLRP3 A439V Mutation in a Large Family with Cryopyrin-associated Periodic

Syndrome: Description of Ophthalmologic Symptoms in Correlation with Other Organ Symptoms. The Journal of Rheumatology. 2016; jrheum.150681

Sokolowska M.,Chen L. Y.,Liu Y.,Martinez-Anton A.,Qi H. Y.,Logun C.,Alsaaty S.,Park Y. H.,Kastner D. L.,Chae J. J. and Shelhamer J. H. Prostaglandin E2 Inhibits NLRP3 Inflammasome Activation through EP4 Receptor and Intracellular Cyclic AMP in Human Macrophages. J Immunol. 2015; 194: 5472-5487

Song N.,Liu Z.-S.,Xue W.,Bai Z.-F.,Wang Q.-Y.,Dai J.,Liu X.,Huang Y.-J.,Cai H.,Zhan X.-Y.,Han Q.-Y.,Wang H.,Chen Y.,Li H.-Y.,Li A.-L.,Zhang X.-M.,Zhou T. and Li T. NLRP3 Phosphorylation Is an Essential Priming Event for Inflammasome Activation. Mol Cell. 2017; 68: 185-197.e186

Song Y.,An O.,Ren X.,Chan T. H. M.,Tay D. J. T.,Tang S. J.,Han J.,Hong H.,Ng V. H. E.,Ke X.,Shen H.,Pitcheshwar P.,Lin J. S.,Leong K. W.,Molias F. B.,Yang H.,Kappei D. and Chen L. RNA editing mediates the functional switch of COPA in a novel mechanism of hepatocarcinogenesis. Journal of Hepatology. 2021; 74: 135-147

Srikanth S.,Woo J. S.,Wu B.,El-Sherbiny Y. M.,Leung J.,Chupradit K.,Rice L.,Seo G. J.,Calmettes G.,Ramakrishna C.,Cantin E.,An D. S.,Sun R.,Wu T. T.,Jung J. U.,Savic S. and Gwack Y. The Ca(2+) sensor STIM1 regulates the type I interferon response by retaining the signaling adaptor STING at the endoplasmic reticulum. Nat Immunol. 2019; 20: 152-162

Stagg S. M.,Gürkan C.,Fowler D. M.,LaPointe P.,Foss T. R.,Potter C. S.,Carragher B. and Balch W. E. Structure of the Sec13/31 COPII coat cage. Nature. 2006; 439: 234-238

Stanley P. Golgi glycosylation. Cold Spring Harb Perspect Biol. 2011; 3: a005199

Starokadomskyy P.,Gemelli T.,Rios J. J.,Xing C.,Wang R. C.,Li H.,Pokatayev V.,Dozmorov I.,Khan S.,Miyata N.,Fraile G.,Raj P.,Xu Z.,Xu Z.,Ma L.,Lin Z.,Wang H.,Yang Y.,Ben-Amitai D.,Orenstein N.,Mussaffi H.,Baselga E.,Tadini G.,Grunebaum E.,Sarajlija A.,Krzewski K.,Wakeland E. K.,Yan N.,de la Morena M. T.,Zinn A. R. and Burstein E. DNA polymerase-α regulates the activation of type I interferons through cytosolic RNA:DNA synthesis. Nat Immunol. 2016; 17: 495-504

Stecher G.,Tamura K. and Kumar S. Molecular Evolutionary Genetics Analysis (MEGA) for macOS. Mol Biol Evol. 2020; 37: 1237-1239

Steimle V.,Otten L. A.,Zufferey M. and Mach B. Complementation cloning of an MHC class II transactivator mutated in hereditary MHC class II deficiency (or bare lymphocyte syndrome). Cell. 1993; 75: 135-146

Steiner A.,Reygaerts T.,Pontillo A.,Ceccherini I.,Moecking J.,Moghaddas F.,Davidson S.,Caroli F.,Grossi A.,Castro F. F. M.,Kalil J.,Gohr F. N.,Schmidt F. I.,Bartok E.,Zillinger T.,Hartmann G.,Geyer M.,Gattorno M.,Mendonça L. O. and Masters S. L. Recessive NLRC4-Autoinflammatory Disease Reveals an Ulcerative Colitis Locus. J Clin Immunol. 2021;

Stempel M.,Chan B.,Juranić Lisnić V.,Krmpotić A.,Hartung J.,Paludan S. R.,Füllbrunn N.,Lemmermann N. A. and Brinkmann M. M. The herpesviral antagonist m152 reveals differential activation of STING-dependent IRF and NF-κB signaling and STING's dual role during MCMV infection. Embo j. 2019; 38:

Stenbeck G.,Harter C.,Brecht A.,Herrmann D.,Lottspeich F.,Orci L. and Wieland F. T. beta'-COP, a novel subunit of coatomer. Embo j. 1993; 12: 2841-2845

Su K. H.,Cao J.,Tang Z.,Dai S.,He Y.,Sampson S. B.,Benjamin I. J. and Dai C. HSF1 critically attunes proteotoxic stress sensing by mTORC1 to combat stress and promote growth. Nat Cell Biol. 2016; 18: 527-539

Su M.-Y.,Fromm S. A.,Zoncu R. and Hurley J. H. Structure of the C9orf72 ARF GAP complex that is haploinsufficient in ALS and FTD. Nature. 2020; 585: 251-255

Suckale J.,Sim R. B. and Dodds A. W. Evolution of innate immune systems*. Biochem Mol Biol Educ. 2005; 33: 177-183

Sudo H.,Tsuji A. B.,Sugyo A.,Kohda M.,Sogawa C.,Yoshida C.,Harada Y. N.,Hino O. and Saga T. Knockdown of COPA, identified by loss-of-function screen, induces apoptosis and suppresses tumor growth in mesothelioma mouse model. Genomics. 2010; 95: 210-216

Sugawara S.,Uehara A.,Nochi T.,Yamaguchi T.,Ueda H.,Sugiyama A.,Hanzawa K.,Kumagai K.,Okamura H. and Takada H. Neutrophil proteinase 3-mediated induction of bioactive IL-18 secretion by human oral epithelial cells. J Immunol. 2001; 167: 6568-6575

Sun B.,Sundström K. B.,Chew J. J.,Bist P.,Gan E. S.,Tan H. C.,Goh K. C.,Chawla T.,Tang C. K. and Ooi E. E. Dengue virus activates cGAS through the release of mitochondrial DNA. Sci Rep. 2017; 7: 3594

Sun H.,Huang Y.,Mei S.,Xu F.,Liu X.,Zhao F.,Yin L.,Zhang D.,Wei L.,Wu C.,Ma S.,Wang J.,Cen S.,Liang C.,Hu S. and Guo F. A Nuclear Export Signal Is Required for cGAS to Sense Cytosolic DNA. Cell Rep. 2021; 34: 108586

Sun L.,Wu J.,Du F.,Chen X. and Chen Z. J. Cyclic GMP-AMP synthase is a cytosolic DNA sensor that activates the type I interferon pathway. Science. 2013; 339: 786-791

Sun M.-S.,Zhang J.,Jiang L.-Q.,Pan Y.-X.,Tan J.-Y.,Yu F.,Guo L.,Yin L.,Shen C.,Shu H.-B. and Liu Y. TMED2 Potentiates Cellular IFN Responses to DNA Viruses by Reinforcing MITA Dimerization and Facilitating Its Trafficking. Cell Reports. 2018; 25: 3086-3098.e3083

Sun W.,Li Y.,Chen L.,Chen H.,You F.,Zhou X.,Zhou Y.,Zhai Z.,Chen D. and Jiang Z. ERIS, an endoplasmic reticulum IFN stimulator, activates innate immune signaling through dimerization. Proc Natl Acad Sci U S A. 2009; 106: 8653-8658

Sun Z.,Anderl F.,Fröhlich K.,Zhao L.,Hanke S.,Brügger B.,Wieland F. and Béthune J. Multiple and stepwise interactions between coatomer and ADP-ribosylation factor-1 (Arf1)-GTP. Traffic. 2007; 8: 582-593

Sürün D.,Schneider A.,Mircetic J.,Neumann K.,Lansing F.,Paszkowski-Rogacz M.,Hänchen V.,Lee-Kirsch M. A. and Buchholz F. Efficient Generation and Correction of Mutations in Human iPS Cells Utilizing mRNAs of CRISPR Base Editors and Prime Editors. Genes (Basel). 2020; 11:

Sutterwala F. S.,Mijares L. A.,Li L.,Ogura Y.,Kazmierczak B. I. and Flavell R. A. Immune recognition of Pseudomonas aeruginosa mediated by the IPAF/NLRC4 inflammasome. J Exp Med. 2007; 204: 3235-3245

Sutton C.,Brereton C.,Keogh B.,Mills K. H. and Lavelle E. C. A crucial role for interleukin (IL)-1 in the induction of IL-17-producing T cells that mediate autoimmune encephalomyelitis. J Exp Med. 2006; 203: 1685-1691

Suzuki T.,Franchi L.,Toma C.,Ashida H.,Ogawa M.,Yoshikawa Y.,Mimuro H.,Inohara N.,Sasakawa C. and Nuñez G. Differential regulation of caspase-1 activation, pyroptosis, and autophagy via Ipaf and ASC in Shigella-infected macrophages. PLoS Pathog. 2007; 3: e111

Symington L. S. and Gautier J. Double-strand break end resection and repair pathway choice. Annu Rev Genet. 2011; 45: 247-271

Symons J. A.,Young P. R. and Duff G. W. Soluble type II interleukin 1 (IL-1) receptor binds and blocks processing of IL-1 beta precursor and loses affinity for IL-1 receptor antagonist. Proc Natl Acad Sci U S A. 1995; 92: 1714-1718

Sysoeva T. A. Assessing heterogeneity in oligomeric AAA+ machines. Cellular and Molecular Life Sciences. 2017; 74: 1001-1018

Sze A.,Belgnaoui S. M.,Olagnier D.,Lin R.,Hiscott J. and van Grevenynghe J. Host restriction factor SAMHD1 limits human T cell leukemia virus type 1 infection of monocytes via STING-mediated apoptosis. Cell Host Microbe. 2013; 14: 422-434

Szul T. and Sztul E. COPII and COPI Traffic at the ER-Golgi Interface. Physiology. 2011; 26: 348-364

Tabeta K.,Hoebe K.,Janssen E. M.,Du X.,Georgel P.,Crozat K.,Mudd S.,Mann N.,Sovath S.,Goode J.,Shamel L.,Herskovits A. A.,Portnoy D. A.,Cooke M.,Tarantino L. M.,Wiltshire T.,Steinberg B. E.,Grinstein S. and Beutler B. The Unc93b1 mutation 3d disrupts exogenous antigen presentation and signaling via Toll-like receptors 3, 7 and 9. Nat Immunol. 2006; 7: 156-164

Takada H.,Nomura A.,Ohga S. and Hara T. Interleukin-18 in hemophagocytic lymphohistiocytosis. Leuk Lymphoma. 2001; 42: 21-28

Takaoka A.,Wang Z.,Choi M. K.,Yanai H.,Negishi H.,Ban T.,Lu Y.,Miyagishi M.,Kodama T.,Honda K.,Ohba Y. and Taniguchi T. DAI (DLM-1/ZBP1) is a cytosolic DNA sensor and an activator of innate immune response. Nature. 2007; 448: 501-505

Tameling W. I.,Vossen J. H.,Albrecht M.,Lengauer T.,Berden J. A.,Haring M. A.,Cornelissen B. J. and Takken F. L. Mutations in the NB-ARC domain of I-2 that impair ATP hydrolysis cause autoactivation. Plant Physiol. 2006; 140: 1233-1245

Tamura T.,Thotakura P.,Tanaka T. S.,Ko M. S. and Ozato K. Identification of target genes and a unique cis element regulated by IRF-8 in developing macrophages. Blood. 2005; 106: 1938-1947

Tanabe T.,Chamaillard M.,Ogura Y.,Zhu L.,Qiu S.,Masumoto J.,Ghosh P.,Moran A.,Predergast M. M.,Tromp G.,Williams C. J.,Inohara N. and Núñez G. Regulatory regions and critical residues of NOD2 involved in muramyl dipeptide recognition. Embo j. 2004; 23: 1587-1597

Tanaka Y. and Chen Z. J. STING specifies IRF3 phosphorylation by TBK1 in the cytosolic DNA signaling pathway. Sci Signal. 2012; 5: ra20

Tang C. H.,Zundell J. A.,Ranatunga S.,Lin C.,Nefedova Y.,Del Valle J. R. and Hu C. C. Agonist-Mediated Activation of STING Induces Apoptosis in Malignant B Cells. Cancer Res. 2016; 76: 2137-2152

Tang X.,Li H.,Liu H.,Xu H.,Yang H.,Liu J. and Zhao S. Etiologic spectrum of interstitial lung diseases in Chinese children older than 2 years of age. Orphanet J Rare Dis. 2020a; 15: 25

Tang X.,Xu H.,Zhou C.,Peng Y.,Liu H.,Liu J.,Li H.,Yang H. and Zhao S. STING-Associated Vasculopathy with Onset in Infancy in Three Children with New Clinical Aspect and Unsatisfactory Therapeutic Responses to Tofacitinib. J Clin Immunol. 2020b; 40: 114-122

Tanjore H.,Blackwell T. S. and Lawson W. E. Emerging evidence for endoplasmic reticulum stress in the pathogenesis of idiopathic pulmonary fibrosis. Am J Physiol Lung Cell Mol Physiol. 2012; 302: L721-729

Tapia-Abellán A.,Angosto-Bazarra D.,Martínez-Banaclocha H.,de Torre-Minguela C.,Cerón-Carrasco J. P.,Pérez-Sánchez H.,Arostegui J. I. and Pelegrin P. MCC950 closes the active conformation of NLRP3 to an inactive state. Nat Chem Biol. 2019; 15: 560-564

Taveira-DaSilva A. M.,Markello T. C.,Kleiner D. E.,Jones A. M.,Groden C.,Macnamara E.,Yokoyama T.,Gahl W. A.,Gochuico B. R. and Moss J. Expanding the phenotype of COPA syndrome: a kindred with typical and atypical features. J Med Genet. 2019; 56: 778-782

Teng S.,Srivastava A. K.,Schwartz C. E.,Alexov E. and Wang L. Structural assessment of the effects of amino acid substitutions on protein stability and protein protein interaction. Int J Comput Biol Drug Des. 2010; 3: 334-349

Tenthorey J. L.,Kofoed E. M.,Daugherty M. D.,Malik H. S. and Vance R. E. Molecular basis for specific recognition of bacterial ligands by NAIP/NLRC4 inflammasomes. Mol Cell. 2014; 54: 17-29

Tenthorey J. L.,Chavez R. A.,Thompson T. W.,Deets K. A.,Vance R. E. and Rauch I. NLRC4 inflammasome activation is NLRP3- and phosphorylation-independent during infection and does not protect from melanoma. Journal of Experimental Medicine. 2020; 217:

Tenthorey J. L.,Haloupek N.,López-Blanco J. R.,Grob P.,Adamson E.,Hartenian E.,Lind N. A.,Bourgeois N. M.,Chacón P.,Nogales E. and Vance R. E. The structural basis of flagellin

detection by NAIP5: A strategy to limit pathogen immune evasion. Science. 2017; 358: 888-893

Thaivalappil S. S.,Garrod A. S.,Borowitz S. M.,Watkin L. B. and Lawrence M. G. Persistent Unexplained Transaminitis in COPA Syndrome. J Clin Immunol. 2021; 41: 205-208

The French F. M. F. C.,Bernot A.,Clepet C.,Dasilva C.,Devaud C.,Petit J.-L.,Caloustian C.,Cruaud C.,Samson D.,Pulcini F.,Weissenbach J.,Heilig R.,Notanicola C.,Domingo C.,Rozenbaum M.,Benchetrit E.,Topaloglu R.,Dewalle M.,Dross C.,Hadjari P.,Dupont M.,Demaille J.,Touitou I.,Smaoui N.,Nedelec B.,Méry J.-P.,Chaabouni H.,Delpech M. and Grateau G. A candidate gene for familial Mediterranean fever. Nature Genetics. 1997; 17: 25-31

Thor F.,Gautschi M.,Geiger R. and Helenius A. Bulk flow revisited: transport of a soluble protein in the secretory pathway. Traffic. 2009; 10: 1819-1830

Thorand B.,Kolb H.,Baumert J.,Koenig W.,Chambless L.,Meisinger C.,Illig T.,Martin S. and Herder C. Elevated levels of interleukin-18 predict the development of type 2 diabetes: results from the MONICA/KORA Augsburg Study, 1984-2002. Diabetes. 2005; 54: 2932-2938

Tian R.,Pan Y.,Etheridge T. H. A.,Deshmukh H.,Gulick D.,Gibson G.,Bao G. and Lee C. M. Pitfalls in Single Clone CRISPR-Cas9 Mutagenesis to Fine-Map Regulatory Intervals. Genes. 2020; 11: 504

Ting J. P.,Lovering R. C.,Alnemri E. S.,Bertin J.,Boss J. M.,Davis B. K.,Flavell R. A.,Girardin S. E.,Godzik A.,Harton J. A.,Hoffman H. M.,Hugot J. P.,Inohara N.,Mackenzie A.,Maltais L. J.,Nunez G.,Ogura Y.,Otten L. A.,Philpott D.,Reed J. C.,Reith W.,Schreiber S.,Steimle V. and Ward P. A. The NLR gene family: a standard nomenclature. Immunity. 2008; 28: 285-287

Todd A. G.,Lin H.,Ebert A. D.,Liu Y. and Androphy E. J. COPI transport complexes bind to specific RNAs in neuronal cells. Hum Mol Genet. 2013; 22: 729-736

Tomalka J.,Ganesan S.,Azodi E.,Patel K.,Majmudar P.,Hall B. A.,Fitzgerald K. A. and Hise A. G. A novel role for the NLRC4 inflammasome in mucosal defenses against the fungal pathogen Candida albicans. PLoS Pathog. 2011; 7: e1002379

Trautwein M.,Dengjel J.,Schirle M. and Spang A. Arf1p provides an unexpected link between COPI vesicles and mRNA in Saccharomyces cerevisiae. Mol Biol Cell. 2004; 15: 5021-5037

Trottestam H.,Horne A.,Aricò M.,Egeler R. M.,Filipovich A. H.,Gadner H.,Imashuku S.,Ladisch S.,Webb D.,Janka G. and Henter J. I. Chemoimmunotherapy for hemophagocytic lymphohistiocytosis: long-term results of the HLH-94 treatment protocol. Blood. 2011; 118: 4577-4584

Tsagkogeorga G.,Parker J.,Stupka E.,Cotton James A. and Rossiter Stephen J. Phylogenomic Analyses Elucidate the Evolutionary Relationships of Bats. Current Biology. 2013; 23: 2262-2267

Tsu B. V.,Beierschmitt C.,Ryan A. P.,Agarwal R.,Mitchell P. S. and Daugherty M. D. Diverse viral proteases activate the NLRP1 inflammasome. Elife. 2021; 10:

Tsui J. L.,Estrada O. A.,Deng Z.,Wang K. M.,Law C. S.,Elicker B. M.,Jones K. D.,Dell S. D.,Gudmundsson G.,Hansdottir S.,Helfgott S. M.,Volpi S.,Gattorno M.,Waterfield M. R.,Chan A. Y.,Chung S. A.,Ley B. and Shum A. K. Analysis of pulmonary features and treatment approaches in the COPA syndrome. ERJ Open Res. 2018; 4:

Tu B. P. and Weissman J. S. Oxidative protein folding in eukaryotes: mechanisms and consequences. J Cell Biol. 2004; 164: 341-346

Tu D.,Zhu Z.,Zhou A. Y.,Yun C. H.,Lee K. E.,Toms A. V.,Li Y.,Dunn G. P.,Chan E.,Thai T.,Yang S.,Ficarro S. B.,Marto J. A.,Jeon H.,Hahn W. C.,Barbie D. A. and Eck M. J. Structure and ubiquitination-dependent activation of TANK-binding kinase 1. Cell Rep. 2013; 3: 747-758

Tufan A.,Avanoğlu Güler A. and Matucci-Cerinic M. COVID-19, immune system response, hyperinflammation and repurposing antirheumatic drugs. Turk J Med Sci. 2020; 50: 620-632

Tunyasuvunakool K.,Adler J.,Wu Z.,Green T.,Zielinski M.,Žídek A.,Bridgland A.,Cowie A.,Meyer C.,Laydon A.,Velankar S.,Kleywegt G. J.,Bateman A.,Evans R.,Pritzel A.,Figurnov M.,Ronneberger O.,Bates R.,Kohl S. A. A.,Potapenko A.,Ballard A. J.,Romera-Paredes B.,Nikolov S.,Jain R.,Clancy E.,Reiman D.,Petersen S.,Senior A. W.,Kavukcuoglu K.,Birney E.,Kohli P.,Jumper J. and Hassabis D. Highly accurate protein structure prediction for the human proteome. Nature. 2021; 596: 590-596

Uhlorn B. L.,Gamez E. R.,Li S. and Campos S. K. Attenuation of cGAS/STING activity during mitosis. Life Sci Alliance. 2020; 3:

Unterholzner L.,Keating S. E.,Baran M.,Horan K. A.,Jensen S. B.,Sharma S.,Sirois C. M.,Jin T.,Latz E.,Xiao T. S.,Fitzgerald K. A.,Paludan S. R. and Bowie A. G. IFI16 is an innate immune sensor for intracellular DNA. Nature Immunology. 2010; 11: 997-1004

Uzé G.,Schreiber G.,Piehler J. and Pellegrini S. The receptor of the type I interferon family. Curr Top Microbiol Immunol. 2007; 316: 71-95

Vajjhala P. R.,Lu A.,Brown D. L.,Pang S. W.,Sagulenko V.,Sester D. P.,Cridland S. O.,Hill J. M.,Schroder K.,Stow J. L.,Wu H. and Stacey K. J. The Inflammasome Adaptor ASC Induces Procaspase-8 Death Effector Domain Filaments. J Biol Chem. 2015; 290: 29217-29230

van Oers M. M.,Pijlman G. P. and Vlak J. M. Thirty years of baculovirus–insect cell protein expression: from dark horse to mainstream technology. Journal of General Virology. 2015; 96: 6-23

Van Opdenbosch N.,Van Gorp H.,Verdonckt M.,Saavedra P. H. V.,de Vasconcelos N. M.,Gonçalves A.,Vande Walle L.,Demon D.,Matusiak M.,Van Hauwermeiren F.,D'Hont J.,Hochepied T.,Krautwald S.,Kanneganti T. D. and Lamkanfi M. Caspase-1 Engagement and TLR-Induced c-FLIP Expression Suppress ASC/Caspase-8-Dependent Apoptosis by Inflammasome Sensors NLRP1b and NLRC4. Cell Rep. 2017; 21: 3427-3444

Vance J. E. Phospholipid synthesis in a membrane fraction associated with mitochondria. J Biol Chem. 1990; 265: 7248-7256

Vece T. J.,Watkin L. B.,Nicholas S.,Canter D.,Braun M. C.,Guillerman R. P.,Eldin K. W.,Bertolet G.,McKinley S.,de Guzman M.,Forbes L.,Chinn I. and Orange J. S. Copa Syndrome: a Novel Autosomal Dominant Immune Dysregulatory Disease. J Clin Immunol. 2016; 36: 377-387

Velazquez-Villarreal E. I.,Maheshwari S.,Sorenson J.,Fiddes I. T.,Kumar V.,Yin Y.,Webb M. G.,Catalanotti C.,Grigorova M.,Edwards P. A.,Carpten J. D. and Craig D. W. Single-cell sequencing of genomic DNA resolves sub-clonal heterogeneity in a melanoma cell line. Communications Biology. 2020; 3: 318

Vembar S. S. and Brodsky J. L. One step at a time: endoplasmic reticulum-associated degradation. Nature Reviews Molecular Cell Biology. 2008; 9: 944-957

Verma V.,Gupta S.,Kumar P.,Yadav S.,Dhanda R. S.,Gaind R.,Arora R.,Frimodt-Møller N. and Yadav M. Involvement of NLRP3 and NLRC4 Inflammasome in Uropathogenic E. coli Mediated Urinary Tract Infections. Front Microbiol. 2019; 10:

Viganò E.,Diamond C. E.,Spreafico R.,Balachander A.,Sobota R. M. and Mortellaro A. Human caspase-4 and caspase-5 regulate the one-step non-canonical inflammasome activation in monocytes. Nature Communications. 2015; 6: 8761

Vincent M. J.,Martin A. S. and Compans R. W. Function of the KKXX motif in endoplasmic reticulum retrieval of a transmembrane protein depends on the length and structure of the cytoplasmic domain. J Biol Chem. 1998; 273: 950-956

Vispé S.,Cazaux C.,Lesca C. and Defais M. Overexpression of Rad51 protein stimulates homologous recombination and increases resistance of mammalian cells to ionizing radiation. Nucleic Acids Research. 1998; 26: 2859-2864

Voeltz G. K.,Rolls M. M. and Rapoport T. A. Structural organization of the endoplasmic reticulum. EMBO Rep. 2002; 3: 944-950

Volker-Touw C. M.,de Koning H. D.,Giltay J. C.,de Kovel C. G.,van Kempen T. S.,Oberndorff K. M.,Boes M. L.,van Steensel M. A.,van Well G. T.,Blokx W. A.,Schalkwijk J.,Simon A.,Frenkel J. and van Gijn M. E. Erythematous nodes, urticarial rash and arthralgias in a large pedigree with NLRC4-related autoinflammatory disease, expansion of the phenotype. Br J Dermatol. 2017; 176: 244-248

Volkman H. E.,Cambier S.,Gray E. E. and Stetson D. B. Tight nuclear tethering of cGAS is essential for preventing autoreactivity. Elife. 2019; 8:

Volpi S.,Tsui J.,Mariani M.,Pastorino C.,Caorsi R.,Sacco O.,Ravelli A.,Shum A. K.,Gattorno M. and Picco P. Type I interferon pathway activation in COPA syndrome. Clin Immunol. 2018; 187: 33-36

Volpi S.,Insalaco A.,Caorsi R.,Santori E.,Messia V.,Sacco O.,Terheggen-Lagro S.,Cardinale F.,Scarselli A.,Pastorino C.,Moneta G.,Cangemi G.,Passarelli C.,Ricci M.,Girosi D.,Derchi M.,Bocca P.,Diociaiuti A.,El Hachem M.,Cancrini C.,Tomà P.,Granata C.,Ravelli A.,Candotti F.,Picco P.,DeBenedetti F. and Gattorno M. Efficacy and Adverse Events During Janus Kinase Inhibitor Treatment of SAVI Syndrome. J Clin Immunol. 2019; 39: 476-485

von Moltke J.,Trinidad N. J.,Moayeri M.,Kintzer A. F.,Wang S. B.,van Rooijen N.,Brown C. R.,Krantz B. A.,Leppla S. H.,Gronert K. and Vance R. E. Rapid induction of inflammatory lipid mediators by the inflammasome in vivo. Nature. 2012; 490: 107-111

Wada T.,Kanegane H.,Ohta K.,Katoh F.,Imamura T.,Nakazawa Y.,Miyashita R.,Hara J.,Hamamoto K.,Yang X.,Filipovich A. H.,Marsh R. A. and Yachie A. Sustained elevation of serum interleukin-18 and its association with hemophagocytic lymphohistiocytosis in XIAP deficiency. Cytokine. 2014; 65: 74-78

Walker J. E.,Saraste M.,Runswick M. J. and Gay N. J. Distantly related sequences in the alpha- and beta-subunits of ATP synthase, myosin, kinases and other ATP-requiring enzymes and a common nucleotide binding fold. Embo j. 1982; 1: 945-951

Walsh C. T.,Garneau-Tsodikova S. and Gatto G. J., Jr. Protein posttranslational modifications: the chemistry of proteome diversifications. Angew Chem Int Ed Engl. 2005; 44: 7342-7372

Wang L.,Wen W.,Deng M.,Li Y.,Sun G.,Zhao X.,Tang X. and Mao H. A Novel Mutation in the NBD Domain of NLRC4 Causes Mild Autoinflammation With Recurrent Urticaria. Frontiers in Immunology. 2021a; 12:

Wang X.,Feuerstein G. Z.,Gu J. L.,Lysko P. G. and Yue T. L. Interleukin-1 beta induces expression of adhesion molecules in human vascular smooth muscle cells and enhances adhesion of leukocytes to smooth muscle cells. Atherosclerosis. 1995; 115: 89-98

Wang X.,Eno C. O.,Altman B. J.,Zhu Y.,Zhao G.,Olberding K. E.,Rathmell J. C. and Li C. ER stress modulates cellular metabolism. Biochem J. 2011; 435: 285-296

Wang Y.,Wang F. and Zhang X. STING-associated vasculopathy with onset in infancy: a familial case series report and literature review. Ann Transl Med. 2021b; 9: 176

Wang Y.,Ouellette A. N.,Egan C. W.,Rathinavelan T.,Im W. and De Guzman R. N. Differences in the electrostatic surfaces of the type III secretion needle proteins PrgI, BsaL, and MxiH. J Mol Biol. 2007; 371: 1304-1314

Wang Y.-C.,Peterson S. E. and Loring J. F. Protein post-translational modifications and regulation of pluripotency in human stem cells. Cell Research. 2014; 24: 143-160

Warner J. D.,Irizarry-Caro R. A.,Bennion B. G.,Ai T. L.,Smith A. M.,Miner C. A.,Sakai T.,Gonugunta V. K.,Wu J.,Platt D. J.,Yan N. and Miner J. J. STING-associated vasculopathy develops independently of IRF3 in mice. J Exp Med. 2017; 214: 3279-3292

Waters M. G.,Serafini T. and Rothman J. E. 'Coatomer': a cytosolic protein complex containing subunits of non-clathrin-coated Golgi transport vesicles. Nature. 1991; 349: 248-251

Watkin L. B.,Jessen B.,Wiszniewski W.,Vece T. J.,Jan M.,Sha Y.,Thamsen M.,Santos-Cortez R. L.,Lee K.,Gambin T.,Forbes L. R.,Law C. S.,Stray-Pedersen A.,Cheng M. H.,Mace E.

M.,Anderson M. S.,Liu D.,Tang L. F.,Nicholas S. K.,Nahmod K.,Makedonas G.,Canter D. L.,Kwok P. Y.,Hicks J.,Jones K. D.,Penney S.,Jhangiani S. N.,Rosenblum M. D.,Dell S. D.,Waterfield M. R.,Papa F. R.,Muzny D. M.,Zaitlen N.,Leal S. M.,Gonzaga-Jauregui C.,Boerwinkle E.,Eissa N. T.,Gibbs R. A.,Lupski J. R.,Orange J. S. and Shum A. K. COPA mutations impair ER-Golgi transport and cause hereditary autoimmune-mediated lung disease and arthritis. Nat Genet. 2015; 47: 654-660

Watson R. O.,Manzanillo P. S. and Cox J. S. Extracellular M. tuberculosis DNA targets bacteria for autophagy by activating the host DNA-sensing pathway. Cell. 2012; 150: 803-815

Weber A.,Wasiliew P. and Kracht M. Interleukin-1 (IL-1) pathway. Sci Signal. 2010; 3: cm1

Wegmann D.,Hess P.,Baier C.,Wieland F. T. and Reinhard C. Novel Isotypic γ/ζ Subunits Reveal Three Coatomer Complexes in Mammals. Molecular and Cellular Biology. 2004; 24: 1070-1080

Wei J.,Lian H.,Guo W.,Chen Y.-D.,Zhang X.-N.,Zang R.,Zhong L.,Yang Q.,Hu M.-M.,Luo W.-W.,Shu H.-B. and Li S. SNX8 modulates innate immune response to DNA virus by mediating trafficking and activation of MITA. PLOS Pathogens. 2018; 14: e1007336

Wei J. H. and Seemann J. Golgi ribbon disassembly during mitosis, differentiation and disease progression. Curr Opin Cell Biol. 2017; 47: 43-51

Weiss E. S.,Girard-Guyonvarc'h C.,Holzinger D.,de Jesus A. A.,Tariq Z.,Picarsic J.,Schiffrin E. J.,Foell D.,Grom A. A.,Ammann S.,Ehl S.,Hoshino T.,Goldbach-Mansky R.,Gabay C. and Canna S. W. Interleukin-18 diagnostically distinguishes and pathogenically promotes human and murine macrophage activation syndrome. Blood. 2018; 131: 1442-1455

Weissbrod L.,Marshall F. B.,Valla F. R.,Khalaily H.,Bar-Oz G.,Auffray J.-C.,Vigne J.-D. and Cucchi T. Origins of house mice in ecological niches created by settled hunter-gatherers in the Levant 15,000 y ago. Proceedings of the National Academy of Sciences. 2017; 114: 4099-4104

Wekell P.,Berg S.,Karlsson A. and Fasth A. Toward an Inclusive, Congruent, and Precise Definition of Autoinflammatory Diseases. Frontiers in Immunology. 2017; 8: 497

Welzel T. and Kuemmerle-Deschner J. B. Diagnosis and Management of the Cryopyrin-Associated Periodic Syndromes (CAPS): What Do We Know Today? J Clin Med. 2021; 10:

Wen J.,Xuan B.,Liu Y.,Wang L.,He L.,Meng X.,Zhou T. and Wang Y. Updating the NLRC4 Inflammasome: from Bacterial Infections to Autoimmunity and Cancer. Frontiers in Immunology. 2021; 12:

Wendler P.,Ciniawsky S.,Kock M. and Kube S. Structure and function of the AAA+ nucleotide binding pocket. Biochimica et Biophysica Acta (BBA) - Molecular Cell Research. 2012; 1823: 2-14

White T. E.,Brandariz-Nuñez A.,Martinez-Lopez A.,Knowlton C.,Lenzi G.,Kim B.,Ivanov D. and Diaz-Griffero F. A SAMHD1 mutation associated with Aicardi-Goutières syndrome uncouples the ability of SAMHD1 to restrict HIV-1 from its ability to downmodulate type I interferon in humans. Hum Mutat. 2017; 38: 658-668

Wieland F. T.,Gleason M. L.,Serafini T. A. and Rothman J. E. The rate of bulk flow from the endoplasmic reticulum to the cell surface. Cell. 1987; 50: 289-300

Williams M. A.,O'Callaghan A. and Corr S. C. IL-33 and IL-18 in Inflammatory Bowel Disease Etiology and Microbial Interactions. Front Immunol. 2019; 10: 1091

Wilson D. W.,Lewis M. J. and Pelham H. R. pH-dependent binding of KDEL to its receptor in vitro. J Biol Chem. 1993; 268: 7465-7468

Wisniewski J. R.,Zougman A.,Nagaraj N. and Mann M. Universal sample preparation method for proteome analysis. Nat Methods. 2009; 6: 359-362

Wortzel I.,Koifman G.,Rotter V.,Seger R. and Porat Z. High Throughput Analysis of Golgi Structure by Imaging Flow Cytometry. Scientific Reports. 2017; 7: 788

Wu H. J. and Wu E. The role of gut microbiota in immune homeostasis and autoimmunity. Gut Microbes. 2012; 3: 4-14

Wu J. and YAN N. Gain-of-function STING mutations induce T cell death in the SAVI mouse. The Journal of Immunology. 2018; 200: 166.129-166.129

Wu J.,Fernandes-Alnemri T. and Alnemri E. S. Involvement of the AIM2, NLRC4, and NLRP3 inflammasomes in caspase-1 activation by Listeria monocytogenes. J Clin Immunol. 2010; 30: 693-702

Wu J.,Sun L.,Chen X.,Du F.,Shi H.,Chen C. and Chen Z. J. Cyclic GMP-AMP is an endogenous second messenger in innate immune signaling by cytosolic DNA. Science. 2013; 339: 826-830

Wu J.,Chen Y. J.,Dobbs N.,Sakai T.,Liou J.,Miner J. J. and Yan N. STING-mediated disruption of calcium homeostasis chronically activates ER stress and primes T cell death. J Exp Med. 2019; 216: 867-883

Wu X.,Wu F.-H.,Wang X.,Wang L.,Siedow J. N.,Zhang W. and Pei Z.-M. Molecular evolutionary and structural analysis of the cytosolic DNA sensor cGAS and STING. Nucleic Acids Research. 2014; 42: 8243-8257

Xia S.,Zhang Z.,Magupalli V. G.,Pablo J. L.,Dong Y.,Vora S. M.,Wang L.,Fu T. M.,Jacobson M. P.,Greka A.,Lieberman J.,Ruan J. and Wu H. Gasdermin D pore structure reveals preferential release of mature interleukin-1. Nature. 2021; 593: 607-611

Xie W.,Lama L.,Adura C.,Tomita D.,Glickman J. F.,Tuschl T. and Patel D. J. Human cGAS catalytic domain has an additional DNA-binding interface that enhances enzymatic activity and liquid-phase condensation. Proceedings of the National Academy of Sciences. 2019; 116: 11946-11955

Xin F. and Radivojac P. Post-translational modifications induce significant yet not extreme changes to protein structure. Bioinformatics. 2012; 28: 2905-2913

Xu H.,Yang J.,Gao W.,Li L.,Li P.,Zhang L.,Gong Y.-N.,Peng X.,Xi J. J.,Chen S.,Wang F. and Shao F. Innate immune sensing of bacterial modifications of Rho GTPases by the Pyrin inflammasome. Nature. 2014; 513: 237-241

Xu Y.,Zhang Y.,Sun S.,Luo J.,Jiang S.,Zhang J.,Liu X.,Shao Q.,Cao Q.,Zheng W.,Chen N.,Meurens F. and Zhu J. The Innate Immune DNA Sensing cGAS-STING Signaling Pathway Mediates Anti-PRRSV Function. Viruses. 2021; 13:

Yamashiro L. H.,Wilson S. C.,Morrison H. M.,Karalis V.,Chung J. J.,Chen K. J.,Bateup H. S.,Szpara M. L.,Lee A. Y.,Cox J. S. and Vance R. E. Interferon-independent STING signaling promotes resistance to HSV-1 in vivo. Nat Commun. 2020; 11: 3382

Yan N.,Chai J.,Lee E. S.,Gu L.,Liu Q.,He J.,Wu J.-W.,Kokel D.,Li H.,Hao Q.,Xue D. and Shi Y. Structure of the CED-4–CED-9 complex provides insights into programmed cell death in Caenorhabditis elegans. Nature. 2005; 437: 831-837

Yan Y.,Jiang W.,Liu L.,Wang X.,Ding C.,Tian Z. and Zhou R. Dopamine Controls Systemic Inflammation through Inhibition of NLRP3 Inflammasome. Cell. 2015; 160: 62-73

Yang H.,Wang H.,Ren J.,Chen Q. and Chen Z. J. cGAS is essential for cellular senescence. Proc Natl Acad Sci U S A. 2017; 114: E4612-e4620

Yang H.,Guan L.,Li S.,Jiang Y.,Xiong N.,Li L.,Wu C.,Zeng H. and Liu Y. Mechanosensitive caveolin-1 activation-induced PI3K/Akt/mTOR signaling pathway promotes breast cancer motility, invadopodia formation and metastasis in vivo. Oncotarget. 2016; 7: 16227-16247

Yang J.,Zhao Y.,Shi J. and Shao F. Human NAIP and mouse NAIP1 recognize bacterial type III secretion needle protein for inflammasome activation. Proc Natl Acad Sci U S A. 2013; 110: 14408-14413

Yang L.,Wang L.,Ketkar H.,Ma J.,Yang G.,Cui S.,Geng T.,Mordue D. G.,Fujimoto T.,Cheng G.,You F.,Lin R.,Fikrig E. and Wang P. UBXN3B positively regulates STING-mediated antiviral immune responses. Nature Communications. 2018; 9: 2329

Yashiro T.,Yamamoto M.,Araumi S.,Hara M.,Yogo K.,Uchida K.,Kasakura K. and Nishiyama C. PU.1 and IRF8 Modulate Activation of NLRP3 Inflammasome via Regulating Its Expression in Human Macrophages. Frontiers in Immunology. 2021; 12:

Ye Z.,Lich J. D.,Moore C. B.,Duncan J. A.,Williams K. L. and Ting J. P. ATP binding by monarch-1/NLRP12 is critical for its inhibitory function. Mol Cell Biol. 2008; 28: 1841-1850

Yin Q.,Tian Y.,Kabaleeswaran V.,Jiang X.,Tu D.,Eck M. J.,Chen Z. J. and Wu H. Cyclic di-GMP sensing via the innate immune signaling protein STING. Mol Cell. 2012; 46: 735-745

Yokota S.,Imagawa T.,Nishikomori R.,Takada H.,Abrams K.,Lheritier K.,Heike T. and Hara T. Long-term safety and efficacy of canakinumab in cryopyrin-associated periodic syndrome: results from an open-label, phase III pivotal study in Japanese patients. Clin Exp Rheumatol. 2017; 35 Suppl 108: 19-26

Yoneyama M.,Kikuchi M.,Matsumoto K.,Imaizumi T.,Miyagishi M.,Taira K.,Foy E.,Loo Y. M.,Gale M., Jr.,Akira S.,Yonehara S.,Kato A. and Fujita T. Shared and unique functions of the DExD/H-box helicases RIG-I, MDA5, and LGP2 in antiviral innate immunity. J Immunol. 2005; 175: 2851-2858

York A. G.,Williams K. J.,Argus J. P.,Zhou Q. D.,Brar G.,Vergnes L.,Gray E. E.,Zhen A.,Wu N. C.,Yamada D. H.,Cunningham C. R.,Tarling E. J.,Wilks M. Q.,Casero D.,Gray D. H.,Yu A. K.,Wang E. S.,Brooks D. G.,Sun R.,Kitchen S. G.,Wu T. T.,Reue K.,Stetson D. B. and Bensinger S. J. Limiting Cholesterol Biosynthetic Flux Spontaneously Engages Type I IFN Signaling. Cell. 2015; 163: 1716-1729

Yoshimoto T.,Takeda K.,Tanaka T.,Ohkusu K.,Kashiwamura S.,Okamura H.,Akira S. and Nakanishi K. IL-12 up-regulates IL-18 receptor expression on T cells, Th1 cells, and B cells: synergism with IL-18 for IFN-gamma production. J Immunol. 1998; 161: 3400-3407

Yu C. H.,Davidson S.,Harapas C. R.,Hilton J. B.,Mlodzianoski M. J.,Laohamonthonkul P.,Louis C.,Low R. R. J.,Moecking J.,De Nardo D.,Balka K. R.,Calleja D. J.,Moghaddas F.,Ni E.,McLean C. A.,Samson A. L.,Tyebji S.,Tonkin C. J.,Bye C. R.,Turner B. J.,Pepin G.,Gantier M. P.,Rogers K. L.,McArthur K.,Crouch P. J. and Masters S. L. TDP-43 Triggers Mitochondrial DNA Release via mPTP to Activate cGAS/STING in ALS. Cell. 2020; 183: 636-649.e618

Yu X.,Acehan D.,Ménétret J.-F.,Booth C. R.,Ludtke S. J.,Riedl S. J.,Shi Y.,Wang X. and Akey C. W. A Structure of the Human Apoptosome at 12.8 Å Resolution Provides Insights into This Cell Death Platform. Structure. 2005; 13: 1725-1735

Yu X.,Zhang L.,Shen J.,Zhai Y.,Jiang Q.,Yi M.,Deng X.,Ruan Z.,Fang R.,Chen Z.,Ning X. and Jiang Z. The STING phase-separator suppresses innate immune signalling. Nature Cell Biology. 2021; 23: 330-340

Zaki M. H.,Man S. M.,Vogel P.,Lamkanfi M. and Kanneganti T. D. Salmonella exploits NLRP12-dependent innate immune signaling to suppress host defenses during infection. Proc Natl Acad Sci U S A. 2014; 111: 385-390

Zamboni D. S.,Kobayashi K. S.,Kohlsdorf T.,Ogura Y.,Long E. M.,Vance R. E.,Kuida K.,Mariathasan S.,Dixit V. M.,Flavell R. A.,Dietrich W. F. and Roy C. R. The Birc1e cytosolic pattern-recognition receptor contributes to the detection and control of Legionella pneumophila infection. Nat Immunol. 2006; 7: 318-325

Zanetti G.,Pahuja K. B.,Studer S.,Shim S. and Schekman R. COPII and the regulation of protein sorting in mammals. Nature Cell Biology. 2012; 14: 20-28

Zeller T.,Haase T.,Müller C.,Riess H.,Lau D.,Zeller S.,Krause J.,Baumert J.,Pless O.,Dupuis J.,Wild P. S.,Eleftheriadis M.,Waldenberger M.,Zeilinger S.,Ziegler A.,Peters A.,Tiret L.,Proust C.,Marzi C.,Munzel T.,Strauch K.,Prokisch H.,Lackner K. J.,Herder C.,Thorand B.,Benjamin

E. J.,Blankenberg S.,Koenig W. and Schnabel R. B. Molecular Characterization of the NLRC4 Expression in Relation to Interleukin-18 Levels. Circ Cardiovasc Genet. 2015; 8: 717-726

Zerangue N.,Malan M. J.,Fried S. R.,Dazin P. F.,Jan Y. N.,Jan L. Y. and Schwappach B. Analysis of endoplasmic reticulum trafficking signals by combinatorial screening in mammalian cells. Proc Natl Acad Sci U S A. 2001; 98: 2431-2436

Zhang B.-c.,Nandakumar R.,Reinert L. S.,Huang J.,Laustsen A.,Gao Z.-l.,Sun C.-l.,Jensen S. B.,Troldborg A.,Assil S.,Berthelsen M. F.,Scavenius C.,Zhang Y.,Windross S. J.,Olagnier D.,Prabakaran T.,Bodda C.,Narita R.,Cai Y.,Zhang C.-g.,Stenmark H.,Doucet C. M.,Noda T.,Guo Z.,Goldbach-Mansky R.,Hartmann R.,Chen Z. J.,Enghild J. J.,Bak R. O.,Thomsen M. K. and Paludan S. R. STEEP mediates STING ER exit and activation of signaling. Nature Immunology. 2020; 21: 868-879

Zhang C.,Shang G.,Gui X.,Zhang X.,Bai X.-c. and Chen Z. J. Structural basis of STING binding with and phosphorylation by TBK1. Nature. 2019; 567: 394-398

Zhang L.,Chen S.,Ruan J.,Wu J.,Tong A. B.,Yin Q.,Li Y.,David L.,Lu A.,Wang W. L.,Marks C.,Ouyang Q.,Zhang X.,Mao Y. and Wu H. Cryo-EM structure of the activated NAIP2-NLRC4 inflammasome reveals nucleated polymerization. Science. 2015; 350: 404-409

Zhang P.,Liu Y.,Hu L.,Huang K.,Hong M.,Wang Y.,Fan X.,Ulevitch R. J. and Han J. NLRC4 inflammasome–dependent cell death occurs by a complementary series of three death pathways and determines lethality in mice. Science Advances. 2021; 7: eabi9471

Zhang X. and Wigley D. B. The 'glutamate switch' provides a link between ATPase activity and ligand binding in AAA+ proteins. Nature Structural & Molecular Biology. 2008; 15: 1223-1227

Zhang X.,Shi H.,Wu J.,Zhang X.,Sun L.,Chen C. and Chen Z. J. Cyclic GMP-AMP containing mixed phosphodiester linkages is an endogenous high-affinity ligand for STING. Mol Cell. 2013; 51: 226-235

Zhang X.,Wu J.,Du F.,Xu H.,Sun L.,Chen Z.,Brautigam C. A.,Zhang X. and Chen Z. J. The cytosolic DNA sensor cGAS forms an oligomeric complex with DNA and undergoes switch-like conformational changes in the activation loop. Cell Rep. 2014; 6: 421-430

Zhang Z.,Yuan B.,Bao M.,Lu N.,Kim T. and Liu Y.-J. The helicase DDX41 senses intracellular DNA mediated by the adaptor STING in dendritic cells. Nature Immunology. 2011; 12: 959-965

Zhang Z.,Meszaros G.,He W. T.,Xu Y.,de Fatima Magliarelli H.,Mailly L.,Mihlan M.,Liu Y.,Puig Gámez M.,Goginashvili A.,Pasquier A.,Bielska O.,Neven B.,Quartier P.,Aebersold R.,Baumert T. F.,Georgel P.,Han J. and Ricci R. Protein kinase D at the Golgi controls NLRP3 inflammasome activation. J Exp Med. 2017; 214: 2671-2693

Zhao B.,Du F.,Xu P.,Shu C.,Sankaran B.,Bell S. L.,Liu M.,Lei Y.,Gao X.,Fu X.,Zhu F.,Liu Y.,Laganowsky A.,Zheng X.,Ji J. Y.,West A. P.,Watson R. O. and Li P. A conserved PLPLRT/SD motif of STING mediates the recruitment and activation of TBK1. Nature. 2019; 569: 718-722

Zhao L.,Helms J. B.,Brunner J. and Wieland F. T. GTP-dependent Binding of ADP-ribosylation Factor to Coatomer in Close Proximity to the Binding Site for Dilysine Retrieval Motifs and p23*. Journal of Biological Chemistry. 1999; 274: 14198-14203

Zhao L.,Helms J. B.,Brügger B.,Harter C.,Martoglio B.,Graf R.,Brunner J. and Wieland F. T. Direct and GTP-dependent interaction of ADP ribosylation factor 1 with coatomer subunit β. Proceedings of the National Academy of Sciences. 1997; 94: 4418-4423

Zhao X.,Lasell T. K. and Melançon P. Localization of large ADP-ribosylation factor-guanine nucleotide exchange factors to different Golgi compartments: evidence for distinct functions in protein traffic. Mol Biol Cell. 2002; 13: 119-133

Zhao Y.,Yang J.,Shi J.,Gong Y. N.,Lu Q.,Xu H.,Liu L. and Shao F. The NLRC4 inflammasome receptors for bacterial flagellin and type III secretion apparatus. Nature. 2011; 477: 596-600

Zheng D.,Liwinski T. and Elinav E. Interaction between microbiota and immunity in health and disease. Cell Research. 2020a; 30: 492-506

Zheng D.,Liwinski T. and Elinav E. Inflammasome activation and regulation: toward a better understanding of complex mechanisms. Cell Discovery. 2020b; 6: 36

Zhong B.,Yang Y.,Li S.,Wang Y. Y.,Li Y.,Diao F.,Lei C.,He X.,Zhang L.,Tien P. and Shu H. B. The adaptor protein MITA links virus-sensing receptors to IRF3 transcription factor activation. Immunity. 2008; 29: 538-550

Zhong F. L.,Robinson K.,Teo D. E. T.,Tan K. Y.,Lim C.,Harapas C. R.,Yu C. H.,Xie W. H.,Sobota R. M.,Au V. B.,Hopkins R.,D'Osualdo A.,Reed J. C.,Connolly J. E.,Masters S. L. and Reversade B. Human DPP9 represses NLRP1 inflammasome and protects against autoinflammatory diseases via both peptidase activity and FIIND domain binding. J Biol Chem. 2018; 293: 18864-18878

Zhong L.,Hu M.-M.,Bian L.-J.,Liu Y.,Chen Q. and Shu H.-B. Phosphorylation of cGAS by CDK1 impairs self-DNA sensing in mitosis. Cell Discovery. 2020; 6: 26

Zhou H.,Watts J. D. and Aebersold R. A systematic approach to the analysis of protein phosphorylation. Nature Biotechnology. 2001; 19: 375-378

Zhou J.,Wang Y.,Chang Q.,Ma P.,Hu Y. and Cao X. Type III Interferons in Viral Infection and Antiviral Immunity. Cellular Physiology and Biochemistry. 2018a; 51: 173-185

Zhou R.,Xie X.,Li X.,Qin Z.,Wei C.,Liu J. and Luo Y. The triggers of the cGAS-STING pathway and the connection with inflammatory and autoimmune diseases. Infection, Genetics and Evolution. 2020; 77: 104094

Zhou W.,Mohr L.,Maciejowski J. and Kranzusch P. J. cGAS phase separation inhibits TREX1-mediated DNA degradation and enhances cytosolic DNA sensing. Mol Cell. 2021; 81: 739-755.e737

Zhou W.,Whiteley A. T.,de Oliveira Mann C. C.,Morehouse B. R.,Nowak R. P.,Fischer E. S.,Gray N. S.,Mekalanos J. J. and Kranzusch P. J. Structure of the Human cGAS-DNA Complex Reveals Enhanced Control of Immune Surveillance. Cell. 2018b; 174: 300-311.e311

Zhuang S.,Lynch M. C. and Kochevar I. E. Caspase-8 mediates caspase-3 activation and cytochrome c release during singlet oxygen-induced apoptosis of HL-60 cells. Exp Cell Res. 1999; 250: 203-212

Zierhut C. and Funabiki H. Regulation and Consequences of cGAS Activation by Self-DNA. Trends in Cell Biology. 2020; 30: 594-605

Zierhut C.,Yamaguchi N.,Paredes M.,Luo J. D.,Carroll T. and Funabiki H. The Cytoplasmic DNA Sensor cGAS Promotes Mitotic Cell Death. Cell. 2019; 178: 302-315.e323

Zink S.,Wenzel D.,Wurm C. A. and Schmitt H. D. A link between ER tethering and COP-I vesicle uncoating. Dev Cell. 2009; 17: 403-416

Curriculum vitae

Education

12/2017 – current	**Doctor of Philosophy (PhD)** Jointly awarded PhD: Bonn & Melbourne Research and Graduate School (IRTG 2168) Thesis title: “Investigation of novel pathways causing autoinflammatory disease” Supervisors: A/Prof. Dr. Seth L. Masters Inflammation Division, Walter and Eliza Hall Institute of Medical Research, University of Melbourne, Australia Prof. Dr. Matthias Geyer Institute of Structural Biology, University of Bonn, Germany
10/2012 – 09/2015	**Molecular Medicine, Master of Science (M.Sc.)** Friedrich Schiller University Jena, Germany Thesis title: “Analysis of putative SALL4-interacting proteins in mouse testis and establishment of a spermatogonial stem cell culture system” Supervisor: Dr. Maren Godmann; Friedrich Schiller University Jena, Germany
10/2009 – 07/2012	**Human Biology, Bachelor of Science (B.Sc.)** Ernst Moritz Arndt University Greifswald, Germany Thesis title: „Occurrence and meaning of *Talpidae*- and *Soricidae*-associated Hantaviruses in Germany” Supervisor: PD Dr. Rainer G. Ulrich; Friedrich Loeffler Institute (FLI) Federal Research Institute for Animal Health, Riems, Germany

Internships & work experience

02/2017 – 06/2017	**Internship** Translational Research & Development CSL Limited, Bio21, Melbourne, Australia
10/2015 – 04/2016	**Internship** Biomedical Research and Project Evaluation Department of Technology and Innovation Management, Global R&D Fresenius Medical Care Germany GmbH, Bad Homburg, Germany
08/2015 – 09/2015	**Graduate Laboratory Assistant** Laboratory of Dr. Maren Godmann Institute for Biochemistry Friedrich Schiller University Jena, Germany
08/2013 – 02/2014	**Internship** Laboratory of A/Prof. Dr. Elena Jones Mesenchymal Stem Cell Research Group NIHR Leeds Musculoskeletal Biomedical Research Unit University of Leeds, United Kingdom
07/2012 – 09/2012	**Internship** Molecular Biology Quality Control IDT Biologika GmbH Dessau-Rosslau, Germany

Appendix

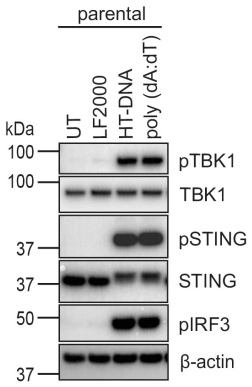

Suppl. Figure 1 | The cGAS-STING pathway is functional in parental HeLa cells used in this study. Parental HeLa cells were transfected with cGAS activators HT-DNA (2 µg/ml) and poly (dA:dT) (1 µg/ml) for 90 min and immunoblotted for detection of cGAS-STING signalling pathway proteins. A representative result of n=3 is shown. Lipofectamine 2000, LF2000; untreated, UT.

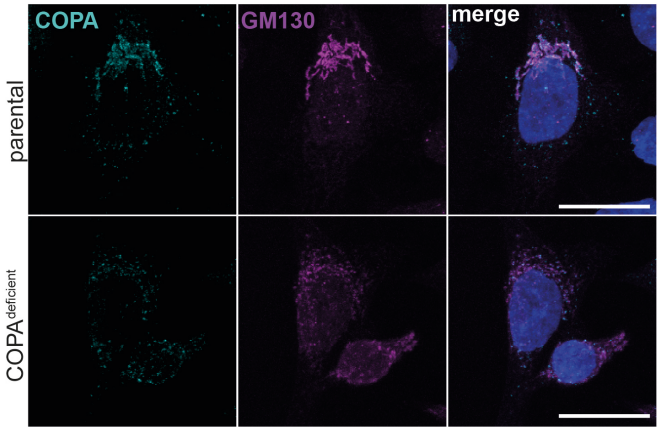

Suppl. Figure 2 | Deletion of COPA results in Golgi dispersal. Immunofluorescence analysis of parental and COPA^{deficient} HeLa cells after 72 hrs Doxycycline treatment stained for COPA (cyan), *cis*-Golgi marker GM130 (magenta) and DAPI (blue). Pictures are representatives of n=3 independent experiments. Scale bar represents 20 µm.

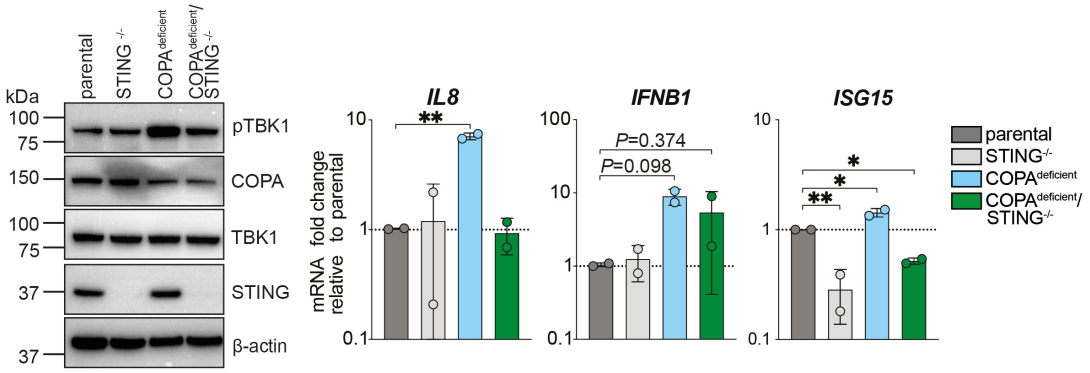

Suppl. Figure 3 | Inflammatory signalling in COPA^{deficient} HeLa cells is STING-dependent. CRISPR/Cas9 gene editing was performed to genetically delete STING in parental and COPA^{deficient} HeLa cells. Protein expression levels of phosphorylated TBK1 (pTBK1) were assessed by immunoblot analysis of unstimulated cells (72 hrs Dox). A representative experiment of n=3 is shown. Inflammatory pathway activation was also investigated by qRT-PCR analysis of proinflammatory gene transcription at baseline. Data were pooled from n=2 independent experiments. Error bars represent SD. Statistical analysis by one-way ANOVA and Dunnett's multiple comparison testing. *P*-values are indicated by numbers or as: * *P*<0.05, ** *P*<0.01.

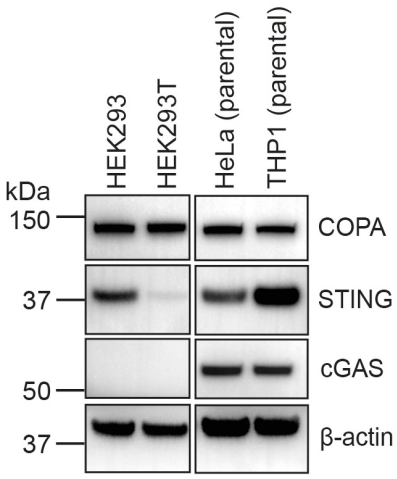

Suppl. Figure 4 | Endogenous cGAS and STING expression levels in cell lines. Representative immunoblot analysis of endogenous STING and cGAS expression levels in HEK293, HEK293T, parental HeLa and THP-1 cell lines used in this study.

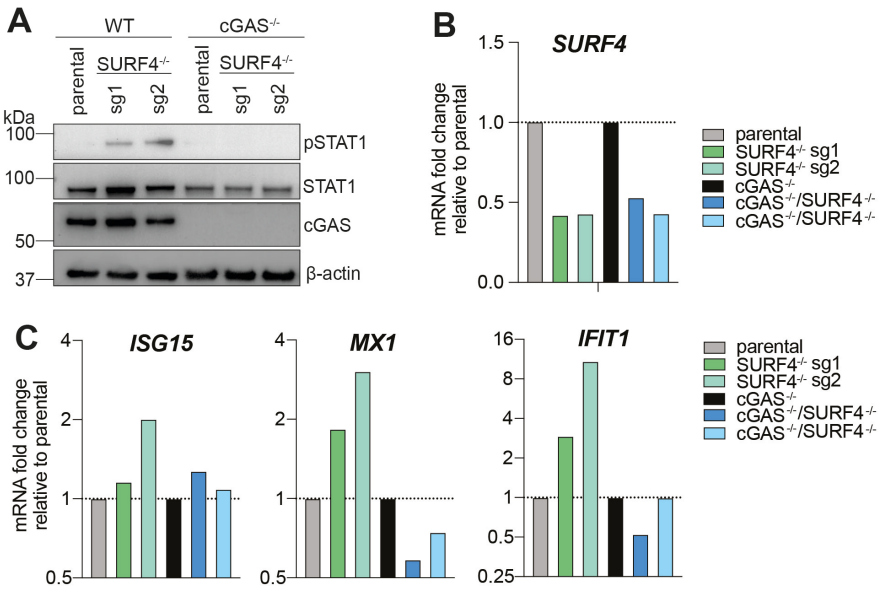

Suppl. Figure 5 | Genetic deletion of adapter protein SURF4 induces inflammatory signalling in a cGAS-dependent manner. A) Immunoblot analysis of inflammatory signalling in parental (WT) and monoclonal cGAS$^{-/-}$ THP-1 cells following genetic deletion of SURF4 using two different sgRNAs (sg1 and sg2), n=1. **B)** qRT-PCR analysis of *SURF4* transcription levels of cell lines used in A), data shown as mean from 2 technical replicates, n=1. **C)** qRT-PCR analysis of ISG transcription levels in THP-1 cell lines used in A) and B), n=1.

Suppl. Table 1 | Literature review of COPA syndrome patients. Patient demographics, clinical presentation, parameters of systemic inflammation, type I IFN signature and treatment are summarized**.** Due to the number of case reports the table was split into two parts: **Suppl. Table 1 A and 1 B**. If available from the original publication, the number of patients presenting with a certain condition is indicated in brackets. In a screening of childhood interstitial lung disease (chILD), Tang et al., identified a COPA patient, however since a detailed description of the clinical presentation and identified COPA mutation was lacking this patient is not included in the table below (Tang et al 2020a).
Abbreviations: interstitial lung disease (ILD), diffuse alveolar hemorrhage (DAH), anti-nuclear autoantibodies (ANAs), anti-neutrophil cytoplasmic antibodies (ANCAs), rheumatoid factor (RF), anti-citrullinated protein (CCP), avascular necrosis (AVN), months (m), years (y), juvenile idiopathic arthritis (JIA), rheumatoid arthritis (RA), polyarticular arthritis (PA), glomerulonephritis (GN), alanine transaminase (ALT), aspartate transaminase (AST), non-steroid anti-inflammatory drugs (NSAIDs), macrophage activation syndrome (MAS), gastroesophageal reflux disease (GERD), Golimumab (G), Etanercept (E), Adalimumab (A), Abatacept (Ab), Tocilizumab (T), Rituximab (Ri), Leflunomide (L), Azithromycin (Az), Hydroxychloroquine (H), Methotrexate (M), Thymoglobin (Th), Tacrolimus (Ta), Mycophenolate mofetil (Mm), Cyclophosphamide (C), Naproxen (N), Salazopyrin (S), Baricitinib (B), Ruxolitinib (R), Upadacitinib (U), Sirolimus (Si), not available (N/A), [#] R233H mutation identified in 2 unrelated families, [##] patients/families were not distinguished according to mutation, [###] disease onset occurred earlier and more severe in successive generations, [####] study contained 2 additional previously reported families that are not listed again, † deceased.

Suppl. Table 1 A:

	Watkin et al., 2015 Vece et al., 2016 Tsui et al., 2018	Jensson et al., 2017	Volpi et al., 2018	Noorelahi et al., 2018	Brennan et al., 2017 (oral abstract)	Taveira-DaSilva et al., 2019	Boulisfane-El Khalifi et al., 2019	Prenzel et al., 2020
Cohort								
Families	5	1	1	1	1	1[###]	1	3
Total No. of mutation carriers	30	3	1	1	1	4	5	4
Male	16	1	-	1	-	2	3	1
Female	14	2	1	-	1	2	2	3
Symptomatic carriers	21	3	1	1	1	4	4	3, 1 N/A
Male	8	1	-	1	-	2	3	1
Female	13	2	1	-	1	2	1	2
Age of onset	16 < 5 y	18 m, 11 y, 32 y	3 y	12 y	4 y	1y, 16 y, 26 y, 56 y	10 y, 50 y, N/A (2)	9 y, 14 y, 2 y (age of diagnosis)
Genetics								
COPA mutation	p.R233H[#] p.D243G p.E241K p.K230N	p.E241K	p.R233H	p.W240R	p.D243N	p.R233H	p.R233H	p.R281W p.W240L p.W240S
Clinical presentation								
Lung disease	21	3	1	1	1	4	2	3; 1 N/A
ILD	21	3	Yes	Yes	Yes	Yes		3
DAH	7	1	-	Yes	-	-	2	N/A
Lung carcinoma	-	-	-	-		1	-	N/A
Musculoskeletal	JIA/RA/PA (20) AVN (1)	J(R)A (3)	Polyarticular JIA	Polyarticular joint pain	Polyarticular JIA	RA (1), AVN (1)	Transient arthralgia (2)	RA (1)
Kidney disease	Fibrosis GN (3) IgA nephropathy (1)	-	-	-	-	Acute pyelonephritis (1) carcinoma (1), kidney stones (1)	GN (2) Lupus-like nephritis	N/A
Skin	-	Skin rash (1)	-	-	-	-	-	-
Neurological	Dyskinesia (2)		-	-	-	neuromyelitis optica (1),	-	Disruptive behaviour disorder (1)
Other organs	-	Respiratory infections (3)	-	Growth retardation (1)	GERD, MAS, SLE	Meningitis (1), respiratory infection (1)	Facial edema	Delayed puberty (1)

Suppl. Table 1 A continued:

	Watkin et al., 2015 Vece et al., 2016 Tsui et al., 2018	Jensson et al., 2017	Volpi et al., 2018	Noorelahi et al., 2018	Brennan et al., 2017 (oral abstract)	Taveira-DaSilva et al., 2019	Boulisfane-El Khalifi et al., 2019	Prenzel et al., 2020
Autoantibodies	18	3	1	1	1	2	2	3; 1 N/A
ANAs	14	3	1	1	1	-	-	3
ANCAs	15	-	-	-	-	-	2	2
RF	9	3	1	1	-	2	-	1
CCP	-	2	-	1	-	-	-	-
Other parameters								
Type I IFN	N/A	N/A	↑PBMC Type I IFN gene signature	N/A	N/A	N/A	↑PBMC Type I IFN gene score	N/A
Inflammatory parameters	N/A	N/A	N/A	↑ESR, ↑CRP,	N/A	↑CRP normal ESR	↑ESR (1), ↑CRP (1)	N/A
Therapy								
Corticosteroids	21	3	1	1	1	N/A	N/A	3; 1 N/A
Immuno-suppressants	C, Ri, M, A, Az, E	Az (1), Mm (3), M (2), anti-TNF (1)	M, Ab, Mm, H, anti-TNF	M, A	M, C, Ri, Mm, H	C, H	Ri (1), Mm (1), N/A (2)	N/A
NSAIDs	N	-	-	N	-	-	N/A	N/A
Others	-	S (3)	-	-	prophylactic antibiotics	ACE inhibitors	N/A	N/A
Transplantation	2 (lung), 1 (kidney)	2 (lung)	-	-	-	-	1 (kidney)	-

Suppl. Table 1 B:

	Krutzke et al., 2019	Thaivalappil et al., 2021	Guan et al., 2021	Mallea et al., 2020	Fremond et al., 2020	Kato et al., 2021	Psarianos et al., 2021	Lepelley et al., 2020[####]	Patwardhan et al., 2019
Cohort									
Families	1	1	2[##]	1	1	1	1	2[##]	1
Total No. of mutation carriers	1	1	3	1	2	4	1	3	2
Male	-	1	3	-	-	3	1	1	2
Female	1	-	-	1	2	1	-	2	-
Symptomatic carriers	1	1	2	1	1	4	1	2	2
Male	-	1	2	-	-	3	1	1	2
Female	1	-	-	1	1	1	-	1	-
Age of onset	2 y	9 m	7 y, 3 m	24 y	2 y	Infancy (3), 53 y (1)	3 y	2.5 y, 7 y	6 m, 7 y
Genetics									
COPA mutation	p.R233H	p.A239P	p.H199R p.K238E	N/A	p.R233H	p.V242G	p.A239P	p.R233H p.D243N	p.E241A
Clinical presentation									
Lung disease	1	1	2	1	1	4	1	2	2
ILD	Yes	-	-	Yes	Yes	Yes	yes	Yes	2
AH	-	-	-	Yes	Yes	-	-	-	2
Lung carcinoma	-	-	-	-	-	-	-	-	-
Musculoskeletal	PA (1)	-	PA (1)	Arthritis (1)	-	Arthritis (4)	-	Arthritis Arthralgia Myalgia (1)	PA (1)
Kidney disease	-	-	Proteinuria (1)	Immune-mediated kidney disease (1)	-	-	-	-	-
Skin	-	-	Eczema/urticaria (2)	-	-	-	Eczema	vitiligo	Eczema (1)
Neurological	-	-	-	-	-	-	-	-	-
Others	GERD	Persistent transaminitis, Growth retardation	Recurrent pneumonia (1), Growth retardation (1)	GERD	Multiple respiratory infections	Multiple bacterial infections Thyroid cancer (1)	Failure to thrive Food allergy Transient ↑ALT, AST	MAS (1), Hepatitis, Cardiac hyperthrophy (1)	Afebrile pneumonia (1), Growth retardation

Suppl. Table 1 B continued:

	Krutzke et al., 2019	Thaivalappil et al., 2021	Guan et al., 2021	Mallea et al., 2020	Fremond et al., 2020	Kato et al., 2021	Psarianos et al., 2021	Lepelley et al., 2020####	Patwardhan et al., 2019
Autoantibodies	1	1	2	1	1	4	1	2	2
ANAs	1	-	2	-	-	4	1	2	2
ANCAs	-	-	-	1	-	-	1	1	2
RF	1	1	1	-	1	2	-	-	-
CCP	1	-	2	-	-	-	-	-	-
Other parameters									
Type I IFN	N/A	N/A	↑PBMC Type I IFN genes	N/A	↑PBMC Type I IFN gene score, ↑serum IFNα	↑PBMC Type I IFN gene score,	N/A	↑PBMC Type I IFN gene score, ↑serum IFNα	N/A
Inflammatory parameters	N/A	N/A	↑ESR, CRP	N/A	N/A	N/A	↑CRP, ESR	N/A	↑ESR, CRP
Therapy									
Corticosteroids	1	1	2	1	1	4	1	1	1
Immuno-suppressants	G, E, A, Ab, T Ri, L, Az	Ri, H, Az	M	Ri, Th, Ta, IVIG	H, Az, Mm, C	T, anti-TNF	H, Mm	M, H (2), Mm, Anti-CD20-mAb	M, Az, Mm, H, E, A
NSAIDs	N/A	N/A	-	-	-	-	-	-	-
Others	B	N/A	Si	Plasma-pheresis	R	B (1), U (1)	-	B (1), R (1)	-
Transplantation	-	-	-	1 (lung)	-	2 (lung) †	-	Listed candidate (lung, 1)	-

Suppl. Table 2 | Literature review of reported NLRC4-AID patients. Demographics, clinical presentation, treatment, outcome and methods of experimental validation are summarized**.** Clinical classification based on the respective case report or following the classification by Wang et al., 2021a. Due to the number of case reports, this table was split into two parts: **Suppl. Table 2 A and 2 B.**Abbreviations: days (d), weeks (w), months (m), years (y), C-reactive protein (CRP), serum amyloid A (SAA), erythrocyte sedimentation rate (ESR), alanine transaminase (ALT), aspartate transaminase (AST), autoinflammation with infantile enterocolitis (AIFEC), macrophage activation syndrome (MAS), nonsteroidal anti-inflammatory drugs (NSAIDs), nucleotide-binding domain (NBD), Helical domain (HD), winged helix domain (WHD), leucin-rich repeat domain (LRR), familial cold autoinflammatory syndrome-4 (FCAS4), neonatal-onset multisystem inflammatory disease (NOMID), inflammatory bowel disease (IBD), diffuse alveolar hemorrhage (DAH), not available (N/A), [#] conference talk, [##] autopsy findings, patient (P); base pair (bp); intestinal epithelial cells (IEC), mutant allele frequency (MAF), monocyte-derived macrophage (MDM), untreated (UT), sensorineural hearing loss (SHL), ulcerative colitis (UC), inflammatory bowel diseases (IBD), central nervous system (CNS), gastrointestinal tract (GIT), laboratory (lab.), Epstein-Barr virus (EBV), intravenous immunoglobulin (IVIG), Cyclosporine (Cy), Dexamethasone (Dex), Corticosteroids (CS), Colchicine (Col), Anakinra (An), Glucocorticoids (GC), Anti-human IFNγ antibody (NI-0501, anti-IFNγ), Prednisone (P), Canakinumab (Can), Infliximab (In), Vedolizumab (Ve), Albumin infusion (AI), Antibiotics (AB), Etoposide (Et), Cetirizine (Cet), bone marrow transplant (BMT), myeloablative conditioning (MAB), Eculizumab (Ecu), Tocilizumab (Toc), Ceftriaxone (Cef), Rapamycin (Rap), Sulfamethoxazole (Sul), Trimethoprim (Tri), Acetaminophen (Ace), Cefuroxime (Cr), Ibuprofen (Ib), Paracetamol (Par).

Suppl. Table 2A:

Reference	Romberg et al., 2014	Canna et al., 2014	Kitamura et al., 2014	Bracaglia et al., 2015[#]	Liang et al., 2017	(Kashiwagi et al., 2008, Kawasaki et al., 2017, Kawashima et al., 2007	Canna et al., 2017	Bardet et al., 2021
Families	1	1	1	1	1	1	1	2, unrelated
No. of Patient	3	1	13	1	1	1	1	2
Male	3	-	7	1	-	1	-	-
Female	-	1	6	-	1	-	1	2
Age of onset	10 d, 3 d, < 2 w	6 m	2-3 m	20 d	*in utero*	at birth	6 w	20 d (1), 3 y (1)
Genetics								
NLRC4 mutation	V341A	T337S	H443P	T337N	S171F	T177A	V341A	P1:R207K,P2:T337N
Genotype	Germline mutation; heterozygous	heterozygous	Germline; heterozygous	heterozygous	Somatic mosaic (25 % MAF); heterozygous	Somatic mosaic; heterozygous	heterozygous	P1:N/A P2:heterozygous
Mutation origin	*de novo* in father, inherited	*de novo*	inherited	*de novo*	*de novo*	*de novo*	*de novo*	N/A
Protein domain I	HD1	HD1	WHD	HD1	NBD	NBD	HD1	NBD/HD1
Clinical presentation								
Phenotypic classification	AIFEC	MAS	FCAS4	MAS	MAS + GIT inflammation	NOMID	AIFEC	P1:Vasoplegic shocks+GIT inflammation +lab. MAS; P2:MAS
Trigger	Physical, emotional stress (1)	N/A	cold	N/A	N/A	N/A	Respiratory infection	Potentially Infections (*E.coli* pyelonephritis)
Temperature	Fever	Fever	Fever	Fever	Fever	Fever	Fever	Fever (2)
GIT	Diarrhea (2), enterocolitis (1) Bowel autolysis[##] (1)	Loose stools, Mild duodenitis, Vomiting	-	-	Chronic enteropathy Enterocolitis	-	Secretory diarrhea, mucosal, Ulcerations, Enterocolitis	Diarrhea (2), Pain (1), Bloating (1) Focal enteritis (1)
Lung	DAH[##] (1) Acute respiratory distress (1)	-	-	-	Respiratory distress, Necrotizing bronchopneumonia[##], Lung infections[##]	-	Respiratory infection	
Kidney	Acute renal failure (1)	-	-	-	-	-	-	-
CNS	Subarachnoid hemorrhage (1), Macrophagic meningitis[##](1)	-	-	-	Pontosubicular necrosis	Mental retardation, Aseptic meningitis, SHL, Brain atrophy	-	-
Musculoskeletal	Arthralgia (1), Myalgia (1), Psoriatic arthritis (1)	-	Arthritis	-	-	-	-	-
Skin	Maculopapular rash (1), Erythematous plaques (1), Psoriasis (1)	Rash	Urticaria-like rash	Rash	-	Erythema urticaria	Erythrodermic rash	Urticarial rash (1) Diffuse erythema (1)
Blood	Anaemia (2) Thrombocytopenia (1) Pancytopenia (1) Coagulopathy (2)	Chronic anaemia, Leucopenia, Thrombocyto-penia	-	Pancytopenia	Anaemia Splenomegaly Thrombocytopenia	-	Coagulopathy, Thrombocytopenia, Anaemia	Vasoplegic shock(1) Pancytopenia

Suppl. Table 2 A continued:

Reference	Romberg et al., 2014	Canna et al., 2014	Kitamura et al., 2014	Bracaglia et al., 2015#	Liang et al., 2017	(Kashiwagi et al., 2008, Kawasaki et al., 2017, Kawashima et al., 2007	Canna et al., 2017	Bardet et al., 2021
Others	Cholecystitis (1) Failure to thrive (3) Splenomegaly# (2)	Poor growth Splenomegaly	-	Hepatospleno-megaly Liver insufficiency	Placental vasculopathy, Hepatospleno-megaly	Saddle nose Frontal bossing Poor growth	-	Splenomegaly (1) EBV infection (1)
Immunological parameters								
Inflammatory parameters	↑ferritin (3), ↑CRP (3) ↑ESR (1), ↑transaminases(1)	↑transaminitis ferritin, triglycerides, CRP	-	↑triglycerides, ↑ferritin	↑ferritin ↑triglycerides	↑CRP, ↑SAA	↑CRP, ↑ferritin	↑ferritin (2) ↑triglycerides (2)
Cytokines (measured in serum/plasma)	↑IL-18 (2)	↑IL-18	N/A	↑IL-18, IFNγ, CXCL9, CXCL10	↑ IL2R	↑ IL-18, IL6	↑ IL-18, CXCL9	P1:↑ IL-18 P2: N/A
Plasma/serum IL-18 concentration	$1x10^4$ pg/ml	0.8-1.7 $x10^4$ pg/ml	N/A	N/A	N/A	4500-6700 pg/ml	**Total:** $1x10^5$ pg/ml **Free:** 50 pg/ml	P1:↑ IL-18 (~18000 pg/ml)
Therapy								
	IVIG, Cy, Dex	CS, Col, An	NSAIDs for pain relieve	GC, Cy, anti-IFNγ	N/A	NSAIDs, An, P, Can	CS, An, In, Cy, Ve	CS, IVIG, AI, AB, Et, Cy, Ri
Outcome								
Successful treatment and survival	Alive at 7 and 46 years, Deceased on day 23 due to DAH (1)	Complete control of flares since An treatment was started at age 8 y	Symptoms mostly resolved without treatment, Alive in adulthood	Recovered at 4.5 m with anti-human IFNγ antibody	Deceased at 60 d of age	An successful, followed patient to 19 y of age	Limited An effect, Combined anti-IL-1β + rhIL-18BP, partial weaning off anti-IL-1β successful	**P1:** An from 6 m of age, switched to Can, complete control of flares **P2:** 17 y now, treatment with IL1β or IL-18 BP considered
Experimental validation								
In vitro system *In vivo* model	**HEK293:** ↑ caspase-1 cleavage, ↑ ASC specks **Patient MDMs:** ↑ ASC speck formation; +LPS:↑ cytokine, cell death	**Patient MDM:** ↑ASC speck, + LPS+intracellular Flagellin: ↑IL-1β, IL-18 + LPS+ATP:↑IL-1β, IL-18, **THP-1:**↑ caspase-1 cleavage, **THP-1 macrophages**: ↑IL-1β, IL-18	**HEK293T:** BNP oligomer formation, ↑cleaved caspase-1, ↑ IL-1β **PBMCs:** + PrgI: ↑IL-1β ***in vivo:*** **Transgenic NLRC4^{H443P} mice:** skin, bone, joints affected, splenomegaly, spontaneous + cold-induced	-	-	**Patient skin fibroblast-derived iPSC clones**: differentiated into monocytes, identified somatic mosaicism, +LPS: ↑ IL-1β, CRISPR/Cas9-mediated KO of NLRC4 confirmed phenotype	Transcriptional analysis of whole blood	-

Suppl. Table 2 B:

Reference	Wang et al., 2021a	Volker-Touw et al., 2017	Goddard 2007#	Moghaddas et al., 2018	Barsalou et al., 2018	Chear et al., 2020	Siahanidou et al., 2019	Jeskey et al., 2020	Ionescu et al., 2021
Families	1	1	1	2, unrelated	1	1	1	1	1
No. of Patient	2	13	1	2	1	1	1	2	1
Male	1	3	-	1	1	-	1	1	-
Female	1	10	1	1	-	1	-	1	1
Age of onset	6 m, adolescence	Infancy	8 d	11 d, 18 m	12 d	2 w	20 d	5-6 y	47 y **Late-onset**
Genetics									
NLRC4 mutation	G172S	S445P	R207K	W655C	V341L	Q657L	V341A	p.G753_L783del	S171F
Genotype	Germline; heterozygous	heterozygous	N/A	heterozygous	heterozygous	heterozygous	heterozygous	N/A	Somatic mosaicism (2-4 % MAF)
Mutation origin	inherited	inherited	*De novo*	*De novo*	*De novo*	*De novo*	*De novo*	inherited	*De novo*
Protein domain	NBD	WHD	NBD	LRR	HD1	LRR	HD1	LRR	NBD
Clinical presentation									
Phenotypic classification	FCAS4	FCAS4	AIFEC	MAS and GIT inflammation	AIFEC	skin erythema, inflammatory arthritis	AIFEC	FCAS4	Systemic inflammation with GIT symptoms
Trigger	Cold	Infections, stress, cold	N/A	N/A	N/A	N/A	Cow's milk protein allergy as suspected trigger for GIT onset	Cold	N/A
Temperature	Fever (1)	Fever	Fever	Fever	Fever	Fever	Fever	Fever	Fever
GIT	-	Late-onset: UC (1P, 75 y old), IBD (1)	Autoimmune enteropathy, duodenitis	Secretory diarrhea (1) Diarrhea + abdominal pain (1)	Bloody diarrhea Necrotic intestinal Mucosa in stool	Abdominal pain Vomiting, GIT Inflammation	Enterocolitis, Perianal abscess, Chronic rectal inflammation,	Chronic oral ulcers exacerbated by flares	Abdominal pain, Diarrhea, Gastritis
Lung	-	-	Respiratory distress	Bronchopneumonia (1)	-	Respiratory tract infections	Respiratory distress	Chest pain	N/A
Kidney	-	Chronic insufficiency (1)	Renal failure	Acute renal injury (1)	Acute kidney failure	-	↓ Glomerular filtration rate	-	N/A
CNS	-	SHL (1)	Encephalopathy	P2; *Sphingomonas paucimobilis* infection	-	-	-	SHL	Prior onset: SHL
Musculoskeletal	Arthralgia (2) Joint swelling (1)	Arthralgias, Myalgias Polyarthritis + tendinitis + osteoarthritis (1)	-	-	-	Inflammatory arthritis	-	Myalgia, Arthralgia	Myalgias Arthralgias
Skin	Urticaria or erythematous patches and flakes (1)	**Adults:** erythematous nodes with urticarial patches **children:** urticarial rash	Rash	Urticaria-like rash (1) Maculopapular skin rash (1)	Macular erythematous rash	Abscesses, Erythematous itchy nodules	-	Persistent facial rash, pronounced during flare Rosacea	N/A

Suppl. Table 2 B continued:

Reference	Wang et al., 2021a	Volker-Touw et al., 2017	Goddard 2007#	Moghaddas et al., 2018	Barsalou et al., 2018	Chear et al., 2020	Siahanidou et al., 2019	Jeskey et al., 2020	Ionescu et al., 2021
Blood	-	Anaemia (1)	Thrombocy-topenia	Pancytopenia (1) Thrombocytopenia (1)	Anaemia Thrombocytopenia Hypereosinophilia T cell lymphopenia	Leucocytosis	Leucocytosis Thrombocytopenia Coagulopathy	N/A	N/A
Others	-	Conjunctivitis, Fatigue	Tachycardia, Poor feeding	Hepatosplenomegaly (2), Lymphadenopathy (1)	Metabolic acidosis, Hepatosplenomegaly	Middle ear effusion (*S.aureus)* Hepatosplenomegaly	Metabolic acidosis Hypothermia Mild hepatosplenomegaly	Hypotension Ménière's disease Fatigue	adenopathy
Immunological parameters									
Inflammatory parameters	Normal CRP, ESR	↑ CRP (3), ESR (2)	↑ ferritin, ↑transaminitis	↑ CRP, ferritin, triglyceride, transaminases	↑ triglycerides, ferritin	↑ ESR, CRP, ferritin	↑ CRP, SAA, transaminases, ferritin	N/A	↑ ESR, triglyceride normal ferritin, AST, ALT
Cytokines (measured in serum/plasma)	↑IL-18, IL-1β, IL-6	↑ IL-18 (8), normal for IL-1β, IL-6, IL-10, TNF, IFNγ	Cytokine storm after BMT:↑IL-6, IL8, IL-10, TNF, IFNγ	↑ sIL-2R (1), IL-18 (2)	↑ IL-18	↑ IL-18, IL-18BP, CXCL9	↑ IL-18	N/A	↑ IL-18
Plasma/serum IL-18 concentration	**P:** 1600 pg/ml; mother normal	Range in 8 patients: 3097-13984 pg/ml	N/A	**P1:** Total: $6x10^4$-$9x10^4$ pg/ml; Free :$2x10^4$-$6x10^4$ pg/ml **P2:** Total: $1.8x10^4$ pg/ml,	Total: $8x10^4$ pg/ml	Total IL-18: between ~10^4-10^5 pg/ml IL-18BP: ~10^3-10^5 pg/ml	Total IL-18: ~$3.5x10^4$ pg/ml, persistently elevated	N/A	~Total: 2000 pg/ml
Therapy									
	Cet, CS, NSAIDs	An (3)	CS, IVIG, An, BMT + MAB	CS, Ec, An, Toc, IVIG, Cef	CS, An, Rap	Sul, Tri, Ace, Cr,Ib, Par, Ib, Par, Col	AB, An	CS	Col, Ib, P
Outcome									
Successful treatment and survival	Alive at 4 y and 42 y (patient's mother=allele carrier)	Varied An response: good to none, deceased (1),other patients alive at 6-88 y	Alive at 6 m after BMT, tapered off CS and An	P1: unresponsive to An, slight improvement with rhIL-18BP, deceased at 11 w P2: deceased at 18.5 m	An + Rap Alive at 7 m →IL-18 plasma levels reduced	Col treatment was effective, Alive at 12 y	Alive at 2 y with An treatment, cow's milk-free diet → GIT remission unclear if due to An or naturally resolved	Father alive (age unknown) Patient alive at 41 y and about to receive An	Good control with An and Can
Experimental validation									
In vitro system *In vivo* model	**PBMCs:** + LPS: ↑ IL-1β, IL-6 but IL-18 release not increased; ↑ caspase-1 cleavage	-	-	**HEK293T:** ↑ ASC specks **THP-1:** ↑ IL-1β + cell death; + P3CSK4: ↑ IL-1β	**Patient MDM:** UT and LPS priming + NLRP3 or NLRC4 stimulation: ↑ IL-1β and IL-18	-	-		**HEK293T:**↑ oligomerization,↑ ASC specks **monocytes:**↑ ASC specks **PBMCs:**UT:↑ IL-18, slightly ↑IL-18 following NLRC4 stimulation, ↓ IL-1β, ↓ *IL1B* mRNA